The developmental polarity and morphogenesis of a single cell

Daria Bonazzi

Université Paris Descartes

Ecole doctorale interdisciplinaire européenne Frontières du Vivant

Equipe de recherche: Organisation spatiale de la cellule

Institut Jacques Monod, 13 Rue Helene Brion 75013 Paris

The developmental polarity and morphogenesis of a single cell

Par Daria BONAZZI

Thèse de doctorat de biologie cellulaire

Dirigée par Nicolas MINC

Présentée et soutenue publiquement le 06 Mars 2015

Devant un jury composé de :

COUDREUSE, Damien	Directeur de recherche	Rapporteur
WEDLICH SOLDNER, Roland	Directeur de recherche	Rapporteur
BOCELYN-GALLEGO, Evelyne	Directeur de recherche	Examinateur
PROST, Jacques	Directeur de recherche	Examinateur
BOUADOUD, Arezki	Directeur de recherche	Membre invite
MINC, Nicolas	Directeur de recherche	Directeur de these

a Marilena

…Anche se non ci sei tu sei sempre con me
per antiche abitudini
perchè ti rivedrò dovunque tu sia…
Franco Battiato

Acknowledgements

I would like to thank the members of the jury for kindly accepting to evaluate my work: the president Jacques Prost, the examiners Evelyne Bloch-Gallego and Arezki Boudaoud and especially my reviewers Damien Coudreuse and Roland Wedlich-Soldner for revising the manuscript.

I would like to thank Nicolas for having welcomed me in his new-born team: it has been great to work with you, you're a brilliant, efficient and passionate scientist with a never-ending stream of ideas! Under your guidance, I have learned a unique way of doing research and I grew up both professionally and personally. Thank you also for pushing me hard to improve myself: I think you care a lot about people in your team, you want the best for all of them, and that's really special.

I thank all the collaborators who contributed to my PhD work: Arezki Boudaoud and his PhD student Jean-Daniel Julien for building up the mechanical model in the first paper and giving me inspiring suggestions; Maryse Romao, for her expertise in electron microscopy; Rima, for brilliantly starting the spore project before me and for all the professional and personal chats we had along these last three years; finally Delphine Salort, for her mathematical model on cell polarity and its relationship with cell geometry in the second paper.

I would like to thank all the people of the lab for their help and support during my PhD: Hiro, for your naturally wise and calm attitude, with some more extravagant moments in front of a beer (but no ninja ties, I promise!); Armin, for your patience in listening to me sooo many times and for your jokes, that sometimes I don't get but well, that's funny anyway ;). Anaëlle, for your very very very special personality, sometimes a bit scary but well that's Xxxẍxxxland, with all its cats and unicorns! Valeria, perché hai illuminato questi ultimi mesi di tesi tesa! E per il tuo singhiozzo che tiene davvero compagnia, e mi mancherà. Moreover, I would like to thank all the people that worked in the Minc's lab in the past: Alexis, I miss your jajaja warm laugh and your jokes about my locura; Yonatan, having you as the first student in my life has been a super

enriching and enjoyable experience; Henry and Marguerite, les deux super stagiaires à l'opposé, bref la musique rock contre la classique.

Moreover, I thank Sebastien and his team with whom we pleasantly share the lab space here at the IJM, the colleagues of the third floor, all the people with whom I had nice discussions during common labmeetings, seminars and young scientist clubs; Je voudrais aussi remercier Mireille pour m'avoir aidée à faire face à l'administration francaise, et Patricia pour son travail essentiel de preparation des milieux et des boites. I thank also all the people of the Imagoseine platform, in particular Orestis, France, Xavier and Vincent, for their help with the microscopes and for being always super nice! Finally, I thank Kim and Antonin for taking care of organizing some regular aperos at the IJM, it is always a great opportunity to get to know people from other labs in a relaxed atmosphere.

I need also to thank numerous people in Curie, with whom I shared my daily lab life for about two years: first Matthieu, thanks for accepting my application as a Leonardo da Vinci student, the interdisciplinary atmosphere of your lab and the great research project I had to tackle both contributed to my decision of staying in Paris to start a PhD in cell biology. Next, I thank all the Piel's lab members: Hawa, my big friend in and beyond Curie, you are a perfect mixture of sensitivity and fun, thanks for always encouraging me, for your suggestions (scientific and not) and for all the time we spent together, inside or outside or around the lab: I wish you all the best for your US adventure! Paolo, con annessi Chiara e Mauro e Giovanna, la mia famiglia parigina d'adozione, vi voglio bene! Franzi, the best counselor ever, you really have a special emotional intelligence for both happy and sad things! Emmanuel, it took me some time to get to know you but it was really worth it, you and I are quite similar isn't it? Ewa, we had very funny moments together, I wish you all the best for your future and I hope we will keep in touch! Nico, merci pour être aussi bizarregeek, pour ton aide au labo et pour toutes les soirées chez toi à jouer aux jeux-vidéo, c'était super sympa! Julie, merci pour ton aide avec les microscopes et pour ton soutien pendant les moments plus durs de travail; Mael, tu as été un très bon supervisor pendant mon stage et un collègue excellent après! Yan Jun, thanks for your kindness and your daily smile; Melanie, les pauses cigarettes ne seraient pas étées les même sans ta drôle compagnie! Clotilde, on a pas encore fait de la musique ensemble mais on peut toujours récupérer; Matthew, we just quickly crossed before I moved to IJM but it has been nice to meet you!

I would like to thank some other people in Curie with whom I have shared some very nice moments: the fantastic Tran's and Paoletti's team, especially Phong, Anne, Merce, Kathleen, Sergio and Imene, thanks for sharing your pombe's expertise, the strains and the microfabrication hood, and thanks for being always so enjoyable and kind! I thank all the people of the third floor, in particular the Perez's and Houdusse's teams, and the fifth too, with your fantastic smoking balcony. A special thanks goes to Lamine, you are a really great and funny friend! Last but not least, I thank all the people in the Nikon Imaging center who helped me so many times with the microscopes, in particular Lucie and Vincent.

I thank also all the people that contribute to create a passionate and novel working atmosphere in my ED "Frontieres du Vivant", and my TAC supervisors, Phong and Claire, for being very supportive and positive about my work.

This PhD would not have been the same without the very unique experience of the Physiology Course in Woods Hole: two months of hard work in an amazing environment, surrounded by excellent and diverse people! I want to especially thank the three supervisors I've got the chance to work with, Clare, Wallace and Hari, the colleagues (and friends) Tamara, Felix, Alexis and Einat, and Nicolas again for sending me there!

To conclude, I want to thank all the people that encouraged me out of the lab: among my friends in Paris, a special thanks goes to Irene, i compagnoni italiani di lab (in particolare Giulia e Davide!), i mitici pareggiani (in particolare la Michi e Michi) e i membri di Argo, Michele, Matthieu e Rafael. Ringrazio i miei compagni di studi chimici a Bologna, Tea, Magna, Vale, Manu e Tommi, perché anche se siamo un po' sparsi in giro non ci perdiamo mai (troppo) di vista! Ringrazio anche il gruppo degli elettrocomici al Ciamician, in particolare Stefi, con cui mi sono avventurata per la prima volta nel mondo della biologia. E poi salto a Reggio, e allora ringrazio le mie amiche storicissime e insostituibili: Lollipoppy, Laura, Alle, Chiara, Sara ed Elly, é sempre un piacere ritrovarvi quando torno nell'Emilia paranoica! Un grazie speciale va a Luca, per avermi fatto scoprire storie e pensieri attorno alla scienza che restano purtroppo alieni agli scienziati, e per tutto quello che abbiamo condiviso.

Vorrei infine ringraziare la mia fantastica famiglia, per tutto il sostegno e l'affetto che non mi hanno mai fatto mancare: papà, Giuli e Aldo, Tati e Ferni, vi voglio bene!

Et là pour finir vraiment, je remercie Matthieu encore une fois, avec tout mon cœur.

Abstract

The developmental polarity and morphogenesis of a single cell

How cells establish their proper shapes and organization is a fundamental biological problem. In this thesis, I investigated the dynamic development of cellular form and polarity in the rod-shape fission yeast cell. These studies are based on monitoring how small symmetric fission yeast spores grow and self-organize to break symmetry for the definition of their very first polarity axis. In a first part, I studied interplays between surface mechanics of the spore cell wall and the stability of Cdc42-based polarity domains which control spatio-temporal aspects of spore symmetry breaking. In a second part, I studied mechanisms by which these polarity domains control their width and adapt it to cell surface geometry, a process likely relevant to understand how functional cortical domains scale to cell size. Overall these novel investigations focusing on how cells dynamically develop their form and polarity *de novo* highlight complex feedbacks in morphogenesis that cannot be evidenced by looking at cells at "steady state" or with genetics.

Resumé

Développement de la morphogenèse et de la polarité d'une cellule unique

Comment les cellules établissent leurs formes et organisations internes est un problème biologique fondamental. Au cours de cette thèse, j'ai étudié le développement de la forme cellulaire et de la polarité chez la cellule de levure fissipare. Ces études sont fondées sur l'exploration de la façon dont les petites spores symétriques de levures se développent et s'organisent pour briser la symétrie pour la définition de leur tout premier axe de polarité. Dans une première partie, j'ai étudié les couplages entre la mécanique de surface de la paroi cellulaire des spores et la stabilité de domaines de polarité de Cdc42 qui contrôlent les aspects spatio-temporelles de la brisure de symétrie de ces spores. Dans une seconde partie, j'ai étudié les mécanismes par lesquels ces domaines de polarité contrôlent leur taille et l'adapte à la géométrie

de la cellule, un processus vraisemblablement pertinents pour comprendre comment des domaines fonctionnels corticaux s'adaptent à la taille des cellules. Globalement, ces nouvelles recherches focalisant sur la façon dont les cellules développent dynamiquement leur forme et polarité *de novo*, permettent de mettre en évidence des couplages complexes dans la morphogenèse qui ne peuvent pas être testés en regardant les cellules à « l'état stationnaire» ou avec des outils génétiques.

Table of contents

List of abbreviations

cAMP/PKA: Cyclic AMP / protein kinase A

AP: Anterior-posterior

Arp2/3: Actin related protein 2/3

ATP: Adenosine triphosphate

BAR: Bin–Amphiphysin–Rvs

CAT: Conidial anastomosis tube

CRIB: Cdc42- and Rac-interactive binding

CWI: Cell wall integrity

ECM: Extracellular matrix

EF: Electric field

EMT: Epithelial-mesenchymal transition

ER: Endoplasmic reticulum

FSM: Forespore membrane

GAP: GTPase-activating protein

GDI: Guanine nucleotide-dissociation inhibitor

GDP: Guanosine diphosphate

GEF: Guanine nucleotide-exchange factor

GFP: Green Fluorescent Protein

GPCR: G protein-coupled receptor

GTP: Guanosine triphosphate

HOG: High osmolarity glycerol

LEP: Leading edge protein

MAPK: Mitogen activated protein kinase

MT: Microtubule

MTOC: Microtubule organizing center

NDR: Nuclear dbf2-related

NETO: New end take off

NSF: N-ethylmaleimide-sensitive factor

NMY-2: Non-muscle myosin II

NPF: Nucleation promoting factor

OSW: Outer spore wall

PAR: Partitioning-defective

PDMS: Polydimethylsiloxane

PI: Phosphatidylinositol

PIP: Phosphatidylinositol phosphate

PM: Plasma membrane

RD: Reaction diffusion

RGS: Regulator of G protein signaling

SASP: Small acid-soluble protein

SEM: Scanning electron microscopy

SNARE: Soluble NSF Attachment Protein

SPB: Spindle pole body

TEM: Transmission electron microscopy

WASp: Wiskott–Aldrich syndrome protein

List of figures

List of movies

Movie 1: Phase-contrast time lapse of the development of a wild-type fission yeast spore, Related to Figure 1 of Paper 1. The green outline corresponds to an automatically detected cell contour. Note the change in phase contrast at germination and the elongation of the polar tube at outgrowth. Time is in hr:min.

Movie 2: Phase-contrast time lapse of the development of a wild-type fission yeast spore going through three rounds of cell cycle, related to Figure 1 of Paper 1. Note that the first "mother" cell remains monopolar and grows away from the spore body. Time is in min.

Movie 3: Time-lapse phase-contrast and epifluorescence images of several developing spores expressing the polarized growth marker GFP-bgs4, related to Figure 2 of Paper 1. The signal in the fluorescent channel has been renormalized at each time point, and the scale bars may vary between successive movie. Note the phases of polar cap assembly and disassembly at successive locations and the stabilization at outgrowth. Time is in hr:min.

Movie 4: Time-lapse phase-contrast and epifluorescence images of a developing spore expressing the polarized growth marker GFP-bgs4, related to Figure 2 of Paper 1. Polarity cap drives local sites of polar growth at the spore surface during the wandering phase. GFP-bgs4 cap is indicated by white arrows, and subsequent local growth sites are indicated by red arrows. Time is in hr:min.

Movie 5: Time-lapse phase contrast of a group of four daughter spores attached to each other assuming the shape of the mother ascus, which germinate and outgrow, related to Figure S3 of Paper 1.

Movie 6: *In silico* simulation of growing spores, related to Figure 4 of Paper 1. The white semidisc represents the polar cap. The colored annulus represents the OSW, and values of strains in the OSW are represented with a color code (increasing from blue to red). When the OSW

breaks, the transparent annulus represents the inner cell wall superimposed on the OSW, for simplicity of representation. Note that the OSW ruptures where the strain reaches the red zone.

Movie 7: Time lapse of three spores expressing GFP-bgs4, related to Figure 6 of Paper 1. One spore is ablated at the site of bgs4 cap, another one is ablated away from the polar cap, and the third one is not ablated. The movie starts at the moment of laser ablation. Red arrows and dots point to sites of ablations, and black arrows point at outgrowing tubes. Time is in hr:min.

Movie 8: *In silico* simulation of growing spores with a hypothesis of positive feedback that biases the stabilization of the polar cap toward sites of maximal surface expansion rates, related to Figure 7 of Paper 1.

Movie 9: *In silico* simulation of growing spores with isotropic growth, related to Figure 6 of Paper 1. Note how the OSW ruptures at many locations.

Movie 10: *In silico* simulation of growing spores with no feedback hypothesis between polar cap and wall mechanics or geometry, related to Figure 7 of Paper 1.

Movie 11: *In silico* simulation of growing spores with a hypothesis of positive feedback that stabilizes the polar cap at sites of minimal surface stress, related to Figure 7 of Paper 1.

Movie 12: *In silico* simulation of growing spores with a hypothesis of positive feedback that stabilizes the polar cap at sites of maximal curvature, related to Figure 7 of Paper 1.

Movie 13: *In silico* simulation of growing spores with a hypothesis of positive feedback that stabilizes the polar cap at sites of maximal surface expansion rates.

Movie 14: Confocal images of several developing spores expressing the polarity marker CRIB-GFP, related to Figure 1 of Paper 2. Scale bar, 1μm. Note the phases of polar cap assembly and disassembly at successive locations and the corresponding variation in pole cap width. Time frame is 5 min.

Movie 15: 3D reconstruction of several developing spores expressing the polarity marker CRIB-GFP, related to Figure 1 and S1 of Paper 2. Confocal z-stacks were acquired with a 0.2μm z-step over 5μm range. Note the differences in pole cap size for spores with various local radii of curvature.

Movie 16: Maximal z-projections of confocal z-stacks of several developing spores expressing the LifeAct-mCherry, related to Figure 4 of Paper 2. Confocal z-stacks were acquired with a 0.2μm z-step over 5μm range. Time frame is 30sec. Note that actin structures, both cables and patches, are highly dynamic.

Movie 17: 3D reconstruction of several developing spores expressing CRIB-GFP and LifeAct-mCherry, related to Figure 4 of Paper 2. Confocal z-stacks were acquired with a 0.2μm z-step over 5μm range. Note the differences in pole cap size for spores with various local radii of curvature, and the corresponding reorganization of the actin cables network.

Movie 18: Phase-contrast time lapse of the development of two *bgs4Δ/pbr1–8* fission yeast spores, Related to Discussion. Time is in hr:min.

AIMS

Cells come in a wide range of forms and sizes. Cell shape and organization influences many of the basic cellular functions, such as growth, migration or division, and defects in cell morphogenesis can give rise to many diseases.

But how does a cell develop and maintain its shape?

The unicellular fission yeast *Schyzosaccharomyces pombe* is an excellent model organism to address such kind of questions, as it grows in a simple rod-shape by tip elongation and divides in the middle when it reaches 14 μm of length. Moreover, genetic manipulation allows to generate mutants with abnormal shapes, from round to bent or branched ones, hence shedding light on the molecular mechanisms responsible of cell shape regulation. Fission yeast cells grow at cell tips by targeting components such as the Rho-type GTPase Cdc42, and actin nucleators, which promote secretion needed for new membrane addition at cell tips.

In absence of nutrients, fission yeast cells develop to generate spores, as in the case of bacteria, plants, algae and other fungi. Spores are round, symmetric and dormant: moreover, they are encased in a very rigid shell, called outer spore coat, which is responsible of their high resistance to environmental stress, for very long periods of time.

In my PhD thesis, I have investigated how fission yeast spores germinate, grow and regenerate a rod-shaped vegetative cell. In a first part, I have characterized the coordination between polarity cap stabilization, growth and surface mechanics in this symmetry breaking event, in order to specify cell shape. In a second part, I have addressed how polarity domains, built around active-Cdc42, may define their size, and how they may adapt their size with cell size or cell shape.

These studies aim to define general principles for spontaneous polarization in eukaryotes, and how this process may be related to cell mechanics and geometry.

INTRODUCTION

1.

PRINCIPLES OF CELL MORPHOGENESIS

In this chapter, I will describe some general features of cell morphogenesis. I will start with a short description of how to define cell shape. I will then present some examples to illustrate the relationship between cell form and cell function and its general impact on cell physiology and disease, both at the uni- and multi-cellular level. Hence, I will illustrate in detail the main regulators of cell morphogenesis: first, cell polarity, with a historical introduction of the concept, a description of the main molecular players for eukaryotic cell polarity, and finally a classification of cell polarization processes that can be guided either by extrinsic or intrinsic cues. Second, cell mechanics, with a short historical overview followed by a general description of how forces can shape single cells and tissues. Hence, I will discuss the main sets of principles that have been proposed to generate spontaneous symmetry breaking. To conclude, I will briefly talk about another aspect of cell morphogenesis: cell size regulation, as a result of the balance between growth and division.

1.1 How to define cell shape?

The term "cell morphogenesis" refers to the processes that generate the forms of cells in the course of their growth, division, or development. The complex structure of a living cell is critical for cellular function. Yet relatively little is known about the mechanisms that produce the complex spatial organization of a living cell. On one hand, cells specify a certain form by integrating signals from the extracellular environment and/or their intracellular spatial organization and establishing a certain polarity axis. On the other hand, cell shape can also be viewed as the result of the mechanical balance of the forces exerted on the cell membrane by intracellular components (in particular, the cytoskeleton in animal cells and the cell wall in plants, fungi and bacteria) and the outside environment. Cell polarity and cell mechanics are highly regulated and interconnected through feedbacks loops to finally achieve a certain shape: in a multi-cellular context, cellular mechanical properties and gene expression/protein activation are coordinated among neighboring cells, to achieve global tissue shaping. It is also to be noted that while many aspects of cell shape and polarity may be determined by external cues, this does not preclude the possibility of self-organizing through spontaneous symmetry breaking. To conclude, another simple and fundamental aspect of cell morphogenesis is size regulation, which results from the balance between cell growth and cell division, and is an important determinant of cellular physiology. From this conceptual landscape, is it possible to identify any general organizational principle in cellular complexity, ranging from free-living cells to cells in tissues?

1.2 Cell shape and cell function

In all living organisms, from prokaryotes to eukaryotes, cells show a high degree of reproducible, non-random geometrical order, together with an extraordinary diversity in cell shapes, the most striking being the elaborate structural specializations of some free-living single-celled organisms. Many of the most complex-looking cells are protists, eukaryotic microorganisms with an elaborate anatomy which includes structures such as sensory bristles, photoreceptors, beating cilia, leg-like appendages, mouth parts, stinging darts, and muscle-like contractile bundles (Figure 1) (Marshall, 2011).

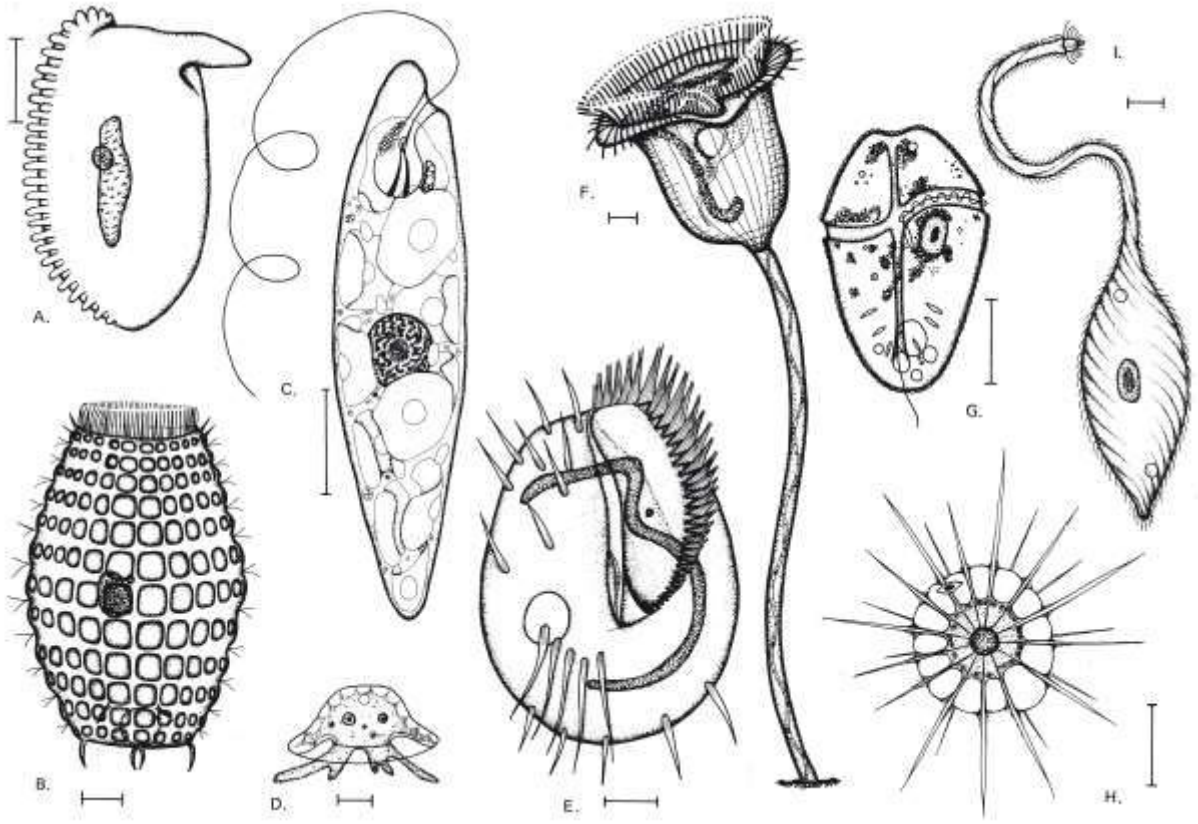

Figure 1: The complexity of cell shape in an assortment of diverse protists. The organisms in ***A***, ***B***, ***E***, ***F***, and ***I*** are ciliates; ***C*** is a euglenoid; ***D*** is an amoeba; ***G*** is a dinoflagellate; ***H*** is a heliozoan. Scale bars, 10 μm. (Sleigh, 1973).

Different cell shapes are not just an eccentricity of nature, but are also coupled to specialized cell functions (Figure 2): in higher eukaryotes, muscle cells have a fusiform shape and can stretch and relax, in order to release tension, support high stresses and at the same time maintain contractility; neurons can harbor extensions, reaching lengths of many meters, to communicate between tissues over long distances; epithelial cells possess rectangular shapes to build up barriers that regulate ionic homeostasis between different biological compartments. In case of infection, immune cells efficiently change shape to accomplish specific tasks, in particular finding and eliminating pathogens: for instance, lymphocytes that migrate throughout the body to get to the site of infection can squeeze through narrow pores in order to cross tightly packed tissues such as the endothelium, while neutrophils engulf bacteria and viruses by 'swallowing' them. A very last example of cell shape diversity is given by the two unique players of the fertilization process: on one hand, sperm cells, that are very small, with a long tail-like structure,

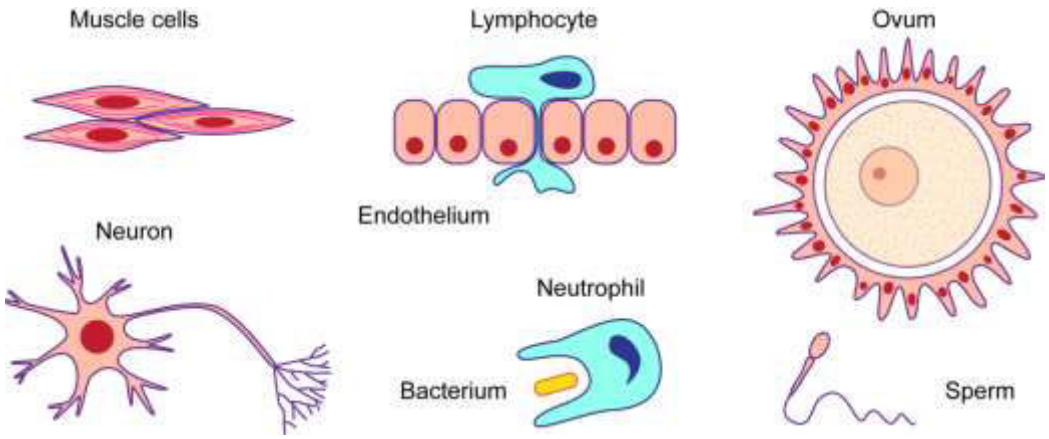

Figure 1: Examples of animal cells with unique shapes, directly related to specific cell functions. A brief description of each specific case can be found in the text.

called flagellum, to propel themselves and swim over long distances; on the other hand, egg cells, that are round, immobile and big.

As the cell is the functional unit of any living tissue, all shape changes in the organism are driven by events at the cellular level. In combination with cell division, growth and death, changes in individual cell shape are central to tissue morphogenesis and homeostasis. Shape change of individual cells, independent of their neighbors, contributes to different morphogenetic processes in development, such as the migration of single primordial germ cells towards the gonad (Blaser et al., 2006). However, in most morphogenetic events, cell shape change is coordinated amongst hundreds of neighboring cells and drives shrinkage, extension, folding and movement of tissues.

1.3 Cell shape and cell polarity

Today, we know that most cell types of metazoans, but also unicellular organisms, such as yeast and ciliated protozoa can polarize. Even in the case of prokaryotes, the notion of bacterial cells as unorganized bags of proteins has been abandoned, leaving space to the concepts of high spatial organization and asymmetric protein distribution. Cell polarity is essential for a great number of cellular functions, such as differentiation, polarized cell growth, activation of the immune response, directional cell migration, and vectorial transport of molecules across cell layers (Figure 3) (Drubin and Nelson, 1996). For example, the bacterium *Caulobacter crescentus* shows

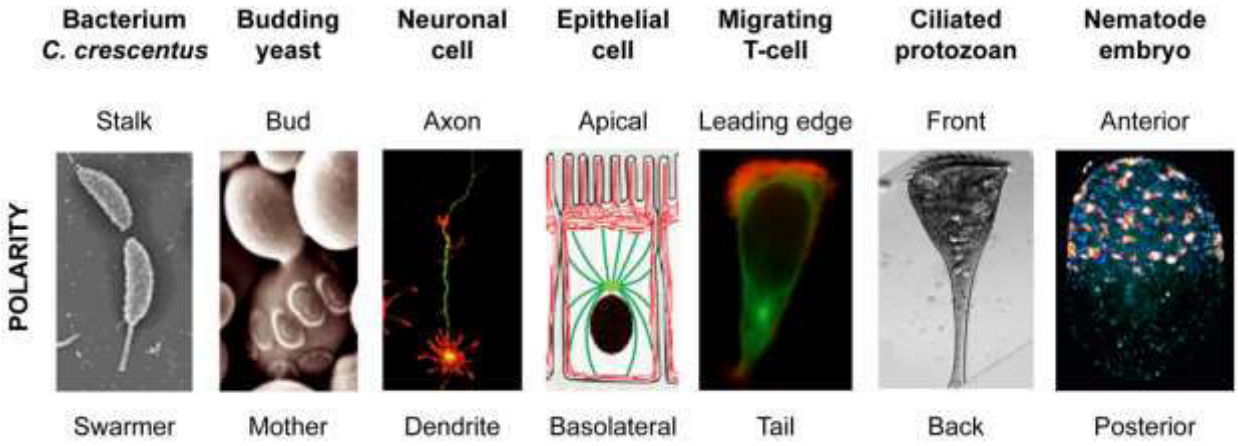

Figure 3: Diverse polarized cells. In the neuron picture, F-actin is marked in red and the axonal marker Tau in green; in both the epithelial cell drawing and the migrating T-cell picture, actin is marked in red and microtubules in green; in the *C. elegans* embryo picture, the early-endosome-associated protein EEA1 is marked in blue and the nonmuscle myosin II NMY-2 is marked in red (Amberg, 1998; Arkowitz and Iglesias, 2008; Thanbichler and Shapiro, 2006).

polarized distributions of the flagellum and stalk structures, leading to asymmetric cell division; the budding yeast *Saccharomyces cerevisiae* displays also pronounced cellular asymmetries during its normal growth cycle, that allow to distinguish mother from daughter cells; polarized hippocampal neurons can polarize by growing dendrites at the postsynaptic side and axonal outgrowths at the presynaptic side; cells in epithelial tissues possess a distinctive polarized internal organization, that is essential for the assembly of specific membrane domains, termed apical and basolateral; migrating cells such as T-cells establish a protrusive front, called leading edge, and a contractile rear, to achieve directional movement; finally, some uni- and multi-cellular organisms define an anterior-posterior (or front-back) polarity early during development.

A surprising feature of cell polarity is that it gives rise to this diversity of cell shapes and functions from a basic set of evolutionarily conserved and adapted core mechanisms, including localized assembly of signaling complexes, cytoskeleton remodeling, mobilization of proteins from intracellular pools, and targeted vesicle delivery to sites of membrane growth. (Nelson, 2003).

In tissues, the organization of cells relies on the integration of polarizing signals from different interdependent biological processes (Bryant and Mostov, 2008). First, cells must sense their environment, including where they are in relation to their neighbors, by direct interaction of cells with the extracellular matrix (ECM) through various receptors. Cells can also communicate

with other cells through adhesion molecules, such as cadherins, and the sensing of diffusible factors, such as morphogens. These combined cues function as instructions for cells to orient and coordinate the asymmetrical distribution of polarity complexes, in order to establish and enforce the generation of an axis of asymmetric organization at the tissue level. Cell polarity is thus crucial for patterning and morphogenesis at the multicellular scale, for development and tissue homeostasis. (Nelson, 2003). Loss of cell polarity can cause developmental disorders and cancer. For example, most human tumours are derived from epithelial tissues, with the common feature of a simultaneous dysregulation of apico-basal cell polarity and cell growth (Wodarz and Nathke, 2007).

1.3.1 Cell polarity: an (old) lesson from eggs

Cell polarity has long been recognized as a fascinating biological phenomenon, related to a number of properties such as cell shape, position, and size; historically, studies in the fields of embryology and developmental biology have been fundamental for the debut of this wide topic. In 1896, in his book "The cell in development and inheritance", Edmund Beecher Wilson

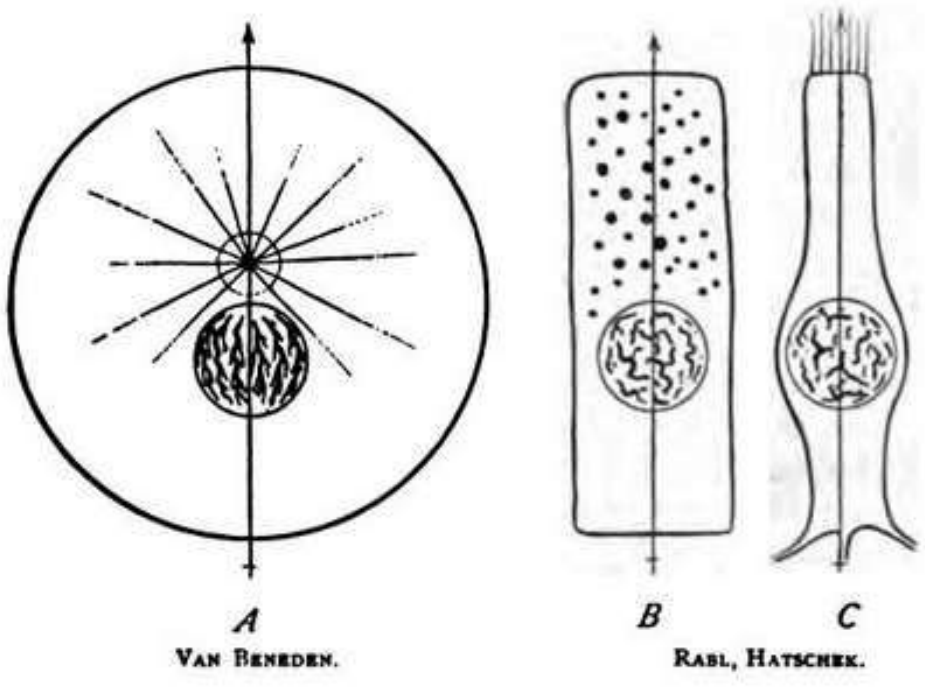

Figure 4: Historical diagrams of cell polarity. ***A.*** Schematic of Van Beneden's morphological polarity, based on the definition of an axis passing through nucleus and centrosome. ***B. C.*** Schematic of Rabl's and Hatschek's physiological polarity, ***B.*** in a gland cell, and ***C.*** in a ciliated cell (Wilson, 1896).

summarizes the two main currents of thought regarding the concept of cell polarity: one that is based on purely morphological considerations, and another with a more physiological perspective (Wilson, 1896). On the one hand, the Belgian embryologist Edouard Van Beneden conceived cell polarity as a primary morphological attribute of the cell, where the organic axis is identified as a line drawn through the center of the nucleus and the centrosome (Figure 4A) (Beneden, 1883). This view is in agreement with Carl Rabl's theory about nuclear polarity, according to which the chromosome loops converge towards the centrosome and consequently the nuclear axis coincides with the cell axis, giving rise to polarity of the whole egg, an essential factor in development (Rabl, 1885). Moreover, Heidenhain proposed that all the structures of the cell have a definite relation to the primary polarity axis, and that this relation is determined by conditions of tension in the astral rays focused at the centrosome (Heidenhain, 1893). On this basis, he endeavors to explain more mechanistically the position and movements of the nucleus, the succession of division planes and related phenomena. Berthold Hatschek together with Rabl, on the other hand, advanced a quite different hypothesis based on physiological considerations: for these authors, "cell polarity" didn't mean a predetermined morphological arrangement of parts in the cell, but a polar differentiation of the cell substance arising secondarily through adaptation to the cell's environment in tissues, and having not necessary relation with the polarity of Van Beneden (Figure 4, Panels *B.* and *C.*) (Hatschek, 1888). This is typically shown in the epithelium, where the free and basal ends of the cells differ widely in relation to the food-supply, and show a corresponding structural differentiation. Although these two conceptions of polarity have entirely different points of departure, Wilson proposed that there may be some cases leading to the same result; in other words, cells where the morphological and physiological polarity axes coincide. In the particular case of epithelial cells, he then suggested then that the position of the centrosome, and hence the direction of the polarity axis, is related to the cell environment.

Altogether, these studies introduce various concepts that have been developed and confirmed in more recent years: first, the definition of cell polarity as the result of a vectorial axis that directs the internal organization of a cell; second, its direct link with cell shape and cell function, in particular in the context of a tissue; finally, the possibility of environmental conditions to be sensed and transduced by the polarity machinery.

1.3.2 The biochemical revolution: vectorial physiology

In the second half of the 20th century, advances in the fields of biochemistry had important consequences on the conception of cell polarity. In 1963 Mitchell coined the term "vectorial metabolism" to describe chemical reactions that have a direction in space, and proposed that such reactions underlie many biological transport processes (Mitchell, 1963). The spatial dimension entered into biochemistry not only through biomembranes in the so-called chemiosmotic theory, but also through sliding filaments: in this case, the most familiar example is undoubtedly the contraction of muscle, where actin and myosin filaments run antiparallel while the directional cycling of the myosin heads generate mechanical force upon actin filaments (Figure 5) (Huxley, 1969). Few years later, eukaryotic MT-based structures such as cilia and flagella were identified as another example of the conversion of scalar free energy into vectorial mechanical force. All these cytoskeletal filaments possess an intrinsic polarity, due to the intrinsic asymmetry of each monomer: for instance, MTs elongate and shrink preferentially at the free "plus" end (Kirschner and Mitchison, 1986), while actin filaments grow by monomers addition to the anchored "barbed" end (Pollard and Cooper, 1986). In the same years, the motor proteins that are

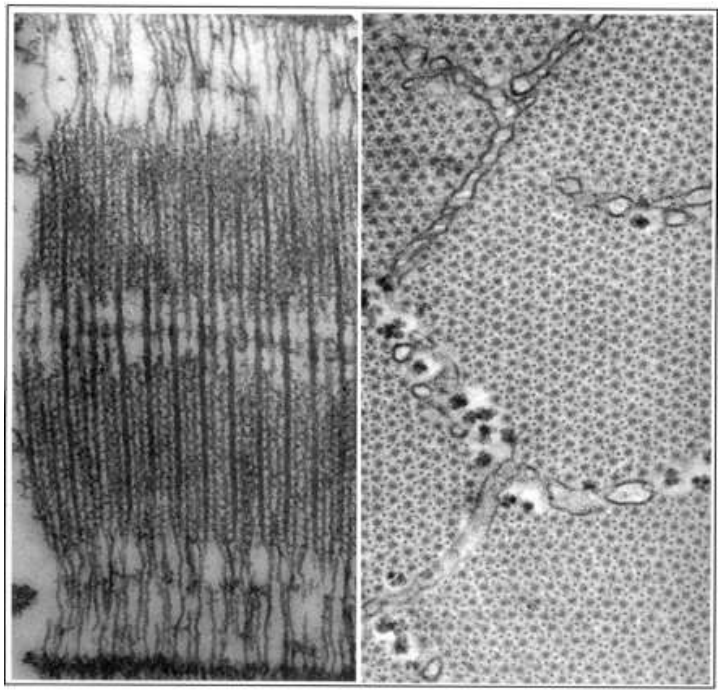

Figure 5: Images of rabbit skeletal muscle, in a longitudinal (on the left) and cross-section (on the right) view, demonstrating the relative positions of thin and thick filaments in a fixed sarcomere. In this system, the actomyosin contractile force is generated in the region of overlap between thick and thin filaments, leading to muscle contraction (Huxley, 1957).

responsible of mediating filaments movement were recognized to possess their own intrinsic vectoriality: in nerve axons, for example, kinesin is the motor for anterograde movement of vesicles (from the cell body towards the growth cone), whereas dynein drives retrograde movement (Vale, 1987; Vallee and Shpetner, 1990). Even if self-assembly from initial monomers is an important feature of cytoskeletal filaments, the cell precisely regulates these structures through a complex signaling network: the way organisms bridge the gap between the molecular and the cellular scale has been defined as "vectorial physiology" (Harold, 1991).

Today, cell polarity is specified by the interplay between the asymmetric accumulation of mobile components (often regulatory molecules) in the cell and the orientated organization of inherently polar cytoskeletal filaments (particularly actin and microtubules) along the cell polarity axis. (Li and Gundersen, 2008).

1.3.3 Conserved molecular players for cell polarization

As I have previously described, cell polarity defines the ability of the cell to localize specific proteins to specific regions of the membrane, generating domains. In molecular terms, the orientation of the polarity axis is initially defined by asymmetric cues acting at the cell surface, that can be sensed by a large family of cell-surface receptors, called G-protein-coupled receptors (GPCRs), leading in turn to local activation of a trimeric GTP-binding protein (G protein). Extrinsic and intrinsic cues have then to be recognized and interpreted by signaling molecules (in particular small GTPases and polarity complexes) to be transduced in the cell interior, leading to

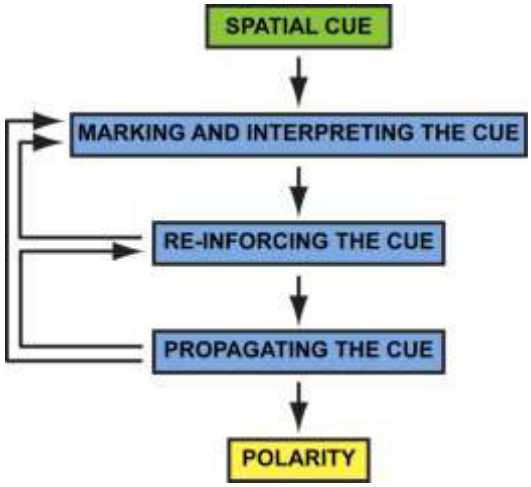

Figure 6: Schematic representation of the general pathway for the establishment of cell polarity. Adapted from (Arkowitz and Iglesias, 2008; Drubin and Nelson, 1996).

the asymmetric activation and/or distribution of downstream effectors. This signaling network results in cytoskeleton rearrangement, polarized vesicles transport and global changes in cell organization. Concomitantly, sorting compartments of the secretory apparatus reorient in the cytoplasm along the axis of polarity relative to the cue. Delivery of newly synthesized proteins to targeting patches at the cell surface reinforces and stabilizes the molecular and structural asymmetry of the cell initiated by the spatial cue. Feedback regulation results in the maintenance of cell polarity (Figure 6) (Drubin and Nelson, 1996).

1.3.3.1 Signal transduction through GPCRs and G proteins

G-protein-coupled receptors (GPCRs) form the largest family of cell-surface receptors, and mediate most responses to signals from the external world, as well as signals from other cells, including hormones, neurotransmitters, and local mediators (Alberts B., 2002). They are found in all eukaryotes, and also in some unicellular organisms, like the receptors for secreted mating pheromones in yeast. Even if activating signal molecules are chemically and functionally diverse, all GPCRs possess a similar structure, mainly composed of a single polypeptide chain which crosses the lipid bilayer seven times. GPCRs have a characteristic orientation in the plasma membrane, and they all use G proteins to relay the signal into the cell interior. G proteins are composed of three protein subunits - α, β, and γ. In the inactive state, Gα is bound to Gβγ dimer and GDP (Figure 7, on the left). Activation by a ligand leads to a GPCR conformational change

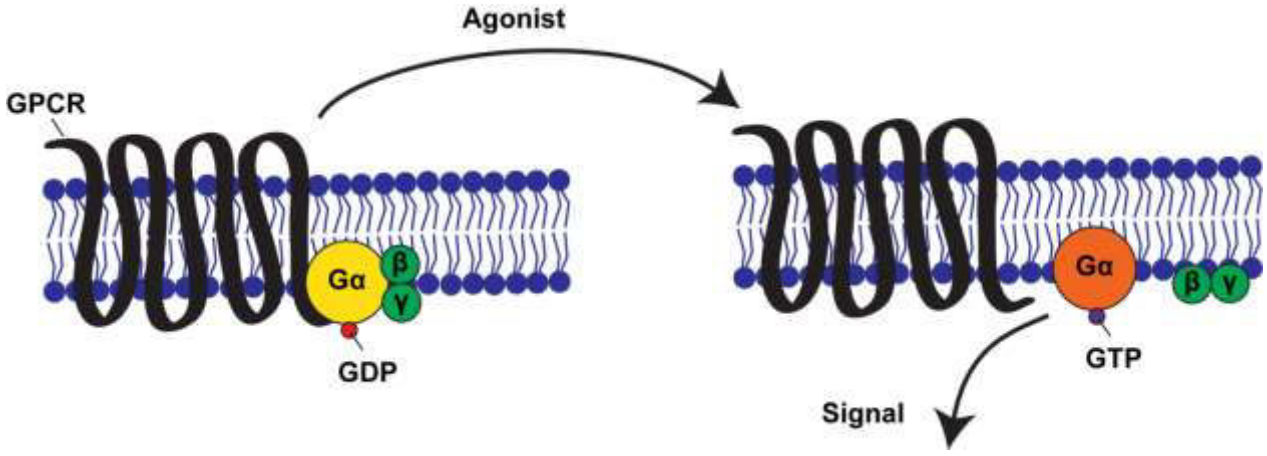

Figure 7: Schematic of the activation of the Gα subunit of a GPCR. In absence of an extracellular cue, Gα (yellow circle) interacts with GDP, Gβγ (green circles) and a GPCR (black loops). Upon receptor stimulation by a ligand, the receptor's state changes: Gα dissociates from the GPCR and Gβγ, and GTP is exchanged with GDP. As a result, Gα is activated (orange circle) and in turn leads to the activation of other molecules in the cell. Adapted from (Amberg, 1998; Li et al., 2002).

and activation of a G protein by promoting the exchange of GDP/GTP associated with the Gα subunit (Figure 7, on the right). As a result, the Gβ/Gγ dimer dissociates from Gα, and its moieties can act upon their downstream effectors at the cytoplasmic face of the plasma membrane, and thereby initiate specific intracellular signaling responses. GTPase activity of the Gα subunits may also be controlled by regulators of G proteins signaling, called RGS proteins, as well as effectors.

1.3.3.2 The core proteins of cell polarity: small GTPases

In the context of cell polarity and cell morphogenesis, all signals coming from diverse cell-surface receptors seem to converge on a group of closely related monomeric G proteins that are part of the Rho protein family - Cdc42, Rac, and Rho. Like all GTPases, these proteins act as molecular switches to control cell processes by cycling between an active, GTP-bound state and an inactive, GDP-bound state (Figure 8) (Iden S, 2008). Rho proteins are activated by guanine nucleotide-exchange factors (GEFs) and/or inactivated by GTPase-activating proteins (GAPs). Moreover, the release of GDP from the GTPase is blocked by guanine nucleotide-dissociation inhibitors (GDIs), which can also sequester Rho GTPases in the cytoplasm by masking their C-terminal motifs, required for Rho GTPases to interact with anchoring phospholipids in the plasma membrane. In addition to the high number of regulators, numerous Rho GTPase effector proteins have been described, especially kinases that function as scaffolding proteins to couple the activation of Rho GTPases to downstream signaling pathways.

Moreover, Rho GTPases can regulate cytoskeletal organization, vesicle transport and the

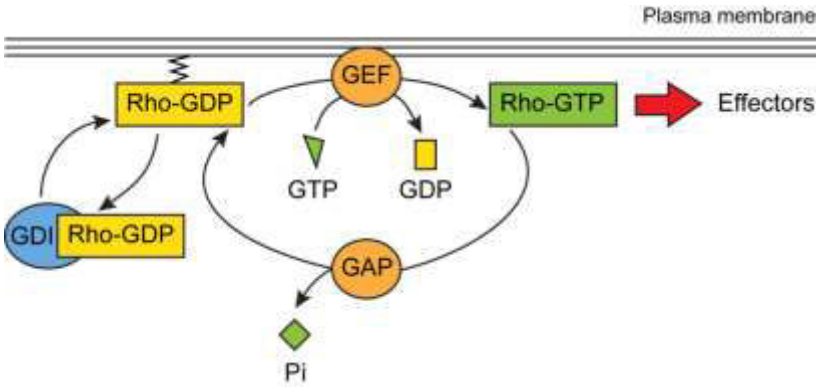

Figure 8: Rho GTPases can cycle between an active, GTP-bound (green rectangle) and an inactive, GDP-bound (yellow rectangle) conformation. This cycle is regulated by activators (GEFs, orange circles) and inhibitors (GAPs, orange circles, and GDIs, blue circles). In the active state, Rho GTPases can interact with various effectors. Adapted from (Etienne-Manneville and Hall, 2002).

localization of cytoplasmic proteins, primarily by controlling the phosphorylation of phospholipids, called phosphoinositides, which serve as specific docking sites for proteins at the cell membrane. Finally, they can also regulate each other's activity through crosstalk. The temporal and spatial balance between the activities of different small GTPases is crucial for many cellular processes, such as cell growth, cell-cell and cell-matrix adhesions, cell migration, cell polarization and epithelial-mesenchymal transition (EMT). Previous studies have identified 20 different Rho-GTPases in mammals, while there are six of them in yeast. In particular, Cdc42, a small GTPase of the Rho family, stands out as key regulator of cell polarity establishment and maintenance in all eukaryotic cells, in particular of polarized growth in yeast (Etienne-Manneville, 2004).

1.3.3.3 The cytoskeleton

Actin filaments and microtubules are polar polymers that are composed, respectively, of globular actin (G-actin) subunits that bind and hydrolyze ATP, and α- and β- tubulin heterodimeric subunits that bind and hydrolyze GTP. Polarity results from head-to-tail association of protein subunits, resulting in alignment of the subunits along the polymer lattices and structural differences between the two ends (Figure 9).

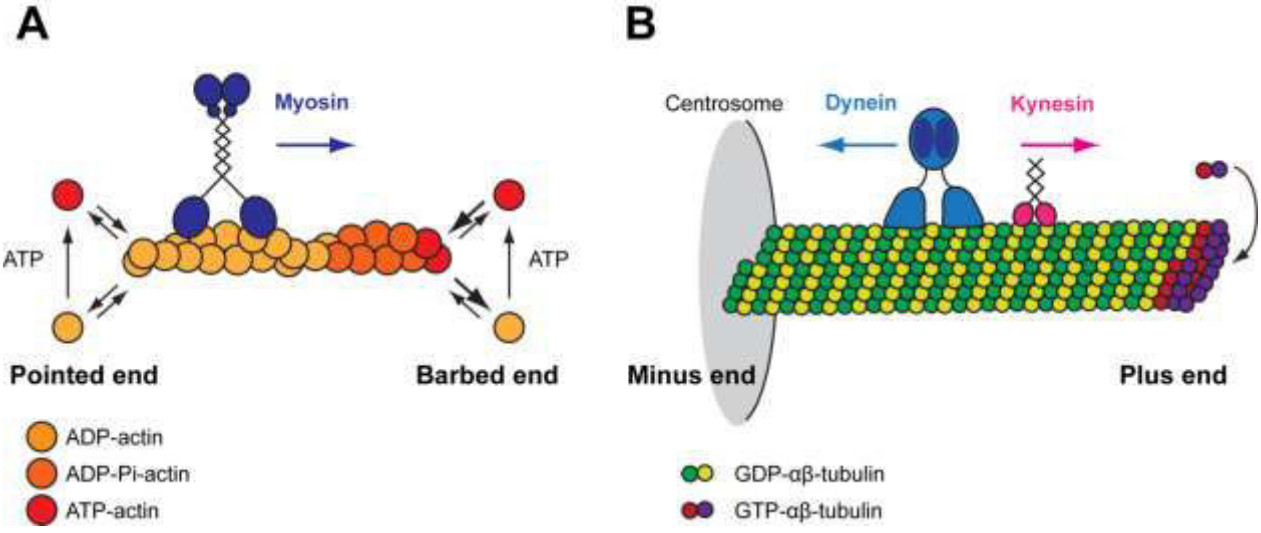

Figure 9: Basic properties of actin filaments and microtubules. ***A.*** Actin filaments are made of orientated subunits, resulting in a polarized surface polymer, responsible of the motors (myosins) unidirectionality, and two structurally different ends, with distinct nucleotide states and subunits kinetics. ***B.*** MTs are composed of α- and β-tubulin heterodimeric subunits orientated in the same direction, resulting in a polarized surface polymer, responsible of the motors (kinesins and dynein) unidirectionality, and two structurally different ends, with distinct polymerization/depolymerization rates related to the tubulin-bound nucleotide state. Adapted from (Li R, 2008).

Actin and microtubules are also dynamic, as they can either polymerize or depolymerize, with different rate constants for growth and shrinkage at the opposite ends. The ability to undergo fast turnover and assembly enables actin and microtubules to reorganize rapidly and locally in response to polarity signals.

A class of cytoskeleton-associated proteins that are particularly important for cell polarity are the motor proteins, characterized by unidirectional movement along actin filaments or microtubules by irreversibly moving from one tightly bound conformation to another using ATP hydrolysis as energy source. Myosins are motor proteins for actin, and most members of this superfamily move towards actin barbed ends, with the exception of myosin-VI. Some myosins, such as myosin-V, display processive movement along actin filaments (that is, they move many consecutive steps before dissociating from the filament) and are thus optimal for transport over long distances. Other myosins, in particular myosin-II, exhibit low processivity but can dimerize to generate contractile forces through the sliding of actin filaments. MT motors encompass kinesins and dynein. Most kinesins move towards MT plus ends with varying degrees of processivity, whereas dynein moves processively towards MT minus ends in the presence of the dynactin complex. In principle, cargo molecules or organelles can be trafficked by motor proteins to specific cellular locations once a cell has established oriented actin or MT arrays.

Cytoskeletal polymers carry out polarized trafficking or localized functions by assembling

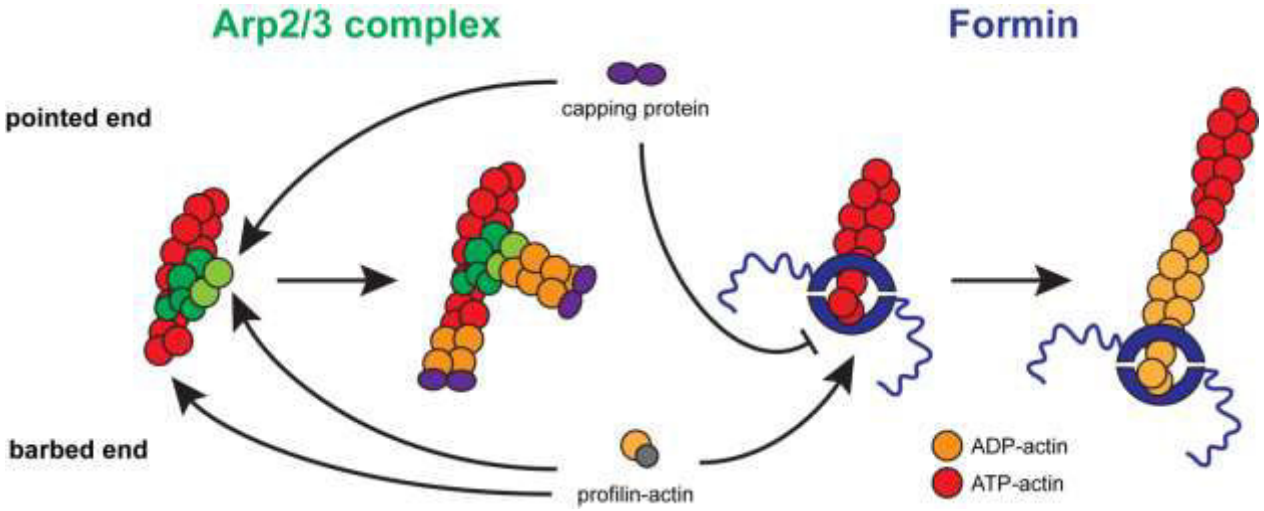

Figure 10: Establishment of orientated actin arrays. There are two main classes of actin filament nucleation factors, Arp2/3 complex and formins. Formins promote the assembly of long-straight filaments by remaining continually bound to the elongating barbed end, whereas Arp2/3 complex facilitates the assembly of short-branched filaments by nucleating filaments from the side of a pre-existing filament that are quickly capped. Adapted from (Li R, 2008)

actin and MTs into organized arrays. The rate-limiting step for spontaneous actin and MT polymerization is nucleation, which is the formation of small oligomers that can rapidly elongate. In the case of MTs, the alternation between growth and shrinkage, known as dynamic instability, contributes to locally regulate cell polarity.

A key mechanism in the assembly of polarized actin arrays is the activation of actin-nucleation factors, such as the actin-related protein-2/3 (Arp2/3) complex and formin-family proteins, at defined locations (Fig 10). Arp2/3 complex produces branched filaments by anchoring the new one to the pre-existing actin network, in order to push forward the leading edge of motile cells and for endocytosis (Pollard and Borisy, 2003): the free end of the new filament elongates until a capping protein terminates growth. On the other hand, formins produce unbranched filaments for actin bundles found in filopodia and the cytokinetic contractile ring (Wallar and Alberts, 2003). The formin remains associated with the growing end of the filament, providing an anchor and protection against capping. Membrane-bound Rho-family GTPases activate actin-nucleation factors either directly or indirectly through nucleation-promoting factors (NPFs). Through these upstream regulatory factors, Arp2/3 complex- or formin-based actin nucleation occurs maximally near the membrane at sites of Rho GTPase activation (Li and Gundersen, 2008).

Whereas nucleation is the principal mechanism that regulates actin during cell polarization, nucleation of MTs usually occurs near the cell center at the centrosome (or other MT-organizing centers, MTOCs), far from membrane-derived signals that stimulate cell polarity. As a consequence, the initial events that localize and orientate MTs during cell polarization mainly involve factors that regulate the dynamic plus ends. For instance, MTs are frequently captured by cortical factors that increase the stability of the plus ends and/or generate pulling forces: this process increases local MT density and also provides a means to enhance the delivery of cargoes to specific sites. Other cases include alterations in the assembly properties and bundling of MTs.

In animal cells, the actomyosin cytoskeleton plays a central role in the dynamic regulation of cell shape (Salbreux et al., 2012). Actin is also essential for the translocation of secretory vesicles towards the membrane and internalization of endocytic vesicles.

Apart from their contribution to directed vesicle trafficking in large cells, MTs also play a common role in the establishment or maintenance of cortical polarity but are not required for

polarity induction per se (Siegrist and Doe, 2007). Similar to the case of migrating cells, in neuronal growth MTs are also essential for positioning the site of protrusion within a growth cone, but not for extension itself (Siegrist and Doe, 2007).

To conclude, interactions between actin and microtubules promote cortical asymmetry to polarize cells for differentiation, division and migration. Some examples of this communication are the establishment of anterior-posterior polarity in the early *C. elegans* embryo, the mechanisms that polarize *Drosophila* neuroblasts and mediate spindle positioning, the establishment of polarity in migrating cells and the regulation of cytokinesis by interactions between the mitotic spindle and the cortex (Akhshi et al., 2014).

1.3.3.4 Membrane remodeling: exocytosis and endocytosis

Polarized distribution of proteins at the plasma membrane often results from a balance of vesicle delivery and fusion with the plasma membrane ("exocytosis"), diffusion at the plasma membrane, and internalization and membrane recycling ("endocytosis") (Figure 11). Exocytosis controls the release of molecules into the extracellular space and results in the addition of new membrane material, which essentially leads to cell growth: for secretion to occur over relatively long distances in cells, vesiscle transport relies on the work of molecular motors along cytoskeletal tracks. By restricting secretion to specific sites, growth is polarized and takes place exclusively at these sites. Endocytosis describes the process of internalization of extracellular material and membrane proteins by invagination of the plasma membrane (PM), eventually resulting in the formation of endocytic vesicles and endosomes, that can either be degraded as lysosomes or

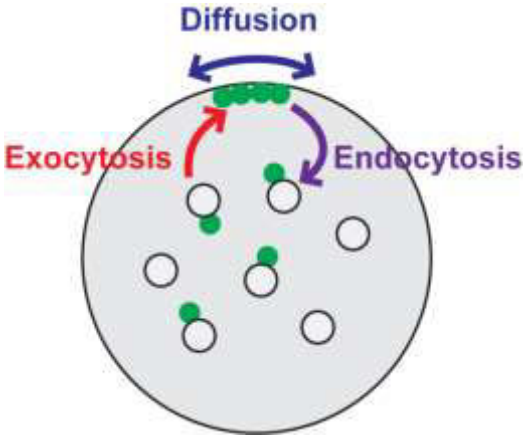

Figure 11: Schematic of the minimal requirements for cell polarization through intracellular trafficking.

recycled back to the plasma membrane.

For cell polarity to take place, intrinsic mechanisms sort membrane proteins into different vesicles, and deliver these vesicles to different membrane domains (through cytoskeleton-mediated targeting, vesicle tethering through exocyst complexes and annexins) for membrane fusion (SNARE - Soluble *N*-ethylmaleimide-sensitive factor Attachment Protein Receptor - proteins). Protein complexes at the plasma membrane (the Par, Crumbs and Scribble complexes) control the identity and distribution of functionally and structurally unique PM domains from the cytosolic face. Moreover, membrane lipid composition regulate secretion and recycling (Orlando and Guo, 2009): for instance, phosphatidylinositol (PI) and phosphatidylinositol phosphates (PIPs) are highly compartmentalized in different organelles, and these local asymmetries in the phospholipid content of plasma membrane domains affect localization of Rho-GTPases such as Cdc42. Finally, extrinsic cues provided by cell adhesion to the ECM and by other cells control the orientation of cell polarity. All these different levels of regulation of cell polarity are integrated into a single network. (Mellman and Nelson, 2008).

1.3.3.5 Polarity complexes

In multicellular tissues there is clearly an increase of complexity, as in the case of epithelial cells, where the fundamental generators of cell polarity have to establish the difference between the apical and basal poles, and they have to do so in a properly oriented way, in accordance with the cell's environment. Cell polarization is achieved by the concerted actions of polarity proteins. These molecules are conserved throughout evolution and can react to extrinsic or intrinsic polarity cues (for example, growth factor gradients or the MT cytoskeleton, respectively). By assembling multiprotein complexes, they induce downstream signalling to trigger the establishment of cellular asymmetry. Of the three described polarity protein complexes - partitioning defective (PAR), Crumbs and Scribble - the PAR complex has the broadest function. In some polarization processes, these complexes cooperate to induce polarity, whereas in other systems they antagonize each other, thereby establishing or maintaining cellular asymmetry.

The crosstalk between polarity proteins and Rho GTPases is essential for the establishment and maintenance of mammalian cell polarization in different cell types, including neuronal, epithelial and T cells (Iden and Collard, 2008): here, I will briefly discuss the case of PAR genes, as they play a fundamental role not only in asymmetric cell division in the early

embryo, but in many other processes such as epithelial cell polarity, cell migration, oriented cell division and axon specification (Figure 12A) (Goldstein and Macara, 2007).

The PAR genes were initially identified by Jim Priess and Ken Kemphues in a screen for maternal-effect genes that are embryonically lethal in the nematode *Caenorhabditis elegans* (Kemphues et al., 1988): following fertilization, the one-cell embryo polarizes along an anterior–posterior axis to prepare for asymmetric division. PAR-3 and PAR-6 segregate to the anterior domain, whereas PAR-1 and PAR-2 distribute to the posterior domain.

Moreover, the asymmetric distribution of polarity proteins before cell division correlates with local differences in contractility, which is regulated by Rho protein activity: in other words, the initially uniform actomyosin network becomes restricted to the anterior pole, thereby generating a contractile anterior and a non-contractile posterior domain. Sperm entry leads to a local weakening of the contractile network by inhibiting Rho activation: this asymmetry is then amplified through positive feedback loops acting on the actomyosin contractile machinery and thePAR and Rho polarity modules, finally resulting in the establishment of an anterior-posterior

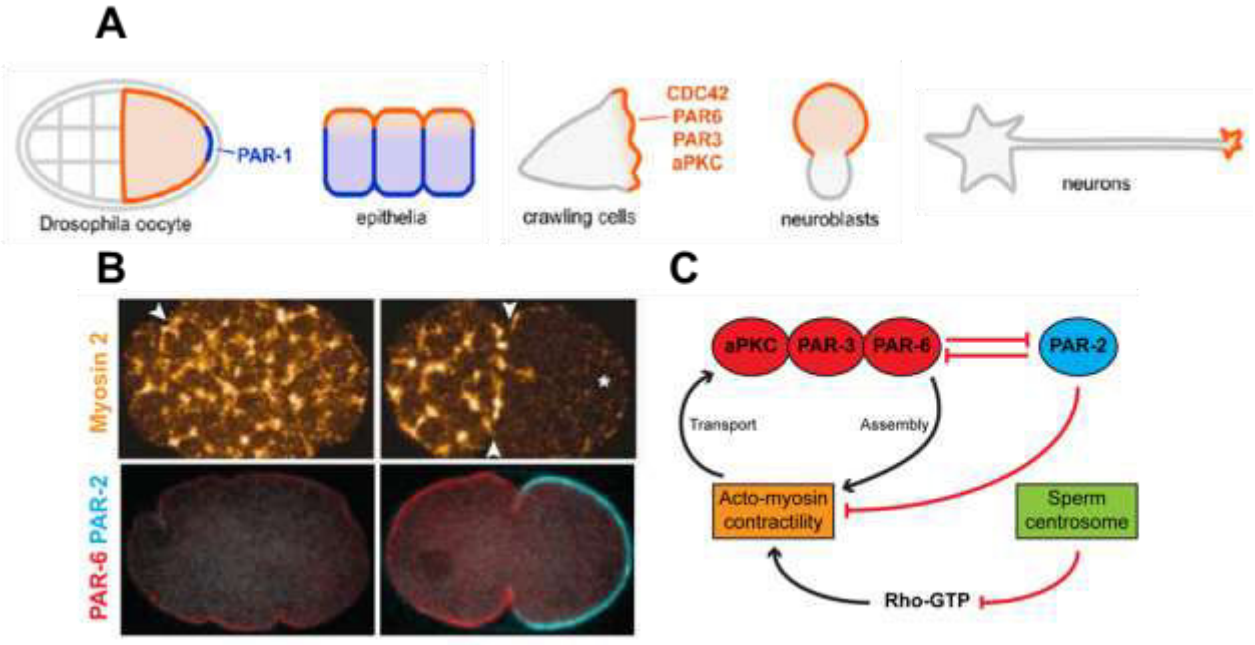

Figure 12: Interplay between PAR proteins and the polarity machinery ***A.*** PAR Localization in Multiple Systems. Adapted from (Goldstein and Macara, 2007). ***B.*** and *C.* Symmetry in a *C. elegans* one-cell embryo. *B.* Cortical network of myosin-II (on top) and PAR-2/PAR-6 localization (on bottom), before (left) and after (right) symmetry breaking. Arrowheads indicate furrows on the egg surface. An asterisk marks the site of sperm entry. (Goehring et al., 2011; Munro et al., 2004). ***C.*** Schematic of the crosstalk between PAR proteins, Rho-GTPases and the cytoskeleton for polarity establishment in *C. elegans.* Adapted from (Li R, 2008; Uyttewaal et al., 2010).

polarity axis (Figure 12B - C).

In conclusion, cell polarization is achieved by intricate communication between different classes of proteins, including small GTPases, polarity proteins and cytoskeletal components, which are mutually regulated and differentially distributed within a cell.

1.3.4 Cell polarization: with or without a cue?

As I described in the first section, cell polarity has first been defined as an organizing property of the cell, with an orientation that may be set by a pre-existing cue at the membrane. There are numerous signals that cells can sense and that may compete with each other *in vivo* (Drubin and Nelson, 1996): these are either localized cues that come from the environment, or spatial landmarks that the system has inherited (Li and Bowerman, 2010). Among the best characterized examples of extracellular signals there are gradients of signaling molecules, sites of cell adhesion, mechanical signals and electric fields. On this basis, the first explanations for the origin of cell polarity had largely focused on the molecular basis of these pre-existing cues and how their signals are propagated.

These extrinsic signals, though important in their physiological contexts, are not always necessary for symmetry breaking: in some cases, asymmetry occurs along random axes even when the cues are removed (Figure 13). For example, cells undergoing chemotaxis such as the social amoeba *Dictyostelium discoideum* and mammalian neutrophils move in random directions in the presence of a uniform concentration of chemoattractant (Kortholt et al., 2013); budding yeast cells, which naturally bud adjacent to the previous bud scar, are still able to polarize in random orientations when the genes responsible of bud site selection are deleted (Johnson et al., 2011); the zygotes of algae from the genus *Fucus* undergo an asymmetric first division in the absence of an external signal that normally defines the axis of polarity (Brownlee and Bouget, 1998). Similarly, in the *Xenopus laevis* egg dorsoventral axis is normally defined by the sperm entry point, but can also be established in eggs that are activated in the absence of sperms (Gerhart et al., 1989). Altogether, these observations suggest that the final asymmetric pattern is entirely self-regulating and that the initial asymmetric cue only provides a bias to orient the pattern correctly with respect to an intrinsic or extrinsic signal.

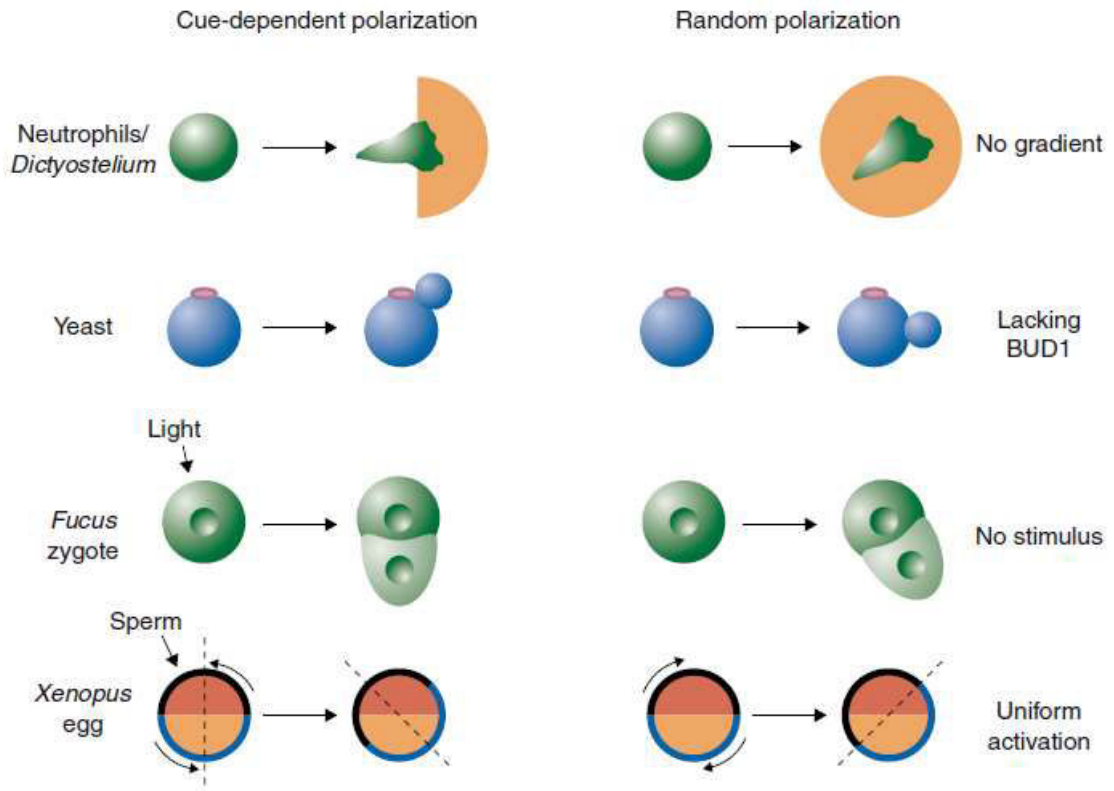

Figure 13: Cue-dependent and random cell polarization in different organisms. A general description of each single case can be found in the main text (Arkowitz and Iglesias, 2008; Wedlich-Soldner and Li, 2003).

1.4 Cell shape and cell mechanics

Cell shape is also determined by cellular mechanics: the main structures that are responsible for providing cell stiffness, resisting external mechanical stresses and opposing to intracellular osmotic pressure are cell walls in plants, fungi and bacteria, and the actin cortex in animal cells. Moreover, force generators inside the cell such as molecular motors and the cytoskeleton are crucial for directing fundamental processes in cells, including orientation of cell division, directional migration and polarized growth. The dynamic plasticity of all these structures is a key feature of cell morphogenesis in a changing extracellular environment, as it allows cells to rapidly adapt shape, move, and exert forces. Further, disruptions in mechanical sensing and/or function have been implicated in several diseases, such as osteoporosis, atherosclerosis and cancer.

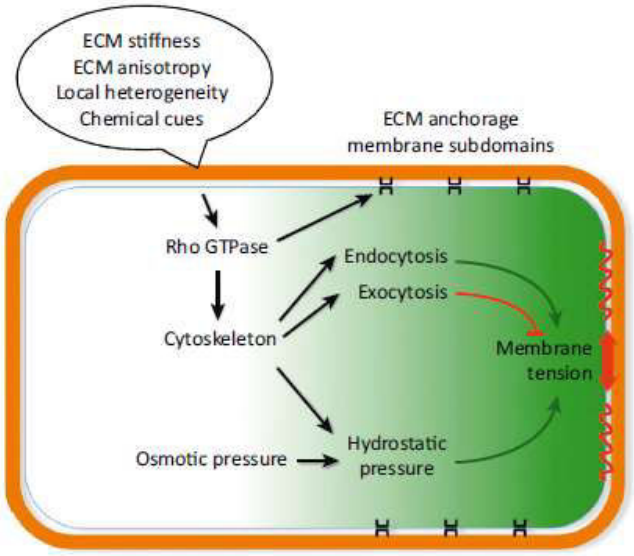

Figure 14: Integration of mechanical stress in the cell polarity pathway. The main actors of the signaling pathway for cell polarity establishment (e.g., Rho GTPase, cytoskeleton, vesicle traffic) are presented together with mechanical inputs (e.g., ECM stiffness) that may trigger activation of the pathway and mechanical outputs (e.g., membrane tension), which can consolidate and even drive polarity establishment (Asnacios and Hamant, 2012).

Cell polarity is also related to the mechanical properties of the cell: for instance, a mechanical signal can be transduced by the cell into a polarizing cue, conversely a polarization process can lead to local changes in the cell mechanics. This interdependence is key for the regulation of cell morphogenesis (Figure 14).

During development, mechanical forces cause changes in size, shape, number, position, and gene expression of cells, acting as integral components of any morphogenetic processes. In animals, force generation by actomyosin networks and force transmission through adhesive complexes are two self-organizing phenomena driving tissue morphogenesis (Heisenberg and Bellaiche, 2013): coordination and integration of forces by long-range force transmission and cells mechanosensing within tissues result in large-scale tissue shape changes. Extrinsic mechanical forces also control tissue patterning by modulating cell fate specification and differentiation.

In a mechanical perspective, biological tissues have two contradictory properties: they have a robust architecture that is required for their stability and resistance to stress, yet they exhibit a remarkable plasticity that allows remodeling (Lecuit and Lenne, 2007). Tissue

homeostasis depends on the balance between this two material features, and its disruption is an important step in the formation of several types of cancer (Huang and Ingber, 2005).

To conclude, the interplay between tissue mechanics and biochemical signaling orchestrates tissue morphogenesis and patterning in development and homeostasis.

1.4.1 On growth and form

In 1917, D'Arcy Thompson proposed for the first time the idea that biological forms likewise reflect the action of physical forces on formless protoplasm: "The form… of any portion of matter, whether it be living or dead, and the changes of form which are apparent in its movements and in its growth, may in all cases alike be described as due to the action of force. In short, the form of an object is a 'diagram of forces' in this sense, at least, that from it we can judge or deduce the forces that are acting or have acted upon it" (Thompson, 1945). Following this idea, cells owe their form to the application of physical forces acting both at the molecular and supramolecular level, most commonly mechanical ones. For instance, he noted that in mitosis dividing cells look like iron filings between the poles of a magnet, in other words like a force field. Moreover, D'Arcy Thompson proposed a link between cell polarity, defined by Van Beneden as "*morphological* polarity", and a "*dynamical* polarity", represented by the distribution

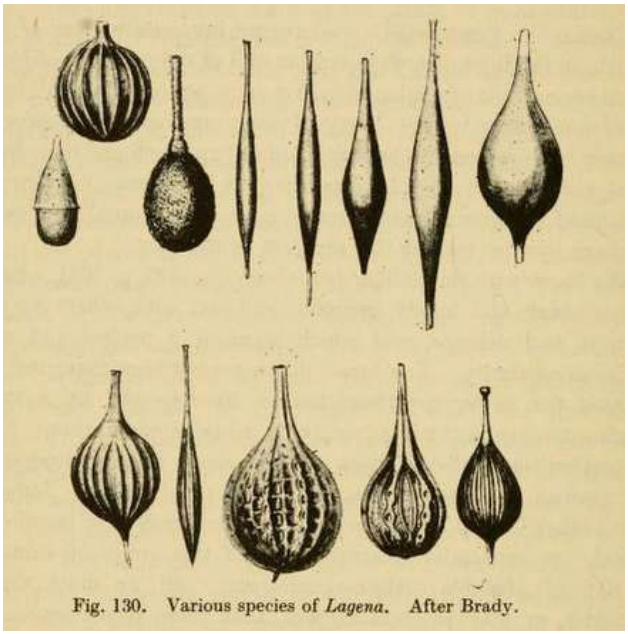

Figure 15: Examples of cell shapes in protists of the *Foraminifera* family which can be explained by the law of minimal surface area, based on surface tension (Thompson, 1945).

of forces acting upon the cell.

Thompson devoted one chapter to the forms of unicellular organisms, which turns on the proposition that many common biological shapes result from surface tension. In objects governed by surface tension, the shape will be the one which has the smallest surface area compatible with volume and mechanical constraints: the simplest and most familiar shape of this type is the sphere, but it is not the only one. What makes this biologically relevant is that many cells and unicellular organisms exhibit forms compatible with the law of minimal surface area: spheres are especially common (bacterial and fungal protoplasts, many algal cells, eggs), as are cylinders (fungal hyphae and algal filaments), but unduloids and catenoids can also be found among the protists (Figure 15). Thompson's idea that surface tension alone would determine cell shape was extended to account for morphogenesis in bacteria and fungi, in the so-called surface stress theory (Koch, 2001). Finally, Thompson proposed that in multicellular organisms, cells influence each other's shapes with triangles of forces, meaning that their shape will depend on the vectorial sum of forces acting upon them.

To conclude, this book marked an important step in defining how mechanical forces influence cell morphogenesis and polarity.

1.4.2 Conserved molecular players for cell mechanics

The relationship between cell shape and cell mechanics is not only based on a purely passive response, but relies on a general sequence of active steps: a mechanosensing stage, where the cell mechanically probe the surrounding environment; a mechanotransduction machinery, which in turn converts the mechanical signal in a biochemical signaling cascade; finally, cell remodeling in response to the mechanical cue. Moreover, most cells can respond to extracellular signals of different nature by remodeling their own mechanical properties, in order to attain a certain goal, such as growing/dividing/migrating in a certain direction; in some cases, intrinsic mechanical instabilities can lead to symmetry breaking and cell polarization. In the following, I will discuss these different aspects of cell mechanics in relationship with cell morphogenesis, and compare the case of cells which possess or not a cell wall.

1.4.2.1 Sensing and transducing a mechanical cue

To induce polarization in response to mechanical cues, cells must be able to sense their mechanical environment. The field of mechanotransduction has been characterized by a significant amount of revealing works in the past 20 years, especially in animal systems (Orr et al., 2006). Mechanoperception mainly relies on transmembrane proteins, mechanosensitive channels (such as stretch-activated channels in plants and fungi (Monshausen and Gilroy, 2009)), and cytoskeletal and adhesion proteins (such as β-catenin in the *Drosophila* embryo (Farge, 2003)), and they simply act through protein conformation change; moreover, small forces can be amplified by transmitting the strain to larger structures, such as the elements of the ECM. By these means, mechanical cues can eventually be transmitted to the polarity machinery.

It is now well established that in animal cells, the attachment to adhesion sites contributes to the mechanotransduction and recruitment of cytoskeletal proteins in a polar way. In particular, stretching the fibronectin can expose binding sites for integrins, which in turn undergo conformational changes that impact upon a molecular cascade involving cytoskeleton regulators. Moreover, mechanotransduction involves the extension of molecules from adhesion complexes composed of α-catenins and cadherins for polarization of multicellular systems. Within an epithelial tissue, intercellular surface tension results from the opposite effects of cortical tension - exerted by an actomyosin contractile network - that reduces the surface of contact, and of adhesion that increases the surface of contact. The prevalence of one element over the other can generate a force field that drives complex morphogenetic events in development: for example, apical upregulation of cortical tension by myosin-II can lead to apical constriction, a crucial

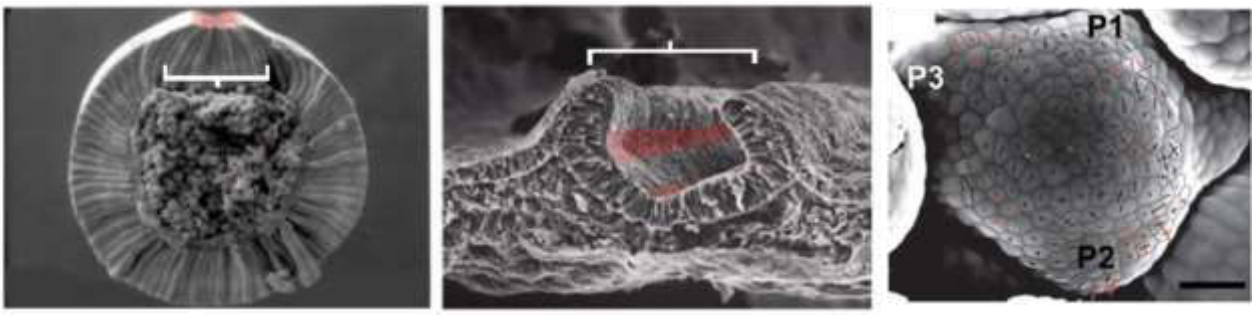

Figure 16: Examples of tissue development guided by mechanical cues. On the left, mesoderm invagination in the *Drosophila* embryo relies on furrowing of the ventral epithelium and corresponding cell shape changes in the apical constriction (indicated in red) of invaginating cells (square bracket). In the middle, vertebrate neurulation corresponds to bending of the neuro-epithelium (square bracket) and apical constriction in specific regions ((indicated in red). On the right, patterns of anisotropy in the plant shoot apical meristem (Lecuit and Lenne, 2007; Uyttewaal et al., 2010).

feature in *D. melanogaster* mesoderm invagination and neurulation in vertebrates (Lecuit and Lenne, 2007) (Figure 16, on the left and in the middle).

In plant tissues, organogenesis can be triggered by expression of PIN proteins at specific cell sides to drive the polar flux of auxin: in the shoot apical meristem for instance, it has been shown that neighboring cells might sense mechanical stress, and in turn locally modulate auxin content, thereby triggering PIN polarity and organ development at specific locations (i.e., phyllotaxis) (Figure 16, on the right) (Hamant et al., 2008).

1.4.2.2 Structural elements of the cells

In walled cells, such as plants, fungi and bacteria, the cell wall is an essential structure to support a proper shape: these cells are characterized by a high internal turgor pressure, which needs to be counterbalanced by the presence of a stiff shell. As turgor is isotropic, cell wall physical properties and the spatiotemporal regulation of cell wall remodeling are key factors for cell morphogenesis (Cosgrove, 2005). The material in the cell wall varies between species, and can also differ depending on cell type and developmental stage: the main components of the cell wall are peptidoglycans for bacteria, other polysaccharides (glucans, mannans etc.) and chitin for fungi, cellulose and pectins for plants. Localized secretion of "softer" cell wall material or of agents affecting the properties of the existing cell wall are considered necessary for cell shape generation in some walled cells (Smith and Oppenheimer, 2005). Moreover, cortical microtubules play a similar role than the actomyosin system in metazoans as they are essential for anisotropic growth, by guiding the deposition of cellulose microfibrils on the cell wall: however, they have a negligible mechanical role to maintain cell shape (Mirabet et al., 2011).

In animal cells, the plasma membrane and the actomyosin cortex, a thin network of actin filaments attached to the membrane, control surface mechanics and determine cell surface tension. Tension in the actomyosin cortex primarily arises from myosin-generated stresses and depends strongly on the ultrastructural architecture of the network, while plasma membrane tension is controlled mainly by the surface area of the membrane relative to cell volume and can be modulated by changing membrane composition, shape and the organization of membrane-associated proteins (Salbreux et al., 2012).

The main differences related to cell shape in plant and animal cells might reflect differences in the characteristic timescale over which the change in shape occurs, and this

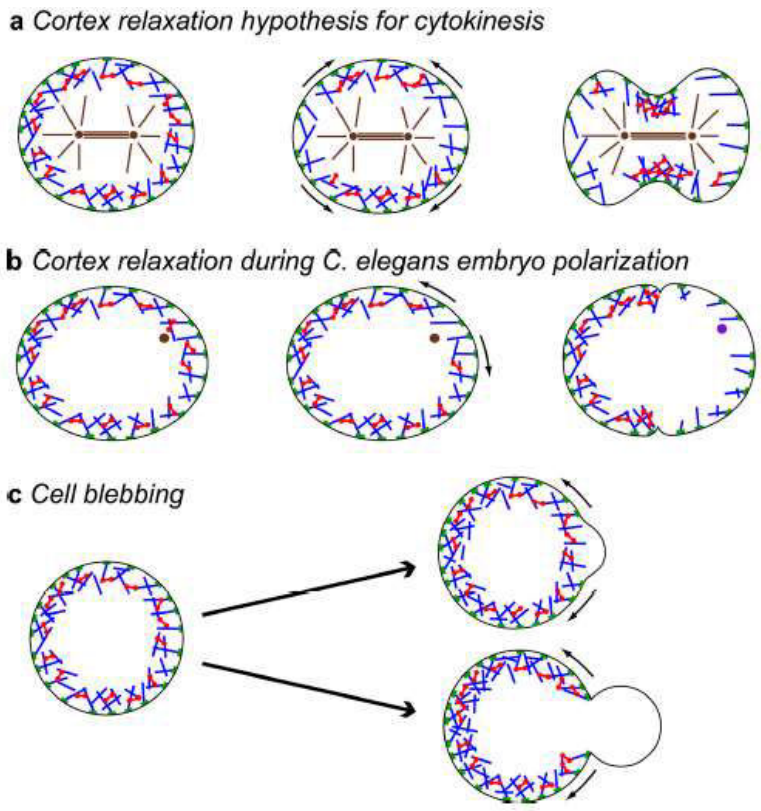

Figure 17: Scheme of different cases of cortex relaxation in different physiological contexts. In blue, actin filaments; in red, myosin fibers; in green, membrane attachments; in brown, MTs and centrosomes. Curved arrows indicate the direction of cortex flows. ***A.*** At the onset of cytokinesis, spindle microtubules cause cortex relaxation at the poles of the cell. The relaxed regions expand, leading to cleavage furrow formation. ***B.*** In the *C. elegans* embryo, shortly after meiosis II, the sperm centrosome moves toward the site of sperm entry, where it triggers cortex relaxation. The cortex then flows away from the relaxed region, leading to polarity protein segregation and pseudocleavage furrow formation. ***C.*** Blebs form at sites of local detachment of the membrane from the cortex (top) or at sites of local cortex rupture (bottom). Legend extracted from (Paluch et al., 2006b).

arguably can be related to the nature of the load (osmotic pressure)-bearing mechanical structure, either a solid wall in plant cells with a Young modulus in the MPa-GPa range, or a compliant and dynamic kPa acto-myosin cortex in animal cells (Asnacios and Hamant, 2012).

The cell wall and the actin cortex determine not only the static shape of the cell, but also cell deformations. In the case of walled cells, polarized growth is achieved by a local softening of the cell wall (Harold, 2002), that in turn is obtained by direct transport of vesicles containing cell wall-loosening enzymes to specific growth sites at the cell periphery; this process requires a polarized cytoskeleton (Wedlich-Soldner et al., 2003). In animal cells, shape changes are required for cell migration, division or epithelial morphogenesis (Clark et al., 2014): for instance, at the

onset of cytokinesis actomyosin flows take place and probably play role for cleavage furrow formation (Figure 17A) (Cao and Wang, 1990; DeBiasio et al., 1996). Another process that is thought to depend on local cortex relaxation is the polarization of the one-cell *C. elegans* nematode embryo. Here, the sperm provides the external cue: after fertilization, the sperm centrosome moves toward the point of sperm entry, where it locally relaxes cortical contractility (Cowan and Hyman, 2004). As during cytokinesis, the cortex flows away from the relaxed region, transporting polarity proteins and shaping the pseudo-cleavage furrow (Figure 17B) (Munro et al., 2004). Furthermore, polarization by cortex relaxation may precede cell migration in some cells (Paluch et al., 2006a). Even in the absence of any spatial cue, the cortical tension can also relax spontaneously, for example during cell blebbing (Figure 17C) (Paluch et al., 2005). Hence, cell polarization can locally regulate cell mechanics but can also be driven by a mechanical instability.

At the multi-cellular scale, cell-shape changes and cell contacts are remodelled by the opposite actions of cortical tension and adhesion (Lecuit et al., 2011).

1.4.2.3 Mechanical forces generated by the cytoskeleton

Cells across kingdoms reorganize their cytoskeleton to resist mechanical stimuli, thus consolidating cell polarity: as I have previously described, animal cells use the contractile actomyosin cortex to oppose to hydrostatic pressure and keep a certain shape. Moreover, they regulate cytoskeleton remodeling in response to mechanical cues: for example, cells of the amoeba *Dictyostelium* subject to hydrodynamic shear stress can reorient actin polymerization at the side that is against the flow (Dalous et al., 2008); furthermore, most cells modulate the actomyosin-dependent traction forces exerted on a substrate depending on its rigidity, meaning that they pull more on rigid substrates (Mitrossilis et al., 2010). In particular, human mesenchymal stem cells grown on substrates with different rigidities strikingly differentiate into specific cell types with diverse morphologies and functions, ranging from neurons to osteoblasts (Engler et al., 2006). Such a correlation between cell shape, traction forces, and gene expression may finally be due to a different compressing force exerted on the nucleus (Swift et al., 2013).

In animal cells, both the extracellular matrix and the cytoskeleton act on membrane tension, which in turn can promote and/or consolidate polarity: this idea has been demonstrated in a recent study which combines both micromechanical and osmotic manipulation to show that

in neutrophils, protrusion at the front increases membrane tension, and thus constrains the sides and the rear of the cell, thereby inducing polarization (Houk et al., 2012).

As previously described, the cytoskeleton also regulates vesicle transport in all mentioned cell types, possessing or not a cell wall, and contributes to cell polarization and cell shape: interestingly, vesicle trafficking may also regulate, and be regulated by, membrane tension, as previous studies have shown that endocytosis is inhibited in highly tense membrane, whereas exocytosis relaxes this tension (Gauthier et al., 2011).

In contrast, the main structural element of cells in plants, fungi and bacteria is the cell wall: in this case, the cytoskeleton plays a different role in the mechanics of cell morphogenesis. Apart from directing polarized trafficking, MTs in plants act as mechanosensors, as they orient under externally applied mechanical stress (Figure 18). Consequently, plant cells resist the maximal stress direction and use MTs to deposit new cell wall parallel to this direction, generating an overall mechanical anisotropy of the cell wall structure (Hamant et al., 2008). Hence, the cytoskeleton also plays a crucial role for cell morphogenesis in walled cells by orienting growth anisotropy.

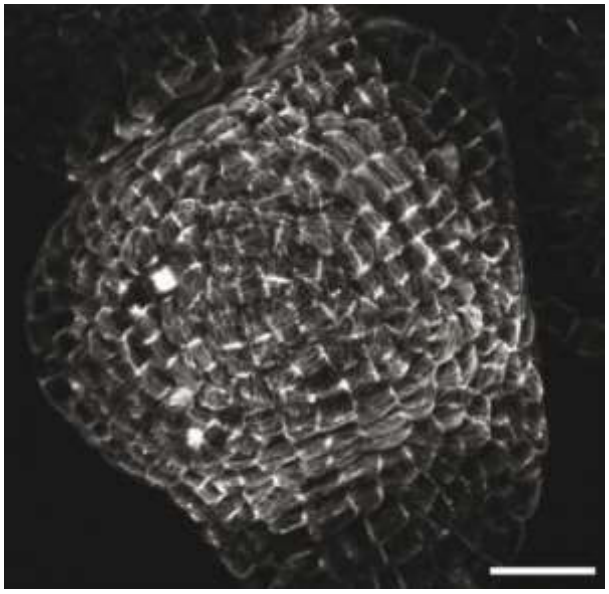

Figure 18: MT spatial organization in the shoot apical meristem. MT orientations correlate with the pattern of cells shapes and anisotropies, in other words they align along predicted principal stresses: in particular, MTs display rotary movements at the tip, while aligning circumferentially at the periphery (Hamant et al., 2008).

1.5 General principles of symmetry breaking

The phenomenon of random polarization in biology is a great example of how stochastic fluctuations or small and transient initial asymmetries, can potentially be amplified to reach a stable system-wide asymmetry. Among the possible amplification mechanisms we find positive feedback loops, which result from intrinsic biochemical and mechanical interactions between regulatory molecules and structural (cytoskeletal and membrane) components. Several mathematical models have been developed to describe how an initially symmetric structure can be transformed into an asymmetric, polarized one.

1.5.1 Reaction-Diffusion systems

A first central set of principles to explain self-organization phenomena came out from the paper "The chemical basis of morphogenesis" by Alan Turing, published in 1952: in there, Turing suggested "that a system of chemical substances, called morphogens, reacting together and diffusing through a tissue, is adequate to account for the main phenomena of morphogenesis" (Turing, 1990). By morphogenesis, Turing was thinking of the spatial patterning of biological tissues - like in the case of spots arrangement on a leopard's skin or a butterfly's wing, or the stripes periodicity on a seashell or a fish's body. A first important point he made was the idea that developmental events are regulated by informational molecules, called "morphogens", whose spatial distribution provides a pre-pattern for the formation of biological structures: today, it is widely accepted that morphogens distribution constitutes a kind of map, which give instructions to a population of cells about their future development (Kondo and Miura, 2010).

Another revolutionary insight of Turing's reaction-diffusion (RD) model relied on the concept of spontaneous generation of spatial patterns once two reacting species diffuse at different rates. Even if intuition would suggest that diffusion smoothes out concentration differences, Turing showed that with some specific kinetic constraints, random fluctuations arising within a homogeneous region can be spontaneously amplified, a stable local maxima and minima of reagent concentration. In his paper, Turing gave a specific example of a reaction-diffusion mechanism in which a slowly diffusing, 'local' activator and a rapidly diffusing 'long-range' inhibitor, through their mutual interactions, reached steady-state concentrations that varied with position with a well-defined spatial period. Later on, Gierer and Meinhardt showed that a

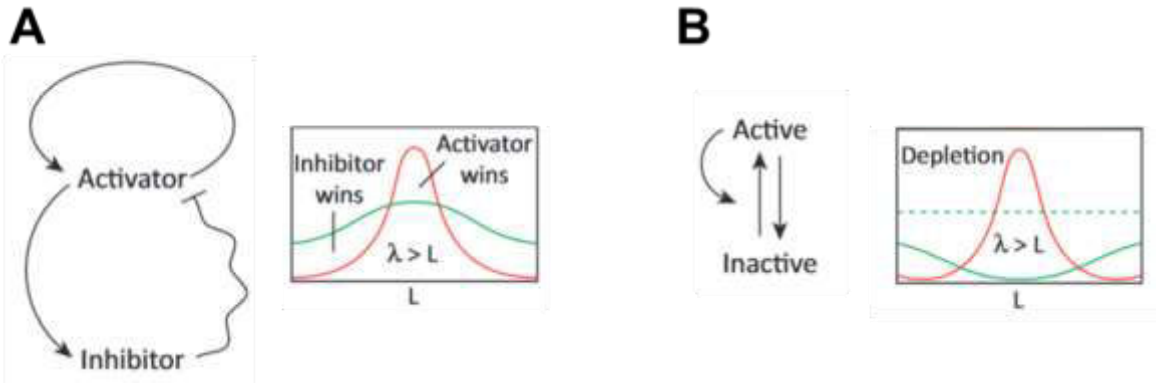

Figure 19: Pattern formation in chemical systems. ***A.*** In an activator-inhibitor system, a slow-diffusing activator stimulates production of both itself via autocatalysis and a fast-diffusing inhibitor. As a result, activation in a defined zone is achieved, with a concomitant suppression beyond. If the distance over which the inhibitor can effectively exert its activity is larger than the system ($\lambda > L$), inhibition will spread throughout the system, leading to a single activation peak. ***B.*** Long-range inhibition can also occur through depletion of a diffusible molecule; for instance, if a molecule that stimulates its own conversion from an inactive, rapidly diffusing state to an active, slowly diffusing state. Rapid diffusion ensures that local conversion events result in system-wide reduction in the concentration of inactive molecules, again restricting activation to a single zone. Adapted from (Goehring and Grill, 2013).

system needs only to include a network that combines "a short-range positive feedback with a long-range negative feedback" to generate a Turing pattern or simply polarize in a random static direction (Gierer and Meinhardt, 1972; Meinhardt and Gierer, 1974) (Figure 19A). In classic Turing-like systems, the resulting spatial pattern is specified by differences in the diffusivities of the slower activating molecule and the faster inhibitor, leading to polarized patterns (Figure 19A). However, a diffusible inhibitor is not strictly required, as its role can be performed by a freely diffusing component that is depleted as part of the signal amplification process (Figure 19B).

The demonstration that spatial order can in principle arise spontaneously, brought morphogenesis in the world of physical sciences. RD equations have been used for instance to model Rho GTPase dynamics and spatial redistribution, as the inherent ability to robustly polarize a cell depends on the cycling between active, membrane-bound and inactive cytosolic forms of these proteins, and the local interactions with their regulators (Mori et al., 2008). This simple view gives rise to a cytoskeleton-independent, positive feedback loop that enhances the recruitment of activators to the polar cap. Polarized growth by budding in the yeast *Saccharomyces cerevisiae* is a particularly illustrative case of an activator-depletion mechanism that allows actin-independent symmetry breaking, that I will discuss in detail in the next chapter.

1.5.2 Transport-based positive feedback loop

Works in different organisms, and especially in neutrophils, *Dictyostelium* and budding yeast, have highlighted the key role of the cytoskeleton (in particular F-actin) together with Rho-type GTPases for self-polarization mechanisms. In the case of yeast, although Cdc42 activity is required for the formation of a polarized actin network, actin in turn plays an important role in the polar localization and stability of Cdc42 (Pruyne et al., 2004; Wedlich-Soldner et al., 2004), by providing the structures necessary for intracellular transport, with cables acting as the transport routes, whereas patches are the ports where membrane components are recycled back from the cortex. In other words, actin polarization requires polarized Cdc42, whereas Cdc42 may in turn be transported and recycled via actin to achieve its polarized distribution, generating a cytoskeleton-dependent positive feedback loop that leads to an asymmetry (Fig. 20). This mechanism is sufficient for symmetry breaking, presumably through amplification of stochastic fluctuations in Cdc42 or actin distribution (Wedlich-Soldner et al., 2003).

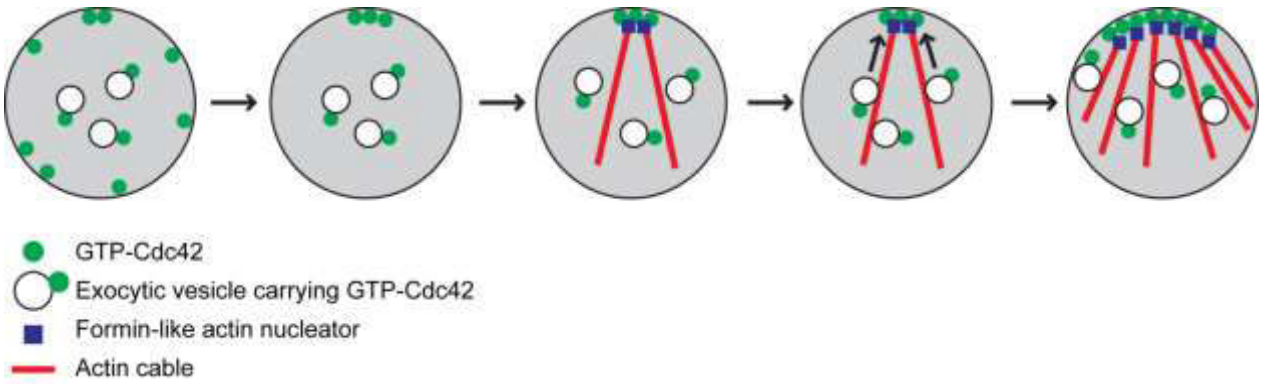

Figure 20: Actin-dependent positive feedback loop. Initial stochastic accumulation of Cdc42-GTP triggers nucleation of actin cables by formin family proteins. This in turn leads to transport of internal Cdc42 to the polarizing site, resulting in further nucleation of actin cables. (Amberg, 1998; Slaughter et al., 2009)

1.5.3 Breaking symmetry mechanically

As I have previously mentioned, recent works have suggested that spontaneous polarization can also be driven by a mechanical instability of the actomyosin cortex of cells. A simple system for studying cortex symmetry breaking consists of actin gel layers which grow around beads coated with an activator of actin polymerization and placed in a medium that reconstitutes actin assembly (Figure 21 Panel A) (van der Gucht and Sykes, 2009). An actin gel grows around the

bead through activation of actin polymerization at the surface: during this process, new monomers are incorporated at the bead surface underneath the pre-existing gel, which is consequently pushed outward and stretched because of the curved surface. As a result, stresses build up and the actin shell is under tension. The shell initially grows homogeneously, and after some time breaks spontaneously: a notch forms at the external surface of the actin gel, which grows inward and expands laterally with a velocity of a few micrometers per minute. After several minutes, the hole is big enough for the bead to escape from the gel, and the bead starts to move, trailing an actin comet. This symmetry breaking can also be triggered by a local disruption of the actin gel. Altogether, these observations strongly suggest that symmetry breaking is driven by the release of elastic energy. Suck kind of phenomenon is also observed in blebbing cells, where spontaneous rupture or detachment from the membrane leads to the expulsion of membrane bulges in the weakened regions, driven by the pressure generated by contraction of the actomyosin cortex (Figure 21 Panel B) (Paluch et al., 2005). In conclusion, the nature of the symmetry breaking instability can be also mechanical, based on a release of stored elastic energy.

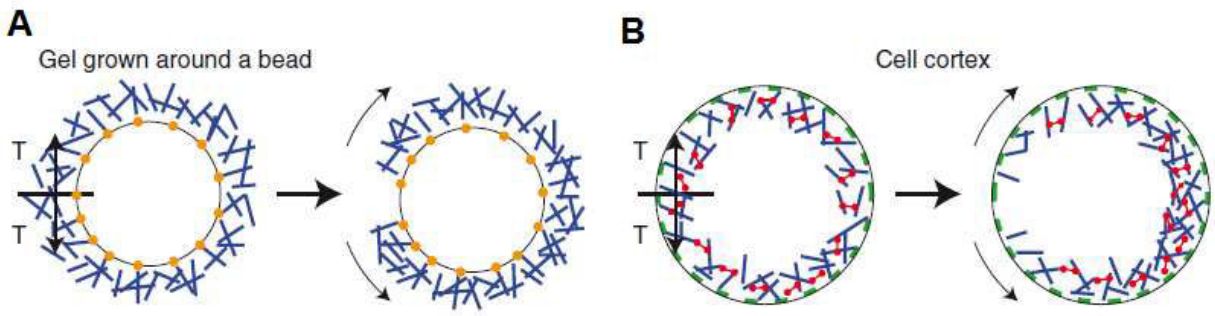

Figure 21: Schematic view of the symmetry breaking of ***A.*** an actin gel growing from the surface of a bead or ***B.*** the breakage of the cell cortex. Actin filaments are represented in blue, myosin fibers in red, membrane attachments in green, and actin polymerization activators in orange. In both cases, a tension (T) builds up because of polymerization in curved geometry for the gel on the bead and because of the presence of myosin motors in the cortex. Rupture of the gel leads to actin shell or cortical movement (indicated by curved arrows) (van der Gucht and Sykes, 2009).

1.5.4 Mechanochemical patterning

Interestingly, Turing also realized the importance of mechanics - stress, motion and elasticity - in morphogenesis, even though he did not know about the molecular basis of biological force generation (Turing, 1990). Indeed, it is clear today that active mechanical processes, such as transport along cytoskeletal filaments, cytoplasmic flow and endocytosis, also have essential

roles in patterning at the cell and tissue levels. These processes provide mechanisms beyond simple diffusion for transporting signals through space (Howard et al., 2011). Although cell polarity can emerge from systems that are largely either chemical or mechanical, in many, if not most, cases, cell polarization depends critically on the interplay between the two.

One well-studied example of such kind of mutual interaction is the establishment of the anterior-posterior (AP) polarity axis in one-celled *C. elegans* embryos, which, as I described previously, depends on both mechanical (through actomyosin) and biochemical (through PAR proteins) networks. On one hand, mutually antagonistic negative feedback between the anterior and posterior PARs yields a locally self-amplifying feedback loop, as a molecule's inhibition of its own inhibitor effectively constitutes an auto-activation pathway. On the other hand, a contractile asymmetry in this network along the AP axis results in a long range flow of cortex from posterior to anterior, which in turn entrains the motion of the cell cytoplasm, creating a fluid flow towards the anterior along the inner surface of the membrane (Hird and White, 1993). Goehring and colleagues recently showed that the diffusive properties of anterior PAR proteins at the membrane are such that these flows can induce a significant redistribution of PAR proteins within the cell through advection (Goehring et al., 2011). Consequently, anterior PARs, which are initially enriched at the membrane, will be preferentially transported towards the anterior,

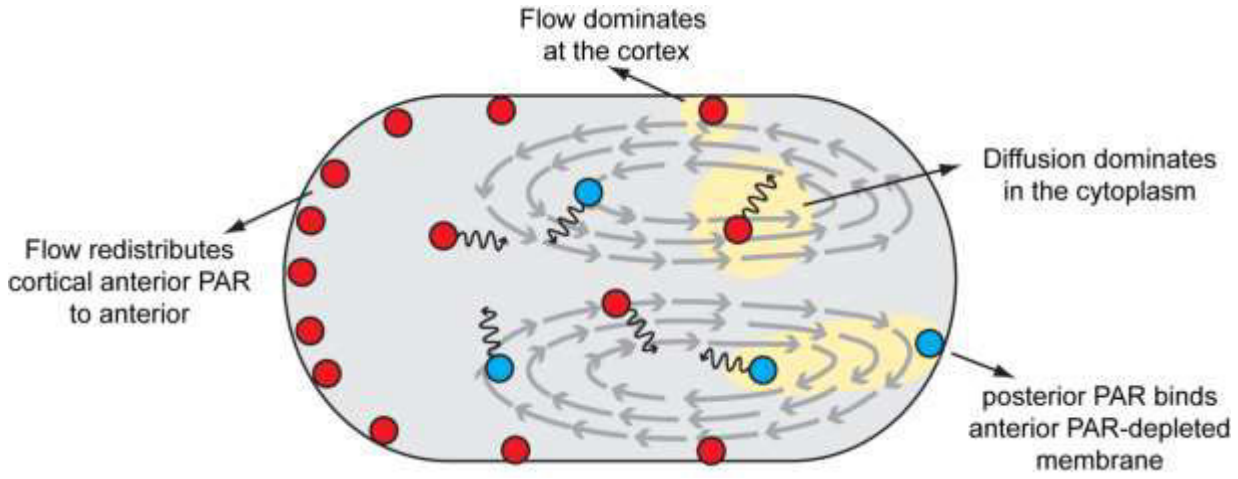

Figure 22: Coupling of mechanical and chemical elements in polarization of the *C. elegans* embryo. Pattern formation is induced by advection of membrane-associated anterior PAR proteins by actomyosin-dependent cytoplasmic flow. This allows membrane binding of posterior PARs, resulting in an asymmetry that can be amplified by the self-organizing characteristics of the PAR reaction-diffusion system, which comprises local self-enhancing feedback and long-range inhibition of two antagonistic groups of PAR proteins (represented in red and blue respectively). Adapted from (Goehring and Grill, 2013).

thus depleting anterior PARs from the posterior membrane (Figure 22). Freely diffusing posterior PARs in the cytoplasm can then take advantage of this local depletion to associate with the posterior membrane. Once asymmetry is established, biochemical reaction–diffusion processes can take over to drive the system to the stably polarized state. In conclusion, this polarization process can be understood as a chemical pattern-forming system based on local self-amplification and long-range inhibition processes that are intrinsic to the PAR network, combined with a mechanical symmetry-breaking event.

1.6 Cell shape and cell size

In "On growth and form" again, D'Arcy Thompson opens the second chapter by defining cell shape as a matter of magnitude, referring to its dimensions in space, and growth, which is related to its dimensions in space and time (Thompson, 1945). Today, we know that that cell size is another fundamental aspect of cell morphogenesis, and its regulation is given by the coupling of growth and division.

In nature, cells can be as small as 0.2 μm (e.g., *Mycoplasma gallicepticum*) and as large as 0.1 m (e.g., *Syringammina fragilissima*), spanning almost six orders of magnitude. Individual organisms, however, show much narrower size distributions, and under constant conditions most single-celled microorganisms change their size by only two-fold between birth and division, suggesting that cells have specific mechanisms to maintain stable size.

In 1958, Schaechter, Maaloe, and Kjeldgaard established a general underlying principle in microbial physiology known as the "growth law" (Schaechter et al., 1958), which states that the average cell size is exponentially proportional to the average nutrient-imposed growth rate. But what determines the actual cell size, and how cells maintain their size under a given growth condition is still a matter of investigation.

Historically, cell size homeostasis has been discussed in the context of two major paradigms: sizer, in which the cell actively monitors its size and triggers the cell cycle once it reaches a critical size, and timer, in which the cell attempts to grow for a specific amount of time before division. Most cells, ranging from bacteria to yeast to animal cells, are thought to regulate their size and cell cycle through critical size thresholds (Turner et al., 2012) or a combination of different control modules, but currently the mechanisms appear diverse (Figure 20): for instance,

work in budding yeast has shown that G1 phase can be separated into two independent steps, a size-sensing module and a size-independent timing module (Di Talia et al., 2007); in fission yeast, Chang and his collaborators recently proposed that cells sense their surface area as part to control size, and enter mitosis at a certain surface, as opposed to a certain volume or length (Pan et al., 2014); finally, a recent study on the model bacterial organisms *E. coli*, which divides symmetrically, and *C. crescentus*, known for asymmetric cell division and cellular differentiation, suggests that size homeostasis can also be obtained by cells adding a constant size between birth and division, irrespective of the birth size (Campos et al., 2014).

Why do cells care how big or small they are? First, cell size matters because the basic processes of cell physiology, such as flux across membranes, are by their nature dependent on cell size. As a result, changes in cell volume or surface area will have profound effects on metabolic flux, biosynthetic capacity, and nutrient exchange. Consequently, cell size can be an important selective trait for survival in changing, nutrient-limited environments. Second, cell size may be optimized in order for the cell to have a highly efficient mitotic machinery, which is in turn dictated by the dynamic properties of MTs. Finally, in both animals and plants, cells must fit together to form tissues and organs, meaning that a cell has to have a size appropriate to its position within the overall tissue (Marshall et al., 2012).

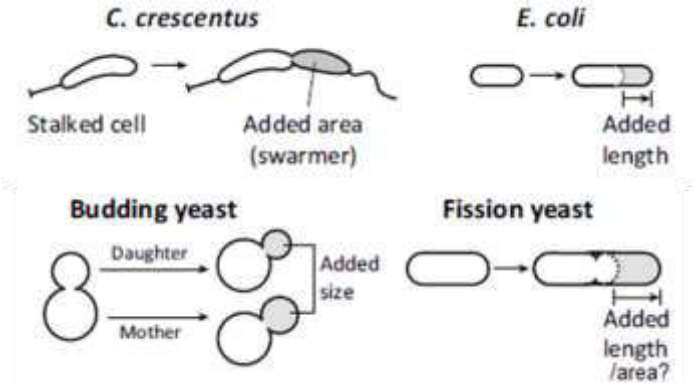

Figure 23: Mechanisms of cell size homeostasis in different organisms. Adapted from (Jun and Taheri-Araghi, 2015)

2.

CELL MORPHOGENESIS IN YEAST

In this chapter, I will focus on different aspects of cell polarization and cell morphogenesis in the eukaryotic unicellular organism fission yeast *Schyzosaccharomyces pombe.* As in the previous section, I will start with an historical perspective on this model organism, followed by a general overview of yeast models in the study of cell morphogenesis. Moreover, I will highlight the importance of cell mechanics for shape establishment in walled cells, and introduce some simple theoretical concepts regarding the link between cell morphogenesis and the balance between turgor pressure and wall remodeling. I will then narrow to rod shape generation by different means, and the particular case of fission yeast. Next, I will describe the main molecular players that are involved in the regulation of fission yeast cell polarity. To conclude, I will describe polarization processes that are guided by extrinsic cues and intrinsic ones in fission yeast, and illustrate the different classes of core principles that have been proposed to generate spontaneous symmetry breaking, in the specific context of yeast polarity.

2.1 Why yeast as a model organism?

Historically, two established yeast systems, *Saccharomyces cerevisiae* (also known as budding yeast) and *Schyzosaccharomyces pombe* (also known as fission yeast) have been widely used by researchers as models to address basic biological questions. For instance, the basis of the cell cycle, a molecular clock driving alternative rounds of growth and division, was initially described in *S. pombe* by Paul Nurse, and for this work he received the Nobel Prize in Physiology and Medicine together with Leland Hartwell and Tim Hunt in 2001. Moreover, *S. pombe*'s genome has been fully sequenced in 2002, and found to contain large conserved regions compared to the human genome: thus fission yeast provides an excellent model system to study numerous cellular processes, such as DNA damage and repair (for instance the function of heterochromatin proteins, origins of replication, centromeres, telomeres, gene splicing), checkpoint controls, and the cell cycle.

Saccharomyces cerevisiae is found in vineyards, a habitat that led to its major impact on human economy in brewing and winemaking. Yeasts, important for these human activities, were proposed to represent domesticated strains initially derived from natural habitats such as trees exudates (Fay and Benavides, 2005). By contrast, the ecology of *S. pombe* remains largely unknown: the organism was initially isolated from millet beer imported from East Africa, and more recently again from alcoholic beverages or cultivated fruits, but almost nothing is known about its natural niches, nor about its influence on the fermentation of human drinks (Figure 24).

S. cerevisiae and *S. pombe* belong to the largest fungal phylum, the ascomycetes, defined by the presence of an ascus, a sac within which spores develop. While the ascomycetes form a monophyletic group, these two species are very divergent within this group: the archiascomycete lineage, which includes *S. pombe*, is estimated to have diverged from the rest of the ascomycetes between 400 and 1200 million years ago, a divergence roughly as large as that between humans and nematode (Heckman et al., 2001; Taylor and Berbee, 2006). Accordingly, the two species diverge significantly in their shapes and physiologies. The study of both systems thus reveals commonalities tracing back to the origins of the ascomycetes, but can also highlight differences reflecting the inherent diversification of cell biological processes.

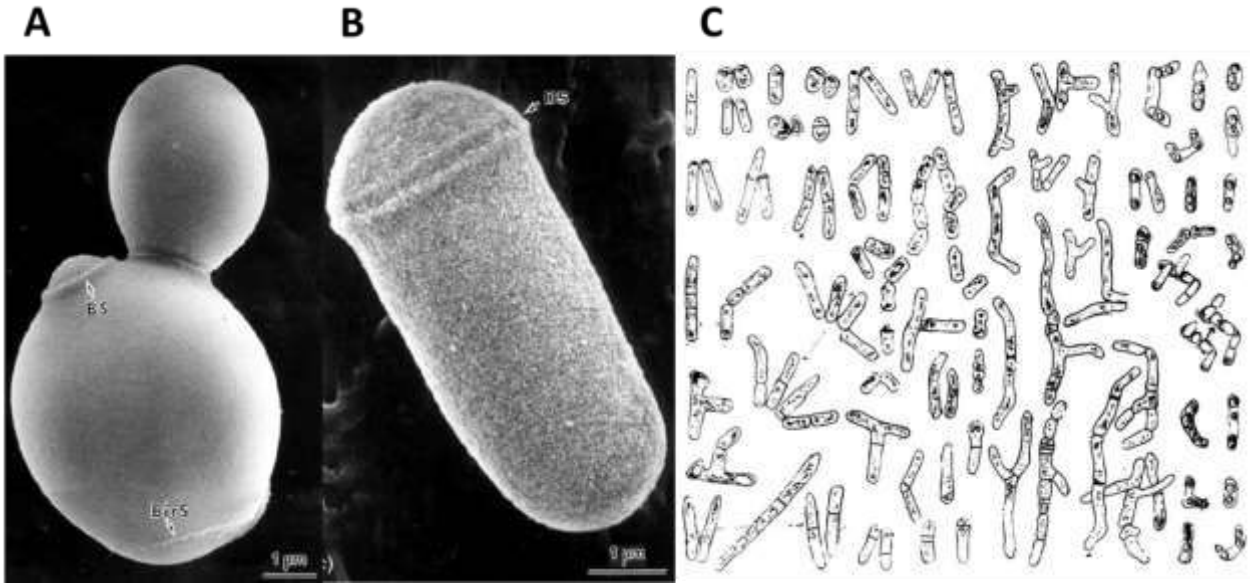

Figure 24: Yeast as a model system. ***A.*** EM picture of a budding yeast cell. ***B.*** EM picture of a fission yeast cell. ***C.*** Drawing of the various developmental stages of the yeast *S. pombe*, in the first description of this species published in the German brewery weekly *Wochenschrift für Brauerei* (Lindner, 1893).

2.2. Cell morphogenesis in fission yeast

The fission yeast *S. pombe* is an attractive, simple unicellular model organism for studying cell morphogenesis. These are rod-shaped cells with highly invariant shape: they maintain a constant diameter (3-4 μm), grow in length by tip extension (from 7 to 14 μm), and divide by medial fission. The stereotypical shape and unicellularity of this system have facilitated the identification of a large number of morphological mutants through genome-wide screenings and automated image analysis, leading to an ever-increasing understanding of cell polarization (Graml et al., 2014; Hayles et al., 2013).

In contrast to *S. cerevisiae*, *S. pombe* is most of the time in a haploid state, with only a transient stage of diploid growth during sexual differentiation. Its genome contains 5123 genes on three large chromosomes (Wood et al., 2002). The division cycle is quite rapid, with a generation time of about 2 hours. In exponential phase, G2 phase is particularly long, with G1, S phase (DNA replication) and M phase (Mitosis) each taking about 10% of the total division time.

During the mitotic cell cycle, fission yeast cells exhibit several polarity transitions: in early G2 phase, cells extend in a monopolar fashion at their old end and, later in G2, a switch to a

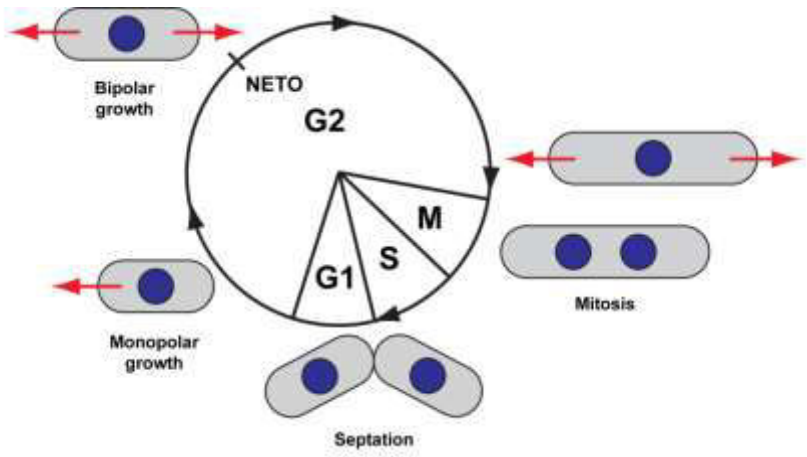

Figure 25: The mitotic cell cycle of fission yeast haploid cells. A brief description of the single stages can be found in the main text.

bipolar growth, named NETO (New End Take Off), is triggered (Mitchison and Nurse, 1985). At the end of G2, when cells reach a critical size, growth ceases and cells enter mitosis. In early mitosis, a contractile actomyosin ring, comprising of actin and several other proteins, is assembled in the cell middle. The position and the orientation of this ring determine the site of septum synthesis, while the growth machinery is redirected towards the cell equator. Septum cleavage produces two equally sized daughter cells that are released in early G2 phase (Figure 25).

Upon nitrogen starvation, haploid fission yeast cells exit the mitotic cell cycle and enter

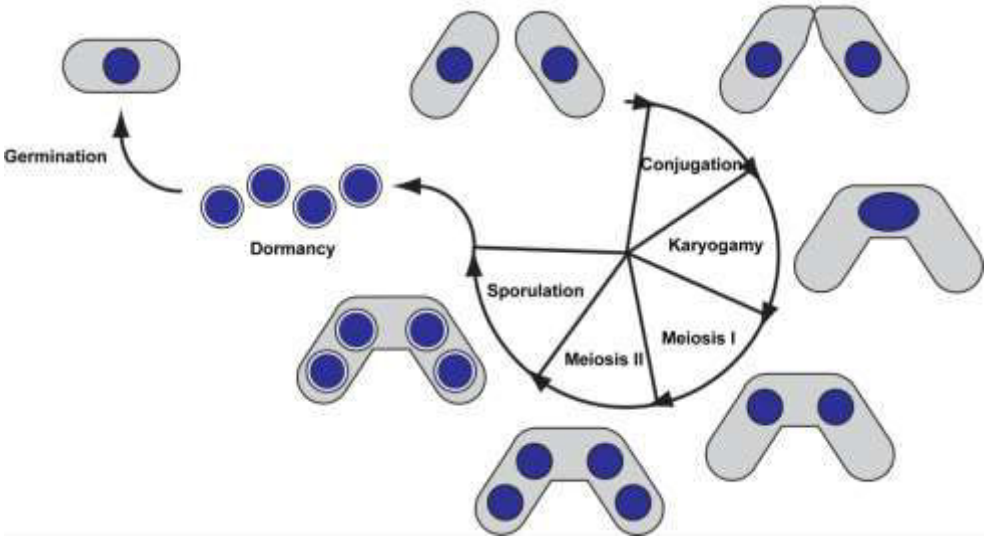

Figure 26: The meiotic cell cycle of fission yeast cells, followed by spore germination and re-entry to the vegetative cell cycle. A brief description of the single stages can be found in the main text.

stationary phase: if cells of opposite mating types, called h^+ and h^-, are present, cells enter the meiotic cell cycle (Figure 26). Therefore, two neighboring cells grow towards each other by forming an extension, named shmoo: once they contact each other, fusion and nuclear congression occur, in a process called karyogamy, and a diploid zygote is formed. In specific nutrient conditions, this diploid can grow and divide as a vegetative cell: however, this state is very unstable, and usually after nuclear fusion, diploid zygotes undergo two consecutive rounds of nuclear division, meiosis I and II, giving rise to four haploid ascospores encapsulated in the ascus. These spores can stay dormant for very long periods of time, and resist to harsh environmental conditions; in the presence of nutrients, spores re-enter the cell cycle in a process called germination to regenerate a rod-shaped vegetative cell.

2.3 Cell shape and cell polarity in fission yeast

As wild-type fission yeast cells are highly reproducible in shape and size, mutants that are defective in cell morphology have been identified through genetic screenings (Brunner and Nurse, 2000; Chang and Martin, 2009; Verde et al., 1995). In particular, specific defects in the polarity and growth machineries can lead to characteristic shape changes (Figure 27): mutants with elongated rod-shapes are typically related to cell cycle regulation, while rounded phenotypes represent essential genes for cell polarization, including the small GTPases Cdc42 and Ras, and their regulators. Mutants defective in MTs and MT-associated factors are generally bent or branched; finally, mutants in actin and actin regulators often form partially depolarized dumpy, fat cells, and have primary defects in cytokinesis.

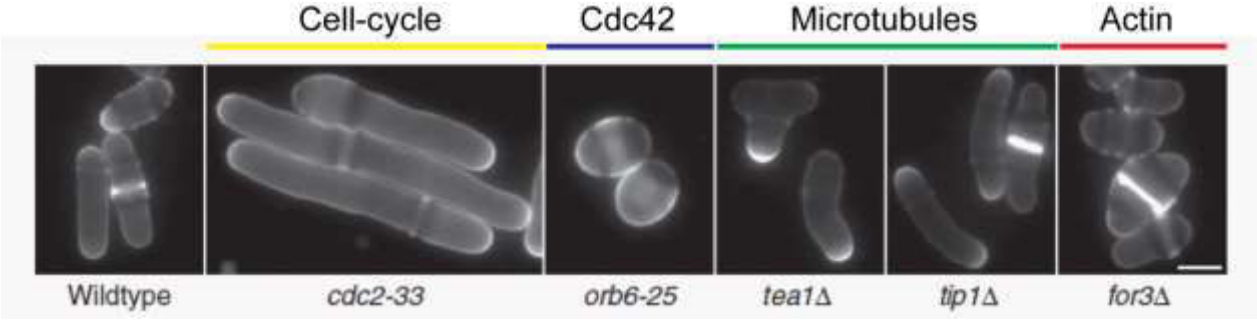

Figure 27: Morphological fission yeast mutants. The calcofluor staining shows the normal rod shape of wild-type cells and the aberrant elongated, round, T, curved, and dumpy shapes of the mutants indicate underneath each picture. Bar, 5 μm. Adapted from (Chang and Martin, 2009).

2.3.1 Molecular players in fission yeast cell polarity

Most of the core components of the eukaryotic polarity machinery are shared between yeast and animals. In this section, I will describe the major polarization mechanisms used by *S. pombe*, reviewing the role of small Rho-family G-proteins, the cytoskeleton, membrane composition and fluxes, and scaffold proteins in generating polarized states.

2.3.1.1 Sensing the partner: GPCRs, G-Proteins and mating

Cell polarization induced by external signals is a fundamental cellular property that relies on cytoskeletal and membrane re-organization in response to specific cues. Many cell types exhibit chemotaxis or chemotropism in response to external signals: unicellular yeast models exhibit chemotropism in response to pheromones produced by partner cells during the mating process. In fission yeast, sexual differentiation is triggered by starvation when compatible mating partners are present: this leads to arrest in G1 phase of the cell cycle, mating-type specific pheromones and pheromone receptor production and polarized growth in the direction of pheromone source for fusion of mating partners. Peptide pheromones are recognized by specific G-protein coupled receptors expressed on the surface of cells of the opposite mating type and this binding stimulates the activation of receptor-associated heterotrimeric G-proteins, which in turn promote the activation of a conserved mitogen-activated protein kinase (MAPK) module. By ultimately activating a specific transcription factor, MAPK cascade components modulate the expression of mating-specific genes, thus promoting cell cycle arrest, polarized morphogenesis in the direction

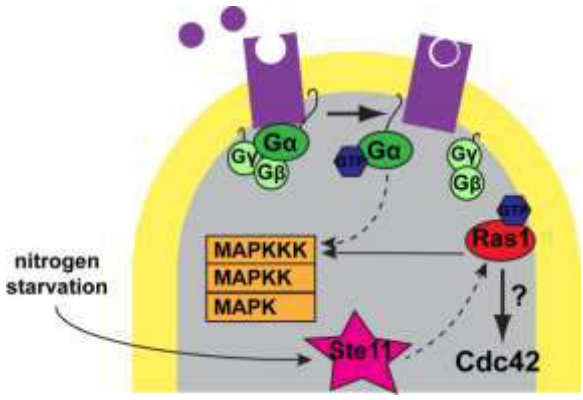

Figure 28: Mating signaling in fission yeast. The transcription factor Ste11 is activated upon nitrogen starvation and regulates the expression of essential signalling genes. Gα is responsible for signal transmission and appears to activate the MAPK cascade cooperatively with Ras1. Dashed arrows indicate hypothetical interactions. Adapted from (Merlini et al., 2013).

of the partner cell (a process known as shmooing), cell–cell fusion and karyogamy to produce a diploid zygote.

In fission yeast, pheromones (P- and M-factors, produced by h^+ and h^- cells, respectively) are bound by the receptors Mam2 and Map3 (for P- and M-factor, respectively), which are presumably coupled to the same components of a heterotrimeric G-protein (Figure 28): in particular, the Gα protein Gpa1 is responsible for the activation of the MAPK pathway. Upon nitrogen starvation, the transcription factor Ste11 acts as a developmental switch: moreover, as it both activates pheromone signalling (by directly stimulating pheromone production and pheromone receptor expression) and is induced by it, it provides a positive feedback for the mating response, where pheromone signalling components cooperate with Ste11 itself, to enhance their own expression and to promote the transcription of other Ste11-dependent genes. Complex feedback loops that involve the small GTPases Ras1 and Cdc42 regulate this pathway to activate mating signaling and initiate polarized growth towards the partner.

2.3.1.2 Small Rho G-Proteins in fission yeast polarized growth

As I have already described, conserved Rho GTPases play a central role in cell polarization. Like *S. cerevisiae*, *S. pombe* also has six genes coding for Rho GTPases, named Rho1 to Rho5 and Cdc42, this last one being the core protein of the polarity machinery in all eukaryotes. The activity of these proteins is tightly regulated by activators (GEFs) and inactivators (GAPs and RDIs), which dictate when, where, and how long the GTPase is active.

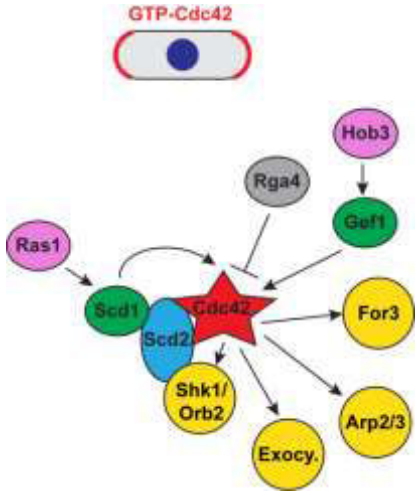

Figure 29: Schematic depiction of the Cdc42 signaling module in fission yeast. asActive, GTP-bound Cdc42 localizes to sites of active growth and to the division site. Adapted from (Chang and Martin, 2009).

In fission yeast, Cdc42 is essential for viability: loss of Cdc42 function results in strong cell polarity defects. Cdc42 activity is controlled by two GEFs located at the tips, Scd1 and Gef1, the scaffold protein Scd2, and one GAP located along the cell sides, Rga4, which restricts the distribution of active Cdc42 (Figure 29). Recent work has established the collaborative role of Rga4 and Scd1–Scd2 in the regulation of cell diameter (Kelly and Nurse, 2011b). Although cells lacking Rga4 or Scd1 may have significantly different levels of active Cdc42, in both cases cells are wider and the double mutants are almost round, suggesting that specific spatial regulation of Cdc42 activity is essential for normal cell shape. Scd1 and Gef1 are regulated by the small GTPase Ras1 and the BAR-domain protein Hob3 respectively (Coll et al., 2007; Das et al., 2009). The different interactions of Rho GTPases with their activators and effectors constitute positive and negative feedback loops, activating and concentrating polarity proteins to a specific site, that correspond then to a growth site.

A second small GTPase, Rho1, is essential for viability in both *S. cerevisiae* and *S. pombe*, as it plays a critical role in activating 1,3-β-glucan synthase, a major structural component of the cell wall (Arellano et al., 1996; Drgonova et al., 1996; Qadota et al., 1996).

In their GTP-bound form, Cdc42 and Rho1 activate a series of effectors to organize cell polarization: GTP-Cdc42 specifically binds CRIB-containing proteins such as the PAK kinases. In addition, Cdc42, Rho1, and other Rho GTPases activate actin nucleators of the formin family, in particular For3, to promote the formation of actin cables: this formin can be in a autoinhibited conformation, but upon Cdc42 binding together with the actin-associated protein Bud6, it gets relieved, leading to formin activation and localization at cell tips (Martin et al., 2007). Cdc42 may also activate Arp2/3 actin nucleation at actin patches to regulate endocytosis, even if the orthologue of the mammalian nucleation activator WASp, Wsp1, seems not able to directly interact with Cdc42. These Rho-family GTPases also bind the exocyst components Sec3 and Exo70 to promote exocytosis (Bendezu and Martin, 2011; Bendezu et al., 2012). Recent studies have shown that Cdc42 is also implicated in endosome to vacuole fusion, and consequently in endocytic uptake (Estravis et al., 2011). Other polarity modules are represented by the orb kinases. One key Cdc42 effector is the essential Ste20-like kinase Orb2/Shk1, which forms a complex with Scd1 and Cdc42, while the NDR kinase Orb6 represents the most downstream effector of a signaling network called MOR (morphogenesis Orb6 network) which spatially regulates Cdc42 (Gupta and McCollum, 2011).

The size of the growth zone, which in turn defines the final cell width, is modulated by regulators of Cdc42 activity. Deletion of the main Cdc42 GEF Scd1 or of the scaffold Scd2, both localizing at cell tips, results in a substantial widening of the zone of growth, producing almost round cells (Kelly and Nurse, 2011b). Similarly, deletion of the Cdc42 GAP Rga4, which on the contrary localizes to cell sides, results in wider cells, which is additive to that observed in *scd1Δ* cells (Das et al., 2007; Kelly and Nurse, 2011b). Altogether, these proteins function to restrict and concentrate active Cdc42 to the cell poles, thereby defining the proper growth dimension. Moreover, disruption of actin cable-mediated transport, in *for3Δ* or *myo52Δ* cells, or partial disruption of the actin cytoskeleton with low-dose LatA treatments, leads to wider cells, although the specific effects on the distribution of active Cdc42 are unclear (Feierbach and Chang, 2001; Kelly and Nurse, 2011b). Thus far, only the mutant *rga2Δ* has been reported to yield thinner cells, and thus smaller growth zones (Villar-Tajadura et al., 2008). Rga2 encodes a GAP for Rho2, but also associates with Cdc42 and somehow indirectly promotes its activation. Cdc42 oscillations between the two cell poles may also contribute to defining the width of the growth zone, but their precise role remain unclear (Das et al., 2012).

In summary, Cdc42 is critical for cell polarity via reorganization of the actin cytoskeleton, secretion, and cell wall remodeling.

2.3.1.3 The cytoskeleton: building up polarity domains

As in other eukaryotes, the fission yeast MT and actin cytoskeletons function in delivery and removal of plasma membrane components and organelle positioning (Figure 30). In both budding and fission yeast, the actin cytoskeleton is critical for polarity, by marking the sites of endocytosis and exocytosis. MTs however are not used for vesicle transport, but they are crucial for various nuclear functions including nuclear migration and division. Moreover, differently from *S. cerevisiae*, where it is dispensable for cell polarization, the MT cytoskeleton plays a central role in *S. pombe* shape polarization, by defining the position of growth zones at the distal ends of cell tips.

The fission yeast actin cytoskeleton is quite simple, as it is composed of only three actin structures for growth – actin patches, actin cables, and the contractile ring. An additional actin structure is also used during mating (Figure 31).

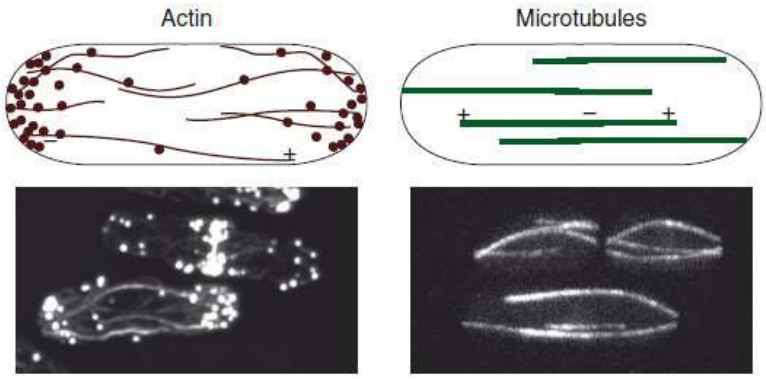

Figure 30: Cytoskeleton organization in fission yeast interphase cells. Adapted from (Chang and Martin, 2009).

Fission yeast express three formins at different cell cycle stages, each one specialized in building up actin cables for specific purposes: first, the formin Cdc12 initiates the cytokinetic ring upon entering mitosis, through the nucleation of actin filaments; these filaments then associate with tropomyosin Cdc8 and undergo rapid elongation, whereas final ring contraction comes from the work of Myo2 motors. Second, For3 forms actin cables in vegetative cells to provide polarized tracks for type V myosin-directed delivery of vesicles and organelles to the expanding cell tips. This formin is activated and recruited by Cdc42 and Bud6 to nucleate and elongate cables that are composed of bundles of short parallel actin filaments, and myosin motors may also affect cables shape by transporting cargoes and exerting physical pulling forces (Lo Presti et al., 2012). Finally, the formin Fus1 concentrate and rearrange actin cables at the projection tips of mating cells, for local cell wall degradation and fusion. In contrast, actin patches that assemble at sites of endocytosis strictly depend on Arp2/3-complex-mediated actin assembly. These patches assemble, to allow cell wall synthesis and remodeling in correspondence of growth zones, *e.g.* at the tips of interphase cells and at the centers of dividing cells. As in animal cells, actin assembly cooperates with BAR (Bin–Amphiphysin–Rvs) and F-BAR proteins to promote membrane invagination and scission. In summary the actin cytoskeleton regulated by Rho-GTPases performs important functions during polarized growth, in particular endocytosis and exocytosis, two processes that orchestrate the remodeling of the membrane.

In *S. pombe*, MTs are organized in bundles oriented along the long axis of the cells during interphase and in bundles comprising the mitotic spindle in mitosis (Marks et al., 1986). The interphase bundles contain MTs overlapping in an antiparallel configuration and attached to the nuclear envelope at multiple sites near the middle of the cell (Tran et al., 2001). The plus ends of

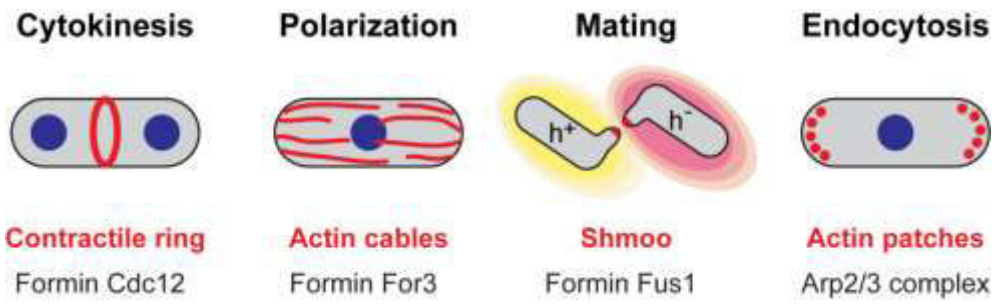

Figure 31: The fission yeast actin cytoskeleton. Adapted from(Kovar et al., 2011)

MTs constantly probe the cell tips, through the alternation of MT growth and shrinkage. In fission yeast, MTs regulate polarity by transporting and depositing landmarks, such as Tea1 and Tea4, to cell tips (Figure 32) (Chang and Martin, 2009). These polarity factors are transported by MT plus ends via a +TIP complex consisting of EB1 Mal3, CLIP-170 Tip1 and kinesin Tea2. A classical example of cytoskeletal crosstalk emerges from the observation that For3 is one of the major targets of the Tea1/Tea4 complex: upon deposition at the cell tip through the Mod5 receptor, the Tea1/Tea4 complex recruits polarity factors including the formin For3 and the For3 activators Rho-GTPase Cdc42, Bud6 and Pob1. Hence the assembly site for actin cables can be initially established by MTs.

2.3.1.4 Membrane remodeling: polarized transport

The targeting and maintenance of the flux of membrane material, integral membrane proteins, and secreted proteins to and from the plasma membrane to a specific site underlies polarized growth. Exocytosis is important for the delivery of membrane-associated proteins necessary for polarized growth, such as Rho G-proteins as well as the subsequent delivery of cell wall-remodeling enzymes. Two recent studies in budding yeast reveal that sites of endocytosis and exocytosis are distinct with exocytic sites being surrounded or corralled by a region of endocytosis, suggesting that this spatial organization may be crucial for polarity establishment and maintenance (Jose et al., 2013; Slaughter et al., 2013). Moreover, the lipid composition of the membrane plays an important role for the organization of membrane trafficking, which in turn influences cell polarity and cell morphogenesis: interestingly, in budding yeast, phosphatidylinositols and phosphatidylserine levels peak upon bud emergence, and in both yeasts block of phosphatidylserine synthesis leads to aberrant cell shapes, suggesting it is required for

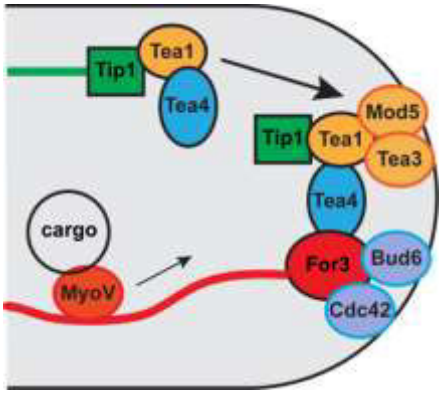

Figure 32: Microtubule-dependent polarization in fission yeast (Chang and Martin, 2009).

polarized growth (Cottrell et al., 1981; Fairn et al., 2011; Matsuo et al., 2007). These results indicate that phosphatidylserine-and presumably its polarization-are required for optimal Cdc42 targeting and activation during cell division and mating.

Polarized secretion in fission yeast is achieved by two independent pathways: the actin-based delivery of secretory vesicles and the PIP-2 dependent asymmetric localization of the exocyst complex (figure 33). Disruption of the transport along actin cables or interfering with the exocyst function alone does not abolish polarized growth; however, when both pathways are affected, cells grow isotropically (Bendezu and Martin, 2010). The exocyst is a conserved multiprotein complex which plays a role in the transport between the Golgi apparatus and the plasma membrane. In fission yeast, the localization of the exocyst complex relies on Cdc42 and PIP-2 but is largely independent of actin cables. Similarly to budding yeast, Sec3 and Exo70 are recruited to the plasma membrane, while other subunits are loaded onto vesicles and transported along actin cables (He and Guo, 2009). Sec8 is another component that plays a key role in delivery of secretory vesicles in a number of organisms, including *S. pombe* (Bendezu and Martin, 2011; Grindstaff et al., 1998; TerBush et al., 1996; Ting et al., 1995). Recently, the GTPase Rho3 was found to be implicated in secretion, suggesting that it may regulate the exocyst independently of Cdc42 (Estravis et al., 2011).

Actin patches dominantly assemble at cell tips in interphase cells, suggesting that endocytosis may participate in polarized growth in fission yeast, by using cargoes such as receptors, transporters and SNAREs (Gachet and Hyams, 2005). Cells lacking the early endocytic factor Sla2/End4 display an aberrant morphology with shorter and fatter cells but the mechanism for the relationship between endocytosis and morphogenesis has not been understood yet

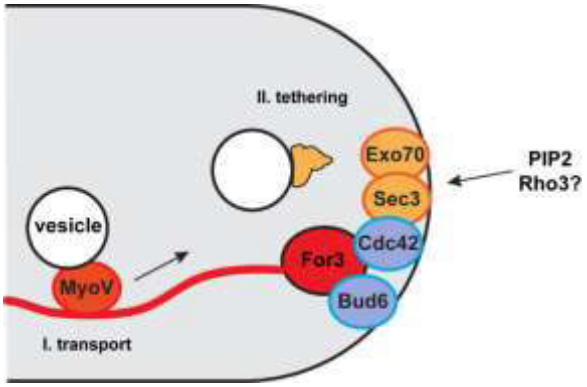

Figure 33: Polarized secretion in fission yeast. For3-dependent actin cables and asymmetric localization of the exocyst complex constitute two independent pathways

(Castagnetti et al., 2005). We can speculate that this recycling mechanisms allows to define the spatial precision and morphology of the polarized state, as it has been proposed for *S. cerevisiae* (Marco et al., 2007). The various steps of the endocytosis process are quite similar in the two yeast models (Kovar et al., 2011). Patch assembly starts with recruitment of early patch components that are thought to promote initial membrane invagination: first clathrin, followed by the endocytic adaptor proteins End4/Sla2 and Pan1. Arp2/3 complex-mediated actin polymerization is required for internalization, probably to overcome the high turgor pressure (Basu et al., 2014): its ability to drive actin assembly is stimulated by the proteins Pan1, Wsp1 and Myo1, whereas membrane deformation may be regulated by BAR and F-BAR proteins. Moreover, patches are rich in fimbrin to prevent binding of tropomyosin Cdc8, which otherwise would interfere with patch internalization and turnover. Activation of Arp2/3 complex results in a burst of branched actin filament assembly culminating in patch internalization: at this stage, the actin network rapidly disassembles for vesicle fusion and actin recycling, mostly thanks to cofilin that severs filaments and dissociates Arp2/3 complex-anchored actin branches. After internalization, patches can undergo either directed or undirected movement, depending on their stochastic association with actin cables. To conclude, regulation of membrane trafficking is very important in fission yeast cell polarity and morphogenesis.

2.3.2 Cell polarization: with or without a cue?

Yeast models are very suitable to compare different polarization pathways, which correspond to specific developmental stages, and in particular to investigate how cells switch from an internally programmed polarized growth process to one dictated by an external cue (Figure 34).

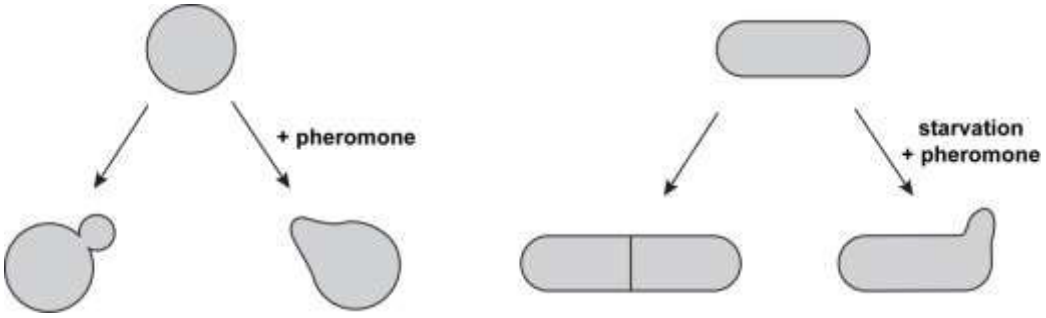

Figure 34: Decision making for polar growth in budding and fission yeast.

For instance, during budding yeast vegetative growth, haploid cells bud at a specific site next to their previous bud site, resulting in a characteristic axial budding pattern (Chant and Pringle, 1995). However, this internal signal generated during budding is overridden upon exposure to a mating pheromone gradient, allowing cells to orient growth towards their mating partner (Madden and Snyder, 1992). These polarity pathways share the same set of core Rho-GTPases proteins and downstream effectors, but the cell can select either one or the other depending on specific upstream regulators that will locally recruit the polarity machinery: in particular, Bud1 will indicate the budding site, while in presence of pheromone binding to Gβγ, by depletion of Axl2 and Bud4, both of which are required for axial budding, Far1 and Cdc24 will create a landmark for growth towards an external signal

In fission yeast, cells generally proliferate asexually as haploids, and undergo sexual differentiation in conditions of starvation. If nitrogen is depleted, cells arrest in G1 after one or two mitotic divisions, express pheromone and pheromone receptor, and polarize growth toward a partner (a process called shmooing) for cell fusion, meiosis, and formation of resistant spores. Compared to *S. cerevisiae*, less is known about the mechanisms regulating the switch between vegetative growth and shmoo formation in *S. pombe*: however, also in this case shmooing simply requires the polarity machinery to switch from using the mitotic growth sites to using the new zones generated from the pheromone gradient. Ras1 is probably involved in relaying positional information to the Cdc42p pathway following pheromone stimulation, while down-regulation of Tea1 facilitates the removal of positional information coming from the cell tips (Fukui et al., 1986; Mata and Nurse, 1997).

In conclusion, the direction of polarized growth in fission yeast vegetative cells is determined by an internal program, producing defined growth patterns; by contrast, the

orientation of mating projections is caused by an external signal (a source of mating pheromone). This change from internal to external induced programs correlates with the degradation of proteins involved in producing the internal landmarks.

2.3.3 External control of cell polarity in fission yeast

In eukaryotic cells MTs and actin filaments help to generate the spatial organization of the cytoplasm that is required for polarity and shape.

2.3.3.1 Manipulation of cell shape

Recent work in fission yeast demonstrates that changing cell shape in turn reorganizes the cytoskeleton and cell polarization machinery (Figure 35). These cells have already a cylindrical shape at the moment of birth, immediately after septation, with defined cell tips and ordered cytoskeletal arrays. It is known that the organization of microtubules along the long axis of the cell depends on its cylindrical shape, as mutant cells with altered morphology also have disorganized microtubule bundles but the causality between cytoskeletal organization and cell shape has not yet been established (Hayles and Nurse, 2001).

Minc et al. and Terenna et al. used novel micro-fabricated chambers to achieve rapid changes in cell shape of wild-type cylindrical yeast cells (Minc et al., 2009b; Terenna et al., 2008). In both cases, bending fission yeast cells by physical means has immediate effects on MT organization. In particular, at a certain bending threshold MT cannot reach any more the cell tips and undergo catastrophe upon contact with the cell cortex at the outer curvature of the bent cells: Minc et al. suggest that specific microtubule attachment sites, called "hot spots", may exist and lead to stalling and subsequent catastrophe upon interaction with MT tips (Minc et al., 2009b). When MTs contact lateral cortical sites, polarity determinant molecules such as Bud6, Tea1, Mod5, the activated form of Cdc42 and For3 are recruited to these sites in a MT-dependent manner, leading to the assembly of actin cables and patches. Thus, these new sites were primed for growth. The pathway for localizing these polarity determinants to ectopic sites in bent cells is novel and independent of Tea1/Tea4: in fact the localization of Bud6 at ectopic sites involves the plus-end-localized EB1 homolog Mal3, the Cdc42- and For3-binding protein Moe1 and the formin For3 itself (Minc et al., 2009b). On the other hand, Terenna et al. show that morphological mutants with a disorganized MT cytoskeleton and mislocalized polarity factors,

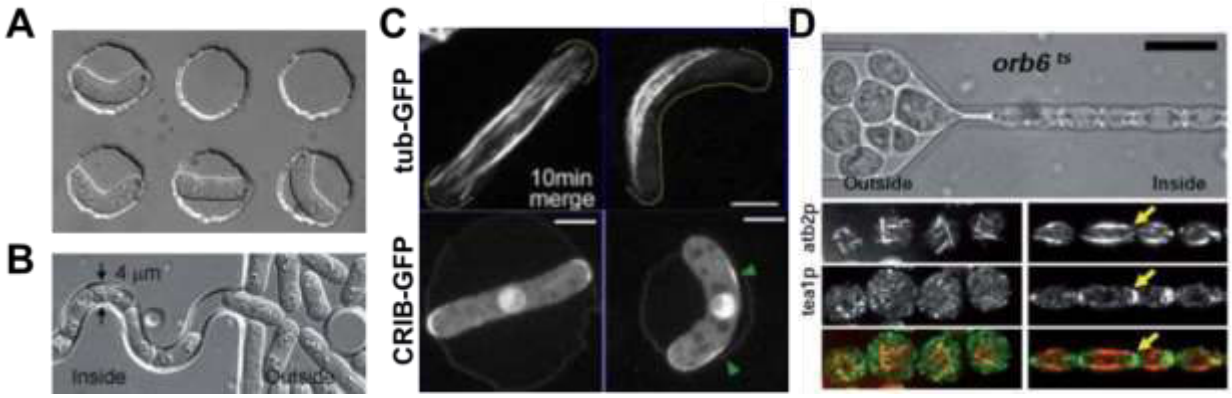

Figure 35: External manipulation of fission yeast cell shape (Minc et al., 2009b; Terenna et al., 2008)

such as *orb6*^{ts}, revert to an ordered MTs array and correct localization of polarity determinants when constrained to grow into cylindrical shapes (Terenna et al., 2008). These experiments establish the existence of a strong feedback loop between cell shape and the cytoskeleton.

Finally, these studies offer novel ways of manipulating cell shape, to investigate the fundamental relationship between cell morphology and its morphogenetic determinants.

2.3.3.2 Electrical control of cell polarity

As I have previously described, the application of exogenous electric fields can direct polarity in most cells, ranging from bacteria, fungi, and amoebas to animal cells, by orienting polarized growth, migration, or division respect to this external cue (Campetelli et al., 2012).

Minc and collaborators recently showed that application of an EF on fission yeast cells causes a reorientation of their growth axis by bending perpendicular to the EF, creating cells with a bent morphology, in a For3- and Cdc42-dependent manner (Figure 36) (Minc and Chang, 2010). Interestingly, the authors further identified a conserved plasma membrane ion pump, the proton ATPase Pma1, a pH and membrane potential regulator in yeast and fungi, as a mediator of EF effects: the rapid proton flux of Pma1and its localization pattern along cell sides may generate a polarized current of ions throughout the cell, maintaining an acidic pH at growing tips that could be important for targeting of Cdc42. Modeling and experimental data suggest that the EF reorients cell polarity by altering the spatial regulation of membrane potential and generating local pH effects: these upstream signals may in turn recruit the polarity machinery, resulting in an overall reorganization of the cell polarity axis. One interesting result is that pma1, cdc42 and for3 mutants still orient to the EF but in the wrong direction, toward the anode of the EF: this effect

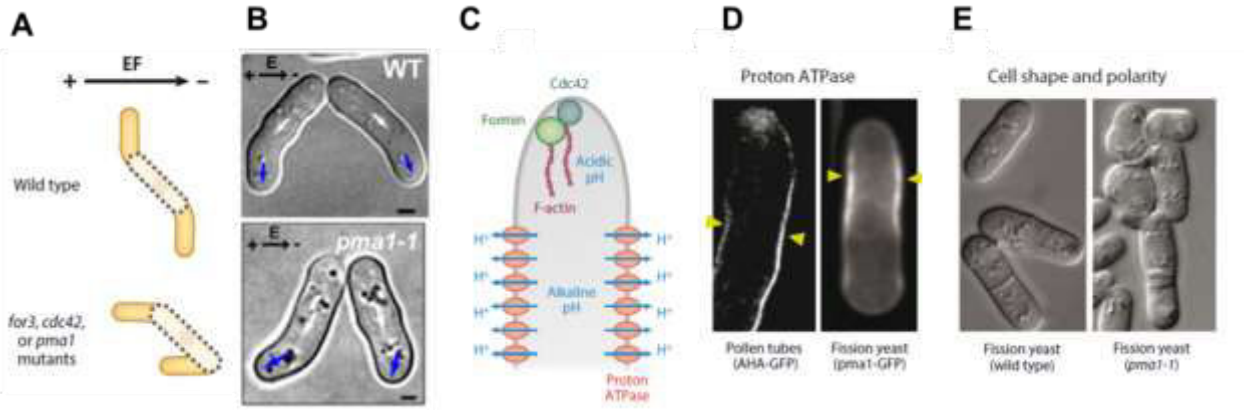

Figure 36: Electrical regulation of fission yeast polarity (Chang and Minc, 2014; Minc and Chang, 2010)

may depend on the anodal electrophoresis of transmembrane cell wall enzymes that possess negatively charged extracellular domains, such as Bgs synthases (Minc and Chang, 2010).
Altogether, these results suggest that external control of cell polarity can uncouple overlapping pathways for cell shape regulation, and hence give new insights on the mechanisms of cell morphogenesis.

2.4 Cell shape and cell mechanics in fission yeast

In plants, fungi and bacteria, cell shape is also determined by two biophysical players: the cell wall and turgor pressure. These features have interested physicists and biologists in understanding cell morphogenesis since a long time ago, as the interplay between the two is tightly regulated by the cell in order to grow. Hence, key elements of walled cell morphogenesis include the physical properties of the cell wall and the processes responsible for its synthesis and remodeling, and the balance of forces between cell-wall extension and turgor pressure.

In the following, I will discuss mechanical aspects of cell form, with a particular focus on the fission yeast case.

2.4.1 Cell wall structure

The cell wall surrounds the plasma membrane and has a prominent role in the shape and growth behavior of walled cells. It provides structural support during development and protection against stress. By cell wall biogenesis, cells can assume a variety of characteristic morphologies to suit a

wide variety of functions: vegetative growth, substrate colonization, reproduction, dispersal, survival, host penetration, animal predation, etc. In the past, researchers even proposed that the morphological development of walled cells may be reduced in simplified terms to a question of cell wall morphogenesis (Harold, 2002).

The composition of the cell wall varies between species, and can also differ depending on cell type and developmental stage, but it generally includes polysaccharides (such as peptidoglycans in bacteria or pectins in plants), structural proteins and cell wall synthases. In fungi, the cell wall has been defined as "a fabric of interwoven microfibrils embedded in or cemented by amorphous matrix substances" (Bartnicki-Garcia, 1968). In yeast and the vast majority of fungi, chitin and glucans are the skeletal components of the cell wall. Proteins and various polysaccharides (glucans, mannans, galactans, heteropolysaccharides) are probably the cementing substances which bind together the different structural components of the wall into macromolecular complexes.

In budding yeast, the vegetative wall consists of two major layers, an inner layer (closer

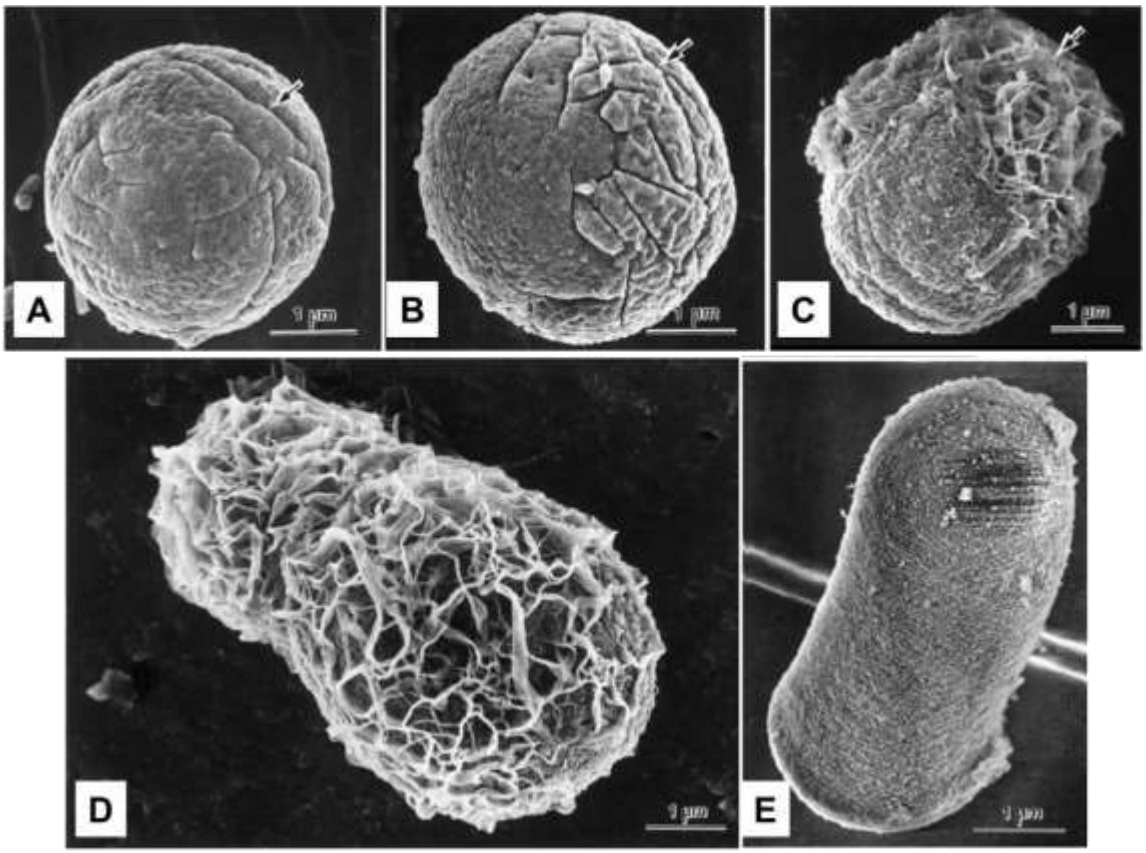

Figure 37: Cell wall regeneration in a fission yeast protoplast (Osumi, 2012)

to the plasma membrane) consisting primarily of β-glucan (chains of β -1,3-linked glucose) with some chitin (β-1,4-linked N-acetylglucosamine) and an outer "mannan" layer consisting of proteins that have been heavily glycosylated with primarily mannose side chains.

In fission yeast, the cell wall is mainly composed of two glucose homopolymers: (1,3)β-D-glucan with 2-4% of (1,6)β-D-glucan branches, which constitutes 50-54% of total cell wall polysaccharides; and (1,3)-α-D-glucan with 7% of (1,4)-α-D-glucans bonds, which constitutes 28%-32% of total polysaccharides (Bush et al., 1974; Kopecka et al., 1995). Galactomannan is a non-structural polymer that represents 9-14% of the cell wall polysaccharides and is linked to proteins to form glycoproteins. Chitin, a critical cell wall component for budding yeast and various pathogenic fungi, seems to be poorly present in fission yeast (de Groot et al., 2007), and specifically associated to ascospore maturation (Arellano et al., 2000; Matsuo et al., 2004).

Ultrastructural studies have shown that fission yeast cell walls have a three-layered structure, with two electron-dense layers separated by a non-dense one. Enzymatic digestion of the entire cell wall in hyperosmotic medium leads to the formation of membrane-encased round cells, called spheroplasts or protoplasts (Figure 37): studies on the cell wall regeneration in these conditions have shown that (1,3)- β-D-glucan is the first layer to be synthetized, forming a microfibrillar network composed of long parallel microfibrils that result in interwoven ribbon-shaped bundles (Osumi et al., 1998). This inner layer is mainly responsible for the mechanical strength of the wall, while -α-glucans and galactomannans are deposited later in more external locations (Ishiguro, 1998). Interestingly, during regeneration protoplasts polarize, and fibrillary networks appear at a pole, extending outwards until they cover the surface of the protoplast and regenerating the cylindrical shape.

2.4.2 Cell wall biosynthesis

Like root hairs, pollen tubes, and algal rhizoids, fungi spatially organize wall deposition. To this aim, secretion and vesicle transport are functionally polarized at a cellular scale, providing an ideal example of "vectorial physiology" (Harold, 1991): cell shape is then determined by the manner and the sites of surface expansion.

In *S. pombe*, synthesis of linear (1,3)β-D-glucan in the cell wall is accomplished by (1,3)β-D-glucan synthase (GS). It is formed by at least two components: a regulatory and a catalytic subunit. As in other fungi, GTP-bound Rho1 is an essential regulatory subunit of this

activity, and is also involved in other morphogenetic processes, such as organization of the actin cytoskeleton and genesis of the growing regions (Arellano et al., 1999; Drgonova et al., 1996). *S. pombe* contains four putative GS catalytic subunits named Bgs1-4 (Perez and Ribas, 2004). Bgs1, also called Cps1, is an essential gene implicated in the coordination between cytokinesis and cell cycle, with an important role in septum synthesis (Cortes et al., 2002). In contrast, Bgs2 expression is induced during sporulation and required for correct ascospore wall maturation and survival (Liu et al., 2000; Martin et al., 2000). Finally, Bgs3 and Bgs4 are essential genes required for cell wall biosynthesis and cell elongation in fission yeast (Cortes et al., 2005; Martin et al., 2003). In particular, Bgs4 is the first subunit that shows a direct in vivo involvement in cell wall (1,3)-β-D-glucan synthesis and GS activity, and that is required in numerous developmental stages such as vegetative growth, septation, cytokinesis, mating, sporulation and spore germination. Cdc42 participates in membrane trafficking, endosome recycling, and vacuole formation, and is required for the correct transport/recycling to the plasma membrane of the glucan synthases Bgs1 and Bgs4 (Estravis et al., 2011).On the other hand, the small GTPase Rho2 controls (1,3)- α-D-glucan synthesis through regulation of the major (1-3)-α-D-glucan synthase, Mok1/Ags1 (Arellano et al., 1996; Calonge et al., 2000; Perez and Rincon, 2010). Highly branched (1,6)-β-glucan is also a component of the cell wall: as low molecular α-1,3-glucan is transported through the secretory pathway to the cell membrane where the synthase is located, and then synthesized into higher molecules, this other polysaccharide may be also synthetized in the endoplasmic reticulum-Golgi system, and finally form highly branched

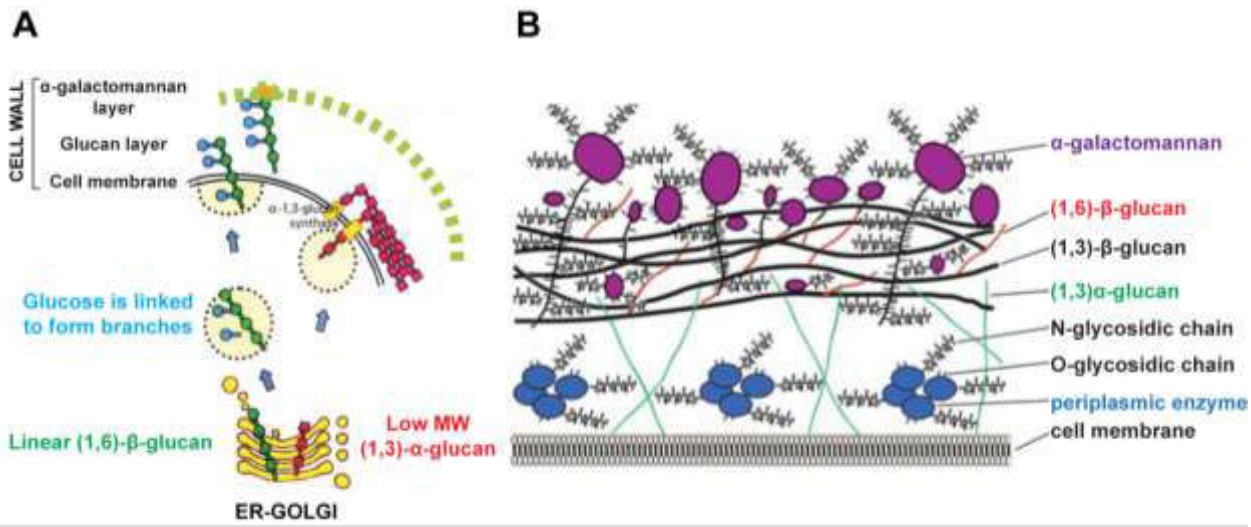

Figure 38: Schematic of fission yeast cell wall biosynthesis and structure (Osumi, 2012)

structures on the cell membrane. Those glucans and α-galactomannan are characteristic components of this yeast (Figure 38).

In response to harsh environmental conditions, the yeast cell wall is remodeled in a highly regulated and polarized manner, mainly through the cell wall integrity (CWI) signaling pathway: in *S. pombe*, little is known about the upstream signals that initiate the stress response. However, this pathway relies again on the activity of Rho1, which mobilizes a physiological response through a variety of effectors, such as the two PKC homologues, Pck1 and Pck2, and the MAPK signaling cascade.

2.4.3 Cell wall mechanics

Cell shape is strictly related to cell wall mechanics: broken walls retain the shape of the cell from which they came, whereas enzymatic walls removal generates spherical protoplasts.

The elasticity of an object can be described in terms of stress and strain. Stress is defined as the force applied per unit area, while strain is the resulting amount of deformation per unit length. The ratio of stress to strain (for an elastic material following Hooke's law) is defined as the elastic modulus (E), and describes the mechanical resistance of a material during elongation or compression. A large E implies a stiff material, while a small E implies a softer material.

In mechanical terms, the cell wall is a very versatile structure: at the same time very rigid and very elastic, it can support high stresses until a certain threshold, called rupture point, which is characteristic of its material properties. However, the cell wall is not a static structure: polarized growth is associated with local remodeling, to allow incorporation of new material, and this in turn impacts the wall's mechanical properties, leading to different cell shapes. In the case of plant cells, it has been established that growth is similar to plastic deformations (Cosgrove, 1986): the wall behaves as an elastic material below a critical strain and grows above it yielding to stress. So, the wall can be modeled as a perfectly plastic material, which can extend under the isotropic force exerted by intracellular turgor pressure.

In a recent work, researchers succeeded in estimating the elasticity of the cell wall in fission yeast (Figure 39) (Minc et al., 2009a). To this aim, cells were pushed into stiff PDMS chambers smaller than the cell length, and consequently forced to bend. By considering this buckling transition, the estimated Young's elastic modulus is around 32 ± 9 MPa, similar to values obtained in budding yeast by compression experiments (Smith et al., 2000).

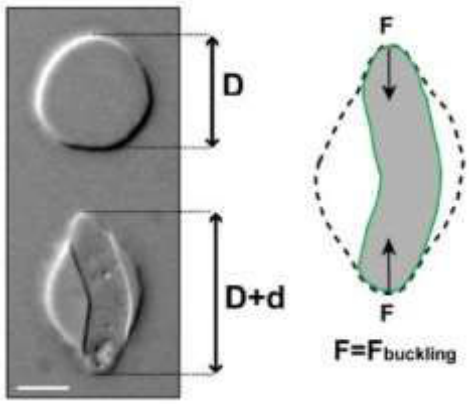

Figure 39: Illustration of the method used to compute chamber deformation (Minc et al., 2009a)

2.4.4 Turgor pressure

Walled microorganisms are also commonly, perhaps universally, subject to turgor, due to a difference in solute concentration between the interior and the exterior, and their shape must be such as to withstand the stress. This hydrostatic pressure may reach 10 or more atmospheres, about five times that in the average car tire; moreover, it is vital as it provides much of the mechanical rigidity of these living organisms. Of course, the problem of enlarging the wall in a controlled manner is exacerbated by the fact that a growing cell is under pressure: the stress is carried by the cell wall, and failure in retaining this stress can easily cause cell bursting. The surface stress theory, developed by A. L. Koch to explain bacterial cell morphogenesis, proposes that turgor is not only the problem but also part of the solution (Koch, 2001). Hydrostatic pressure supplies the driving force for surface enlargement by exerting tension upon the wall, hence counteracting the cohesive forces that hold the wall together. Cells yield to this force by controlled expansion at particular loci, through the insertion of new units into the existing wall (Harold, 1990). The central place of hydrostatic pressure as the driving force for growth, and its implication in morphogenesis, is generally accepted by plant physiologists: in this case, water influx is restrained by the wall, which is consequently subjected to considerable hydrostatic pressure; net influx ceases when the two forces balance. Enlargement depends, then, on controlled expansion of the surface, and the spatial constraints upon this process mold the form of the cell. Turgor pressures in fungal infection structures, in combination with powerful adhesives, if elevated above those of host cells, could play a significant role to exert mechanical forces during penetration: a recent study estimated the magnitude of turgor in melanized appressoria of

M. grisea - an astonishing 80 bars (over 10^3 psi) - for penetration of different Mylars (Howard et al., 1991).

However, if turgor drives morphogenesis, it must be finely tuned: yeast has evolved an ability to control turgor by monitoring the environment and adjusting its internal osmolarity. When budding yeast cells are exposed to media of high osmolarity, the HOG (high-osmolarity glycerol) signaling pathway is activated, resulting in increased production of glycerol and a reduction in glycerol export (O'Rourke et al., 2002). Mutations in HOG pathway components lead to cessation of growth in hyperosmotic media, consistent with turgor being required for yeast growth. In contrast, upon a shift from high to low osmolarity, yeast cells stimulate a different MAP kinase cascade, the cell integrity pathway (CIW) (Hohmann, 2002).

The fission yeast *S. pombe* possesses a signaling pathway very similar to the *S. cerevisiae* HOG pathway: in this, Sty1 is stimulated by osmotic shock and controls expression of genes important for osmoadaptation, such as Gpd1 (glycerol-3-phosphate dehydrogenase), whose product is involved in glycerol biosynthesis. In contrast with the HOG pathway, Sty1 phosphorylation and Sty1-dependent responses are not specific to osmotic shock, but can be stimulated by a whole range of stress conditions, including osmotic upshift, heat shock, exposure to hydrogen peroxide or other oxidative stress agents, UV light and alkylating agents, nitrogen and carbon starvation (Hohmann, 2002). Moreover, the Sty1 pathway is a cell cycle regulator: for instance, it is required to arrest vegetative cells in G1 upon nitrogen starvation, to activate Ste11 for pheromone production in order to undergo mating. In conclusion, walled cells have developed mechanisms for osmoadaptation and osmoregulation, which may play an important role in cell growth and morphogenesis.

The central role of turgor for cell growth has been confirmed in plants, algae and filamentous fungi, but the case of smaller cells such as yeasts and bacteria remains quite mysterious. Recently, Minc and colleagues investigated the role of turgor pressure in fission yeast growth (Minc et al., 2009a): to this aim, vegetative cells are subjected to an increase of the extracellular osmolarity, that results in a decrease of internal turgor pressure. Upon sorbitol addition, wild-type cells initially shrink, but fast recover their initial turgor thanks to a compensatory osmotic stress response. This recovery is dependent on the synthesis of intracellular glycerol, catalyzed by Gpd1 (Aiba et al., 1995; Hohmann, 2002). *gpd1Δ* cells are viable, but sensitive to hyperosmotic medium: in these mutant, low sorbitol concentrations are

sufficient to completely block cell growth, suggesting that internal turgor pressure is the main force generator for cell growth in fission yeast. On the contrary, a recent study on *Escherichia coli* bacterial cells suggest that the rate of cell wall expansion is determined by the rate of peptidoglycan insertion which is in turn not directly dependent on turgor pressure, even if pressure does play a basic role whereby it enables full extension of recently inserted peptidoglycan (Rojas et al., 2014). Furthermore, it has been shown that turgor pressure generates a high outward force which may potentially oppose to specific cellular processes in fission yeast, such as cytokinesis and endocytosis: in these cases, cells have evolved unique mechanisms to overcome such a mechanical obstacle (Basu et al., 2014; Proctor et al., 2012). Very surprisingly, fission yeast mutant cells in the kinase Pck2 required for activation of β-1,3-glucan biosynthesis, present cell wall defects, and show an amoeboid-like migration through repeated cycles of protrusion driven by internal turgor pressure, accompanied by weak cell wall rupture and repair (Flor-Parra et al., 2014).

Hence, different mechanisms of "localized compliance with the global force of turgor pressure" regulate morphogenesis in walled cells (Harold, 2002).

2.4.5 The mechanics of cell growth

As I have previously suggested, turgor pressure is the key force generator for growth in walled cells. However, as turgor is isotropic in space and commonly constant over short time periods, the generation of complex cellular geometries relies on the mechanics of the cell wall, which is in turn constantly remodeled through polarized secretion. In 1965, Lockhart proposed a first mathematical model to explain plant cell expansion (Lockhart, 1965): in his view, cells need to overcome a barrier (the intrinsic wall yield threshold), beyond which plastic expansion takes place.

Various plants, fungi and bacteria possess a mechanism of apical growth that allows them to extend at a specific point along a directional axis, called tip extension. In this way, cells can penetrate through other tissues (such as in the case of pollen tubes) or through the soil (as in the case of root hairs). Moreover, mechanical forces are key factors in fungal pathogenesis (Bastmeyer et al., 2002): plant pathogen fungi form specialized structures, called appressoria, which raise turgor pressure to breach the plant cell wall for host invasion; *Candida albicans* can pierce the membranes of macrophages (Gow et al., 2002). To investigate if invasion may rely on

mechanical force, besides chemical mechanisms, it is very interesting to investigate how much of such force can be exerted by a growing fungal tip.

Recently, Minc and colleagues used the same setup of PDMS microchambers to measure the force exerted by the growth of single fission yeast cells (Minc et al., 2009a): the different rates of cell growth and chamber deformation provided an estimate of the stalling force, *e.g.* the external force required to stall growth, of 11 ± 3 μN. Moreover, these measured values can be introduced into mathematical models, which can estimate the fission yeast typical size on the basis of its mechanical properties (Boudaoud, 2003). In a similar theoretical approach, the simple geometry of tip-growing cells is obtained via the assembly and expansion of cell wall in the apical region of the cell: this irreversible expansion can be modeled as the extension of an inhomogeneous viscous fluid shell under the action of turgor pressure, fed by a material source in the neighborhood of the growing tip. By this means, it is possible to determine theoretically the radius of the cell and its growth velocity in terms of the turgor pressure and the secretion rate and rheology of the cell wall material (Boudaoud, 2003; Campas and Mahadevan, 2009). Another theoretical work which aims at understanding how shape is regulated and maintained in fission yeast takes into account the feedback between a growth signal and cell shape, and how this might affect cell diameter (Drake and Vavylonis, 2013): to this aim, Vavylonis and his collaborators included in the model the relationship between Cdc42 signal width and cell diameter which has been experimentally characterized in a recent paper (Kelly and Nurse, 2011b), and then investigated the potential role of a MT-based exploration mechanism for the maintenance of the cell diameter

In conclusion, growing fission yeast cells exert a considerable mechanical force, 100-

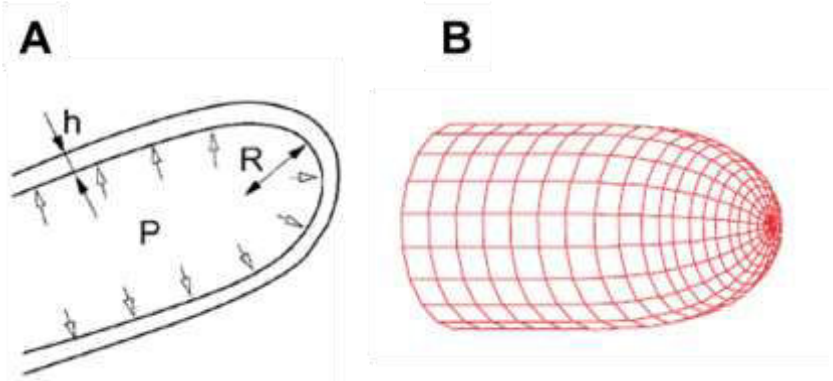

Figure 40: Physical model of cell growth by tip elongation (Boudaoud, 2003).

1000 times higher than the ones generated at the leading edge of migrating animal cells, which are on the order of 10-100 nN (du Roure et al., 2005; Minc et al., 2009a). Altogether, these results suggest that the impressive mechanical growth forces from the fungal tip can be a major factor in driving penetration and host invasion.

2.4.6 Another possible force generator: the cytoskeleton

In advance respect to his time, Harold foresaw a larger role for actin flow and cortical mechanics in the localization of growth and predicted that in morphogenesis, "spatial localization and temporal control of secretory processes are especially critical" (Harold, 1990, 2002). Given the new insights on the important roles the cytoskeleton plays during morphogenesis, it has been recently proposed that cytoskeletal forces in addition to turgor may drive cell growth (Slaughter and Li, 2006). One possible example is the force generated by actin polymerization, given that actin filaments in patches and cables are highly dynamic and their barbed ends face the plasma membrane at sites of growth. Actin polymerization is widely considered as a force generator, for instance to drive the propulsion of the intracellular pathogenic bacteria *Listeria monocytogenes*, and to guide edge protrusion in motile cells (Gouin et al., 2005; Mogilner A, 1996). Consequently, it is conceivable that actin polymerization in patches or cables directly may cause stress on the cell surface or modulate the turgor-induced surface stress: for instance, formation of endocytic membrane invagination, driven by the force from actin polymerization, at the time of glucan synthase activation could provide local and transient stress relief, allowing new glucan bonds to form, resulting in local compliance and growth (Slaughter and Li, 2006).

However, in most walled cells turgor pressure can itself generate much higher forces that the ones obtained by the actin cytoskeleton, and thereby guide growth: in the case of fission yeast, cells don't need actin cables for force production, as growth rate is unaffected in *for3Δ* mutants (Minc et al., 2009a), suggesting that the cytoskeleton don't play any mechanical role on cell morphogenesis.

2.5 Building up a rod-shaped cell

The rod, a radially symmetric cylinder with rounded ends, represents a relatively simple geometry that is ubiquitous in unicellular walled organisms. Well-studied examples include

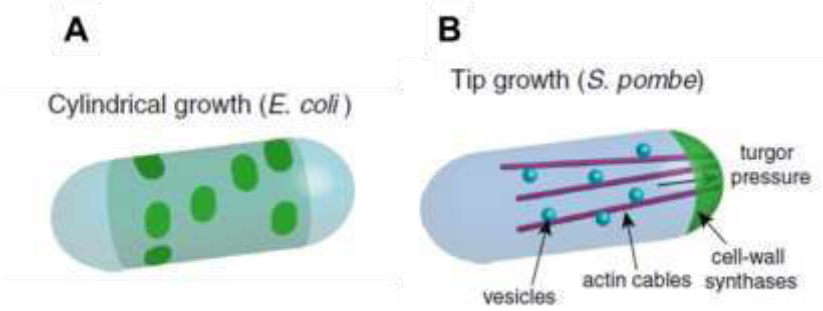

Figure 41: Comparison of different growth patterns for rod-shaped cells (Chang and Huang, 2014)

bacteria (*Escherichia coli*, *Bacillus subtilis*), fungi (*Schizosaccharomyces pombe*, *Aspergillus nidulans*), and plants (pollen tubes, stem and root axis epidermal cells in *Arabidopsis thaliana*) (Figure 41). In particular, *E. coli* and *S. pombe* have also similar aspect ratios (length is approximately four times width), despite a nearly 100-fold difference in volume and qualitatively different spatial patterns of growth. A common feature of all walled cells is that the cell wall and turgor pressure are crucial for cell shape: however, *E. coli* and *B. subtilis* grow by inserting cell wall material along the length of the cylindrical portion of the cell, whereas *S. pombe*, plant pollen tubes, and certain other bacteria grow by insertion of new wall material at cell tips (Daniel and Errington, 2003; Mitchison and Nurse, 1985; Rojas et al., 2011). Given the ubiquity of rod-shaped organisms across kingdoms, it is tempting to speculate that the rod shape represents some kind of geometric optimum, which has independently evolved multiple times (Chang and Huang, 2014).

The simplest physical view of a walled cell considers it as a thin viscoelastic shell, uniformly inflated by turgor pressure. The ends of rod-shaped cells are roughly hemispherical, with dimensions in accordance with the cylindrical portions of the cell, and may be mainly produced by the mechanics of turgor pressure inflation onto the cell wall. In order to predict the resulting cell shape of a specific growth pattern, it is necessary to consider three main parameters: the distribution of forces related to turgor pressure, the counterbalancing forces of the wall stretching, and the way the wall couples those forces to the degree of extension. On this basis, the circumferential and longitudinal strains should be linearly dependent on width and turgor pressure and inversely dependent on wall thickness. By measuring the degree of cell shrinkage along the longitudinal and radial direction when turgor pressure is reduced, the fission yeast cell wall appears to be an isotropic material. In contrast, the *E. coli* cell wall exhibits mechanical anisotropy, with greater stiffness in the circumferential relative to the longitudinal direction (Yao

et al., 1999). This polarized arrangement of cell wall components can be directly related to the resulting rod-shape: on the contrary, in the case of tip growth, physical models have proposed that the rod shape is obtained by inserting softer gel-like wall at the very tip of the cell, which then matures into a stiffer network on the sides of cells (Campas and Mahadevan, 2009; Goriely and Tabor, 2003). Consistent with this model, in pollen tubes and in *S. pombe*, cell-wall synthases are localized to growing cell tips where they introduce new wall material, potentially generating gradients of cell wall stiffness, with soft growing tips (Rojas et al., 2011).

Rod-shaped cells need to face multiple challenges for a correct morphogenesis: first, they need to maintain a constant cell width during growth. This can be accomplished in tip-growing cells by keeping a constant growth zone. In fission yeast, actin-dependent delivery of Cdc42 and its local regulation by Cdc42 activators and inhibitors set the width of the polarity domain: this can be achieved by establishing a gradient of active Cdc42 within the cellular tip plasma membrane, which depends on the GAP Rga4 and the GEF Scd1, hence determining the cell growth-zone size and normal cell width (Figure 42) (Kelly and Nurse, 2011b). In contrast, bacteria such as *E. coli* must coordinate growth with extension so that width is maintained as cell length increases. Second, rod-shaped cells need to maintain a linear axis of growth during

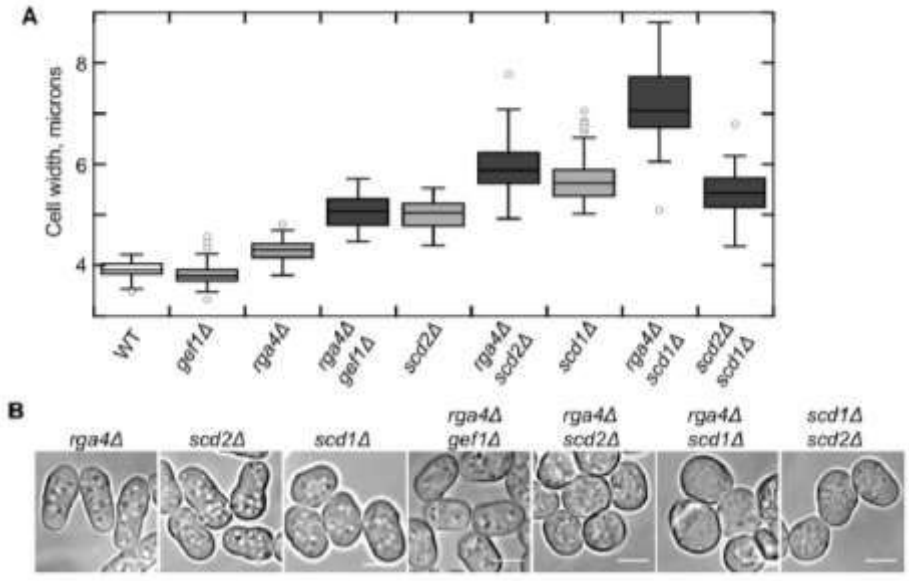

Figure 42: Control of cell width in fission yeast ***A.*** Cell-width defects of double mutants *scd2Δ rga4Δ* and *scd1Δ rga4Δ* and *gef1Δ rga4Δ* are additive, but the *scd1Δ scd2Δ* double mutant resembles *scd1Δ*. Box-and-whiskers plot of cell widths for each strain in exponential growth. All differences are statistically significant by a Student's t test with $p < 0.0001$; at least 50 cells were measured for each genotype. ***B.*** Exponentially growing cells, bright-field microscopy. Scale bars: 5 μm. (Kelly and Nurse, 2011)

elongation: in *E. coli* cells, the actin-like MreB cytoskeleton localizes preferentially to regions of negative Gaussian curvature, suggesting that MreB polymers sense cell curvature and actively straighten the cell by directing cell-wall insertion to specific sites on the cell surface based on local geometry (Ursell et al., 2014). In *S. pombe*, the MT cytoskeleton may keep cells straight by coordinating cell-wall growth at the cell tips; MTs extend across the cell length and transport polarity factors, such as the Tea proteins, to the tips (Mata and Nurse, 1997). Taken together, in both prokaryotes and eukaryotes, the cytoskeleton is at least partially responsible for maintaining cell shape by coordinating local growth patterns with global morphology.

Among the possible benefits of a rod-like shape, we can find the inherent breaking of symmetry, that allows the cell to concentrate molecules at specific cellular zones, and to divide properly; and the relatively simple related growth pattern, which consists in extension along one dimension.

2.5.1 From round to rod-shaped: spheroplast regeneration

All along the vegetative cell cycle, both *E. coli* and *S. pombe* cells keep on having a polarized rod-shape, and consequently a polarization axis. However, these organisms can regenerate a rod-shape even from an initially spherical state: for instance, enzymatic treatments can lead to the formation of round cells which completely lack a cell wall, called spheroplasts or protoplasts or L-forms in the case of bacteria. As there is no more structure to counterbalance the internal turgor pressure, these cells are very fragile and survive only in in hyperosmotic media to avoid bursting.

In fission yeast, newly formed spheroplasts possess a disorganized cytoskeleton and depolarized growth proteins (Kelly and Nurse, 2011a). Very interestingly, in specific growth conditions, these unpolarized cells can recover by forming new growth zones, resume polarized growth and finally regenerate a rod-shaped vegetative cell. As I have described previously, *S. pombe* spheroplasts first resynthetize new cell wall on the entire cell surface (Osumi, 2012): by these means, they become resistant to osmotic shock but still possess a round shape and a disorganized polarity machinery. Later on, a symmetry breaking process occurs, which is again centered around Cdc42 and its regulators: for instance, the scaffold Scd2 forms a polarized patch in the rounded spheroplast, whereas the GAP Rga4 switches from an initial homogeneous distribution at the membrane to a specific exclusion from the growth zone after a stable patch of Scd2 forms. As in the case of vegetative cells, either *rga4Δ* or *scd1Δ* spheroplasts regenerate

wider tips, suggesting that growth zones with normal width and protein localization can form *de novo* through sequential organization of cellular domains, and that the size of these growth zones is genetically controlled, independent of preexisting cell shape (Figure 43) (Kelly and Nurse, 2011a, b).

Similarly, *E. coli* L-forms can revert to rod-like shapes, through the localization of MreB to negatively curved regions of the cell, which in turn drives synthesis of new cell wall (Billings et al., 2014). Thus, in both yeast and bacteria the same machinery that is responsible for the maintenance and propagation of a rod-like morphology is also capable of establishing the rod-like shape *de novo*.

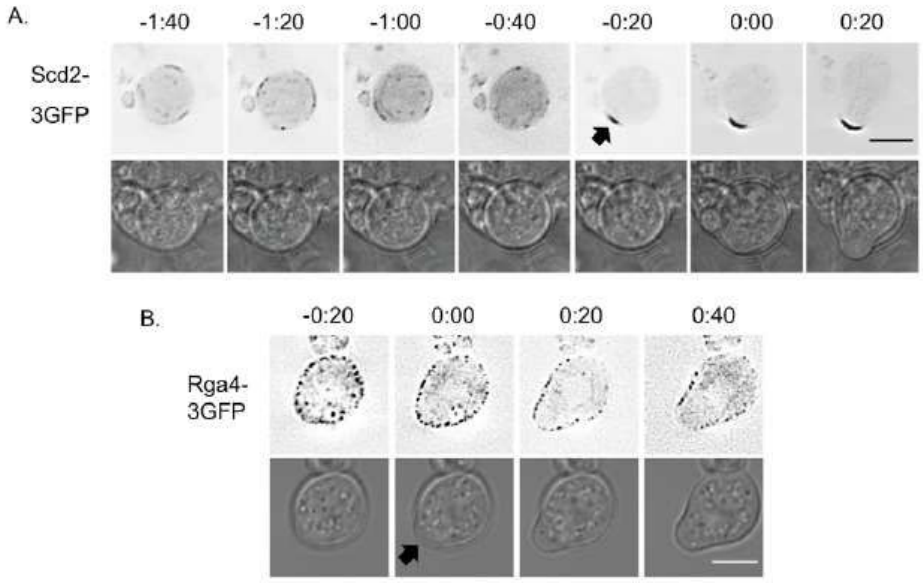

Figure 43: Protein polarization accompanies spheroplast recovery. ***A.*** Scd2 polarizes before cell shape changes. Time-lapse series of Scd2-3GFP in a spheroplast as it undergoes the transition to polarized growth. The black arrow indicates the appearance of a bright patch of Scd2-3GFP that formed before the shape of the spheroplast changed. ***B.*** Rga4 is excluded as the growth zone forms. Time-lapse series of Rga4-3GFP in a spheroplast as it undergoes the transition to polarized growth. Black arrow indicates the initiation and location of polarized growth. Fluorescence images are single planes, best fluorescent signal, with inverted LUTs, and time is displayed in hours:minutes from spheroplast polarization. Scale bars, 5 μm. (Kelly and Nurse, 2011a)

2.6 Symmetry breaking in yeast models

As I have previously described, polarity establishment in most eukaryotes employs an evolutionarily ancient machinery centered around the conserved Rho family GTPase Cdc42 (Park and Bi, 2007). The budding yeast *S. cerevisiae* is a particularly attractive model organism as it displays pronounced cell polarity in response to intracellular and extracellular cues, starting from a quasi-symmetric shape. Cells of budding yeast undergo polarized growth during various phases of their life cycle, such as budding during vegetative growth, mating between haploid cells of opposite mating types, and filamentous growth upon deprivation of nutrients. The most prominent feature in all these different growth patterns is the organization of the polarized actin cytoskeleton, which guides secretion towards one specific site at the membrane, resulting in polarized cell growth. The process of budding is controlled both spatially and temporally: bud emergence occurs at a particular site in the cell cortex and at a particular time in the cell cycle. First, a specific site for polarized growth is determined in the bud site selection step, by the Ras family GTPase Rsr1/Bud1 and its regulators. Second, the assembly of components required for bud formation, such as Cdc42 and its activators and inactivators, takes place at the chosen site to restrict cell growth to that position. As in the case of fission yeast, Cdc42 interacts with several proteins to trigger downstream processes, including polarization of the actin cytoskeleton and secretion towards the sites of cell growth.

One of the key issues concerning the role of Cdc42 in polarity development is to understand how Cdc42 itself becomes polarized and how its polarization state is maintained during the cell cycle. In fact, this protein localizes to sites of polarized growth even in the absence of spatial cues: in other words, when the bud site selection machinery is not functional, mutant cells bud at random sites. This case of spontaneous symmetry breaking in a relatively simple unicellular eukaryote has brought researchers to investigate the core principles that are needed for GTPase clustering at a random location. To this aim, two main strategies have been used to remove predetermined cues, leading to a random budding pattern. One way consists in the removal of the protein Rsr1, the essential spatial landmark for bud site selection (Irazoqui et al., 2003). Another approach involves expression of $Cdc42^{Q61L}$, a mutant that cannot hydrolyze GTP and is thus constitutively activated (Wedlich-Soldner et al., 2003). In both cases, clusters of concentrated Cdc42 spontaneously form at random locations. However, the polarization process

depends differently on actin, resulting in some controversies about the actual mechanism of symmetry breaking.

In the following paragraphs, I will discuss the different models that have been proposed for spontaneous polarization in yeast, with some insights on related processes in fission yeast.

2.6.1 Simple Cdc42-based positive feedback

Recently, Altschuler and colleagues formulated a model where a generalized term for Cdc42 self-recruitment serves as the central source for positive feedback, with no explicit pathway for global inhibition. In this context, signaling molecules comprising a single species move between non recruiting, cytoplasmic states and recruiting, plasma-membrane bound states without mechanisms of directed transport (Altschuler et al., 2008). In the model, redistribution of signalling molecules is determined by four transport mechanisms: (1) recruitment of cytoplasmic molecules to the locations of membrane-bound signalling molecules (k_{fb}); (2) spontaneous association of cytoplasmic molecules to random locations on the plasma membrane (k_{on}); (3) lateral diffusion of molecules along the membrane (D); and (4) random disassociation of signaling molecules from the membrane (K_{off}) (Figure 44). This work suggests that an intrinsic stochastic mechanism through positive feedback alone is sufficient to create and maintain a highly localized cortical distribution required for activation of downstream biological processes, through complex signalling networks with small numbers of molecules.

These results open a fundamental question about the definition of a polarized state in mathematical modeling and in biology, suggesting that transient symmetry breaking events generated by random fluctuations may be sufficient to initiate polarity in biological systems.

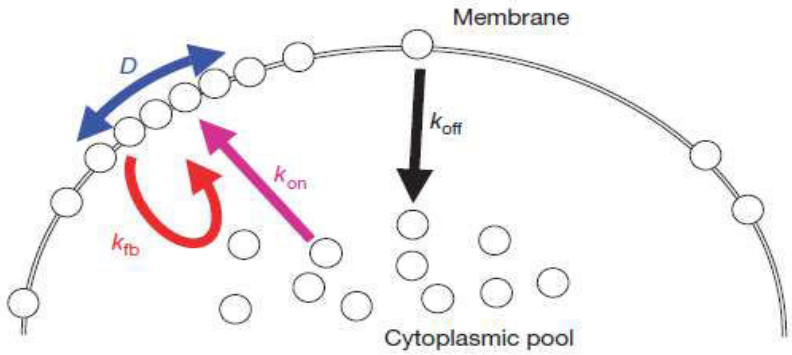

Figure 44: Minimal model of a positive feedback circuit (Altschuler et al., 2008)

2.6.2 Positive feedback via GEF-effector complexes

In the continuity of Turing's work, various theoretical studies have proposed that positive feedback can be generated by amplification of stochastic fluctuations in the concentration of specific molecules along an initially homogeneous cell cortex. Analysis of the genetic requirements for polarization in *rsr1Δ* cells led to the identification of the scaffold protein Bem1 as an essential factor for symmetry breaking (Irazoqui et al., 2003). Polarization depends on this protein and its binding partners: the GEF that activates Cdc42, Cdc24, and a Cdc42 effector called p21-activated kinase (PAK) (Kozubowski et al., 2008). Similar complexes are found in many other cells, including *S. pombe* (Endo et al., 2003). The model in budding yeast is the following: at the membrane, Cdc42 can switch between GDP- and GTP-bound forms, in a regulated manner through GEFs and GAPs. The active, GTP-bound form can bind to a cytoplasmic Bem1-Cdc24 complex: consequently, the GEF-effector complex can bind to pre-existing GTP-Cdc42 via the effector, leading to activation of neighboring GDP-Cdc42 via the GEF. As a result of this loop, a cluster of active Cdc42 grows at the membrane, providing a mechanism for Turing-like actin-independent positive feedback (Figure 45) (Johnson et al., 2011). In order to raise the local GTP-Cdc42 concentration above that of the surrounding GDP-Cdc42, a GDI extracts GDP-Cdc42 from the membrane, by forming a complex that can exchange between the membrane and the cytoplasm. This reaction enables the local build-up of a GTP-Cdc42 cluster (Johnson et al., 2011).

In addition to positive feedback, theoretical analyses have shown that diffusion plays an essential role in symmetry-breaking, and experimental evidences have confirmed these hypotheses in the case of GTPase domain formation. For example, GTP-Cdc42 in yeast can be

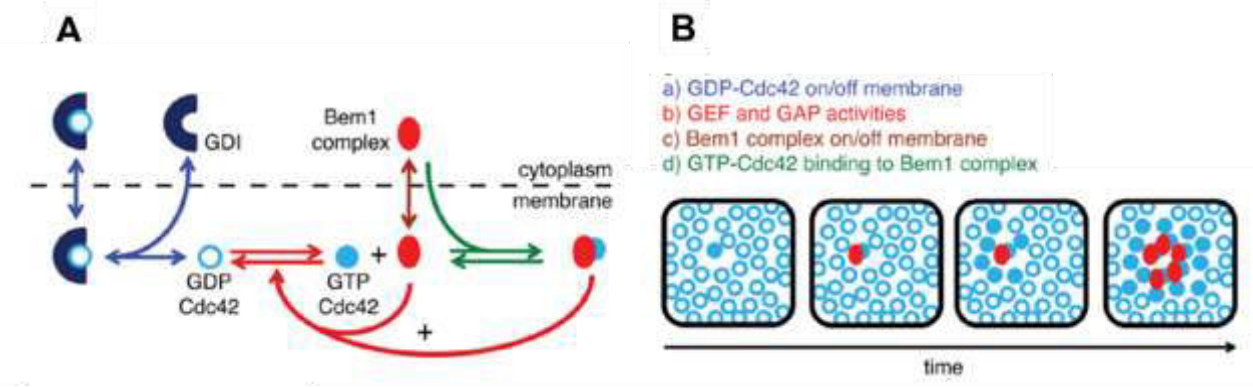

Figure 45: Cdc42 polarization via reaction-diffusion mechanism (Savage et al., 2012)

considered to be a Turing-type activator: it diffuses very slowly in the PM and promotes local accumulation of more GTP-Cdc42 (Johnson et al., 2011). On the other hand, the GEF–effector complex has characteristics of a Turing-type substrate: it diffuses rapidly in the cytoplasm, from which it is depleted due to recruitment to the growing GTP-Cdc42 cluster. Mathematical modeling of this system shows that the uniform Cdc42 steady state exhibits Turing-type instability to spatial perturbation, evolving to a stable polarized distribution of Cdc42 (Goryachev and Pokhilko, 2008). In the model as in yeast cells, the polarized Cdc42 distribution is stable, although single Cdc42 molecules cycle rapidly in and out of the polarization site (Goryachev and Pokhilko, 2008; Wedlich-Soldner et al., 2004): Cdc42 cycling between the membrane and the cytoplasm is regulated by the Bem1 complex and the GDI, finally resulting in local growth and maintenance of a concentrated patch of GTP-Cdc42. To conclude, this model consists in a diffusion-based feedback loop that represents a specific case of a more general "substrate depletion" class of pattern formation models (Meinhardt and Gierer, 1974).

2.6.3 Positive feedback via actin-mediated transport

Another possible mechanism of spontaneous symmetry breaking in budding yeast relies on polarized vesicle trafficking on actin tracks (Marco et al., 2007; Wedlich-Soldner et al., 2003). As I have previously described, active Cdc42 regulate the localization of formins, in particular Bni1 in interphase budding yeast cells, responsible of actin cables nucleation and Myosin V-dependent vesicle delivery along these cables, leading to vesicle fusion with the plasma membrane at the growth site. As secretory vesicles carry Cdc42, polarized vesicle delivery could potentially lead to local enrichment of Cdc42 at the cell front: in this scenario, Cdc42 would be at the same time required for the formation of a polarized actin network, and regulated by actin itself for its localization (Wedlich-Soldner et al., 2004). This model is in accordance with experiments where depolymerization of actin by treatment with the inhibitor Latrunculin A (LatA) or inhibition of actin cable assembly using tropomyosin mutations resulted in reduced efficiency and stability of Cdc42 polarization (Pruyne et al., 2004; Wedlich-Soldner et al., 2004). Moreover, both cable stability and vesicle transport are crucial for the efficiency of cell polarization (Wedlich-Soldner et al., 2004; Zajac et al., 2005). Mathematical modelling shows that a balance of directed transport, endocytosis and diffusion at the membrane is sufficient to accurately describe budding yeast morphologies (Figure 46) (Marco et al., 2007); in particular, the maintenance of a steady

state distribution of polarized proteins requires a stable window of actin-dependent directed transport. The feedback loop between polarity regulators, such as Cdc42, and the formation of actin cables play an important role in the maintenance of this transport window, leading to relatively high rates of actin cable attachment in regions of high Cdc42 concentration and detachment in regions of low Cdc42 (Marco et al., 2007).

Crucially to this model, recent studies found that endocytosis and membrane organization serve to maintain Cdc42 concentration in the polar cap (Jose et al., 2013; Slaughter et al., 2013). In the first case, it was shown that cell polarity can be established via the spatial coordination of opposing membrane trafficking activities, which consists in endocytic vesicles corralling a central exocytic zone, and tightening it to a vertex (Jose et al., 2013). In the second case, researchers presented evidence that Cdc42 diffusion in endocytic and exocytic regions is considerably different, resulting in membrane microdomains with locally concentrated Cdc42 (Slaughter et al., 2013). Similar observations have recently been reported as a widely occurring phenomenon for PM-associated proteins in yeast (Dodgson et al., 2013).

Although a role for membrane transport in polarity establishment has been widely established, its relevance for budding yeast polarization is still controversial: in particular, it has been proposed that actin may be a negative regulator in cell polarity (Ozbudak et al., 2005). A major criticism is related to the idea that in a vesicle-delivery model, the concentration of Cdc42 on secretory vesicles must exceed that at the polarization site, to avoid Cdc42 dilution after

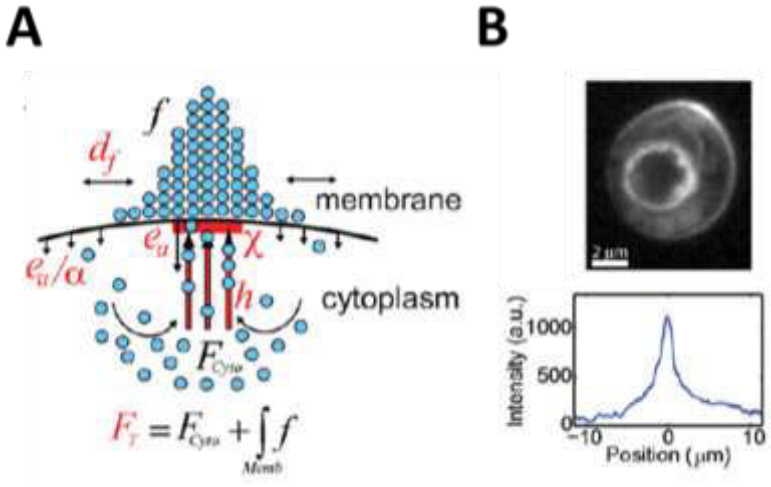

Figure 46: Actin-based mathematical model for the dynamic redistribution of polarized membrane proteins. ***A.*** Schematic model of dynamically polarized membrane proteins (blue circles) incorporating diffusion, directed transport, and endocytosis. ***B.*** Example of polarized membrane protein, GFP-Cdc42^{Q61L} cap and its membrane intensity in arbitrary units (a.u.). (Marco et al., 2007)

vesicle fusion. Mathematical modeling recently proposed that vesicle trafficking of Cdc42 would destroy, rather than contribute to, polarization (Layton et al., 2011): in this scenario, combination of a reaction-diffusion system with positive feedback via the Cdc42-directed GEF and vesicle traffic targeted by GTP-Cdc42 produces a reduced local polarity factor concentration. This is due to the slow rate of vesicle delivery to the plasma membrane, which may underlie a competition between the reaction diffusion system (which recruits more factors) and vesicle delivery (which adds more membrane) (Savage et al., 2012). On the contrary, in another recent stochastic model for yeast polarity establishment through actin- and GDI- mediated recycling of Cdc42, correct polarity establishment is achieved through coupling of these multiple feedback loops: in this case, authors suggest that the slow actin-mediated loop provides stability, whereas a faster Bem1-dependent feedback loop provides rapid responsiveness to inductive signals (Freisinger et al., 2013).

2.6.4 Winner-takes all competition

In principle, positive feedback could lead to the simultaneous growth of several polarity domains: however, when most cells polarize they generate only one front. One way of explaining this phenomenon considers that cells may contain a small absolute number of molecules of a key polarity factor, which leads to a low probability of initiating an autocatalytic loop. In other words, it would be highly improbable for a cell to develop more than one cluster within a relevant timeframe; however, these conditions lead also to a very low probability to form just one polarity cluster, resulting in a significant increase in thw time required for cell polarization. Another possibility is that multiple clusters do develop frequently, but there is some way to ensure that

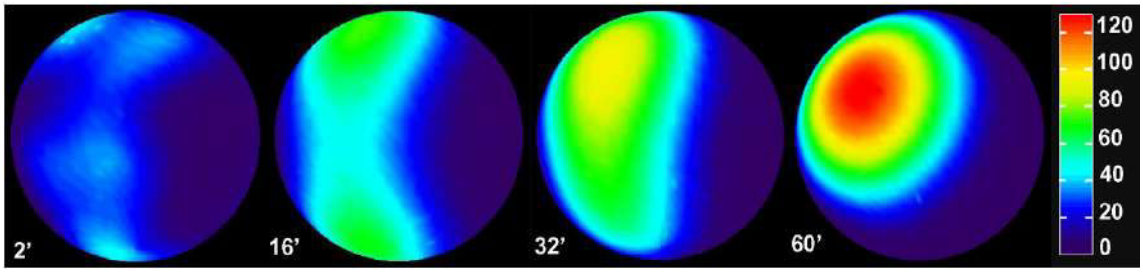

Figure 47: A single Cdc42 cluster forms in the simulations with molecular noise. A 3D view on the surface of a yeast cell shows the distribution of the activated Cdc42 on the membrane. In the absence of landmark proteins, spontaneous activation of individual Cdc42 molecules on the membrane can induce the cluster formation. At first, RT accumulates at multiple random locations (2 min). Subsequently, two well-defined cluster nuclei form (16 min). The top nucleus consumes the slower-growing lower nucleus (32 min). By 1 h the Cdc42 cluster is near the steady-state. (Goryachev and Pokhilko, 2008).

only one cluster persists. One way that this could occur is through competition: imaging polarity establishment at high spatiotemporal resolution in *S. cerevisiae* has revealed that many cells initially grow more than one small cluster of Cdc42, but this state is very unstable and rapidly one cluster grows while the others shrink, leaving at the end a single large domain (Howell et al., 2012). This behavior strongly suggests that the clusters compete with each other.

The number of domains generated by Turing models depends on the size of the cell, meaning that in large cells various domains can coexist without "sensing" each other (Meinhardt and Gierer, 2000). However, Goryachev's mathematical model predicts that coexisting clusters will compete due to the continuous membrane-cytoplasmic exchange of the Cdc42 cluster components and their consequent depletion from the cytoplasm, giving rise to a "winner-takes-all" competition between clusters which is independent on cell size (Figure 47) (Goryachev and Pokhilko, 2008).

The singularity of symmetry breaking has also been investigated in the case of a transport-based feedback loop (Freisinger et al., 2013): in this case, the establishment of a stable and unique polarization axis requires coordination of two pathways. Actin-mediated recycling of Cdc42 is very robust, but does not reliably result in formation of a single-polarization site on its own. In contrast, GDI-dependent recycling is sensitive to changes in the GTPase cycle of Cdc42 but faithfully generates a unique polarization site. By combining the two recycling pathways, yeast cells ensure reliable establishment of a single polarity axis.

2.6.5 Coexisting cortical domains

To understand singularity in budding yeast symmetry breaking, researchers rewired the signaling cascade that directs Cdc42 polarization, by replacing the normally cytosolic Bem1 with a Bem1 that is fused to the yeast v-SNARE Snc2, an integral membrane protein (Howell et al., 2009). As Bem1-overexpressing cells, these cells take longer to resolve multiple foci, and often become multibudded, suggesting that the efficiency of competition is reduced when Bem1 mobility is slowed down (Houk et al., 2009).

While budding yeast polar growth is restricted to one site (Figure 48A), other fungi can naturally develop two or more growth zones, each with its own GTPase-based domain (Figure 48B, C and D.). The cylindrical fission yeast provides an optimal example of transition from one to two coesisiting polarity domains: as in *S. cerevisiae*, depolarized *S. pombe* cells (round spores

or regenerating spheroplasts) break symmetry and form a single domain enriched in Cdc42 which initiates polar growth (Figure 48B). Then the reproducible pattern of vegetative growth is triggered, with a first period of monopolar growth at the old end, followed by a period of bipolar growth at both ends. The NETO transition might be triggered by a time- or size-dependent cue. A

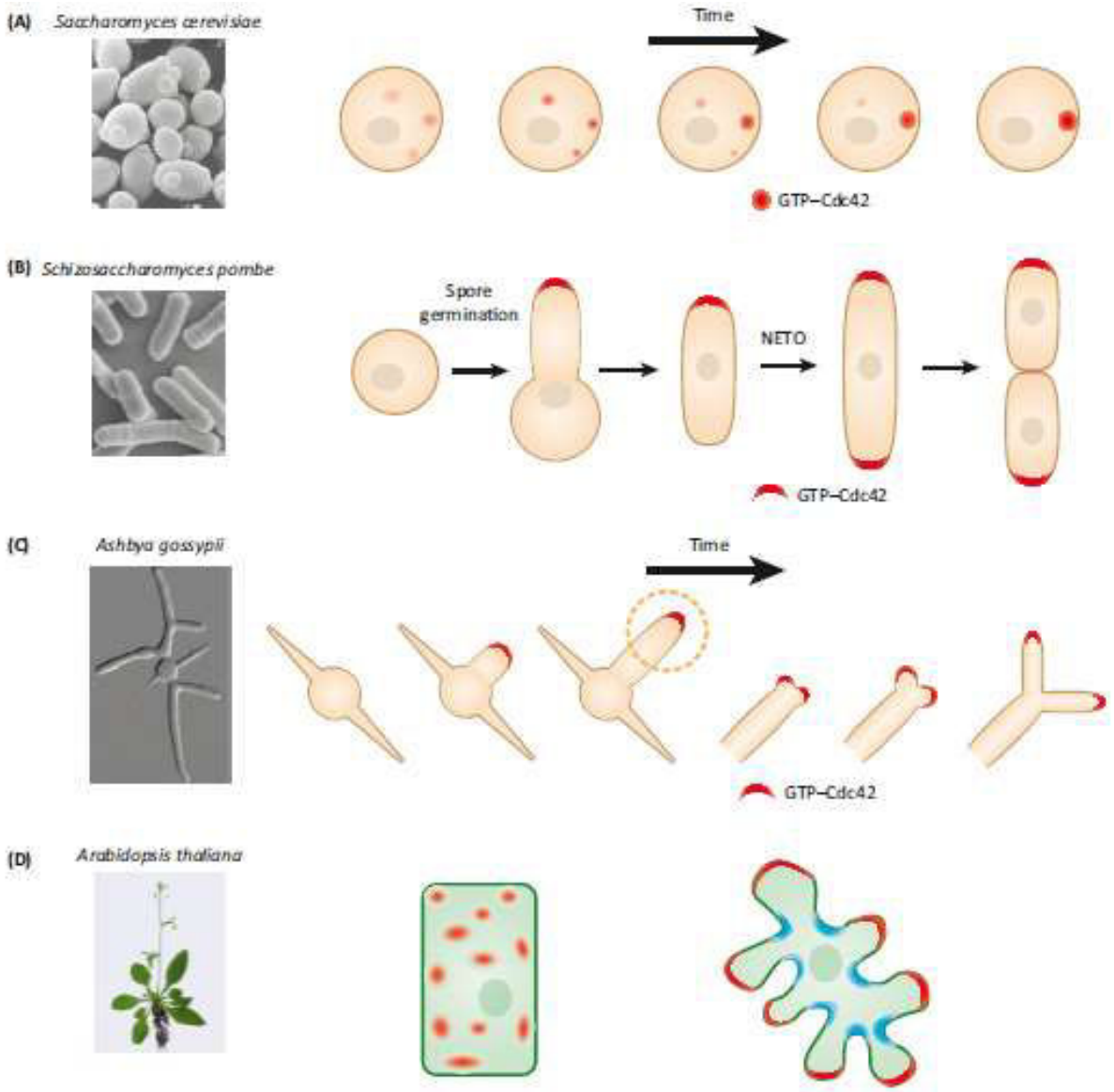

Figure 48: Competition and coexistence among GTPase clusters. **A.** In *S. cerevisiae* cells breaking symmetry, clusters of Cdc42 compete until a single winner emerges. **B.** In *S. pombe*, initial symmetry-breaking is followed by stereotypical cycles of old-end growth and NETO (new end take-off) leading to bipolar growth. **C.** In *Ashbya gossypii*, initial symmetry-breaking is followed by hyphal branching (not shown) and then apical branching that involves the splitting of one Cdc42 cluster into two. **D.** In *A. thaliana*, expression of GTPase Rop11 and its GEF and GAP in non-xylem plant cell types leads to formation of multiple dispersed clusters containing Rop11–GTP and its GEF (left). In leaf pavement cells, mutually inhibitory clusters of Rop2/Rop4 and Rop6 GTPases establish zones of growth versus indentation (right). (Wu and Lew, 2013)

simple idea to explain NETO that have not been experimentally tested yet, considers the interaction between positive feedback, competition, and saturation. Assuming that some 'tip factor' promotes local Cdc42 recruitment by positive feedback, both tips would recruit Cdc42 and its regulators until a limiting cytoplasmic factor becomes depleted, leading to tips competition. Mathematical modeling indicates that, with suitable positive feedback and saturation, this system proceeds from monopolar to bipolar growth via a bistable intermediate in which either monopolar or bipolar solutions are attainable.

Transitions from one to two or more growth zones are also common in filamentous fungi such as *Ashbya gossypii*, which grows from needle-shaped spores to form extended multi-nucleated mycelia (Figure 48C). Following spore germination, symmetry-breaking creates a single growth site. As hyphae grow, they either initiate new polarity sites in the shafts that become side-branches, or split their tip in two, leading to adjacent ‘apical’ branches.

A last case considers the coexistence of multiple, dispersed GTPase domains in a single cell, for example of Rop11 and its regulators in several plants, or the puzzle appearance of *Arabidopsis* leaf pavement cells, in which localized outgrowth in one cell is coordinated with localized inhibition of outgrowth of the adjacent cell to form interdigitating lobes and indentations (Figure 48D) (Fu et al., 2005; Oda and Fukuda, 2012). However, these clusters coexist instead of competing to yield a single winner.

2.6.6 Oscillations of Rho-GTPases

Even in absence of any competitor, GTPase domains sometimes disappear. In budding yeast *rsr1Δ* cells, the winning Cdc42 cluster that emerges from rapid competition then disperses and reforms in an oscillatory manner (Ozbudak et al., 2005). Similarly, in fission yeast cells undergoing bipolar growth after NETO, Cdc42 accumulates at one tip, then disperses from that tip while simultaneously accumulating at the other tip in an oscillatory manner (Figure 49) (Das et al., 2012). In plants, the GTPase Rop1 undergoes oscillatory accumulation and dispersal at the tips of growing pollen tubes (Hwang et al., 2005). In bacteria, the oscillatory Min system positions the site of division at the cell middle by inhibiting division at the cell poles. Oscillatory behaviors in biological systems are thought to require the presence of a delayed negative feedback loop, such that initial activation triggers subsequent inactivation. Altogether, these

observations suggest that clustered polarity regulators such as GTPases may trigger their own dispersal via some form of negative feedback.

In the case of fission yeast, it was shown that active Cdc42, detected through localization of a reporter composed of a CRIB (Cdc42/Rac interactive binding) domain fused to green fluorescent protein (CRIB-GFP), oscillated between the two cell poles in an anticorrelated manner (Das et al., 2012). Oscillations in Cdc42 activity happened not only in bipolar cells but also in cells that had not undergone NETO and were still monopolar. Cdc42 oscillations thus suggest a previously unknown way that cells could regulate the transition from monopolar to bipolar growth. In the proposed mathematical model, authors made three major assumptions: first, positive feedback promotes the accumulation of Cdc42 at a defined location; second, the positive feedback is combined with a delayed negative feedback to promote oscillations; and finally, limiting amounts of Cdc42 regulatory factors ensure that the cell poles would compete for these factors and exhibit anticorrelative behavior. In fission yeast, mechanisms of positive feedback may be similar to the budding yeast case and could involve the scaffold Scd2, the Cdc42 GEF Scd1, and the PAK kinase Pak1 (also known as Orb2 or Shk1), as these three proteins form a complex with Cdc42 (Chang et al., 1999; Endo et al., 2003). Negative feedback mechanisms in Cdc42 oscillations are less well characterized: *tea1Δ* cells still display Cdc42

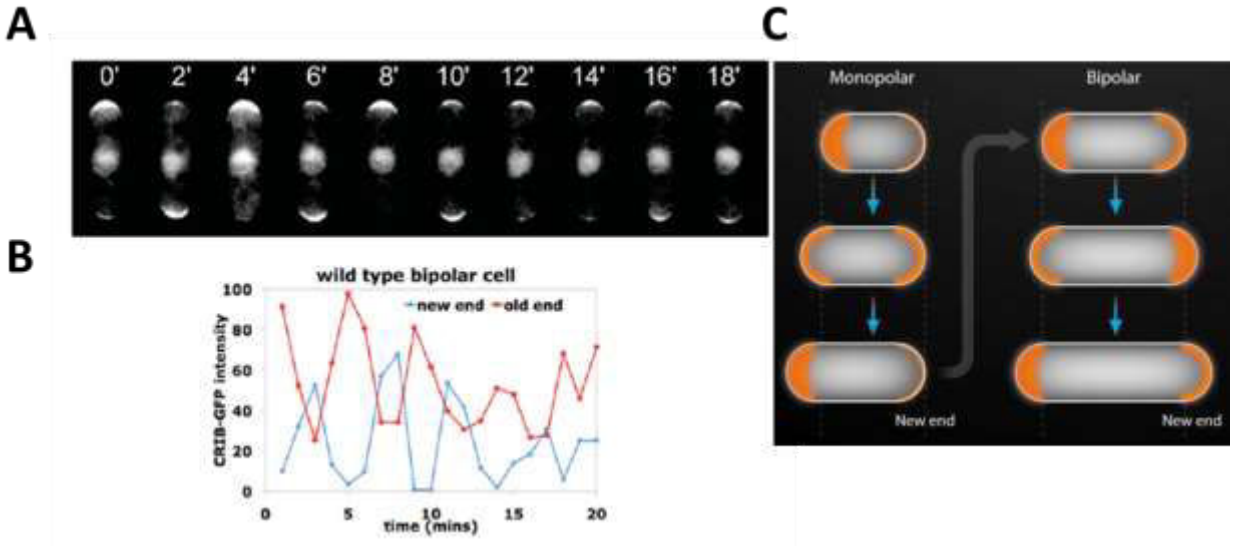

Figure 49: Cdc42 oscillatory pattern in fission yeast. ***A.*** Oscillatory behavior of activated Cdc42 as visualized by CRIB–GFP at the tips of a bipolar fission yeast cell. ***B.*** Quantitative analysis of cells shown in A. ***C.*** Schematic of Cdc42 oscillations during monopolar and bipolar growth (Bendezu and Martin, 2012; Das and Verde, 2013)

oscillations, but with very asymmetric amplitudes, similarly to the *pak1* mutant, suggesting that Tea1 could be involved in a negative feedback loop, maybe as a substrate of Pak1.

The existence of oscillations suggests that the NETO transition may occur stochastically between two existing potential states, likely helped by intrinsic noise, potentially explaining the requirement of a minimal cell length (Mitchison and Nurse, 1985). One zone of active Cdc42 can be seen as a local sink for activators, which exerts long range inhibition, preventing the formation of a new growth site (Csikasz-Nagy et al., 2008). By increasing the total pool of Cdc42 GEFs and other factors while maintaining a constant cell tip size, cell growth may simply increase the availability of GEFs for both poles, which would trigger symmetric oscillations of activated Cdc42 at both cell tips, allowing bipolar growth. Another possibility relies on the observation that bipolar growth depends also on passage through S-phase and localization of the molecular landmarks Tea1, Tea4, and Pom1 (Martin and Chang, 2005): in fact, G1-arrested cells remain monopolar, despite substantial growth in length, which, according to the model, should result in sufficient GEF abundance for symmetric accumulation of active Cdc42 and bipolarity. Moreover, other specific mutant combinations may have symmetric Cdc42 localization, yet maintain monopolar growth (Tatebe et al., 2008).

Cdc42 oscillations in budding and fission yeast display many similarities: for example, they employ similar feedback mechanisms and both occur with 5-min periods. However, the two systems also display fundamental differences in cell geometry and in the physiological role of oscillations: The *S. cerevisiae* studies make use of mutant backgrounds lacking protein landmarks to define the incipient bud site, where the oscillations are transient and occur in an almost spherical mother cell, which does not grow considerably. By contrast, the oscillations in *S. pombe* occur throughout interphase in growing wild-type cells, which do not break symmetry per se, because the growth sites are already defined by the localization of protein landmarks and the cells are naturally rod-shaped.

Another interesting example of Cdc42 dynamic relocation at the cell periphery in the two yeast models deals with shmooing cells. In the case of *S. cerevisiae*, cells exposed to non-saturating concentrations of pheromone assemble a polarity domain that wanders around the cell cortex in an actin-dependent manner (Dyer et al., 2013). Similarly in *S. pombe* cells, low-level pheromone signaling promotes a novel polarization state, where active Cdc42, its GEF Scd1, and scaffold Scd2 form colocalizing dynamic zones that sample the periphery of the cell, by

overcoming cell pole polarity landmarks (Bendezu and Martin, 2013). In both cases, exploration may represent a fundamental self-organizing mechanism for accurate and flexible gradient sensing, orientation along this gradient and mating partner choice.

In conclusion, a design of competing feedback regulation loops combines efficient polarization with the ability to dynamically respond to varying intracellular or environmental conditions.

2.6.7 Roles of negative feedback

As I have previously mentioned, in *rsr1Δ* yeast cells that bud randomly, a continuous change of the polarization axis has been observed, in the form of traveling waves of activated Cdc42 randomly exploring the cell periphery (Ozbudak et al., 2005). These findings reveal a mechanism for negative feedback that competes with the aforementioned positive feedback loops to regulate Cdc42 activity and confer dynamic responsiveness on the robust initiation of cell polarization.

Negative feedback can potentially have multiple functions: for instance, it may buffer the system against fluctuations in polarity protein concentration, providing robustness to the polarity circuit (Howell et al., 2012). In addition, negative feedback could significantly change the dynamics of competition, for example by accelerating the disappearance of the losing cluster. Unexpectedly, mathematical modeling reveals that as concentrations of polarity factors increase and clusters grow larger, it is possible to enter a regime where smaller clusters could survive to the competition, and in turn grow very large. This feature may potentially explain the apical branching of fungal hyphae, where the system may transition from a regime where GTPase clusters compete (yielding one winner) to a regime where they equalize (splitting to form two clusters) (Wu and Lew, 2013). Another role for negative feedback could be to allow repositioning of the polarity cluster. Relocation may be advantageous for cells that need to grow towards specific targets. Intriguingly, recent studies suggest that polarity site relocation is important for partner selection in both *S. cerevisiae* and *S. pombe* (Bendezu and Martin, 2013; Dyer et al., 2013): in particular, Cdc42 wandering in budding yeast shmooing cells is actin dependent, and may depend on negative feedback through vesicle fusion, as a vesicle that fuses off-center from the polarity peak will locally dilute polarity factors, producing a shift of the polarity peak away from the fusion site because of positive feedback (Dyer et al., 2013).

Negative feedback does not simply reflect the presence of negative regulators (e.g., GAPs) that are constitutively present: rather, accumulation of an active GTPase must induce its own inactivation and/or dispersal. In principle, this might occur via GTPase-mediated stimulation of GAP activity, or inhibition of GEF activity (Kuo et al., 2014). One proposed model relies derives from the observation that Cdc42 oscillations in budding *rsr1Δ* cells and in shmooing wild-type cells is actin-dependent: in this scenario, a key feature of polarized growth would act as a negative feedback, by fusion of the secretory vesicles locally which may locally dilute the GTPases at the polarity domain (Dyer et al., 2013; Howell et al., 2012; Ozbudak et al., 2005).

However, additional actin-independent sources of negative feedback must be present, as oscillatory clustering of Rop1 in pollen tubes and even of Cdc42 in budding yeast continue even after actin depolymerization (Howell et al., 2012; Hwang et al., 2005). Oscillatory growth of pollen tubes is accompanied by periodic changes in tip Ca2+ levels, which may participate in negative feedback (Qin and Yang, 2011). Another potential negative feedback mechanism is suggested by findings from the basidiomycete *Ustilago maydis*. In that system a GTPase effector phosphorylates the GEF, triggering its degradation and hence a reduction in GTPase activity, but it is still unknown if a similar mechanism occurs in yeast (Frieser et al., 2011). A quite similar explanation has been proposed for *S. pombe*, where delayed negative feedback may be driven by the activity of the effector Pak1, the same PAK kinase involved in positive feedback. Pak1 can phosphorylate both itself and the scaffold Scd2, either of which could potentially lead to a decrease in active Cdc42. Alternatively, negative feedback could also result from the activation of an inhibitor, for instance a GAP of Cdc42: however, in *rga4Δ* cells that are lacking the only known GAP for Cdc42 in *S. pombe*, Cdc42 oscillations are similar to those observed in wild-type cells (Das et al., 2012). To conclude, additional mechanisms of negative feedback remain to be elucidated.

2.7 Cell size regulation in fission yeast

Cells of a particular type, whether making up a specific tissue or growing as single cells, often maintain a constant size. Cell size maintenance is crucial for coordination of cell cycle progression with attainment of a critical size. Yeasts have been used in this context as they both

possess different mechanisms to monitor cell size and use this information to regulate progression through events of the cell cycle.

In the past, most biologists considered that form and size, like other aspects of cell structure and function, are genetically determined. In 1971, Hartwell published the first study on temperature-sensitive mutants of yeast that are blocked at specific stages of cell division (Hartwell, 1971). These mutants, called *cdc* for cell division cycle, were identified by the criterion that at the restrictive temperature each cell would cease to grow at the same point in the cycle, indicating at which point the product of the defective gene is required. The approach was brilliantly successful: since then, about 60 *cdc* mutants of *S. cerevisiae* have been described, and *S. pombe* has contributed as many again, and further mutants with lesions in cytoskeletal proteins and wall synthesis have been generated by gene disruption.

In the case of fission yeast, cell size regulation occurs primarily during G2 but can operate in G1, and for budding yeast it occurs during G1 (Hartwell, 1974; Nurse, 1975). Cdc2 (Cdk1) kinase activity drives entry into mitosis and thus determines the length of G2. Wee1 catalyzes inhibitory phosphorylation of Cdc2 and is antagonized by the phosphatase Cdc25. Cell size information is transduced via Cdr1 and Cdr2, inhibitors of Wee1 that localize to cortical nodes at the center of the cell. Pom1 is a kinase that inhibits Cdr1/Cdr2, thus alleviating inhibition of Wee1. Few years ago, two studies independently provide evidence that in fission yeast a spatial gradient of the protein Pom1 emanating from cell tips may regulate mitotic entry, thereby directly

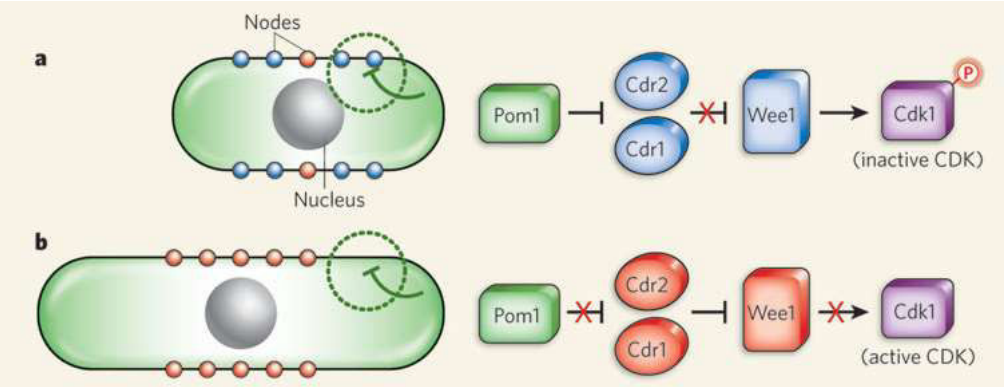

Figure 50: A spatial gradient links cell size to cell division in fission yeast. Pom1 is localized to the cell cortex, with the highest concentration at the cell tips, whereas Cdr2, Cdr1 and Wee1 are present in cortical nodes in the middle of the cell. ***A.*** In small cells, the Pom1 gradient reaches most of the cortical nodes. Pom1 inhibits Cdr2, preventing Cdr2 and Cdr1 from inhibiting Wee1, and allowing Wee1 to phosphorylate Cdk1, thus inactivating cyclin-dependent kinase (CDK) activity and preventing entry into mitosis. ***B.*** In long cells, the Pom1 gradient does not reach the cortical nodes, and therefore Cdr2 and Cdr1 remain active in the nodes. Cdr2 and Cdr1 inhibit Wee1, preventing phosphorylation of Cdk1 and thereby leading to activation of CDK and mitotic entry. (Sawin, 2009).

linking cell size with cell division (Figure 50) (Martin and Berthelot-Grosjean, 2009; Moseley et al., 2009). The idea is strikingly simple: in small cells the 'tail' of the Pom1 gradient overlaps with the medial Cdr2–Cdr1–Wee1 network and there is sufficient Pom1 to inhibit Cdr2, allowing active Wee1 to prevent mitotic entry (Figure 50 A.). However, as the cell grows and the distance between the tips and medial region increases, a crucial length is reached at which the Pom1 gradient no longer overlaps sufficiently with Cdr2–Cdr1–Wee1; Pom1 can therefore no longer inhibit Cdr2, which is free to inhibit Wee1, leading to activation of CDK and entry into mitosis (Figure 50B.). In this way the size of the cell regulates mitotic entry.

These results show that of course there is a connection between genes and form, but it is oblique, as morphogenesis is especially a matter of large-scale spatial organization. However, other unknown mechanisms may operate to measure size and integrate this information into cell cycle control: for instance, Chang and his collaborators recently proposed that Cdcr2 may also act as a cortical sizer to probe the surface area of the cell (Pan et al., 2014). Moreover, additional factors affecting cell size are mechanical considerations such as cell wall stress and turgor pressure (Chang and Huang, 2014): in fact, an increase in cell width would be coupled to an increase in stress that would entail an increase in stretching of the wall. It will be interesting to determine how the mechanical properties and wall thickness vary across closely related species of different sizes, such as the larger fission yeast *S. japonicus*. Each species may thus attain a certain size that benefits its mechanical and growth properties.

To conclude, the mechanisms for cell size regulation still need to be further investigated to understand what are the optimal means associated to a specific cell size, shape or function.

3.

THE MYSTERIOUS CASE OF SPORES

Spores are ubiquitous structures that can resist to harsh environmental conditions. In this chapter, I will discuss the main features of spores, by specifically discussing the function and structure of the outer spore coat. Then I will describe the sequence of events which characterize the fission yeast spore's life: how it is formed (the sporulation stage), its ability to survive in extreme conditions throughout dormancy, and then its re-entry into the cell cycle and growth to finally regenerate a rod-shaped vegetative cell. This is an intriguing example of development in a unicellular organism: moreover, the transition from a quasi-symmetric to a polarized shape occurs through a symmetry breaking process. Finally, I will distinguish known cases where the final direction of polarized growth is set by an extrinsic cue and few evidences of spontaneous polarization in spores.

3.1 The discovery of spores

The first observation of microrganisms came together with the design and development of the first microscope, in particular by Antonie Van Leeuwenhoek (1632–1723) and Robert Hooke, who coniated the term "cell". Later on, the investigations of Lazzaro Spallanzani (1729–1799) and especially Louis Pasteur (1822–1895) demonstrated that life doesn't emerge spontaneously from non-living substances and supported Robert Koch's germ theory (1875), which states that some diseases are caused by microorganisms, too small to see without magnification. In the same years, the German botanist Brefeld reported growing fungal colonies from single spores on gelatin surfaces (Figure 51). On the other hand, Ferdinand J. Cohn observed bacteria (which he called *Bacillus subtilis*) that appeared after boiling in cheese infusions, and theorized that there might be a special developmental stage or germ that survived the boiling: he then proposed that these oval, strongly refractive little bodies could be "real spores, from which new Bacilli may develop". In 1876, Cohn, Koch, Brefeld, Pratzmowski, van Tieghem, de Bary and others confirmed the discovery of spore germination in various species.

Figure 51: Historical drawing of all characterized developmental stages of a single fungal species. The large central figure in this plate shows a number of specimens of *Asterophora lycoperdoides* growing on a dark brown mushroom of the species *Russula nigricans*. In the painting you can see that the upper surfaces of some of the caps are breaking up. In fact the cap surfaces will eventually break down into a brown, powdery mass. Each granule is a chlamydospore (Brefeld, 1872).

3.2 General features of spores

Spores are nature's ultimate survival package. The term derives from the ancient Greek word *σπορά* (spora), meaning "seed, sowing". These are reproductive structures, adapted for dispersal and surviving for extended periods of time in unfavorable conditions, forming part of the life cycles of many bacteria, plants, algae, fungi, slime molds and some protozoa (Figure 52). The earliest evidence of plant life on land comes from envelope-enclosed spore tetrads, dating from ~470 million years ago (Wellman and Gray, 2000). Moreover, spores of the *Bacillus* bacterium that were preserved for 25 to 40 million years in extinct bees buried in Dominican amber were surprisingly revived and cultured, highlighting the incredible ability of spores to come back to life (Cano and Borucki, 1995).

Spores are usually haploid and unicellular, as they result from sexual reproduction by meiosis; in some cases asexual spores can be produced by mitosis, like in the case of chlamydospores. In bacteria, spores are not part of any sexual cycle, but they are produced in a process called endosporulation to provide a structure with high resistance to stress.

In the case of fungi, approximately 50,000 species produce spores, and most of them can generate both sexual and asexual ones: some species of rust fungi have five different spore types. Fungal spores are very diverse in morphology and range from 1-2 to 200 μm in size. Due to the high diversity among species, different criteria have been proposed to classify spores: the most common is based on the structure responsible of spore production, used also to distinguish different taxons of fungi (Figure 53). On this base, for example we can identify ascospores as spores produced by an ascus, characteristic of ascomycetes. One member of this category is fission yeast: conditions of nutrients deprivation lead vegetative cells to exit the haploid cell cycle and mate with each other, forming a transient diploid, or zygote, that proceeds through meiosis to produce four spores into a tetrad ascus. Other common classes in this classification are: sporangiospores, produced by a sporangium, which is a sac-like sporophore found in plants, algae and fungi; aeciospores, produced by an aecium, a cluster-cup or fruiting body of certain rust fungi usually found on lower leaf surfaces of plants; conidia, produced by a conidiophore; and basidiospores, produced by a basidium, a spore-producing structure found on the hymenophore of fruiting bodies in some rust fungi.

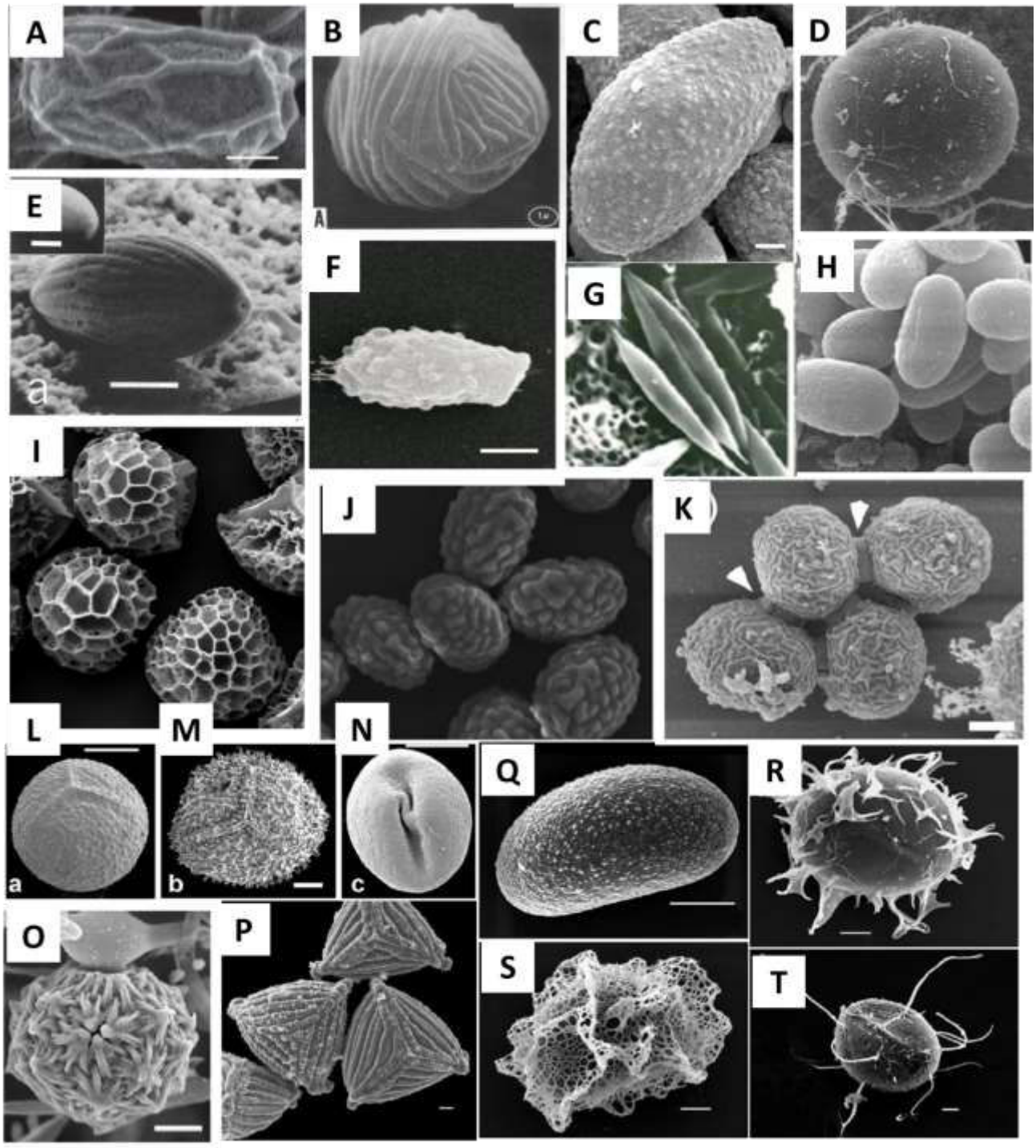

Figure 52: Diversity of spore morphology in nature. All pictures are scanning electron micrographs (SEM). **A.** Spore of the bacterium *Bacillus subtilis*. **B.** Spore of the mold *Rhizopus stolonifer*. **C.** Spore of the pathogenic zygomycete *Mucor circellinoides*. **D.** Spore of the arbuscular mycorrhizal fungus *Scutellospora heterogama.* **E.** Spore of the ascomycete *Neurospora crassa*. **F.** Spore of the pathogenic tremellomycete *Cryptococcus neoformans*. **G.** Spores of the acomycete *Rosellinia bunodes* belonging to the family of *Xylariace*. **H.** Spores of the social amoeba *Dictyostelium discoideum.* **I.** Spores of the club moss *Lycopodium*

clavatum. **J.** Spores of the ascomycete *Schyzosaccharomyces pombe*. **K.** Daughter spores of the ascomycete S*accharomyces cerevisiae*, connected by interspore bridges. **L.** Spore of the eusporangiate fern *Angiopteris*, showing proximal triradiate mark. **M.** Spore of the eusporangiate fern *Osmunda imperialis*, showing proximal triradiate mark. **N.** Pollen grain of the cycad *Stangeria eriopus*, showing distal surface with prominent folds. **O.** Zygospore of the pathogenic zygomycete *Mucor circellinoides*. **P.** Y-shaped fern spores of *Anemia aspera*. **Q.** Smooth fern spore of *Lomariopsis japurens*. **R.** Crested fern spore of *Lomariopsis sorbifolia.*. **S.** Lacy fern spore of *Lomariopsis hederacea*. **T.** Spiny fern spore of *Lomariopsis prieuriana.* References: **A.** (Sahin et al., 2012); **B.** (Van Etten et al., 1974); **C. O.** (Li et al., 2011); **D.** (Jeffries et al., 2007); **E.** (Seale, 1973); **F.** (Botts et al., 2009); **G.** (Suwannasai et al., 2012); **H.** (Repass et al., 2007); **I.** (Diego-Taboada et al., 2014); **J.** (Fukunishi et al., 2014); **K.** (Coluccio and Neiman, 2004); **L. M. N.** (Rudall and Bateman, 2007); Authors of **P.**: Robbin Moran; Authors of **Q. R. S.**: Judith Garrison Hanks and Robbin Moran; Authors of **T.**: Donald McClelland

Another principle of spore distinction is based on spore motility, which in turn depends on two main features: first, the presence of flagella, like in the case of zoospores; second, the ability to be discharged from the fungal fruiting body, either actively (for example most basidiospores,also named ballistospores) or inactively (such as statismospores for puffballs). Spore dispersal over long distances is essential for the organism's survival and proliferation.

Finally, spores can be classified on the basis of their function: for instance, chlamydospores are typically resting structures produced to survive unfavorable conditions, while parasitic spores aim to infect a host, either by germinating inside it or being released externally to invade other hosts (Figure 54). For instance, dormant spores of the pathogenic bacteria *Bacillus anthracis* can survive in soil for long periods, but upon inhalation or ingestion germinate and begin to replicate, finally resulting in toxin release and infection. Another example of spore-based invasion mechanism comes from the eukaryotic unicellular parasites *microsporidia*, and is based on a strange extrusion apparatus, the polar tube, which can discharge explosively upon contact with an appropriate host cell: by these means, the spore penetrates plasma membrane and delivers its content inside the host cytoplasm, where the parasite replicates to form up to a hundred progeny. Eventually, the progeny mature into spores and the host cell lyses to release them. In the case of the fungus *M. grisea*, host invasion is initiated by a germinating conidium: the germ tube apex swells after a short period of growth and forms a separate single cell, the appressorium, from which develops the penetration peg; this structure serves to carry the pathogen through the surface of the host into an underlying plant epidermal cell; after penetration, the fungus begins to develop yet another distinct structure, the infection hypha.

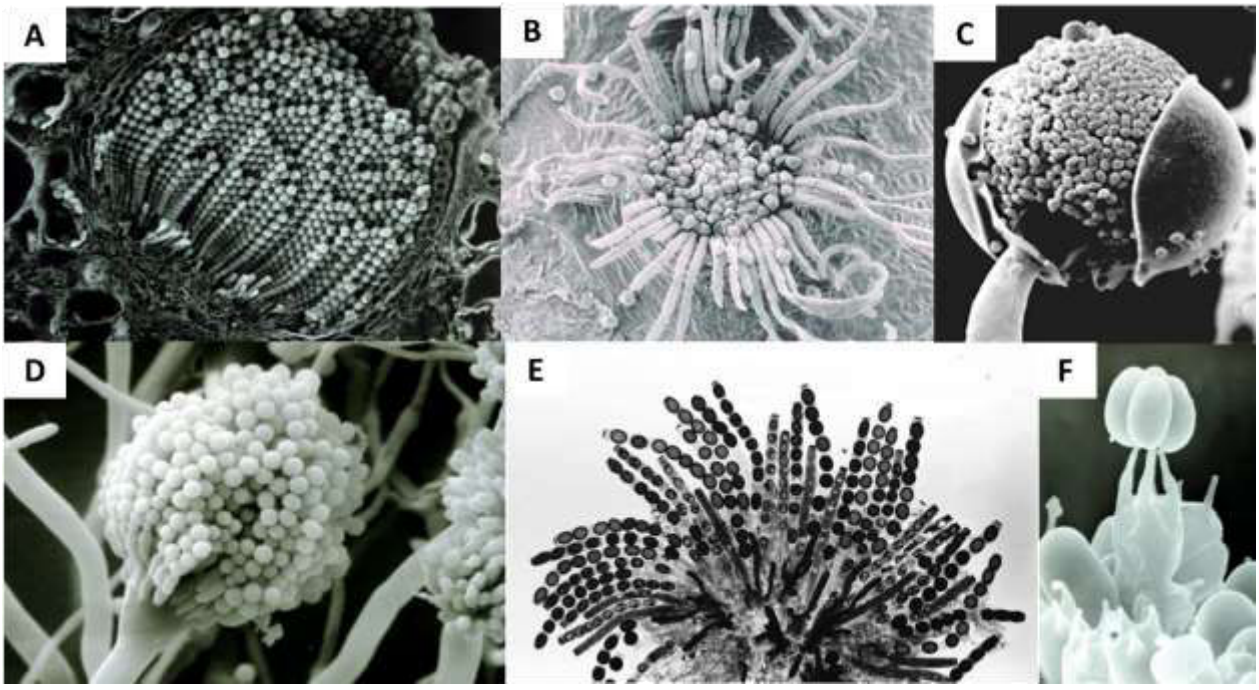

Figure 53: Examples of spores-forming structures. All pictures are transmission electron micrographs, eith the exception of panel E, which is a scanning electron micrograph.. ***A.*** Section of a mature rust aecium filled with spores; ***B.*** Aecium containing germinating spores; ***C.*** Sporangium of *Gilbertella persicaria* releasing sporangiospores; ***D.*** Mature conidiophore of *Aspergillus nidulans*; ***E.*** Rosette of maturing ascii of *Neurospora crassa*; ***F.*** Basidiospores emerging from a basidium. Authors: ***A. C. D. F.*** Charles Mims; ***B.*** Steve Kronmiller and Tom Arndt; ***E.*** Namboori B. Raju and David Perkins.

Even if the mentioned organisms are very different one to the other, their spores have a common feature that is essential for stress resistance: the spore coat (Figure 55). This structure is assembled *de novo* after the completion of prospore membrane closure, in order to generate a tight multilayered shell, mainly composed by polysaccharides and glycoproteins. Thanks to this shell, spores are commonly resistant to heat, ultraviolet and ionizing radiation, pressure, and chemical agents.

In a harsh environment, spores can survive for very long periods in a unique developmental state, called dormancy, where need for metabolic energy is minimized. Apart from the outer wall, spore resistance during dormancy also depends on other factors, including the relative impermeability of the spore's membrane, and mechanisms of DNA repair and protection (for example in bacteria, by saturation with α/β-type acid-soluble spore proteins, SASPs). Once conditions are favorable, the spore can re-enter the cell cycle and develop back into a vegetative cell (in the case of bacteria or fungi) or a gametophyte (in the case of algae and plants). Most

spores have almost spherical shape: after the onset of germination, they start to grow isotropically, and later on initiate polarized growth in a process termed outgrowth (Figure 56).

This event can be viewed as an example of symmetry breaking, where the cell establishes an axis of polarization and then maintains it during tip extension: for instance, round fission yeast spores regenerate rod-shaped vegetative cells. Hence, spore-to-cell development is an essential morphogenetic process, and represents an optimal model system to investigate general features of

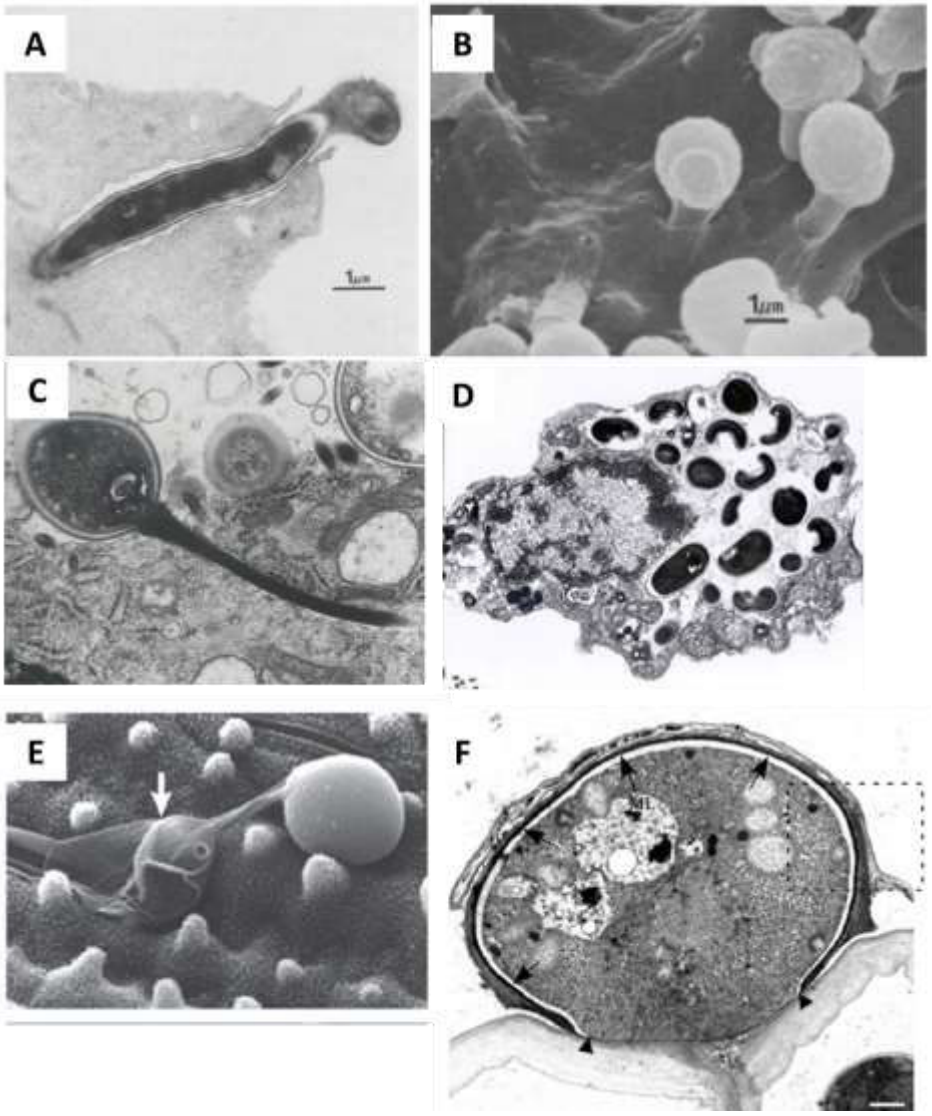

Figure 54: Mechanisms of infection by fungal and microsporidian pathogens. **A.** TEM and **B.** SEM of the fungal pathogen *Candida albicans* invading cultured human vascular endothelial cells (Rotrosen et al., 1985). **C.** TEM of a microsporidian spore with an extruded polar tubule inserted into an eukaryotic cell. The spore injects the infective sporoplasms through its polar tubule. (Source: DPDx - Division of Parasitic Diseases and Malaria) **D.** TEM of an eukaryotic cell with *Encephalitozoon intestinalis* spores and developing forms inside a septated parasitophorous vacuole. (Source: Massimo Scaglia, Laboratory of Clinical Parasitology, University-IRCCS San Matteo, Pavia, Italy). **E.** SEM of a *M. grisea* appressorium (arrow), a cell used by the fungus to infect its host (Source: Nick Talbot, University of Exeter); F. TEM of a *M. grisea* appressorial-like structure (Howard et al., 1991).

cell polarization.

Moreover, during germination the spore needs to crack the external coat to succesfully grow and divide: how the mechanical properties of the outer wall affect spores development and morphogenesis remains a mystery.

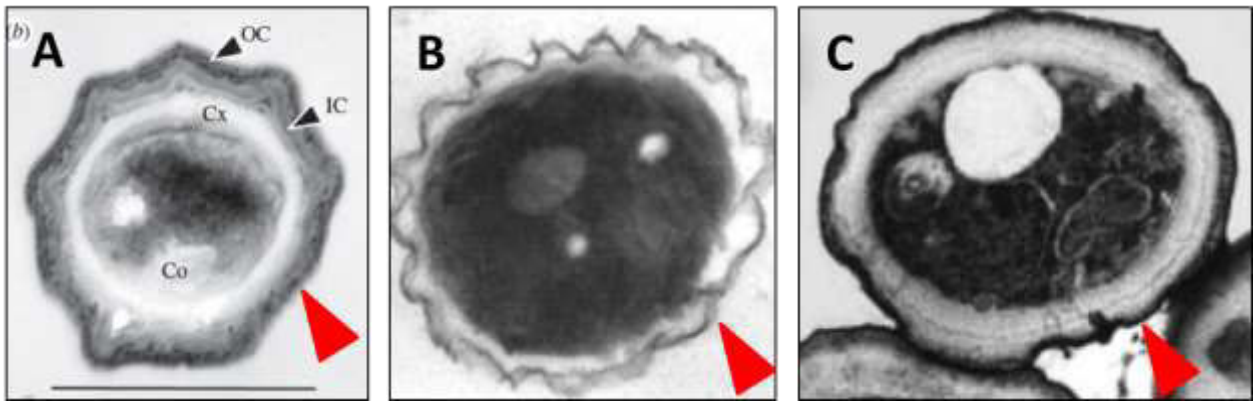

Figure 55: The spore coat encases the spore to protect it from hard environmental conditions. All pictures are transmission electron micrographs. **A.** Spore of the bacterium *B. subtilis* (Sahin et al., 2012). **B.** Spore of the yeast *S. pombe* (Nakamura et al., 2004). **C.** Spore of the yeast *S. cerevisiae* (Kono et al., 2005). In the three cases, the thin black outer layer indicated by the red arrows is the spore coat.

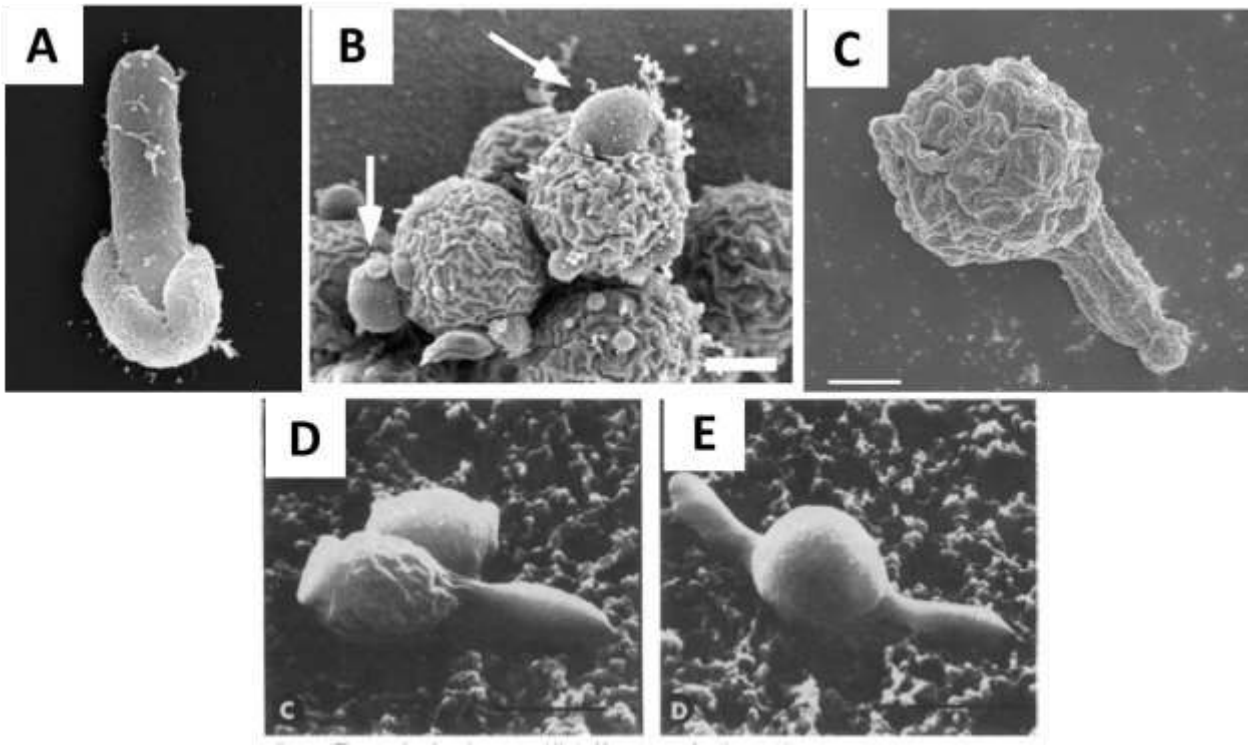

Figure 56: Example of outgrowing spores. All pictures are transmission electron micrographs. **A.** Spore of the bacterium *B. licheniformis.* Authors: Antje Hoenen (SEM Lab, University of Oslo) and Elisabeth H. Madslien (The Norwegian Defence Research Establishment). **B.** Spore of the yeast *S. cerevisiae*. (Coluccio and Neiman, 2004). **C.** Spore of the kelp *Undaria pinnatifida* (Petrone et al., 2011). **D.** Spore of the macroconidia of *N. crassa* (Seale, 1973). **E.** Spore of the macroconidia of *N. crassa* (Seale, 1973).

3.3 The spore wall: composition and biogenesis

The main structure that is responsible for spores high resistance to stress in all mentioned organisms is the outer spore wall, or spore coat.

It is usually composed of several layers of different sugar polymers like mannans and glucans which are associated to glycoproteins. Moreover at least one of these layers is fibrous: some fungi contain cellulose, some others chitin. The composition, structure and number of layers are very different between bacteria, plants, protozoans or fungi.

In the past years, several authors have shed light on spore wall composition and biosynthesis in budding yeast (Figure 57). This structure is composed of four layers of different polymers (Neiman, 2005): the two inner layers (about 70 nm thick) consist mainly of mannoproteins and glucans, and their chemical composition is very similar to that of the vegetative cell wall, while the third and fourth layers (about 30 nm thick) are specific to the spore and comprise chitosan and a dityrosine-containing polymer, respectively (Briza et al., 1988; Briza

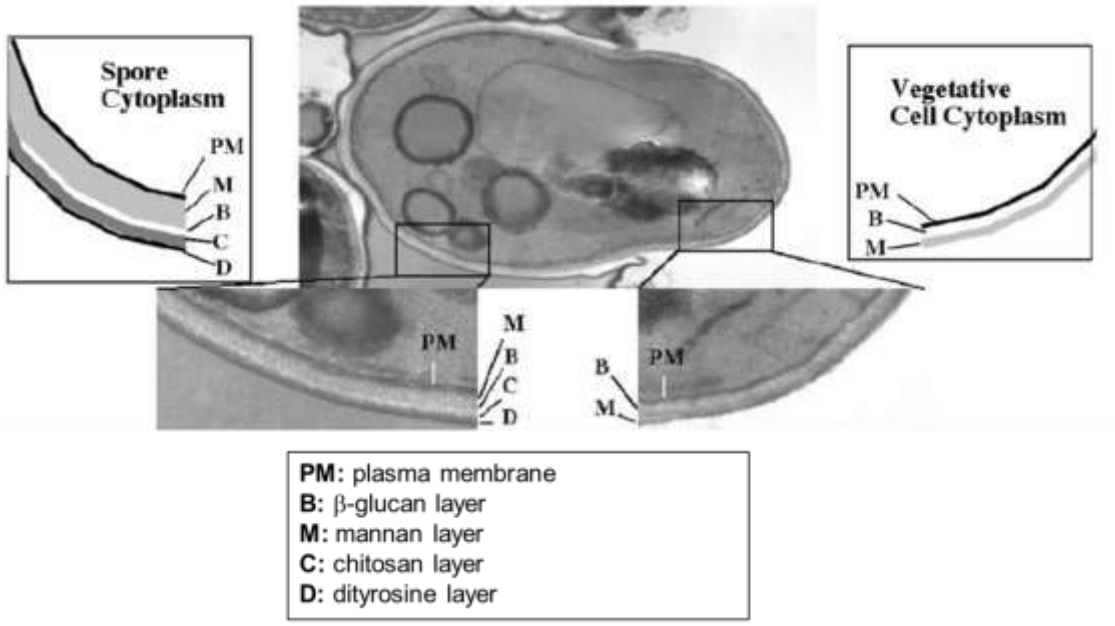

Figure 57: Comparison of the spore wall and the vegetative cell wall. An electron micrograph of a germinating ascospore is shown. On the left side, the cell is surrounded by spore wall with its four layers, mannan, beta-glucan, chitosan, and dityrosine (indicated by M, B, C, and D, respectively). On the right side, the tip of the germinating cell is bounded by vegetative cell wall with its predominant beta-glucan and mannan layers (indicated by B and M). The mannan layer of the cell wall appears to be continuous with that of the spore wall. PM, plasma membrane (Neiman, 2005).

et al., 1986). These two outer wall layers primarily provide the enhanced resistance of the spore to various environmental stresses, for example the passage through the digestive track of *Drosophila* (Coluccio et al., 2008). In *C. albicans*, dityrosine has been identified in the cell wall, and may play a role in allowing pathogenic fungi to survive in the host.

In fission yeast, the exact architecture of the spore wall remains elusive. It is known that the fission yeast spore wall has electron-lucent and electron-opaque materials (Figure 58): the first one represents the inner spore wall and contains β-1,3-glucan, whereas the second corresponds to the outer spore wall and contains amylose-like material that is responsible for the dark brown colour seen with iodine staining. A recent work has shown that α-glucans are more abundant than β-glucans in the ascospore cell wall, either in the form of an abundant polymer with α-1,3-glucan linkages or a minor α-1,4-glucan polymer, which is also able to react with iodine (Garcia et al., 2006).

Biosynthesis of spore wall components is carried out by various proteins during fission yeast sporulation: in the case of β-1,3-glucan, the synthase Bgs2 localizes to the spore periphery and is essential for maturation of the ascospore wall (Liu et al., 2000; Martin et al., 2000): in fact this member of the bgs gene family is the only one that is specifically expressed during sporulation, and its depletion causes thinning of the electron-lucent layer is thinner and spores unviability (Liu et al., 2000; Martin et al., 2000; Mata et al., 2002). The synthesis of cell wall β-1,3-glucan does not only require the enzymatic activity of the synthase complex, as recently

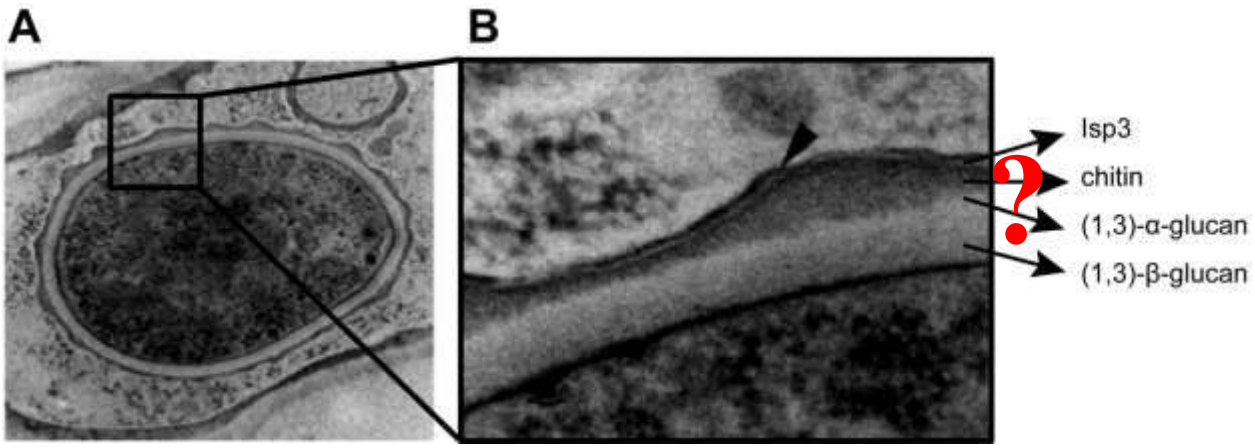

Figure 58: Proposed structure of the fission yeast spore wall. ***A.*** Transmission electron micrograph of a spore; ***B.*** Close-up on the spore coat: on the right, a proposed sequence of layers composition. Adapted from (Fukunishi et al., 2014).

synthesized β-1,3-glucan chains remain unorganized and alkali-soluble until covalent linkages are set up between β-1,3-glucans and other cell wall components (Ram et al., 1998). β-1,3-glucanosyltransferases such as the *S. cerevisiae* Gas1 or the *Aspergillus fumigatus* Gel1, are glycosyl-phosphatidylinositol (GPI)-anchored cell surface proteins that play a role in the elongation of β-1,3-glucan chains. Recently, it has been described that *S. cerevisiae* Gas2 and Gas4 genes are expressed exclusively during sporulation and that both proteins play redundant functions in the maturation of the spore wall (Ragni et al., 2007): a similar result has been obtained in fission yeast, where Gas4 is dispensable for vegetative growth but plays an essential role in spore wall assembly (de Medina-Redondo et al., 2008).

On the other hand, the spore wall maturation process in fission yeast relies on three (1,3)-α-glucan synthase-related genes-Mok12, Mok13 and Mok14, which are paralogues of Mok1/Ags1, an essential gene for cell morphogenesis during vegetative growth (Garcia et al., 2006; Hochstenbach et al., 1998). More specifically, expression of these genes is restricted to sporulating cells and the corresponding proteins localize to the spore envelope but with different timing. Moreover, mutants of each of these genes show peculiar spore wall defects: mutation of Mok12 affects the efficiency of spore formation and spore viability; deletion of Mok13 does not affect spore viability but the spores are less resistant to stress conditions. Finally, mutant spores in Mok14 fail to accumulate the amylose-like spore wall-specific polymer.

Furthermore, it has been suggested that chitin, chitosan or other glucosaminoglycans may be minor components of the spore wall and may constitute a matrix synthesized between other polymers, giving support to the spore wall. In fission yeast, expression and activity of the chitin synthase Chs1 increase significantly during sporulation: mutants in this gene show defect in spore wall synthesis and spore formation, although they do not have any defect during vegetative growth (Arellano et al., 2000). Chitosan is produced by chitin deacetylase from chitin, a polymer of N-acetyl glucosamine, in microorganisms. In *S. cerevisiae*, two chitin deacetylases called Cda1 and Cda2 have been shown to build up the proper ascospore wall by synthesizing chitosan from chitin (Christodoulidou et al., 1999). This chitosan based structure is believed to be important for spores to retain its structural rigidity and resistance to various stresses. Consistantly with these results, the chitin deacetylase Cda1 is also expressed during sporulation in *S. pombe* and required for proper spore formation (Matsuo et al., 2005). Previous studies show that chitin is

also an essential component of vegetative cell walls of hyphae, as well as conidiophores in the filamentous fungus *Aspergillus nidulans* (Fukuda et al., 2009).

Finally, a recent study has investigated the structure of the fission yeast outermost spore surface and found that it is composed of the protein Isp3/Meu4, conferring resistance to various environmental stresses (Fukunishi et al., 2014). The surface morphology of *S. pombe* spores differs considerably from that of *S. cerevisiae*, as it is characterized by the presence of many spikes, whereas *S. cerevisiae* spores have many wrinkles (Coluccio et al., 2004; Nakamura et al., 2004): this may be due to the different composition of the outer spore layer, that is protinaceous in fission yeast and composed of neither protein nor polysaccharide in budding yeast, and finally related to evolution of distinct strategies for surviving drastic changes in the environment and/or adaptation for insect vectors .

As the germ tube develops, new wall material is deposited by vesicles to form the new germ tube wall; at the same time, the old spore wall layers are dissolved or ruptured or both.

3.4 The spore wall mechanics

The spore wall provides great strength and resistance to chemical attack, related to its mechanical and surface properties respectively, which in turn depend on its molecular composition and ultrastructure. The mechanics of the spore wall may also be relevant for wall expansion during germination, as changes in cell wall mechanical properties could affect the emergence of the germ tube. In this context, previous studies have described various spore physical aspect related to spore resistance, such as surface morphology, permeability, adhesive properties and mechanics.

To this aim, various researchers used Atomic Force Microscopy (AFM), to obtain informations about surface topography and rigidity at the same time on such small structures: for example, work on the fungus *Aspergillus nidulans* showed that the spore wall is covered with rodlet structures that confer hydrophobicity, while the underlying wall structure, made of cross-linked polysaccharides, is more rigid and provides great strength. Elastic moduli for the two layers range between 10 and 30 GPa, suggesting that it may be hard for dormant spores to germinate and extrude a germ tube (Zhao et al., 2005). Similar values of elastic moduli have been found for *Aspergillus Niger* dormant spores (10-20 GPa) and for the bilayered wall of the oocyst

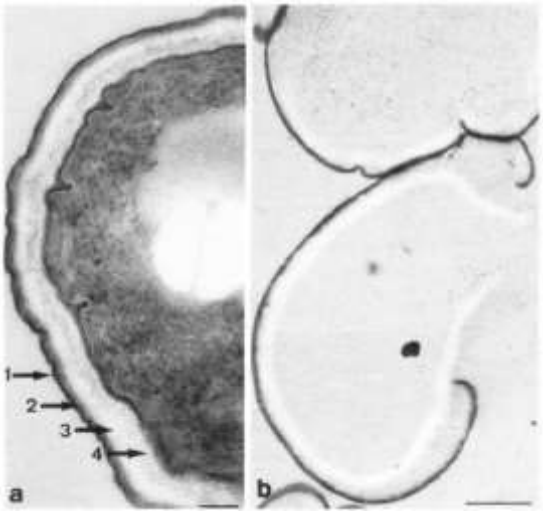

Figure 59: Electron microscopy of yeast ascospores and spore walls. On the right, a budding yeast spore: numbers indicate each of the four spore coat layers. On the left, purified budding yeast spore walls, with a partial detachment of layers 1 and 2 from layers 3 and 4. Note that the spore coat, especially the two outer layers, retain the spore shape, suggesting an intrinsically high rigidity (Briza et al., 1988).

Toxoplasma gondii, suggesting that the overall rigidity of these cells is as high as common plastic materials (Dumetre et al., 2013; Fang et al., 2012). Moreover, also in the case of *Aspergillus fumigatus* dormant spores, a layer of rodlets was observed, as the result of the presence of hydrophobins: germination then corresponds to a progressive disruption of the rodlet layer, revealing hydrophilic inner cell wall structures (Dague et al., 2008). The hydrophobic rodlets are likely to play a central role in promoting spore dispersion by air currents and in mediating adhesion to various surfaces, including host cells; on the contrary, the hydrophilic nature of the germ tube cell wall probably favors hyphal growth through moist environments and especially endothelia and epithelia. As a consequence, changes of surface morphology are related to specific functions of the spores; on the other hand, adhesive properties are crucial for some fungal pathogens to initiate invasion, as in the case of *C. albicans* (Rotrosen et al., 1985). In budding yeast, a recent work reported that the gene Osw3 is necessary for proper construction of the dityrosine layer, in order to act as a barrier blocking the diffusion of soluble proteins out of the spore wall into the cytoplasm of the ascus (Suda et al., 2009): hence, the yeast ascospore can survive extreme conditions, such as ingestion by insects, and even exploit them as vectors for dispersal (Coluccio et al., 2008). Moreover, isolation of *S. cerevisiae* spore walls do not seem to affect their shape, underlining their intrinsically high rigidity (Figure 59).

The design principles that allow the spore coat to be tough but also flexible and, when metabolic activity resumes, to be efficiently shed, are mysterious. These apparently incompatible characteristics may derive from an adaptive mechanical response of the coat. Mahadevan and his collaborators built up a mechanical model that predicts the emergence and dynamics of the folding patterns uniformly seen in *Bacillus* spore coats (Sahin et al., 2012): according to this model, spores carefully harness mechanical instabilities to fold into a wrinkled pattern during sporulation. These wrinkles persist during dormancy and allow the spore to accommodate changes in volume without compromising structural and biochemical integrity (Westphal et al., 2003). The observed architecture and dynamics of the coat and cortex of the dormant spore have important implications for the role of mechanical processes involved in germination. In contrast to the dormant state, the wrinkles disappear in germinating spores: the authors propose that the coat unfolding during germination may be due mostly to degradation of the cortex peptidoglycan, which will in turn facilitate wrinkle disappearance, and not necessarily driven by the expansion of the spore interior. Wrinkles are present in most spore coats of dormant spores and may hence play a role in mechanical adaptation to environmental stress.

To conclude, the spore coat provides high rigidity to the spore, which in turn is essential for resistance and survival.

3.5 Spore development

Spores represent a unique developmental stage of various organisms, where a precise sequence of events involving dramatic physical and chemical modifications takes place: in particular, in the following, I will discuss the main life steps of these structures, with a special attention on the fission yeast case.

3.5.1 Sporulation

Spores are mostly generated through the process of meiosis, even if examples of mitospores in fungi are known. In the case of Ascomycetes, ascospores are generally found in clusters of four or eight spores within a single mother cell, the ascus, as the result of meiosis. The creation of these specialized cells requires a cell division mechanism distinct from that used during vegetative growth of fungal cells. The process of meiotic or ascospore formation appears to be

cytologically close in all Ascomycetes. In particular in fissions yeast, the sporulation process is very similar to that described for *S. cerevisiae*. Despite these similarities, however, conservation of sporulation functions at the level of protein sequence is surprisingly low.

Mutants defective in meiosis and sporulation have been identified in *S. pombe* in a number of different screens, and most of the identified genes are hence named Spo (Bresch et al., 1968; Kishida and Shimoda, 1986). The overall process in fission yeast is summarized in the following (Figure 60) (Tanaka and Hirata, 1982): conjugation of the two haploid cells (step 1) results in a binucleate zygote where karyogamy has occurred by fusion of the two nuclei (step 2). At the presumed prophase in meiosis I, the zygote nucleus is elongated (step 3). Then, a MT spindle connecting nuclear-associated organelles at opposite poles is formed to perform nuclear division (step 4). Consequently, ascospore delimitation first becomes apparent at the start of

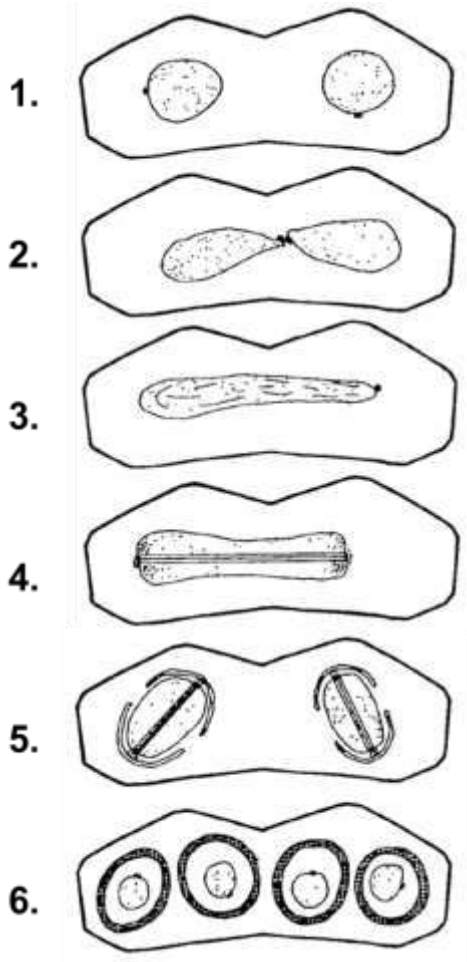

Figure 60: A schematic of meiosis and ascospore development in fission yeast (Tanaka and Hirata, 1982).

meiosis II (step 5) and a four-spored ascus is finally produced (step 6).

The process of spore construction requires two events in which cellular structures are assembled *de novo*: first, prospore membranes must be generated around the daughter nuclei to create prospores; second, the resulting prospores must be surrounded by a protective spore wall.

3.5.1.1 Meiosis

In rich growth medium, *S. pombe* cells are commonly haploid whereas *S. cerevisiae* cells conjugate to generate diploid cells; however, in conditions of nutrients deprivation, both yeasts trigger the sporulation program. In the case of fission yeast, nitrogen starvation leads to haploid cells exit from the mitotic cycle, initiation of conjugation and formation of zygotes. Zygotes can either directly undergo meiosis and generate four haploid spores or grow as diploids if they are transferred to a rich medium immediately after conjugation. However, these diploid cells are instable and also easily enter meiosis and form spores when they exhaust the available nutrients. Whether they are zygotes or diploids, meiotic cells follow essentially the same pathway: they arrest transiently in G1, initiate one round of DNA synthesis, and perform two consecutive nuclear divisions, called first and second meiotic divisions (or meiosis I and meiosis II).

The initiation of meiosis is regulated by two major signal transduction pathways in fission yeast, one responding to the nutritional conditions and the other to the mating pheromones (Harigaya and Yamamoto, 2007). Nutrient starvation results in transcriptional activation of the Ste11 gene, through down-regulation of the activity of cAMP-dependent protein kinase (PKA), which results finally in activation of a number of genes required for mating and meiosis. Binding of the pheromone to its receptor results in activation of a MAPK cascade, which leads to the induction of additional genes required for the mating process. All upstream signals converge to the master regulator of meiosis, Mei2: this RNA-binding protein is required at two distinct stages of meiosis, once prior to premeiotic DNA synthesis and then prior to the first meiotic division (meiosis I). The meiosis-specific gene products are likely to be required to modify the basic cell duplication machinery that operates in the mitotic cell cycle, and to reorganize the cell morphology, which results in the formation of asci containing four haploid spores, the counterparts of gametes in higher eukaryotes.

3.5.1.2 Forespore membrane assembly

The process of spore formation begins during meiosis II. Vesicles are recruited to the cytoplasmic side of each of the four spindle pole bodies, where they fuse to form flattened double membrane sheets termed forespore membranes (FSMs) (Figure 61) (Neiman, 2005). These four prospore membranes expand during the course of meiosis II so that at the time of nuclear division each prospore membrane completely engulfs the nuclear lobe to which it is anchored via the spindle pole body (SPB). Several coiled-coil proteins are specifically recruited to the SPBs and play indispensable roles in FSM assembly. After nuclear division, the open end of each forespore membrane closes off so that each daughter nucleus and its associated cytoplasm are completely encapsulated within a double membrane. The closure of the forespore membranes is a cytokinesis event, generating four autonomous spores. The SPB is a key element for this coordination: spatially it serves as the organizing center so that the FSM is assembled in the vicinity of nuclei, and temporally it determines the timing of FSM assembly during meiosis II through modification of the meiotic outer plaque (MOP), a specialized surface that assembles on the SPBs and is required for the initial fusion of vesicles to form an incipient prospore membrane (Knop and Strasser, 2000). If the SPB is prematurely activated in meiosis I, precocious assembly of the FSM occurs and consequently only two diploid spores are produced. In *S. pombe*, the temperature-sensitive cdc2 mutant forms such diploid spores at permissive temperatures (Nakaseko et al., 1984).

Vesicle trafficking is crucial for FSM assembly, the FSM growing through fusion with ER/Golgi-derived vesicles. In particular, SNARE proteins seem to be necessary for correct FSM formation. Vesicles and target membranes carry v-SNAREs and t-SNAREs, respectively: the specific interaction between v- and t- SNAREs might facilitate both docking and fusion steps. *S. pombe* contains one synaptobrevin v-SNARE homolog, Syb1, which is required for proliferation and localizes to the plasma membrane at growth sites during vegetative growth, and to the FSM during sporulation (Edamatsu and Toyoshima, 2003; Yamaoka et al., 2013). Moreover, the *S.pombe* syntaxin 1 orthologue Psy1 is a t-SNARE also essential for both vegetative growth and spore formation (Maeda et al., 2009), and localizes to the FSM.

Another central step in FSM formation is fusion of secretory vesicles: Neiman and his collaborators reported that sporulation in *S. cerevisiae* requires the late-acting secretion proteins Sec1, Sec4 and Sec8 (Neiman, 1998): Sec1 is a SNARE-complex-binding protein, Sec4 is a Rab-

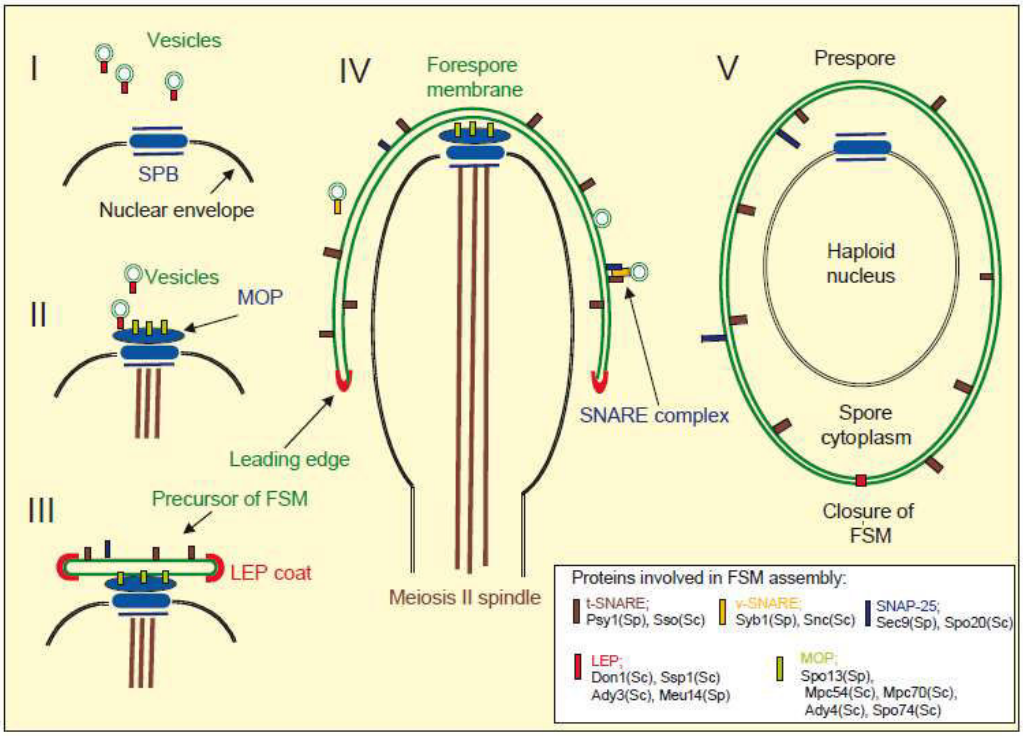

Figure 61: A model for the initiation and development of the FSM on the outer plaque of the SPB. (I) The nucleus contains a three-layered, unmodified SPB. Cytoplasmic vesicles, which carry components of LEPs, are observable. (II) These vesicles gather on the outer plaque of SPBs. Remarkably, the outer plaque develops to be a meiotic outer plaque (MOP), which contains several specific proteins. (III) A FSM precursor is formed by fusion of vesicles. t-SNAREs are recruited to the FSM precursor. A LEP complex is formed at the leading edge of the FSM. (IV) Cells enter anaphase II. The FSM grows by fusion with cytoplasmic vesicles that carry v-SNARE proteins. (V) The FSM engulfs the nucleus and a part of the cytoplasm. Closure of the FSM forms a membrane compartment called the prespore, which contains a haploid nucleus and part of the mother cell cytoplasm (Shimoda, 2004).

family small GTPase, and Sec8 is a component of the exocyst complex. In *S. pombe*, two components of the exocyst complex have also been identified as important regulators in spore formation: in particular, Exo70 is required for proper FSM development, while Sec8 plays a role in mating, and both proteins seem to affect spore wall formation (Sharifmoghadam et al., 2010).

The FSM extension with final encapsulation of each daughter nucleus is another important step in spore formation. Two FSM regions can be distinguished: the SPB attachment site and the leading edge. The leading edge of the FSM is coated with a specific protein complex, while chromosome segregation is coordinated with the growth of the FSM so that the divided nucleus is encapsulated by the FSM. In this context, SPBs act as FSM organizing centers: presumably, septin proteins facilitate construction of the FSM (Fares et al., 1996). Once the

prespore is completed, the FSM is released from the SPB. FSM closure triggers the synthesis of spore wall components, which accumulate in the luminal space of the FSM.

3.5.1.3 Spore wall assembly

The term "prespore" refers to the fragile, newly formed spore precursors, which are bounded by the FSM and bear one haploid nucleus, a set of organelles and some cytosol. Prespores mature through spore wall synthesis. Spore wall components are deposited in the luminal space between the outer and inner leaflets of the FSM (Lynn and Magee, 1970). The inner leaflet becomes the plasma membrane of the spore. The outer leaflet covers the spore walls during early sporulation, but its fate is not known after spore maturation. The *S. cerevisiae* spore wall consists of four layers: two inner polysaccharide layers composed of β-glucan and α-mannan, a central chitosan layer and an outermost layer of crosslinked dityrosine. These layers wall appear to be laid down in a temporal order, suggesting that feedback mechanisms must exist to coordinate the completion of one layer with the beginning of synthesis of the next layer.

The first step in spore wall assembly consists in initiation, to coordinate it with both membrane closure and completion of meiosis II. Following initiation, the first stage of spore wall formation is a deposition of material into the lumen between the two membranes formed from the prospore membrane, to deposit the mannan and β-glucan layers. During this phase, the outer membrane derived from the prospore membrane disappears and spores acquire refractility in the light microscope. This wall components seem to be essential for proper spore formation. Once the β-glucan layer is completed, the spore initiates synthesis of the chitosan layer: to this aim, the synthase Chs3 synthesizes chitin, while two sporulation-specific chitin deacetylases, Cda1p and Cda2p, deacetylate the chitin in the spore wall, converting it to chitosan. The conversion of chitin to chitosan is essential for organization of the outer spore wall layers (Christodoulidou et al., 1999). During proper assembly of the chitosan layer in the wall, interspore bridges are formed (Coluccio and Neiman, 2004), that connect adjacent spores of a tetrad independently of the overlying ascus. The last stage of spore wall formation consists in assembly of the dityrosine layer: this is achieved through the action of a sporulation-specific ATP-dependent transporter, Dtr1, localized in the prospore membrane (Felder et al., 2002). As for the other layers, the exact mechanisms of polymer network assembly and incorporation into the wall remain to be elucidated.

In *S. pombe*, the spore wall consists of an inner, electron-transparent layer and an outer, electron-dense layer (Figure 62): the genes Bgs2, Mok13 and Chs1 are required for spore wall formation, meaning that β-glucan, α-glucan and chitin must be necessary components of spore walls, but the mechanism of layer deposition remains poorly described (Arellano et al., 2000; Garcia et al., 2006; Liu et al., 2000; Martin et al., 2000). The inner layer is probably composed of polysaccharides similar to the wall components of vegetative cells: when a germinated spore commences polarized growth, the outer, electron-dense layer is locally disrupted, and the inner layer protrudes, which indicates that the inner layer is structurally related to the vegetative cell wall and that the outer layer is spore specific.

After the completion of the spore wall, the now anucleate mother cell, which remains

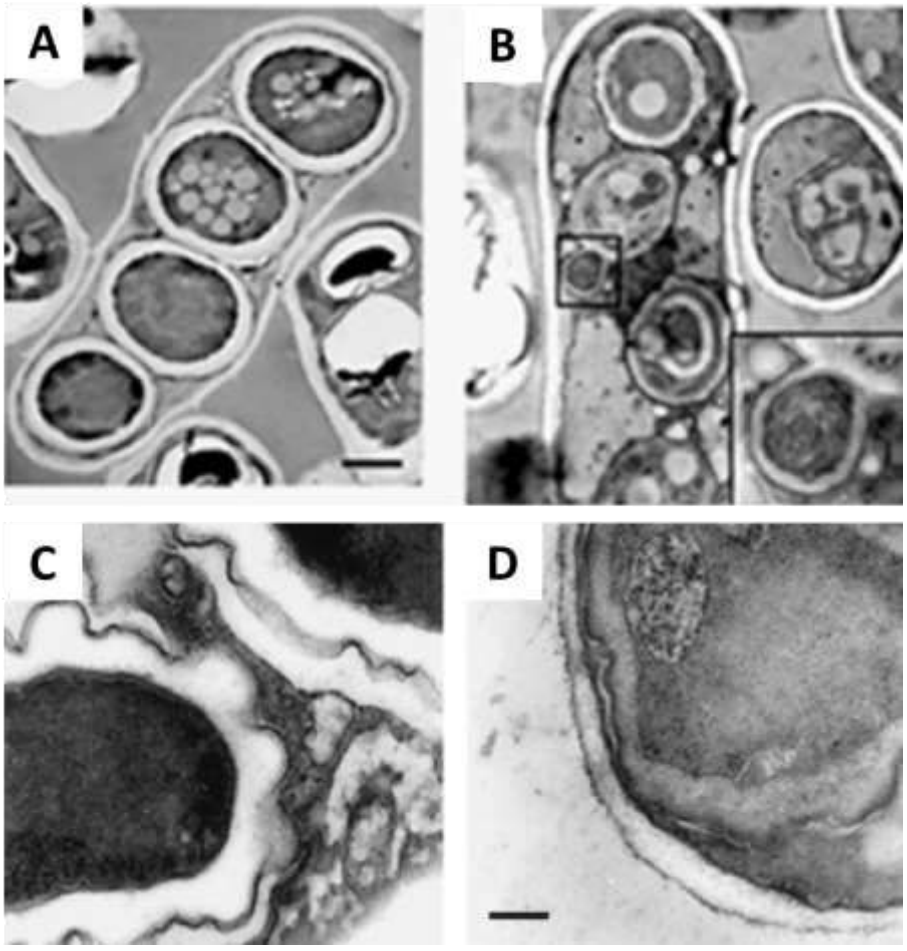

Figure 62: Examples of fission yeast spore wall mutants compared to wild-type. **A.** Wild-type ascus encasing four daughter spores. **B.** *chs1Δ* ascus encasing four daughter spores, with abnormal accumulation of membranes in their cytoplasm and defects in the spore walls. C. Close-up on a wild-type spore. **D.** Close-up on a *bgs2Δ*, showing a thinner electron-transparent layer of the spore wall with an amorphous structure (Arellano et al., 2000)

intact throughout sporulation, is remodeled to serve as an ascus that encapsulates the four spores of the tetrad. A mutation that delays or blocks the shrinking of the ascus around the spore has been described, suggesting that ascal maturation may be an active process, rather than a simple lysis of the anucleate cell (Dekker et al., 2007).

3.5.2 Spore dormancy

Once released, some types of spores will germinate quickly while others will remain dormant for a period a time, which can be very long. For fungal spores, dormancy can be defined as any rest period or any irreversible interruption of the phenotypic development of an organism. Generally, asexual spores are regarded as agents of dispersal, aiding dissemination to fresh substrates: to efficiently accomplish their function, such spores tend to be light, small, in very large numbers and germinate rapidly after formation, but they carry limited stores of nutrients and survival abilities. On the contrary, sexual spores are mostly regarded as survival structures, capable of high resistance and long-life span: in some cases, they require a period of maturation and/or exposure to particular stimuli prior to germination. Spores of the first category are often subject to relatively short-term dormancy and can resume development providing that favourable environmental conditions are present (exogenous dormancy), whereas spores of the second category can survive longer and in unfavorable conditions (constitutive dormancy).

Dormancy is associated with low water content, low respiration rate and low rates of protein and nucleic acid synthesis: dormant spores are surrounded by a rigid shell, the outer spore coat, and possess a very dense cytoplasm. The duration of dormancy may depend on the spore permeability, which in turn relies on the spore wall properties: dehydration is also essential for spore survival, to withstand extreme temperatures.

Furthermore, dormant spores have a high content of energy-storage materials such as lipids, glycogen and trehalose: hence, dormancy may be maintained by the physical separation of metabolic enzymes and substrate: for instance, in *Neurospora tetrasperma* the enzyme trehalase, which cleaves trehalose to glucose, is stored in the spore wall and hence physically separated from the stored substrate until dormancy is broken. Trehalose mobilization may be an important biochemical event in fungal spore germination and related developmental processes, such as the resumption of growth in resting cells: high trehalose levels in fungal spores are also believed to enhance the resistance to extreme environmental conditions.

Dormancy can also be maintained by extracellular pH levels, oxygen concentration, or the presence of biochemical inhibitors: for example, the parent mycelium may express such inhibitors to preventing germination prior to dispersal. Direct evidence on this matter, however, remains scarce.

3.5.3 Spore germination

In 1966, Sussman and Halvorson defined germination as the first irreversible stage with a form recognizably different from the dormant organism, as judged by physiological or morphological criteria. The process of germination requires as a primary event the identification of an extracellular signal which is transformed by signal transduction machinery leading to intracellular changes that break the dormancy of a spore. When germination is triggered, all spores behave in a similar way: the cell becomes hydrated (an event marked by the loss of refractility, or darkening, of the spores), there is a marked increase in respiratory activity, followed by a progressive increase in the rates of protein and nucleic acid synthesis.

During germination, the cell undergoes dramatic changes in cell wall and membrane composition, as well as in gene expression, as during the exit from other resting states, such as stationary phase. Like in these states, germination requires large transcriptional changes in the cell, with about one-sixth of the genome undergoing transcriptional changes (Joseph-Strauss et al., 2007). The transcriptional program that occurs in *S. cerevisiae* during germination can be divided into two stages: first, spores respond to glucose, and second, they respond to other nutritional components, such as amino acids (Joseph-Strauss et al., 2007). The regulated genes reflect the transition towards glucose metabolism, the resumption of growth and the release of stress, with a transient up-regulation of genes involved in protein folding and transport. Components of the mitotic machinery are involved in spore germination but in a distinct pattern: in the case of fission yeast, spores have a protracted G1 period during which there is a well-defined sequence of events to achieve the transition to vegetative growth and cell division: hence, DNA synthesis occurs later on after germination.

However, in both yeasts, the glucose signal is transmitted through Gα/Ras pathways that cause rapid increase in cellular cAMP levels, which in turn activate cPKA catalytic subunits (Hatanaka and Shimoda, 2001; Herman and Rine, 1997). The activation of cPKA leads to activation of trehalose degradation and glycerol synthesis that increase the cell osmotic potential

(Pahlman et al., 2001); moreover, germination initiates two processes essential for cell growth, protein synthesis and signaling through the Ras protein pathway (Herman and Rine, 1997). Germination has also been studied in other fungi, such as *Aspergillus nidulans* and *Neurospora crassa*, and also in these cases the ras/mitogen-activated protein kinase pathway is involved, together with the cyclic AMP/protein kinase A pathway, and the Ca2+/calmodulin-mediated signaling pathway (Osherov and May, 2001).

As for *S. cerevisiae*, *S. pombe* spores initiate germination in response to glucose through the Ras-activated cyclic AMP–PKA pathway (Figure 63) (Hatanaka and Shimoda, 2001). Spores of some plant pathogenic fungi usually germinate even in absence of any nutrients: these spores depend on the limited endogenous resources present within the resting spore for completing all the developmental stages that precede host penetration. On the other hand, when spores exit

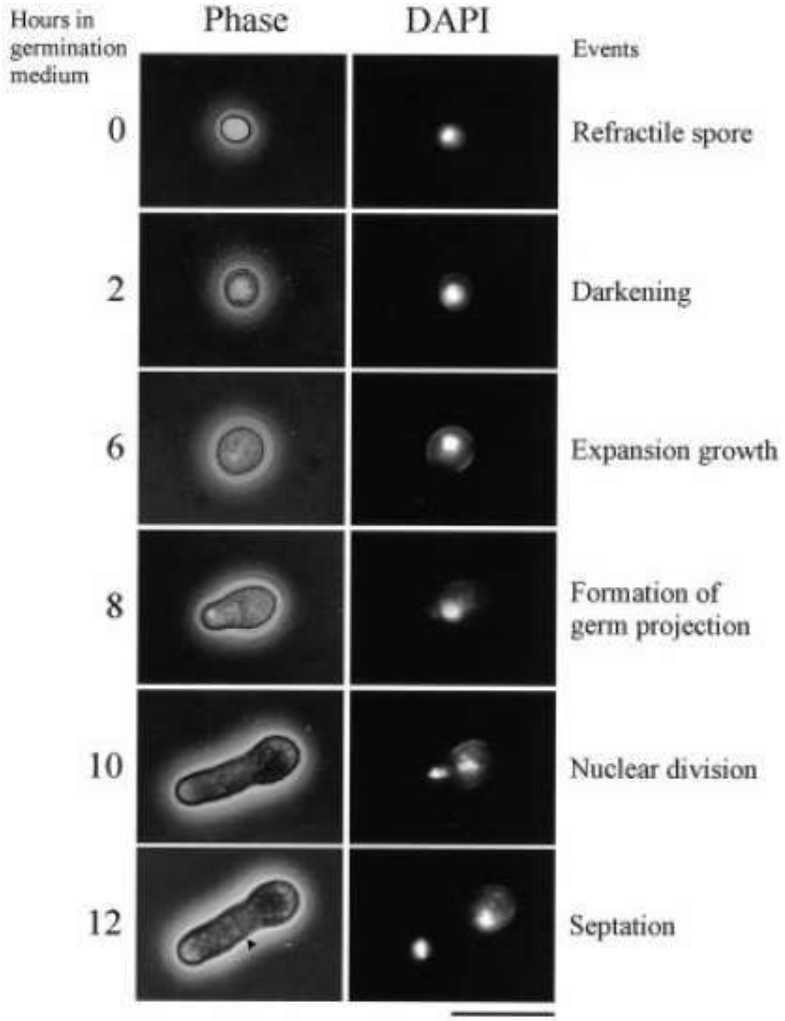

Figure 63: Morphological changes of fission yeast spores during germination and outgrowth. Phase-contrast and DAPI staining acquired every two hours. Bar, 10 μm (Hatanaka and Shimoda, 2001).

dormancy and germinate, they partially lose their extreme resistance properties: germination is thus both an essential part of disease pathogenesis or food spoilage and a major weak spot in these organisms life cycle.

3.5.4 Spore outgrowth

The germination process consists of various stages marked by key morphological changes (Figure 64). Shortly after germination the spores are generally almost round, and grow isotropically: later on, the growth pattern switches from isotropic growth to polarized growth, in a process called outgrowth. Fungal mycelia can be grown from spores of filamentous fungi: again, spores first grow isotropically to generate a spherical germ cell, and then initiate polarized growth which results in formation of the first hyphae and successive branching. In the past, researchers have shown that protein synthesis is required for germ tube emergence, but it is not clear if it also plays a role during the first isotropic growth phase.

Isotropic growth results in a drastically increased volume. Therefore two basic processes need to be monitored by the cell, (i) water uptake and (ii) cell wall integrity, to avoid cell lysis/bursting. During this phase, yeasts and filamentous fungi use a similar pathway, based on the Rho1–Pkc1–MAPK cascade, to control basic processes of cell wall stabilization and generation of turgor pressure (Wendland, 2001). These pathways need to operate also in other growth stages of filamentous fungi and might therefore be controlled in a species-specific manner, e.g., as occurs during the formation of appressoria in *M. grisea.* Particularly, upstream mechanosensors may play a role in the targeting of growth to differential areas of the cell wall and, thereby, could be potential antifungal drug targets. Thereby, the site of final polarization is established by external cues in various physiological contexts, but intrinsic mechanisms could also participate and be sufficient for symmetry breaking.

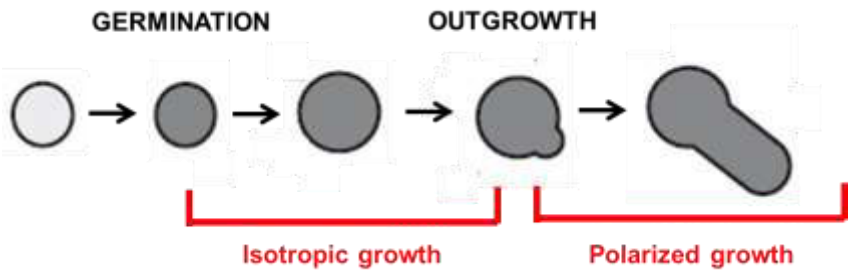

Figure 64: Schematic of spore germination and outgrowth in fission yeast.

The growth transition, that marks an essential step in the developmental morphogenesis of the spore, can be viewed as a symmetry breaking event, where polarity is established *de novo*. Previous studies in budding and fission yeast have highlighted the fact that the cytoskeleton also appears unpolarized during the first isotropic growth phase, and then switches to a polarized organization at the onset of outgrowth, suggesting that regulatory proteins for cytoskeletal rearrangements such as the small GTPases Cdc42 and Rac1 may also be involved in the establishment of germ projection sites (Hatanaka and Shimoda, 2001; Kono et al., 2005).

Another important player in spore symmetry breaking is the spore coat: in fact, it has been observed in various organisms that outgrowth and polarity establishment occur in concomitance with local rupture of the coat, suggesting the potential existence of feedbacks between cell mechanics and polarity.

3.5.4.1 Guidance by an extrinsic cue

Spore development is a polarization process, and the final direction of growth can be established by various environmental signals: for example, the zygote of the brown alga *Fucus* can polarize in response to a unidirectional light, a crucial cue for defining its growth axis in its natural environment. On the other hand, spores of plant pathogenic fungi respond to plant-specific signals, including physico-vchemical characteristics of the plant surface (thigmotropism) and specific plant chemicals such as cuticular waxes, root exudates or plant volatiles, to induce germination and appressorium formation (Podila et al., 1993; Tucker and Talbot, 2001).

Interestingly, most spores contain an abscission scar where they were originally attached to the sporophore: this structure is a remnant of the previous meiotic cell cycles, and could contain specific landmark protein that potentially act as a memory cue for setting the site of outgrowth, in a similar way as budding scars in *S.cerevisiae* vegetative cell cycle. However, evidences for such kind of mechanisms are still missing, and it would be interesting for instance to evaluate the potential role of "separation marks" left over from conidiogenesis as historical landmarks determining sites of tip emergence in filamentous fungi.

Very interestingly, asexual spores (conidia) of the mold *Neurospora crassa* differentiate two types of polarized cell protrusions, germ tubes and conidial anastomosis tubes (CATs), which exhibit negative (germ tube avoidance) and positive (CAT homing) chemotropism, respectively. It is not known how these opposite chemotropic responses from the same cell are

regulated. Researchers provided the first evidence that shared and separate functions of the Rho-type GTPases Cdc-42 and Rac-1 regulate these opposite chemotropisms, by showing that Rac-1 is essential for CAT formation and cell fusion, whereas Cdc-42 is necessary and sufficient for normal germ tube development (Lichius et al., 2014). Cdc42-Rac-interactive-binding (CRIB) reporters were constructed to exclusively label locally activated GTP-bound GTPases (Figure 65).

In conclusion, dormant spores are still sensitive to the surrounding environment, and can initiate germination and polarized growth on the basis of this information.

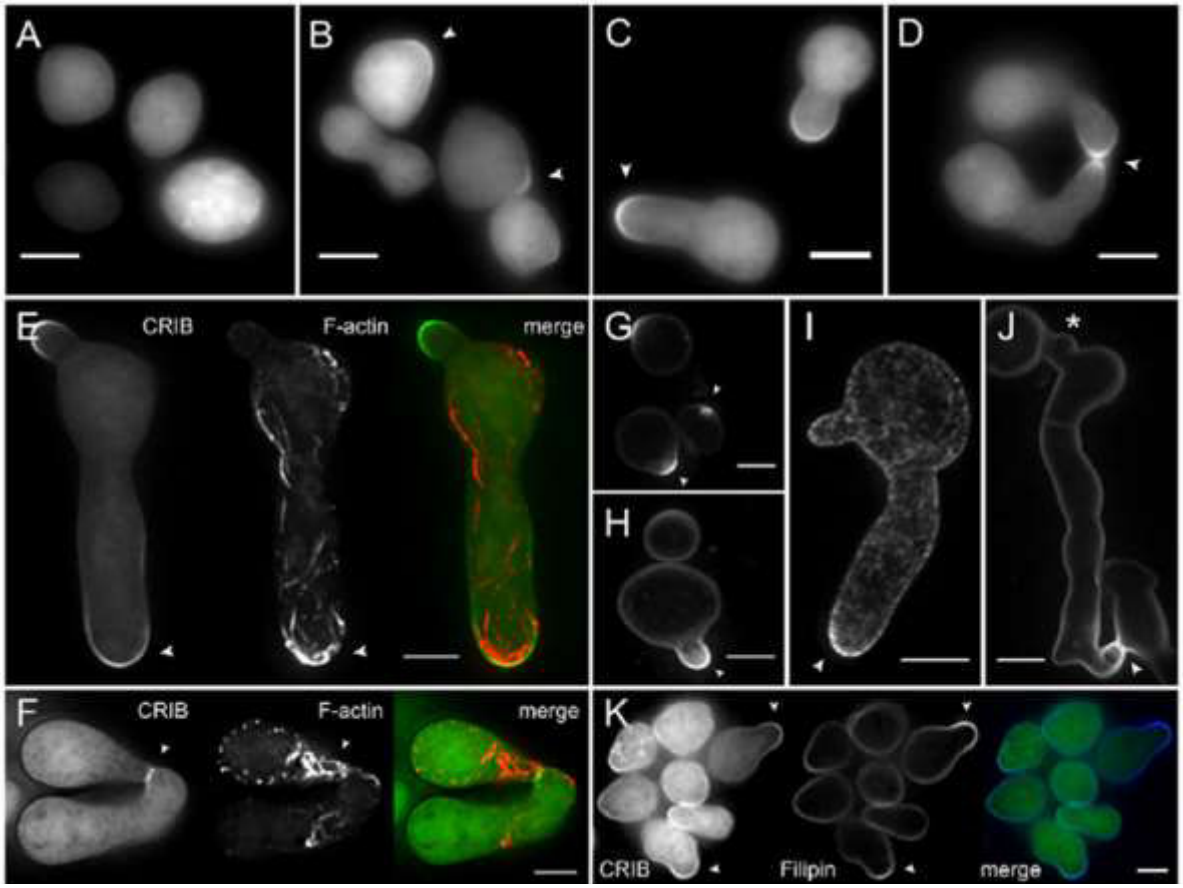

Figure 65: Colocalization of activated GTPases, F-actin and sterol-rich plasma membrane regions constitute sites of polarized growth. ***A.*** In non-polarized conidia, CRIB fluorescence is evenly distributed in the cytoplasm. ***B.*** Cell symmetry breaking coincides with cortical recruitment of the CRIB reporter, indicating localized activation of Rho GTPases prior to polarized protrusions (arrowheads). ***C. D.*** Crescent-shaped caps of activated GTPases mark the tips of growing ***C.*** germ tubes and ***D.*** CATs. ***E. F.*** Co-expression of CRIB–GFP and Lifeact-TagRFP-T shows colocalization of both polarity markers in apical crescents at ***E.*** germ tube tips and ***F.*** CAT fusion sites. ***G. H. I. J.*** Filipin staining highlights sterol-rich regions (arrowheads) ***G.*** at incipient polarization sites, ***H. I.*** during tip protrusion and ***J.*** at newly established CAT fusion sites. ***K.*** Colocalization of filipin-stained sterol-rich plasma membrane regions and the CRIB reporter. Scale bars: 5 µm (A.–D., G.–J.); 4 mm (E.,F.) (Lichius et al., 2014).

3.5.4.2 Spontaneous symmetry breaking: the role of polarity

As described previously, the establishment of cell polarity in various organisms may be either a purely stochastic process independent of internal landmarks, or dependent on MT-mediated deposition of *de novo* landmarks prior to each polarization event, as in the case of fission yeast vegetative cells.

Even in absence of any extracellular cue, various spores can still spontaneously break symmetry: for instance, the *Fucus* zygote, which is initially a sphere with an even distribution of cytological components, can locally grow one developmental, pole, which corresponds to the nascent rhizoid, forming a pear-shaped zygote characterized by a single axis of symmetry, even when no light cue is present. Also in the case of yeast and filamentous fungi, spores appear to be able to enter germination and outgrowth without the need of any extracellular signal: one possible explanation is that a cortical landmark may be set during the meiotic phase and then used as a cue for polarity establishment during spore development, but this hypothesis still needs experimental evidence.

Another intriguing possibility suggests the existence of an intrinsic self-organizing mechanism for spontaneous symmetry breaking in spore germination: indeed the transition from isotropic to polarized growth appears to correlate with a reorganization of the cytoskeleton and the polarity machinery, centered around small GTPases, and hence suggests that the same regulatory modules of vegetative growth are involved in this process.

In the case of the *Fucus* zygote, F-actin and cell wall secretion are localized at the rhizoid pole before any morphological change: moreover, a dense cortical MT network appears to originate from cortical nucleation sites, reorganize from random to a polarised array at the rhizoid pole during polarization, and hence contribute to germination (Figure 66) (Corellou et al., 2005).

Finally, transcellular ion currents of Ca^{2+} enters at the rhizoid pole, circulates around the zygote and leaves the zygote at the opposite pole (thallus), and this pattern of ion concentrations and electric field may contribute in the zygote polarization (Homble and Leonetti, 2007). Such kind of phenomena and their role in initiation of polarized growth has also been described in other systems: for example, in *C. richardii* spores which align their initial rhizoid growth with the gravity vector, researchers observed a calcium current flowing into the bottom and out the top of the spore in the period during which gravity determines the direction of cell polarization; calcium is clearly involved in the early stages of pollen germination and pollen tube growth, which in turn

is defined mostly by using positional signals from the stigma and style as initial growth guides (Bushart and Roux, 2007).

However, as I have previously described, cell polarity in eukaryotes mostly relies on the interplay between small GTPases and the cytoskeleton: hence, it is reasonable to think that this morphogenetic network could play a role also during spore germination. For instance in budding yeast, it has been shown that the actin cytoskeleton is essential for polarized outgrowth from a spore and that localization of actin patches dynamically changes during germination (Kono et al., 2005). In particular, the polarisome complex, composed of the proteins Spa2, Pea2, Bud6 and Bni1, functions for polarized organization of actin patches, while the PAK Cla4 is involved in the following depolarization of actin patches. Finally, Ras2 may be involved in establishment of the actin cytoskeleton whereas Rho1 organizes the polarized actin cytoskeleton, to establish a growth zone enriched in 1,3-β-glucan synthases and regenerate a vegetative cell wall.

Also in the case of fission yeast spores, actin patches are randomly distributed in the cortical region after the onset of germination (Hatanaka and Shimoda, 2001): interestingly, researchers observed that during isotropic growth, actin patches are localized to one side of the expanding spores (Figure 66), and proposed that this the future site of germ projection. These results suggest that cell polarity would be established in unpolarized spores before formation of germ projections, and hence the decision of a site for polarization is done during isotropic growth. Finally, authors proposed that regulatory proteins for the rearrangement of cytoskeletons such as small GTPases are involved in the establishment of germ projection-launching sites.

Such kind of Rho-GTPase morphogenetic network could be essential for *de novo* polarity establishment also during germination of filamentous fungi, as spores of *Ashbya gossypii* need the rhoGAP gene AgBEM2, which is a homolog of the *S. cerevisiae* Bem2 gene, to initiate polarized growth (Wendland and Philippsen, 2000). Moreover, in this fungus deletion of either AgCDC24 or AgCDC42 leads to delocalized actin and isotropically expanding cells, with diameters up to twice the standard size (Wendland and Philippsen, 2001). On the other hand, distinct events during spore germination and outgrowth in this organism appear to be controlled by different Rho-GTPase modules: Cdc42 is essential for polarity establishment, whereas Rho1 plays a role in polarity maintenance and polarized hyphal growth and Rho3 regulates growth at the hyphal tip (Wendland and Philippsen, 2001). Moreover the same polarity modules, centered around Cdc42, also regulate the branching pattern of *A. gossypii* and *Aspergillus nidulans*, where

a second germ tube is produced from the germ cell at a 180° angle after the first has been grown. Furthermore, in the case of *A. nidulans* the isotropic-to-polar growth switch appears also to be related to the plasma membrane organization, suggesting that lipid rafts at the tips of fungal

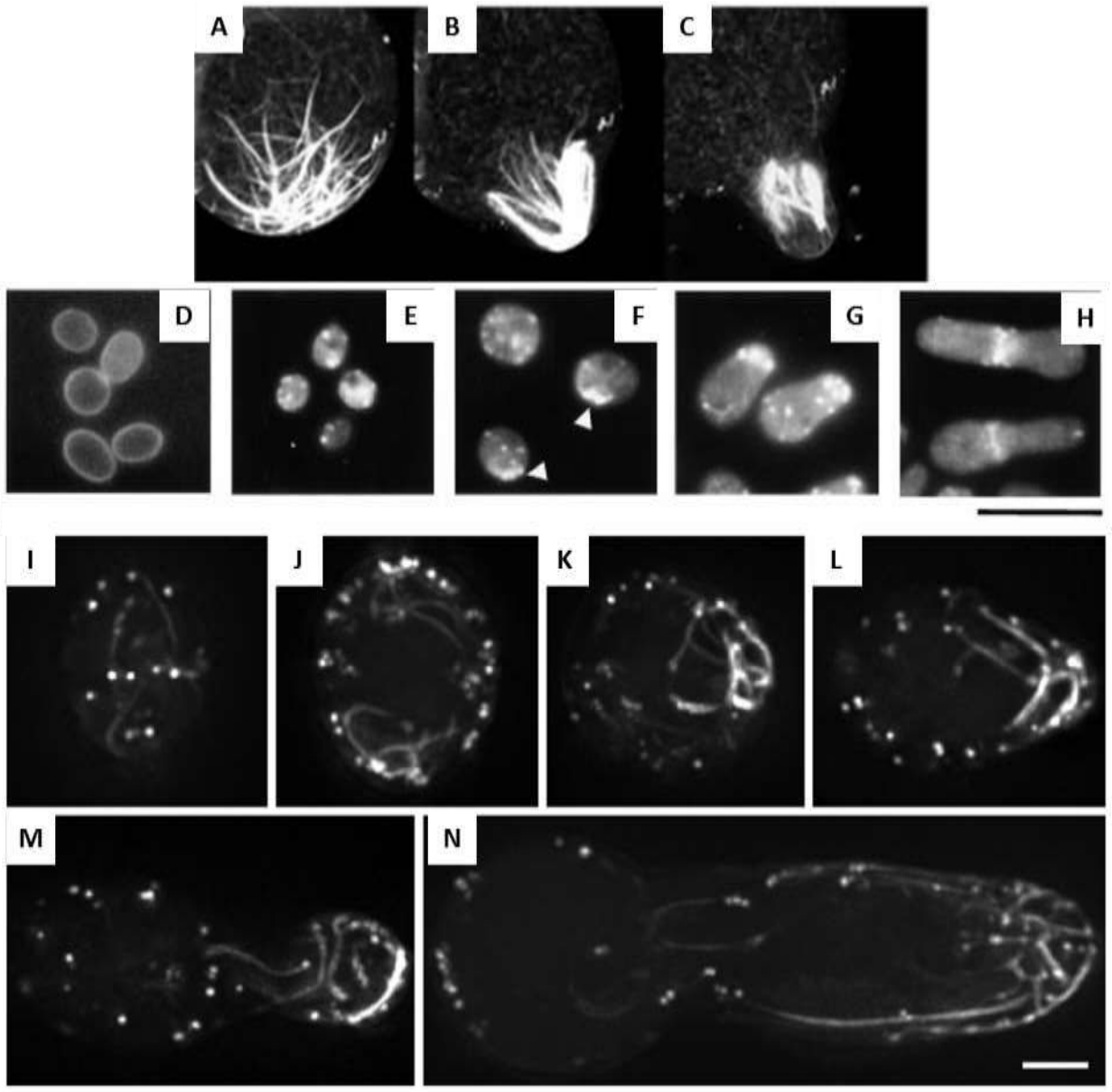

Figure 66: Examples of cytoskeleton remodeling during germination and outgrowth. ***A. B. C.*** Time course of cortical MT array reorganisation during *Fucus* rhizoid germination and growth (Corellou et al., 2005). ***D. E. F. G. H.*** Changes in the phalloidin staining pattern in wild-type fission yeast spores fixed after 2, 4, 6, 8 and 10 hours from nutrients addition. Arrowheads in c indicate localized actin patches (Hatanaka and Shimoda, 2001). Bar, 10 μm. ***I. J. K. L. M. N.*** F-actin remodelling in macroconidia of *N. crassa* expressing Lifeact-GFP. In an ungerminated spore, actin patches and cables are mostly associated with the cell cortex; F-actin arrays always mark the site of GT emergence, and finally persist at sites of active growth. Bar, 2 μm (Berepiki et al., 2010).

hyphae might play a role in sequestering polarity proteins (Cheng et al., 2001).

Dimorphic fungi can switch between polarized apical and isotropic growth. Dimorphic switching requires fungal cells to undergo changes in polarized growth in response to environmental stimuli and during cellular differentiation. *Penicillium marneffei* is an opportunistic human fungal pathogen which at 25C grows apically forming multinucleate, septate, branched hyphae which grow apically (Chan and Chow, 1990), whereas a temperature shift at 37C cell separation occurs along the septal plane to liberate single yeast cells, which are uninucleate and divide by fission. Conversely, upon switching from 37C to 25C, yeast cells elongate, cell and nuclear division uncouple to form multinucleate compartments and grow with a filamentous pattern (Andrianopoulos, 2002). In addition, this fungus is capable of asexual development at 25C, producing uninucleate spores on complex multicellular structures termed conidiophores: this mode of polarized growth differs from that of hyphal or yeast cells and involves cell budding. All these different modes of growth are regulated by in the interplay of three Rho-GTPases: the Ras homologue RasA (Ras), the Cdc42 homologue CflA and the Rac homologue CflB (Boyce et al., 2005).

Moreover, polarized growth for CAT-mediated cell fusion in *N. crassa* is strictly F-actin dependent (Berepiki et al., 2010), and probably involves spatial confinement of a specific polarity. When MTs are disrupted, fungal cells and hyphae still polarize but the corresponding tubes possess unstable polarity axes and are finally not straight, as in the case of fission yeast vegetative mutants in MTs or MT-associated factors (Horio and Oakley, 2005; Riquelme et al., 1998). However, these results rule out MT-mediated de novo deposition of landmark proteins, and thus strongly suggest a stochastic process for the initiation of polarized growth in these species (Lichius et al., 2011).

3.5.4.3 Spontaneous symmetry breaking: the role of mechanics

The process of germination and outgrowth is characterized by profound structural modifications of the spore wall: in the case of budding yeast, a first notable change is a considerable decrease in electron density of the structure, corresponding to typical swelling of the spore. Then, the surface layer is partially disrupted, and consequently the inner layer is exposed as the germinating spore elongates (Figure 67). The inner spore coat then gives rise to the newly grown cell wall, which is also of poorly electron dense and rich in (1,3)-β-glucan (Kono et al., 2005).

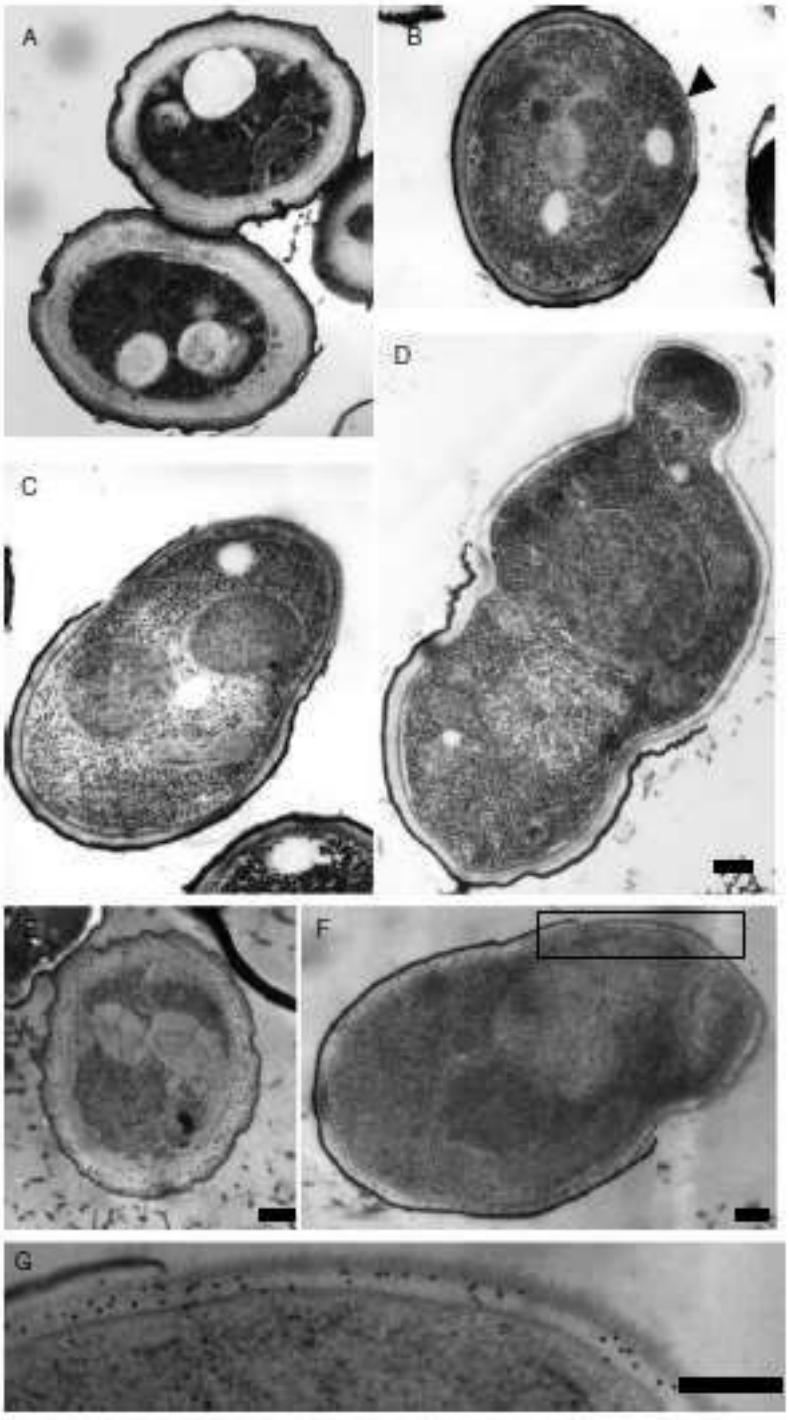

Figure 67: Electron micrographs of germinating spores. The wild-type spores were collected from germination culture at 0 min (A, E), 60 min (B), 120 min (F, G), 180 min (C) and 240 min (D) after germination induction. (G) is an enlarged image of (F). Scale bars = 200 nm. Arrowhead in B indicates the region where the outer layer is digested (Kono et al., 2005).

Local rupture or dissolution of the spore coat at the onset of outgrowth is a common feature of numerous organisms (Figure 68). In the case of *Bacillus subtilis*, the spore is encased in two coats (Santo and Doi, 1974): upon start of germination, the inner spore coat gets

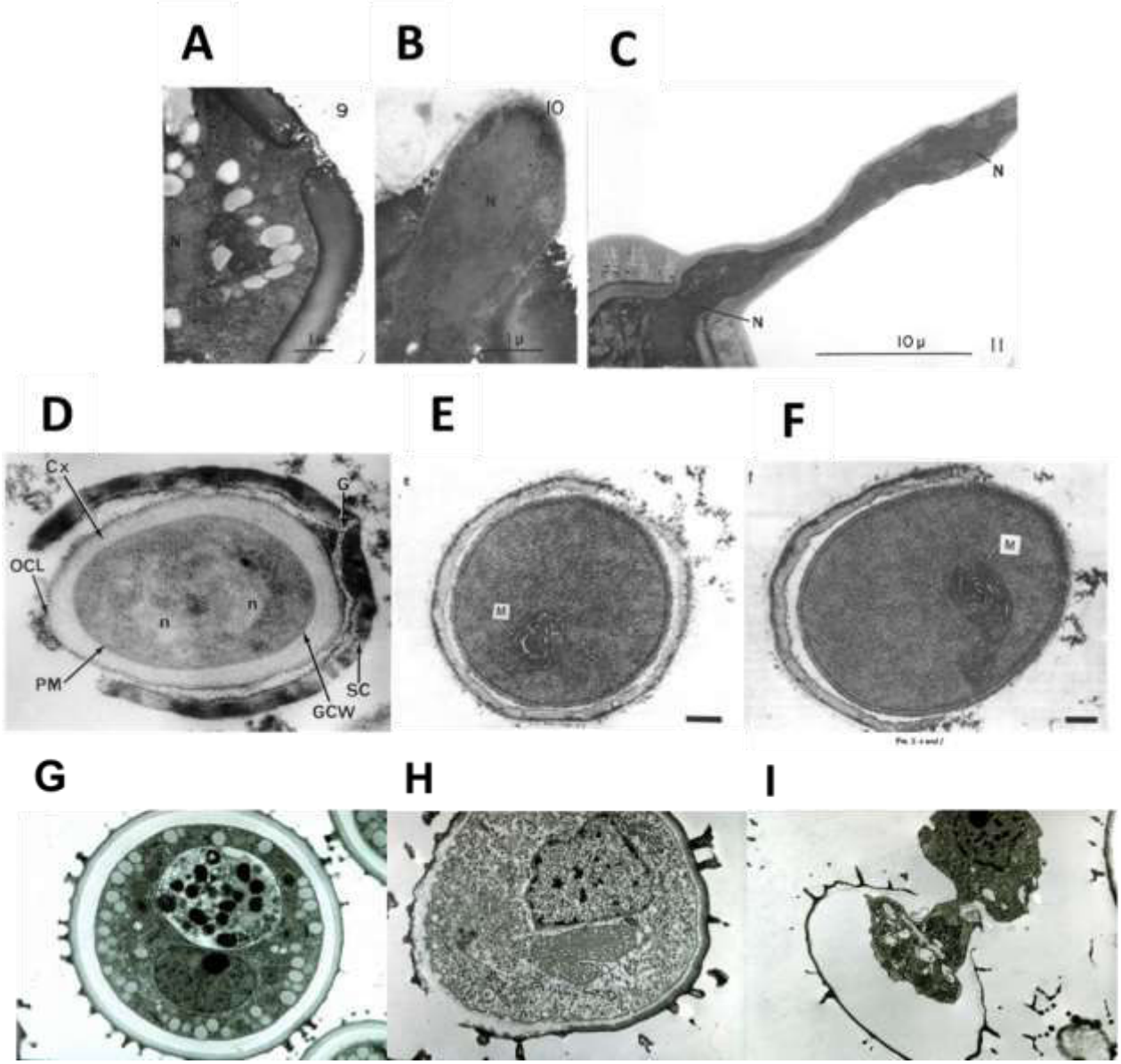

Figure 68: outgrowth corresponds to local rupture or dissolution of the outer spore coat. A. B. C. Aeciospores of *C. fusiforme* at different stages of germination. Note that a germ tube emerges through thin areas in the cell wall, called germ pores, that were dissolved or ruptured: the cytoplasm appears to flow out from the spore, together with nuclei (indicated with N) into the germ tube, concomitantly to synthesis of new cell wall (Walkinshaw et al., 1967). D. TEM of an outgrowing *Bacillus megaterium* spore showing the thick spore coat (SC), outer cortex layer (OCL) and cortex (Cx) germinal cell wall layer (GCW), underlying spore protoplast membrane (PM). Author: John H Freer, University of Glasgow, Scotland. E. F. TEM of *Bacillus subtilis* germinating and outgrowing spores. Scale bars, 0.1 μm (Santo and Doi, 1974). G. H. I. TEM of dormant, early germinating and late germinating spores of a Myxomycete. Author: Charles Mims

progressively nicked and weakened by the activity of some proteolytic enzymes at discrete and almost regular spaces around the spore (maybe deposited during sporulation), whereas the outer spore coat progressively thin out and is finally stripped away evenly. After 50 minutes, outgrowth occurs, so that the cell elongates and enters the first division: fragments of the outer spore coat often remain stuck at cell tips, suggesting that this structure behaves like a passive sticky shell.
All these observations suggest that mechanical anisotropy caused by the breakage may trigger the recruitment of the polarity machinery to initiate polarized growth.

Some fungal spores display one or more small pores in the outer coat, called germ pores, from which the germ tube exits upon germination, as in the case of *Neurospora crassa* and *Cronartium fusiforme* (Figures 68 and 69) (Seale, 1973; Walkinshaw et al., 1967): in the first case, the emerging tip is severely constricted at the pore but then blows out probably under the force of turgor pressure, and finally narrows to an average hyphal diameter, highlighting the ability of the cell to dynamically regulate its width. In the case of *Cronartium fusiforme*, incubation of ungerminated spores of this fungus in chitinase at 20-23C, allows specific disruption of the germ pore while the rest of the spore wall remains intact, resulting in the release of the spore content as a thin stream of protoplasm: these observations suggest that the germ pore can be considered as a weak spot in a very rigid shell, with a different chemical composition, which allows the cell to extrude out a germ tube.

Altogether, these observations highlight a possible feedback between mechanics and polarity for breaking symmetry during spore germination.

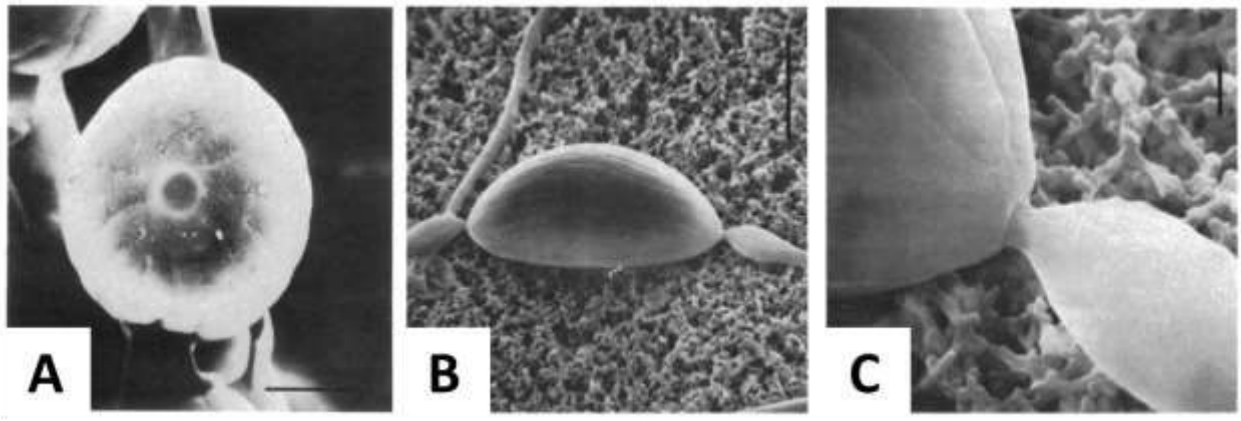

Figure 69: some fungal spores germinate through a germ pore. As an example, the ascospore of *N. crassa* in A. an end view during dormancy showing germination pore (scale bar, 5 μm); B. a top view and (scale bar, 10 μm) C. a close-up (scale bar, 1 μm) during germination (Seale, 1973).

3.6 Spore size control

Another possible explanation of how polarized growth is initiated in spores relies on a cell-size regulator: in other words, spores may need to reach a certain size to enter S phase and establish polarity. Moreover, *S. pombe* vegetative cells grow at one cell end in the early G2 phase and then at both ends through the rest of G2, whereas during spore outgrowth, unidirectional cell elongation occurs throughout the long G1 phase and even during the G2 phase. The question whether there is any link between cell size, cell cycle and polarity establishment in spore development remains to be explored.

RESULTS

1.

Symmetry breaking in spore germination relies on an interplay between polar cap stability and spore wall mechanics

1.1 Summary

Cell morphogenesis relies on the spatial organization of specific proteins and the cytoskeleton, *e.g.* cell polarity, and its coordination with cellular surface mechanics, in order to generate a specific shape. Spore germination represents an intriguing developmental process, during which small round cells reorganize to establish *de novo* their first polarity axis and initiate polarized growth; however, the mechanisms remain largely unknown.

In this work, I have developed novel approaches which integrate live-cell imaging, quantitative image analysis and mathematical modeling to understand how outgrowth is regulated in the genetically tractable unicellular organism fission yeast.

Very surprisingly, I have found that germinating spores first grow isotropically for about 6 hours before breaking symmetry and initiating polarized growth: in the first growth phase, a polarity domain is assembled at the membrane and wanders around, but growth is hindered by the presence of a mechanical barrier, the outer spore coat (Figure 70). Consequently, polarity is destabilized and the cap is disassembled and reassembled in different sites of the spore surface. As soon as the spore has grown enough, for instance has doubled in volume, the spore coat

reaches a certain threshold strain that allows its local rupture, resulting in polarity stabilization and outgrowth. Spore wall breakage and polarity establishment are linked, as the local fragilisation of the coat by laser ablation leads to stabilization of the polarity cap and inititation of polarized growth at smaller spores volumes. Numerical simulations allow to reproduce spore morphogenesis and to make predictions in different experimental conditions. This interdisciplinary approach sheds light on a novel general principle which links cell polarity to cell growth.

In conclusion, the developmental morphogenesis of single spores is a great example of a self-organizing process regulated by the interplay between cell polarity and cell mechanics

Highlights

- Gradual growth of fission yeast spores determines an abrupt developmental transition
- Mechanical stress caused by spore growth ruptures the outer spore wall (OSW)
- OSW rupture converts an initial unstable wandering polarity into stable polarization
- OSW rupture thus locks self-organizing polarity for subsequent growth and developmen

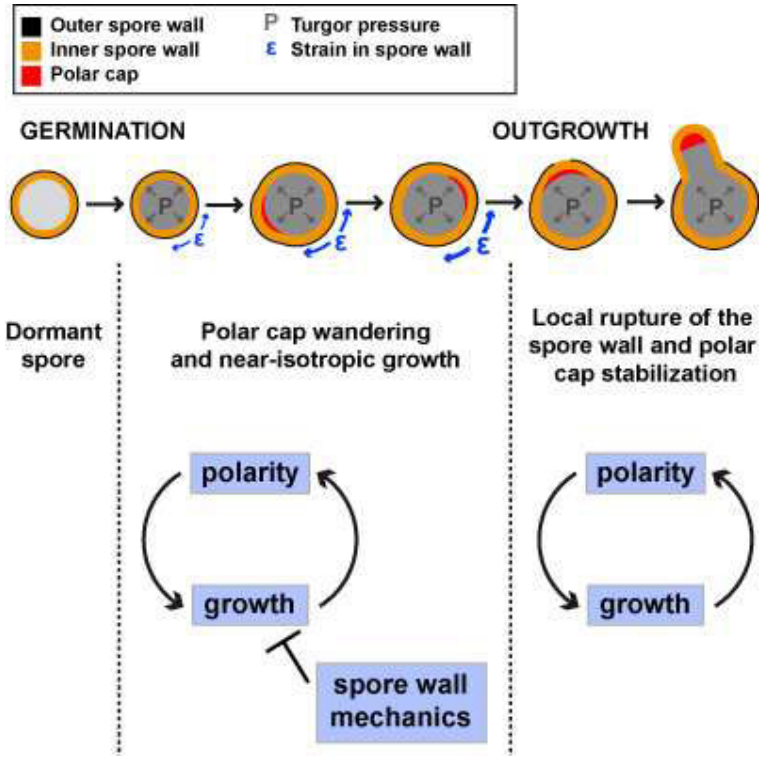

Figure 70: schematic of the mechanism for fission yeast spore germination and outgrowth.

1.2 Paper

Bonazzi Daria, Julien Jean-Daniel, Romao Maryse, Seddiki Rima, Piel Matthieu, Boudaoud Arezki, Minc Nicolas:

Symmetry Breaking in Spore Germination Relies on an Interplay between Polar Cap Stability and Spore Wall Mechanics;

(2014); *Dev Cell*; 28(5):534-46.

Developmental Cell
Article

Symmetry Breaking in Spore Germination Relies on an Interplay between Polar Cap Stability and Spore Wall Mechanics

Daria Bonazzi,[1,2,6] Jean-Daniel Julien,[3,4,5,6] Maryse Romao,[2] Rima Seddiki,[1] Matthieu Piel,[2] Arezki Boudaoud,[3,5,*] and Nicolas Minc[1,*]
[1]Institut Jacques Monod, 15 rue Hélène Brion, 75205 Paris Cedex 13, France
[2]Institut Curie, UMR 144 CNRS/IC, 26 rue d'Ulm, 75248 Paris Cedex 05, France
[3]Laboratoire Joliot-Curie, CNRS, ENS de Lyon, Université de Lyon, 46 Allée d'Italie, 69364 Lyon Cedex 07, France
[4]Laboratoire de Physique, CNRS, ENS de Lyon, UCBL Lyon I, 46 Allée d'Italie, 69364 Lyon Cedex 07, France
[5]Reproduction et Développement des Plantes, INRA, CNRS, ENS de Lyon, UCBL Lyon I, 46 Allée d'Italie, 69364 Lyon Cedex 07, France
[6]These authors contributed equally to this work
*Correspondence: arezki.boudaoud@ens-lyon.fr (A.B.), minc@ijm.univ-paris-diderot.fr (N.M.)
http://dx.doi.org/10.1016/j.devcel.2014.01.023

SUMMARY

The morphogenesis of single cells depends on their ability to coordinate surface mechanics and polarity. During germination, spores of many species develop a polar tube that hatches out of a rigid outer spore wall (OSW) in a process termed outgrowth. However, how these awakening cells reorganize to stabilize this first growth axis remains unknown. Here, using quantitative experiments and modeling, we reveal the mechanisms underlying outgrowth in fission yeast. We find that, following an isotropic growth phase during which a single polarity cap wanders around the surface, outgrowth occurs when spores have doubled their volume, concomitantly with the stabilization of the cap and a singular rupture in the OSW. This rupture happens when OSW mechanical stress exceeds a threshold, releases the constraints of the OSW on growth, and stabilizes polarity. Thus, outgrowth exemplifies a self-organizing morphogenetic process in which reinforcements between growth and polarity coordinate mechanics and internal organization.

INTRODUCTION

Organisms ranging from bacteria to fungi and plants can produce spores. These are dehydrated cells adapted for survival in harsh environments over very long periods of time ranging from weeks to thousands of years in some bacteria (Cano and Borucki, 1995; McKenney et al., 2013; Neiman, 2005). Spore resistance is associated with a rigid protective extracellular shell deposited at sporulation, called the outer spore wall (OSW) or spore coat (Arellano et al., 2000; García et al., 2006; Klobutcher et al., 2006; Wallace et al., 2011). Once conditions are favorable, spores germinate to exit dormancy, resume growth, and develop a single polarized tube that hatches out of the OSW, in a process termed outgrowth (Hatanaka and Shimoda, 2001; Kono et al., 2005; Pandey et al., 2013). Because of its particular cell cycle, de novo protein synthesis, and exit from prolonged period of dormancy, outgrowth poses an outstanding morphogenetic puzzle, which is to understand how these awakening symmetric cells may reorganize their interior to stabilize their very first polarized growth axis.

Polarized growth involves the formation of cortical polar caps of the GTP-bound form of a GTPase, such as Cdc42p in yeast (Drubin, 1991). These caps may be spatially stabilized by extrinsic cues, or can self-assemble at random positions by positive feedback (Drubin, 1991; Howell et al., 2012; Wedlich-Soldner et al., 2003; Wu and Lew, 2013). Yet, it becomes increasingly clear that mechanisms regulating cap establishment and/or stabilization may largely vary between different periods of cellular life cycles, even in a single given organism (Bendezú and Martin, 2013; Das et al., 2012; Dyer et al., 2013; Wu and Lew, 2013). In yeast and fungal cells, polar caps serve as platforms to direct local membrane addition and cell-wall remodeling, needed for surface expansion (Chang and Martin, 2009; Drubin, 1991). Growth itself involves mechanical work from high internal osmotic pressure that allows deforming newly synthesized cell wall (Bastmeyer et al., 2002; Boudaoud, 2003; Minc et al., 2009a). Thus, the morphogenesis of these single cells ultimately relies on an integration of biochemical and biomechanical signals (Harold, 1990; Slaughter and Li, 2006).

Here, we use quantitative time-lapse microscopy to understand how single spores break symmetry to become rod shaped in the model fission yeast *Schizosaccharomyces pombe*. We show that germination is followed by a long period of near-isotropic growth during which a single polar cap of active-cdc42p wanders around and drives small local growth sites that fail to progress, disassemble, and reform at a new position. We demonstrate that this unstable behavior is associated with the presence of the rigid OSW, which acts as a mechanical barrier that hinders growth and destabilizes polarity, and that cap stabilization occurs at outgrowth when the OSW ruptures. We develop a computational model that fully reproduces spore development in silico. This work demonstrates that the switch in polar cap stability at outgrowth can be explained by a simple positive-feedback loop between growth and polar cap stabilization.

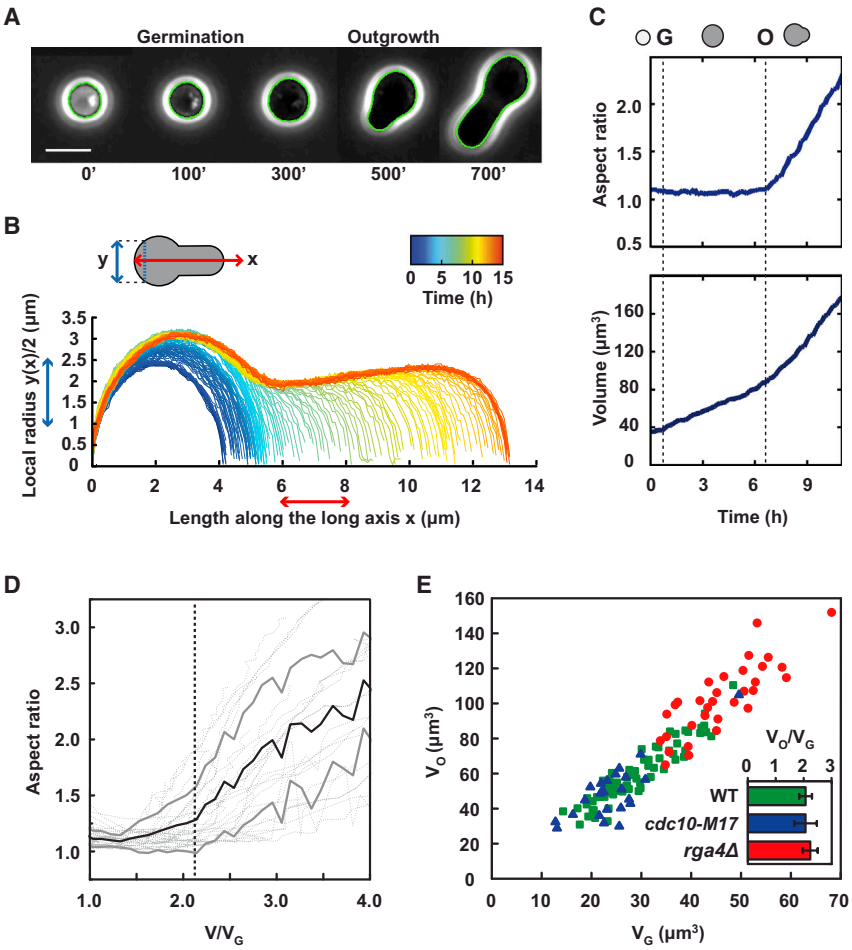

Figure 1. Spore Outgrowth Onset Correlates with a Robust Size-Increase Threshold

(A) Phase-contrast time-lapse superimposed with automated shape contour detection of a wild-type fission yeast spore germinating and outgrowing.

(B) Morphogenetic plot representing the temporal evolution of cell morphogenesis.

(C) Evolution of single-cell aspect ratio and volume as a function of time.

(D) Integrated morphogenesis at the population level (n = 25 spores). The black line depicts the averaged cell aspect ratio as a function of the averaged cell volume normalized with the volume at germination. Thick gray lines delimit the SD, and thin gray lines are plots arising from individual spore morphogenesis tracking.

(E) Volume at the onset of outgrowth, V_0 plotted as a function of the volume at germination, V_G. These volumes are measured from time-lapse phase images. The onset of outgrowth is defined as the inflexion point of the aspect ratio curve. Green, blue, and red data points, respectively, correspond to single WT, *cdc10-M17* at restrictive temperature (37°C), and *rga4Δ* spores. Error bars represent SDs. Scale bars, 5 µm. See also Figure S1 and Movies S1 and S2.

RESULTS

The Developmental Morphogenesis of Single Fission Yeast Cells

We quantitated the morphogenetic development of single fission yeast spores by performing long (over 10 hr) time-lapse phase-contrast microscopy with frequencies down to 5 min (Figure 1A; Movie S1 available online). Spores were rapidly transferred from starvation media to agar pad containing rich media. Phase contrast allowed delineating germination onset, which is characterized by a bright-phase to dark-phase transition (Figure S1A) (Hatanaka and Shimoda, 2001). Spores then grew in a near-isotropic manner for about 6–8 hr and entered outgrowth, which corresponds to the definition and stabilization of the first polarized growth axis characterizing the rod-shaped fission yeast cell (Hatanaka and Shimoda, 2001) (Figure 1A). The cells then kept on growing for another 3–4 hr before entering mitosis. Outgrowing cells kept their bottle-like shape and remained monopolar, growing away from the spore body for several cell cycles (Movie S2). Phase images were segmented and analyzed to quantitate single spore dimensions, aspect ratios, and volumetric growth rates (Figures 1B–1D; Experimental Procedures). At outgrowth, the aspect ratio depicted a sharp increase, which marked the extension of the polarized tube, and single-cell growth rates also increased abruptly by a factor of 2.4 ± 0.4 on average (Figure S1B).

Outgrowth Onset Is Associated with a Robust Fold Change in Cell Size

We used this approach to investigate whether outgrowth could correlate with an internal timer, a size increase, or a specific spore size (Mitchison and Nurse, 1985). The absolute time from germination to outgrowth depicted cell-to-cell variation of around 30% in the same field of observation. Not surprisingly, this timing was also largely dependent on temperature, humidity, as well as strain background (data not shown). We thus used cell volume as an indicator of spore developmental progression, to generate an averaged morphogenetic development at the cell population level (Figure 1D). This analysis revealed that the onset of outgrowth correlated with a fixed spore volume increase. We thus computed the volume at germination (V_G) and at the onset of outgrowth (V_O) for individual spores. This showed that the volume at outgrowth can vary up to 3- to 4-fold in a wild-type (WT) population and revealed a linear scaling between V_O and V_G (R^2 = 0.87) with a slope of 2.07 ± 0.12 (n = 67). This scaling was similar in spores with larger initial volumes like those produced by the fat mutant *rga4Δ* (volume ratio, $< V_O/V_G > =$ 2.22 ± 0.13, n = 32) (Figure 1E) (Das et al., 2007; Tatebe et al., 2008). This size increase was also independent on G1/S cell-cycle transition, which is known to occur around these stages of spore development (Hatanaka and Shimoda, 2001; Mitchison and Nurse, 1985), as spores of the *cdc10-M17* mutant, which arrest in G1 at restrictive temperature (Nurse et al., 1976), depicted similar volume ratios ($<V_O/V_G> = 2.07 \pm 0.20$, n = 23) (Figures 1E, S1C, and S1D). Thus, outgrowth correlates with spore

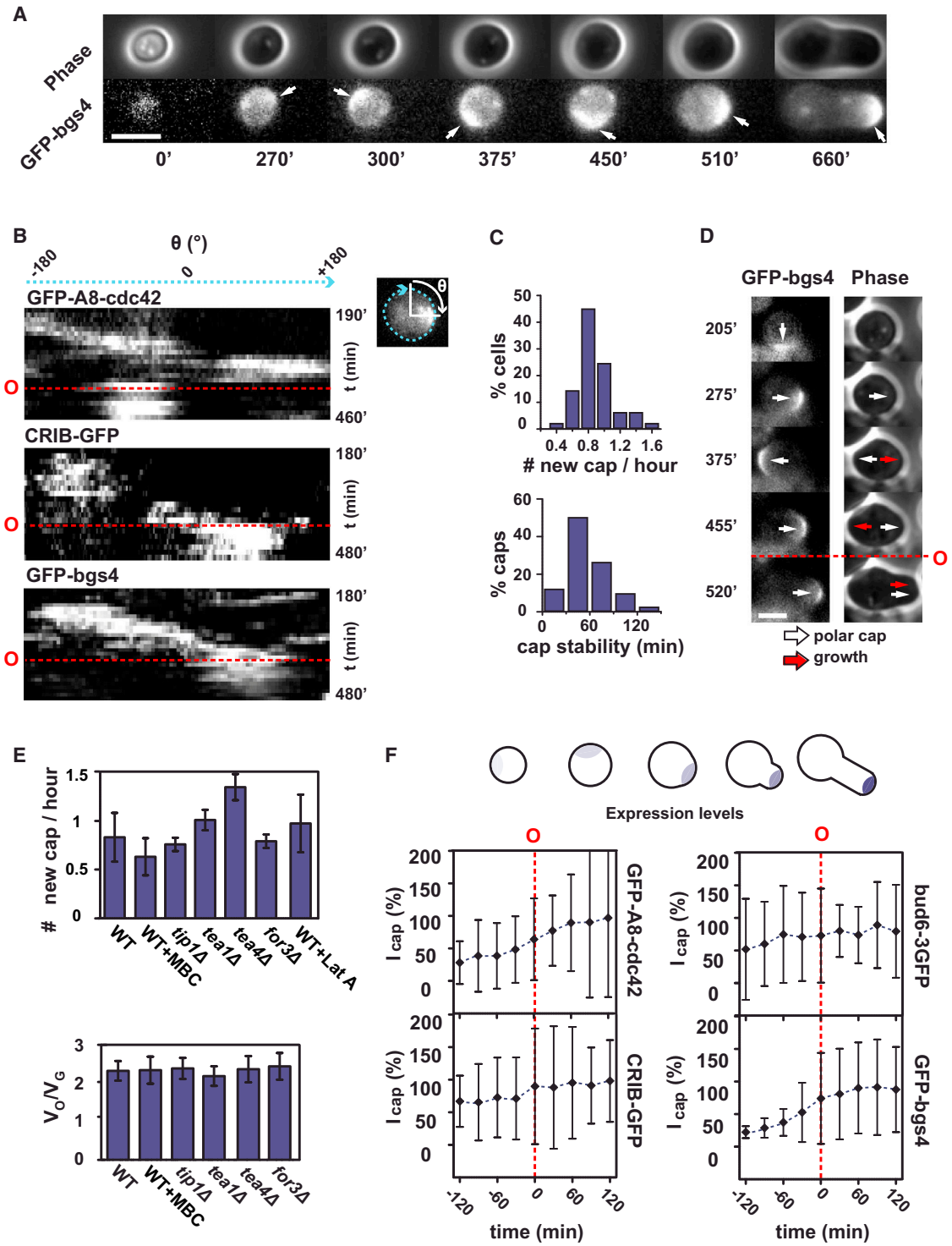

Figure 2. A Polarity Cap Wanders around the Symmetric Spore and Finally Stabilizes to Promote Outgrowth

(A) Time-lapse phase-contrast and epifluorescence images of a developing spore expressing the polarized growth marker GFP-bgs4. White arrows point at newly assembled caps.

(B) Cell kymographs representing the changes of localization over time of the polarity factors GFP-A8-cdc42, CRIB-GFP (a marker for active GTP-cdc42), and GFP-bgs4. Kymographs for GFP-bgs4 and GFP-A8-cdc42 are computed from epifluorescence time lapse, whereas those for CRIB-GFP are computed from confocal single midslices.

(C) Quantification of polar cap frequency and stability in time (n = 50 spores). A new polar cap is defined as a newly assembled cap at a different location than the previous one. Final stable outgrowth caps are not counted. Cap stability corresponds to the time between assembly and disassembly.

(legend continued on next page)

volume doubling, independently of absolute size or cell-cycle progression.

A Wandering Polar Cap Becomes Stable at Outgrowth

To understand polarity establishment and stabilization in spores, we then imaged fluorescently tagged canonical polarity markers throughout spore development. For polarized growth, vegetative fission yeast cells assemble clusters of polarity proteins into a polar cap at their growing tips (Chang and Martin, 2009). This cluster includes the small GTPase cdc42p, actin regulators, and cell-wall remodeling factors, which promote tip growth. We followed the localization of GFP-tagged cdc42p (Rincón et al., 2009) and its active GTP-bound form using the CRIB-GFP fusion (Tatebe et al., 2008), the actin-associated marker bud6-3GFP (Glynn et al., 2001) and the membrane glucan synthase GFP-bsg4, which marks sites of cell-wall synthesis (Cortés et al., 2005). Strikingly, all these factors assembled into a single cap long before outgrowth (first visible between 1 and 3 hr after germination), which disassembled and reassembled at successive locations, yielding a stochastic wandering motion around the spore surface, and finally stabilized to promote outgrowth (Figures 2A, 2B, S2A, and S2B; Movie S3). In some cases, the polar cap completely disassembled to reform at a new location, whereas, in other cases, the cap displayed local sliding or rearrangement in a restricted area of the spore surface (Movie S3). This unstable behavior was reminiscent of oscillating states of polarity in budding yeast, vegetative fission yeast, and in adherent mammalian cells (Bendezú and Martin, 2012, 2013; Das et al., 2012; Fink et al., 2011; Howell et al., 2012; Wedlich-Soldner et al., 2003). However, in these spores, a large fraction of caps appeared to be stable for a comparatively longer time period (ranging from 30 to 90 min) (Figure 2C). This yielded an average frequency of about 0.75 newly assembled caps per hour and a total of three to four transient unstable caps visible in the plane of focus between germination and outgrowth. We did not note dampening of cap wandering behavior before stabilization. Rather, the transition between wandering and definitive docking of the cap appeared to be abrupt in most cases (Figures 2B and S2A).

Importantly, all these polarity components colocalized two by two, and cowandered together (Figure S2C). In addition, transient cap formation led in ~65% of cases to small localized growth sites that extended out of the rounded spore and failed to progress (Figure 2D; Movie S4). Local growth followed the assembly of a new GFP-bgs4 polar cap with a time delay ranging from 5 to 20 min typically (Figure 2D; Movie S4). Thus, the upstream polarity machinery appears to be properly assembled and competent for polar growth soon after germination, but destabilizing elements may hinder polarity maintenance until the spore has increased its volume sufficiently.

Cap Stabilization Does Not Involve NETO Factors, Memory Cues, or Polarity Protein Levels

We next tested if elements that spatially stabilize polarity in vegetative cells could contribute to cap maintenance at outgrowth. One class of such characterized factors are those that promote polarity establishment at the new end (NETO, New End Take Off) in vegetative cells, such as microtubules (MTs) and MT + TIP factors (Chang and Martin, 2009). MTs in spores were short and disorganized until after outgrowth, and treatment with a microtubule-inhibitory drug (MBC), which blocks MT polymerization in spores and cells neither blocked wandering nor altered volume-doubling required for stabilization. In addition, mutants in MT-based polarity pathways defined by tip1p, tea1p, and tea4p and mutants defective in actin cables assembly such as in the formin for3p all showed similar behavior as WT (Figures 2E, S3A, S3C, and S3E). Complete depolymerization of actin with Latrunculin A halted spore growth but did not block wandering, as seen in other cell types exhibiting polarity oscillations (Figures 2E, S3B, and S3D) (Howell et al., 2012).

Cap stabilization did not appear to involve fixed spatial cues in the spore (Chang and Martin, 2009; Drubin, 1991). Spores that remained attached to each other assuming the shape of the mother ascus outgrew along an axis independent of the previous meiotic division axis (Figure S3F; Movie S5). Additionally, in a subset of time lapses we saw the polar cap exploring several times the incipient site of outgrowth, before stabilizing (see Movie S4, for an example). These data suggest that outgrowth involves different polarity stabilizing elements than in vegetative cells.

We also quantified the concentration of these polarity factors in the cap with confocal microscopy, to test a hypothesis in which polarity proteins that are being de novo synthesized in spores may need to reach a saturating level to stabilize. This showed that the expression levels were noisy with 5- to 10-fold variations in protein concentration at the cap between different spores at a given time, so that some outgrowing spores could display concentrations lower than spores at earlier stages. Also, the overall increase in expression did not obviously saturate at outgrowth and continued to rise until the first mitosis (Figure 2F). Although these data do not rule out the existence of a concentration threshold in an uncharacterized cytoplasmic factor that may stabilize the cap, they do not support a cap maturation model needed for stabilization.

The Outer Spore Wall Encases the Spore and Displays a Singular Rupture at Outgrowth

We thus turned our attention to factors that are specific to this spore-to-cell transition. One specific feature of spores is the encasing OSW. The fission yeast OSW is deposited onto the inner cell wall during sporulation, and is also composed of polysaccharides, but it features different crosslinking and the

(D) Time-lapse phase-contrast and fluorescence images of GFP-bgs4 cap wandering and corresponding local growth site.
(E) Frequency of newly assembled successive GFP-bgs4 polar caps, in the indicated conditions and mutants, and corresponding outgrowth volume ratio V_0/V_G ($n > 25$ spores for each condition).
(F) Quantification of changes in fluorescence levels of different polarity factors (see Experimental Procedures): GFP-A8-cdc42, CRIB-GFP, bud6-3GFP, and GFP-bgs4 from 2 hr before to 2 hr after outgrowth ($n > 10$ spores for each marker). Error bars represent SDs.
Scale bars, 5 μm. See also Figures S2 and S3 and Movies S3 and S4.

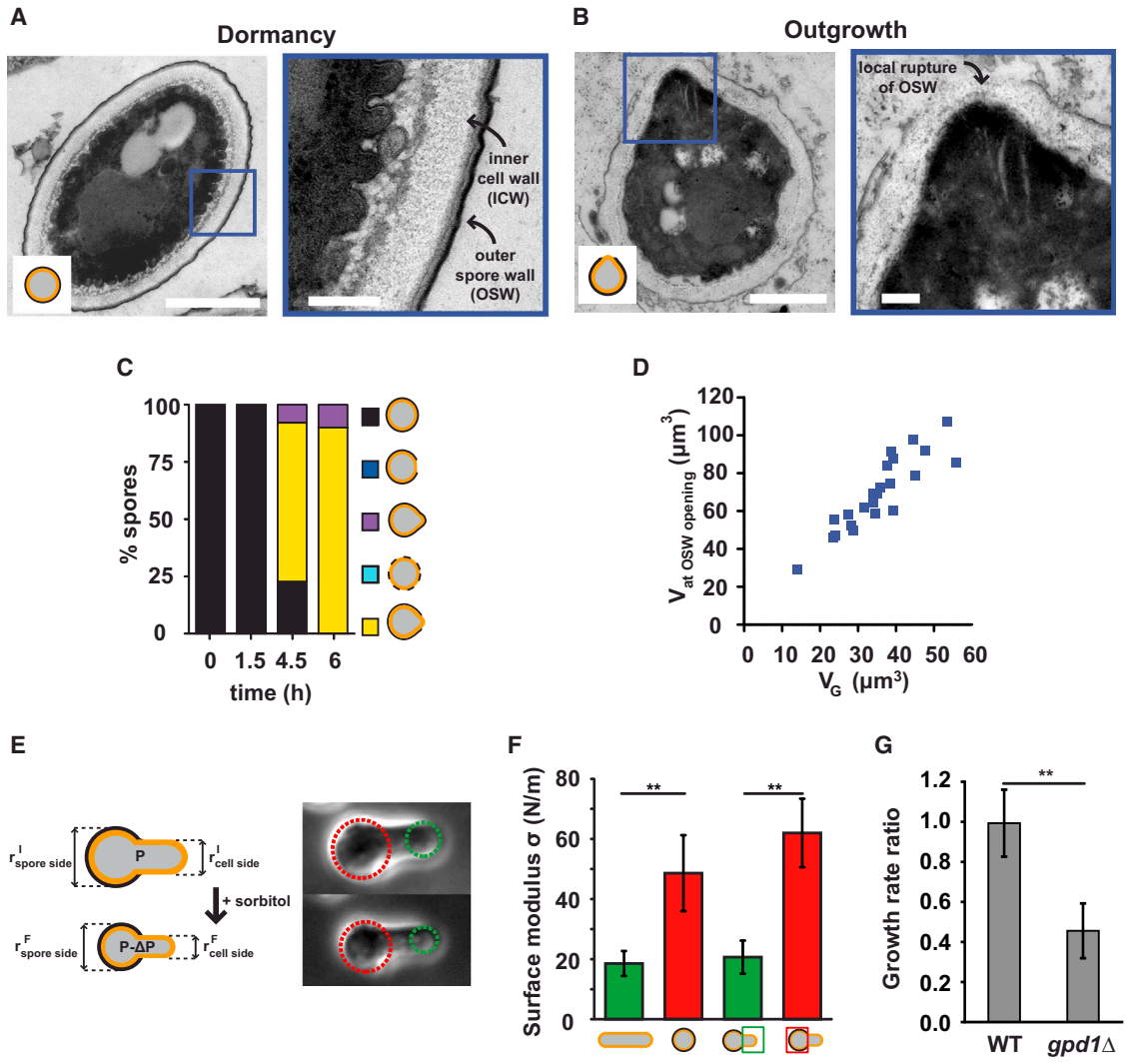

Figure 3. The Outer Spore Wall Is Rigid and Displays a Singular Rupture at the Time and Location of Outgrowth

(A) Transmission electron microscopy picture of a dormant spore and corresponding close-up view on OSW.

(B) Outgrowing spore after 6 hr of incubation at 30°C and corresponding close-up view on the outgrowth site, which displays a local rupture in the OSW (scale bars in large view, 1 µm; and in close-ups, 200 nm).

(C) Quantification of the phenotypes of outer wall rupture at different times from germination (n = 52 spores).

(D) Volume at the moment of OSW rupture, as assayed by growing spores in medium supplemented with an inner/vegetative cell-wall digestion mix, plotted as a function of the volume at germination for WT spores.

(E) Stress-strain approach used to measure the elastic properties of the inner and outer wall.

(F) Cell-wall surface moduli for vegetative cells, spores, and the two sides of an outgrown spore (n > 10 cells or spores).

(G) Ratio between growth rate before and after treatment with sorbitol measured in WT and *gpd1Δ* spores (n = 7 spores for each condition). Error bars represent SDs.

**p < 0.01, Student's t test. See also Figure S3.

presence of chitin, both of which may confer atypical properties that allow this layer to protect spores from harsh environment (Arellano et al., 2000; García et al., 2006; Tanaka and Hirata, 1982). We visualized the OSW at gradual time intervals using transmission electron microscopy (TEM). In dormant spores, the OSW was visible as a homogeneous electron-dense multilayered structure, about 15–20 nm thick. This thickness remained nearly constant throughout development (data not shown). Yet, we noted that the OSW often appeared wrinkled at early stages and flatter at later stages (Figures 3A and S4A), suggesting that these wrinkles may unfold as a result of spore growth, without drastic remodeling of the OSW.

Interestingly, at timing corresponding to outgrowth, we observed a local rupture/dissolution of the OSW at the site of tip emergence (Figures 3B, 3C, and S4A). Rupture of the wall was only obvious in spores with an outgrowing tip, and we did not note major opening at earlier time points, or at sites away from the growth zone. At later time points, the OSW appeared

to remain intact at the back of the outgrown cell (Figure S4A). By contrast, the inner cell wall appeared to be continuous with the emerging vegetative cell wall. To monitor the opening of the OSW in live spores, we grew spores in medium supplemented with an inner/vegetative wall digestion enzyme mix, which rapidly causes the death of outgrown spores and vegetative cells but does not affect spores protected by an intact OSW (Figure S4B). Spores developed normally in the enzyme mix and abruptly died at a volume ratio of $< V_{OSW\ opening}/V_G > = 1.97 \pm 0.22$ (n = 24) (Figures 3D and S4B), suggesting that the OSW opens when spores have doubled their volume. Thus, outgrowth is concomitant with a singular rupture in the OSW at the site of polar tube emergence.

The Outer Spore Wall Is Very Stiff and May Hinder Growth

To understand how the OSW may influence spore development, and how it may rupture at outgrowth, we assessed its mechanical properties using cellular stress-strain experiments (Figures 3E and S4C). This assay consists in applying a dose-dependent negative osmotic pressure by rinsing cells placed in microfluidic chambers with different concentrations of sorbitol and measuring the consequent changes in local curvature (see Experimental Procedures) (Misra et al., 2013). This assay showed that the OSW behaves as an elastic material whose surface modulus is approximately 2.3 times larger than that of the inner cell wall, yielding a bulk modulus 30 times larger (Figures 3E and 3F; Experimental Procedures). These properties remained nearly constant even after rupture (Figure 3F). Thus, the OSW is much stiffer than the inner/vegetative cell wall.

The presence of this rigid structure encasing the spore may influence growth, by reducing the effective stress generated by internal turgor pressure on the remodeling inner wall (Minc et al., 2009a). To test this, we reduced turgor by changing external osmolarity in a *gpd1Δ* mutant, which impairs osmoadaptation and found that this led to a significant reduction in growth rate, suggesting that growth in spores is powered by internal turgor as in vegetative cells (Minc et al., 2009a) (Figure 3G). We note that the simplest model for pressure-driven growth in walled cells predicts that growth rates are proportional to the surface modulus of the wall (Minc et al., 2009a). The changes in growth rate at outgrowth (increase by a factor 2.4; Figure S1B) are indeed comparable to the ratio between OSW and inner/vegetative cell-wall surface moduli ($\sigma_o/\sigma_i \approx 2.3$). Thus, these data suggest that the OSW may act as a mechanical barrier that slows down growth.

A Computational Model Reproduces Spore Morphogenesis and Predicts Variations in Outgrowth Onset with Changes in Wall Mechanics

Because the OSW is not majorly remodeled during spore development and behaves as an elastic material, it may accumulate elastic strain (equivalently mechanical stress) as the spore volume increases. As for most materials, the OSW may rupture if this strain exceeds a threshold that corresponds to the local failure stress (also known as ultimate strength of the material), and the volume increase needed to rupture it at outgrowth may relate to this threshold in strain (Figure 4A). To test this hypothesis, we developed numerical simulations of growing spores, using the following assumptions: (1) growth is powered by turgor pressure, (2) the inner wall is viscoelastic over the polarity cap because of remodeling, and elastic outside the cap (Minc et al., 2009a), (3) the OSW is elastic but may rupture when elastic strain (equivalently mechanical stress) exceeds a threshold, and (4) the cap center undergoes a random walk, which we use as a proxy for cap wandering by successive assembly/disassembly (Figure 4A; Supplemental Model). In simulations, we observed that spores remained roughly spherical until the OSW ruptured at a specific location, after which a polar tube began to elongate (Figures 4B and S5A; Movies S6 and S8). Starting from various initial conditions (n = 50 simulations), we found that the OSW ruptured when the ratio of spore volume to initial volume exceeded a well-defined threshold, thus reproducing experimental behavior (Figure 4C). In the model, this outgrowth threshold increased with the elastic strain (equivalently mechanical stress) threshold for OSW rupture and with the ratio of elastic moduli between OSW and inner wall (Figures 4D and S5B).

Mutants with Defective Spore Wall Hasten Outgrowth

A direct prediction of this mechanical model is that spores with defective spore wall structure or mechanical properties should outgrow at smaller volume ratio than wild-type spores. To test these aspects, we characterized spore wall mechanics and spore development in two mutants specifically defective in spore wall synthesis: *mok13Δ*, a mutant in an α-glucan synthase (García et al., 2006) and *chs1Δ*, a mutant in a chitin synthase (Arellano et al., 2000). These mutants depicted a marked reduction in the surface modulus of the OSW but no major difference in inner wall mechanics (Figure 4E), and indeed did outgrow at volume ratios that were significantly lower than WT: $< V_O/ V_G > = 1.46 \pm 0.10$ (n = 58) for *mok13Δ* and $< V_O/ V_G > = 1.57 \pm 0.11$ (n = 36) for *chs1Δ* (Figure 4F). This suggests that OSW mechanical properties contribute to the timing of outgrowth.

A Single Polar Cap Is Required for Singular Rupture in the OSW

An additional prediction of the model is that the threshold for rupture at outgrowth is first attained at the polar cap location, because mechanical stress in the OSW is enhanced by local growth (Figure 4A). Accordingly, simulations predicted that the OSW should rupture at many sites if growth is diffuse and not restricted to a single cap (Figure 5A). To experimentally test this, we assayed spores of the *orb6-25* mutant, a mutant in the NDR kinase orb6p, which shuts off polarity establishment at a downstream level when grown at restrictive temperature (Das et al., 2009). These spores grew in a perfectly isotropic manner, with polarity factors diffusely distributed around the surface, and remained round many hours after the typical timing corresponding to WT outgrowth (Figures 5B and 5C). We then performed TEM at different time points and indeed observed that, 6 hr after germination, this mutant presented multiple sites of spore wall rupture (Figure 5D). The number and size of holes in the OSW increased over time, as in the simulations (Figures 5E and S5D). Initial opening of the OSW in this mutant appeared at a volume ratio of $< V_{OSW\ opening}/V_G > = 2.18 \pm 0.40$ (n = 24), slightly higher than WT (Figure S5C).

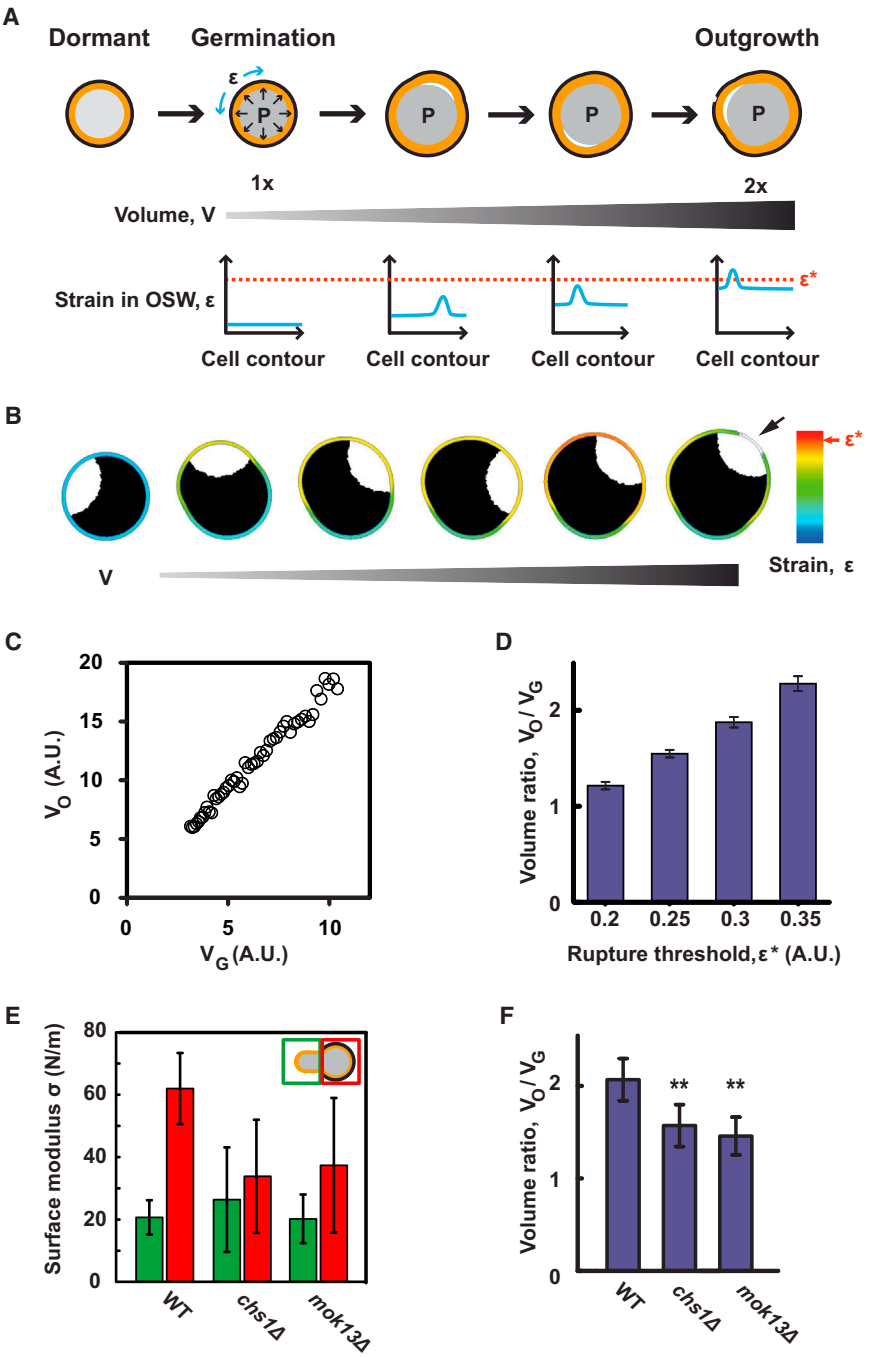

Figure 4. A Mechanical Model of Stress in the Outer Spore Wall Predicts Size-Increase Threshold for Wall Rupture and Outgrowth

(A) Schematic representing the geometry and inputs of the mechanical model. The spore grows under pressure, and is enclosed within the inner wall (orange) and the OSW (black). Growth is restricted to the polar cap. The OSW is under elastic strain ε, which increases globally as the spore grows, and locally at sites of polarized growth. The OSW ruptures above an elastic strain threshold ε^* corresponding to the failure stress of the material.

(B) Spores growing in silico. Colors in the OSW correspond to local strain values. Elastic moduli are assumed to be constant, and therefore the color code for strain also indicates the stress in the OSW.

(C) Theoretical prediction of volume doubling at outgrowth for a specific value of the threshold for rupture (n = 50 simulations).

(D) Dependence of volume ratio on the rupture threshold.

(E) Surface moduli for the walls on the spore (red bars) and cell (green bars) sides in outgrown spores of WT and *chs1Δ* and *mok13Δ* mutants (n > 10 spores for each condition).

(F) Volume ratios between outgrowth and germination for WT, *chs1Δ*, and *mok13Δ* mutants (n > 30 spores for each condition). Error bars represent SDs.

**p < 0.01, Student's t test. See also Figure S5 and Movie S6.

Thus, our mechanical model can predict both temporal and spatial rupture in the OSW at outgrowth and suggests a picture in which local growth at the cap locally increases the stress in the OSW until the failure stress is reached and the OSW ruptures (Figure 4A).

Local Laser-Induced Fragilization of the OSW Is Sufficient to Trigger Polar Cap Stabilization and Outgrowth

We next asked if the rupture in the OSW at outgrowth could influence polar cap stabilization. To directly assess this hypothesis, we developed a UV-laser assay to weaken the OSW with an intense pulse concentrated at a diffraction-limited spot on the spore surface. We optimized this assay to selectively weaken the OSW but not the inner wall (Figures S4B, S5E, and S5F; Experimental Procedures). We then filmed spores expressing GFP-bgs4 at early time points after germination and ablated the OSW either away from the polarity cap or at its exact location. Strikingly, the fragilization of the OSW at the cap caused it to stabilize and promoted the extension of a polarized tube at timings and volumes much smaller than in control nonablated spores in the same field of view (Figures 6A and 6B; Movie S7). Importantly, this effect was likely due to the mechanical fragilization of the OSW and not to a stress-activated recruitment or stabilization of polarity components (Kono et al., 2012). Spores ablated away from the cap did not show obvious recruitment at ablation sites and kept on wandering to stabilize at an independent location at similar timing and volumes as nonablated controls. These data suggest that the OSW has destabilizing effects on polarity, and that rupturing the OSW is sufficient to trigger cap stabilization and outgrowth.

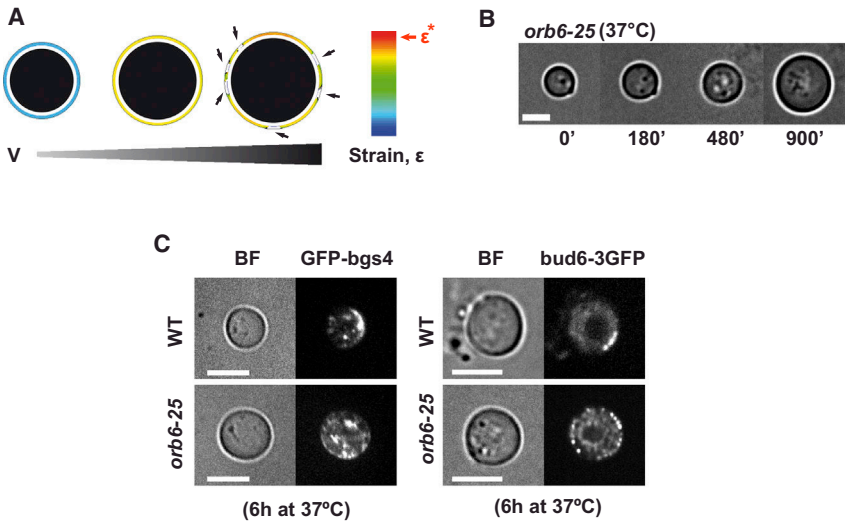

Figure 5. Polar Cap Assembly Is Required for Singular Rupture in the Spore Wall at Outgrowth

(A) Numerical simulations predicting multiple sites of rupture in spores with diffuse polarity.

(B) Time-lapse bright-field images of spore development in an *orb6-25* mutant grown at restrictive temperature (37°C) (scale bars, 5 μm).

(C) Single confocal midslices of WT and *orb6-25* spores expressing the polarity markers GFP-bgs4 or bud6-3GFP, 6 hr after germination at 37°C (scale bars, 5 μm).

(D) TEM of an *orb6-25* mutant spore 6 hr after germination at 37°C (scale bars, 1 μm) and close-up (scale bars, 200 nm). The black arrows point at sites of OSW ruptures.

(E) Quantification of phenotypes of OSW rupture at different times after germination at 37°C (n = 65 spores).

See also Figure S5.

A Positive Feedback between Growth and Polarity Can Account for the Switch in Polar Cap Stability at Outgrowth

To understand how the changes in the OSW could impact changes in polarity behavior, we turned to our numerical simulations to assess different hypotheses of feedbacks on polarity. We biased the random walk of the polar cap toward a location determined by (1) minimal stress, (2) maximal curvature, or (3) maximal surface expansion rate. Although all three hypotheses seem to be qualitatively in agreement with experimental observations, we found that with hypothesis (1) the cap does not stop wandering, whereas with hypothesis (2) the tube is immediately curved. Only hypothesis (3) reproduced observations, yielding the most robust behavior after outgrowth (Figures 7A and 7B; Movie S8). These modeling results thus suggest that a feedback from surface growth on the position of the polarity cap can explain polar cap stabilization at outgrowth.

To experimentally validate this prediction, we halted growth either by depolymerizing actin with Latrunculin A or by confining the growth of single spores in round microchambers. In these experiments, the controls (spores treated with DMSO or in large microchambers) displayed cap wandering and then stabilized, whereas the caps in nongrowing spores kept on wandering for several hours passed the timing of outgrowth in the control, exhibiting a marked increase in the number of unstable caps (Figures 7C and 7D). Thus, growth is required for cap stabilization. Furthermore, the coordinated OSW rupture and cap stabilization at outgrowth may be accounted for by a positive-feedback loop between growth and polarity, in which the cap promotes local growth while being preferentially stabilized at regions with higher surface growth rate.

DISCUSSION

By dynamically studying the developmental polarity and morphogenesis of single fission yeast spores, we develop and test here a simple quantitative model linking changes in the OSW with the spatial stability of polar caps needed for outgrowth. We propose that the OSW acts as a mechanical barrier, which hinders growth and destabilizes polarity. A rupture in this barrier generated by local polar growth when spores have grown enough releases inhibition by the OSW, stabilizes the cap, and coordinates spatial and temporal aspects of outgrowth. Instead of sensing absolute size (Turner et al., 2012), outgrowth appears to be triggered upon a fold change in volume. A function of this sensing system might be to prevent the reorganizing spores to exit the spore protective shell too early, as well as to regulate the timing and cell sizing at outgrowth in the absence of a tight cell-cycle regulation (Hatanaka and Shimoda, 2001). Through modeling and experimental tests, we demonstrate that a positive feedback between growth and polarity can account for a switch from unstable to stable polar cap behavior. Spatial landmarks from previous cell cycles, or MT-based targeting do not appear to be required at these early stages. MTs are also dispensable for de novo tip growth in rounded fission yeast spheroplasts or in mutants branching from cell sides (Kelly and Nurse, 2011; Sawin and Snaith, 2004). In addition, many cellular systems display transient oscillation of polar caps, which then stabilize at a fixed position even in the absence of directional cues (Bendezú and Martin, 2013; Dyer et al., 2013).

Polarity Cap Oscillations

The initial polarity cap establishment in these spores is likely to involve an interplay between reaction-diffusion-based positive and negative feedbacks that promote the self-assembly of a

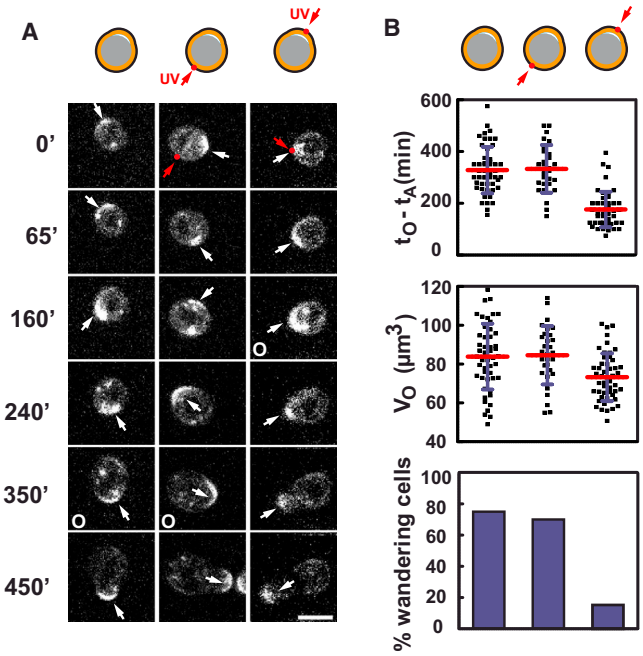

Figure 6. Rupturing the Outer Spore Wall Is Sufficient to Spatially Stabilize the Polar Cap

(A) Time-lapse single confocal midslices of germinating spores expressing GFP-bgs4 in the following conditions: not photoablated, photoablated away from the cap, and photoablated at the cap location with a UV laser. White arrows point at polar cap positions, and red arrows and dots indicate the photoablation site.

(B) Time of outgrowth with reference to laser irradiation, absolute volume at outgrowth, and percentage of spores depicting cap oscillations in the 2 hr following laser irradiation for the same three conditions as in (A).

Red bars: mean values; blue bars: SDs. Scale bars, 5 μm. See also Figure S5 and Movie S7.

single front of active-cdc42p (Bendezú and Martin, 2012; Das et al., 2012; Wu and Lew, 2013). We found that actin-based transport was not required in spores, although we note that actin inhibition caused a reduction in cap size (Figure S3B). The observed cap oscillations could be by-products of intrinsic mechanisms of polarization systems (Bendezú and Martin, 2012; Wu and Lew, 2013). Alternatively, they may function as a search mechanism when polarity needs to be redirected (Bendezú and Martin, 2013). In spores, the stochastic wandering of the cap could serve to identify a "weak spot" in the spore wall. Although our inspection of electron microscopy images of the OSW in fission yeast did not reveal obvious opening in the OSW in dormant spores (Figures 3A and S4A), certain fungal species display germ pores, which are small defects in the OSW from which the polar tube may emerge (Walkinshaw et al., 1967). Similarly, pollen tubes exit from specific apertures in the walls of pollen grains (Furness and Rudall, 2004) and early embryos of the marine brown algae *Fucus* use cues from the cell wall for polarity and outgrowth (Quatrano and Shaw, 1997). Our mechanism, whereby polar cap stability is amplified by growth, could serve to explain how these cells may polarize using mechanical cues from the cell wall.

Crosstalks between Growth and Polarity

Our work directly evidences the requirement of growth to spatially stabilize a polarity front. Similar growth-polarity feedbacks have been recently proposed in plants to regulate auxin-driven patterning of the shoot apex (Nakayama et al., 2012). Different tip-growing walled cells display variation in elongation rate that can range over almost two orders of magnitude (Knechtle et al., 2003; Qin and Yang, 2011). It is thus plausible that they have evolved mechanisms to monitor growth rate and link it to polarity machineries. A failure to do so could yield deleterious variations in cell-wall thickness and risks of cell death by bursting, or growth arrest (Campàs and Mahadevan, 2009). These growth-polarity feedbacks may underlie switching behavior such as oscillatory growth and contact sensing seen in fungal hyphae and pollen tubes (Kumamoto and Vinces, 2005; Qin and Yang, 2011; Rojas et al., 2011). Recent work in *S. cerevisiae* suggests models by which transport and fusion of vesicles may dilute polarity caps thereby causing them to disassemble (Layton et al., 2011). A reduction of surface expansion rate would yield similar dilution effects at a constant vesicle flux, and destabilize polarity. Conversely, the constraining effect of the OSW on surface expansion could restrict the available space needed for sufficient new membrane or inner wall addition necessary to stabilize the polar cap. In addition, we speculate that growth rates could impact polarity stability through a differential monitoring of cellular dimensions by intracellular gradients (Howard, 2012; Moseley and Nurse, 2010). Further work will be needed to fully characterize complex interplays between these essential morphogenetic cellular parameters.

Mechanochemical Coupling in Cell Polarity

Our data in conjunction with others support the existence of self-organizing processes coupling surface mechanics, growth, and internal organization. In animal cells, the micromechanical property of the actin cortex has been proposed to act as an important element to control polarity and shape changes during migration or cytokinesis (Paluch et al., 2006; Salbreux et al., 2012; Sedzinski et al., 2011). In addition, recent studies in migrating neutrophils suggest that membrane tension may have global inhibitory effects on polarity that function to maintain a singular active domain at the cell front (Houk et al., 2012). Thus, our work adds to a growing appreciation of mechanochemical feedbacks that serve to pattern cell shape and polarity (Asnacios and Hamant, 2012; Howard et al., 2011). The steady-state morphogenesis of a cell, like the rod shape of fission yeast, is likely to involve many types of feedbacks (Minc et al., 2009b; Terenna et al., 2008), which cannot be dissected with genetics. Thus, in addition to large-scale studies of gene products regulating cell shape and polarity (Hayles et al., 2013), dynamic studies like the one we performed here promise to pave the way for integrated models of morphogenesis.

EXPERIMENTAL PROCEDURES

Yeast Strains, Media, and Genetic Methods

Standard methods for *S. pombe* media and genetic manipulations were used (http://www-bcf.usc.edu/~forsburg/). Strains used in this study are

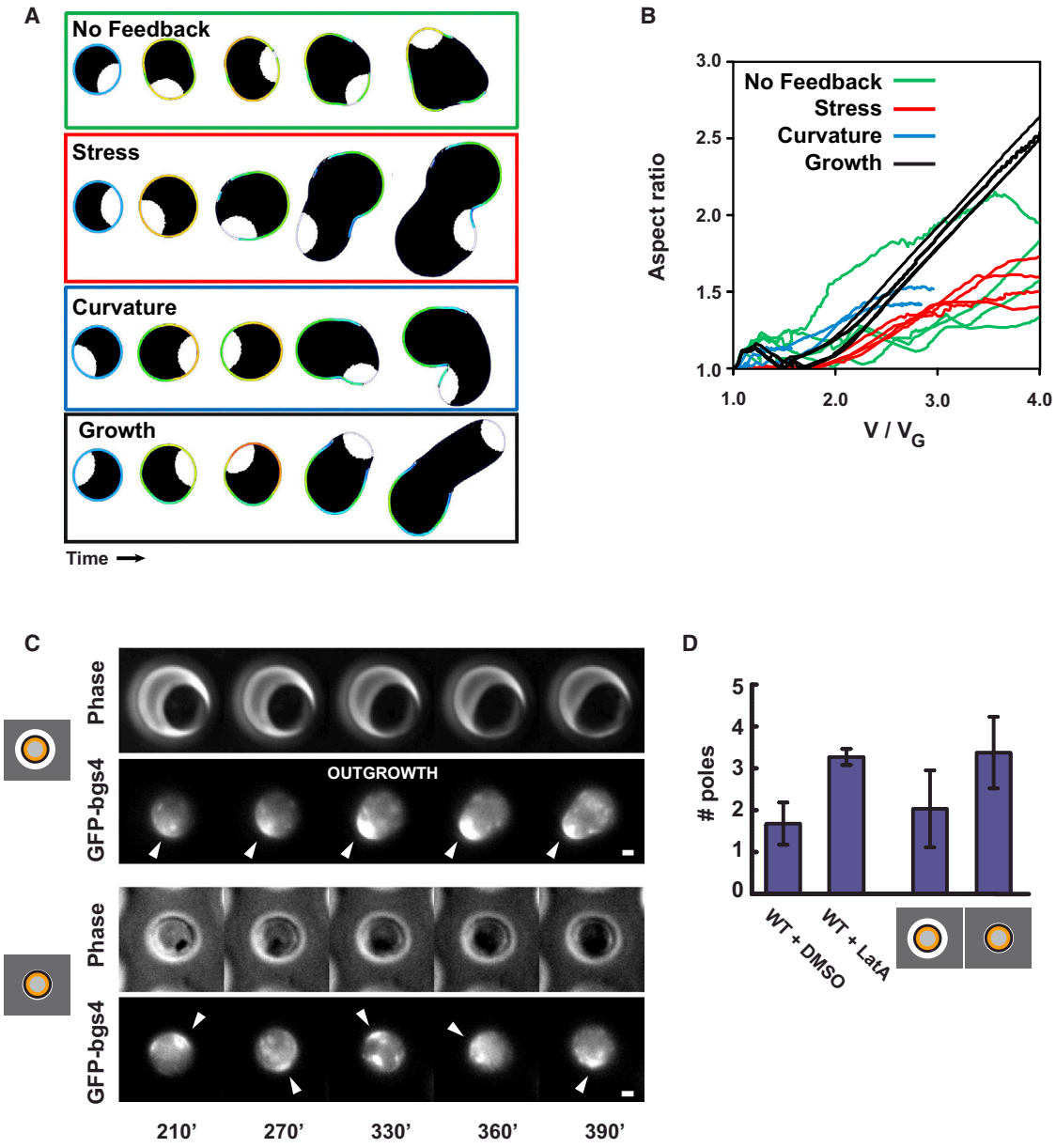

Figure 7. Outgrowth Involves a Positive-Feedback Loop between Growth and Polarity

(A) Numerical simulations testing different sources of feedback for polarity stabilization at outgrowth: no feedback, feedback on minimal mechanical stress, feedback on maximal curvature, feedback on maximal surface expansion rate (growth).

(B) Model prediction for the evolution of the aspect ratio as a function of normalized volume in the same conditions as in (A).

(C) Epifluorescence time-lapse of germinating spores expressing GFP-bgs4 arising from the same population, placed in large (on top) or small confining (on bottom) PDMS microchambers. White arrows point at successive polarity cap positions.

(D) Total number of observed successive polar caps for spores expressing CRIB-GFP treated with DMSO or 100 μM of Latrunculin A, which halts growth, and for spores expressing GFP-bgs4 in large or confining microchambers (n > 15 spores for each condition). Error bars represent SDs.

Scale bars, 1 μm. See also Movie S8.

listed in Table S1. Spores were obtained from homothallic h90 strains, or from diploids when indicated. Freshly growing cells were sporulated on malt extract (ME) solid media for 3 days. Spores were then digested 1 hr at room temperature in 1/200 glusulase solution in water to kill vegetative cells, and the enzyme was washed out three times in water. Digestion with glusulase did not influence morphogenetic and polarity events (size sensing and cap wandering) described in the manuscript (data not shown).

Pharmacological Inhibitors

Methyl-2-benzimidazole carbamate (MBC, Sigma) was used at a final concentration of 50 μg/ml from a 100× stock solution made fresh in DMSO. Latrunculin A (LatA, Sigma) was used at a final concentration of 100 μM from a 100× stock in DMSO. The efficiency of these treatments in rapidly depolymerizing microtubules and actin, respectively, was assessed by treating a mixed population of spores and cells for 10 min and imaging atb2-GFP for microtubules and the actin patch marker crn1-GFP (Figures S3C and S3D).

Microscopy

For long-term imaging, spores in water solution were placed on 2% agar YE5S pads and covered with a coverslip. For some applications, spores were placed in microfluidic chambers between a dialysis membrane and a coverslip, which allowed live fluid exchange (Charvin et al., 2008). Spore development was imaged at room temperature (23°C–25°C), with controlled humidity, with an inverted epifluorescence microscope provided with a motorized stage and automatic focus (Nikon Ti-Eclipse), and an EM-CCD camera (Hamamatsu). Movies were generally acquired at 100× magnification with 5 or 10 min time intervals, using phase contrast and epifluorescence when necessary. GFP-tagged polarity markers were also imaged with a spinning-disk confocal fluorescent microscope (Yokagawa, CSU-X1 spinning head) equipped with an EM-CCD camera (Evolve, Photometrics) and a 100× oil immersion objective (Nikon S Fluor 100× 0.5–1.3 NA). Images were acquired with Micromanager or Metamorph and processed and analyzed with Image J and MATLAB (MathWorks).

Image Analysis

Morphogenetic parameters of single developing spores were extracted from phase-contrast time-lapses using home-built MATLAB scripts (available upon request). Cell contours were segmented from the phase images, at each time point and oriented along the future outgrowth axis, yielding the morphogenesis color plots depicted in Figure 1B. The precision in contour segmentation was calibrated using spores expressing a plasma membrane marker GFP-psy1. The long axis was identified at each time point, and the aspect ratio was computed as the ratio between the length along this axis and the largest perpendicular diameter. Volumes were computed by assuming a prolate geometry (rotational symmetry around the long axis of the cell). The long axis was thus sliced in local diameters y(x) every pixel (Figure 1B, inset) which served to compute the areas of the sections of the prolate $S(x) = \pi^*(y(x)/2)^2$, and the volume was computed as the sum of these areas along all the pixels of the long axis. We estimate imprecisions associated to these methods (including errors in the z, segmentation, and prolate approximation), to be lower than 5% for length and aspect ratio and on the order of 10% for the volume.

The frequency of new caps during the initial phase of near-isotropic growth (Figures 2C and 2E) was visually quantified from time-lapse epifluorescence movies of cells expressing GFP-bgs4. Only fully reassembling new caps were counted, and the number of caps was divided by the time between first cap appearance and outgrowth. The last stable cap-promoting outgrowth was not counted.

Quantification of relative concentration evolution of polarity factors at the cap (Figure 2F) was inferred from computing the mean signal at the polar cap from a merged confocal stack of six z-sections time-lapsed on individual spores. Growing spores were imaged together with vegetative cells, to normalize the concentration in spore caps with the concentration in vegetative bipolar caps. Photobleaching was accounted for by quantifying the loss of signal in fixed cells expressing the same marker, and autofluorescence was accounted for by imaging WT spores and cells with no marker.

Transmission Electron Microscopy

Wild-type spores were grown in liquid YE5S at 30°C for different amounts of time and subsequently fixed in 2% glutaraldehyde in YE5S for 30 min on ice. *orb6-25* mutants spores were grown at 37°C for different amounts of times and fixed in same conditions. Spores were then transferred to 0.1 M PBS + 2% glutaraldehyde and stirred overnight at 4°C. The spore pellet was then dehydrated in ethanol and embedded in Epon resine. Ultrathin sections were made with an ultramicrotome (Leica), deposited onto electron microscopy grids, and contrasted with uranyl acetate in lead citrate. Images were taken using a FEI CM120 electron microscope (FEI Company), equipped with a numeric camera (Keen View; Soft Imaging System, SIS).

Laser Ablation of the Outer Spore Wall

The laser ablation assay uses a pulsed 355 nm ultraviolet laser interfaced with an iLas system (Roper Scientific) in the "Mosquito" mode. This allows irradiating at multiple positions in the field with laser spots having a fixed area of about 500 nm. This system is mounted on a confocal spinning disk (Yokagawa CSU-X1 spinning head on a Nikon Eclipse Ti inverted microscope) equipped with an EM-CCD camera (Evolve, Photometrics) and a 100× oil immersion objective (Nikon S Fluor 100× 0.5–1.3 NA). We calibrated the irradiation time to optimize the selectivity of the assay in fragilizing the spore wall but not the inner wall. To this aim, spores were placed in microfluidic flow chambers, irradiated, and subsequently rinsed with a mix of two vegetative cell-wall (inner wall) digestion enzymes (0.5 mg/ml Zymolase and 10 mg/ml Novozyme). Rinsing with these enzymes yields the death of all vegetative cells and outgrown spores in 10–30 min but does not affect spores (Figure S4B). Using this assay, we identified the laser time of exposure that did not yield spore death without enzyme treatment, but that yielded death of irradiated spores after enzyme treatment. The optimal exposure time in our conditions was found to be 80 ms. The photoablation assay as presented in Figure 6 was then performed in these same conditions on spores expressing the polarity marker GFP-bgs4, that were germinated in YE5S liquid for 3 hr before laser irradiation.

Stress-Strain Experiment to Measure Rigidity of the OSW and Inner Cell Wall

To compute surface moduli of cell walls, spores, outgrown spores, and vegetative cells were placed in microfluidic chambers in YE5S media. The media was then exchanged rapidly and replaced by YE5S with a given concentration of sorbitol. This created a relative change in the internal osmotic pressure computed as $\Delta p = C_s RT$, with C_s the sorbitol concentration, R the gas constant, and T the temperature. This change in osmolarity caused the spores and cells to shrink, which serves as a measure of strain. Local changes in curvature radii, r, (before and 5 min after treatment) were tracked using homemade MATLAB scripts (Figure 3E). This assay was then repeated with dose-dependent addition of sorbitol (C_s = 2 M, 1.5 M, 1 M, 0.5 M), which allowed us to derive a stress-strain curve (Figure S4C). This curve was found to be linear within the regime probed, which reflects elastic behavior of both inner and outer spore wall, on short timescales. The slopes were then extracted to compute the average surface moduli of spores, using the following formula:

$$\frac{\Delta P}{\Delta r} = 4\frac{\sigma}{r^2}$$

This assay was used to derive average surface moduli of spores, vegetative cells, the back of outgrown spores (where the OSW is still encasing the inner wall) and the tip of outgrown spores (which only have vegetative wall) (Figure 3E). In vegetative cells, this analysis led to a value of the surface modulus of the cell wall of $\sigma_{Veg} = 18.6\ N.m^{-1}$, which closely agrees with measurement achieved by other means (Minc et al., 2009a). The surface modulus of the back of the spores was found to be $\sigma_{back} = 62.0\ N.m^{-1}$, and the surface modulus at the tip of the emerging tube was very close to the vegetative value: $\sigma_{tip} = 20.6\ N.m^{-1}$. Because the back of the spore has superimposed inner and outer wall, $\sigma_{back} = \sigma_i + \sigma_o$, whereas $\sigma_{tip} = \sigma_i$. Thus, the ratio between the surface moduli of the outer and the inner wall can be computed from $\sigma_o/\sigma_i = \sigma_{back}/\sigma_{tip} - 1 \approx 2.3$. Because the thickness, h_0, of the outer wall is approximately 15 nm and the thickness of the inner wall, h_i, is around 200 nm, the ratio in bulk moduli $E_o/E_i = (h_O\sigma_o)/(h_i\sigma_i)$ is around 30. The same assay and analysis were then used to characterize rigidity of spore walls in *chs1Δ* and *mok13Δ* mutants defective in spore wall synthesis (Figure 4E).

Assessment of the Role of Turgor Pressure in Spore Growth

Spores of either WT or *gpd1Δ* were first germinated and grown at 30°C for 2 hr in liquid YE5S. Spores were then placed in microfluidic chambers and covered with a semipermeable dialysis membrane. Single spore growth rates were monitored from time-lapse imaging during 2 hr, after which the spores were rinsed with 1 M sorbitol to decrease internal turgor, and growth rates were measured again for another 2 hr. Growth rate ratio before and after treatment was then computed for each single spore and averaged to plot the bar graph presented in Figure 3F.

Microchambers Operation

Microchambers were fabricated by the use of standard soft-lithography methods (Minc et al., 2009a, 2009b). Chambers are round, are 3–4 μm deep, and have diameters varying between 3 and 10 μm. Spores expressing the polarity marker GFP-bgs4 were germinated and grown for 3 hr 30 min, and a

1 μl drop of spore suspension was then placed at the bottom of a round fluorodish (WPI). The polydimethylsiloxane (PDMS) block containing the chambers was activated with a plasma cleaner and subsequently placed, holes facing down, on top of the spores in the dish and let to bind to the glass bottom. This forced many spores into single microchambers, some constraining, and some much larger than the spore diameter, that were used as controls. Time-lapses at different positions were then recorded to monitor polar cap wandering in different conditions.

SUPPLEMENTAL INFORMATION

Supplemental Information includes supplemental model, five figures, one table, and eight movies and can be found with this article online at http://dx.doi.org/10.1016/j.devcel.2014.01.023.

ACKNOWLEDGMENTS

We thank the Coudreuse, Martin, Perez, Ribas, Valdivieso, Sanchez, Chang, Tran, and Paoletti labs for sharing strains and materials. D.B. was supported by an Institut Curie PhD fellowship in the initial period of this work. A.B. is supported by a European Research Council starting grant (PhyMorph, #307387). N.M. acknowledges support from CNRS, FP7 (CIG and ITN programs), ANR (grant 10PDOC00301), FRM (grant AJE20130426890), and a Mairie de Paris "Emergence grant."

Received: September 24, 2013
Revised: January 6, 2014
Accepted: January 23, 2014
Published: March 10, 2014

REFERENCES

Arellano, M., Cartagena-Lirola, H., Nasser Hajibagheri, M.A., Durán, A., and Henar Valdivieso, M. (2000). Proper ascospore maturation requires the chs1+ chitin synthase gene in Schizosaccharomyces pombe. Mol. Microbiol. *35*, 79–89.

Asnacios, A., and Hamant, O. (2012). The mechanics behind cell polarity. Trends Cell Biol. *22*, 584–591.

Bastmeyer, M., Deising, H.B., and Bechinger, C. (2002). Force exertion in fungal infection. Annu. Rev. Biophys. Biomol. Struct. *31*, 321–341.

Bendezú, F.O., and Martin, S.G. (2012). Cdc42 oscillations in yeasts. Sci. Signal. *5*, pe53.

Bendezú, F.O., and Martin, S.G. (2013). Cdc42 explores the cell periphery for mate selection in fission yeast. Curr. Biol. *23*, 42–47.

Boudaoud, A. (2003). Growth of walled cells: from shells to vesicles. Phys. Rev. Lett. *91*, 018104.

Campàs, O., and Mahadevan, L. (2009). Shape and dynamics of tip-growing cells. Curr. Biol. *19*, 2102–2107.

Cano, R.J., and Borucki, M.K. (1995). Revival and identification of bacterial spores in 25- to 40-million-year-old Dominican amber. Science *268*, 1060–1064.

Chang, F., and Martin, S.G. (2009). Shaping fission yeast with microtubules. Cold Spring Harb. Perspect. Biol. *1*, a001347.

Charvin, G., Cross, F.R., and Siggia, E.D. (2008). A microfluidic device for temporally controlled gene expression and long-term fluorescent imaging in unperturbed dividing yeast cells. PLoS ONE *3*, e1468.

Cortés, J.C., Carnero, E., Ishiguro, J., Sánchez, Y., Durán, A., and Ribas, J.C. (2005). The novel fission yeast (1,3)beta-D-glucan synthase catalytic subunit Bgs4p is essential during both cytokinesis and polarized growth. J. Cell Sci. *118*, 157–174.

Das, M., Wiley, D.J., Medina, S., Vincent, H.A., Larrea, M., Oriolo, A., and Verde, F. (2007). Regulation of cell diameter, For3p localization, and cell symmetry by fission yeast Rho-GAP Rga4p. Mol. Biol. Cell *18*, 2090–2101.

Das, M., Wiley, D.J., Chen, X., Shah, K., and Verde, F. (2009). The conserved NDR kinase Orb6 controls polarized cell growth by spatial regulation of the small GTPase Cdc42. Curr. Biol. *19*, 1314–1319.

Das, M., Drake, T., Wiley, D.J., Buchwald, P., Vavylonis, D., and Verde, F. (2012). Oscillatory dynamics of Cdc42 GTPase in the control of polarized growth. Science *337*, 239–243.

Drubin, D.G. (1991). Development of cell polarity in budding yeast. Cell *65*, 1093–1096.

Dyer, J.M., Savage, N.S., Jin, M., Zyla, T.R., Elston, T.C., and Lew, D.J. (2013). Tracking shallow chemical gradients by actin-driven wandering of the polarization site. Curr. Biol. *23*, 32–41.

Fink, J., Carpi, N., Betz, T., Bétard, A., Chebah, M., Azioune, A., Bornens, M., Sykes, C., Fetler, L., Cuvelier, D., and Piel, M. (2011). External forces control mitotic spindle positioning. Nat. Cell Biol. *13*, 771–778.

Furness, C.A., and Rudall, P.J. (2004). Pollen aperture evolution—a crucial factor for eudicot success? Trends Plant Sci. *9*, 154–158.

García, I., Tajadura, V., Martín, V., Toda, T., and Sánchez, Y. (2006). Synthesis of alpha-glucans in fission yeast spores is carried out by three alpha-glucan synthase paralogues, Mok12p, Mok13p and Mok14p. Mol. Microbiol. *59*, 836–853.

Glynn, J.M., Lustig, R.J., Berlin, A., and Chang, F. (2001). Role of bud6p and tea1p in the interaction between actin and microtubules for the establishment of cell polarity in fission yeast. Curr. Biol. *11*, 836–845.

Harold, F.M. (1990). To shape a cell: an inquiry into the causes of morphogenesis of microorganisms. Microbiol. Rev. *54*, 381–431.

Hatanaka, M., and Shimoda, C. (2001). The cyclic AMP/PKA signal pathway is required for initiation of spore germination in Schizosaccharomyces pombe. Yeast *18*, 207–217.

Hayles, J., Wood, V., Jeffery, L., Hoe, K.L., Kim, D.U., Park, H.O., Salas-Pino, S., Heichinger, C., and Nurse, P. (2013). A genome-wide resource of cell cycle and cell shape genes of fission yeast. Open Biol. *3*, 130053.

Houk, A.R., Jilkine, A., Mejean, C.O., Boltyanskiy, R., Dufresne, E.R., Angenent, S.B., Altschuler, S.J., Wu, L.F., and Weiner, O.D. (2012). Membrane tension maintains cell polarity by confining signals to the leading edge during neutrophil migration. Cell *148*, 175–188.

Howard, M. (2012). How to build a robust intracellular concentration gradient. Trends Cell Biol. *22*, 311–317.

Howard, J., Grill, S.W., and Bois, J.S. (2011). Turing's next steps: the mechanochemical basis of morphogenesis. Nat. Rev. Mol. Cell Biol. *12*, 392–398.

Howell, A.S., Jin, M., Wu, C.F., Zyla, T.R., Elston, T.C., and Lew, D.J. (2012). Negative feedback enhances robustness in the yeast polarity establishment circuit. Cell *149*, 322–333.

Kelly, F.D., and Nurse, P. (2011). De novo growth zone formation from fission yeast spheroplasts. PLoS ONE *6*, e27977.

Klobutcher, L.A., Ragkousi, K., and Setlow, P. (2006). The Bacillus subtilis spore coat provides "eat resistance" during phagocytic predation by the protozoan Tetrahymena thermophila. Proc. Natl. Acad. Sci. USA *103*, 165–170.

Knechtle, P., Dietrich, F., and Philippsen, P. (2003). Maximal polar growth potential depends on the polarisome component AgSpa2 in the filamentous fungus Ashbya gossypii. Mol. Biol. Cell *14*, 4140–4154.

Kono, K., Matsunaga, R., Hirata, A., Suzuki, G., Abe, M., and Ohya, Y. (2005). Involvement of actin and polarisome in morphological change during spore germination of Saccharomyces cerevisiae. Yeast *22*, 129–139.

Kono, K., Saeki, Y., Yoshida, S., Tanaka, K., and Pellman, D. (2012). Proteasomal degradation resolves competition between cell polarization and cellular wound healing. Cell *150*, 151–164.

Kumamoto, C.A., and Vinces, M.D. (2005). Alternative Candida albicans lifestyles: growth on surfaces. Annu. Rev. Microbiol. *59*, 113–133.

Layton, A.T., Savage, N.S., Howell, A.S., Carroll, S.Y., Drubin, D.G., and Lew, D.J. (2011). Modeling vesicle traffic reveals unexpected consequences for Cdc42p-mediated polarity establishment. Curr. Biol. *21*, 184–194.

McKenney, P.T., Driks, A., and Eichenberger, P. (2013). The Bacillus subtilis endospore: assembly and functions of the multilayered coat. Nat. Rev. Microbiol. *11*, 33–44.

Minc, N., Boudaoud, A., and Chang, F. (2009a). Mechanical forces of fission yeast growth. Curr. Biol. *19*, 1096–1101.

Minc, N., Bratman, S.V., Basu, R., and Chang, F. (2009b). Establishing new sites of polarization by microtubules. Curr. Biol. *19*, 83–94.

Misra, G., Rojas, E.R., Gopinathan, A., and Huang, K.C. (2013). Mechanical consequences of cell-wall turnover in the elongation of a Gram-positive bacterium. Biophys. J. *104*, 2342–2352.

Mitchison, J.M., and Nurse, P. (1985). Growth in cell length in the fission yeast Schizosaccharomyces pombe. J. Cell Sci. *75*, 357–376.

Moseley, J.B., and Nurse, P. (2010). Cell division intersects with cell geometry. Cell *142*, 184–188.

Nakayama, N., Smith, R.S., Mandel, T., Robinson, S., Kimura, S., Boudaoud, A., and Kuhlemeier, C. (2012). Mechanical regulation of auxin-mediated growth. Curr. Biol. *22*, 1468–1476.

Neiman, A.M. (2005). Ascospore formation in the yeast Saccharomyces cerevisiae. Microbiol. Mol. Biol. Rev. *69*, 565–584.

Nurse, P., Thuriaux, P., and Nasmyth, K. (1976). Genetic control of the cell division cycle in the fission yeast Schizosaccharomyces pombe. Mol. Gen. Genet. *146*, 167–178.

Paluch, E., van der Gucht, J., and Sykes, C. (2006). Cracking up: symmetry breaking in cellular systems. J. Cell Biol. *175*, 687–692.

Pandey, R., Ter Beek, A., Vischer, N.O., Smelt, J.P., Brul, S., and Manders, E.M. (2013). Live cell imaging of germination and outgrowth of individual bacillus subtilis spores; the effect of heat stress quantitatively analyzed with SporeTracker. PLoS ONE *8*, e58972.

Qin, Y., and Yang, Z. (2011). Rapid tip growth: insights from pollen tubes. Semin. Cell Dev. Biol. *22*, 816–824.

Quatrano, R.S., and Shaw, S.L. (1997). Role of the cell wall in the determination of cell polarity and the plane of cell division in Fucus embryos. Trends Plant Sci. *2*, 15–21.

Rincón, S.A., Ye, Y., Villar-Tajadura, M.A., Santos, B., Martin, S.G., and Pérez, P. (2009). Pob1 participates in the Cdc42 regulation of fission yeast actin cytoskeleton. Mol. Biol. Cell *20*, 4390–4399.

Rojas, E.R., Hotton, S., and Dumais, J. (2011). Chemically mediated mechanical expansion of the pollen tube cell wall. Biophys. J. *101*, 1844–1853.

Salbreux, G., Charras, G., and Paluch, E. (2012). Actin cortex mechanics and cellular morphogenesis. Trends Cell Biol. *22*, 536–545.

Sawin, K.E., and Snaith, H.A. (2004). Role of microtubules and tea1p in establishment and maintenance of fission yeast cell polarity. J. Cell Sci. *117*, 689–700.

Sedzinski, J., Biro, M., Oswald, A., Tinevez, J.Y., Salbreux, G., and Paluch, E. (2011). Polar actomyosin contractility destabilizes the position of the cytokinetic furrow. Nature *476*, 462–466.

Slaughter, B., and Li, R. (2006). Toward a molecular interpretation of the surface stress theory for yeast morphogenesis. Curr. Opin. Cell Biol. *18*, 47–53.

Tanaka, K., and Hirata, A. (1982). Ascospore development in the fission yeasts Schizosaccharomyces pombe and S. japonicus. J. Cell Sci. *56*, 263–279.

Tatebe, H., Nakano, K., Maximo, R., and Shiozaki, K. (2008). Pom1 DYRK regulates localization of the Rga4 GAP to ensure bipolar activation of Cdc42 in fission yeast. Curr. Biol. *18*, 322–330.

Terenna, C.R., Makushok, T., Velve-Casquillas, G., Baigl, D., Chen, Y., Bornens, M., Paoletti, A., Piel, M., and Tran, P.T. (2008). Physical mechanisms redirecting cell polarity and cell shape in fission yeast. Curr. Biol. *18*, 1748–1753.

Turner, J.J., Ewald, J.C., and Skotheim, J.M. (2012). Cell size control in yeast. Curr. Biol. *22*, R350–R359.

Walkinshaw, C.H., Hyde, J.M., and van Zandt, J. (1967). Fine structure of quiescent and germinating aeciospores of Cronartium fusiforme. J. Bacteriol. *94*, 245–254.

Wallace, S., Fleming, A., Wellman, C.H., and Beerling, D.J. (2011). Evolutionary development of the plant and spore wall. AoB Plants *2011*, plr027.

Wedlich-Soldner, R., Altschuler, S., Wu, L., and Li, R. (2003). Spontaneous cell polarization through actomyosin-based delivery of the Cdc42 GTPase. Science *299*, 1231–1235.

Wu, C.F., and Lew, D.J. (2013). Beyond symmetry-breaking: competition and negative feedback in GTPase regulation. Trends Cell Biol. *23*, 476–483.

Developmental Cell, Volume *28*

Supplemental Information

Symmetry Breaking in Spore Germination Relies on an Interplay between Polar Cap Stability and Spore Wall Mechanics

Daria Bonazzi, Jean-Daniel Julien, Maryse Romao, Rima Seddiki, Matthieu Piel, Arezki Boudaoud, and Nicolas Minc

SUPPLEMENTAL MODEL

The simulations presented in Figures 4,5 and 7 were obtained based on a mechanical model of the growing spore. We accounted for the following hypotheses: (i) growth is powered by turgor, (ii) the inner wall is viscoelastic over the polarity cap because of inner wall remodeling, and elastic outside the cap, (iii) the OSW is elastic but may rupture when elastic strain (equivalently stress) exceeds a threshold, and (iv) the cap center undergoes a walk that is either fully random or biased by specific feedbacks (see below). To easily explore model parameters, we considered a 2D model where a disc of inner wall is initially surrounded by a thin annulus of OSW. In the figures and supplementary movies presented throughout the manuscript, the OSW and the inner wall are superimposed, but have different colors: the OSW is depicted as an opaque colored layer (in which the colors correspond to local values of the strain in the OSW), while the inner wall is shown in white over the polar cap (the growing region) and in black outside of the cap. The initial state in the simulation assumes that both the inner and outer cell walls are homogeneously stressed by internal pressure. To allow the system to grow at the polar cap where the inner cell wall is being remodeled, we assume that this wall behaves as a viscoelastic material whose viscosity is infinite outside the polar cap and finite at the cap. The OSW is on the other hand supposed to behave as a purely elastic, brittle material that breaks when the elastic strain exceeds a fixed threshold ε^*. Above this strain, the OSW can then deform plastically.

The simulations consist of iterative loops; the strain and the position of the polarity cap are computed at each iteration. The polarity cap width is set to a fixed value. In the first set of simulations (Figure 4), the center of the polarity cap is assumed to follow a random walk, of a step length chosen to match the observed frequency of new caps (Figure 2C). In the second set of simulations (Figure 7), the polarity cap was moved according to one of the specific hypotheses of feedback, (i) to the position of maximal curvature (assuming the existence of putative curvature sensors), (ii) to the position of minimal stress (assuming the existence of putative stress sensors, like stretch activated ion channels for instance), or (iii) to the position of maximal growth rate; in this second set, a small noise on polar cap location was added to prevent the simulations from being deterministic. The minimal input parameters needed for the default model, as presented in Figure 4 are thus: the normalized radius of the polar cap r^*, the characteristic time of the random walk, t^*, the normalized Young's modulus of the OSW E_0^*, the normalized Young's modulus of the inner wall Ei^* (the pressure P^* is set as a unit),

the viscosity η of growing regions of the inner wall, the rupture strain threshold of the OSW ε*, which corresponds to the failure stress through the constitutive relation. For prediction of rupture in the OSW, the parameters r* and t* do not influence predictions; the viscosity η influences the absolute timing but not the sizes and morphologies; finally the parameters ε* and the ratio E_0*/Ei* have a strong influence (Figure 4D and Figure S5B).

More specifically, we assumed the cell wall to be viscoelastic, and modeled it as an isotropic Maxwell material. By separating the plastic ε_p and elastic ε_{el} parts of the strain tensor ε, we write:

$$\frac{d\boldsymbol{\epsilon}}{dt} = \frac{d\boldsymbol{\epsilon_p}}{dt} + \frac{d\boldsymbol{\epsilon_{el}}}{dt} = \frac{\boldsymbol{\sigma}}{\eta} + \frac{1}{E}\frac{d\boldsymbol{\sigma}}{dt}$$

where σ is the stress tensor, η the viscosity and E the young modulus of the material. Here, the characteristic timescale of the material, η/E, is assumed to take two values: infinity where no growth occurs, and a constant finite value where growth occurs; this finite value sets the unit of time in the simulations. At each time step, the stress due to internal pressure is computed by solving the stationary Cauchy momentum equation:

$$div(\boldsymbol{\sigma}) = f$$

where f is the body force due to internal pressure. The Hooke's law gives the relationship between the strain tensor and the stress tensor:

$$\boldsymbol{\sigma} = \frac{E\nu}{(1+\nu)(1-2\nu)} tr(\boldsymbol{\epsilon_{el}})\boldsymbol{I} + \frac{E}{(1+\nu)}\boldsymbol{\epsilon_{el}}$$

where ν is the Poisson's ratio and I the identity tensor.

We employ an incremental and discrete approach to growth. After computing the elastic strain, the increment of plastic strain is equated with the elastic strain. In the limit of small strains, this is exactly equivalent to defining a Maxwell material for which the characteristic time scale, η/E, is equal to the time step of the simulation. The inner wall is viscoelastic in the domain corresponding to the polar cap and purely elastic outside of this domain. The OSW deforms elastically as long as the largest eigenvalue of the elastic strain ε is smaller than the threshold strain ε*. When and where this threshold is reached, the OSW is irreversibly ruptured, and then it is assumed to be viscoelastic. In the simulations, the spore is a disc of typical radius R*=1 and Young's modulus Ei* surrounded by an annulus of thickness R*/10 and Young's modulus Eo*. The polar cap is computed as a disc of radius r*=0.9R* whose

center is located on the boundary of the spore, unless for the simulation of Figure 5A where r*>>R*, to account for a diluted polarity.

To test hypothesis of polar cap stabilization from wall mechanics, we assess possible sources of positive feedback. Because the polar cap yields local growth, that results in reducing surface stress, increasing curvature and increasing surface expansion rates; we implement in the model a feedback so that at each time step, the polar cap moves to a new position determined by:
(o) a random walk of step time t*=30,
(i) the minimal value of stress σ,
(ii) the maximal value of curvature of the OSW,
(iii) or the maximal surface growth (computed as the normal velocity of the wall).
In order to avoid completely deterministic simulations with hypotheses (i-iii), an intrinsic white noise of amplitude 5% is added to the variable that defines the location of the polar cap; the value of this noise is unimportant as long as it is small.

Numerically, the elastic problem is solved with the finite elements method implemented in a FreeFem++ program. After each time step, the domain is re-meshed to keep a mesh size equal to 1/10 in the inner wall domain and 1/50 in OSW domain.

Values of parameters used in the model are:
- Ei*=14 in all simulations
- Eo*= 42 for simulations presented in Figures 4B, 4C, 4D, 5A, 7A, 7B and S5A, and 28<Eo*<42 for Figure S5B
- ν=0.3 for all simulations;
- R*=1 for Figures 4B, 4D, 5A, 7A, 7B, S5A and S5B, and 0.8<R*<1.2 for Figure 4C
- ε*=0.3 for Figures 4B, 4C, 5A, S5A and S5B, and 0.2< ε*<0.35for Figure 4D
- P*=1, for all simulation

DB_146	h90	wt	leu1-32 ura4-D18 his3-D1	Figs 1,3,4,S1,S3,S4,S5
DB_147	h+/h-	wt	ade-M210/ade-M216 leu1-32 ura4-D18	Not shown
NM 436	h90	leu:GFP-Psy1	leu1-32 ura4-D18	Not shown
NM 422	h+/h-	cdc10-M17	ade-M210/ade-M216	Figs 1,S1
DB_124	h90	bgs4::ura GFP-bgs4:leu	leu1-32 ura4-D18	Figs 2,3,5,6,7,S2,S3,S6
DB_166	h90	rga4::KanMX bgs4::ura GFP-bgs4:leu	leu1-32 ura4-D18	Figs 1,S1
DB_163	h90	rga2::KanMX bgs4::ura GFP-bgs4:leu	leu1-32 ura4-D18	Figs S1
DB_169	h90	bud6-3GFP:KanMX	leu1-32 ura4-D18	Figs 2,5,S2
DB_228	h90	GFP-A8-cdc42:KanMX	leu1-32 ura4-D18	Figs 2,5,S2
DB_214	h90	CRIB-GFP:ura	leu1-32 ura4-D18	Figs 2,5,S2
DB_226	h90	CRIB-GFP:ura bud6-Tomato:NatMX	leu1-32 ura4-D18	Figs 7,S2,S3
DB_287	h90	CRIB-GFP:ura bgs4::ura RFP-bgs4:leu	leu1-32 ura4-D18	Figs S2
DB_221	h90	bgs4::ura RFP-bgs4:leu bud6-3GFP:kan	leu1-32 ura4-D18	Figs S2
NM 376	h90	crn1-GFP::KanMX	ade6-M216	Figs S3
DB_201	h90	leu1-32:SV40:GFP-atb2[leu1+]		Figs S3
DB_182	h90	tea1:NatMX bgs4::ura GFP-bgs4:leu	leu1-32 ura4-D18	Figs 2, S3
DB_236	h90	tip1::kanMX bgs4::ura GFP-bgs4:leu	leu1-32 ura4-D18	Figs 2, S3
DB_181	h90	for3::KanMX bgs4::ura GFP-bgs4:leu	leu1-32 ura4-D18	Figs 2, S3
DB_234	h90	tea4::kanMX bgs4::ura GFP-bgs4:leu	leu1-32 ura4-D18	Figs 2, S3
DB_197	h90	mok13::kanR	leu1-32 ura4D-18 his3-D1	Figs 4
DB_186	h90	chs1::his3+	leu1-32 ura4D-18 his3-D1	Figs 4
DB_218	h90	orb6-25 bgs4::ura GFP-bgs4:leu	ade6-M216 leu1-32 ura4-D18	Figs 5, S5
DB_216	h90	gpd1::ura	ura4-D18	Figs 3
DB_323	h90	orb6-25 bud6-3GFP: KanMX	ade6-M216 leu1-32	Figs 5

Supplementary Table S1 (Related to Experimental procedures): Fission yeast strains used in this study

SUPPLEMENTAL FIGURES

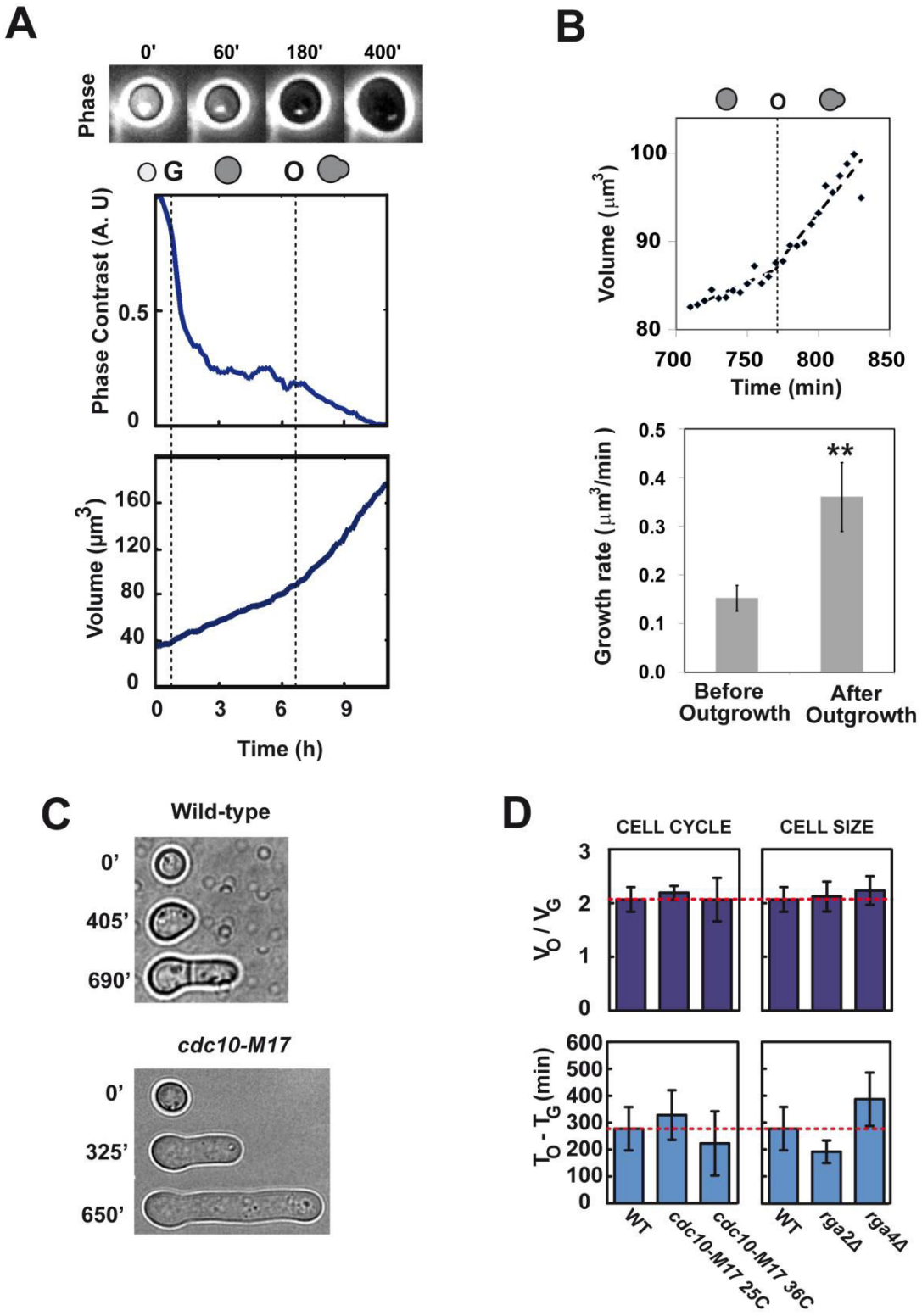

Figure S1

Supplemental Figure 1(Related to Figure 1): Characterization of morphogenetic changes at germination and outgrowth.

(A) Evolution of phase contrast intensity as a function of spore development, and corresponding volume evolution (bottom). High phase contrast signal corresponds to bright spores. **(B)** Growth rate increases at the onset of outgrowth. Top: Cell volume as a function of time. The dotted line corresponds to the linear fits of growth rates before and after outgrowth (indicated by the black dotted line). Bottom: Mean growth rates computed 1h before and 1h after outgrowth (n=13 spores). **(C)** Time-lapse bright field images of WT and *cdc10-M17* mutant spores grown at 37°C. Both strains do outgrowth at similar size increase, but *cdc10-M17* fails cell cycle progression and keeps elongating without dividing. **(D)** Volume-doubling for outgrowth is conserved in mutants defective in cell cycle progression and cell size. Mean volume ratios (dark blue bars) and mean germination to outgrowth times (light blue bars), of indicated mutants ($n > 30$ for each condition). Error bars correspond to standard deviations. ** $p<0.01$, Student's t-test.

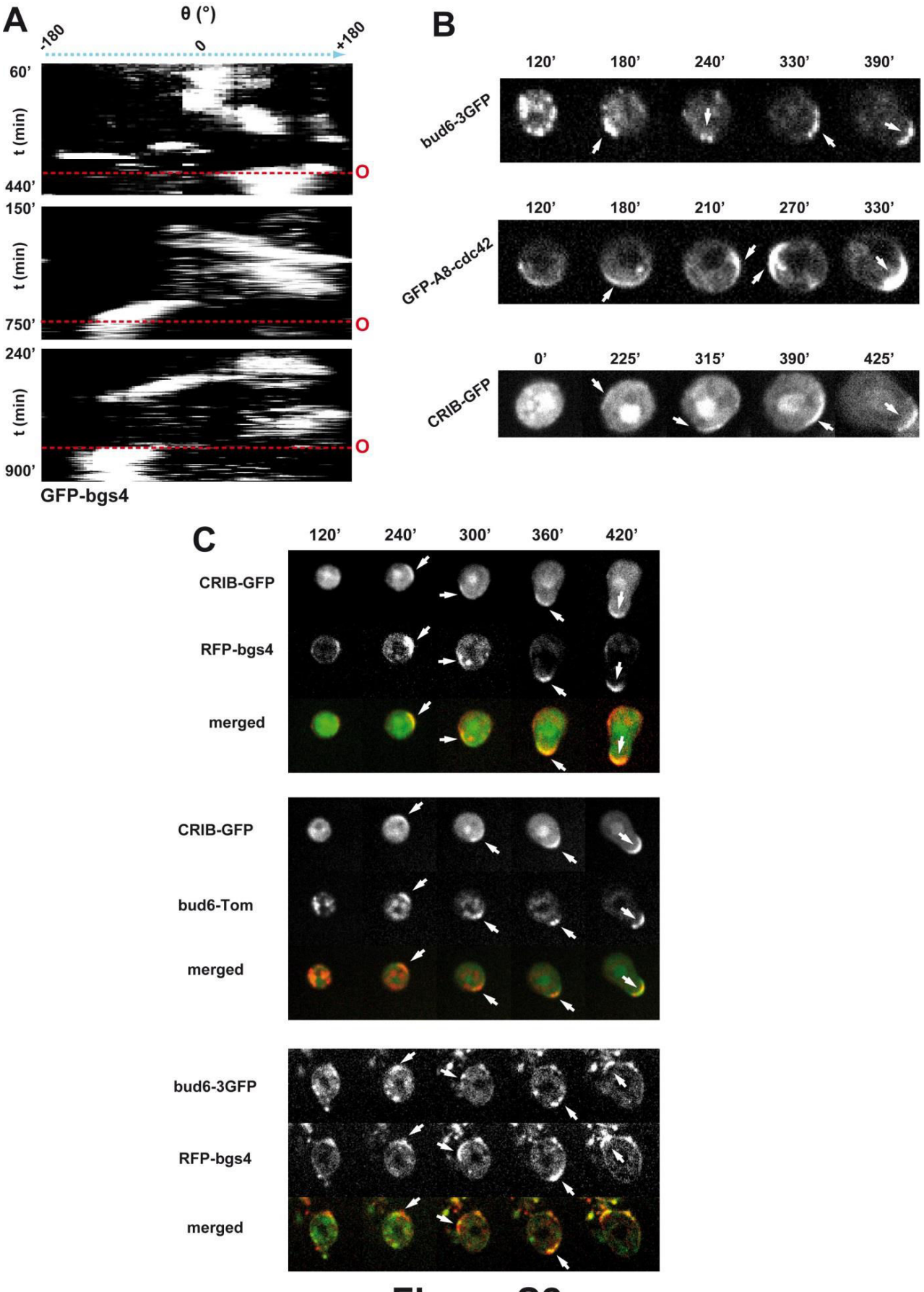
A
θ (°)
-180
0
+180
60'
t (min)
440'
150'
t (min)
750'
240'
t (min)
900'
GFP-bgs4
B
120'
180'
240'
330'
390'
bud6-3GFP
120'
180'
210'
270'
330'
GFP-A8-cdc42
0'
225'
315'
390'
425'
CRIB-GFP
C
120'
240'
300'
360'
420'
CRIB-GFP
RFP-bgs4
merged
CRIB-GFP
bud6-Tom
merged
bud6-3GFP
RFP-bgs4
merged

Figure S2

Supplemental Figure 2 (Related to Figure 2): Polarity components wandering

(A) Cell kymographs of three independent spores representing the changes of localization over time of the polarity factor GFP-bgs4 extracted from epifluorescence time-lapse. Red dotted lines mark the onset of outgrowth. **(B)** Time-lapse single confocal mid-slices of different polarity markers wandering around the spore surface before outgrowth. White arrows point at successive polar cap positions. Note that the nuclear localization of CRIB-GFP is a by-product of the probe, similarly observed in vegetative cells. **(C)** Time-lapse single confocal mid-slices of spores co-expressing the indicated polarity components. Note how polarity components co-wander two by two.

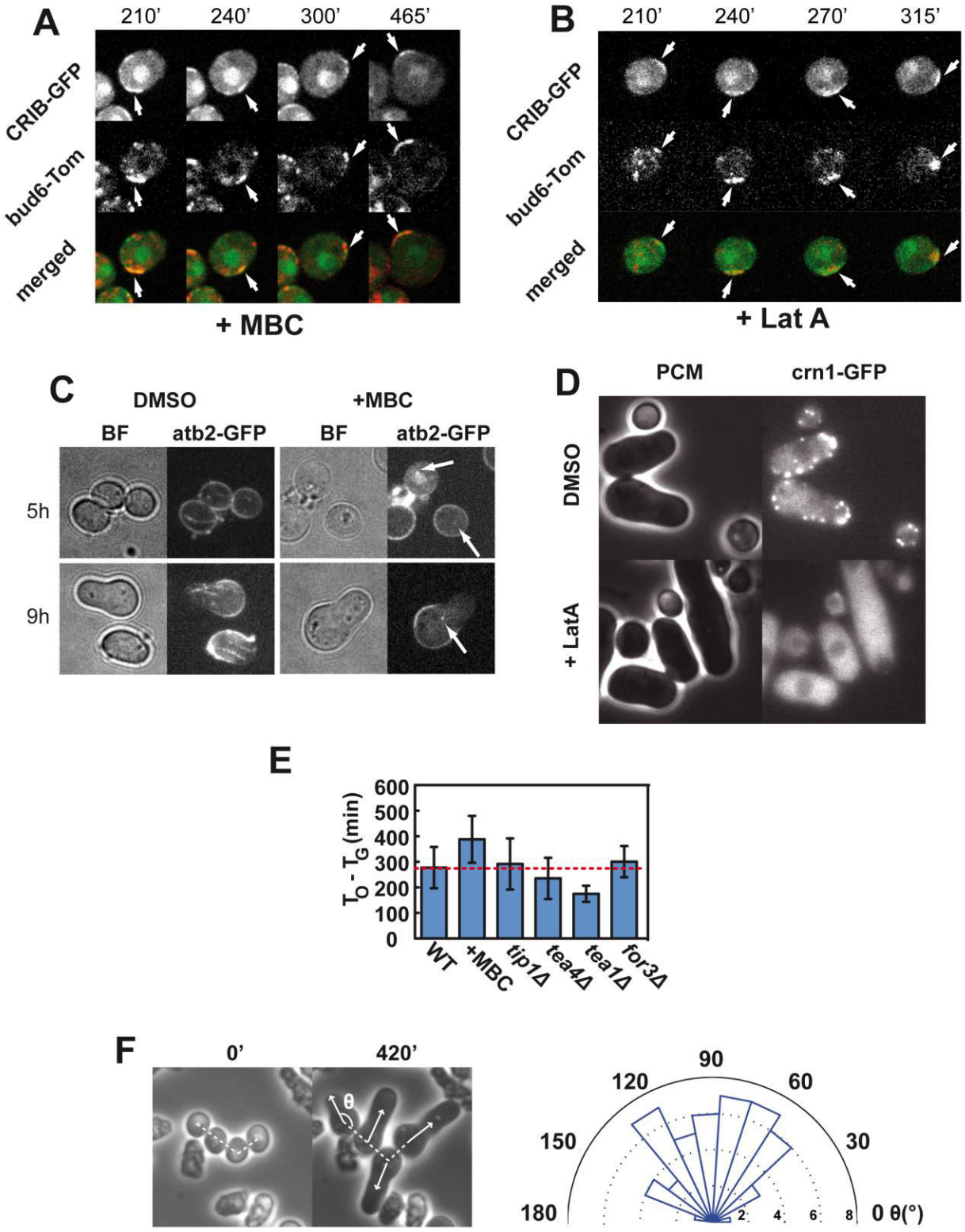
A
210'
240'
300'
465'
CRIB-GFP
bud6-Tom
merged
+ MBC
B
210'
240'
270'
315'
CRIB-GFP
bud6-Tom
merged
+ Lat A
C
DMSO
+MBC
BF
atb2-GFP
BF
atb2-GFP
5h
9h
D
PCM
crn1-GFP
DMSO
+ LatA
E
$T_O - T_G$ (min)
600
500
400
300
200
100
0
WT
+MBC
tip1Δ
tea4Δ
tea1Δ
for3Δ
F
0'
420'
θ
90
120
60
150
30
180
0 θ(°)
2
4
6
8

Figure S3

Supplemental Figure 3 (Related to Figure 2): Polar cap establishment, wandering and stabilization at outgrowth are independent on MTs, MT -associated factors, actin and memory cues

(A) Polar cap wandering is independent of microtubules: Time-lapse single confocal mid-slices of MBC-treated spores expressing CRIB-GFP and bud6-Tomato. White arrows point at the polar cap positions. **(B)** Polar cap wandering is independent of actin. Time-lapse single confocal mid-slices of LatA-treated spores expressing CRIB-GFP and bud6-Tomato. **(C)** Controls for the effect of the Microtubule depolymerizing drug MBC in spores. Bright-field and merged 12 z-stacks of spores expressing GFP-atb2, grown from germination in DMSO (control) or MBC. **(D)** Controls for the effect of Latrunculin A in spores. Phase contrast and epifluorescence images of control and LatA treated spores expressing crn1-GFP, a marker of actin patches. Addition of LatA, causes equal disappearance of actin structures in vegetative cells and in spores. **(E)** Mean germination to outgrowth times of indicated mutants (n>30 for each condition). Note the large variation in absolute time between different mutants. **(F)** Outgrowth direction is independent of previous meiotic division position. Left: Group of daughter spores derived from a mother ascus before germination and after outgrowth. The angle θ, represents the angle between the final growth direction (indicated by the white arrows) and the division axis between two close spores (indicated by the white dotted line). Right: Rose plots integrating angles from 80 different spores. Error bars correspond to standard deviations.

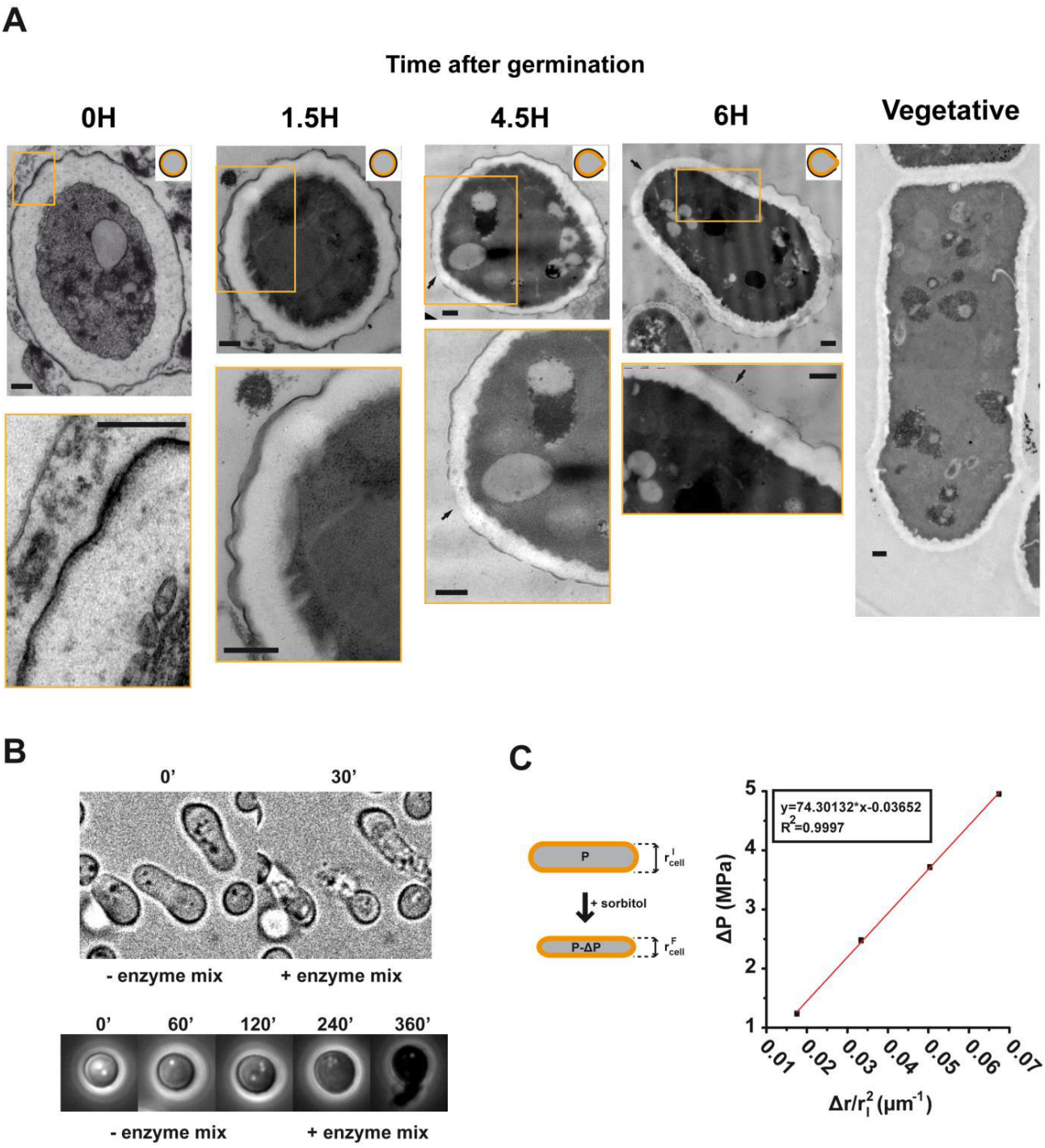
A
Time after germination
0H
1.5H
4.5H
6H
Vegetative
B
0'
30'
- enzyme mix
+ enzyme mix
0'
60'
120'
240'
360'
- enzyme mix
+ enzyme mix
C
P
+ sorbitol
P-ΔP
y=74.30132*x-0.03652
R2=0.9997
ΔP (MPa)
Δr/r1^2 (μm^-1)

Figure S4

Supplemental Figure 4 (Related to Figure 3): Evolution of spore cell walls during spore development and mechanics of cell walls.

(A) Transmission Electron Microscopy images of spores at different times after germination, with corresponding phenotype drawings and close-ups. Black arrows point at sites on the spores surface with no apparent OSW. Scale bars, 200 nm. **(B)** (Top) Description of the death assay used to monitor the presence of an intact spore outer spore wall. The time-lapse depicts the effect of the addition of an inner cell wall enzyme mix on spore (protected by the OSW) and outgrown spores where the tip is not protected anymore. Spores survive but outgrown spores burst and die within less than 30 minutes. (Bottom) Phase contrast time lapse of a single wild-type spore grown in microfluidic chambers from germination. The inner wall enzyme mix is added 3h after germination. At time 6h, note how the spore burst and dies because of the enzyme mix digesting the inner wall not protected anymore by the opened OSW. **(C)** (Left) Stress-strain experimental approach used to measure the elastic properties of vegetative walls: vegetative cells are exposed to different concentrations of sorbitol and the corresponding deformation at the tip side is measured, by tracking changes in local radius of curvature; (Right) Cell deformation scales linearly with osmotic pressure drops caused by dose-dependent sorbitol addition. Pressure drop is plotted as a function of local deformation of the tip for the case of WT vegetative cells. The surface modulus of the cell wall can be extracted from the linear fit (indicated by the red line), as described in experimental procedures.

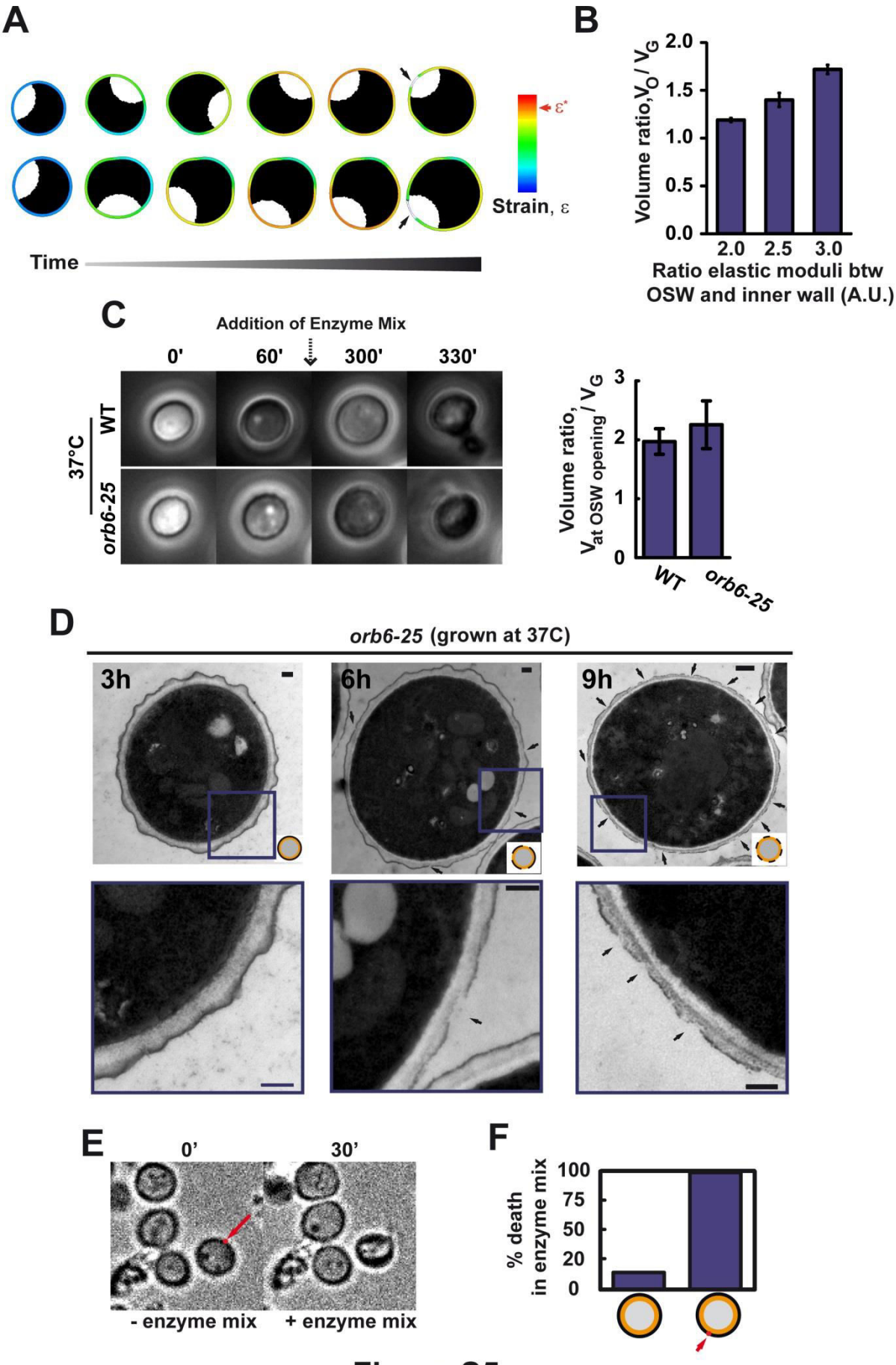
A
Time
Strain, ε
B
Volume ratio, V_O / V_G
2.0
1.5
1.0
0.5
0.0
2.0 2.5 3.0
Ratio elastic moduli btw
OSW and inner wall (A.U.)
C
Addition of Enzyme Mix
0'
60'
300'
330'
37°C
WT
orb6-25
Volume ratio,
$V_{at\ OSW\ opening} / V_G$
3
2
1
0
WT
orb6-25
D
orb6-25 (grown at 37C)
3h
6h
9h
E
0'
30'
- enzyme mix
+ enzyme mix
F
% death
in enzyme mix
100
75
50
20
0

Figure S5

Supplemental Figure 5 (Related to Figures 4, 5 and 6): Spatio-temporal control of rupture in the OSW; and optimization of the specificity of UV laser assay in fragilizing the outer spore wall but not the inner wall.

(A) Spores growing *in silico*. Colors in the OSW correspond to local strain/stress values in the OSW. Note the local rupture in the OSW marked by the arrow when the strain reaches the red zone. **(B)** Influence of the ratio between elastic moduli of inner and outer spore wall on volume ratio for outgrowth, as predicted from numerical simulations. **(C)** Growth in enzyme mix assay for wild-type and *orb6-25* spores (grown at 37°C). (Left) Phase contrast time-lapses of spores growing and bursting at the moment of OSW opening. (Right) Volume ratio between spore volumes right before death, corresponding to OSW opening, and volume at germination. **(D)** Representative examples of TEM images of *orb6-25* spores grown at 37°C at different times after germination with corresponding phenotype drawings. Black arrows point at sites on the spores surface with openings in the OSW. Scale bars, 200 nm. Error bars correspond to standard deviations. (**E)** Use of enzyme mix death assay to optimize the selective effect of laser photoablation on the spore outer wall but not inner wall. The spore indicated by the arrow is photoablated, and the three other spores serve as controls. After rinsing with the enzyme mix, only the photoablated spore dies. **(F)** Death assay quantification in photo-ablated spores: percentage of dying spores in the enzyme mix in the case of photoablated and non-photoablated spores (n=37 spores).

2.

Actin-based transport adapts polarity domains size to local curvature

2.1 Summary

Cells of different size and shape can assemble polarity domains, which are generally constituted of small Rho-GTPases, such as Cdc42; these domains are built up through the dynamic exchange of thousands of molecules between the cytoplasmic pool and the membrane, and their size appears to scale with cell size itself. This is a fundamental yet poorly understood paradigm likely relevant to most cells, as large eggs of 100 µm in diameters specify Rho GTPases polarity domains which have typical width of 30-50 µm; while small cells of 3-4 µm in diameters, define domains of 1-2 µm in width.

In this work, I aimed at defining scaling laws for how polarity domain adapt to cell geometry: as I have shown in my first paper, in fission yeast spores a polar cap is assembled early during germination, and wanders around the round spore surface (Bonazzi et al., 2014): very interestingly, I observed that its width evolves over time, as the spore increases in size, and changes shape, making this system optimal for investigating how polarity domains may adapt to local cell geometry (Figure 71). Thanks to a novel quantitative approach, I found a strong correlation between polar cap width and local radius of curvature. A similar behavior was observed also in the case of mutants with defective size (bigger or smaller), and by manipulating cell shape, either by deforming spores into microchannels or by enzymatic removal of cell wall in vegetative cells to obtain spheroplasts. The scaling was neither dependent on absolute size, nor

on the concentration of active Cdc42 at the membrane, suggesting that a local geometry-dependent cap spreading mechanism is involved.

To obtain mechanistic insights of this scaling phenomenon, I computed these effects in the presence of cytoskeleton drugs. Strikingly, this correlation is lost in the absence of actin, resulting in a significant decrease in pole cap size. These results suggest that actin functions in spreading the cap and adapting it to local curvature. Mutants in a formin, for3, which lack actin-cable, and secretion mutants displayed similar loss of scaling as LatA treatment, suggesting that actin controls polar cap size through cable based transport of vesicles to the membrane.

In parallel to the experimental approach, we developed mathematical models to understand how actin-based events at the molecular scale regulate cap size scaling: in the model, reaction-diffusion of Cdc42 associated components and actin-cable based vesicular trafficking can generate polarization states, but the actin-mediated process only appears to affect the size of the polarity domain. Live-imaging of LifeAct-mCherry in germinating spores shows that actin cables mostly distribute at the spore surface, suggesting that vesicles need to get to from the cytoplasm to the surface to be efficiently transported at the pole cap. Hence, the actin-mediated pole cap scaling may result from the local surface/volume ratio of the dome defined by cables.

In conclusion, this work investigates a scaling phenomenon which allows the cell to locally probe its geometry in an actin-dependent manner to assemble a polarity domain of the appropriate size, and may be relevant for cells in different physiological conditions.

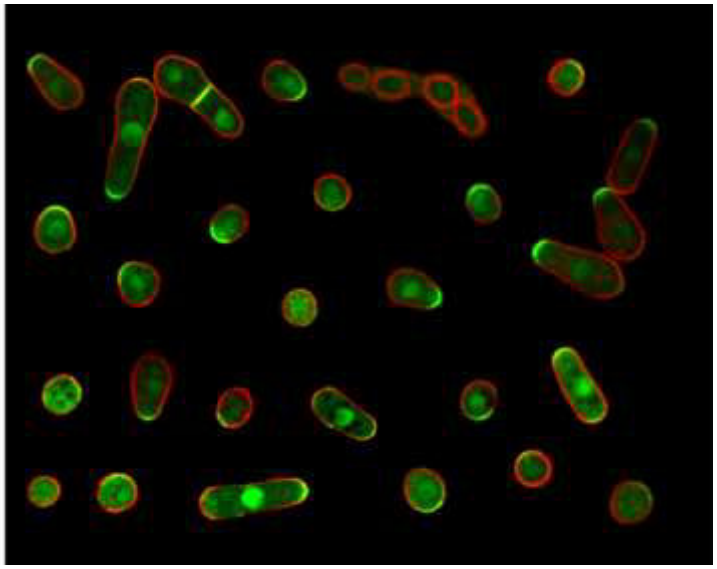

Figure 71: Example of fission yeast spores at different developmental stages. Spores express the polarity marker CRIB-GFP and the membrane marker Psy1-mCherry. Note the diverse shapes cells can assume, and the corresponding adaptation of pole cap size.

2.2 Paper

Bonazzi Daria, Salort Delphine, Minc Nicolas

Actin-based transport adapts polarity domains size to local curvature

Manuscript in preparation

ACTIN-BASED TRANSPORT ADAPTS POLARITY DOMAINS SIZE TO LOCAL CELLULAR CURVATURE

Daria Bonazzi[1], Delphine Salort[2] and Nicolas Minc[1*]

Affiliations: [1] Institut Jacques Monod, 15 rue Hélène Brion, 75205 Paris cedex 13, France

Tel: +331-572-780-52, Fax : +331 572-780-26

[2] Université Pierre et Marie Curie, 15, Rue de l'Ecole de Médecine, 75205 Paris cedex 06, France

* Corresponding author: Nicolas Minc, minc@ijm.univ-paris-diderot.fr

ABSTRACT

Cells polarize by clustering membrane-bound proteins to subcellular cortical domains. These domains are built around conserved Rho-GTPases, such as Cdc42, but can vary in size over two orders of magnitude in different cells. By tracking oscillating GTP-Cdc42 domains at the surface of growing fission yeast spores, we find that domain size scales with local radii of cellular curvature. Using experiments and modelling, we show that reaction-diffusion sets a minimal domain size, and that vesicle transport along cortical actin cables spread the domain to scale it to local curvature. This work suggests that actin networks may act as micrometric curvature sensors, and uncovers a general morphogenetic principle for how polarity domains adapt their size to particular cellular morphologies.

ONE SENTENCE SUMMARY

Actin filaments probe local cellular curvature to scale Cdc42 polarity domains to cell size or shapes.

Main Text: Cells in a wide range of shapes and sizes must define asymmetric functional polarity domains for orienting growth, migration or division. In eukaryotic cells, these domains are assembled near the cell surface as a consequence of the clustering of the active form of a Rho-type GTPase, such as Cdc42p (*1*). Localized GTPase activity instructs downstream reorganization of cytoskeletal elements and trafficking machineries for polarized behavior. Work in yeast and other systems, has suggested that the establishment of a polarity domain, of active Cdc42p for instance, may involve a combination of actin-mediated transport and reaction-diffusion mechanisms, both of which function in positive-feedback loops to amplify fluctuations in Cdc42p concentration into mature cellular-scale domains (*2-5*). Although generic principles and molecular modules appear to be conserved, polarity domains built around very similar molecules, may vary up to 2 orders of magnitude in different cells. For instance, large mouse oocytes display GTP-cdc42 domains that extend up to ~20-30μm in width, while small yeast cells have GTP-cdc42 domains that are typically ~2-3μm in width (*2, 6, 7*). The size of these domain is an important parameter for morphogenesis, as it patterns cell shape during polarized growth or daughter cell size in asymmetric divisions (*6-8*). In general, how these domains made of thousands of dynamic proteins may define their size and adapt it to cellular geometry, is not understood.

To address how cells may control the size of a polarity domain, we exploited the successive assembly and disassembly of active GTP-Cdc42 domains in fission yeast spores (*9*). During initial spore growth and development, which occurs within an extended G1 phase, single GTP-Cdc42 domains oscillate around the cell surface (*9*). These domains establish within a defined cellular size and geometry with a typical timing of around 10-15 min, and remain stable for

about 20-40 min to eventually disassemble and reform at another random location (Figure 1A and Supplementary movie S1). To visualize GTP-Cdc42 we used a Cdc42/Rac interactive binding domain labelled with three GFPs, CRIB-3GFP (*10*). Domain width was computed as the full width at half maximum, FWHM, from a gaussian fit of the intensity profile along the cell surface (Figure 1A). By performing this analysis in wild-type spores of various shapes and sizes, we found a striking positive correlation between domain width and cellular local radius of curvature, Rc , measured at the domain location. This correlation was well represented by an affine scaling such that: FWMH= 1.0μm + 1.2*Rc (n=142 cells, R^2= 0.489) (Figure 1B). In contrast, domain width was not correlated with cell volume (R^2= 0.0811), surface area (R^2= 0.087), CRIB-3GFP intensity at the cap (R^2= 0.0223) or timing after germination (Supplementary Figure 1A-1D). Similar scaling was obtained in vegetative cells which re-establish polarity at old ends soon after cytokinesis, suggesting this effect was not a particular property of spores (Figure 1B). Other upstream polarity components, including the Cdc42 GEF scd1p, the scaffold protein scd2p, the actin associated protein bud6p, and the glucan wall synthase bgs4p co-wandered with GTP-cdc42, and co-scaled their width to local curvature (*9, 11-13*) (Supplementary Figure 2A-H). 3D reconstructions revealed that domains had circular shapes in most instances, although we did observe a fraction of ellipsoidal domains in spores with flattened 3D shapes. The major axes of these ellipsoidal domains appeared to scale with corresponding principal radii of curvature in 3D (Supplementary Figure 3A and Supplementary movie S2). Analysis of spores of the Rho GAP mutants *rga4Δ* and *rga2Δ* which are respectively bigger and smaller than WT spores (*9*) allowed to extend the range of validity of this scaling, and suggested that domain width scaling is independent of fine-tuned Cdc42 activity (Figure 3C) (*7, 10, 14, 15*).

To directly manipulate local curvature independently of cell size, we first analyzed domain size in repolarizing WT spheroplast generated by enzymatic digestion of the cell wall (*8, 16*). Those spheroplasts come with similar volume as vegetative cells but significantly larger radius of curvature at the site of Cdc42 domain assembly. Domains were much larger than those at cell tips of control cells, and also scaled with local radii of curvature (Figure 1D). We also deformed spores into oblong geometries by forcing them into linear micro-channels (*17, 18*). Domains wandered around this particular geometry and became small when assembling at the curved tip and large when forming on the flat side of the deformed spore (Figure 1E). This very local effect was also observed in naturally anisotropic spores suggesting that domains adapt to cellular geometry, and not as a consequence of mechanical stress or confinement in chambers (Supplementary Figure 3B). Pulling together those different conditions, we could validate domain sizing over a 5-fold range in radii of curvature (from R_C= 0.8μm to R_C= 4.3μm), with FWMH= 0.75 μm + 1.37*Rc (n=588 domains, R^2= 0.72) (Supplementary Figure 3C). Thus, GTP-Cdc42 domains can probe local surface geometry to adapt their width to micrometric cellular curvatures.

Cytoskeleton-based transport has been proposed to contribute to the assembly of polarity domains (*19*). In fission yeast spores, although microtubule depolymerization did not impact domain size and scaling; we found that complete actin disassembly with 100μM Latrunculin A (LatA) had a major impact on domain size. GTP-cdc42 domains still displayed oscillating behavior, but were significantly smaller than in controls. Importantly, these LatA treated

domains did not adapt their widths to curvature, but remained similarly small independently of cell geometry (Figure 2A and 2B). Similar effect of LatA treatment on domain size were obtained by visualizing scd1-3GFP and scd2-GFP caps (Figure 2C). Dynamic LatA wash-in experiments showed that domains shrank within ~20-30min to a minimal size independently of their initial width (Figure 2D). Conversely, LatA wash-outs, yielded domain expansion, albeit slower than in wash-in experiments, and width recovery adapted to local radius of curvature (Figure 2E). All together, these results suggest that an actin-independent system may set a minimal polarity domain size and that actin dynamically extend these domains to adapt them to local cellular curvature.

To understand the contribution of actin-independent and actin-dependent processes to polarity domain size scaling, we developed mathematical models for computing Cdc42 polarity domain size; using previous theoretical frameworks established for budding yeast polarity (*20-22*). The model is reduced to one-dimension representing the cell surface, by assuming a rotational symmetry and an infinite diffusion in the cytoplasm. The model incorporates: (i) a reaction-diffusion based mechanisms for Cdc42 activation at the membrane which involves a positive feedback loop with an activation complex (GEF-scaffold) and local removal of inactive-Cdc42 by Guanine Dissociation factors (Rdi) (*22*); (ii) actin-cable based directed transport along secretory vesicle transporting more Cdc42 to the domain by exocytosis; and (iii) actin-dependent endocytosis which recycle Cdc42 from the membrane into nascent vesicles (*20, 21*) (Supplementary Figure 4A and 4B, and Supplementary models). These simulations showed that both reaction-diffusion alone, and reaction-diffusion coupled with actin-based transport and recycling could yield spontaneous Cdc42 domain formation from an initial un-polarized state, in

agreement with previous work (*20-22*) (Figure 3A and 3B). Interestingly, the predicted size of these domains were significantly smaller without the actin contribution in the model; in close agreement with LatA experiments (Figure 3A and 3B). By tuning independent parameters in the model, we could predict dose-dependent effects of actin-based transport on domain size. In general, an increase in vesicle transport rate along actin cables or vesicle fusion events or an improved cable nucleation yielded broader caps, suggesting that secretory vesicle flux along actin cables could play a central role in regulating domain size (Supplementary Figure 4C-4F).

To experimentally test these predictions, we used specific drugs and mutants, which display characterized defects, in actin nucleation, exocytosis and endocytosis. Strikingly, we found that in *for3Δ* spores, which lack for3-nucleated actin cables (*23*), Cdc42 domain size was smaller than wild-type, and did not scale with cellular radius of curvature (Figure 3C, Supplementary figure 5A). A *sec8-1* mutant which blocks secretory vesicle fusion at restrictive temperature (*24*), displayed similar phenotype as *for3*Δ, with even smaller domains (Figure 3C, Supplementary Figure 5B). The overall variation in mean domain size between WT, WT + LatA (no actin cables and no endocytic actin patch), *for3Δ* (no actin cable) and *sec8-1* (no vesicle fusion) was qualitatively captured by changing corresponding parameters in the model (Figure 3D, Supplementary figure 4C-F). In contrast, endocytosis did not appear to grossly impact domain size and scaling to local cell curvature. Characterized endocytic mutants in the adaptor protein End4p (*25*) and in the WASp-like protein Wsp1p (*26*) or short-time treatment with 100μM of CK666 which disrupt Arp2/3-nucleated actin endocytic patches (*27*), all displayed similar domain size behavior as WT controls (Figure 3C, Supplementary Figure 5C). In addition, GTP-cdc42 binding rates and/or diffusion properties at the membrane did not change significantly

with cellular curvature as assayed by FRAP experiments of scd2-GFP which binds active GTP-cdc42 (Supplementary figure 5D and 5E) (*28*). Together, these results suggest that secretory vesicles transported along actin cables, which carry more Cdc42 to the domain, may function to extend polar domains to adapt them to local cellular curvature.

We next asked how cellular curvature could influence the dynamics and/or organization of actin-cable based transport. To that aim, we visualized actin cables growing from GTP-Cdc42 domains, in spores expressing LifeAct-mCherry and CRIB-3GFP (*29*). Actin cables were relatively straight, with varying lengths and were quite dynamic (Figure 4A, Supplementary movie 3 and 4). Notably, 3D analysis of cables location revealed that the vast majority of actin cables were restricted to a cortical region within 0.4μm underneath the plasma membrane, in agreement with previous report in budding yeast (Figure 4B and 4C) (*30*). Similar cortical actin cable confinement was also observed in vegetative cells (Figure 4C and Supplementary figure 6A). This actin cable arrangement at the cell cortex may thus represent an optimal configuration to probe cellular surface geometry.

Actin cable nucleation by the formin for3, did not appear to be sensitive to cell curvature. For3 exhibited a dotty patterns clustered in a single domain, which scaled with local radius of curvature, and with near constant dots density (Supplementary figure 6B-6D) (*31*). We also sought to compute cable length distributions as a function of cellular curvature. Because actin patches obscured the visualization of short cables around the polarity domain, we treated cells with CK666, which does not influence domain size (Figure 3C), to selectively disassemble actin

patches, and imaged actin cables within 5 min of treatment. Although this treatment oftentimes yielded one large stable bundle in the spores, the rest of the cable network appeared to be similar as untreated cell (Figure 4D) (*27*). Actin cables lengths, computed in 3D, exhibited an exponential distribution reminiscent of *in vitro* measurement (*32*). The majority of cables had a length of 1-2μm, and only few cables extended up to 5-6μm. Importantly, this length distribution was unchanged with local curvature (Figure 4E). Together these result suggest that in varying cell surface geometry, actin cable networks may grow with similar nucleation density and length distribution into a dome-like shape that follows the local curvature surrounding GTP-cdc42 domain (Figure 4G) (*33*). We envision that the geometry of this dome-like network could influence secretory vesicle trafficking efficiency carrying Cdc42 to the polar domain. For instance, by analyzing the variation of geometrical parameters of actin domes, such as solid angles, surfaces or local volumes (Supplementary model), we found that the local surface/volume defined had the most significant increase with Rc in the range of cable length and radius probed in this study (Figure 4F). Since secretory vesicles diffuse in bulk cytoplasm, their ability to bind an actin cable at the surface could be significantly influenced by local surface/volume effects (*34*). We thus propose that this pure geometrical effect could account for domain size scaling with curvature (Figure 4G).

In sum, our quantitative analysis of oscillating GTP-cdc42 domains in fission yeast spores allowed us to propose novel models for the determination of polarity domain size. While most studies to date have assumed that cellular morphogenetic parameters, such as the cell diameter in fission yeast, was a defined output of the size of GTP-Cdc42 polarity domains (*7, 8*), our data demonstrate that these domains can also probe local geometry in an autonomous manner to

define their own size. The steady cell cycle state of spores combined with significant changes in cell size and shape, and domains oscillations provides an optimal system to test and dissect this mechanism. We thus suggest that the definition of domain size and cell shape may be intricately coupled within feedbacks mechanisms, which may underlie a homeostasis in cell shape control. It will be interesting to assess this feedback in mutants with irregular diameters such as skittled- or bottled-shaped mutants (*35*). An important finding of our study is that GTP-cdc42 domain size may be purely guided by local surface curvature, rather than absolute cell volume, cell cycle progression or Cdc42 concentration. Although the sizes of these domains could be tuned by the regulation of Cdc42 activity by GAPs and GEFs for instance (*7*), our data support a mechanism independent on this fine-tune activity, plausibly closer to a spontaneous self-assembling system. Although actin was not required for domain formation, we found significant evidence that actin filaments-based vesicle trafficking back to the domain mediate local cellular curvature sensing. We suggest that actin cable network assembly on a curved surface may yield sufficient variations in local surface/volume ratios in the global network to influence the kinetics of vesicle attachment. Alternative effects of curvature could be on the detachment or rupture of filaments themselves which grow and curve on the surface (*36*). Curvature sensing for cap size determination may thus not be encoded at the level of protein or polymer structural properties (*37*), but rather as a result of self-organization on a defined geometry (*38*). Actin networks have been proposed to be sensitive to surface geometry in several *in vitro* and *in vivo* contexts (*39-41*). Because most eukaryotic cells share the use of Rho GTPase and actin-based systems to cluster functional cortical polarity domains, our study promise to have broad relevance to the understanding of geometry-polarity feedbacks needed for morphogenesis.

ACKNOWLEDGMENTS

The authors acknowledge S. Martin , M. Balasubramanian and A. Paoletti for sharing strains. We thank members of the Minc Laboratory, G. Romet-Lemonne, A. Jegou and D. Tareste for technical help and discussions. Our laboratory is supported by the CNRS, and grants from the FRM (AJE20130426890), the FP7 CIG program and ITN "FungiBrain" and the "Mairie de Paris emergence" program.

EXPERIMENTAL PROCEDURES

Yeast Strains, Media, and Genetic Methods: Standard methods for *S. pombe* media and genetic manipulations were used (http://www-bcf.usc.edu/~forsburg/). Strains used in this study are listed in Table S1. Spores were obtained from homothallic h90 strains. Freshly growing cells were sporulated on malt extract (ME) solid media for 3 days. Spores were then digested 1h at room temperature in 1/200 glusulase solution in water to kill vegetative cells and the enzyme was washed out 3 times in water. For measurements of local radii of curvature and domain widths, spores were germinated and grown in liquid YE5S for 3h at 30°C before imaging.

***Pharmacological Inhibitors*:** Methyl-2-benzimidazole carbamate (MBC, Aldrich) was used at a final concentration of 50µg/ml from a 100X stock solution made fresh in DMSO. Latrunculin A (LatA, Sigma) was used at a final concentration of 100µM from a 100X stock in DMSO. The Arp2/3 inhibitor CK666 (Tocris Bioscience) was used at a final concentration of 100 µM from a 10-mM stock solution in DMSO.

Microscopy: For long-term imaging, spores in water solution were placed on 2% agar YE5S pads and covered with a coverslip. For drug treatment, spores were placed in a home-made glass channel coated with poly-lysin and lectin: in this setup, spores stick to the surface allowing live fluid exchange. Spore development was imaged at room temperature (23°C –25°C), with controlled humidity, with an inverted Spinning-Disk confocal microscope provided with a motorized stage and automatic focus (Nikon Ti-Eclipse), and an EM-CCD camera (Hamamatsu).

Images were generally acquired with a 100X oil immersion objective (Nikon S Fluor 100x 0.5-1.3 NA), occasionally using an additional 2.5X lens for improved spatial resolution. Time-lapses of CRIB-3GFP were acquired at the mid focal plane. 3D localizations of CRIB-3GFP and LifeAct-mCherry were performed by acquiring 26 z-stacks with a 0.2µm step. Full-tip and half-tip FRAP experiments were performed on the same microscope, using an iLas system and manually drawing a region corresponding to the full or half cap respectively. Images were acquired with Metamorph.

Image Analysis: Morphogenetic parameters of single developing spores were extracted from confocal fluorescence images using recent home-built Matlab scripts (*9, 18*). Quantification of local radius of curvature at the polarity domain was computed by drawing a line scan on the CRIB-GFP image and by fitting it with a circle using a semi-automated Matlab Script. Quantification of pole cap width was computed by drawing a line scan around the CRIB-3GFP domain and performing a Gaussian fit on the signal intensity to compute the full cap width at half maximum (FWHM) using a semi-automated Matlab Script. Local concentration of Cdc42p at the pole cap was measured from the average intensity of CRIB-3GFP at the domain after background subtraction. Temporal averaging of single confocal For3-3GFP images was performed by projecting 30 single images over a 30 sec mid-plane confocal time-lapse. For3-3GFP stable dots number were identified and quantified from kymographs along a line contour around the for3 domain. Measurement of actin cables length in 3D was performed using Imaris software.

Micro-channels operation: Micro-channels were fabricated using standard soft-lithography and PDMS methods (*18*). The PDMS channels were pierced, and was washed along with a glass coverslip, with acetone, isopropanol, water, and air-dried. PDMS and glass were activated with a plasma cleaner (Harrick). The PDMS channels were subsequently placed, holes facing down, onto the glass coverslip for bonding. Channels were subsequently baked for 1h at 65°C to improve binding. Channels have a rectangular section, are ~3µm deep and 2.5µm wide. *rga4Δ* **s**pores expressing CRIB-3GFP were germinated and grown for 3h, and a 10µl drop of spore suspension was then pushed into the channel hole using a syringe. This caused many spores to

deform into single micro-channels, thereby adopting an ellipsoidal shape. Pictures at different positions were then rapidly recorded to monitor polar domain wandering in deformed spores.

Spheroplasts protocol: Spheroplast generation was performed by using Lallzyme MMX protocole (*16*). Cell wall digestion was obtained by adding 0.1g/ml enzyme to wild-type cells in SCS buffer at room temperature. In these conditions, most cells lost their wall after 10-20 min treatment. The spheroplasts were then incubated during 2h in EMM + supplements with 1M sorbitol, and transferred onto glass slides for imaging. In these conditions, many spheroplasts initiated to re-assemble a single GTP-cdc42 polarity domain.

Mathematical Model for Cdc42 polarity: Details of the model are presented in supplementary material. Briefly, the model describes the dynamics of Cdc42 concentration along a one-dimension representing the cell surface (*20, 21*). The model is built around reaction-diffusion equations and mass conservations with parameters extracted from the literature or assessed in dose-dependent manner (see Table S2). The equations incorporate:
(1) An actin-independent system where Cdc42 exist at the membrane, in the cytosol, and in a complex form with Rdi1. Cytosolic elements have infinite diffusion coefficients, while membrane-bound proteins have finite diffusion. The concentration of active GTP-Cdc42 at the membrane is set to be proportional to Cdc42 at the membrane. A non-linear cubic term which accounts for positive feedback around GTP-cdc42, allows to break symmetry (*42*).
(2) An actin-dependent loop, where Cdc42 also exist in endocytic and secretory vesicles. The efflux and influx of these vesicles happens along actin structures with defined rates. Actin cables and patches are nucleated within the GTP-cdc42 domain in proportion with the local concentration of GTP-cdc42 which provides another feedback system for symmetry breaking.

FIGURE LEGENDS

Figure 1: GTP-cdc42 domains scale their widths to local cellular radius of curvature

(A) (Top) Confocal time-lapse of a germinating wild-type spore expressing the GTP-cdc42 marker CRIB-GFP. A polarity domain is initially assembled at one cortical site and dynamically explores the entire spore geometry by subsequent assembly dis-assembly. The red dotted line

indicates the cell contour at the pole cap location. (Bottom) Corresponding intensity profiles (red dots) and Gaussian fits (blue line) along a surface line contour for each time frame of the above time-lapse. The blue double-headed arrow indicates the full cap at half maximum (FWHM) of the Gaussian fit. **(B)** (Top) Confocal image of wild-type (WT) cells (blue) expressing CRIB-GFP at the onset of monopolar growth after cytokinesis, and spores of different shapes (red). The white arrow and corresponding circle representing the fitting used to compute local radius of curvature at the polarity domain, Rc. (Bottom) GTP-cdc42 domain FWHM plotted as a function of Rc, for wild-type cells reestablishing polarity (n=32) and spores (n=142). **(C)** (Top) Confocal images of *rga2Δ*, WT and *rga4Δ* spores expressing CRIB-GFP. (Bottom) GTP-cdc42 domain FWHM plotted as a function of Rc, for *rga2Δ* (n=72), WT (n=142) and *rga4Δ* (n=110) spores. **(D)** (Top) Confocal images of wild-type spheroplasts expressing CRIB-GFP. (Bottom) Schematic of cell shape manipulation by enzymatic wall digestion, and plot of GTP-cdc42 domain FWHM as a function of Rc, for WT spheroplasts (n=50) and WT spores (n=142). **(F)** (Top) Confocal images of CRIB-GFP expressing *rga4Δ* spores, outside (green) and inside (blue) micro-fabricated longitudinal channels. (Bottom) Schematic of cell shape manipulation using microchannels, and plot of GTP-cdc42 domain FWHM as a function of Rc, for non-deformed *rga4Δ* spores (n=50) and *rga4Δ* spores deformed in channels (n=119). Scale bars, 1 μm.

Figure 2: Actin mediate polar domain scaling to cellular curvature.

(A) Confocal merged stacks of wild-type spores expressing CRIB-GFP and LifeAct-mCherry in the presence of DMSO or 100μM Latrunculin A (LatA). **(B)** GTP-cdc42 domain FWHM plotted as a function of Rc, for control (n=142) and LatA treated (n=50) spores. Dotted lines represent linear fits with resulting slopes, s **(C)** Linear regression slopes, s, of domain size scaling as a function of Rc , for CRIB-3GFP, Scd1-3GFP and Scd2-GFP, in controls (n=142, for CRIB-GFP; n=19, for Scd1-3GFP; n=55, for Scd2-GFP) and LatA treated spores (n=50, for CRIB-GFP; n=13, for Scd1-3GFP; n=19, for Scd2-GFP). Error bars represent 95% confidence intervals. **(D)** (Top) Confocal time-lapse of a spore expressing CRIB-3GFP, 10 min before and 20 minutes after LatA treatment. (Bottom) Evolution of GTP-Cdc42 domain FWHM as a function of time, following LatA wash-in for 10 individual wild-type spores with various sizes. **(E)** (Top) Confocal time-lapse of a spore expressing CRIB-3GFP, before LatA treatment, 20 min after

LatA wash in and 60 min after wash out. (Bottom) Evolution of GTP-Cdc42 domain FWHM as a function of time, following LatA treatment and wash out for 6ndividual wild-type spores with various sizes. Scale bars, 1µm.

Figure 3: Actin cables-dependent secretory vesicle scale polarity domain to local curvature (A) Simulations of steady-state active GTP-Cdc42 concentration at the cell membrane contour (represented in 1D) resulting from pure reaction-diffusion (green) or reaction diffusion with actin-based transport and endocytosis (red). The blue line depicts the initial homogenous state **(B)** Kymographs representing the time evolution (in arbitrary unit) of GTP-Cdc42 along the cell membrane contour in the same conditions as in 3A. **(C)** Linear regression slopes, s, of CRIB-3GFP domain size scaling as a function of Rc, in the indicated mutants and drug treatment (n>20 in all conditions). Error bars represent 95% confidence intervals. **(D)** (left) Confocal image of wild-type, *for3Δ* and *sec8-1* (37C) spores expressing CRIB-3GFP. (Rigth) Experimental values and theoretical predictions of polarity domain sizes for control wild-type (n=142), wild-type treated with LatA (n=50), *sec8-1* (n=29) and *for3Δ* spores (n=97), Scale bars, 1µm.

Figure 4: A cortical actin-cable dome probes local cell surface geometry to scale polarity domains to local radii of curvature. (A) Confocal time-lapse of a wild-type spore expressing CRIB-GFP and LifeAct-mCherry. LifeAct images are maximal projections of confocal z-stacks taken at 0.2 µm internal. Arrows point at the pointed end of a growing actin bundle, nucleated from the polarity domain. **(B)** Confocal slices of spores expressing LifeAct-mCherry, at the bottom, mid and top focal plane. White arrows point at actin cables. **(C)** Quantification of actin cables distribution at the cell surface or interior, for spores and vegetative cells. Error bars represent standard deviations (n>10 in each condition). **(D)** (top) Confocal mid-planes images of CRIB-3GFP and corresponding 3D reconstruction of LifeAct-mCherry of CK-666 treated wild-type spores. Red lines indicate actin cables tracked in 3D. **(E)** Distribution of lengths of actin cables growing from GTP-cdc42 domains in CK-666 treated wild-type spores binned with respect to local radius of curvature. **(F)** Evolution of actin dome's surface to volume ratio as a function of local radius of curvature computed and weighted to account for actin cables length distribution in fission yeast spores. **(G)** Deformation of actin network by local surface curvature may account for polarity domain size adaptation to local curvature. An initial domain of GTP-

Cdc42 is assembled by reaction diffusion; actin cables then grow from this domain following the local curvature of the surface and define a dome-like network where they fetch vesicles that move to the domain, bringing more Cdc42 to expand the domain. The Surface/Volume ratio may influence the binding of vesicles from bulk cytoplasm to actin cables at the surface. As a consequence, an actin networks grown on a flat surface may bring more Cdc42 containing vesicles to the domain than on a curved surface, yielding a broader polarity domain. Scale bars, 1µm.

BIBLIOGRAPHY

1. D. G. Drubin, *Cell* **65**, 1093 (Jun 28, 1991).
2. R. Wedlich-Soldner, S. Altschuler, L. Wu, R. Li, *Science* **299**, 1231 (Feb 21, 2003).
3. F. Motegi, G. Seydoux, *Philosophical Transactions of the Royal Society B: Biological Sciences* **368**, 20130010 (2013).
4. A. Mogilner, J. Allard, R. Wollman, *Science* **336**, 175 (Apr 13, 2012).
5. J. E. Irazoqui, A. S. Gladfelter, D. J. Lew, *Nat Cell Biol* **5**, 1062 (Dec, 2003).
6. B. Dehapiot, V. Carriere, J. Carroll, G. Halet, *Dev Biol* **377**, 202 (May 1, 2013).
7. F. D. Kelly, P. Nurse, *Mol Biol Cell* **22**, 3801 (Oct, 2011).
8. F. D. Kelly, P. Nurse, *PLoS One* **6**, e27977 (2011).
9. D. Bonazzi *et al.*, *Dev Cell* **28**, 534 (Mar 10, 2014).
10. H. Tatebe, K. Nakano, R. Maximo, K. Shiozaki, *Curr Biol* **18**, 322 (Mar 11, 2008).
11. E. C. Chang *et al.*, *Cell* **79**, 131 (Oct 7, 1994).
12. E. Wheatley, K. Rittinger, *Biochem J* **388**, 177 (May 15, 2005).
13. J. M. Glynn, R. J. Lustig, A. Berlin, F. Chang, *Curr Biol* **11**, 836 (Jun 5, 2001).
14. M. A. Villar-Tajadura *et al.*, *Mol Microbiol* **70**, 867 (Nov, 2008).
15. M. Das *et al.*, *Mol Biol Cell* **18**, 2090 (Jun, 2007).
16. I. Flor-Parra, J. Zhurinsky, M. Bernal, P. Gallardo, R. R. Daga, *Yeast* **31**, 61 (Feb, 2014).
17. C. R. Terenna *et al.*, *Curr Biol* **18**, 1748 (Nov 25, 2008).
18. Y. Zegman, D. Bonazzi, N. Minc, in *Methods in Cell Biology*. (Academic Press, 2015).
19. R. Li, G. G. Gundersen, *Nat Rev Mol Cell Biol* **9**, 860 (Nov, 2008).
20. E. Marco, R. Wedlich-Soldner, R. Li, S. J. Altschuler, L. F. Wu, *Cell* **129**, 411 (Apr 20, 2007).
21. S. E. Smith *et al.*, *J Cell Biol* **202**, 1091 (Sep 30, 2013).
22. N. S. Savage, A. T. Layton, D. J. Lew, *Mol Biol Cell* **23**, 1998 (May, 2012).
23. B. Feierbach, F. Chang, *Curr Biol* **11**, 1656 (Oct 30, 2001).
24. H. Wang *et al.*, *Mol Biol Cell* **13**, 515 (Feb, 2002).
25. T. Iwaki, N. Tanaka, H. Takagi, Y. Giga-Hama, K. Takegawa, *Yeast* **21**, 867 (Jul 30, 2004).
26. W. L. Lee, M. Bezanilla, T. D. Pollard, *J Cell Biol* **151**, 789 (Nov 13, 2000).
27. T. A. Burke *et al.*, *Curr Biol* **24**, 579 (Mar 3, 2014).
28. N. S. Gov, *Phys Rev E Stat Nonlin Soft Matter Phys* **73**, 041918 (Apr, 2006).
29. J. Huang *et al.*, *J Cell Biol* **199**, 831 (Nov 26, 2012).
30. J. H. Yu, A. H. Crevenna, M. Bettenbuhl, T. Freisinger, R. Wedlich-Soldner, *J Cell Sci* **124**, 1533 (May 1, 2011).
31. S. G. Martin, F. Chang, *Curr Biol* **16**, 1161 (Jun 20, 2006).
32. S. Romero *et al.*, *Cell* **119**, 419 (2004).
33. D. W. Pruyne, D. H. Schott, A. Bretscher, *J Cell Biol* **143**, 1931 (Dec 28, 1998).
34. P. Rangamani *et al.*, *Cell* **154**, 1356 (Sep 12, 2013).
35. J. Hayles *et al.*, *Open Biol* **3**, 130053 (2013).
36. M. P. Murrell, M. L. Gardel, *Proc Natl Acad Sci U S A* **109**, 20820 (Dec 18, 2012).
37. T. S. Ursell *et al.*, *Proc Natl Acad Sci U S A* **111**, E1025 (Mar 18, 2014).
38. N. Minc, D. Burgess, F. Chang, *Cell* **144**, 414 (Feb 4, 2011).
39. A. Bernheim-Groswasser, S. Wiesner, R. M. Golsteyn, M. F. Carlier, C. Sykes, *Nature* **417**, 308 (May 16, 2002).
40. A. C. Reymann *et al.*, *Nat Mater* **9**, 827 (Oct, 2010).
41. M. Thery, A. Pepin, E. Dressaire, Y. Chen, M. Bornens, *Cell Motil Cytoskeleton* **63**, 341 (Jun, 2006).
42. A. B. Goryachev, A. V. Pokhilko, *FEBS Lett* **582**, 1437 (Apr 30, 2008).

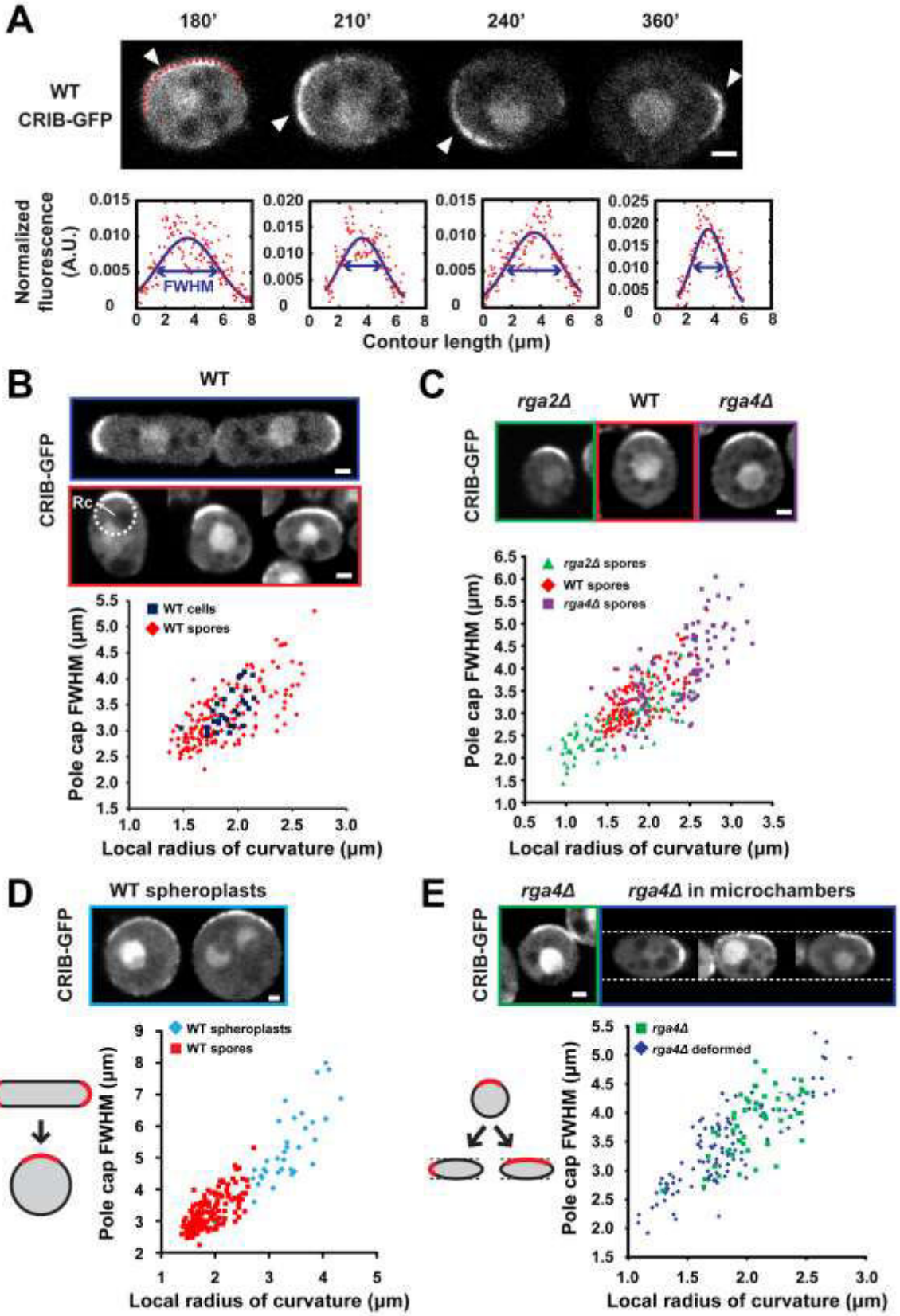
A
180'
210'
240'
360'
WT
CRIB-GFP
Normalized fluorescence (A.U.)
FWHM
Contour length (μm)
B
WT
CRIB-GFP
Rc
WT cells
WT spores
Pole cap FWHM (μm)
Local radius of curvature (μm)
C
rga2Δ
WT
rga4Δ
CRIB-GFP
rga2Δ spores
WT spores
rga4Δ spores
Pole cap FWHM (μm)
Local radius of curvature (μm)
D
WT spheroplasts
CRIB-GFP
WT spheroplasts
WT spores
Pole cap FWHM (μm)
Local radius of curvature (μm)
E
rga4Δ
rga4Δ in microchambers
CRIB-GFP
rga4Δ
rga4Δ deformed
Pole cap FWHM (μm)
Local radius of curvature (μm)

Figure 1

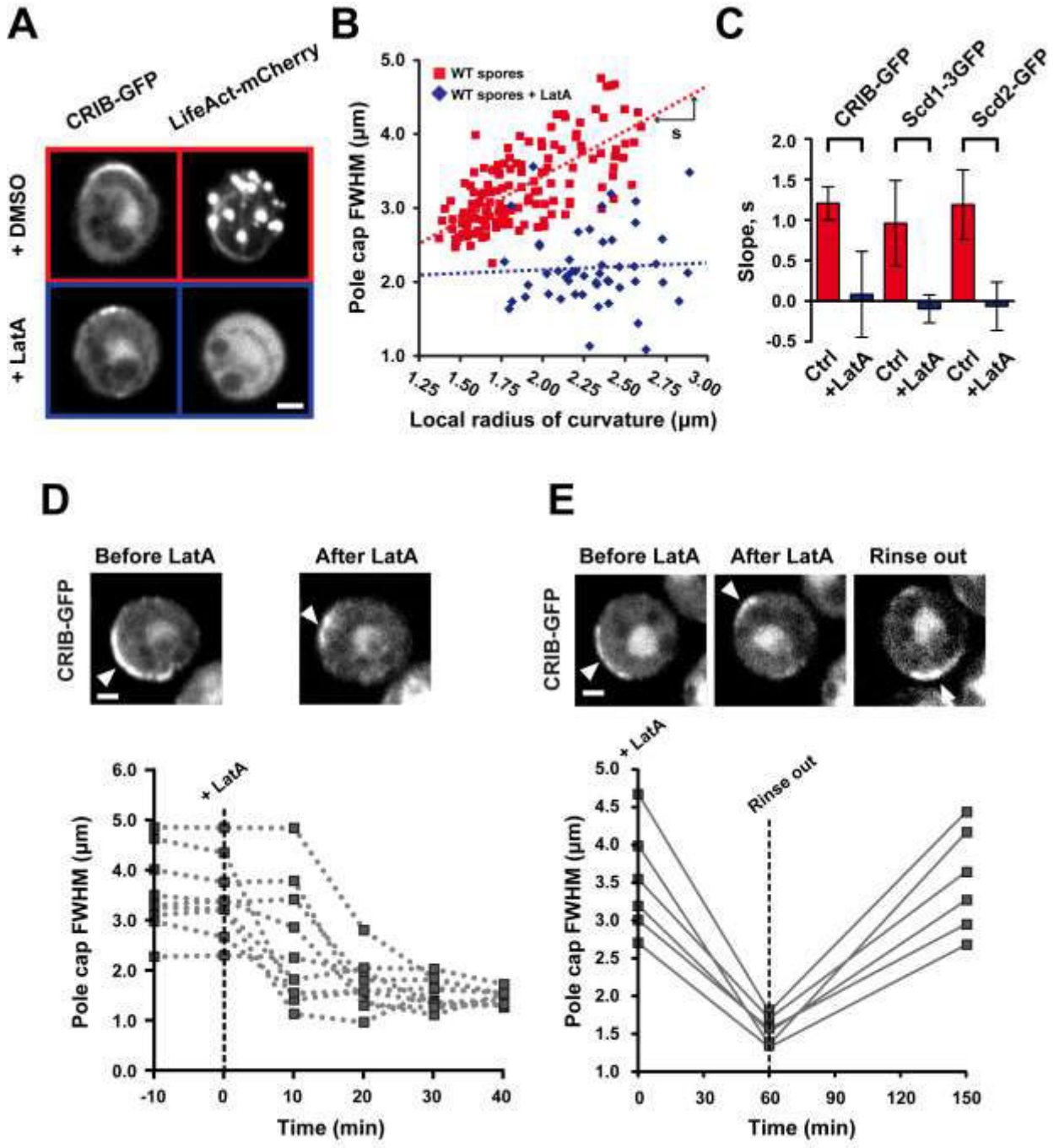
A
CRIB-GFP
LifeAct-mCherry
+ DMSO
+ LatA
B
WT spores
WT spores + LatA
Pole cap FWHM (µm)
Local radius of curvature (µm)
s
C
CRIB-GFP
Scd1-3GFP
Scd2-GFP
Slope, s
Ctrl
+LatA
D
Before LatA
After LatA
CRIB-GFP
+ LatA
Pole cap FWHM (µm)
Time (min)
E
Before LatA
After LatA
Rinse out
CRIB-GFP
+ LatA
Rinse out
Pole cap FWHM (µm)
Time (min)

Figure 2

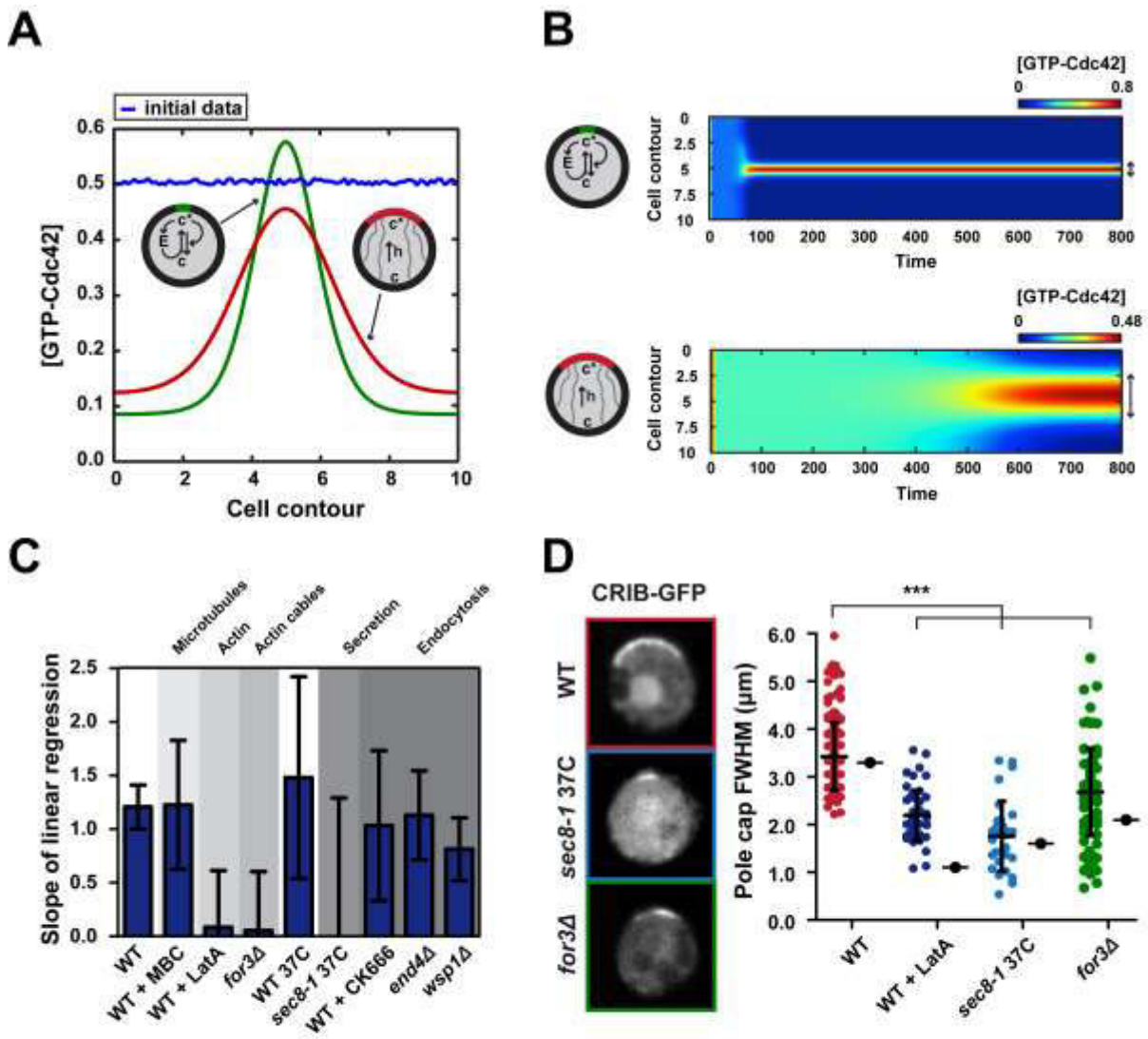
A
initial data
[GTP-Cdc42]
Cell contour
B
[GTP-Cdc42]
Cell contour
Time
C
Microtubules
Actin
Actin cables
Secretion
Endocytosis
Slope of linear regression
WT
WT + MBC
WT + LatA
for3Δ
WT 37C
sec8-1 37C
WT + CK666
end4Δ
wsp1Δ
D
CRIB-GFP
WT
sec8-1 37C
for3Δ
***
Pole cap FWHM (µm)
WT
WT + LatA
sec8-1 37C
for3Δ

Figure 3

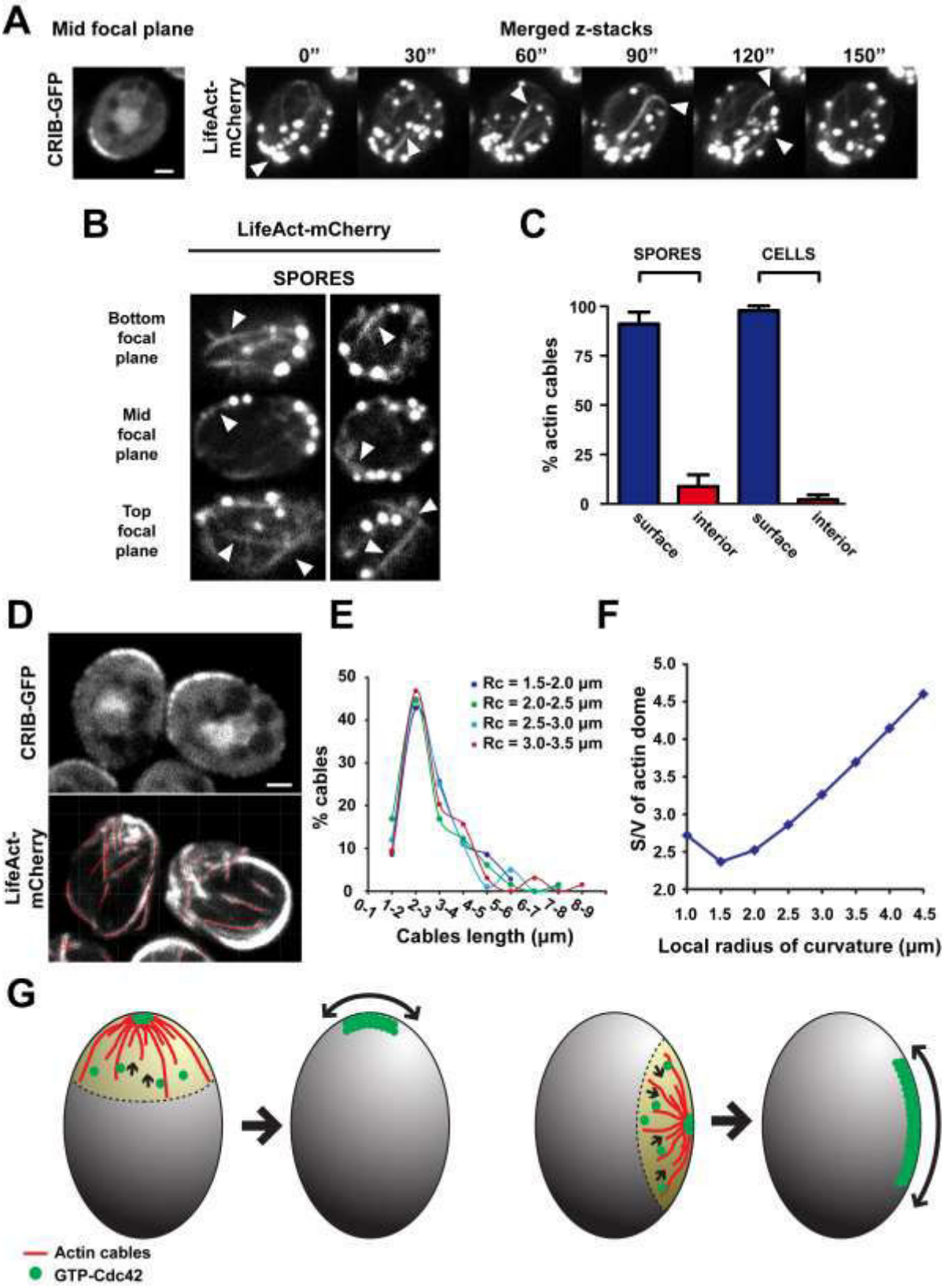
A
Mid focal plane
Merged z-stacks
0"
30"
60"
90"
120"
150"
CRIB-GFP
LifeAct-mCherry
B
LifeAct-mCherry
SPORES
Bottom focal plane
Mid focal plane
Top focal plane
C
SPORES
CELLS
% actin cables
100
75
50
25
0
surface
interior
surface
interior
D
CRIB-GFP
LifeAct-mCherry
E
% cables
Rc = 1.5-2.0 µm
Rc = 2.0-2.5 µm
Rc = 2.5-3.0 µm
Rc = 3.0-3.5 µm
Cables length (µm)
F
S/V of actin dome
Local radius of curvature (µm)
G
Actin cables
GTP-Cdc42

Figure 4

SUPPLEMENTAL INFORMATION

This file contains:

2 Supplementary models

Table S1

Supplemental Figure Legends S1-S6

Supplemental Figures S1-S6

1- Mathematical model for GTPCdc42 spatiotemporal evolution at the membrane

The aim of this mathematical model is to test how different components of reaction-diffusion and actin-transport loops may influence GTP-cdc42 domain size. We use previously established frameworks to derive differential equations, guiding the spatio-temporal dynamics of Cdc42 concentration at the membrane (*1-5*). We focus our output on domain size, rather than on the existence of polarity state. In other word, the model is already constraint by its ability to generate a clustered activity of Cdc42 at the membrane.

The model is kept as simple as possible, by making the following assumptions:

- The membrane of the cell is modeled as a straight line of fixed length, L.
- The diffusion of Cdc42 and vesicles in the cytoplasm is assumed to be infinite (*2, 4, 5*). This allows us to reduce the equations to a one dimensional problem where the space variable modeling the cell membrane is [0;L].

a- Actin-independent model

First, we model the Cdc42 symmetry breaking dynamics in the absence of actin-based transport and recycling. To this aim, we consider the following one dimensional model inspired from (*1*) defined on $(0,+\infty)\ [0;L]$ by:

$$\partial_t u(t,x) = \gamma A\big(u(t,x)\big)^2 C_b(t) - \theta u(R-\gamma C_b(t)) + a\partial_x^2 u(t,x), \qquad \text{(Eq 1)}$$

with boundary conditions: $u(t,0) = u(t,L); \partial_x u(t,0) = \partial_x u(t,l),$

and mass conservation:

$$\frac{d}{dt}C_b(t) = -\gamma A C_b(t)\int_0^L u^2(t,x)dx + \theta(R-\gamma C_b(t))\int_0^L u(t,x)dx \qquad \text{(Eq 2)}$$

- $u(t,x)$ represents the concentration of active GTP-Cdc42 at the membrane that we assume to be proportional to the membrane concentration Cdc42.
- $C_b(t)$ is the concentration of Cdc42 in the cytosol.
- R is the total concentration Rdi1which is set as a constant and is portioned between free Rdi1 and Rdi1 in a complex with Cdc42

- The concentration of Rdi1-Cdc42 is assumed to be proportional to Cb, via the fraction γ , with $0 < \gamma < 1$, so that the concentration of free Rdi1 is given by $(R - \gamma C_b(t))$

In Equation (Eq 1), the first term $\gamma A u^2 C_b$ accounts for a positive-feedback loop (GEF-adaptor) where more Cdc42 is recruited as a result of more activity at the membrane. The quantity of Cdc42 extracted from the membrane to the cytosol by Rdi1 is given by $\theta u(R - \gamma C_b(t))$ and the final term represent Cdc42 on the membrane with a diffusion coefficient a. Using previous report we fix parameters in this model as : $a = 0.01$, $\gamma = 0.4$, $\theta = 0.2$, $R = 0.6$, $L = 10$.

b- Model accounting for actin-based transport and membrane recycling

We then add to the above model actin-dependent endocytosis to extract Cdc42 in endocytic vesicles and actin-dependent transport and exocytosis where secretory vesicles carrying Cdc42 are directed toward the membrane along actin cables. To this aim, we introduce two novel functions:

- $C_v(t)$ which models the total concentration of Cdc42 in the vesicles
- $\chi(t, x)$ defines an actin-based transport window which describes the probability of an actin cable to be attached at position x at time t.
- For actin-patch mediated endocytosis, we assume that $\chi(t, x)$ also represents the probability to have an actin patch at the position x and time t; and we also allow patches to assemble away from the transport window with a probability $\frac{1}{\alpha}(1 - \chi)$. The extraction rate of Cdc42 by endocytic patches is given by the constant CC.

In the spirit of (*2*), we assume that the function $\chi(t, x)$ depends on $u(t, x)$ via the two parameters Ω and β, which respectively influence attachment and detachment rates of actin cables so that:

$$\partial_t \chi = (1 - \chi)\Omega u - \chi e^{-\beta u} \qquad \text{(Eq 3)}$$

The quantity of Cdc42 transported of secretory vesicles along actin cables is proportional to $C_v(t)\chi(t, x)$ via the directed exocityc rate constant h. In addition, we posit that exocytosis can occur in a non-polarized homogenous manner via the constant rate Ex.

Finally, we also assume a transfer from vesicle-bound Cdc42, C_v to cytoplasmic Cdc42 C_b via a constant rate dil. The new spatiotemporal evolution of Cdc42 at the membrane is thus given by the sets of differential equations (3)-(6):

$$\partial_t u = \gamma A u^2 C_b - \theta u(R - \gamma C_b) + a\partial_x^2 u - uCC\left(\chi + \frac{1}{\alpha}(1-\chi)\right) + ExC_v + hC_v\chi \quad \text{(Eq 4)}$$

with mass conservations equations on Cdc42 (Eq 5) and vesicles (Eq 6)

$$\frac{d}{dt}C_b = -\gamma A C_b \int_0^L u^2(x)dx + \theta(R - \gamma C_b)\int_0^L u(x)dx + dilC_v \quad \text{(Eq 5)}$$

$$\frac{d}{dt}C_v = -dilC_v - L\,Ex\,C_v + CC\int_0^L \left(u\chi + \frac{1}{\alpha}(1-\chi)\right)dx - hC_v\int_0^L \chi(x)dx \quad \text{(Eq 6)}$$

c- Numerical simulations for the model

In all the simulations we start with an initial homogenous concentration of GTP-Cdc42 with small fluctuations so that:

$$u(0,x) = 0.5 + 0.01rand(0,1)(x), \qquad C_b(0) = 1, \qquad C_v(0) = 0$$

Where $rand(0,1)(x)$ returns a random value between 0 and 1 at each x.

The simulations were then run using python, with a time step dt=0.005 and a length step dx=0.1 returning typical dynamic evolution of GTP-Cdc42 concentration at the membrane presented in Figure 3.

References

1. S. E. Smith *et al.*, *J Cell Biol* **202**, 1091 (Sep 30, 2013).
2. E. Marco, R. Wedlich-Soldner, R. Li, S. J. Altschuler, L. F. Wu, *Cell* **129**, 411 (Apr 20, 2007).
3. A. T. Layton *et al.*, *Curr Biol* **21**, 184 (Feb 8, 2011).
4. N. S. Savage, A. T. Layton, D. J. Lew, *Mol Biol Cell* **23**, 1998 (May, 2012).
5. A. B. Goryachev, A. V. Pokhilko, *FEBS Lett* **582**, 1437 (Apr 30, 2008).

Geometrical calculations for actin cable domes.

Based on our observation that actin cables grow from Cdc42 membrane domains with constant nucleation density and length distribution both independent of local curvature, we test here how the growth of this network on differently curved surface could influence its ability to transport vesicles. Our hypothesis is that actin cables are highly dynamic on the time-scale of polarity domain formation, so that they scan the local surface in an isotropic manner with lengths that distribute following measure length distribution (Figure 4)
For a spherical dome made of many cables with fixed length L_{cable} which runs along a curved surface of radius of curvature R_c, the surface, S_{dome} of the dome is given by:

$$S_{dome}(R_c, L_{cable}) = 2\pi {R_c}^2 (1 - \cos\left(\frac{L_{cable}}{R_C}\right))$$

the volume is given by:

$$V_{dome}(R_c, L_{cable}) = \frac{\pi}{3} {R_c}^3 (1 - \cos\left(\frac{L_{cable}}{R_C}\right))^2 * \ (2 + \cos\left(\frac{L_{cable}}{R_C}\right)),$$

and the solid angle is given by:

$$\Omega_{dome}(R_c, L_{cable}) = 2\pi(1 - \cos\left(\frac{L_{cable}}{R_C}\right))$$

For a given Rc we compute these geometrical values weighted by the probability density of filament length $p(L_{cable})$ obtained experimentally (Figure 4) .For instance the mean surface explored over time by an actin dome at a radius Rc is obtained by:

$$< S_{dome}(R_c) >= \int p(L_{cable})\, S_{dome}(R_c, L_{cable})$$

By performing these calculations, we find that the surface/volume ratio defined by the actin dome gives a correct scaling with Rc. We envision this effect to be a result of a switch from vesicle diffusion in bulk cytoplasm and binding at the surface on an actin cable in the dome.

Supplementary Table S1: Strains used in this study

DB_301	h90	wt CRIB-GFP::Ura	ade6-M216 leu1-32
DB_292	h90	rga4::KanMX CRIB-GFP::Ura	ade6-M216 leu1-32
DB_295	h90	rga2::KanMX CRIB-GFP::Ura	ade6-M216 leu1-32
DB_333	h90	for3::KanMX CRIB-GFP::Ura	ade6-M216 leu1-32
DB_339	h90	sec8-1 CRIB-GFP::Ura	
DB_335	h90	end4::KanMX CRIB-GFP::Ura	ade6-M216 leu1-32
DB_351	h90	wsp1::Leu CRIB-GFP::Ura	ade6-M216
DB_337	h90	wt CRIB-GFP::Ura Pact1-Lamcherry::Leu	ade6-M216
DB_364	h90	wt for3-3GFP::Ura	ade6-M216 leu1-32
DB_405	h90	wt bgs4::Ura GFP-bgs4-leu Pact1-Lamcherry::Leu	ade6-M216
DB_378	h90	wt scd1-3GFP::KanMX	
DB_377	h90	wt scd2-GFP::NatMX	
DB_228	h90	wt GFP-A8-cdc42::KanMX	
DB_124	h90	wt bgs4::Ura GFP-bgs4::Leu	
DB_287	h90	wt CRIB-GFP::Ura bgs4::Ura RFP-bgs4::Leu	
DB_327	h90	wt bud6-Tomato::NatMX bgs4::Ura GFP-bgs4::Leu	
DB_415	h90	wt sec6-GFP::Ura Pact1-Lamcherry::Leu	
DB_416	h90	wt sec8-GFP::Ura Pact1-Lamcherry::Leu	

SUPPLEMENTAL FIGURE LEGENDS

Supplementary Figure 1: Polarity domain width in spores is independent on cell volume, surface, Cdc42 concentration and timing after germination.

(A) Plot of CRIB-3GFP polarity domain FWHM as a function of cell surface in wild-type spores (n=142). **(B)** Plot of CRIB-3GFP polarity domain FWHM as a function of cell volume in wild-type spores (n=142). **(C)** Plot of CRIB-3GFP polarity domain FWHM as a function of CRIB-3GFP intensity at the cap in wild-type spores (n=142) **(D)** (Left) Phase contrast and confocal CRIB-3GFP time-lapse of wild-type germinating and outgrowing spores. (Right) Temporal evolution of polarity domain FWHM and local radius of curvature for a population of wild-type spores. Time zero corresponds to outgrowth onset. Each data point is averaged on 20 spores and error bars correspond to standard deviations.

Supplementary Figure 2: Canonical polarity marker all form polarity domain which scale with local radius of curvature.

(A) (Left) Polarity domain FWHM plotted as a function of Rc, for wild-type spores expressing Scd1-3GFP (n=19). Black dotted line indicates the result of linear regression analysis. (Rigth) Confocal mid-plane image of a spore expressing Scd1-3GFP. A light blue dotted line indicates the cell contour. **(B)** (Left) Polarity domain FWHM plotted as a function of Rc, for wild-type spores expressing Scd2-GFP (n=54). (Right) Confocal mid-plane image of a spore expressing Scd2-GFP. **(C)** (Left) Polarity domain FWHM plotted as a function of Rc, for wild-type spores expressing GFP-A8-Cdc42 (n=28). (Right) Confocal mid-plane image of a spore expressing GFP-A8-Cdc42. **(D)** (Left) Polarity domain FWHM plotted as a function of Rc, for wild-type spores expressing GFP-Bgs4 (n=47). (Right) Confocal mid-plane image of a spore expressing GFP-Bgs4. **(E)** (Left) Linear regression slopes, s, of domain size scaling as a function of Rc for different polarity markers. Error bars represent 95% confidence intervals. (Right) Polarity domain size measured with different polarity marker. Averages and Standard deviations are indicated in black (n>19 in all conditions). **(F)** (Left) Polarity domain FWHM plotted as a function of Rc, for wild-type spores expressing CRIB-3GFP and Bud6-Tomato, with corresponding values indicated in green and red respectively. (Right) Confocal mid-plane image of a spore expressing CRIB-GFP and Bud6-Tomato (n=20). **(G)** (Left) Polarity domain FWHM plotted as a function of Rc , for wild-type

spores expressing CRIB-GFP and RFP-Bgs4, with corresponding values indicated in green and red respectively. (Right) Confocal mid-plane image of a spore expressing CRIB-GFP and RFP-Bgs4 (n=20). **(H)** Ratio of polar domain FWHM obtained with each expressing polarity marker in single cells, for spores co-expressing CRIB-GFP and Bud6-Tomato or CRIB-GFP and RFP-Bgs4 (n=20).

Supplementary Figure 3: 3D adaptation of polarity domains, and validation of domain sizing over multiple conditions

(A) 3D reconstructions of confocal images of wild-type spores expressing CRIB-3GFP with different geometries. Side view, front view and segmented front view are shown for each cell. **(B)** (Left) Confocal mid-slices of naturally anisotropic *rga4Δ* spores expressing CRIB-3GFP. (Rigth) Polarity domain FWHM plotted as a function of Rc, for *rga4Δ* spores, *rga4Δ* spores deformed in microchambers and naturally anisotropic *rga4Δ* spores, indicated in green, blue and red respectively. **(C)** Combined data of polarity domain FWHM plotted as a function of Rc, for all indicated conditions (n=588 domains). Scale bars, 1μm.

Supplementary Figure 4: Mathematical models predicting domain size evolution from pure reaction diffusion and as a function of actin transport parameters.

(A) Schematic representing the mathematical model used to predict the assembly and size of an active GTP-Cdc42 domain at the membrane, based on pure reaction diffusion. **(B)** Schematic representing the mathematical model used to predict the assembly and size of an active GTP-Cdc42 domain at the membrane, accounting for actin-based transport and endocytosis. **(C-F)** Theoretical dependence of GTP-cdc42 domain FWHM on the following model parameters: **(C)** Exocytic rate via actin cables, h; **(D)** Exocytic rate without actin cables, Ex; **(E)** Probability of detachment of an actin cable, β; **(F)** Probability of attachment of an actin cable, Ω.

Supplementary Figure 5: Actin cables and vesicle fusion contribute to scale polarity domains to curvature, but endocytosis appears dispensable

(A) Polarity domain FWHM plotted as a function of Rc, for wild-type (n=142) and *for3Δ* (n=97) spores, indicated in red and green respectively. Dotted lines correspond to linear fits. **(B)** Polarity domain FWHM plotted as a function of Rc, for wild-type (n=19) and *sec8-1* (n=29) spores grown at 37°C, indicated in red and light blue respectively. Dotted lines correspond to linear fits. **(C)** Polarity domain FWHM plotted as a function of Rc, for wild-type (n=142), CK666-treated wild-type (n=18), *end4Δ* (n=53) and *wsp1Δ* (n=42) spores, indicated in red, green, purple and blue respectively. Dotted lines correspond to linear fits. **(D)** Fluorescence recovery half-times after full polarity domain photobleaching, for the indicated polarity markers (n>15 in all conditions). Average values and standard deviations are indicated in black. **(E)** Plot of recovery half-time as a function of local radius of curvature for wild-type spores expressing Scd2-GFP, for full domains (indicated in red) or half-domains (indicated in blue) photobleaching.

Supplementary Figure 6: Cortical actin cables in vegetative cells and for3 nucleator density as a function of local curvature.

(A) Confocal slices of vegetative cells expressing LifeAct-mCherry, at the bottom, mid and top focal plane. White arrows point at actin cables. **(B)** (Top) Single confocal image of a spore expressing For3-3GFP; (Bottom) Corresponding temporally averaged picture, obtained by a projection of 30 single images taken every 1 second over a 30 sec time lapse. **(C)** Polarity domain FWHM plotted as a function of Rc, obtained by quantification of temporally averaged For3-3GFP domains (n=46). Linear fit is depicted as a blue dotted line. **(D)** Polarity domain FWHM plotted as a function of For3-3GFP stable dots number. Mean values and corresponding standard deviations are shown (n>10 in all conditions).

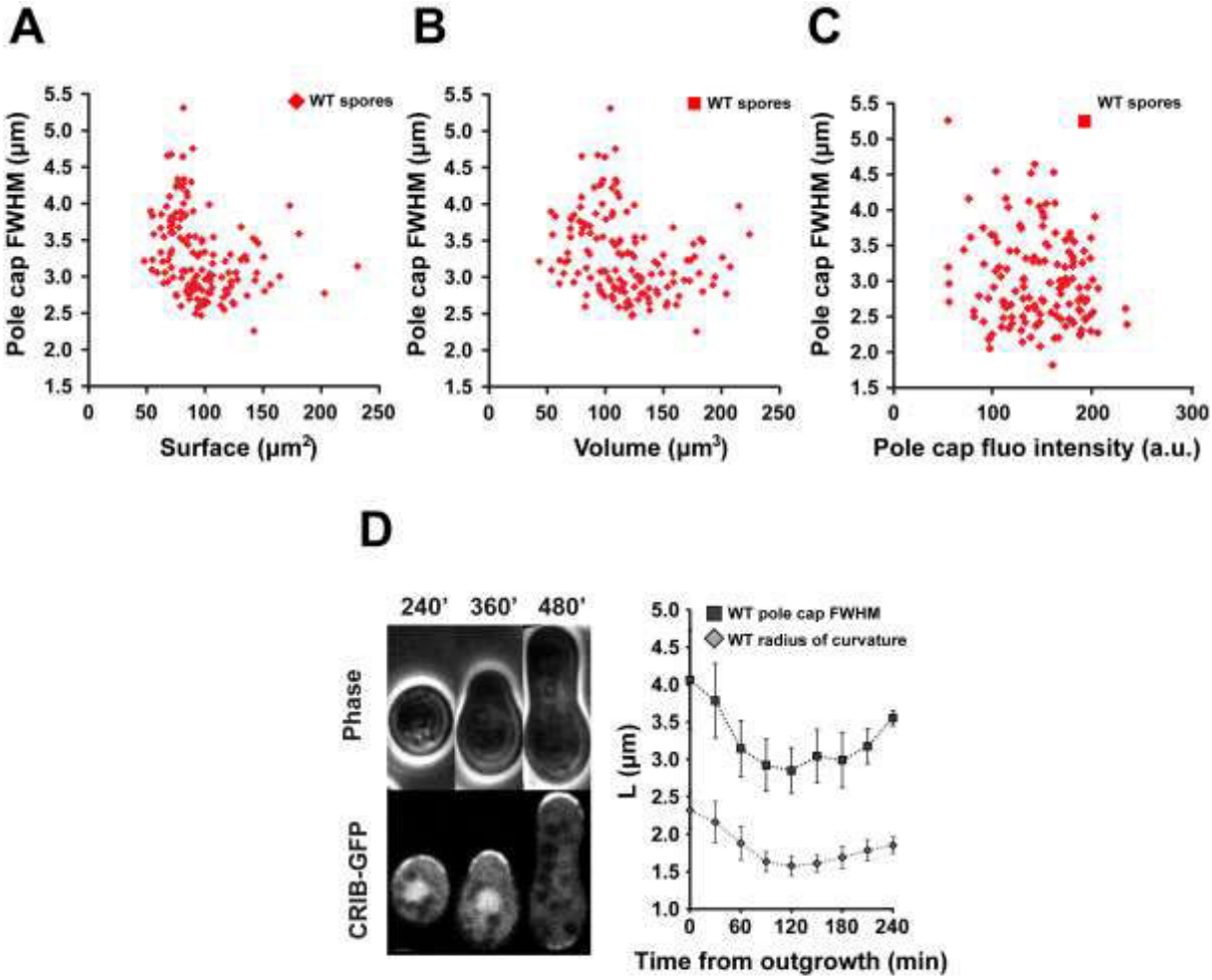

Supplementary Figure 1

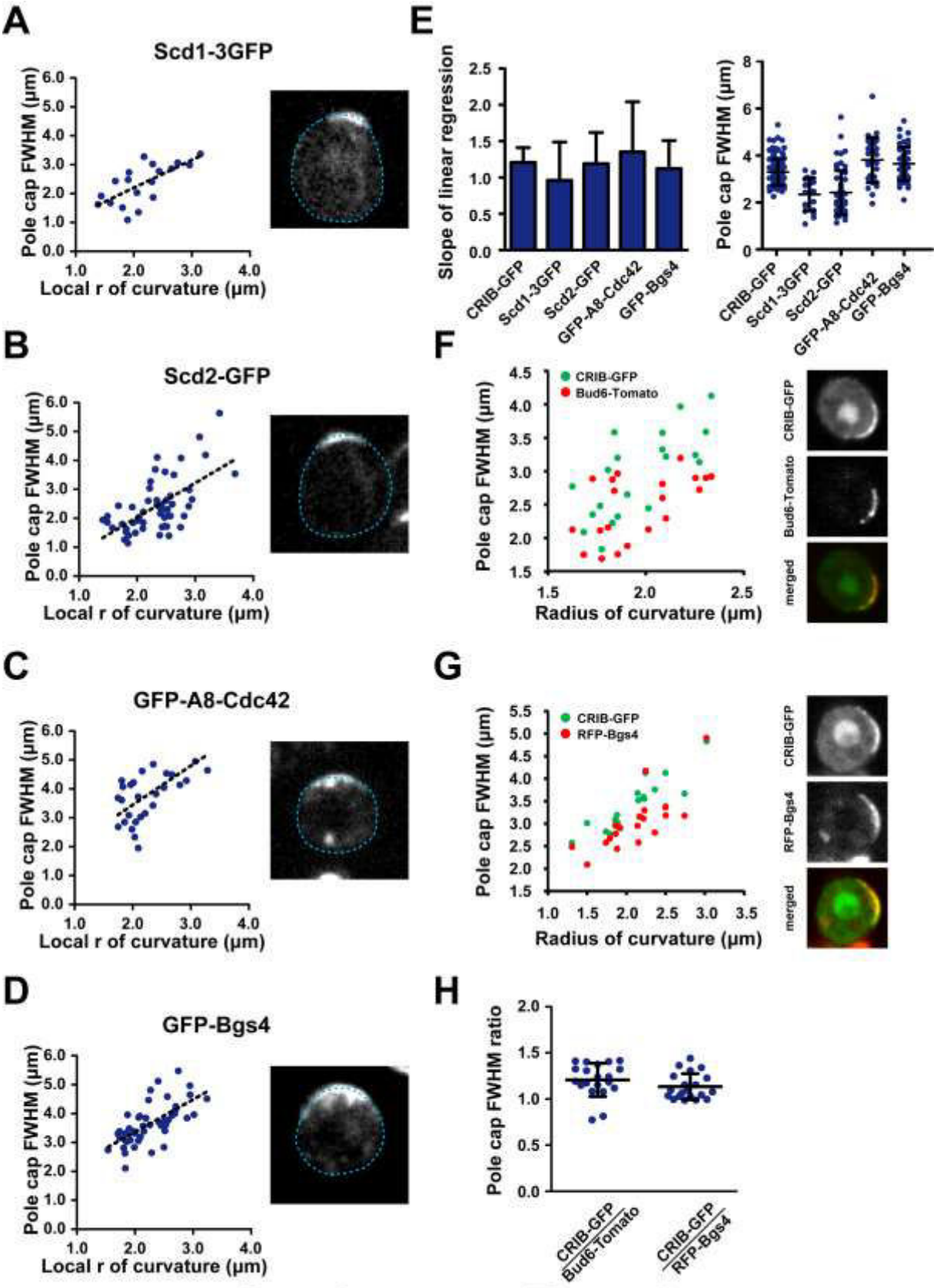

Supplementary Figure 2

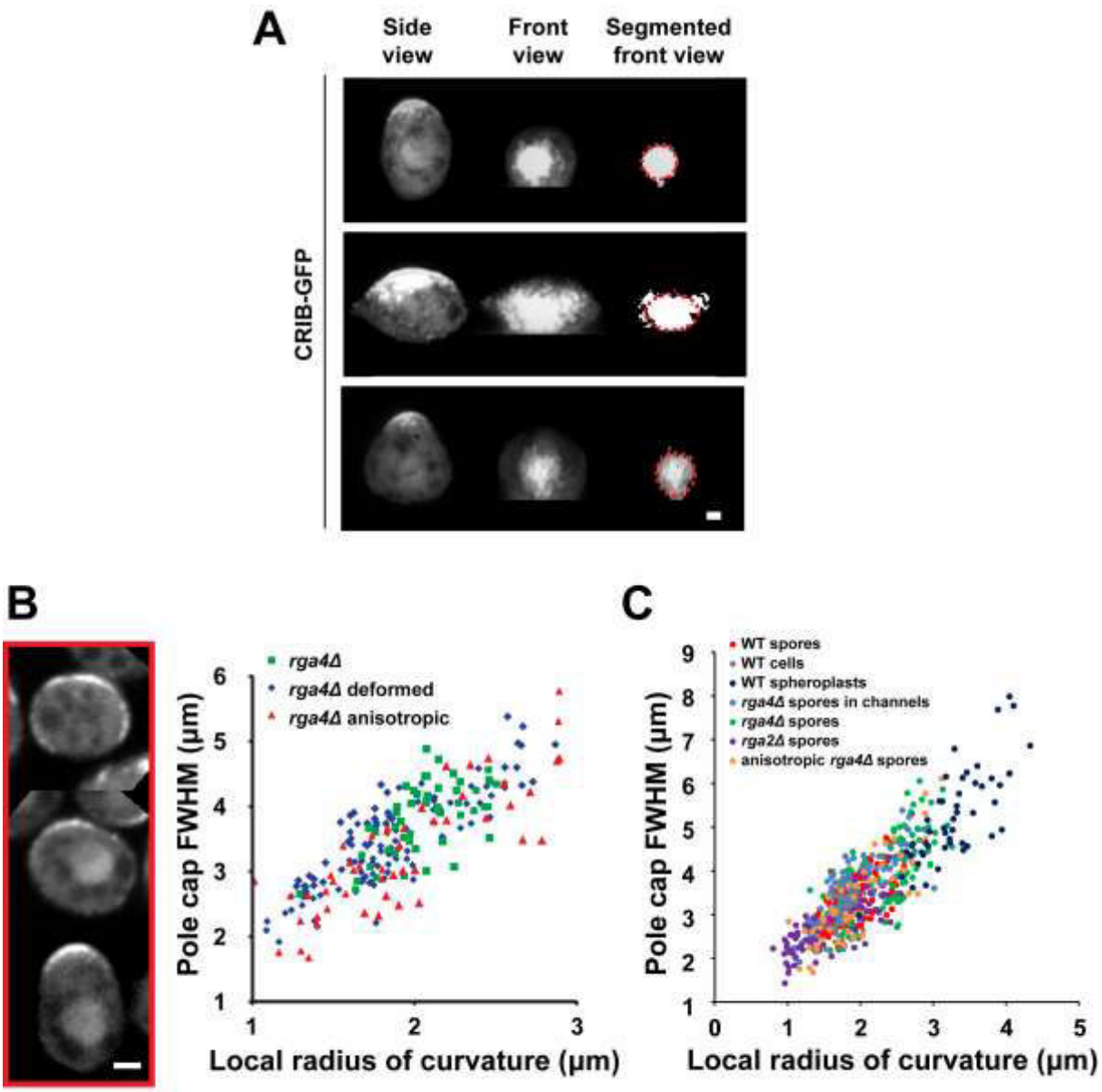

Supplementary Figure 3

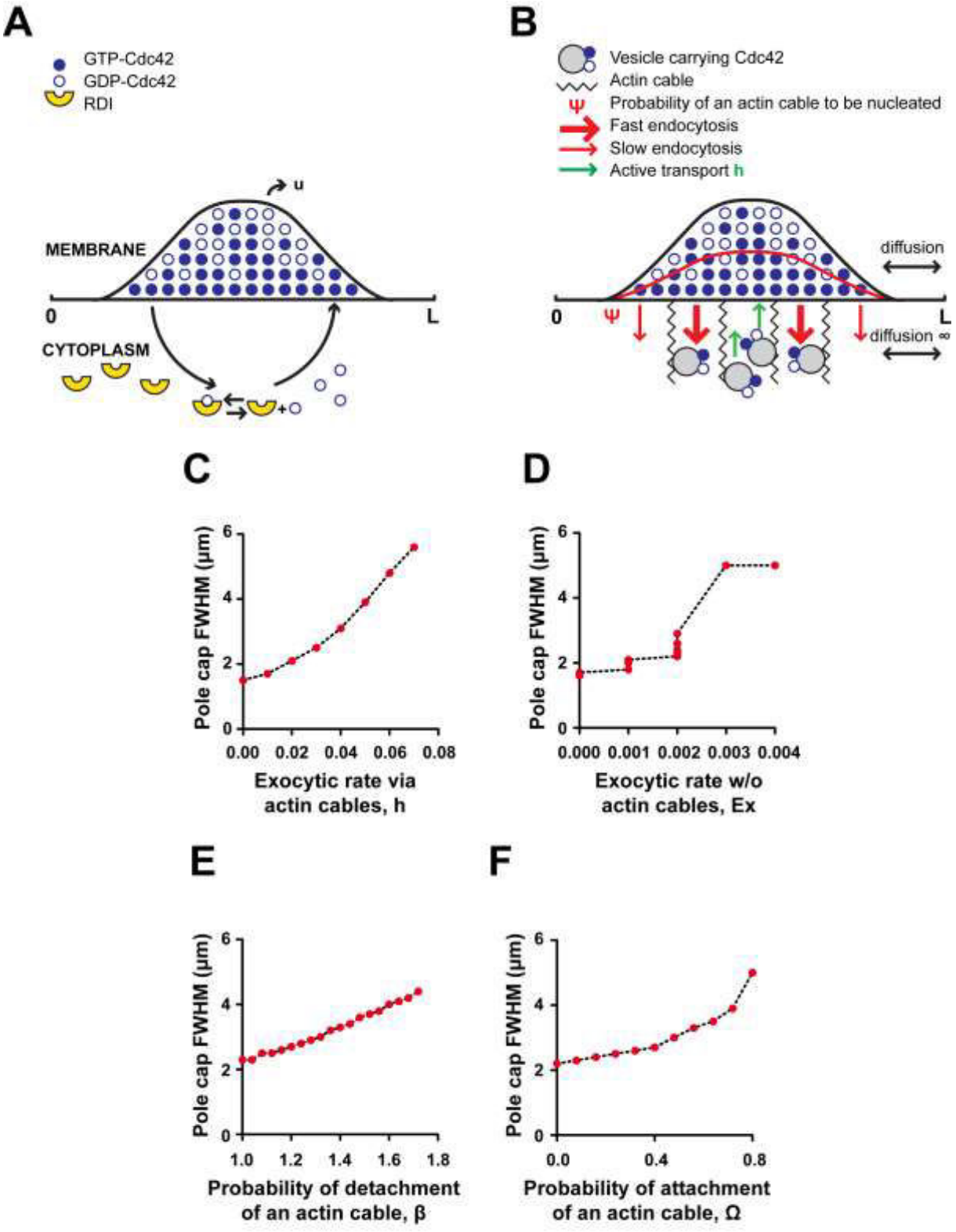

Supplementary Figure 4

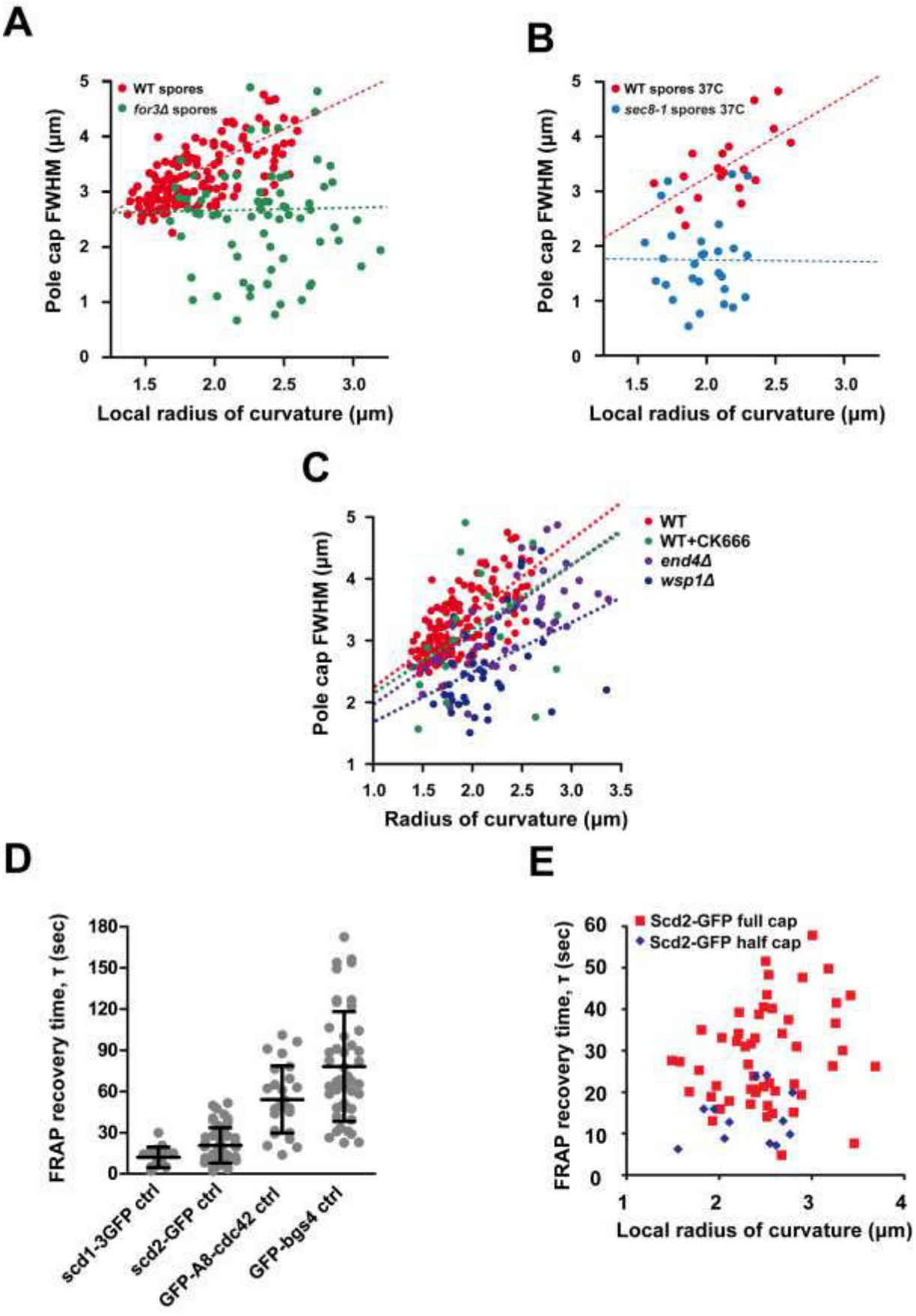

Supplementary Figure 5

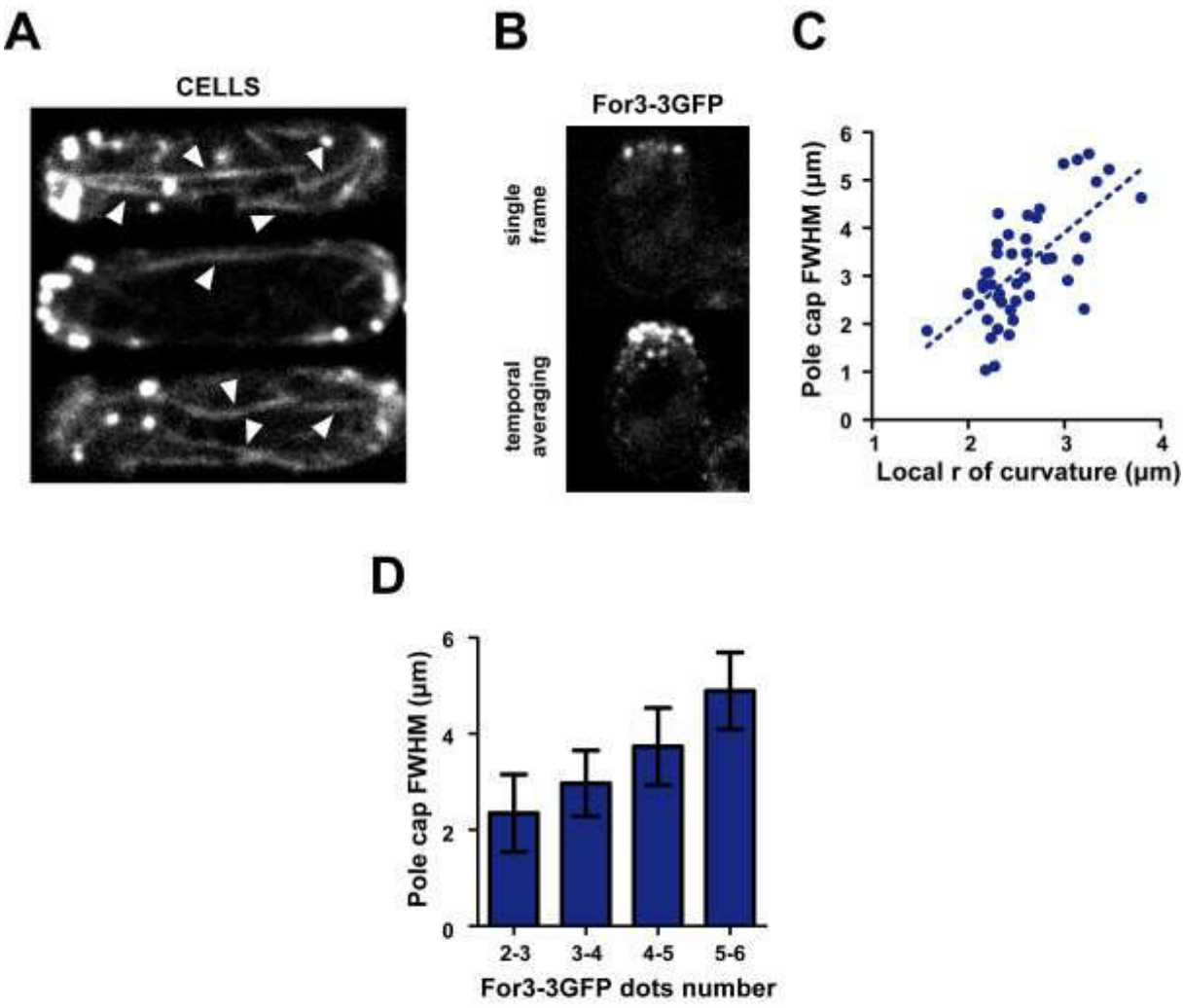

Supplementary Figure 6

DISCUSSION

During my PhD, I have investigated different aspects of cell polarity and cell morphogenesis in fission yeast spore germination. In here, I will briefly discuss some major points that remain to be investigated, and that mainly arose through numerous discussions with research colleagues.

I have shown that outgrowth as a symmetry breaking event may be set by a feedback between polarity cap stability and the spore outer wall mechanics. Differently from vegetative cell case, outgrowth is not triggered by absolute spore size; in contrast, a fold change in volume precisely predicts the initiation of polarized growth: I propose that this "relative sizer" is related to the material properties of the spore wall, in particular ultimate strength or failure stress. Such a robust regulation through a passive encasing shell may be important to avoid a premature cell exit from the reorganizing phase, as well as to regulate timing and sizing at outgrowth without a tight cell-cycle regulation.

Another important question that emerged from this work concerns the mechanism of spore wall rupture at outgrowth: more specifically, if the breakage is purely mechanical, or based on local digestion by some specific enzymes. To date, although many enzymatic activities have been associated with building the OSW at sporulation, no enzyme has been shown to influence its remodeling after germination or outgrowth. EM inspection was in agreement with this result, as no major remodeling of the outer spore wall was observed during germination. More specifically, I did not observe any notable thinning of the OSW, and even many hours after outgrowth, the OSW appeared relatively intact at the back of the outgrown cell. The most significant change that I could qualitatively observe is a time-dependent variation in spore surface wrinkles. As the spore grows these wrinkles appear to flatten out in the EM images. This wrinkles' unfolding, could in principle serve as surface reservoir, as it has been proposed in the case of *B. subtilis* spores (Sahin et al., 2012). Altogether, these observations suggest that local OSW rupture may be a purely mechanical event.

A very intriguing phenomenon during spore germination is the wandering dynamics of the polarity cap: as shown previously, MTs and MT-associated factors do not seem to be required

for these oscillations, and to influence the transition from an unstable to a stable polarity domain, which corresponds to a switch from isotropic to polarized growth. Imaging of the GFP-tagged Atb2 marker at different stages of spore germination shows that MTs are very scarce in early germinating spores, then form 2-3 bundles in a disorganized pattern during the late phase of isotropic growth and finally start to polarize at the onset of outgrowth. Consequently, the MT-dependent pathway, which is known to play a central role in polarity establishment and maintenance of fission yeast cells, is dispensable in the case of spores. Also actin is not necessary for pole cap wandering, although it is essential for cell growth.

Altogether, these results suggest that oscillations of the polarity domain may be a "natural" byproduct of a symmetry breaking process: in other words, the polarity machinery could be intrinsically unstable, due to the properties of a reaction diffusion mechanism that regulate Cdc42 exchange between the cytoplasm and the membrane, and need the action of a positive feedback in order to stabilize at one site. But what can generate such an effect on polarity establishment? As previously described, the case of spores is quite peculiar as they are encased in a rigid shell: for this reason, we can imagine that cell growth is hindered compared to the case of a "freely" growing vegetative cell, and this acts as a negative feedback on the polarity machinery. In other words, the presence of the outer spore coat may enhance the innate instability of the polarity machinery, and the morphogenetic switch to polarized growth in turn highlights the central role of actual growth for the transition to a stable pole cap. In this scenario, the wandering of the polarity cap that is observed during the isotropic phase of growth is directly related to the ability of cells to grow. In support to this hypothesis, spores that are not able to grow either by chemical treatment or by physical confinement continue to assemble polarity domains that wander around and never stabilize. The results obtained with the photoablation setup strongly support this hypothesis, as a direct local fragilisation of the OSW is sufficient to stabilize the pole cap at that site and trigger outgrowth. A recent study has also shown that *C. Albicans* hyphae which perpendicularly encounter an obstacle stop growing for a short time window, during which the Spitzenkörper (Spk) laterally oscillates, suggesting that this destabilization of the polarity machinery may be relevant for growth reorientation in filamentous fungi (Thomson et al., 2014). On the other hand, an *A. nidulans* SIK1 mutant, which is defective in the activation of the HOG pathway, growth can be strongly slowed down by salt addition in the media. In these conditions, SIK1 mutants show a growth pattern of increased hyphal branching, suggesting that growth is

required for maintenance of a single growing tip (Han and Prade, 2002). In the case of budding yeast, it has been recently found that old bud scars are never reused as new bud sites thanks to the presence of some memory cues which act as negative feedback on the polarity machinery (Meitinger et al., 2014): moreover, removal of these inhibitory cues lead to cell polarization exactly within old division sites. To explain this phenomenon, it has been proposed that, similarly to the case of fission yeast spores, the polarity cap could be destabilized at the rigid chitin-enriched rings and consequently ensure accumulation of Cdc42 in the ring center (Wedlich-Soldner, 2014).

The idea of a positive feedback between growth and polarity could also explain how this wandering mechanism may serve to probe the spore surface and find a weak spot in the spore coat, for instance a germ pore. In this scenario, it will be sufficient for the spore to grow faster at a certain location in order to stabilize its pole cap there, and consequently to generate a reproducible site of outgrowth. In the case of fission yeast spores, it would be interesting to test this hypothesis by locally fragilizing the OSW at earlier stages and then follow the germination process, to observe if by giving enough time the spore is now able to detect the artificial weak spot and outgrowth at that location.

A very intriguing question for the next future is to investigate the mechanism for how cell growth may actually stabilize polarity. Theoretical studies have shown that in tip-growing walled cells, growth is the result of the balance between local secretion rate and the rheology of the cell wall, in order to keep a good cell wall width, and avoid bursting or growth arrest by either thinning or thickening of the cell wall (Campas and Mahadevan, 2009). One example of how such a dysregulation may affect cell shape and cell wall integrity emerged by observing germination of fission yeast *bgs4Δ* spores: in this case, spores enter germination and grow isotropically as for wild-type, but as soon as they double in volume, they either burst out from one site or enter outgrowth, immediately fail to maintain a rod shape, and grow a bud which finally explodes. These results suggest that the first phase of growth is at the same time hindered and protected by the outer spore coat: as soon as a local rupture occurs, if the newly synthetized cell wall is not too fragile, the spore will still be able to initiate tip growth, as the spore coat defines the initial boundaries for the emerging tip. However later on, the imbalance between cell growth and cell wall mechanics/deformability will lead to cell death.

The way local growth may act as a positive feedback on cell polarity, may rely on pathways for cell wall reparation: in fact we can imagine that as soon as the cell grow, it locally deforms the cell wall and consequently weakens it, leading to the activation of the CWI pathway. A recent study in budding yeast has shown indeed that the polarized cytoskeleton and the secretory machinery can be redirected to the damage site upon photoablation (Kono et al., 2012), but the possibility that a similar mechanism could be important for yeast growth in physiological conditions has not been investigated yet.

In the course of a second work, I have shown that pole cap size scales with local radii of curvature, and that this process depends on actin. This simple observation is probably relevant for most eukaryotes, as it focuses on the dynamic assembly of Rho-GTPases-based polarity domains, such as for Cdc42, which are highly conserved among species and play crucial roles in cell polarity for different functions, from cell migration to polarized growth, axon specification, development and tissue organization. Spores represent an ideal system to address this question, as the polarity cap explores the cell surface and dynamically adapts to the local geometry.

In a first part, I have characterized this scaling phenomenon in wild-type spores and mutants of smaller or bigger sizes: moreover, cell shape manipulation leads to fast adaptation of the polarity domain to the newly formed local cell geometry. This process depends on actin, and more specifically on actin cables mediated vesicles transport and fusion at the membrane: A very puzzling question consists in understanding how vesicle transport through actin cables scales pole cap size to the local cell geometry. In a recent work, Huang and colleagues have shown that in *E. coli* growing cells the MreB actin-like cytoskeleton is preferentially localized at regions of negative cell wall curvature, and this feedback on growth zones is in turn crucial for rod-shape morphogenesis, in particular for rod straightness (Ursell et al., 2014). The authors propose that this curvature sensing may be based on the mechanics of MreB polymers, which could potentially impose some geometric preferences: moreover, various transmembrane proteins have been found to be curvature sensitive, and to regulate local curvature for the initiation of processes such as endocytosis. However, in the case of fission yeast spores, local radii of curvature vary within a range that is too big to be sensed by either cytoskeletal polymers or transmembrane proteins and vesicles. Hence, there has to be a different mechanism for actin cables network to size the polarity domain: a possibility, as described in the paper, is that this network, which

defines a dome around the pole cap at different local radii of curvature, may generate sufficiently different surface to volume ratios to affect the efficiency of vesicle attachment.

To conclude, this work highlights a feedback between cell geometry and polarity which appears to play a central role in cell morphogenesis.

CONCLUSION

This thesis aims at investigating some of the fundamental principles which regulate cell polarity and cell shape establishment, by addressing how these cells first establish polarity and morphogenesis, in their very first cell cycle after germinating from dormant spores. To this aim, I have developed novel methods which integrate detailed live-cell imaging, quantitative image analysis and mathematical modeling to understand how polarity components self-organize to stabilize a polarity axis and define a cell with proper dimension and morphogenesis. In particular, I have found out that local changes in cell mechanics or cell geometry can in turn affect cell polarity establishment and size definition of polarity domains.

These studies put forward the fission yeast spore as a novel model system to address general questions on cell polarity and morphogenesis: in fact these cells are characterized by a transition form an unstable to a stable polarity domain, which in turn corresponds to a switch from isotropic to polarized growth. Thanks to the profound changes in cell shape that characterize their development, and to the dynamics of pole cap wandering that allows the cell to locally probe its geometry, spores appear as a very powerful tool to assess the basic principles of symmetry breaking in a biological system.

Moreover, during my PhD I have found out that spore wall mechanics plays a crucial role on polarity establishment, and finally sets outgrowth at a precise fold-change in spore volume: these results highlight the complex network feedbacks between cell growth, polarity and mechanics to finally regulate cell morphogenesis. However, the mechanisms for how growth may act as a positive feedback loop on the polarity machinery remains to be explored: to this aim, fission yeast is again a very powerful tool as it allows not only genetic manipulation, but also control of other physical parameters such as turgor pressure (which in turn will affect growth rate).

Finally, I have shown that fission yeast spores can probe the local geometry of the cell and adapt the polarity domain size to it. This mechanism may be essential for generating and maintaining a certain shape: in other words, cell form is established by the size of the growth

zone, which in turn depends on the cortical domain containing upstream polarity factors such as Cdc42. In this context, it would be interesting to assess if some morphological mutants fail in this scaling process, by observing pole cap wandering in the corresponding spores. On the other hand, it would be interesting to have more mechanistic insights on how actin cables may probe local geometry: for this aim, I believe the best approach would be to integrate mathematical modeling in 3D with more detailed analyses of actin cables and vesicles dynamics, in wild-type spores and mutants in some regulatory proteins of actin cable assembly, disassembly, severing and bundling.

To conclude, I believe that these results may be relevant for very different cell types, and give important insights on how polarity is established from an initial symmetric state. They reveal that the final morphogenesis of a cell arises from the integration of interdependent and diverse parameters, such as cell polarity, cell mechanics, cell growth and cell geometry itself.

METHODS

In this section, I will describe some specific experimental setups which I developed in the course of my thesis, and that have not been detailed in the aforementioned papers.

1. Photoablation

Spores expressing the polarity marker GFP-bgs4 were digested overnight in glusulase, rinsed, grown in YE5S media for 3hours at 30C and finally placed on top of a 2% YE5S agar pad. Spores were imaged on a Spinning Disk confocal microscope equipped with an iLAS system linked to a UV laser, with 100x magnification and an EM-CCD camera. After choosing 3-4 fields of view, spores in each field were photoablated at a small resolution-limit spot of their surface, with the help of the so-called Mosquito tool from the ILas software; then, spore germination and outgrowth were followed by acquiring time-lapses with 20-30 minutes time frame in bright field and the 491 channel for visualization of GFP-bgs4. To ensure that the laser effectively fragilizes the spore coat, I performed a series of calibration experiments to optimize the exposure time for a given laser power and ablation area which allows to immediately kill the cell but not the spore. Moreover, I have coupled a novel death assay method (described below) to the photoablation assay, in order to directly check the efficiency of spore wall fragilisation in this context: I then identified the laser time of exposure that did not lead to spore death without enzyme treatment, but that caused death of irradiated spores after enzyme treatment.

2. Death assay

This method consists in the preparation of a mix of cell wall digesting enzymes (0.5 mg/ml Zymolase and 10 mg/ml Novozyme). Treatment with these enzymes leads to death of all vegetative cells and outgrown spores in 10–30 min but does not affect spores protected by an intact OSW. Moreover, spores can grow for many hours in this mix, and then die when the OSW

opens at the onset of outgrowth. Using this assay, it is thus possible to moonitor the opening of the OSW in live spores.

3. Microchambers setup

Microfabricated round chambers of varying width and 3μm height have been obtained through standard photolithography methods. A replica of the structures was obtained by pouring PDMS (1:10) on top of the silica wafers. The resulting PDMS molds were washed with isopropanol, acetone, and water, dried and plasma treated immediately before the experiment, together with a glass coverslip. Spores expressing the polarity marker GFP-bgs4 were digested overnight in glusulase, rinsed and grown in YE5S media for 3hours at 30C. Spores were then centrifuged and media was discarded in order to resuspend cells in a volume of 10 μl: 1 μl of this solution was then loaded on top of the coverslip, and the PDMS was placed on top, with the microchambers-containing side facing the cells, and gently pushed, to ensure spores entry into the chambers. A small volume of YE5S was added on top of the PDMS, to allow diffusion of nutrients throughout the elastomer and minimize drying. Spores were immediately imaged on a Spinning Disk confocal microscope: as the same molds contained round chambers of different sizes over a small surface, it was possible to image at the same time control and confined spores for about 3 hours.

4. Microchannels setup

Microfabricated channels of 2.5 μm width and 3 μm height were obtained by standard photolitography methods. A replica of the structures was obtained by pouring PDMS (1:10) on top of the silica wafers. The resulting setup was sticked on top of a glass coverslip, after washing the two elements with isopropanol, acetone, and water, successive drying and plasma treatment to ensure a strong adhesion between the two surfaces. Spores expressing the polarity marker CRIB-GFP were digested overnight in glusulase, rinsed and grown in YE5S media for 3hours at 30C. At this point, spores were centrifuged and media was discarded in order to concentrate cells in a volume of 50 μl: this solution was then loaded in the channels, and spores were forced to enter the channels by exerting a mechanical pressure with the help of needle-less syringe. This process was repeatedly performed and checked on an inverted microscope to ensure that a high number of spores were deformed inside the channels. The setup is then ready for imaging: this step was

achieved on a Spinning-Disk confocal microscope, with 100x magnification and a CCD camera, by acquiring z-stacks with 0.2 μm z-step to ensure an optimal visualization of the fluorescence signal. Time-lapses with 10 min time frame allowed to follow the fast adaptation of the polarity domain to the new spore geometry.

Spores can also be grown for longer times inside such kind of microchannels, in order to observe the first generations of resulting vegetative cells: this protocol is accurately described in the method paper at page included at the end of the thesis.

5. Setups for drug treatment and rinse out

In my experiments, I have mainly used two different setups which allow media exchange over time. A first one is based on the use of a PDMS microfluidic channel where cells were stuck down on the bottom coverslip with the help of a dialysis membrane. In these conditions, cells and spores can be monitored for up to three hours, and rapid exchange of YE5S with a given concentration of sorbitol allows to perform stress-strain measurements.

In the case of specific chemical inhibitors such as LatA which have an effect at specific concentrations, I found out that the PDMS assay was not optimal as the final drug concentration inside the chamber was much lower than the bulk one, likely due to the elastomer's hydrophobic properties.

In this case, I have built up home-made glass channels by simply sticking two coverslip one on top of the other: cell or spores were stuck down in the channel by coating the bottom surface with poly-lysin and lectin, allowing imaging for up to 2 hours. Media exchange was performed by bringing near one entrance of the channel a sheet of Kimtech, and simply exploiting capillarity.

6. Fluorescence exclusion method

The robustness and reliability of the phase-contrast based image analysis for measurement of the cell and spore wall Young modulus has been confirmed by implementing a method based on fluorescence exclusion, which allows tracking detailed changes in cell shape upon sorbitol treatment, with spinning-disk confocal microscopy. Because this method tracks the interface between the cell outer contour and the surrounding medium, it ensures that there are no

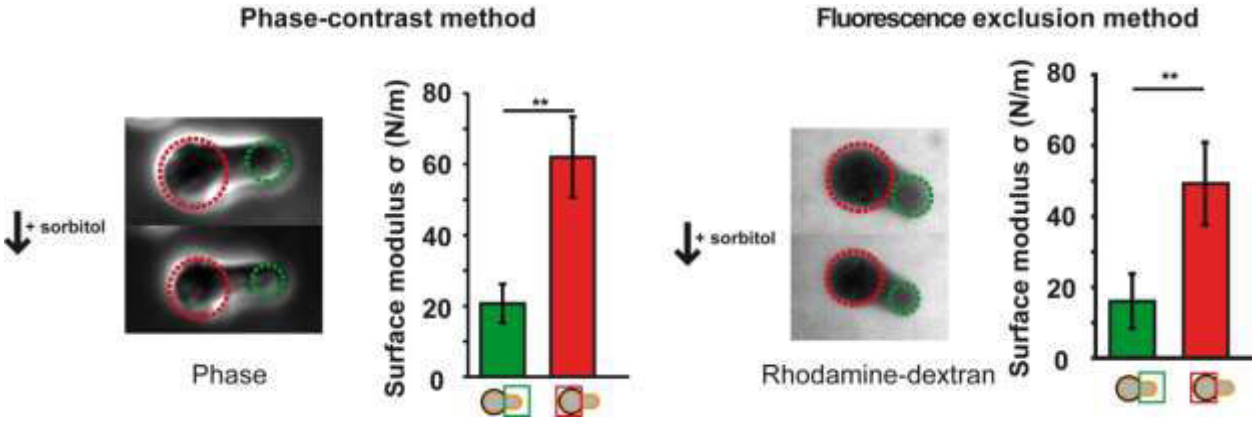

Figure 72: Comparison of phase-contrast based and fluorescence exclusion methods to monitor local changes in cell shape induced by sorbitol addition. On the left, phase-contrast method. On the right, fluorescence exclusion method: the medium is supplemented with Rhodamine-dextran, to dynamically track changes in cell shape/size by tracking the contour of the cell which appears in black.

differential optical effects between inner and outer walls. This analysis yields similar surface modulus values (within SDs) as in the phase-based analysis (Figure 72).

7. Actin imaging and analysis

Observation of LifeAct in live spores was performed on a Spinning disk confocal microscope. Spores were digested overnight, rinsed and grown in YE5S for 3 hours at 30C. Afterwards, spores were placed on a 2% YE5S agar pad: images were acquired by performing z-stacks of 0.2 µm step over a 5 µm range. Image analysis was performed on Imaris (Bitplane), a powerful 3D imaging software which allows to explore and manipulate z-stacks: in particular, I have used the "FilamentTracer" tool to detect actin cables in the spore volume: this module has been optimized to study neurons morphology, specifically for temporal spine analysis. One great advantage of this quantitative approach relies on the combination of automated analysis and operator decision: among the four complementary tracing strategies that the software offers, I have chosen one where manual tracing is accompanied by automated detection over the perpendicular axis of the image as it is visualized: dynamic 3D visualization while analyzing allows to assess the validity of the tracing. Once a set of tracked cables is generated for each spore, the software generates an excel file with informations on counts, branching, size, shape, and intensity.

OTHER PUBLICATIONS

OPEN ACCESS Freely available online

PLOS | BIOLOGY

Electrochemical Regulation of Budding Yeast Polarity

Armin Haupt[1☯], Alexis Campetelli[1☯], Daria Bonazzi[1☯], Matthieu Piel[2], Fred Chang[3]*, Nicolas Minc[1]*

1 Institut Jacques Monod, UMR7592 CNRS, Paris, France, **2** Institut Curie, UMR 144 CNRS/IC, Paris, France, **3** Department of Microbiology and Immunology, Columbia University College of Physicians and Surgeons, New York, New York, United States of America

Abstract

Cells are naturally surrounded by organized electrical signals in the form of local ion fluxes, membrane potential, and electric fields (EFs) at their surface. Although the contribution of electrochemical elements to cell polarity and migration is beginning to be appreciated, underlying mechanisms are not known. Here we show that an exogenous EF can orient cell polarization in budding yeast (*Saccharomyces cerevisiae*) cells, directing the growth of mating projections towards sites of hyperpolarized membrane potential, while directing bud emergence in the opposite direction, towards sites of depolarized potential. Using an optogenetic approach, we demonstrate that a local change in membrane potential triggered by light is sufficient to direct cell polarization. Screens for mutants with altered EF responses identify genes involved in transducing electrochemical signals to the polarity machinery. Membrane potential, which is regulated by the potassium transporter Trk1p, is required for polarity orientation during mating and EF response. Membrane potential may regulate membrane charges through negatively charged phosphatidylserines (PSs), which act to position the Cdc42p-based polarity machinery. These studies thus define an electrochemical pathway that directs the orientation of cell polarization.

Citation: Haupt A, Campetelli A, Bonazzi D, Piel M, Chang F, et al. (2014) Electrochemical Regulation of Budding Yeast Polarity. PLoS Biol 12(12): e1002029. doi:10.1371/journal.pbio.1002029

Academic Editor: Mark D. Rose, Princeton University, United States of America

Received April 10, 2014; **Accepted** November 12, 2014; **Published** December 30, 2014

Data Availability: The authors confirm that all data underlying the findings are fully available without restriction. All relevant data are within the paper and its Supporting Information files.

Funding: This work was supported by funds from the National Institutes of Health (http://www.nih.gov/, GM056836) to FC and the CNRS, ANR (http://www.agence-nationale-recherche.fr/, grant 10PDOC00301), FRM (http://www.frm.org/, grant AJE20130426890), the FP7 CIG and ITN "FungiBrain" (http://ec.europa.eu/research/mariecurieactions/) and the "Mairie de Paris emergence" program (http://www.paris.fr/, LS100805) to NM. The funders had no role in study design, data collection and analysis, decision to publish, or preparation of the manuscript.

Competing Interests: The authors have declared that no competing interests exist.

Abbreviations: EF, electric field; LatA, latrunculin A; PS, phosphatidylserine; TMP, transmembrane potential; WT, wild-type.

* Email: fc99@columbia.edu (FC); minc@ijm.univ-paris-diderot.fr (NM)

☯ These authors contributed equally to this work.

Introduction

Cell polarization arises from the asymmetric accumulation of cellular components near a region of the plasma membrane. Although the roles of polarity proteins such as small GTPases and cytoskeletal elements have been studied extensively [1], much less is known about the possible contribution of electrochemical elements. Recent studies identifying certain ion transporters in regulating processes such as cell migration and polarized cell growth indicate potential roles of local pH, ion fluxes, and membrane potentials at the plasma membrane [2–8]. How these elements interface with established modules of polarity networks remains to be defined.

The importance of electricity in cell polarization is illustrated by the ability of electric fields (EFs) to direct cell polarization. It has been appreciated for decades that most cells—ranging from bacteria, fungi, and amoebas to animal cells—are electrotactic, and robustly orient polarity, migration, or division to applied exogenous EFs [9–14]. EFs of similar intensities as those used in these experiments naturally surround cells in tissues, and even individual cells such as fungal cells [10,15,16]. The physiological relevance of endogenous EFs has been demonstrated in fungal infection [17], immune cell response [18], wound healing, regeneration, and development [6,10,19,20]. These findings have led to the proposal that in addition to responding to chemical and mechanical signals, cells may also be responding to endogenous electrotactic signals to guide cell polarization [20]. The response of cells to exogenous EFs provides a powerful tool to study electrochemical elements in cell polarization.

The molecular mechanisms of cell polarity are currently best understood in the budding yeast, *Saccharomyces cerevisiae*. Polarized cell growth in these cells is tightly controlled by intrinsic and extrinsic spatial cues. Haploid budding yeast cells display an axial budding pattern, in which new buds form adjacent to previous bud sites, while diploid cells exhibit a bipolar pattern, in which buds emerge at sites of previous division or growth [21,22]. During mating, cells of opposite mating type polarize towards each other in response to gradients of secreted pheromones; exogenous application of the pheromone α-factor causes cells to grow a mating projection, forming a pear-shaped "shmoo." The core polarity machinery required for both bud and shmoo formation is organized around the small GTPase Cdc42p, which coordinates actin assembly and exocytosis [23–25]. Bud site selection is specified by a Ras-like protein Rsr1p and its regulators [23]. During mating, these spatial cues used to direct budding are turned off, so that cells can polarize towards the mating partner. This reorientation of polarity involves Far1p and its interactions with the receptor-coupled Gβ protein and Cdc42 GEF [25–27]. As demonstrated by mutants affected in the regulation of only shmoos or only budding [23,28,29], there are specific molecular

Author Summary

The ability of cells to orient towards spatial cues is critical for processes such as migration, wound healing, and development. Although the role of electrochemical signals is well characterized in processes such as neuronal signaling, their function in cell polarity is much less understood or appreciated. Application of exogenous electric fields can direct cell polarization in many cell types, and electric fields of similar magnitude surround cells and tissues naturally. However, the significance and mechanism of these responses remain poorly understood. Here, we introduce budding yeast (*Saccharomyces cerevisiae*) as a powerful model system to study electrochemical regulation of cell polarity. We show that application of electric fields causes budding yeast to polarize in particular directions. We begin to identify key proteins involved in this response, which implicate an electrochemical pathway involving membrane potential, membrane charge, and an ion channel, which ultimately regulate the central polarity factor Cdc42p. These key proteins are not only needed for response to electric fields, but also contribute to cell polarity more generally. To test whether a change in membrane potential is sufficient to control cell polarization, we introduce a light-sensitive ion channel into yeast and show that we can now control the site of polarization simply by using a focused laser beam. Thus, our study shows that electrochemical regulation is an integral component of cell polarity pathways.

differences in the mechanisms governing budding and shmoo polarity. In general, still little is appreciated about electrochemical aspects of cell polarization in this cell type.

Here, we show that cell polarity can be directed by exogenous EFs in budding yeast. Although EFs have been shown to direct polarized growth in *Schizosaccharomyces pombe* [13] and *Candida albicans* [30,31], there have been no reports to date in *S. cerevisiae*. We find that although EFs do not appear to affect wild-type (WT) budding cells, they do have robust effects on cells in the presence of pheromone and on mutants defective in bud site selection. We find a potassium channel and membrane lipid charges as components mediating EF responses. We further show, using a light-activated rhodopsin, that local membrane potential itself is capable of directing polarization. Our results demonstrate the importance of electrochemical signaling in cell polarity and begin to define mechanistically how they contribute to polarized cell growth.

Results

Electrotactic Responses of Budding Yeast Polarity

We tested whether exogenous EFs can influence cell polarization in budding yeast. Yeast cells were grown in the presence of EFs in microfluidic channels, which allow for defined EF lines and heat control [13]. Haploid WT cells were mostly resistant to EF effects and budded at their normal axial position (Figure 1A and 1B). The bud site selection mutant *rsr1*Δ forms buds in random directions, in the absence of EF. In the EF, however, almost all new buds emerged at the cathode-facing side of the *rsr1*Δ cells after 1 h of exposure to an EF of 50 V/cm (Figure 1A and 1B; Movie S1). Cells did not exhibit any major signs of stress, cell death, or stress pathway activation [32], but grew with slightly reduced growth rates and prolonged cell cycle length as controls (Figure S1). Cathodal bud orientation displayed dose dependence on EF intensity and duration of application (Figure S2A and S2C). Diploid WT cells also polarized towards the cathode significantly more than WT haploids; this may reflect a less stringent regulation of budding pattern in diploids (Figure 1B). Thus, the EF was not able to efficiently override the normal spatial cues involved in axial budding, but could direct bud site polarization if these cues were absent or weak.

The application of EFs also directed the site of shmoo tip formation but, surprisingly, in the opposite direction. In the presence of uniform concentrations of α-factor and an EF, budding yeast cells showed a strong polarization towards the anode (Figures 1C, 1D, S2B, S2D, and S2E; Movie S2). Changing the EF direction induced the formation of a second shmoo tip towards the new anode (Figure 1E; Movie S3). To rule out possible effects of adding mating factor exogenously, we also noted similar effects in mating pairs of cells. The EF disrupted mating and caused cells to polarize towards the anode of the EF instead of towards each other (Figures 1G and S2F). Cells that were induced to shmoo without external pheromones, by overexpressing Ste4p, the β subunit of the G protein involved in pheromone response, also polarized toward the anode [33] (Figure 1F and 1G; Movies S4 and S5). Thus, although bud and shmoo formation use many of the same components of the polarity machinery [21,22], there is a striking difference in directionality (cathodal versus anodal) for how budding and shmooing yeasts respond to EFs.

EF Response Involves the Cdc42p-Based Polarity Machinery

We next tested whether cell polarization in response to EF requires the same polarity machinery normally used in budding or shmooing. The highly conserved small GTPase Cdc42p was required to polarize buds and shmoos in the absence or presence of the EF, as assessed with the loss-of-function mutant allele *cdc42-118* (Figures 2A, 2B, and S3A) [34]. In addition, mutants specifically defective in establishing polarity during mating but not budding, such as *bem1-s1* (a point mutant in the scaffold protein Bem1p [29]) and the formin null mutant *bni1*Δ [28], showed similar polarization defects in the absence or presence of the EF (Figures 2B, S3B, and S3E). Imaging GFP-Cdc42 [35] and the associated components Cdc24-GFP [36] (a GEF for Cdc42p) and Bem1-GFP [37] revealed that polarity caps assembled and oriented to the EF prior to bud or shmoo emergence (Figure 2C–2E). Bem1-GFP cap assembly was dependent on Cdc42p in the presence or absence of EF (Figure S3C and S3D). Actin also appeared to similarly mediate cell polarization in both instances. In budding cells, actin was dispensable for EF-induced Bem1-GFP cap cathodal orientation, although actin depolymerization appeared to accelerate polar cap accumulation at the cathodal side. In shmooing cells, actin inhibition caused rapid disappearance of the cap in the presence or absence of the EF [27] (Figures 2D, 2F, and S3F). Together, these data show that the EF acts in reorienting polarized cell growth through the normal polarity machinery, including Cdc42p and its regulators.

To investigate how EF directs mating projections, we tested the role of Far1p and Cdc24p. Mutant *far1-s* and *cdc24-m* cells have a specific orientation defect in response to α-factor, as they are not able to orient appropriately towards gradients of α-factor, and polarize instead using bud site selection cues [25–27]. In saturating concentrations of α-factor, we found that both of these mutants polarized towards the cathode of the EF (the opposite direction as WT cells) (Figure 2G). This reversal was also observed at non-saturating concentrations of pheromones (Figure S3G). As *rsr1Δ* mutants in the absence of α-factor bud towards the cathode, this suggests that *far1-s* and *cdc24-m* mutants may use machinery that orients buds to direct shmoo projections to the cathode.

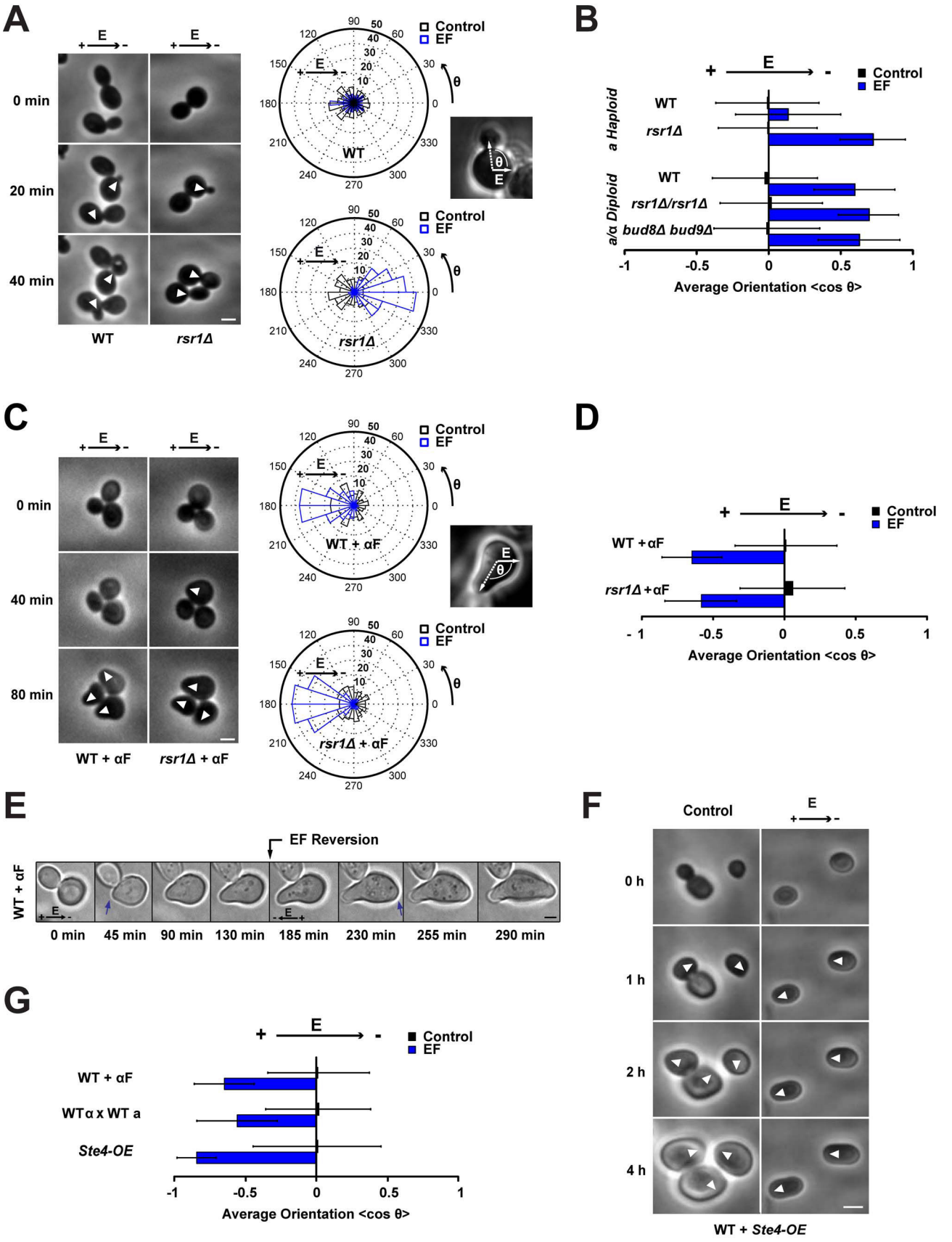
A
E
0 min
20 min
40 min
WT
rsr1Δ
Control
EF
θ
B
Control
EF
WT
rsr1Δ
WT
rsr1Δ/rsr1Δ
bud8Δ bud9Δ
a Haploid
a/α Diploid
Average Orientation <cos θ>
C
0 min
40 min
80 min
WT + αF
rsr1Δ + αF
D
WT + αF
rsr1Δ + αF
E
EF Reversion
WT + αF
0 min
45 min
90 min
130 min
185 min
230 min
255 min
290 min
F
Control
0 h
1 h
2 h
4 h
WT + Ste4-OE
G
WT + αF
WTα x WT a
Ste4-OE

Figure 1. Budding versus shmooing yeast cells polarize in opposite directions in an electric field. (A) Phase contrast time lapse of WT and *rsr1*Δ budding yeast cells growing under an EF of 50 V/cm. White arrowheads point at sites of bud emergence. On the right are radial histograms of polarized growth direction (indicated as the final angle of bud emergence with the EF, θ) for WT and *rsr1*Δ cells in the presence or in the absence of an EF. (B) Average bud orientation, computed as $<\cos\theta>$ after 3 h of growth in the absence or in the presence of an EF, for a population of haploids and diploids of the indicated genotype. A positive average orientation represents an orientation to the cathode (negative electrode of the EF), whereas a negative orientation stands for an orientation to the anode. (C) Phase contrast time lapse of WT and *rsr1*Δ budding yeast cells growing mating projections ("shmoos") in the presence of α-factor (αF) under an EF of 50 V/cm. White arrowheads point at sites of shmoo emergence. On the right are radial histograms of polarized growth direction. (D) Average shmoo orientation after 3 h of mating tip growth in the absence or in the presence of an EF for a population of WT and *rsr1*Δ cells treated with α-factor. (E) Time-lapse images of shmoo reorientation in a WT cell after inverting the EF direction. A second shmoo is formed at the new anodal side after reversing the EF. Blue arrows indicate sites of shmoo emergence. (F) Time lapse of WT cells overexpressing Ste4p (Ste4-OE) in the absence or in the presence of an EF of 50 V/cm. White arrowheads point at sites of polarized growth. (G) Average shmoo orientation after 3 h in the absence or in the presence of an EF for a population of WT cells treated with α-factor, WT mating pairs, and WT cells overexpressing Ste4p. $n>50$ cells for all conditions. Error bars represent standard deviations. Scale bars: 2 μm.
doi:10.1371/journal.pbio.1002029.g001

EF Response Involves the Membrane-Potential-Regulating Potassium Transporter Trk1p

EFs are thought to affect cellular processes at or outside the plasma membrane, but not in the cell interior. They have been postulated to generate subcellular asymmetries in transmembrane potentials (TMPs) [13,38,39], and/or displace charged membrane proteins at the cell surface [40,41]. To test whether membrane transporters mediate EF responses, we screened a set of well-characterized mutants and inhibitors affecting transport at the membrane. We found that calcium, sodium, and proton transport systems are not critical for EF sensing for bud or shmoo reorientation (Figure S4). We found, however, that a potassium transporter mutant *trk1*Δ was defective in the anodal orientation of mating projection, but not in budding orientation; these cells oriented shmoos to the cathode, in a similar manner as *far1-s* and *cdc24-m* mutants (Figure 3A; Movie S6). Trk1p is a high-affinity inward potassium transporter that displays conserved features in bacteria, plants, and fungi. In yeast, Trk1p is a major TMP regulator [42,43], and *trk1*Δ cells exhibit hyperpolarized resting potential (Figure 3B and 3C) [42]. A *trk2*Δ mutant, in the secondary K^+-import system (Trk2p), did not display any orientation defect in the EF, however [44]. Similarly to *far1-s* and *cdc24-m* mutants, *trk1*Δ mutants formed shmoos with normal morphology and timing, but were defective in mating (efficiencies of ~10% of WT; Figure 3D), and displayed significant defects in polarizing in the correct direction in mating pairs (Figure S5B). In contrast, *trk1*Δ had no defects in bud emergence and haploid axial patterns (Figure S5A). We found that Trk1-GFP was located throughout the plasma membrane, but was reduced in emergent growing buds and shmoo tips, in a pattern similar to that of other membrane transporters [45,46]. In shmooing cells, measurements of fluorescence intensity showed a stable back-to-front gradient, with a concentration ratio of about 3-fold (Figures 3E and S5C). In the presence of the EF, we observed a similar depletion of Trk1-GFP at the shmoo tip growing towards the anode, without noticeable change in protein distribution prior to tip growth (Figure S5D and S5E). Together, these data suggest that a natural gradient of Trk1p leading to local differences in potassium import may contribute to polarity regulation for shmoo tip orientation and EF response.

To shed more light on why cells may polarize in these different directions, we performed computational simulations and analytical calculations of the local EF strengths and electric potentials along the membrane of *S. cerevisiae* cells (Figure S6). This showed that sites of bud and shmoo emergence correspond to the minimum and maximum local EF potentials, and to sites of depolarized and hyperpolarized TMPs, respectively. This analysis thus led to the prediction that if EF-induced polarity is sensitive to TMPs, shmoos should emerge at sites of hyperpolarized TMP, while buds should emerge at sites of depolarized TMP.

Asymmetries in Membrane Potential Can Direct Polarity

To directly test the nature of the electrochemical signaling orienting polarity, we developed an optogenetic approach to locally modulate TMPs and/or ion fluxes [47]. Microbial opsins are light-gated transmembrane channels or pumps that have been used to modulate TMPs for neuron activation or silencing [48], as well as in other cell types such as yeast [49,50]. We expressed different opsins tagged with GFP, and found that Halorhodopsin-GFP (NpHR) displayed the most robust expression and plasma membrane targeting, although there was some low level accumulation of Halorhodopsin-GFP in internal membranes, as often seen in other cell types [51] (Figure S7A). Halorhodopsin is a reversible inward chloride pump that causes rapid hyperpolarization of the TMP upon activation with green/yellow light [48]. We confirmed that Halorhodopsin could drive membrane hyperpolarization upon light activation in budding yeast, by measuring changes in global membrane potential in single cells following laser exposure, using the sensitive dye $DiBAC_4(3)$ (Figure S7B and S7C). We implemented a photoactivation assay to locally hyperpolarize mating and budding yeast cells at specific sites on the plasma membrane [52]. Cells were illuminated on a small square-shaped region at the cell surface with a yellow laser for 20 min, and subsequently filmed for 2 h to compute polarized growth orientation (Figure 4A and 4B). Laser exposure did not cause the cells to die or halt growth, but we did note a reduction in growth rate of ~10%–15% in cells exposed to the laser compared to non-exposed controls in the same field. Accordingly, measurement of stress pathway activation revealed a minor stress response that remained negligible compared to typical osmotic stress responses (Figure S8A–S8C).

Strikingly, many cells expressing Halorhodopsin subsequently grew mating projections towards the site of the laser illumination (Figure 4C and 4D). This effect on orientation caused by light was similar to the one caused by 20 min of EF exposure (Figure S2D). Control cells that either did not express Halorhodopsin or expressed an unrelated GFP-tagged transmembrane protein, Hxt3-GFP, with similar localization [53] polarized in directions independent of the laser, showing that this effect was opsin-dependent and not due to cellular damage from the laser itself [54] (Figures 4D and S8D). Similar treatments in budding cells did not orient bud site emergence however (Figure 4D). These data suggest that the direction of mating projections can be controlled by local hyperpolarization of membrane potentials.

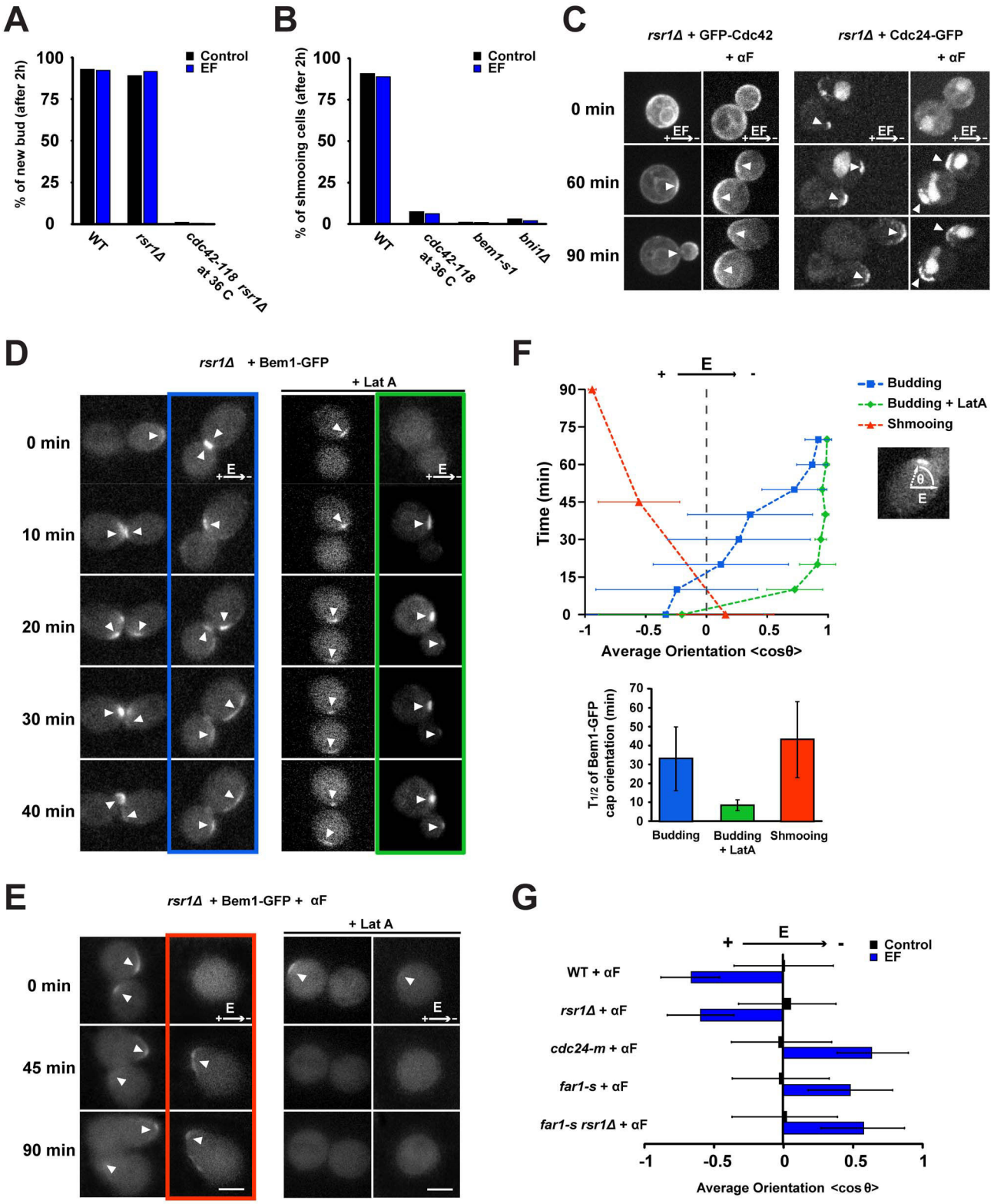
A
% of new bud (after 2h)
100
75
50
25
0
Control
EF
WT
rsr1Δ
cdc42-118 at 36 C
rsr1Δ
B
% of shmooing cells (after 2h)
100
75
50
25
0
Control
EF
WT
cdc42-118 at 36 C
bem1-s1
bni1Δ
C
rsr1Δ + GFP-Cdc42
+ αF
rsr1Δ + Cdc24-GFP
+ αF
0 min
60 min
90 min
EF
D
rsr1Δ + Bem1-GFP
+ Lat A
0 min
10 min
20 min
30 min
40 min
E
F
E
Budding
Budding + LatA
Shmooing
Time (min)
90
75
60
45
30
15
0
-1
-0.5
0
0.5
1
Average Orientation <cosθ>
θ
T1/2 of Bem1-GFP cap orientation (min)
70
60
50
40
30
20
10
0
Budding
Budding + LatA
Shmooing
E
rsr1Δ + Bem1-GFP + αF
+ Lat A
0 min
45 min
90 min
G
E
Control
EF
WT + αF
rsr1Δ + αF
cdc24-m + αF
far1-s + αF
far1-s rsr1Δ + αF
-1
-0.5
0
0.5
1
Average Orientation <cos θ>

Figure 2. EF response involves Cdc42p polarization. (A) Percentage of new bud formation after 2 h in the absence or in the presence of an EF for a population of WT, *rsr1*Δ, and *cdc42-118 rsr1*Δ (at restrictive temperature, 36°C). (B) Percentage of shmoo formation after 2 h in the absence or in the presence of an EF for a population of WT, *cdc42-118* (at restrictive temperature), *bem1-s1*, and *bni1*Δ cells treated with α-factor (αF). (C) Confocal single plane time-lapse images of GFP-Cdc42 and Cdc24-GFP expressed in *rsr1*Δ cells grown under an EF, in the absence or in the presence of α-factor. White arrowheads indicate the successive positions of the protein polar caps. (D) Confocal single plane time-lapse images of Bem1-GFP in control and LatA-treated *rsr1*Δ cells grown in the absence and in the presence of an EF. White arrowheads indicate the successive positions of Bem1-GFP polar caps. (E) Confocal single plane time-lapse images of Bem1-GFP in control and LatA-treated *rsr1*Δ cells grown with or without an EF in the presence of α-factor. Note that LatA treatment induces rapid dispersion of the Bem1-GFP signal at the cap, with or without EF. White arrowheads indicate the successive positions of Bem1-GFP polar caps. (F) Temporal evolution of the average orientation of Bem1-GFP caps with respect to the applied EF in a population of *rsr1*Δ cells, treated with and without LatA or α-factor (top) ($n = 13$ cells for budding [blue], $n = 9$ cells for budding + LatA [green], $n = 4$ cells for shmooing [red]). Half-time ($t_{1/2}$) corresponding to the mean orientation of Bem1-GFP polar caps to the cathode or anode of the EF is shown at the bottom. (G) Average shmoo orientation after 3 h in the absence or in the presence of an EF for a population of WT, *rsr1*Δ, *cdc24-m*, *far1-s*, and *rsr1*Δ *far1-s* cells treated with α-factor. $n > 50$ cells for each condition. Error bars represent standard deviations. Scale bars: 2 μm.
doi:10.1371/journal.pbio.1002029.g002

Membrane Potential May Influence Lipid-Mediated Membrane Surface Charge to Steer Cdc42p Polarity Caps

We next asked how local changes in membrane potential influence the Cdc42-based polarity machinery. Although membrane potential could impact proton transport and local pH [13] or the transport of other ions, our candidate screen did not reveal any obvious role for proton or other ion transport systems other than Trk1p (Figure S4C and S4D). Another way by which membrane potential may affect polarity is through membrane electrostatics by affecting charged lipid flipping [55–57]. PS is a negatively charged lipid that acts as an electrostatic platform at the inner leaflet to regulate membrane binding of proteins including Cdc42p [58]. In budding yeast, PS concentrates at sites of shmoo and bud emergence [58]. A PS synthesis mutant *cho1*Δ has defects in Cdc42p recruitment, shmoo polarity, and mating [58]. We found that this mutant also exhibited an abnormal EF response in that it oriented mating projections to the cathode of the EF, much like *trk1*Δ, *far1-s*, and *cdc24-m* mutants (Figure 5A). Conversely, mutants in a lipid flippase complex, *dnf1-2*Δ or *lem3*Δ, which may have increased PS and negative surface charges [59], showed significant increased anodal shmoo orientation in the EF. PS and membrane charges affected EF response only in shmoos, not in buds (Figure 5B). Next, we imaged PS localization using a GFP-Lact-C2 probe [58,60]. In shmooing cells, PS rapidly accumulated and persisted at the anodal side, long before shmoo appearance. In budding cells, PS also initially accumulated at the anodal side, but then reverted to the cathodal side immediately prior to bud emergence, often leaving a secondary patch at the anodal side (Figure 5C and 5D). Thus, asymmetries in membrane potential may bias the localization of Cdc42p and other polarity factors through effects on PS and membrane charge.

Discussion

These are the first studies, to our knowledge, showing the input of membrane electrochemistry in the regulation of cell polarity in *S. cerevisiae*. We find that EFs direct the site of bud formation and mating projections in different directions. Our optogenetic experiments further show that in shmooing cells, local hyperpolarization of membrane potential is actually sufficient for polarity reorientation (Figure 6). The mating defects of *trk1*Δ and *cho1*Δ mutants [58], for instance, demonstrate that this pathway contributes to cell polarization even in the absence of EFs. Our results suggest a model in which the asymmetric segregation of Trk1p and possibly other transporters produces positive charges at the back of the cell and negative charges on PS lipids at the front of the cell, which promotes the polarized distribution of Cdc42. In the absence of EFs, the asymmetry of Trk1p localization may arise from initial polarization of membrane insertion. These electrochemical pathways may thus represent a positive feedback loop that stabilizes the axis of Cdc42-based polarity for chemotropism.

A surprising finding of this study is the different behavior of budding versus shmooing cells. Although these polarization systems share downstream polarity regulators, we found clear differences in the requirement for upstream electrochemical elements. *rsr1*Δ cells bud towards the cathode, while the same strain shmoos towards the anode. Mutations in Far1, Cdc24, Trk1, and Cho1 all cause cells to shmoo in an abnormal direction in response to EF and have mating defects in the absence of EF, but have little or no effect on bud site selection [27,58]. The cathodal orientation of budding cells in EFs suggests that buds originate at sites of depolarized TMP. However, genetic and optogenetic analysis demonstrate that they may not be dependent on gradients of membrane potential or PS levels, suggesting that regulation of bud site selection is determined by a distinct mechanism. Although it is not yet known what elements act upstream of Cdc42p to drive cathodal growth, a plausible hypothesis is that EFs may localize some charged membrane proteins by direct electrophoresis, as suggested in other systems [13,40]. The EF thus causes a tug-of-war between two competitive pathways that steer polarity in different directions, with the anodal one being dominant in response to mating factors.

The observed responses of cells to exogenously applied EFs lead to a question of whether EFs normally contribute to polarity regulation. Tissues and even individual polarized cells are surrounded by EFs, which may arise from asymmetries in ion transport [61–65]. We speculate that fungi may respond to their own EFs, possibly during mating, in the context of fungal communities such as biofilms, and in their natural environment to guide them during invasion of host tissues, for instance. It would be interesting to examine the role of genes such as Trk1 on various fungal behaviors.

Mechanisms of electrochemical regulation of cell polarity are likely conserved. Our data are consistent with recent findings implicating a similar set of actors in fission yeast, neutrophils, keratocytes, and slime molds [9,10,12,13,40]. Fission yeasts respond to EFs by orienting their growth axis perpendicular to the EF, producing bent morphologies. Cdc42, formins, and the Pma1 proton pump at the plasma membrane are identified as critical elements. Pma1 affects cell polarity and actin assembly even in the absence of exogenous EFs, indicating a role for membrane potential and intracellular pH in regulating normal tip growth [13]. Migrating neutrophils, keratocytes, and slime molds orient migration to exogenous EFs, possibly through effects on membrane potential [10,66]. These responses involve the phosphorylation and charge additions on phosphatidylinositol lipids—mediated by PI3-kinase—that recruit and activate Rho GTPases for polarized migration.

Recent studies on plasma membrane pumps and channels are beginning to reveal the pivotal role of membrane potential, pH, and/or local ion transport in cell migration [67–69], mitotic

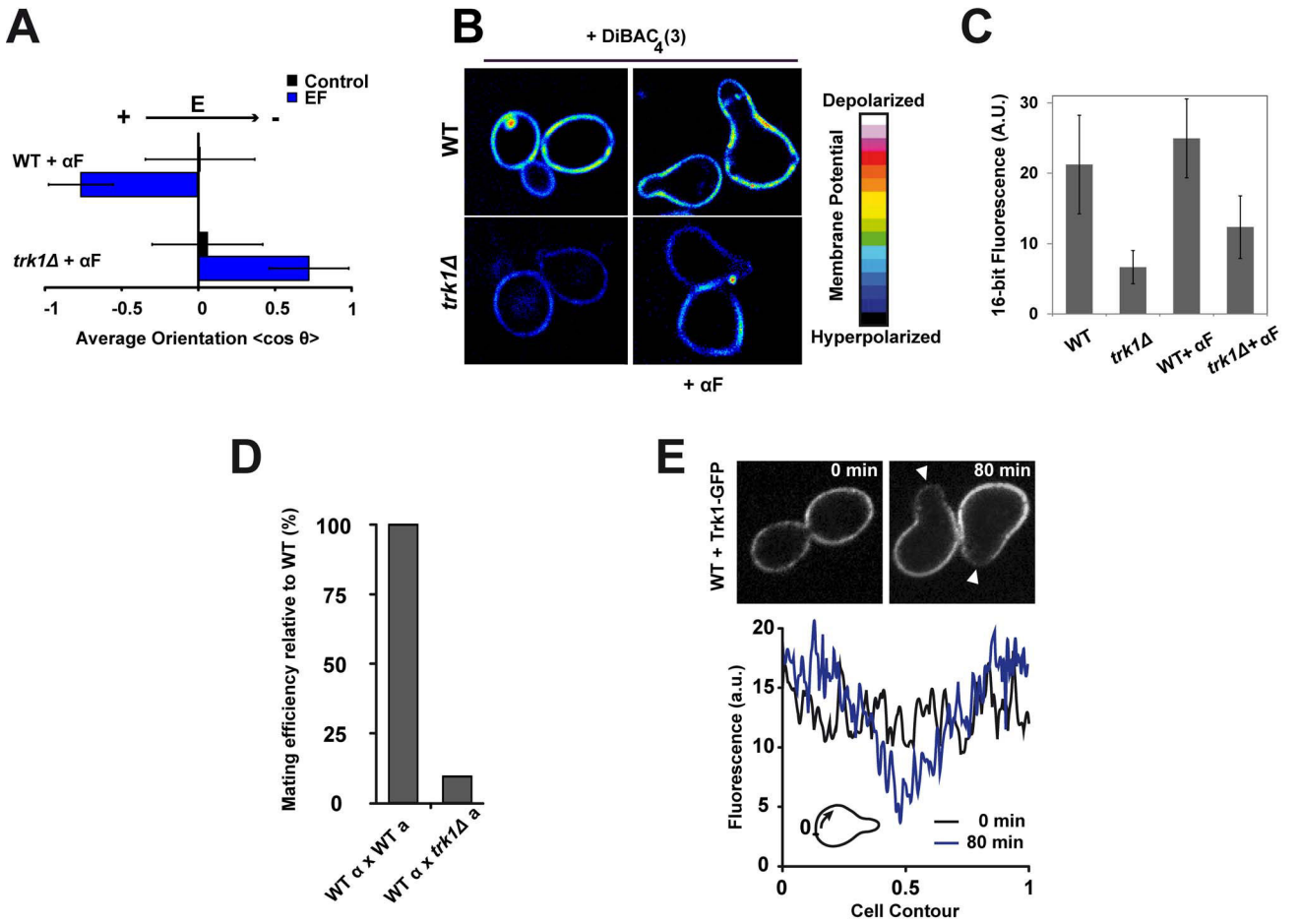

Figure 3. A potassium transporter, Trk1p, mediates EF response in shmoos. (A) Average shmoo orientation after 3 h in the absence or in the presence of an EF for a population of WT and *trk1*Δ cells treated with α-factor (αF) ($n>50$ cells). (B) Sixteen-color images of WT and *trk1*Δ cells stained with the membrane-potential-sensitive dye $DiBAC_4(3)$, which depicts reduced membrane fluorescence upon membrane hyperpolarization. (C) Quantification of $DiBAC_4(3)$ dye membrane staining intensity in WT and *trk1*Δ cells. (D) Mating efficiency of *trk1*Δ cells relative to WT. (E) Confocal single focal plane time-lapse images of Trk1-GFP in WT cells grown in the presence of α-factor. White arrowheads indicate shmoo growth sites. Below is the mean fluorescence intensity along the cell contour at times 0 and 80 min after α-factor treatment, averaged on five independent cells. Distances are normalized between 0 and 1 so that the value 0.5 corresponds to the site of shmoo emergence.
doi:10.1371/journal.pbio.1002029.g003

rounding [70], asymmetric aging [71], and tissue patterning [4,7,72]. A Na^+-H^+ exchanger, Nhe1, is needed for directionality in fibroblast migration; this transporter has been shown to control local pH, which affects the ability of a Cdc42 GEF to bind to the plasma membrane [69,73]. Similarly, the membrane targeting of Dishevelled needed for planar cell polarity activation in fly epithelia may rely on charge interaction and pH [4,69]. An inward-rectifier potassium channel influences patterning of zebrafish skin stripes, leading to a model in which membrane potential controls a directional switch in cell migration and consequent cell–cell arrangement in the tissue [7]. The establishment of a highly tractable system in yeast to study the mechanisms of electrochemical regulation will serve as a foundation to understand the diverse roles of membrane electrochemistry in processes related to cell polarity.

Materials and Methods

Yeast Strains, Media, and Genetic Methods

Standard methods for *S. cerevisiae* media and genetic manipulations were used. Strains and plasmids used in this study are listed in Tables S1 and S2, respectively.

Microscopy

Microscopy was performed at room temperature (23–25°C) with either an inverted wide-field fluorescence microscope or a spinning-disk confocal microscope. Images were acquired, processed, and analyzed with Micro-Manager or Metamorph.

Electric Field Chambers

Chambers to apply the EF to the cells were adapted from previously described methods [13]. Microchannels were approximately 200 μm high, 500 μm wide, and 4 cm long and were fabricated in PDMS. *S. cerevisiae* cells were immobilized by adding 1% of low-melting agarose to the medium. For shmooing experiments with saturating pheromones, 50 μM of α-factor was added to the medium, and cells were placed in the channel 30 min prior to EF application. Because of their slow growth, *cho1*Δ cells were placed in the channel 1 h prior to EF application. Reservoirs connecting electrodes to the channels contained 4% agarose blocks made of medium, which protect cells in the channel from potentially toxic products emanating from the electrodes. Electrodes connected to a generator were immersed in liquid medium added on top of the

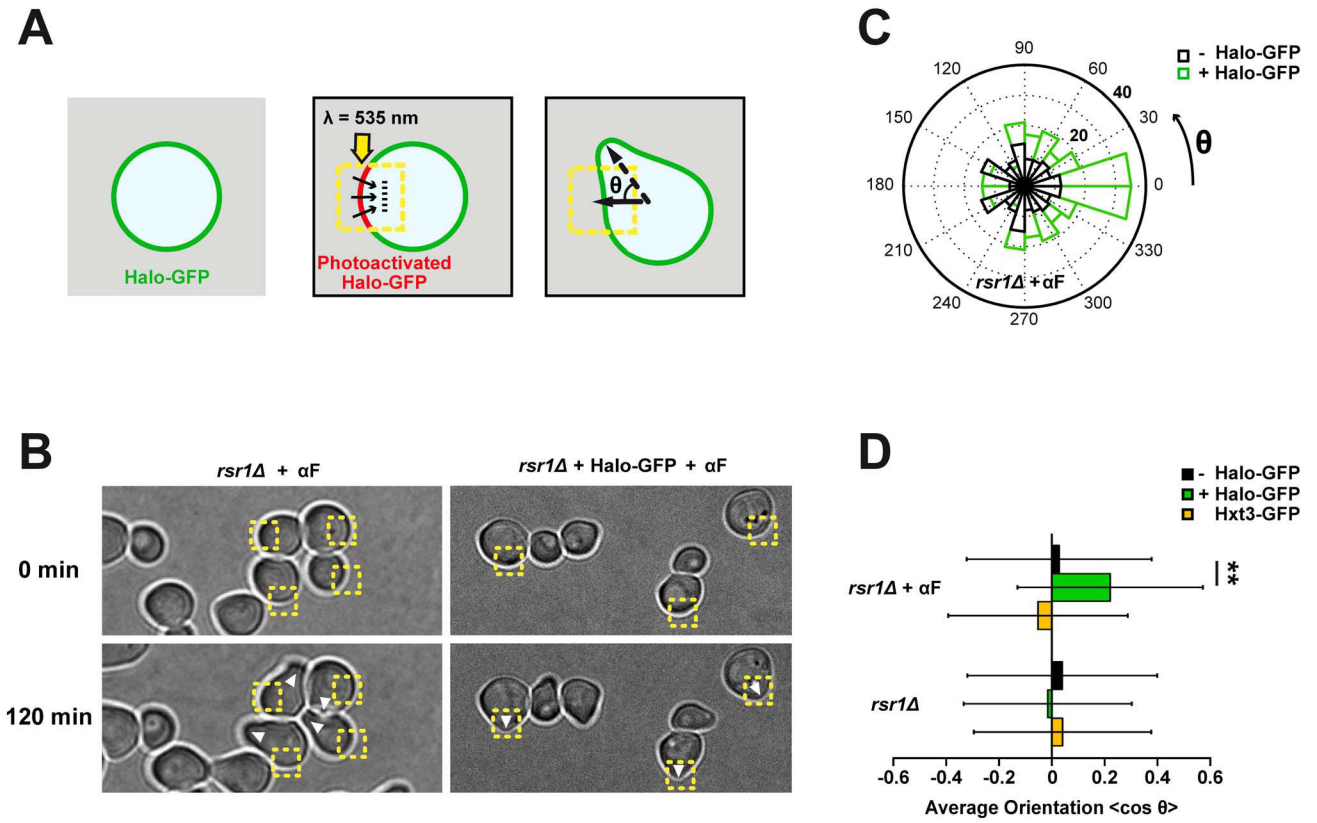

Figure 4. An optogenetic assay shows that asymmetries in membrane potential can direct polarity. (A) Optogenetic assay to generate asymmetries in membrane potential and assess for effect on polarity. Schematic representation of the experimental setup: a yellow laser (λ = 535 nm) is used to photoactivate Halorhodopsin (Halo) in selected regions of *rsr1*Δ cells. θ is the final angle of shmoo or bud emergence with respect to the direction of the photoactivated region. (B) *rsr1*Δ (left) and Halorhodopsin-GFP-expressing *rsr1*Δ (right) cells in the presence of α-factor (αF) and retinal are continuously photoactivated from time 0 to 20 min at the indicated yellow region. After 2 h, shmoos grow and polarity orientation can be quantified with respect to the photoactivated region. White arrowheads indicate sites of shmoo formation. (C) Quantification of optogenetic experiments: radial histogram of polarized growth orientation with respect to photoactivation angle in *rsr1*Δ and *rsr1*Δ + Halorhodopsin-GFP cells treated with α-factor. (D) Average orientation of polarized growth in budding and shmooing cells after 2 h of growth following local photoactivation for a population of *rsr1*Δ, *rsr1*Δ Hxt3-GFP, and *rsr1*Δ + Halorhodopsin-GFP cells ($n>70$ cells gathered from four independent datasets for all conditions and $n=166$ cells gathered from seven independent experiments for *rsr1*Δ + Halorhodopsin-GFP + α-factor). **Student's *t* test, $p<0.05$. Error bars represent standard deviations.
doi:10.1371/journal.pbio.1002029.g004

reservoirs. In these conditions, growth rate and cell cycle periods were almost unaffected, and no significant stress was induced (Figure S1).

Optogenetics

The optogenetic assay used a 535-nm laser, with a power of ~5 mW, interfaced with an iLas system (Roper Scientific) mounted on a confocal spinning disk and a 63× objective. This allowed irradiation of multiple regions of interest (of 20×20 px^2) in a given field of view. Cells were placed on a 2% agar pad containing 20 μM of all-trans retinal and 50 μM of α-factor for shmooing experiments. Cells were put on the pad 30 min prior to laser excitation. The laser was turned on for a continuous period of 20 min, and the cells were subsequently filmed for 2 h to monitor polarized growth. Laser exposure did not induce major changes in growth rate or stress levels (Figure S8A–S8C).

Pharmacological Inhibitors

All inhibitors were prepared at the indicated concentration and applied before EF application. Latrunculin A (LatA) (Sigma) was used at a final concentration of 100 μM from a 100× stock in DMSO. The calcium ionophore A23187 was used at a final concentration of 10 μM. The calcium chelating agent EGTA was used at a final concentration of 2 mM.

Quantitative Mating Assays

Efficiency of mating in *trk1*Δ mutants was assayed by quantitative counting of mating diploids. WT Mat α (AC 131), WT Mat a (AC 129), and *trk1*Δ Mat a (AC 31) cells were grown to mid-log phase in YPD medium and concentrated to 10 OD/ml; WT Mat α cells were incubated at a 10:1 ratio with target WT or *trk1*Δ Mat a cells, and collected into a soft pellet by centrifugation. After 4 h of mating at 30 °C, cells were suspended in liquid YPD, and serial dilutions were plated on medium selective for diploids. Mating efficiency was compared between WT and *trk1*Δ by counting the number of diploid colonies obtained at different dilutions. About 500 colonies were counted for each condition, and the assay was repeated twice.

In addition to this assay, we also counted the number of genuine zygotes by microscopy after 4 h of mating. To this aim, WT Mat

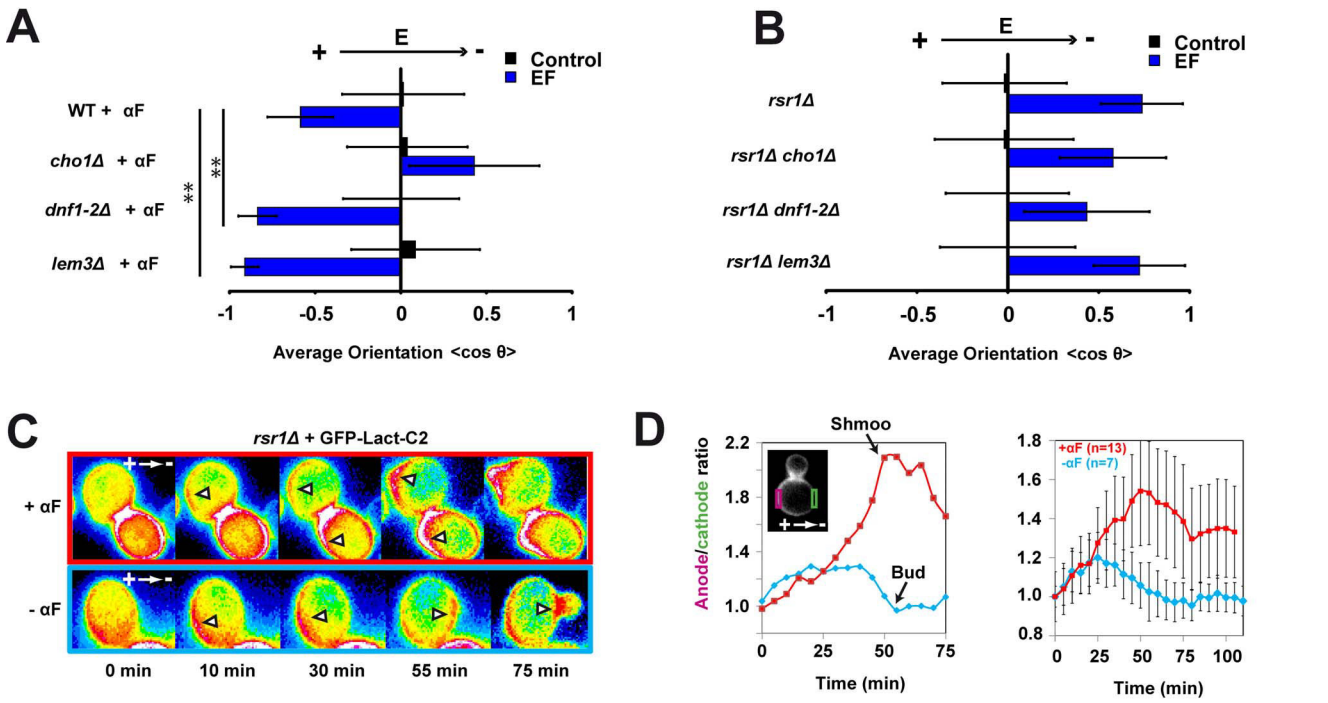

Figure 5. Membrane hyperpolarization orients polarity through local phosphatidylserine accumulation. (A) Average shmoo orientation in the absence or presence of an EF for a population of WT, *cho1*Δ, *dnf1-2*Δ, and *lem3*Δ cells treated with α-factor (αF) ($n>50$ cells). (B) Average bud orientation after 3 h in the absence and in the presence of an EF for a population of *rsr1*Δ, *rsr1*Δ *cho1*Δ, *rsr1*Δ *dnf1-2*Δ, and *rsr1*Δ *lem3*Δ cells ($n>50$ cells). (C) Sixteen-color epifluorescence time lapses of shmooing and budding cells polarizing in EFs and expressing GFP-Lact-C2 probe (a marker for PS). White arrowheads point at sites of PS accumulation. (D) Quantification of PS localization in EFs. The ratio of anodal versus cathodal signal is computed by measuring the total amount at the membrane on both facing sides of the cell. Left: ratio evolution for the depicted sequences in (C). The black arrows indicate the moment when shmoo tip or bud was first visible. Right: average ratio of anodal versus cathodal PS signal for shmooing and budding cells. **Student's *t* test, $p<0.001$. Error bars represent standard deviations.
doi:10.1371/journal.pbio.1002029.g005

α, WT Mat a, and *trk1*Δ Mat a cells were grown in YPD liquid medium to mid-log phase and concentrated to 10 OD/ml. WT Mat α cells were stained with calcofluor for 5 min, subsequently rinsed with YPD, and incubated at a 10:1 ratio with target WT or *trk1*Δ Mat a cells. A 10-µl drop of each mixture was then spotted onto a YPD plate and incubated for 4 h at 30 °C. The mixtures were then imaged on a microscope, and mating efficiency was computed as the ratio of genuine zygotes to the total number of Mat α cells in the field of view. About 500 cells were counted for each condition, and the assay was repeated twice. This assay yielded a mating efficiency in the *trk1*Δ of about 30% of the WT.

Budding Patterns

To test the role of Trk1p in axial budding, we generated a *trk1*Δ strain in the W303 background with a WT copy of the BUD4 gene (AC 134). Cells were then grown to mid-log phase in YPD medium and stained with calcofluor for 5 min to mark bud scars. Axially budding cells were counted when more than three scars were clustered at one site on the surface.

Chemotropism Efficiency in Zygotes

To compare the efficiency of chemotropism in WT versus *trk1*Δ cells, we used a previously described assay that takes advantage of the fact that WT cells grow towards their mating partners irrespective of previous bud site selection, while mutants with defective mating polarity (like *far1-s* or *cdc24-m*) use bud site selection cues to grow shmoos [74]. WT Mat α, WT Mat a, and *trk1*Δ Mat a cells were grown in YPD liquid medium to mid-log phase and concentrated to 10 OD/ml. WT Mat a and *trk1*Δ Mat a cells were stained with calcofluor for 5 min, subsequently rinsed with YPD, and incubated at a 1:1 ratio with target WT Mat α cells. A 10-µl drop of each mixture was then spotted onto a YPD plate and incubated for 4 h at 30°C. The mixtures were then imaged to assess the position of the bud scar relative to the fusion site in each newly formed zygote. Only zygotes with a single fluorescent bud scar were counted. Zygotes were scored as proximal if the bud scar was in the one-third of the cell adjacent to the fusion site, medial for the middle one-third, and distal for the one-third away from the fusion site (Figure S5B).

Membrane Potential Measurement

To measure global membrane potential in single budding yeast cells, we used the membrane potential dye $DiBAC_4(3)$ (Invitrogen), which absorbs in blue light and depicts increased membrane fluorescence upon membrane depolarization, with a sensitivity of nearly 1% per millivolt [7]. Cells were incubated with a concentration of 50 µM dye for 30 min, and images were taken on a confocal spinning disk. Relative membrane potential values were then quantified as membrane signal subtracted from background signal. To assess membrane hyperpolarization by Halorhodopsin, cells were immobilized at the bottom of a microfluidic chamber, between a dialysis membrane and the coverslip [75]. Cells expressing Halorhodopsin-GFP were bleached by long-time exposure with a blue laser. Medium was

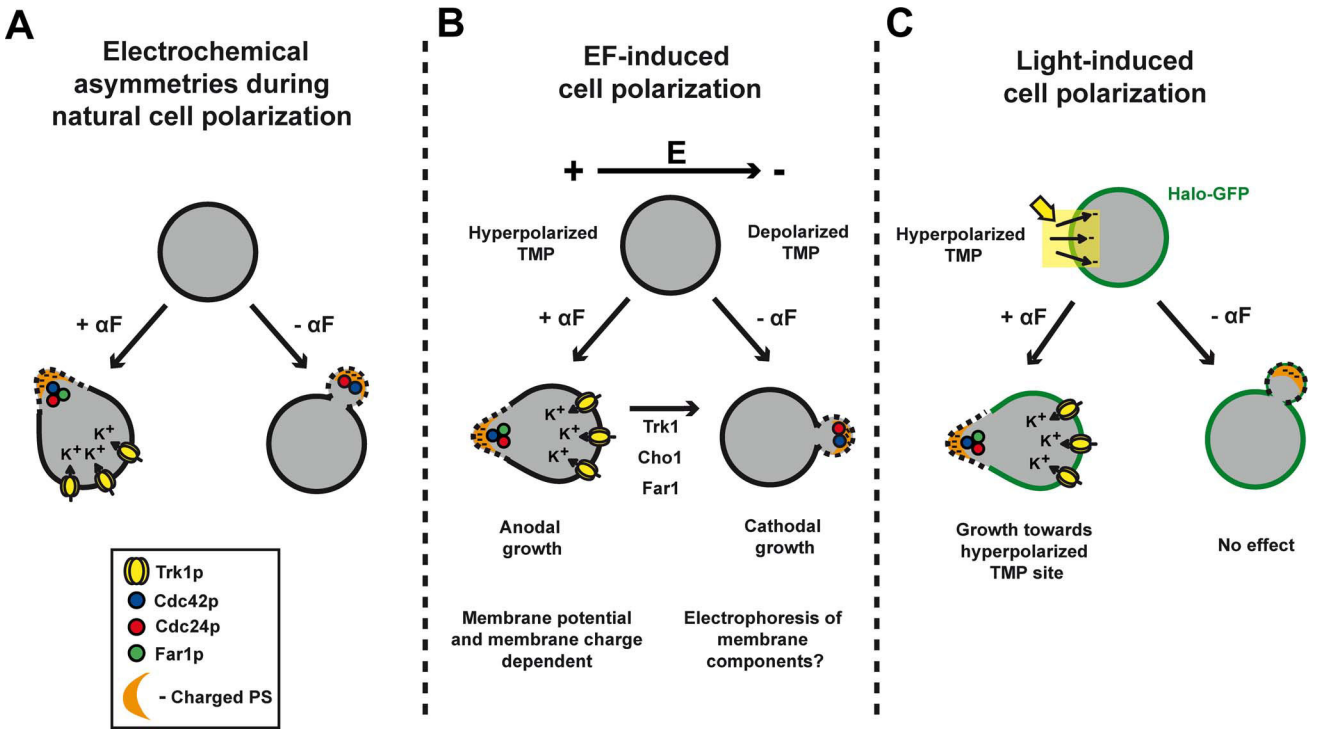

Figure 6. Influence of electrochemical asymmetries on polarity. (A) During normal cell polarization, electrochemical layers segregate to the front and the back of the cell and may influence polarization processes, for instance during mating. (B) In an EF, the anode-facing side has hyperpolarized membrane potential, which drives anodal growth of the shmoos, in a Trk1-, Cho1-, and Far1-dependent manner. The secondary default orientation mode appears to be the cathodal orientation, which drives bud emergence and shmoo growth in *trk1*Δ, *cho1*Δ, and *far1-s* mutants by a yet unknown mechanism. (C) Optogenetic experiments directly suggest that local hyperpolarization of cell membrane potential can drive shmoo polarized growth but not bud site emergence. αF, α-factor.
doi:10.1371/journal.pbio.1002029.g006

subsequently exchanged with YPD containing 50 μM $DiBAC_4(3)$ dye, and the dye was left to stain the cells for 30 min. Dye staining intensity at the membrane was then measured in the same pre-bleached cells at two consecutive time points spaced by 3 min (I_0 and I_1) to compute dye photo-bleaching. These cells were then exposed to the yellow laser for 3 min, and the final dye staining was computed again (I_2). The specific loss of dye staining associated with Halorhodopsin effects on membrane potential was then computed as $\frac{I_2}{I_1} * \frac{I_0}{I_1} - 1$, which is expected to be negative for membrane hyperpolarization and positive for membrane depolarization.

Computer Simulations of EF Effects on Yeast Cells

Computer simulations were performed using the Matlab Partial Differential Equation Toolbox (MathWorks). The cell surfaces as well as the channel sides were considered as perfect insulators, while the cell interior and the surrounding medium as conductors.

Analytical Calculations of EF Effects on Yeast Cells

The electric potential, Φ, created by the applied EF, $\vec{E}$, was analytically computed by solving the Laplace equation: $\Delta\Phi = 0$, with the boundary condition at the insulating membrane $\left(\left(\vec{\nabla}\Phi\right).\vec{n}\right) = 0$, with $\vec{n}$ the vector normal to the membrane, and the limit condition at infinity $\left(\vec{\nabla}\Phi\right)_{\inf} = \vec{E}$. *S. cerevisiae* cells were represented by a sphere, leading to the classical results [76] for the potential at the membrane Φ_m and the field at the membrane $\vec{E}_m$: $\Phi_m = -\frac{3}{2}ER\cos\theta$ and $\vec{E}_m = -\frac{3}{2}E\sin\theta.\vec{e}_\theta$, with R the radius of the sphere and θ the angle with the field.

Supporting Information

Figure S1 EF effects on cell physiology. (A) Effect of EFs on the timing of bud (dose-dependent, left) and shmoo emergence (100 V/cm, right). (B) Effect of EF (100 V/cm for 1 h) on stress levels of cells in presence of 50 μM α-factor as measured by Hog1-GFP nuclear accumulation. Osmotic stress (0.5 M NaCl for 5 min) is used as a positive control for stress. (C) Quantification of Hog1-GFP nuclear to cytoplasmic levels. $n>25$ cells for each condition. Error bars represent standard deviations.
(TIF)

Figure S2 Polarity orientation to EFs displays dose dependence on EF strength and duration of application. (A) Evolution of the average orientation of bud site emergence angles of *rsr1*Δ cells after 2 h under different EF strengths. (B) Evolution of the average orientation of shmoo tip growth angles of WT cells in the presence of α-factor after 2 h under different EF strengths. (C) Evolution of the average orientation of bud site emergence angles of *rsr1*Δ cells under an EF of 50 V/cm as a function of the duration of EF application. Orientation was measured 2 h after start of EF application. (D) Evolution of the average orientation of shmoo tip growth angles of WT cells in the presence of α-factor under an EF of 50 V/cm as a function of the duration of EF application. Orientation was measured 2 h after start of EF application. (E) Shmoo orientation of WT cells in EFs is

independent of pheromone concentration. (F) Images of adjacent cells of opposite mating type in the absence or presence of EFs (left panel). Mat α cells were stained with calcofluor prior to the experiment. Note that control mating pairs polarize towards each other to form a zygote, while cells in EFs grow shmoo tips to the anode, and fail to mate. Right bar graph: percentage of mating cells after 3 h in no EF or an EF of 50 V/cm. $n>50$ cells for each condition. Error bars represent standard deviations. Scale bars: 2 μm.
(TIF)

Figure S3 EF orients polarized growth through canonical downstream polarity effectors. (A and B) Time lapses of indicated mutants grown in the absence or presence of exogenous EFs. Note that mutants that fail to polarize grow in a near isotropic manner, with no bud or shmoo tip emergence. (C and D) Time lapses of Bem1-GFP localization in the indicated mutants grown in the absence or presence of exogenous EFs at the restrictive temperature, 36°C. Note that Bem1-GFP fails to polarize in *cdc42-118rsr1*Δ cells independent of EF presence. White arrowheads indicate the successive positions of Bem1-GFP polar caps. Cells were cultured at 36°C for 1 h prior to EF assay. (E) Average orientation of bud site emergence angles in the indicated mutants ($n>50$ for each condition). (F) Control for the effect of LatA in the microfluidic set-up used for EF applications. Abp1 is a marker for actin patches that becomes diffuse when actin is fully depolymerized. (G) EF-dependent shmoo orientation of WT and *far1-s* cells is independent of pheromone concentration. Error bars represent standard deviations. Scale bars: 5 μm.
(TIF)

Figure S4 Candidate screen for ion transport systems involved in EF response in buds versus shmoos. (A and B) Strain background (W303 versus S2888c) does not impact EF orientation of buds or shmoos. (C) Average orientation of bud site emergence angles in the indicated mutants and drugs in an *rsr1*Δ background. (D) Average orientation of shmoo tip growth angles in the indicated mutants and drugs in the presence of α-factor in a WT background ($n>50$ for each condition). Drug concentrations are indicated in Materials and Methods. Error bars represent standard deviations.
(TIF)

Figure S5 Effects of Trk1 on budding patterns and chemotropism during mating and dynamic localization of Trk1-GFP during bud and shmoo emergence. (A) Axial budding pattern in *trk1*Δ cells expressing a WT BUD4 (strain AC 134). (B) Position of zygote fusion sites compared to previous bud scars in WT and *trk1*Δ cells. (C) Trk1-GFP signal is reduced at shmoo tips. Optical sections spaced by 200 nm were used for maximum intensity projections (left, "MAX"). The 19 individual sections are shown on the right. Three representative individual cells are depicted. (D) Changes of localization of Trk1-GFP during bud emergence in presence (in *rsr1*Δ background) or absence (WT background) of an EF. (E) Changes of localization of Trk1-GFP in shmooing cells exposed to an EF. Note the disappearance of Trk1-GFP at the shmoo tip growing to the anode.
(TIF)

Figure S6 Computational simulation of EF effects on membrane potential predicts a hyperpolarization at the anode-facing side and a depolarization at the cathode-facing side. (A) Computational simulation of the EF-induced electric potential (Φ) landscape around a *S. cerevisiae* cell created by an EF of 50 V/cm. The cytoplasm is set at an arbitrary homogenous reference potential. The lines represent the equipotentials. (B) Predicted local changes in extra-transmembrane potential created by the EF.
(TIF)

Figure S7 Optimization of optogenetic control of membrane potential in *S. cerevisiae*. (A) Images of WT cells expressing different opsins (Archaerhodopsin, Channelrhodopsin, and Halorhodopsin—from left to right) tagged with GFP, after 18 h of induction at 25°C. (B) Assay to monitor Halorhodopsin light-induced membrane depolarization in single cells using $DiBAC_4(3)$. Cells expressing Halorhodopsin-GFP are placed in a microfluidic flow chamber (see Materials and Methods), and the GFP signal is first bleached with 15 stacks of 5-s exposure with a blue laser. Cells are subsequently rinsed with $DiBAC_4(3)$ dye and left to stain for 30 min. Effects of dye photo-bleaching are accounted for by taking single slices spaced apart by 3 min, and measuring membrane intensity subtracted from background before and after the 3-min interval (I_0 and I_1). Hyperpolarization induced by yellow light activation of Halorhodopsin is then assessed by exposing cells to a yellow laser for 3 min, and measuring fluorescence in the green channel (I_2). Specific loss of fluorescence associated with membrane hyperpolarization is computed as $\frac{I_2}{I_1} * \frac{I_0}{I_1} - 1$, which accounts for dye photo-bleaching, and is expected to be positive upon membrane depolarization and negative upon membrane hyperpolarization. (C) Halorhodopsin activation triggers hyperpolarization of *rsr1*Δ cells. Fluorescence changes are computed as described in (B). p-Value is 0.079 as calculated by Student's t test. Error bars represent standard deviations, and $n \geq 32$ cells were analyzed.
(TIF)

Figure S8 Effects of optogenetic assays on cell physiology. (A) Effect of locally restricted yellow light exposure for 20 min on the growth rate of shmoos. (B) Effect of local yellow light exposure (yellow boxes) for 20 min on stress levels of cells in presence of 50 μM α-factor as measured by Hog1-GFP nuclear accumulation. Osmotic stress (0.5 M NaCl for 5 min) is used as a positive control for stress. (C) Quantification of Hog1-GFP nuclear to cytoplasmic levels. (D) Subcellular localization of Hxt3-GFP expressed under its endogenous promoter in *rsr1*Δ cells. $n>25$ cells for each condition. Error bars represent standard deviations.
(TIF)

Table S1 Strains used in this study.
(XLSX)

Table S2 Plasmids used in this study.
(XLSX)

Movie S1 Haploid *rsr1*Δ *S. cerevisiae* cells budding toward the cathode of the EF. Elapsed time = 180 min. Time is in hours: minutes.
(AVI)

Movie S2 Haploid MAT a WT *S. cerevisiae* cells shmoo toward the anode of the EF in the presence of α-factor. Elapsed time = 160 min. Time is in hours: minutes.
(AVI)

Movie S3 Inducing two sites of polarization by switching the direction of the EF. Cell in α-factor and EF. After 140 min, the EF was reversed. Elapsed time = 290 min. Time is in hours: minutes.
(AVI)

Movie S4 WT cells overexpressing Ste4p fail to stabilize polarity at a single place and grow successive shmoos all

around the surface. Elapsed time = 240 min. Time is in hours: minutes.
(AVI)

Movie S5 WT cells overexpressing Ste4p and grown in the EF stabilize shmoo growth towards the anode. Elapsed time = 190 min. Time is in minutes.

Movie S6 Merged movie depicting haploid MAT a WT cells growing shmoos toward the anode of the EF and subsequently haploid MAT a *trk1*Δ cells growing shmoos toward the cathode. Time is in minutes.
(AVI)

Data S1 Excel spreadsheet containing, in separate sheets, the underlying numerical data and statistical analysis for Figures 1B, 1D, 1G, 2A, 2B, 2F, 2G, 3A, 3C, 3D, 3E, 4D, 5A, 5B, 5D, S1A, S1C, S2A, S2B, S2C, S2D, S2E, S2F, S3E, S3G, S4A, S4B, S4C, S4D, S5A, S5B, S7C, S8A, and S8C.
(XLSX)

Acknowledgments

The authors acknowledge members of the Minc and Chang laboratory for discussions and technical assistance. We thank the Kominsky, Arkowitz, Pringle, Kaknosen, Cunningham, Sychrova, Li, Grinstein, Carman, Stillman, Jackson, Leon, Boyden, Han, and Whiteway labs for sharing plasmids, strains, and protocols.

Author Contributions

The author(s) have made the following declarations about their contributions: Conceived and designed the experiments: AH AC FC NM. Performed the experiments: AH AC DB NM. Analyzed the data: AH AC DB NM. Contributed reagents/materials/analysis tools: AH AC DB MP FC NM. Wrote the paper: AH AC DB FC NM.

References

1. Drubin DG, Nelson WJ (1996) Origins of cell polarity. Cell 84: 335–344.
2. Campetelli A, Bonazzi D, Minc N (2012) Electrochemical regulation of cell polarity and the cytoskeleton. Cytoskeleton (Hoboken) 69: 601–612.
3. Schonichen A, Webb BA, Jacobson MP, Barber DL (2013) Considering protonation as a posttranslational modification regulating protein structure and function. Annu Rev Biophys 42: 289–314.
4. Simons M, Gault WJ, Gotthardt D, Rohatgi R, Klein TJ, et al. (2009) Electrochemical cues regulate assembly of the Frizzled/Dishevelled complex at the plasma membrane during planar epithelial polarization. Nat Cell Biol 11: 286–294.
5. Magalhaes MA, Larson DR, Mader CC, Bravo-Cordero JJ, Gil-Henn H, et al. (2011) Cortactin phosphorylation regulates cell invasion through a pH-dependent pathway. J Cell Biol 195: 903–920.
6. Levin M (2009) Bioelectric mechanisms in regeneration: unique aspects and future perspectives. Semin Cell Dev Biol 20: 543–556.
7. Inaba M, Yamanaka H, Kondo S (2012) Pigment pattern formation by contact-dependent depolarization. Science 335: 677.
8. Chang F, Minc N (2014) Electrochemical control of cell and tissue polarity. Annu Rev Cell Dev Biol 30: 317–336.
9. Sun Y, Do H, Gao J, Zhao R, Zhao M, et al. (2013) Keratocyte fragments and cells utilize competing pathways to move in opposite directions in an electric field. Curr Biol 23: 569–574.
10. Zhao M, Song B, Pu J, Wada T, Reid B, et al. (2006) Electrical signals control wound healing through phosphatidylinositol-3-OH kinase-gamma and PTEN. Nature 442: 457–460.
11. Song B, Zhao M, Forrester JV, McCaig CD (2002) Electrical cues regulate the orientation and frequency of cell division and the rate of wound healing in vivo. Proc Natl Acad Sci U S A 99: 13577–13582.
12. Sato MJ, Kuwayama H, van Egmond WN, Takayama AL, Takagi H, et al. (2009) Switching direction in electric-signal-induced cell migration by cyclic guanosine monophosphate and phosphatidylinositol signaling. Proc Natl Acad Sci U S A 106: 6667–6672.
13. Minc N, Chang F (2010) Electrical control of cell polarization in the fission yeast Schizosaccharomyces pombe. Curr Biol 20: 710–716.
14. Bonazzi D, Minc N (2014) Dissecting the molecular mechanisms of electrotactic effects. Adv Wound Care (New Rochelle) 3: 139–148.
15. Jaffe LF, Stern CD (1979) Strong electrical currents leave the primitive streak of chick embryos. Science 206: 569–571.
16. Kropf DL, Caldwell JH, Gow NA, Harold FM (1984) Transcellular ion currents in the water mold Achlya. Amino acid proton symport as a mechanism of current entry. J Cell Biol 99: 486–496.
17. van West P, Morris BM, Reid B, Appiah AA, Osborne MC, et al. (2002) Oomycete plant pathogens use electric fields to target roots. Mol Plant Microbe Interact 15: 790–798.
18. Lin F, Baldessari F, Gyenge CC, Sato T, Chambers RD, et al. (2008) Lymphocyte electrotaxis in vitro and in vivo. J Immunol 181: 2465–2471.
19. Hotary KB, Robinson KR (1992) Evidence of a role for endogenous electrical fields in chick embryo development. Development 114: 985–996.
20. Zhao M (2009) Electrical fields in wound healing—an overriding signal that directs cell migration. Semin Cell Dev Biol 20: 674–682.
21. Drubin DG (1991) Development of cell polarity in budding yeast. Cell 65: 1093–1096.
22. Chang F, Peter M (2003) Yeasts make their mark. Nat Cell Biol 5: 294–299.
23. Chant J, Herskowitz I (1991) Genetic control of bud site selection in yeast by a set of gene products that constitute a morphogenetic pathway. Cell 65: 1203–1212.
24. Martin SG, Arkowitz RA (2014) Cell polarization in budding and fission yeasts. FEMS Microbiol Rev 38: 228–253.
25. Nern A, Arkowitz RA (1998) A GTP-exchange factor required for cell orientation. Nature 391: 195–198.
26. Butty AC, Pryciak PM, Huang LS, Herskowitz I, Peter M (1998) The role of Far1p in linking the heterotrimeric G protein to polarity establishment proteins during yeast mating. Science 282: 1511–1516.
27. Nern A, Arkowitz RA (1999) A Cdc24p-Far1p-Gbetagamma protein complex required for yeast orientation during mating. J Cell Biol 144: 1187–1202.
28. Evangelista M, Blundell K, Longtine MS, Chow CJ, Adames N, et al. (1997) Bni1p, a yeast formin linking cdc42p and the actin cytoskeleton during polarized morphogenesis. Science 276: 118–122.
29. Chenevert J, Corrado K, Bender A, Pringle J, Herskowitz I (1992) A yeast gene (BEM1) necessary for cell polarization whose product contains two SH3 domains. Nature 356: 77–79.
30. Brand A, Shanks S, Duncan VM, Yang M, Mackenzie K, et al. (2007) Hyphal orientation of Candida albicans is regulated by a calcium-dependent mechanism. Curr Biol 17: 347–352.
31. Brand AC, Morrison E, Milne S, Gonia S, Gale CA, et al. (2014) Cdc42 GTPase dynamics control directional growth responses. Proc Natl Acad Sci U S A 111: 811–816.
32. Ferrigno P, Posas F, Koepp D, Saito H, Silver PA (1998) Regulated nucleo/cytoplasmic exchange of HOG1 MAPK requires the importin beta homologs NMD5 and XPO1. EMBO J 17: 5606–5614.
33. Whiteway M, Hougan L, Thomas DY (1990) Overexpression of the STE4 gene leads to mating response in haploid Saccharomyces cerevisiae. Mol Cell Biol 10: 217–222.
34. Kozminski KG, Chen AJ, Rodal AA, Drubin DG (2000) Functions and functional domains of the GTPase Cdc42p. Mol Biol Cell 11: 339–354.
35. Wedlich-Soldner R, Altschuler S, Wu L, Li R (2003) Spontaneous cell polarization through actomyosin-based delivery of the Cdc42 GTPase. Science 299: 1231–1235.
36. Nern A, Arkowitz RA (2000) Nucleocytoplasmic shuttling of the Cdc42p exchange factor Cdc24p. J Cell Biol 148: 1115–1122.
37. Butty AC, Perrinjaquet N, Petit A, Jaquenoud M, Segall JE, et al. (2002) A positive feedback loop stabilizes the guanine-nucleotide exchange factor Cdc24 at sites of polarization. EMBO J 21: 1565–1576.
38. Gross D, Loew LM, Webb WW (1986) Optical imaging of cell membrane potential changes induced by applied electric fields. Biophys J 50: 339–348.
39. Kralj JM, Hochbaum DR, Douglass AD, Cohen AE (2011) Electrical spiking in Escherichia coli probed with a fluorescent voltage-indicating protein. Science 333: 345–348.
40. Allen GM, Mogilner A, Theriot JA (2013) Electrophoresis of cellular membrane components creates the directional cue guiding keratocyte galvanotaxis. Curr Biol 23: 560–568.
41. Jaffe LF (1977) Electrophoresis along cell membranes. Nature 265: 600–602.
42. Madrid R, Gomez MJ, Ramos J, Rodriguez-Navarro A (1998) Ectopic potassium uptake in trk1 trk2 mutants of Saccharomyces cerevisiae correlates with a highly hyperpolarized membrane potential. J Biol Chem 273: 14838–14844.
43. Gaber RF, Styles CA, Fink GR (1988) TRK1 encodes a plasma membrane protein required for high-affinity potassium transport in Saccharomyces cerevisiae. Mol Cell Biol 8: 2848–2859.
44. Calero F, Gomez N, Arino J, Ramos J (2000) Trk1 and Trk2 define the major K(+) transport system in fission yeast. J Bacteriol 182: 394–399.
45. Perez-Valle J, Jenkins H, Merchan S, Montiel V, Ramos J, et al. (2007) Key role for intracellular K+ and protein kinases Sat4/Hal4 and Hal5 in the plasma membrane stabilization of yeast nutrient transporters. Mol Cell Biol 27: 5725–5736.

46. Eldakak A, Rancati G, Rubinstein B, Paul P, Conaway V, et al. (2010) Asymmetrically inherited multidrug resistance transporters are recessive determinants in cellular replicative ageing. Nat Cell Biol 12: 799–805.
47. Adams DS, Tseng AS, Levin M (2013) Light-activation of the Archaerhodopsin H(+)-pump reverses age-dependent loss of vertebrate regeneration: sparking system-level controls in vivo. Biol Open 2: 306–313.
48. Zhang F, Vierock J, Yizhar O, Fenno LE, Tsunoda S, et al. (2011) The microbial opsin family of optogenetic tools. Cell 147: 1446–1457.
49. Hildebrandt V, Fendler K, Heberle J, Hoffmann A, Bamberg E, et al. (1993) Bacteriorhodopsin expressed in Schizosaccharomyces pombe pumps protons through the plasma membrane. Proc Natl Acad Sci U S A 90: 3578–3582.
50. Lang-Hinrichs C, Queck I, Buldt G, Stahl U, Hildebrandt V (1994) The archaebacterial membrane protein bacterio-opsin is expressed and N-terminally processed in the yeast Saccharomyces cerevisiae. Mol Gen Genet 244: 183–188.
51. Arrenberg AB, Del Bene F, Baier H (2009) Optical control of zebrafish behavior with halorhodopsin. Proc Natl Acad Sci U S A 106: 17968–17973.
52. Strickland D, Lin Y, Wagner E, Hope CM, Zayner J, et al. (2012) TULIPs: tunable, light-controlled interacting protein tags for cell biology. Nat Methods 9: 379–384.
53. Ko CH, Liang H, Gaber RF (1993) Roles of multiple glucose transporters in Saccharomyces cerevisiae. Mol Cell Biol 13: 638–648.
54. Kono K, Saeki Y, Yoshida S, Tanaka K, Pellman D (2012) Proteasomal degradation resolves competition between cell polarization and cellular wound healing. Cell 150: 151–164.
55. McNamee MG, McConnell HM (1973) Transmembrane potentials and phospholipid flip-flop in excitable membrane vesicles. Biochemistry 12: 2951–2958.
56. McLaughlin S, Harary H (1974) Phospholipid flip-flop and the distribution of surface charges in excitable membranes. Biophys J 14: 200–208.
57. Hall JE (1981) Voltage-dependent lipid flip-flop induced by alamethicin. Biophys J 33: 373–381.
58. Fairn GD, Hermansson M, Somerharju P, Grinstein S (2011) Phosphatidylserine is polarized and required for proper Cdc42 localization and for development of cell polarity. Nat Cell Biol 13: 1424–1430.
59. Das A, Slaughter BD, Unruh JR, Bradford WD, Alexander R, et al. (2012) Flippase-mediated phospholipid asymmetry promotes fast Cdc42 recycling in dynamic maintenance of cell polarity. Nat Cell Biol 14: 304–310.
60. Yeung T, Gilbert GE, Shi J, Silvius J, Kapus A, et al. (2008) Membrane phosphatidylserine regulates surface charge and protein localization. Science 319: 210–213.
61. Nuccitelli R, Jaffe LF (1976) The ionic components of the current pulses generated by developing fucoid eggs. Dev Biol 49: 518–531.
62. Robinson KR, Jaffe LF (1975) Polarizing fucoid eggs drive a calcium current through themselves. Science 187: 70–72.
63. Peng HB, Jaffe LF (1976) Polarization of fucoid eggs by steady electrical fields. Dev Biol 53: 277–284.
64. Weisenseel MH, Nuccitelli R, Jaffe LF (1975) Large electrical currents traverse growing pollen tubes. J Cell Biol 66: 556–567.
65. Nuccitelli R, Poo MM, Jaffe LF (1977) Relations between ameboid movement and membrane-controlled electrical currents. J Gen Physiol 69: 743–763.
66. Gao RC, Zhang XD, Sun YH, Kamimura Y, Mogilner A, et al. (2011) Different roles of membrane potentials in electrotaxis and chemotaxis of dictyostelium cells. Eukaryot Cell 10: 1251–1256.
67. Choi CH, Webb BA, Chimenti MS, Jacobson MP, Barber DL (2013) pH sensing by FAK-His58 regulates focal adhesion remodeling. J Cell Biol 202: 849–859.
68. Frantz C, Barreiro G, Dominguez L, Chen X, Eddy R, et al. (2008) Cofilin is a pH sensor for actin free barbed end formation: role of phosphoinositide binding. J Cell Biol 183: 865–879.
69. Frantz C, Karydis A, Nalbant P, Hahn KM, Barber DL (2007) Positive feedback between Cdc42 activity and H+ efflux by the Na-H exchanger NHE1 for polarity of migrating cells. J Cell Biol 179: 403–410.
70. Stewart MP, Helenius J, Toyoda Y, Ramanathan SP, Muller DJ, et al. (2011) Hydrostatic pressure and the actomyosin cortex drive mitotic cell rounding. Nature 469: 226–230.
71. Hughes AL, Gottschling DE (2012) An early age increase in vacuolar pH limits mitochondrial function and lifespan in yeast. Nature 492: 261–265.
72. Pai VP, Aw S, Shomrat T, Lemire JM, Levin M (2012) Transmembrane voltage potential controls embryonic eye patterning in Xenopus laevis. Development 139: 313–323.
73. Denker SP, Barber DL (2002) Cell migration requires both ion translocation and cytoskeletal anchoring by the Na-H exchanger NHE1. J Cell Biol 159: 1087–1096.
74. Follette PJ, Arkowitz RA (2009) Chemotropism during yeast mating. Methods Mol Biol 571: 99–110.
75. Charvin G, Cross FR, Siggia ED (2008) A microfluidic device for temporally controlled gene expression and long-term fluorescent imaging in unperturbed dividing yeast cells. PLoS ONE 3: e1468.
76. Cole KS (1969) Membranes, ions and impulses. Berkeley: University of California Press.

CHAPTER

23 Measurement and manipulation of cell size parameters in fission yeast

Yonatan Zegman, Daria Bonazzi, Nicolas Minc[1]

Institut Jacques Monod, CNRS UMR, Paris Cedex 13, France

[1]*Corresponding author: E-mail: minc@ijm.univ-paris-diderot.fr*

CHAPTER OUTLINE

Methods in Cell Biology, Volume 125, ISSN 0091-679X, http://dx.doi.org/10.1016/bs.mcb.2014.10.011

Abstract

Cells usually grow to a certain size before they divide. The fission yeast *Schizosaccharomyces pombe* is an established model to dissect the molecular control of cell size homeostasis and cell cycle. In this chapter, we describe two simple methods to: (1) precisely compute geometrical parameters (cell length, diameter, surface, and volume) of single growing and dividing fission yeast cells with image analysis scripts and (2) manipulate cell diameter with microfabricated chambers and assess for cell size at division. We demonstrate the strength of these approaches in the context of growing spores, which constantly change size and shape and in deriving allometric relationships between cell geometrical parameters associated with G2/M transition. We emphasize these methods to be useful to investigate problems of growth, size, and division in fungal or bacterial cells.

INTRODUCTION

Cell size is a significant cellular property, which influences the maintenance of metabolite concentrations, transport at the cell surface, tissue morphogenesis, and the proper assembly of intracellular structures, such as the mitotic spindle (Lloyd, 2013; Marshall et al., 2012; Turner, Ewald, & Skotheim, 2012). For size homeostasis, cells usually grow to a certain size and enter division, a process which is largely controlled by the cell-cycle machinery. The rod-shaped fission yeast *Schizosaccharomyces pombe* has been instrumental in identifying regulators of cell cycle and size controls (Mitchison & Nurse, 1985). These cells grow along a unicellular axis with a nearly constant diameter and divide at a fixed length of $\sim$14 μm. Mutants in the cell cycle have thus traditionally been identified as being shorter or longer than wild-type cells (Nurse, Thuriaux, & Nasmyth, 1976). Recent studies have suggested a "geometrical control" model for the cell cycle, in which cell length is monitored by gradients of the DYRK kinase pom1p emanating from cell tips. These gradients serve as cellular rulers for G2/M transition (Martin, 2009; Martin & Berthelot-Grosjean, 2009; Moseley, Mayeux, Paoletti, & Nurse, 2009; Moseley & Nurse, 2010).

Despite the prominent role of *S. pombe* in deciphering core mechanisms of size sensing, to date, there is no standardized method to precisely quantitate length, diameter, surface, and volume of single cells. Because mutants associated with the cell cycle can also be defective in polarity and cell shape (e.g. *pom1* for instance (Bahler & Pringle, 1998)), computing parameters such as surface or volume can often be difficult. In addition, many morphogenetic mutants have defective cell length at division; for instance, fat mutants in the Rho GAP rga4p divide shorter, while thin mutants in another Rho GAP rga2p divide longer (Das et al., 2007; Pan, Saunders, Flor-Parra, Howard, & Chang, 2014; Tatebe, Nakano, Maximo, & Shiozaki, 2008; Villar-Tajadura et al., 2008). Disentangling causal effects of geometry onto cell-cycle progression may thus be difficult, and is likely to bring important insights into this fundamental problem.

Here, we describe two relatively simple methods for the study of size-related questions in fission yeast: The first method uses confocal or phase microscopy

and MATLAB-based image analysis script to compute precisely cell length, diameter, surface, and volume in individual growing cells that may change shape and diameter, for instance, and in dividing cells. Outputs of this method include the dynamic evolution of size parameters in single cells (single volumetric or surface growth rates, for instance) and the study of the correlation between different size parameters in populations of dividing wild-type or mutant cells. Second, we describe the use of microfabricated PDMS (polydimethylsiloxane) channels to manipulate cell diameter, and assess impact on cell length at division. This approach may serve to directly address the relationships between geometry and cell-cycle progression.

1. MEASUREMENT OF SIZE PARAMETERS OF SINGLE FISSION YEAST CELLS

This section will describe basic methodologies for sample preparation and the use of a MATLAB script designed to compute the length, diameter, surface area, and volume of outgrowing spores, which continuously change shapes and sizes (Bonazzi et al., 2014), as well as of dividing cells of different mutants with various shapes and dimensions. The method includes cell handling, microscopy, and image analysis protocols.

1.1 DYNAMIC MEASUREMENT OF CELL SIZE PARAMETERS DURING SINGLE SPORE GROWTH AND POLARIZATION

Materials

Glass slide; 22 × 22 mm^2 coverslips; Erlen Meyer; YE5S plates, ME plates, YE5S liquid media; agarose (Euromedex, Ref. D5-C); Sterile water; Glusulase (PerkinElmer, Ref. NEE154001EA); Fission yeast homothallic h90 strains; Block heater for microtubes; Microwave; Centrifuge; Rotating agitator; Wide-field microscope equipped with perfect focus system and a phase 100X objective; Humidifier; Temperature and humidity sensor; Computer equipped with MATLAB and image analysis toolbox (Mathworks); and dedicated script (available upon demand).

1.1.1 Spore preparation for imaging

1. Grow a homothallic h90 colony on a YE5S (Yeast Extract) plate for 1−2 days to obtain a fresh culture and replica on ME (Malt Extract) plates to sporulate cells for at least 3 days at room temperature.
2. Check sporulating efficiency under the microscope by placing a tiny amount of cells in 2 µl water between a glass slide and a coverslip. The spores should account for more than 70% of the population.
3. Digest a relatively large amount of spores for 1 h at room temperature in 200 µl of water solution containing 1/200 glusulase to kill vegetative cells.
4. Wash the spores three times in water to remove the enzyme.
5. In a sterile Erlen Meyer, add agarose to liquid YE5S at a final concentration of 2% w/V. Heat the mix shortly in the microwave to melt the agarose in the solution, mix well, and aliquot in 1 ml microtubes.

6. Melt a tube of 2% agar YE5S at 95 °C for 5 min in the block heater and place it at 65 °C for at least 20 min.
7. Pipette 180 µl of melted agar on a glass slide and spread it by covering the drop with a glass slide perpendicularly to the first one, wait 3 min, and then remove the upper glass slide by gently sliding it laterally.
8. Adjust the dilution of spores under the microscope to obtain a relatively dense concentration of spores, but spores that do not contact each other.
9. Place 1 µl of concentrated spores on top of the agar pad and cover with a coverslip. To avoid air bubble formation, place the coverslip on the side of the agar pad and bring it gently to the surface of the pad by holding it with a razor blade. Small bubbles may appear here and there, and it is advised to start imaging away from those, as they may grow over time and disrupt long-term imaging.

1.1.2 Imaging

1. Place the sample on the inverted microscope with the coverslip side facing the 100X objective.
2. Find a position that optimizes the density of spores (not too dense and not too diluted).
3. Focus on the middle plane by searching for the maximal contour of the spores.
4. Turn on perfect focus.
5. Take time-lapse phase-contrast movies (5−10 min time interval) of germinating spores at room temperature (23−25 °C), and control humidity with a humidifier in the microscopy room. The first cell cycle, from germination to mitosis, may take typically 10−12 h.

1.1.3 Image analysis

General principle of image-analysis script:

Evolution of spore dimensions (diameter, surface, volume, aspect ratio) is measured from phase-contrast time-lapse movies using home-built MATLAB scripts. The software follows a series of steps interacting with the user from selecting and cropping the spore, adapting the threshold, and troubleshooting. It then segments the phase image by applying thresholding and edge-detection methods to extract the cell contour at each time point. From the contour, diameter and aspect ratio can be directly computed and surface and volume are calculated by assuming a prolate geometry (rotational symmetry around the longest axis of the cell). The long axis is identified and sliced in local diameters d(x) at every pixel in order to compute the areas of the sections of the prolate $s(x) = \pi * (d(x)/2)^2$ and their circumferences $c(x) = \pi * d(x)$. Finally, the volume is the sum of the areas, and the surface area is the sum of the circumferences, both integrated along all the pixels of the long axis (Figure 1(A)) (Bonazzi et al., 2014). We estimate imprecisions associated to these methods (including errors in the z, segmentation, and prolate approximation) to be lower than 5% for length and aspect ratio and on the order of 10% for surface and volume. These analyses will be the most accurate if the plane of focus is as close as possible to the midsection of the spore.

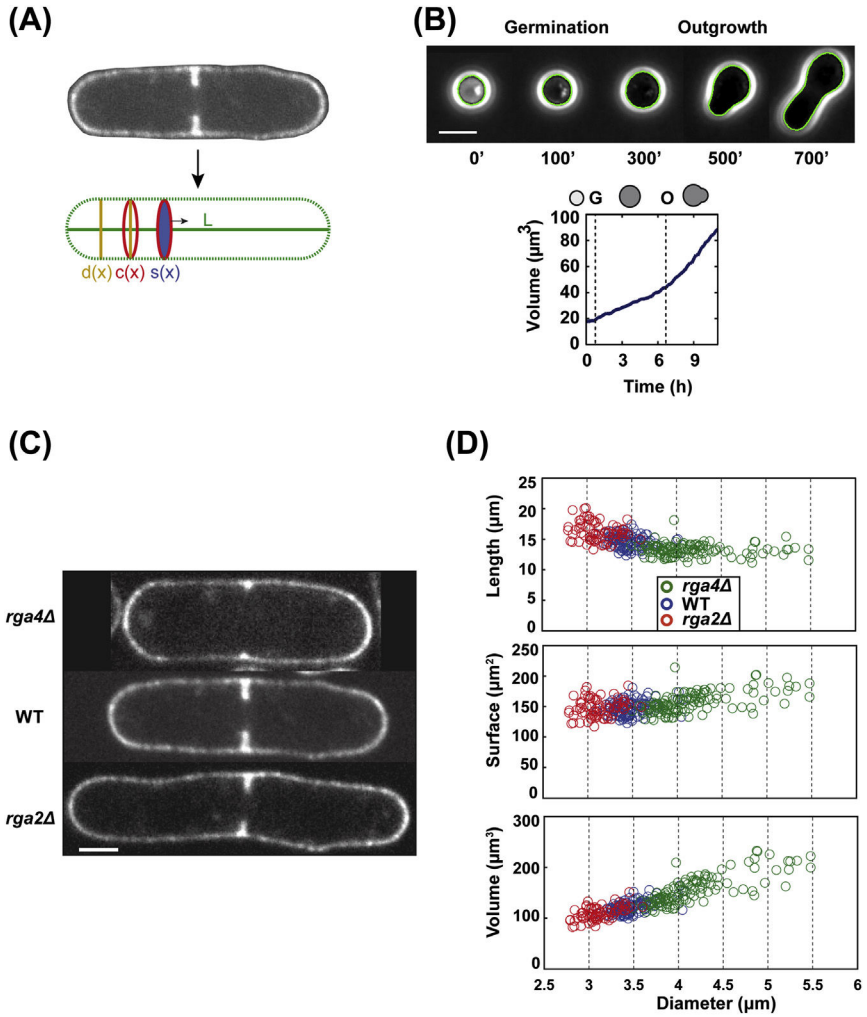

FIGURE 1 Measurement of size parameters of single fission yeast cells.

(A) Fluorescence image of a dividing fission yeast cell expressing GFP-psy1 (to label plasma membrane). The contour is cropped, traced, and measured for length (L, green), as well as local diameters (d(x), yellow), circumferences (c(x), red), and section areas (s(x), blue), which are integrated to give the cell surface and volume. (B) Upper: Phase-contrast time-lapse superimposed with automated shape contour detection (green) of a wild-type fission yeast spore germinating and outgrowing. Scale bar, 5 μm. Lower: Dynamic evolution of single cell volume as a function of time. (C) Midsection confocal images of dividing WT, *rga4*Δ, and *rga2*Δ fission yeast cells expressing GFP-psy1. Dividing cells can be identified from membrane invaginations associated with cytokinesis. Scale bar, 2 μm. (D) Single cell length (upper), surface area (middle), and volume (lower) plotted as a function of diameter (horizontal axis of each), for populations of WT (blue data points), *rga4Δ* (green data points), and *rga2*Δ (red data points) dividing fission yeast cells. (See color plate)

Procedure:

1. Open MATLAB and start the script.
2. The software will open the first- and last-phase images of the corresponding time-lapse: crop a region of interest, in order to select a single growing spore.
3. The automatic tracking will start and progressively display each image of the time-lapse with a green outline of the spore contour, in order to visually check the detection accuracy.
4. As long movies are necessary in order to observe spore germination, background and contrast often change over time in phase images, leading to failure of automatic tracking. In this case, the best solution consists in setting a different threshold value in the edge-detection section for successive subsections of the time-lapse.
5. In addition, if automatic segmentation fails, the script allows selecting failed frames and for each of them, to manually draw the spore contour.

Output:

By integrating the automatic and manual detection in a single time-lapse analysis, the script will calculate a series of geometric parameters (e.g., long axis, local diameter along this axis, surface volume, aspect ratio…) for each spore over time and save these results in a MATLAB file that can be exported as an Excel table. Furthermore, the software will generate a movie of the phase-contrast time-lapse for the cropped spore, with a green outline corresponding to the detected contour (Figure 1(B)). This approach should be applicable to single growing cells that grow and change size or shapes.

1.2 LENGTH, DIAMETER, SURFACE, AND VOLUME OF DIVIDING CELLS

This subsection is dedicated to the precise measurement of cellular dimensions of dividing fission yeast cells. In order to precisely capture the contour of the cell, the plasma membrane should be detectable by fluorescence microscopy. This can be achieved either by using a GFP-tagged plasma membrane marker such as GFP-psy1 (Nakamura, Nakamura-Kubo, Hirata, & Shimoda, 2001) or by applying a fluorescent membrane staining such as $DiBAC_4(3)$, shortly before imaging. Dividing cells can be identified by the ingression of the membrane for cytokinesis (Figure 1(C)). Calcofluor, which stains the cell wall and has increased staining at the division septum may also be used, but could add imprecision in the timing of division as the septum may still be stained when cells have restarted growth. In addition, we note that Calcofluor, which outlines the contour of the cell wall, adds around 0.5 μm in the diameter and length of the cell.

Using this script, we analyzed cell size parameters at division for a number of fission yeast mutants. We measured WT cells, as well as *rga4Δ* and *rga2Δ* mutants, in order to evaluate the evolution of cell length, L_{div}, at division as a function of cell diameter, D (Figure 1(C) and (D)). This analysis revealed an allometric scaling between length and diameter at division, such that $L_{div} \sim 1/\sqrt{R}$. This scaling is

intermediate between previously proposed hypothesis of pure-length sensing for division onset (Martin & Berthelot-Grosjean, 2009; Moseley et al., 2009), and recently proposed surface sensing, $L_{div} \sim 1/R$ (Pan et al., 2014). The origin of this newly found scaling may serve as an interesting subject of further investigation.

Materials:

Glass slide; 22 × 22 mm^2 coverslip; Exponentially growing fission yeast culture; Spinning disk microscope with 100X objective; $DiBAC_4(3)$ dye (LifeTechnologies, Ref. B-438); EMM liquid media (minimal media); Computer equipped with MATLAB and image analysis toolbox (Mathworks); and dedicated script (available upon demand).

1.2.1 Cell preparation for imaging

1. If cells do not express a plasma membrane marker, stain with DiBAC4(3) at a final concentration of 100 μM (1/100 dilution from a stock solution in DMSO) for 10 min, then rinse 3x with EMM, and image immediately after rinsing.
2. Spin down 1 ml of cells and concentrate to 50 μl typically.
3. Place a 1.2−1.5 μl drop of cell suspension on the glass slide and gently cover with a 22 × 22 mm^2 coverslip. To ensure that cells are not flattened by the coverslip, adapt the volume of the drop and observe cells under the microscope; the ideal situation is to have a majority of immobile cells with a small percentage of cells that slowly jiggle around in the field.
4. Quickly go to the spinning disk microscope and take z-stacks of several fields extending 5−7 μm around the cell midsection using a distance between slices of 0.2 μm. The acquisition time of a single stack is ∼15−30 s. The pixel size should be as small as possible (In Figure 1(C), the pixel size is = 59.5 nm).

1.2.2 Image analysis

General principle of image analysis script:

The script used for this application follows similar concepts as previously discussed (Figure 1(A), Section 1.1.3) and allows to sequentially select and crop dividing cells, go through the z-stack to identify the midsection, find the top and bottom of the cell, segment either automatically or manually the cell contour, and output all relevant cellular parameters.

Procedure:

1. Open MATLAB and run the script for a given stack.
2. The script asks and inputs the magnification and z-step.
3. Crop the cell of interest out of the displayed image.
4. Click through the z-stack slices taking note of the slices containing the top and bottom of the cell (in which fluorescence begins to blur away) as well as the slice containing the most extended section of the cell (midplane).
5. Report top-, bottom-, and middle-section slice numbers.
6. Manually click to trace the contour of the cell using the segmented line or use the automatic detection. Use automatic detection when the cell contour is clearly

contrasted from the background and separated from other cells or artifacts in the field, otherwise use manual tracing. The script will display the overlay of the trace with the cell to control for proper segmentation.

7. The script will compute length, diameter, surface area, and volume from the contour shape.
8. Repeat steps 3–7 to measure all dividing cells in this image, then change file and continue analysis.

2. MICROCHANNEL ASSAY FOR CELL DIAMETER MANIPULATION

In this section, we describe a method based on microfabricated channels, which serve to confine and deform spores and let them germinate and grow into cells with a diameter imposed by the channel (Figure 2). Using this approach, we can generate cells with diameter down to 2–2.5 μm. Controls with large and high channels, which largely exceed the cell diameter are used to discriminate putative effects of growing spores/cells in PDMS channels from effects of cell geometry. Although the channels have a defined width and height, cells do deform channels, or may sometimes be slightly tilted in z with respect to the channel wall (for instance, when contacting another cell). We thus couple this method with the size measurement script developed in Section 1.2.2. This method may have applications in dissecting mechanisms of polarity, growth, or morphogenesis. In here, we demonstrate its strength by bringing the abnormally large diameter of *rga4* mutants (4–6 μm) to values similar to WT (3–4 μm). These "thinner" *rga4* mutant cells do not divide anymore at a short length but at a very similar length than WT cells (Figure 2(C) and (D)), and fall within the allometric scaling mentioned before (Section 1.2). This suggests that defects in length at division in this mutant are directly associated with defects in diameter.

2.1 FABRICATING MICROCHANNELS TO MANIPULATE CELL DIAMETER

This section describes the methods used to fabricate PDMS microchannels. The design of the channels was adapted from previous work using microchannels to elongate fission yeast cells round mutants (Terenna et al., 2008) and for studies of cell migration (Faure-Andre et al., 2008; Heuze, Collin, Terriac, Lennon-Dumenil, & Piel, 2011). The fabrication procedure follows two steps: Soft-lithography, PDMS molding and chamber preparation. In what follows, we describe detailed material and procedure for each of these steps.

Materials:

Computer with drawing software; 4-inch-diameter Silicon wafer (University wafers in US and Neyco in France, 4″ N(111) SSP Test Grade Quality); 6 cm-diameter petri dish; SU8-2005 resist and developer (MicroChem); Acetone and Isopropanol; Access to clean room facility (with spin coater, hot plates, and UV lamp); Sylgard 184 base and

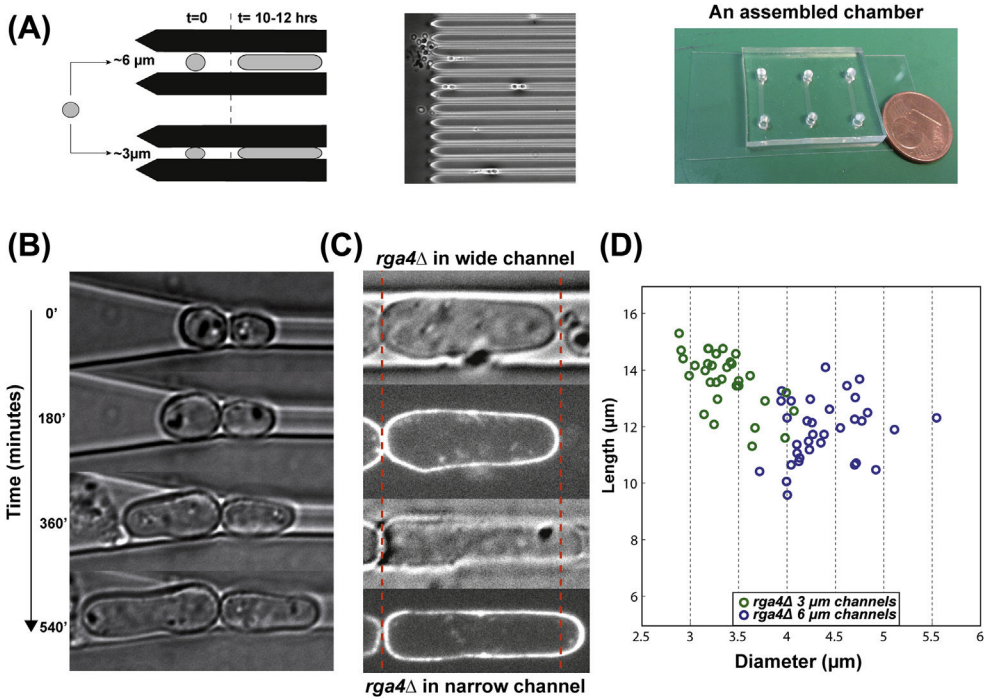

FIGURE 2 Diameter manipulation of fission yeast cells in microchannels.

(A) Left: Scheme representing the installation and elongation of spores inside channels with confining (3 μm) and nonconfining (6 μm) diameters. Spores grown in confining diameters will assume a smaller cell diameter compared to control cells. Middle: Large-view phase-contrast image of spores installed in microchannels. Right: An assembled PDMS chamber containing three channel domains. (B) Time-lapse of spores developing at the channel entry. The right cell is growing into the microchannel and adopts a small diameter, while the left cell is growing out. (C) Bright field and florescence images of dividing *rga4*Δ GFP-psy1 fission yeast cells, in a wide channel (upper pair) and in a narrow channel (lower pair). Extension of length in both conditions is highlighted with red dotted lines. (D) Single *rga4*Δ cell length at division plotted as a function of cell diameter in wide (6 μm) channels (blue data points (gray in print versions)) and narrow (3 μm) channels (green data points (black in print versions)).

curing agent (Fisher, NC9644388); plastic cups; plastic stirring rod; timer; scale; vacuum desiccator; 65 °C oven; Tridecafluoro-(1,1,2,2-Tetrahydrooctyl)-1-trichlorosilane (United Chemical Technologies, Ref. T2492); a scalpel, 2 mm hole-punch screwdriver; tweezers; 24 * 50 mm^2 cover glass; DI Water; Dry air; Plasma Cleaner (Harrick Plasma).

2.1.1 Photomask design

The design of patterns is done on a computer-assisted drawing program (CAD). Available programs include AutoCAD (free for students) and QCAD (freeware). The design includes a long-rectangular region containing the channels, joining two large regions (for entry and exit of spores). The large regions are covered with equally spaced posts (of typically 20 μm in diameter and spaced apart by 20 μm). We recommend to design sets of channels with a range of width (from 2 to 7 μm typically). For these ranges of size, these designs are printed on 5″ quartz mask with a resolution below 0.5 μm (which can be ordered from specialized company, such as Toppan Photomasks).

2.1.2 Photolithography

Channels are made from PDMS using a positive master composed of SU8. Masters are prepared using standard lithography methods for SU8 microfabrication (Weibel, Diluzio, & Whitesides, 2007). A positive master is a hardened structure of SU8 such that the desired geometric shapes extend as posts from a silicon wafer. SU8 is an epoxy-based negative photoresist: when it is exposed to UV light it becomes insoluble to the photoresist developer, while the unexposed portion of the photoresist is dissolved by the developer.

Procedure:

1. Clean the silicon wafer with dry air and bake at 150 °C for 5 min on hot plate.
2. Put SU8 onto the wafer by using a transfer pipette (approximately 1 ml for each square inch) and spin it. Rotation speeds depend on the type of SU8 used as well as desired thickness of the coating. To obtain 5 μm high features, the basic procedure involves an SU8-2005 and a first spin of 20 s at 500 rpm, with an acceleration of 500 rpm/s and a subsequent spin of 45 s at 3000 rpm with the same acceleration. Note that we adapt the height in order to generate channels with squared section.
3. Bake the resist on a hot plate for about 1 min at 65 °C and 1 min at 95 °C.
4. Create patterns on the SU8 by covering the wafer with the quartz mask using a dedicated UV insulator (or mask aligner). It is important to ensure that the mask remains well plastered onto the SU8 layer (this can be achieved by placing a weight on top of the mask). The optimal time of exposure will depend on wavelength and intensity of the light and has to be adapted. A too short exposure will make features that do not stick well to the substrate and detach, while a too long exposure will generate features with poor spatial definition.
5. The sample is then baked again for 1 min at 65 °C and 1 min at 95 °C, immersed in a glass dish containing developer for 2 min, and transferred to another glass dish containing clean developer for 30 s. The wafer is then rinsed with isopropyl

alcohol and dried on the spin coater (1 min at 1000 rpm). A final bake at 150 °C for 10 min is then performed on the hot plate.

6. The master is then observed on a bright-field reflected light microscope to check the shape and size of SU8 channels.
7. An overnight exposure of the master with vapors of silane is then performed to prevent the PDMS from sticking too much to the SU8 (see hereafter). This is done by placing the SU8 masters together with a small flask containing 200 µl of silane in a vacuum desiccator, overnight.
8. Master wafers can be stored in large petri dishes for long time periods and be used repeatedly to produce PDMS structures, for periods up to several years if handled with care (see Section 2.1.3).

2.1.3 Creating PDMS from master

PDMS chambers can be replicated many times from a positive SU8 master.

1. Mix over 50 g of PDMS base and curing agent in a ratio of 5:1. Mix vigorously with a transfer pipette or a plastic rod.
2. Degas mixture by placing into a vacuum desiccator. Apply vacuum until bubbles disappear.
3. Apply a fraction of the PDMS slowly onto the wafer. Once the wafer is coated completely by a few millimeters of PDMS, let it settle onto the wafer for 10 min. Bake at 65 °C for at least 4 h. Note that baking temperature and time will change the rigidity of the PDMS.
4. Cut the PDMS off the masters with a blade and carefully peel it off the master using tweezers. Place the PDMS with the channels facing up in a petri dish. The PDMS slab can be stored for long periods of time.

2.1.4 Assembling the micro channels

The PDMS slab is then pierced and sealed with a coverslip to assemble closed channels in which to manipulate and grow cells.

Procedure:

1. Just before use, pierce holes in the PDMS slab within the square regions at the two channel ends using the hole-punch screwdriver.
2. Cut the PMDS slab around the structure just enough to fit it onto the 24 * 50 mm^2 surface of the coverslip, leaving sufficient edges for adhesion.
3. Clean a 24 * 50 mm^2 coverslip with Acetone, Isopropanol, and DI water and dry with pressurized air.
4. Activate the PDMS channels facing up and the coverslip with a plasma cleaner, for ∼1 min. Place the PDMS channels facing down on top of the coverslip. Check for adhesion by softly pulling on the PDMS. If the PDMS moves, softly press on the PDMS (sparing the channels) to initiate adhesion. Bake the channel at 65 °C for 1−2 h. Once assembled, the chamber can be stored in a clean petri dish for a couple of days before use (Figure 2(A) right).

2.2 CELL DIAMETER MANIPULATION AND IMAGING

This section describes the diameter manipulation of fission yeast cells. This aim is achieved by growing spores inside PDMS channels with confining sections. The method is composed of several steps: sporulation, installation of the spores inside the channels, germination, elongation, division within the channels, and imaging of the manipulated cells. In the following sections, we describe materials and procedures for each of these steps.

Materials:

Resuspended spores (see Section 1.1.1), assembled microchannels (see Section 2.1.4), 10 ml syringe, YE5S media, petri dish, Gel-loading pipette tips, Spinning disk microscope with 100X objective, Computer equipped with MATLAB and image analysis toolbox (Mathworks), and dedicated script (available upon demand).

Procedure:

1. Place 20−50 μl of the YE5S suspended spores inside the channels entry hole (the pierced square region closest to the channels). Use a relatively diluted suspension.
2. In order to widen the syringe exit, assemble a clipped pipette tip onto the needle adapter. Withdraw air into the syringe, hold it vertically on top of the channel entrance, and push the plunger to inflate air and push spores into the channels. Take care (1) not to apply a strong manual pressure directly on top of the channels as they might collapse and (2) to push moderately in order to avoid air penetration into the channels.
3. Mount the chamber on an inverted microscope and check for the presence of spores inside the channels. An optimal installation will have one to two spores in some channels (Figure 2(A) middle). If needed repeat step 2 until achieving a successful installation.
4. Empty entry holes in order to remove excess spores that did not enter the channels and fill them again with fresh YE5S media. Note that this aspiration will note cause spores, which are stuck in channels to move out.
5. Place the chamber in a large petri dish, surrounded by wet kimwipes on the sides, and close the lid of the petri dish.
6. Incubate the petri dish over night at 18 °C. In the morning, most of the spores should be finishing their first cell cycle (Figure 2(B)).
7. Refresh YE5S media in the entry and place the chambers at 25 °C for another 2−3 h.
8. Mount the chamber on a Spinning disk inverted microscope with a 100X objective. Take pictures of dividing cells in channels. Ideally, several chambers in parallel should be prepared (some large channels for controls, and some thin ones) and cells should be imaged every other ∼30 min to capture many cell division events.
9. Follow similar imaging procedure as in Section 1.2.1.
10. Analyze images using the same script as in Section 1.2.2. The script has built-in analysis for situations when the cell have ellipsoidal cross section (for instance, if the channel height is smaller than the width).

CONCLUSIONS

The methods that are described here provide novel material available to the community for the study of cell size-related questions in fission yeast. The imaging method for the measurement of cell dimensions is likely to be adaptable to many situations and to different kinds of tip-growing cells (fungi, bacteria). Microchannels are sizable down to fractions of a micrometer, and could even be fabricated in glass using other methods, to deform much smaller cells such as bacteria (Männik, Driessen, Galajda, Keymer, & Dekker, 2009). Microchambers to control cell diameter may help to decipher which size parameters cells measure for G2/M, and to isolate novel mutants defective in this process.

ACKNOWLEDGMENTS

We thank Rima Seddiki, Emmanuel Terriac, Matthieu Piel, and Anne Paoletti, and members of the Minc Laboratory for their technical help and discussions. Our laboratory is supported by the CNRS, and grants from the ANR (10PDOC00301), the FRM (AJE20130426890), the FP7 CIG program, and ITN "FungiBrain" and the "Mairie de Paris emergence" program.

REFERENCES

Bahler, J., & Pringle, J. R. (1998). Pom1p, a fission yeast protein kinase that provides positional information for both polarized growth and cytokinesis. *Genes & Development, 12*(9), 1356–1370.

Bonazzi, D., Julien, J. D., Romao, M., Seddiki, R., Piel, M., Boudaoud, A., et al. (2014). Symmetry breaking in spore germination relies on an interplay between polar cap stability and spore wall mechanics. *Developmental Cell, 28*(5), 534–546.

Das, M., Wiley, D. J., Medina, S., Vincent, H. A., Larrea, M., Oriolo, A., et al. (2007). Regulation of cell diameter, For3p localization, and cell symmetry by fission yeast Rho-GAP Rga4p. *Molecular Biology of the Cell, 18*(6), 2090–2101.

Faure-Andre, G., Vargas, P., Yuseff, M. I., Heuze, M., Diaz, J., Lankar, D., et al. (2008). Regulation of dendritic cell migration by CD74, the MHC class II-associated invariant chain. *Science, 322*(5908), 1705–1710.

Heuze, M. L., Collin, O., Terriac, E., Lennon-Dumenil, A. M., & Piel, M. (2011). Cell migration in confinement: a micro-channel-based assay. *Methods in Molecular Biology, 769*, 415–434.

Lloyd, A. C. (2013). The regulation of cell size. *Cell, 154*(6), 1194–1205.

Männik, J., Driessen, R., Galajda, P., Keymer, J. E., & Dekker, C. (2009). Bacterial growth and motility in sub-micron constrictions. *Proceedings of the National Academy of Sciences of the United States of America, 106*(35), 14861–14866.

Marshall, W. F., Young, K. D., Swaffer, M., Wood, E., Nurse, P., Kimura, A., et al. (2012). What determines cell size? *BMC Biology, 10*, 101.

Martin, S. G. (2009). Geometric control of the cell cycle. *Cell Cycle, 8*(22), 3643–3647.

Martin, S. G., & Berthelot-Grosjean, M. (2009). Polar gradients of the DYRK-family kinase Pom1 couple cell length with the cell cycle. *Nature, 459*(7248), 852–856.

Mitchison, J. M., & Nurse, P. (1985). Growth in cell length in the fission yeast *Schizosaccharomyces pombe*. *Journal of Cell Science, 75*, 357–376.

Moseley, J. B., Mayeux, A., Paoletti, A., & Nurse, P. (2009). A spatial gradient coordinates cell size and mitotic entry in fission yeast. *Nature, 459*(7248), 857–860.

Moseley, J. B., & Nurse, P. (2010). Cell division intersects with cell geometry. *Cell, 142*(2), 184–188.

Nakamura, T., Nakamura-Kubo, M., Hirata, A., & Shimoda, C. (2001). The Schizosaccharomyces pombe spo3^{+} gene is required for assembly of the forespore membrane and genetically interacts with psy1(+)-encoding syntaxin-like protein. *Molecular Biology of the Cell, 12*(12), 3955–3972.

Nurse, P., Thuriaux, P., & Nasmyth, K. (1976). Genetic control of the cell division cycle in the fission yeast *Schizosaccharomyces pombe*. *Molecular and General Genetics, 146*(2), 167–178.

Pan, K. Z., Saunders, T. E., Flor-Parra, I., Howard, M., & Chang, F. (2014). Cortical regulation of cell size by a sizer cdr2p. *Elife, 3*, e02040.

Tatebe, H., Nakano, K., Maximo, R., & Shiozaki, K. (2008). Pom1 DYRK regulates localization of the Rga4 GAP to ensure bipolar activation of Cdc42 in fission yeast. *Current Biology, 18*(5), 322–330.

Terenna, C. R., Makushok, T., Velve-Casquillas, G., Baigl, D., Chen, Y., Bornens, M., et al. (2008). Physical mechanisms redirecting cell polarity and cell shape in fission yeast. *Current Biology, 18*(22), 1748–1753.

Turner, J. J., Ewald, J. C., & Skotheim, J. M. (2012). Cell size control in yeast. *Current Biology, 22*(9), R350–R359.

Villar-Tajadura, M. A., Coll, P. M., Madrid, M., Cansado, J., Santos, B., & Perez, P. (2008). Rga2 is a Rho2 GAP that regulates morphogenesis and cell integrity in *S. pombe*. *Molecular Microbiology, 70*(4), 867–881.

Weibel, D. B., Diluzio, W. R., & Whitesides, G. M. (2007). Microfabrication meets microbiology. *Nature Reviews Microbiology, 5*(3), 209–218.

Dissecting the Molecular Mechanisms of Electrotactic Effects

Daria Bonazzi[1,†] and Nicolas Minc[1,†,*]

[1]Subcellular Structure and Cellular Dynamics Research Group (UMR 144 CNRS/IC), Institut Curie, Paris, France.
[†]Present address: Institut Jacques Monod (UMR 7592 CNRS), University Paris Diderot, Paris, France.

Significance: Steady electric fields (EFs) surround cells and tissues *in vivo* and may regulate cellular behavior during development, wound healing, or tissue regeneration. Application of exogenous EFs of similar magnitude as those found *in vivo* can direct migration, growth, and division in most cell types, ranging from bacteria to mammalian cells. These EF effects have therapeutic potential, for instance, in accelerating wound healing or improving nerve repair. EFs are thought to signal through the plasma membrane to locally activate or recruit components of the cytoskeleton and the polarity machinery. How EFs might function to steer polarity is, however, poorly understood at a molecular level.

Recent Advances: Here, we review recent work introducing genetically tractable systems, such as yeast and *Dictyostelium* cells, that begin to identify proteins and pathways involved in this response both at the level of ion transport at the membrane and at the level of cytoskeleton regulation.

Critical Issues: These studies highlight the complexity of these EF effects and bring important novel views on core polarity regulation.

Future Directions: Future work pursuing initial screening in model organisms should generate broad mechanistic understanding of electrotactic effects.

Nicolas Minc, PhD

Submitted for publication February 3, 2013. Accepted in revised form April 7, 2013.

*Correspondence: Institut Curie, UMR 144 CNRS/IC, 26 rue d'Ulm, 75248 Paris Cedex 05, France (e-mail: minc.nicolas@ijm.univ-paris-diderot.fr).

Abbreviations and Acronyms

cAMP = cyclic adenosine monophosphate
cGMP = cyclic guanosine monophosphate
EF = electric field
GCA = guanilyl cyclase A
GTPase = guanosine triphosphate hydrolase enzyme
PI3K = phosphatidylinositide 3-kinases
PIP = phosphatidylinositol-phosphate
PIP2 = phosphatidylinositol bisphosphate
PMv = transmembrane potential value
PTEN = phosphatase and tensin homolog
sGC = soluble guanilyl cyclase
WT = wild-type

SCOPE AND SIGNIFICANCE

This review will provide an overview of the recent advances made in understanding the molecular mechanisms of galvanotactic effects, which is the process by which cells sense and utilize small electric fields (EFs) to orient polarity, migration, or division. These effects have long been known to influence many physiological processes, including development and wound healing, and the discovery of gene products regulating these effects promises to open new avenues for medical applications in these contexts.

TRANSLATIONAL RELEVANCE

The study and molecular understanding of EF effects on cell polarity will aid in understanding many medically relevant *in vivo* tissue behaviors. The most important one is wound healing, which is known to be influenced by endogenous EFs *in vivo*. Other *in vivo* relevance also includes nerve regeneration and metastasis.

CLINICAL RELEVANCE

The discovery of genes and proteins regulating electrotaxis will likely provide the driving knowledge to design chemical enhancers of

DOI: 10.1089/wound.2013.0438

wound healing *in vivo*. Additionally, the control over cellular behavior provided by exogenous EFs may serve as a potent tool to drive repair- or target-specific cells to sites of infections.

BACKGROUND

Cell polarization describes the ability of a cell to use external and/or internal stimuli to decide in which direction to grow, migrate, or divide. It is a prerequisite for the development of a multicellular organism and is involved in numerous biological processes such as tissue repair, cancer metastasis, or cell–cell communication.[1] Cell polarity is usually regulated by internal polarity effectors that promote the assembly of actin and microtubule cytoskeleton, which trigger cell movement and shape changes.[2] Conserved polarity hubs include the one regulating the small guanosine triphosphate hydrolase enzyme (GTPase) cdc42p, or the one controlling the phosphorylation state of phosphatidylinositol lipids (phosphatidylinositol-phosphate [PIP]).[3,4] In tissues, these internal polarity modules are usually biased and oriented by external cues, such as chemical gradients, mechanical signals, and electrical signals, which allow cells to organize spatially at the tissue level. Although the effects of extracellular cues on single-cell or tissue polarity have been described in many contexts, the molecular details of the cross-talk between external and internal cues remain unclear in most cases. Here, we review the molecular mechanisms underlying this cross-talk in the context of electrical signals.

Cells and tissues in our body are surrounded by organized electrical currents and ion flux, yet the role of such electrochemical signals in organizing cellular behavior remains poorly appreciated. Steady electrical currents and fields have been measured across epithelial layers and proposed to guide cellular behavior in wound healing, development, and metastasis.[5–9] Even single cells may organize ion flux and electrical currents in large polarized single cells, such as developing eggs or pollen tubes; organized ionic currents around the cell have been measured and are implicated in helping to establish a global order to maintain polarized growth.[10–13]

It has been observed for decades that the exogenous application of an EF on the same order of magnitude as those measured *in vivo* (ranging typically from 0.1 to 10 V/cm) can direct cell polarity, migration, and division in many different cell types ranging from bacteria and fungi to neurons and neutrophils.[9,14–17] This near-universal process is known as galvanotaxis when the cell migrates directionally in the EF, and galvanotropism when the cell reorients its growth axis with respect to the EF. EF effects may have important therapeutic and diagnostic values, for instance, in nerve repair, wound healing, or to control the orientation of cells within tissues. For instance, it has been widely appreciated that EFs may serve as prime directional cues to direct cell migration and division during wound healing, and that their manipulation affects wound closure *in vivo*.[18] Although these effects have long been described and investigated, both molecular and biophysical mechanisms remain elusive. A deep understanding of these EF-sensing mechanisms should enable clinicians and engineers to develop new therapeutic methods for improving wound-healing treatment.

In this article, we review recent advances in the dissection of the molecular mechanisms underlying EF effects on cell polarity, with a particular emphasis on the introduction of genetically tractable organisms and quantitative approaches, which begin to bring understanding of these effects.

DISCUSSION OF FINDINGS AND RELEVANT LITERATURE

Cathode, anode, or perpendicular: which way to polarize in an EF?

Whereas most cell types respond to EFs by reorienting their internal polarity to guide migration, growth, or division, a puzzling result obtained over the years is that different cell types respond by orienting to different directions (Fig. 1A). Most migrating cells, including epithelial cells, fibroblasts, or neutrophils, respond to EFs by migrating to the cathode of the EF (negative electrode).[18] In contrast, breast cancer cells and some endothelial cells migrate to the opposite direction, which is toward the anode of the field.[19–22] Some cells also display additional atypical shape changes that accompany the directional migration phenotype. Mouse fibroblasts depict, for instance, a striking shape elongation perpendicular to the EF and start migrating to the cathode of the EF.[23]

EFs may also orient cellular growth in a nonmotile walled cell that displays polarized growth, such as rod-shape bacteria, filamentous fungi, and the rod-shape fission yeast.[16,24,25] In this situation, the cells reorient their growth axis by bending or branching with respect to the EF direction (Fig. 1C). There again, different cell types appear to reorient differently. Most bacteria grow and bend toward the anode, while some fungi such as *Candida*

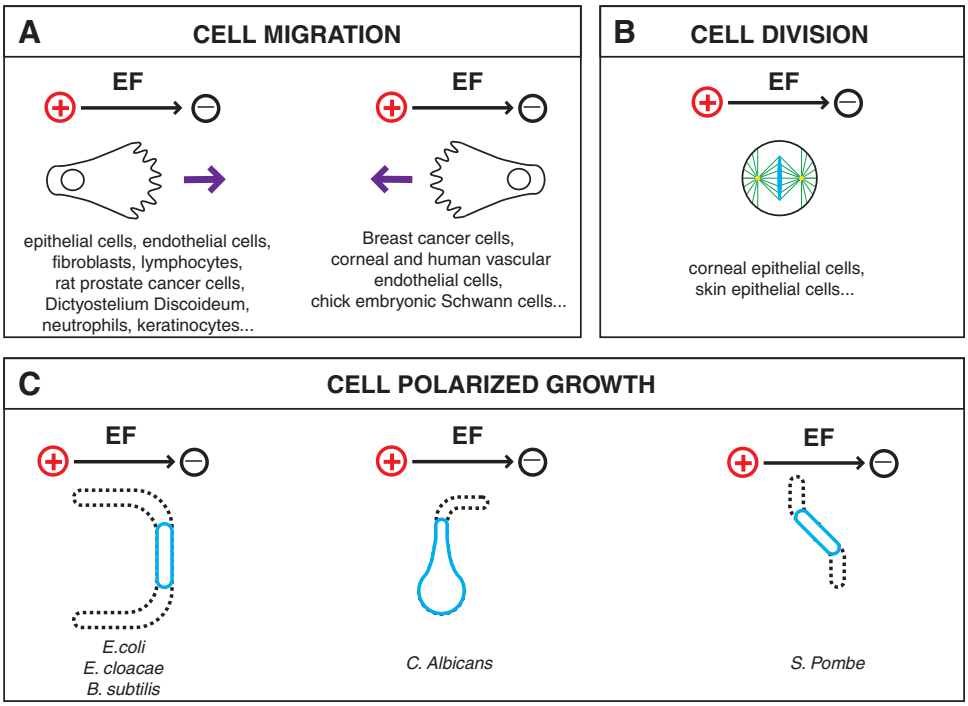

Figure 1. Polarity reorientation of different cell types to exogenous EF. **(A)** Different cell types that show directional migration to the cathode or anode of the EF. **(B)** Cells that depict a perpendicular orientation of the metaphase plate with respect to the EF during division. **(C)** Different cell types that orient their growth axis toward the anode (*left*), the cathode (*center*), or perpendicular to the EF (*right*). EF, electric field. To see this illustration in color, the reader is referred to the web version of this article at www.liebertpub.com/wound

albicans elongate its hyphal tip toward the cathode. Other mycelia fungi and the fission yeast *Schizosaccharomyces pombe*, reorient their polarity and grow perpendicular to the EF.[25,26]

These different orientations, as well as the multiple effects caused by the EF on certain cells, highlight the complexity of these responses and reveal the putative existence of dominant modes that may have a prevalence to steer cells to the cathode versus anode versus perpendicular.

The biophysics of galvanotactic effects

To dig into the understanding of galvanotactic effects, one needs to start asking questions on the biophysical effects that EFs may cause to cells. One well-accepted view is that EFs signal at or through the plasma membrane of cells, which serves as an electrical insulator. In other words, the cell response to EFs is not caused by the movement or direct rearrangement of certain proteins or organelles inside the cytoplasm. Rather, this response may involve a complex signal transduction, which eventually leads to the reorganization of the cytoskeleton and polarity machinery with respect to the EF direction (Fig. 2).

Several biophysical mechanisms for EF effects have been proposed throughout the years and are supported by experimental evidence (Fig. 3). A prevalent model is that the EF causes local inhomogeneity in transmembrane potential values (PMv) around the cell: the cathode-facing side would be depolarized (reduced PMv) and the anode-facing side would be hyperpolarized (increased PMv), while the parts of the cell facing the

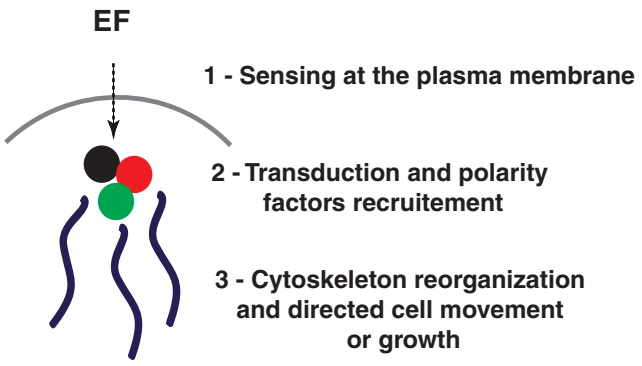

Figure 2. Schematic representation of how EFs may signal to reorganize cell polarity and the cytoskeleton. The EF signal is transduced at or through the plasma membrane, which acts as an electrical insulator. This initial effect may trigger a complex signaling cascade, which eventually leads to the reorganization of the cytoskeleton and polarity machinery with respect to the EF direction. To see this illustration in color, the reader is referred to the web version of this article at www.liebertpub.com/wound

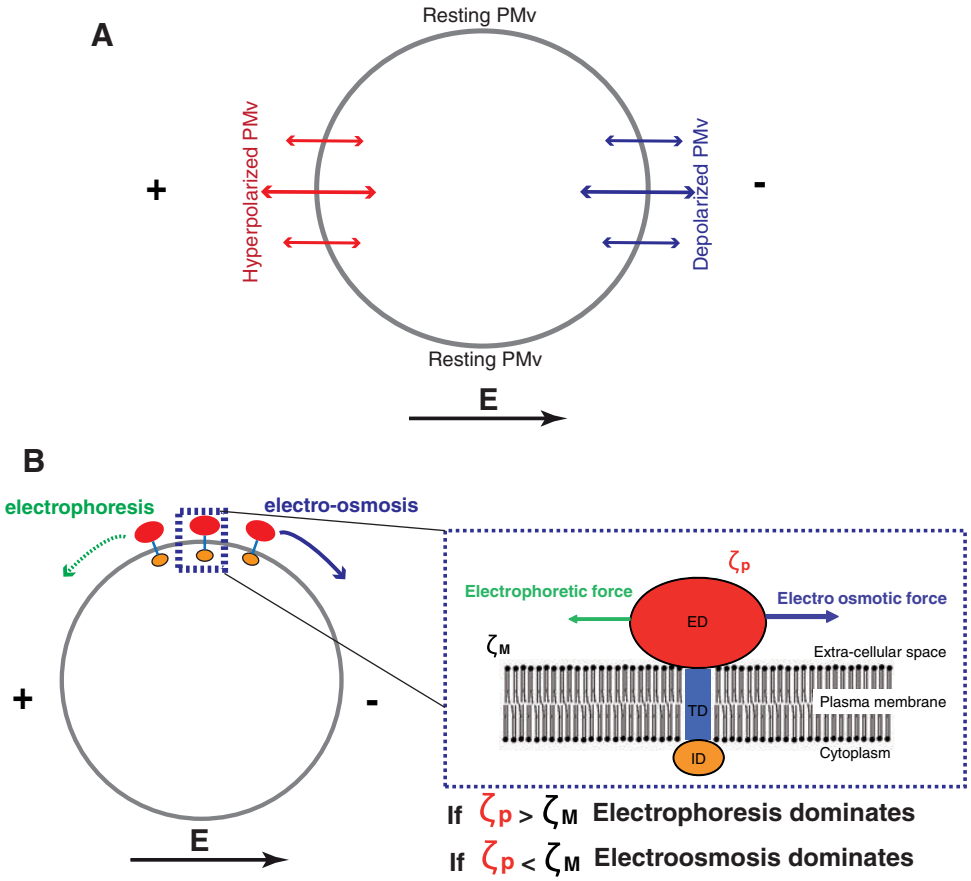

Figure 3. Biophysics of galvanotactic effects. **(A)** EF can cause local inhomogeneity in PMv around the cell, leading to depolarization (reduced PMv) at the cathode-facing side and hyperpolarization (increased PMv) of the anode-facing side. **(B)** EF can cause movements of membrane proteins along the plasma membrane through electrophoresis or electro-osmosis of membrane proteins with a charged extracellular domain. This effect involves competitive forces on the extracellular domain of membrane proteins, and the dominance of steering electrophorectic versus electro-osmotic forces may depend on the surface charge of the domain. PMv, transmembrane potential value. To see this illustration in color, the reader is referred to the web version of this article at www.liebertpub.com/wound

perpendicular axis would stay at their resting PMv (Fig. 3). These changes in PMv may yield local imbalances in ion fluxes, or turn on or off voltage-gated channels, or have other yet uncharacterized effects that would initiate a signaling cascade recruiting polarity component. Quantitatively, the extra-transmembrane potential caused by the EF scales with the intensity of the EF multiplied by the typical size of the cell, and thus, if this effect is dominant in EF experiments, larger cells are expected to respond at smaller EFs, which is most likely true from inspecting values in the literature.[6] These effects on PMv have been directly highlighted using membrane potential dyes[27] and genetically encoded proteins.[28] Best supports for the role of PMv in EF responses come from experiments in which PMv is altered, from changing specific ion concentrations (H^+ or K^+) in or out the cell, or genetically inhibiting membrane potential regulators.[14,25,29]

A second important view is that the EF may cause movements of membrane proteins, along the plasma membrane. These movements may result from the electrophoresis or electro-osmosis of membrane proteins, which have charged extracellular domains protruding the plasma membrane. If the Zeta potential (effective surface charge) of the extracellular domain of the protein is more negative than the local Zeta potential of the surrounding membrane, then the prediction is that the protein should move toward the anode; in the opposite case, the protein will be moved by electro-osmosis toward the cathode. Several models coupled with experimental data depicting movements of different membrane proteins, provide support for this view,[30–32] although very little functional data linking protein movement and polarity reorientation have been reported so far. It is plausible that in any given cell type, some extracellular domains of some proteins may display enough

surface charge to yield movements, but the question is whether these movements really drive polarity downstream. Modeling considerations provide arguments for how this effect would depend on cell size, protein charge, and diffusion constant in the membrane.[31] Trafficking and recycling of these membrane proteins is also likely to bias these modeling predictions, and should be taken into account in future extensions of these models.

How might cells sense and transduce EF?

The hidden side of galvanotactic effects is found in the molecular machinery transducing an EF into a defined internal cell polarity. Until recently, there has not been a complete picture in a single cell type that provides a pathway linking biophysical effects of EFs at the membrane down to cytoskeletal organization. In Table 1, we summarize some of the most important proteins or types of proteins that have been suggested to sense and transduce EF effects and be involved in reorganizing polarity in response.[9,14,21,25,33–38]

Connections between EF effects and downstream cytoskeletal regulators, including the small GTPase cdc42p, the Rho/Rac pathways, integrin signaling, and phosphatidylinositol (PIP) signaling, have been suggested in different cellular systems.[9,25,33–35] A pioneering work, performed in the context of mammalian wound healing, showed that neutrophils and keratinocytes wound-directed migration depended on phosphatidylinositide 3-kinases (PI3K) and on the phosphatase tensin homolog (PTEN) which, respectively, positively and negatively regulate phosphatidylinositol bisphosphate (PIP2) homeostasis.[9,39] Wound-healing relies, in part, on endogenous EFs in the wound, and can be inhibited or accelerated by exogenous application of EFs pointing toward or away from the wound, respectively.[9] In this electrotactic assay, exogenous EFs induce the activation of signaling kinases, including ERK, p38, Src, and Akt. In mouse models lacking the catalytic γ-subunit of PI3K, neutrophils and keratinocytes displayed reduced activation of these kinases, reduced electrotactic migration, and defective wound closure. Conversely, PTEN deletion enhanced EF-induced Akt and Src phosphorylation and directional migration, and accelerated wound healing. Thus, PIP signaling regulates electrotactic migration of cells in the wounded tissue and supports proper healing.[18] It is interesting to note that PIP signaling also regulates chemotaxis in neutrophils.[40] The downstream machinery required for directional migration is thus likely to be similar regardless of the nature of the spatial cue in this situation.

The amoebae *Dictyostelium discoideum* has long served as a genetic model to dissect molecular mechanisms of directional cell migration and chemotaxis.[41,42] When exposed to homogeneous concentrations of cyclic adenosine monophosphate and small EFs, these cells depict striking galvanotaxis, orienting their migration to the cathode of the EF within minutes.[37] This EF response is independent of chemotactic receptors.[43] Downstream signaling modules regulating directional cell migration during chemotaxis include PIP and cyclic guanosine monophosphate (cGMP) signaling. These effectors promote actin polymerization at the leading edge for directed migration.[44,45] In a recent work, Sato *et al.* tested the role of these signaling modules in galvanotaxis.[35] Intracellular cGMP is produced mainly by two enzymes, soluble guanilyl cyclase (sGC) and guanilyl cyclase A (GCA). Mutants lacking the sGC and GCA (gca^-/sgc^-) and mutants lacking the cGMP-binding protein C ($gbpC^-$), which display reduced levels of cGMP, exhibited attenuated cathodal electrotactic migration. Similar phenotypes were obtained when PIP signaling was repressed through PI3-kinase inhibition (Fig. 4). Strikingly, when both PIP2 synthesis and cGMP pathways were knocked down, cells migrated to the opposite direction, to the anode of the EF. These results suggest the existence of parallel pathways participating in regulating electrotaxis and point to the existence of a third pathway promoting anodal migration.[35] These studies support the role of PIP signaling for electrotaxis in another cell type, and provide detailed genetic characterization of the molecular mechanisms involved. Cross-talk between EFs and polarity in these systems have been proposed to be mediated by calcium transport and membrane potential,[23,36,37,46] yet the details of this transduction remain to be studied.

Fungal cells and yeasts are model systems to dissect molecular mechanisms of cell polarity. These nonmigrating cells exhibit polarized growth,

Table 1. *Examples of gene products and putative pathways identified in electric field reponses in different cells*

Cell Type	*Sensing at the Membrane*	*Sensing in the Cytosol*	*References*
Xenopus neuron growth cones	Unknown	Cdc42/Rho/Rac	34,36
Keratinocytes	Integrin	Rac/cAMP	21,33
Dictyostelium discoideum	NHE2/Ca2+	PI3K/PTEN/cGMP	9,35,37
Candida albicans	Cch1	Rsr1/cdc42	14,38
Fission yeast	Pma1	Cdc42/for3	25

cAMP, cyclic adenosine monophosphate; cGMP, cyclic guanosine monophosphate; PI3K, phosphatidylinositide 3-kinases; PTEN, phosphatase and tensin homolog.

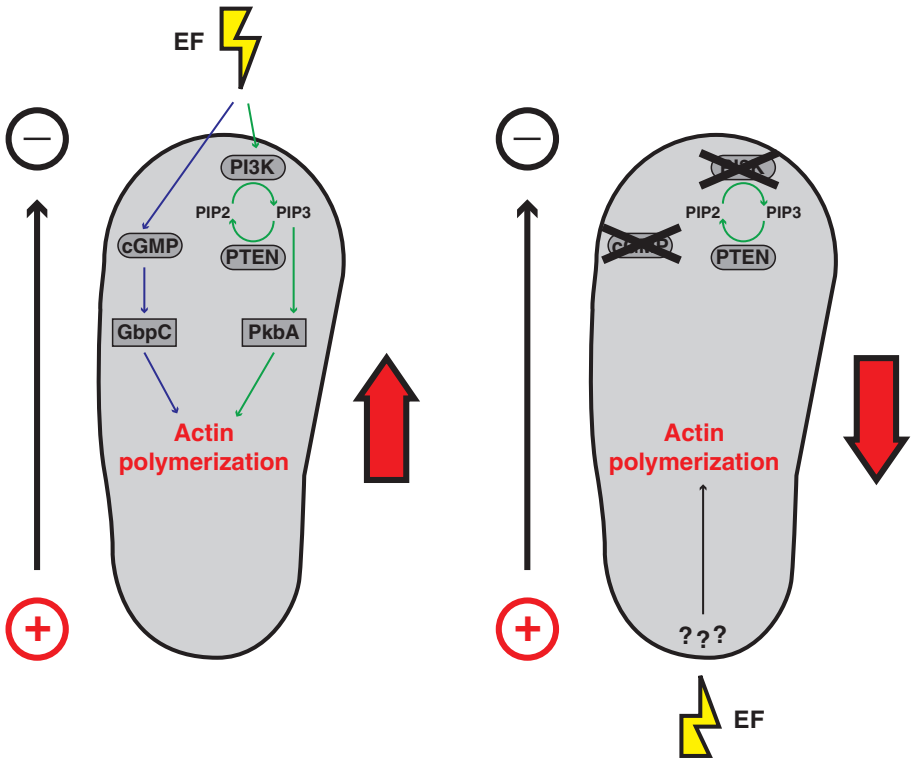

Figure 4. Molecular mechanisms regulating *Dictyostelium discoideum* galvanotaxis. WT cells migrate to the cathode of an applied EF. This polarized migration involves at least two different pathways: The PI3 kinase/PTEN pathway that lead to a polarized distribution of PIP (green arrows); and the cGMP pathway (purple arrows). Mutant cells deficient in the PI3K and cGMP pathway migrate to the anode, suggesting the existence of a third pathway for EF sensing and directional migration. cGMP, cyclic guanosine monophosphate; PI3K, phosphatidylinositide 3-kinases; PIP, phosphatidylinositol-phosphate; PTEN, phosphatase and tensin homolog; WT, wild-type. To see this illustration in color, the reader is referred to the web version of this article at www.liebertpub.com/wound

which involves similar regulatory modules and conserved effectors as many higher eukaryotes.[47] They usually possess a self-sustained internal polarity, which allows them to grow in a highly polarized manner even in the absence of external guiding cues. This polarity machinery may be biased and redirected by chemical gradients, for instance, during mating, or by mechanical signals in processes such as thigmotropism that may have relevance to infection in some hyphal species.[14,38] Fungi and yeast also depict strong galvanotropism.[25,26,48] The physiological relevance of the EF response in fungi is not well-established, but EFs are most likely present in the natural fungal habitat, such as on the surface of plants or in humid soils. Some fungi and molds have further been suggested to target wounds by following ion currents and EFs, and thus, the EF response could also have relevance in infection.[49] Ion transporters and membrane potential regulators are widely shared between fungi and higher organisms, and thus, fungal and yeast cells will likely serve as excellent prototype genetic systems to dissect molecular mechanisms of the EF response at different levels.

One such example can be highlighted from work on the pathogenic fungi *C. albicans*. This single-celled organism grows by budding and switches to highly polarized hyphal growth in certain conditions. EFs can direct both the site of bud emergence and the hyphal polarized growth toward the cathode.[24] Using forward genetic and chemical inhibitors, Brand *et al.* recently demonstrated that the galvanotactic response of *C. albicans* involved the conserved calcium transporter CaCch1p.[14] This voltage-gated calcium channel shares high homology with mammalian homologues and with many other eukaryotes, and may serve to transduce membrane potential changes into calcium transport. Further work should reveal whether its function in EF sensing is conserved in other species. Other work from the same group further implicates the role of the Ras-like GTPase Rsr1 that serves as an internal landmark regulating Cdc42 activation in *C. albicans*.[38] This set of studies begins to identify important regulatory nodes at the membrane and in the cytoplasm, and further work should reveal how these different modules are connected to drive galvanotropism.

The fission yeast *S. pombe* serves as an excellent system to dissect the molecular mechanisms of eukaryotic polarized cell growth and cell form.[50] These cells depict a constant and quantitative rod-shape and grow exclusively at cell tips. Genetic libraries of individual knockout strains are available, and provide a very powerful tool to perform systematic genetic studies of basic biological processes. We recently introduced the use of this model to study EF effects on cell polarity.[25] The EF caused the fission yeast cells to reorient their growth axis by bending to a direction perpendicular to the EF, creating cells with a bent morphology.[25] Candidate genetic screens of mutants in major polarity regulators and in ion transporters suggested that this response depended on the conserved formin for3p and the small GTPase cdc42p, which regulate actin cable polymerization for cell polarity.[51,52] This screen identified a conserved plasma membrane ion pump, the proton ATPase pma1p, as a major regulator of EF effects. One interesting result was that mutants in these different genes still oriented to the EF, but to the wrong direction, toward the anode of the EF (Fig. 5). Coupling simulation of biophysical EF effects with detailed localization of these identified components suggested that the main mode orienting cell growth perpendicular to the EF involved membrane potential and local pH effects that may promote formin activation to nucleate actin cables. In turn, the anodal orientation in pma1 for3 or cdc42 mutants appeared to rely on the anodal electrophoresis of cell wall enzymes, beta-glucan synthases that possess highly charged extracellular domains. The role of

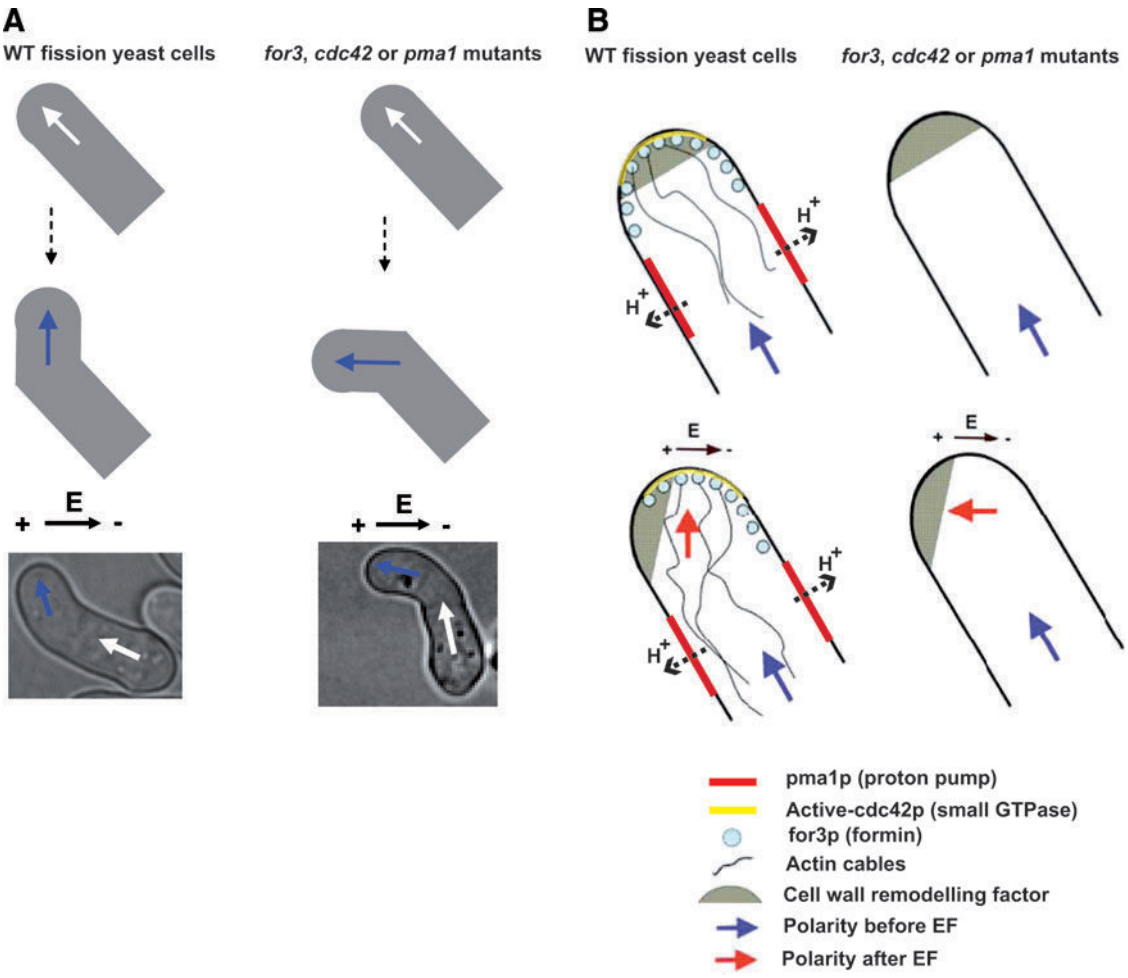

Figure 5. Molecular pathways regulating *Schizosaccharomyces pombe* galvanotropism. **(A)** In fission yeast cells that normally grow in perfect rod-shaped morphology; EF causes WT cells to reorient growth perpendicular to the EF direction. This reorientation depends on the proton ATPase pump pma1p, the small GTPase cdc42p, and the formin for3p. Pma1 functions as a pH regulator and is located on the side of the cell, which may establish putative transcellular proton currents and cortical pH gradients that transduce EF effects to for3p and cdc42p regulation. **(B)** The anodal orientation in pma1 for3 or cdc42 mutants may rely on the anodal electrophoresis of cell wall enzymes, which possess highly charged extracellular domains, and are important regulators of polarized cell growth in these cells. To see this illustration in color, the reader is referred to the web version of this article at www.liebertpub.com/wound

cdc42 and formin are consistent with findings in neuronal growth cone migration, which implicate function for the Cdc42/Rho/Rac pathway.[34]

A very novel aspect of these studies is to promote the role of pH and/or membrane potential in mediating the cross talk between EFs and actin.[25] These layers of regulation may be important even in normal cells as *pma1* mutants depict strong morphogenesis and polarity defects. These studies thus bring important fresh views on general cell polarization mechanisms.

TAKE-HOME MESSAGES

- EFs may influence the spatial behavior of cells and tissues *in vivo*, during processes, such as wound healing, development, and cancer
- Exogenous EFs can direct cell migration, growth, and division in many different cell types, such as bacteria, neutrophils, and neurons.
- Biophysical and molecular mechanisms of EFs are poorly characterized, but may involve complex signal transductions at the plasma membrane.
- Recent work using genetic models such as *Dictyostelium* and yeast cells, begin to identify key molecular players at the level of membrane signaling and in the regulation of the cytoskeleton to direct migration and growth in response to EFs.

All together, these genetic dissections in different organisms suggest downstream transduction of EF effects by small GTPase, lipid signaling, and actin regulation factors. The cross-talk between EFs and some of these polarity modules remains to be clearly defined, although some transporters and ions have been specifically identified in these different systems. Membrane potential, calcium, and pH regulation may play key roles in mediating EF effects into polarized reorganization of cytoskeletal regulators. Genetic studies in *Dictyostelium* and yeast begin to reveal why different cells may polarize to different directions, and suggest that directionality in response to the EF may be sensitive to the expression of a single protein, or a cellular component. These different directional responses found in different mutants support the existence of competing pathways steering the cell in different directions with one dominant mode. When the dominant mode is knocked down, the second pathway takes over to drive polarity in another direction.

Biological significance of galvanotactic effects

These EF effects are likely to reflect physiological events in wound healing, neuron organization, and development. As EFs are present around tissues, studying these effects in isolated cells *in vitro* will reveal important mechanisms of tissue organization and cell behavior *in vivo*. These effects offer one unique manner to control the orientation and shapes of many different cells, and have the potential to open new avenues in bioengineering and medicine.

Beyond their significance in basic biological processes, these galvanotactic experiments bring fundamental understanding in core polarity mechanisms.[53] The fact that most cell types can sense and orient to EFs suggest that galvanotactic effects involve an evolutionarily conserved layer of spatial organization. We speculate that EF effects could reflect the natural electrochemical regulation of polarity and cytoskeletal elements. If this is the case, the EF effect may bias or exacerbate an existing electrical organization, leading to the polarized reorientation in the EF. A specific cytoskeletal regulator may, for instance, naturally bind to portions of the plasma membrane with specific charges,[54,55] or be activated within a narrow pH window; the EF-induced perturbation on the membrane potential, membrane charge, or pH would cause the relocation or reactivation of this element to redirect polarity. It has long been a puzzle to understand how such small EFs, which perturb only 1–5% of the resting membrane potential, could orient polarity in such a striking manner.[6] Positive feedback regulating polarization modules, the cytoskeletons and ion transport may begin to provide answers to these long-standing questions. There are many recent reports that highlight the role of membrane potential, pH gradients, and membrane inner leaflet charges as fundamental regulators of polarity processes in single cells, tissues, and whole organisms (for a recent review, see Campetelli *et al.*[53]). Galvanotactic experiments will thus continue revealing important aspects of general polarization mechanisms, and may provide novel approaches to develop suitable therapeutic alternatives in the context of wound healing, development, and regeneration.

CONCLUSIONS AND FUTURE DIRECTIONS

In sum, the road to understanding the molecular mechanisms regulating galvanotactic effects is still long, before one can provide a system-level detailed understanding of such fascinating effects. Model organisms which allow reliable forward genetic studies, such as yeast or *Dictyostelium*, will help to rigorously identify and characterize gene products that may be involved in the electric response. It will then be possible to test these hits, either in mammalian cells using RNA silencing in cultured cell

lines, or in animal models, and to discern relevant signal transduction mechanisms directly relevant to human care. The identification of specific proteins also promises to pave the way for the synthesis of specific chemical inhibitors, which may be used to enhance the galvanotactic effect to improve healing or nerve repair and to develop accurate therapeutic methods for treating chronic wounds and spinal injury. Besides the genetic investigation of these sensing mechanisms, efforts at the biophysical level need to be made to generate a detailed understanding of the processes at play, and modeling together with detailed dynamic microscopy should help research move in this direction.

ACKNOWLEDGMENTS

N.M. acknowledges financial support from an Agence Nationale de la Recherche (ANR) 'retour post-doctorants' grant ANR-10PDOC-003-01 and a European FP7-People-CIG grant. D.B. is supported by an Institut Curie PhD fellowship.

AUTHOR DISCLOSURE AND GHOSTWRITING

The authors declare no competing financial interests. No ghostwriters were used.

ABOUT THE AUTHORS

Daria Bonazzi studied chemistry at the University of Bologna, discovering a particular interest for bioelectrochemistry. She then moved to the Institut Curie (Paris, France), where she focused on a cell biology research topic. She now is a PhD student at the Institut Curie and Institut Jacques Monod (Paris, France) under the supervision of Nicolas Minc, working on biophysical aspects of cell polarity in yeast. **Nicolas Minc** initially trained in physics and completed his initial training in cell biology during his post-doctorate at Columbia University. He is a CNRS researcher and a group leader at the Institut Jacques Monod (Paris, France). His group focuses on the biophysical studies of cell shape and cell polarity, and conduct these investigations in yeast and early embryos.

REFERENCES

1. Drubin DG and Nelson WJ: Origins of cell polarity. Cell 1996; **84:** 335.
2. Li R and Gundersen GG: Beyond polymer polarity: how the cytoskeleton builds a polarized cell. Nat Rev Mol Cell Biol 2008; **9:** 860.
3. Cain RJ and Ridley AJ: Phosphoinositide 3-kinases in cell migration. Biol Cell 2009; **101:** 13.
4. Iden S and Collard JG: Crosstalk between small GTPases and polarity proteins in cell polarization. Nat Rev Mol Cell Biol 2008; **9:** 846.
5. Djamgoz MBA, Mycielska M, Madeja Z, Fraser SP, and Korohoda W: Directional movement of rat prostate cancer cells in direct-current electric field: involvement of voltagegated Na+ channel activity. J Cell Sci 2001; **114:** 2697.
6. Jaffe LF and Nuccitelli R: Electrical controls of development. Annu Rev Biophys Bioeng 1977; **6:** 445.
7. Mycielska ME and Djamgoz MB: Cellular mechanisms of direct-current electric field effects: galvanotaxis and metastatic disease. J Cell Sci 2004; **117:** 1631.
8. Reid B, Nuccitelli R, and Zhao M: Non-invasive measurement of bioelectric currents with a vibrating probe. Nat Protoc 2007; **2:** 661.
9. Zhao M, Song B, Pu J, Wada T, Reid B, Tai G, Wang F, Guo A, Walczysko P, Gu Y, Sasaki T, Suzuki A, Forrester JV, Bourne HR, Devreotes PN, McCaig CD, and Penninger JM: Electrical signals control wound healing through phosphatidylinositol-3-OH kinase-gamma and PTEN. Nature 2006; **442:** 457.
10. Kropf D, Lupa M, Caldwell J, and Harold FM H: Cell polarity: endogenous ion currents precede and predict branching in the water mold *Achyla*. Science 1983; **220:** 1385.
11. Levin M, Thorlin T, Robinson KR, Nogi T, and Mercola M: Asymmetries in H+/K+-ATPase and cell membrane potentials comprise a very early step in left-right patterning. Cell 2002; **111:** 77.
12. Nuccitelli R, Poo MM, and Jaffe LF: Relations between ameboid movement and membrane-controlled electrical currents. J Gen Physiol 1977; **69:** 743.
13. Weisenseel MH, Nuccitelli R, and Jaffe LF: Large electrical currents traverse growing pollen tubes. J Cell Biol 1975; **66:** 556.
14. Brand A, Shanks S, Duncan VM, Yang M, Mackenzie K, and Gow NA: Hyphal orientation of *Candida albicans* is regulated by a calcium-dependent mechanism. Curr Biol 2007; **17:** 347.
15. McCaig CD, Rajnicek AM, Song B, and Zhao M: Controlling cell behavior electrically: current views and future potential. Physiol Rev 2005; **85:** 943.
16. Rajnicek AM, McCaig CD, and Gow NA: Electric fields induce curved growth of *Enterobacter cloacae*, *Escherichia coli*, and *Bacillus subtilis* cells: implications for mechanisms of galvanotropism and bacterial growth. J Bacteriol 1994; **176:** 702.
17. Robinson KR: The responses of cells to electrical fields: a review. J Cell Biol 1985; **101:** 2023.
18. Zhao M: Electrical fields in wound healing—an overriding signal that directs cell migration. Semin Cell Dev Biol 2009; **20:** 674.
19. Chang PC, Sulik GI, Soong HK, and Parkinson WC P: Galvanotropic and galvanotaxic responses of corneal endothelial cells. J Formos Med Assoc 1996; **95:** 623.
20. McKasson MJ, Huang L, and Robinson KR: Chick embryonic Schwann cells migrate anodally in small electrical fields. Exp Neurol 2008; **211:** 585.
21. Pu J, McCaig CD, Cao L, Zhao Z, Segall JE, and Zhao M: EGF receptor signalling is essential for electric-field-directed migration of breast cancer cells. J Cell Sci 2007; **120:** 3395.
22. Zhao M, Bai H, Wang E, Forrester JV, and McCaig CD: Electrical stimulation directly induces preangiogenic responses in vascular endothelial cells by signaling through VEGF receptors. J Cell Sci 2004; **117:** 397.
23. Onuma EK and Hui SW: Electric field-directed cell shape changes, displacement, and cytoskeletal reorganization are calcium dependent. J Cell Biol 1988; **106:** 2067.
24. Crombie T, Gow NA, and Gooday GW: Influence of applied electrical fields on yeast and hyphal growth of *Candida albicans*. J Gen Microbiol 1990; **136:** 311.

25. Minc N and Chang F: Electrical control of cell polarization in the fission yeast *Schizosaccharomyces pombe*. Curr Biol 2010; **20:** 710.

26. McGillivray A and Gow NAR: Applied electrical fileds polarize the growth of mycelial fungi. J Gen Microbiol 1986; **132:** 2515.

27. Gross D, Loew LM, and Webb WW: Optical imaging of cell membrane potential changes induced by applied electric fields. Biophys J 1986; **50:** 339.

28. Kralj JM, Hochbaum DR, Douglass AD, and Cohen AE: Electrical spiking in *Escherichia coli* probed with a fluorescent voltage-indicating protein. Science 2011; **333:** 345.

29. Pantazopoulos P, Kwong K, Lillycrop W, Wong L, Gao Y, Chalouh S, Samadhin M, Ratnayake WM, Krenosky S, Dumais L, and L'Abbe MR: Trans and saturated fat on food labels in Canada: fact or fiction? Can J Public Health 2011; **102:** 313.

30. Jaffe LF: Electrophoresis along cell membranes. Nature 1977; **265:** 600.

31. Poo M: *In situ* electrophoresis of membrane components. Annu Rev Biophys Bioeng 1981; **10:** 245.

32. Poo M and Robinson KR: Electrophoresis of concanavalin A receptors along embryonic muscle cell membrane. Nature 1977; **265:** 602.

33. Pullar CE, Baier BS, Kariya Y, Russell AJ, Horst BA, Marinkovich MP, and Isseroff RR: Beta4 integrin and epidermal growth factor coordinately regulate electric field-mediated directional migration via Rac1. Mol Biol Cell 2006; **17:** 4925.

34. Rajnicek AM, Foubister LE, and McCaig CD: Temporally and spatially coordinated roles for Rho, Rac, Cdc42 and their effectors in growth cone guidance by a physiological electric field. J Cell Sci 2006; **119:** 1723.

35. Sato MJ, Kuwayama H, van Egmond WN, Takayama AL, Takagi H, van Haastert PJ, Yanagida T, and Ueda M: Switching direction in electric-signal-induced cell migration by cyclic guanosine monophosphate and phosphatidylinositol signaling. Proc Natl Acad Sci USA 2009; **106:** 6667.

36. Pullar CE and Isseroff RR: Cyclic AMP mediates keratinocyte directional migration in an electric field. J Cell Sci 2005; **118:** 2023.

37. Shanley LJ, Walczysko P, Bain M, MacEwan DJ, and Zhao M: Influx of extracellular Ca2+ is necessary for electrotaxis in *Dictyostelium*. J Cell Sci 2006; **119:** 4741.

38. Brand A, Vacharaksa A, Bendel C, Norton J, Haynes P, Henry-Stanley M, Wells C, Ross K, Gow NA, and Gale CA: An internal polarity landmark is important for externally induced hyphal behaviors in *Candida albicans*. Eukaryot Cell 2008; **7:** 712.

39. Zhao M, Pu J, Forrester JV, and McCaig CD: Membrane lipids, EGF receptors, and intracellular signals colocalize and are polarized in epithelial cells moving directionally in a physiological electric field. FASEB J 2002; **16:** 857.

40. Servant G, Weiner OD, Herzmark P, Balla T, Sedat JW, and Bourne HR: Polarization of chemoattractant receptor signaling during neutrophil chemotaxis. Science 2000; **287:** 1037.

41. Devreotes PN and Zigmond SH: Chemotaxis in eukaryotic cells: a focus on leukocytes and *Dictyostelium*. Annu Rev Cell Biol 1988; **4:** 649.

42. Parent CA and Devreotes PN: Molecular genetics of signal transduction in *Dictyostelium*. Annu Rev Biochem 1996; **65:** 411.

43. Song B, Zhao M, Forrester JV, and McCaig CD: Electrical cues regulate the orientation and frequency of cell division and the rate of wound healing *in vivo*. Proc Natl Acad Sci USA 2002; **99:** 13577.

44. Veltman DM, Keizer-Gunnik I, and Van Haastert PJ: Four key signaling pathways mediating chemotaxis in *Dictyostelium discoideum*. J Cell Biol 2008; **180:** 747.

45. Veltman DM and Van Haastert PJ: Guanylyl cyclase protein and cGMP product independently control front and back of chemotaxing *Dictyostelium* cells. Mol Biol Cell 2006; **17:** 3921.

46. Gao RC, Zhang XD, Sun YH, Kamimura Y, Mogilner A, Devreotes PN, and Zhao M: Different roles of membrane potentials in electrotaxis and chemotaxis of dictyostelium cells. Eukaryot Cell 2011; **10:** 1251.

47. Chang F and Peter M: Yeasts make their mark. Nat Cell Biol 2003; **5:** 294.

48. Harold FM, Schreurs WJ, Harold RL, and Caldwell JH: Electrobiology of fungal hyphae. Microbiol Sci 1985; **2:** 363.

49. van West P, Morris BM, Reid B, Appiah AA, Osborne MC, Campbell TA, and Shepherd SJ: Oomycete plant pathogens use electric fields to target roots. Mol Plant Microbe Interact 2002; **15:** 790.

50. Chang F and Martin SG: Shaping fission yeast with microtubules. Cold Spring Harb Perspect Biol 2009; **1:** a001347.

51. Martin SG, Rincon SA, Basu R, Perez P, and Chang F: Regulation of the formin for3p by cdc42p and bud6p. Mol Biol Cell 2007; **18:** 4155.

52. Minc N, Bratman SV, Basu R, and Chang F: Establishing new sites of polarization by microtubules. Curr Biol 2009; **19:** 83.

53. Campetelli A, Bonazzi D, and Minc N: Electrochemical regulation of cell polarity and the cytoskeleton. Cytoskeleton (Hoboken) 2012; **69:** 601.

54. Das A, Slaughter BD, Unruh JR, Bradford WD, Alexander R, Rubinstein B, and Li R: Flippase-mediated phospholipid asymmetry promotes fast Cdc42 recycling in dynamic maintenance of cell polarity. Nat Cell Biol 2012; **14:** 304.

55. Fairn GD, Hermansson M, Somerharju P, and Grinstein S: Phosphatidylserine is polarized and required for proper Cdc42 localization and for development of cell polarity. Nat Cell Biol 2011; **13:** 1424.

MINI-REVIEW ARTICLE
Cytoskeleton, September 2012 69:601–612 (doi: 10.1002/cm.21047)

Electrochemical Regulation of Cell Polarity and the Cytoskeleton

Alexis Campetelli, Daria Bonazzi, and Nicolas Minc*

Institut Curie, UMR 144 CNRS/IC, 26 rue d'Ulm, 75248 Paris Cedex 05, France

Received 9 May 2012; Revised 13 June 2012; Accepted 14 June 2012
Monitoring Editor: Pekka Lappalainen

Cell polarity plays a key role in regulating cell–cell communication, tissue architecture, and development. Both internal and external cues participate in directing polarity and feedback onto each other for robust polarization. One poorly appreciated layer of polarity regulation comes from electrochemical signals spatially organized at the level of the cell or the tissue. These signals which include ion fluxes, membrane potential gradients, or even steady electric fields, emerge from the polarized activation of specific ion transporters, and may guide polarity in wound-healing, development or regeneration. How a given electrochemical cue may influence cytoskeletal elements and cell polarity remains unclear. Here, we review recent progress highlighting the role of electrochemical signals in cell and tissue spatial organization, and elucidating the mechanisms for how such signals may regulate cytoskeletal assembly for cell polarity. © 2012 Wiley Periodicals, Inc.

Key Words: cell polarity, electric fields, pH, membrane potential, cytoskeleton

Electrochemical signals have been widely studied for their role in regulating cell physiology. Proper ion transport through the membrane is a prerequisite for cell survival and defects in this process have been implicated in numerous diseases [Prevarskaya et al., 2010; Hollenhorst et al., 2011; Webb et al., 2011]. Electrochemical aspects of cell biology have also been deeply characterized in neurons, where waves of ion influx and efflux and consequent membrane potential changes allow for the propagation of action potentials. One less understood aspect of cellular electrochemistry stands in the control that electrochemical cues may have on the spatial organization of cells and tissues.

Alexis Campetelli and Daria Bonazzi contributed equally to this work.

*Address correspondence to: Nicolas Minc, Institut Curie, UMR 144 CNRS/IC, 26 rue d'Ulm, 75248 Paris Cedex 05, France. E-mail: nicolas.minc@curie.fr

Published online 11 July 2012 in Wiley Online Library (wileyonlinelibrary.com).

Most cells in our body are surrounded by organized electrical signals. These have relatively small magnitude and depict near steady-state organization, and could serve as guiding cues for spatially regulating cell and tissue behavior [Jaffe and Nuccitelli, 1977; McCaig et al., 2005]. Endogenous electrical currents, fields, and membrane potential gradients have been mapped around epithelial monolayers, developing embryos, and regenerating organisms [Hotary and Robinson, 1992; Szatkowski et al., 2000; Reid et al., 2007; Levin, 2009; Kucerova et al., 2011; Reid and Zhao, 2011]. They have been proposed to participate in directing cell migration, division, and proliferation in these processes [McCaig et al., 2005; Zhao et al., 2006; Levin, 2009]. Organized ionic currents have also been detected around large polarized single cells such as developing eggs or pollen tubes and suggested to help establishing a spatial order for polarized division or growth [Robinson and Jaffe, 1975; Weisenseel et al., 1975; Kline et al., 1983; Schreurs and Harold, 1988]. These currents may be generated by the activation of ion transporters at defined locations around cells or tissues [Feijo et al., 1999; Levin et al., 2002; McCaig et al., 2005; Minc and Chang, 2010]. Application of exogenous electric fields, similar to those measured in vivo can direct polarity in many different cell types, ranging from bacteria, fungi to neutrophils [McCaig et al., 2005].

Very little is known on how this electrical patterning arises in the first place, and how it is transduced to influence cytoskeletal elements for cell polarity. The lack of molecular descriptions has impaired progress in this area and has kept the field outside of mainstream research for many years. In here, we review novel insights into the molecular and biophysical mechanisms linking electrochemical cues such as membrane potential, pH, or external electric fields, to the regulation of cytoskeletal elements and polarity proteins.

Membrane Potential and Tissue Architecture

The membrane potential of a cell results from gradients of charges segregated across the insulating plasma

membrane. Membrane potential is dynamically regulated by ion channels and pumps, which function in exporting and importing anions and cations through the membrane. Values of resting membrane potentials may vary largely between different cell types, ranging from −10 to −150 mV [Levin, 2012]. Some cells globally modify their membrane potential to perform specific functions or during different periods of their life cycle, for instance, during egg fertilization or cell differentiation [Blackiston et al., 2009; Wessel and Wong, 2009]. Metastatic cancer cells usually display depolarized (reduced) membrane potential which has been associated with metastatic potential [Binggeli and Weinstein, 1985; Binggeli et al., 1994]. Membrane potential may feedback on ion transport, intracellular pH, or membrane surface charges at the membrane inner and outer leaflet. It has long been suggested as a cue regulating tissue patterning [Jaffe and Nuccitelli, 1977]. One proposed view is that tissue-scale membrane potential gradients could yield electrophoresis of morphogens through gap junctions or other cell–cell connections [Woodruff and Telfer, 1980; Bohrmann and Gutzeit, 1987; Levin et al., 2002; Esser et al., 2006]. Another one is that membrane potential could indirectly influence downstream cytoplasmic factors organization or even gene transcription [Levin, 2012]. Some recent works which revisit these concepts within the modern knowledge of cell and developmental genetics begin to provide functional evidence for the role of membrane potential, in tissue patterning in embryos and animals.

Developmental fidelity relies on proper localized gene transcription in the embryo. In the *Xenopus* embryo, a group of cells in the anterior neural field specify the activation of eye field transcription factors (EFTF) in the neighboring tissue for eye development (Fig. 1A). Membrane potential may have important inputs in this activation. At stage 17/18, these neural anterior cells have striking hyperpolarized membrane potential as compared to the neighboring tissue cells, that can be qualitatively visualized by sensitive fluorescent imaging of different membrane potential dyes [Pai et al., 2012]. Perturbation of this hyperpolarization pattern, achieved by expressing and locally activating exogenous anionic or cationic channels, yields major defects in eye development or the formation of an ectopic eye in the gut and other caudal areas. In situ visualization of expression patterns, show that membrane potential values correlate with specific gene transcription, and may thus contribute to proper developmental patterning in this tissue.

Similar evidence for the role of membrane potential in tissue patterning has been put forward in regeneration processes [Adams et al., 2007; Levin, 2009; Beane et al., 2011]. Planarians are flat worms which serve as model organisms to study regeneration of tissues, because they exhibit an extraordinary ability to regenerate lost body parts. Regeneration involves a specific timing of events, starting from sensing the tissue cut, regenerating specific cells, and growing back tissues in a proper manner. Hints on the importance of bioelectrical signals on regeneration mechanisms in similar organisms had long been suggested [Marsh and Beams, 1957]. In a recent study, Beane et al. measured membrane potential gradients generated upon amputation of either the head or the tail of a planarian [Beane et al., 2011]. When the head is amputated, cells in the border of the cut, called the head blastemas depict a strongly depolarized membrane, while tail blastemas are typically hyperpolarized (Fig. 1B). These membrane polarization patterns may depend on the differential expression of an H^+-K^+ ATPase pump in these two different parts of the animal. To assess the functional role for membrane voltage as a potential regulator of anterior/posterior polarity, the authors express exogenous ion channels that alter membrane potential values to these border blastema cells. Strikingly, hyperpolarizing tail blastemas yields regeneration of a second head and a bi-headed organism, while depolarization of the head blastemas yields regeneration of a tissue that is neither a tail nor a head (Fig. 1B). These results suggest that membrane potential may act as an upstream signal that allows the organism to discern its global head to tail polarity.

Dose-dependent values of membrane potentials may impose differential expression of specific sets of genes. Several mechanisms have been suggested to transduce membrane potential into specific gene expression patterns. One proposed view is that membrane potential values are transduced via voltage-sensitive calcium channels that indirectly regulate gene expression [Weick et al., 2003]. Another one comes from the identification of voltage sensitive phosphatases that may trigger specific signaling pathways from membrane potential—dependent conformational changes [Villalba-Galea, 2012]. Other examples include membrane-potential dependent affinity between specific ligands and G-protein type receptors [Ben-Chaim et al., 2006], or even movement of signaling molecules through cellular gap junctions [Levin, 2012]. As these different mechanisms may be triggered at different threshold of membrane potential changes, it is likely to expect different dominant mechanisms in different tissues or situations. How specific is the signal-transduction downstream of such electrical cue and how membrane potential patterns are established in tissues in the first place, remain interesting open questions.

Novel work in zebrafish tissues brings an interesting point of view for how cellular membrane potential may help to pattern a tissue or an organism [Inaba et al., 2012]. Zebrafish animals have pigmented skin stripes of alternating blue and gold (for males) and blue and silver (for females) that run along their body (Fig. 1C). Each stripe is typically composed of a pigment cell type. The melanophores compose the gold stripe and the xanthophores are in the blue stripes. Mechanisms for how these

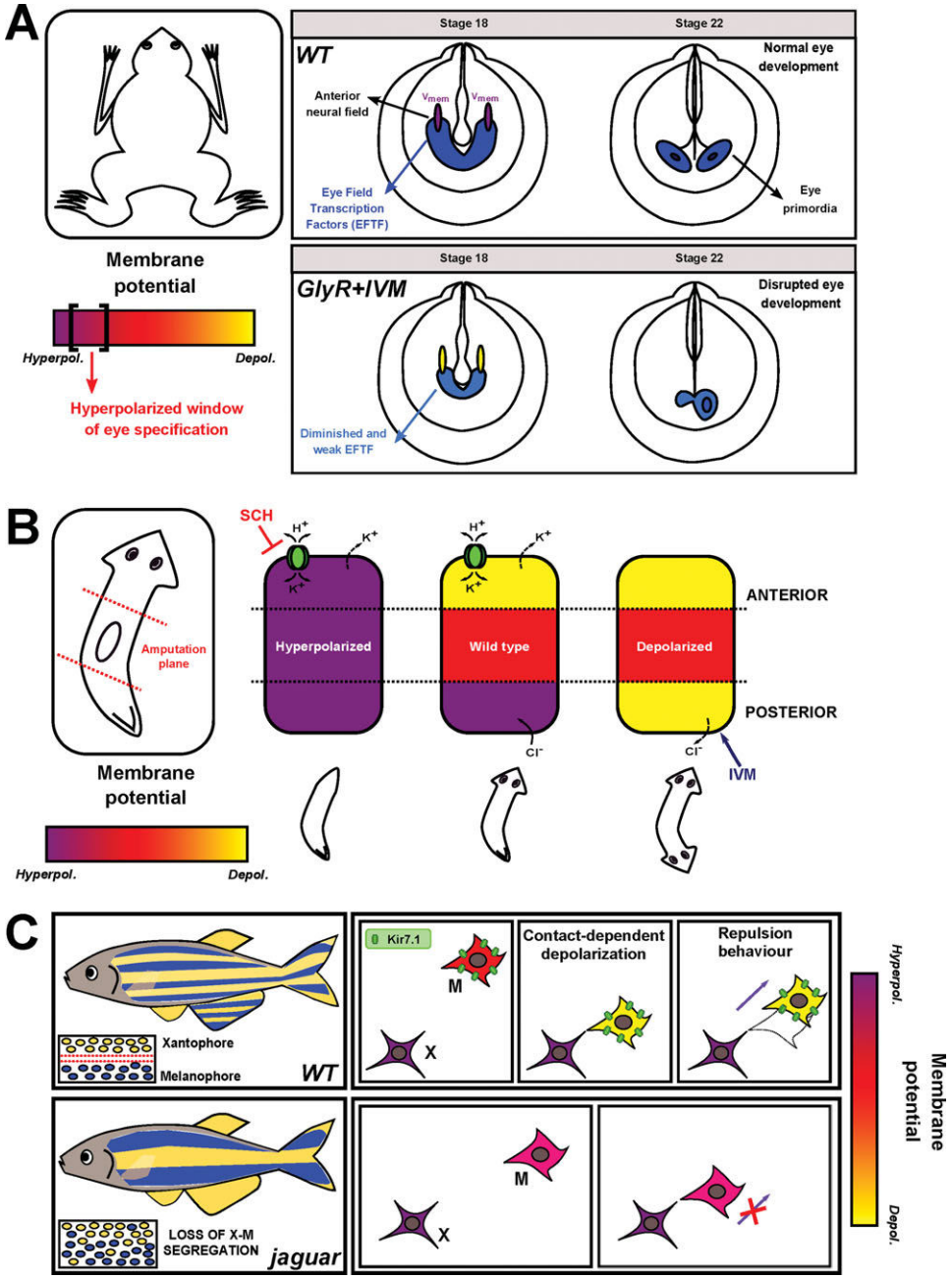

Fig. 1. Influence of membrane potential on embryonic development and tissue architecture. A: Embryonic eye development in *Xenopus laevis* involves the bilateral patterning of EFTFs by two clusters of hyperpolarized cells in the anterior neural field at stage 18 before the formation of eye primordial (stage 22). Disruption of the membrane potential signal results in diminished or lost EFTF signal, leading to disrupted eye development. **B:** Planarian tissue regeneration. Upon amputation of both head and tail, wild-type fragments generate a membrane potential gradient with the head blastema depolarized and the tail blastema less depolarized. H,K-ATPase inhibition with SCH treatment results in relative hyperpolarization and consequent regeneration of a neither tail-nor head structure. On the other hand, ivermectin (IVM) treatment leads to relative depolarization and consequent head formation. **C:** Zebrafish pigment pattern formation. The wild-type (WT) fish is characterized by a regular segregation of blue and yellow stripes on the skins. Pigment cells in these stripes are called melanophores (M) and xanthophores (X), respectively. Stripes may be generated by the repulsive behavior of M contacting X, which is in turn regulated by a contact-dependent membrane depolarization of M. In the homozygous kir7.1 mutant (jaguar), contact-dependent depolarization is malfunctioning, resulting in a lack of repulsive behavior, X-M mis-segregation and defects in the stripe pattern.

two cell types stay apart to regulate stripes patterning are lacking, but several fish mutants that depict defect in stripe patterns have been identified [Maderspacher and Nusslein-Volhard, 2003; Iwashita et al., 2006]. One such mutant, called Jaguar has a mutation in a gene encoding an inward potassium rectifying channel, Kir7.1. This channel regulates the resting membrane potential by promoting the entry of potassium in the cytoplasm, and is

expressed in the melanophores cells of the fish skin. Dynamic tracking of the melanophores membrane potential visualized with fluorescent dyes reveals a Kir7.1-dependent membrane depolarization when these cells contact a xanthophore. This membrane depolarization underlies a contact inhibition process that yields a polarity switch to drive migration away from the xanthophore. Thus, cellular membrane potential values are sensitive to cell–cell contacts and may regulate cell polarity and consequent large-scale tissue patterning. In this situation, it remains to be established whether cellular membrane potential modulation triggering this polarity switch is global or local at the subcellular level.

Electrochemical Cues Regulating Cell Polarity

Other specific electrochemical cues have been involved in organizing tissues and embryos. Large scale ion fluxes originating from the differential expression of ion transporters are found around tissues and cells and regulate the intracellular content of certain ions such as calcium, potassium, and even protons. These intracellular gradients could modulate the activity of intracellular polarity factors [Robinson and Jaffe, 1975; Levin et al., 2002]. Although data correlating these current patterns with polarity abound, mechanisms for achieving and sensing intracellular ion gradients are still poorly defined. Proton currents and consequent pH gradients are particularly interesting, because many cytoskeletal components are thought to be tightly regulated by pH values [Bachewich and Heath, 1997; Denker and Barber, 2002b].

Migrating cells establish a polarization axis by specifying a zone of actin polymerization at the leading edge. This process is regulated by the polarized recruitment and activation of polarity factors such as the conserved Rho-type small GTPase cdc42 [Etienne-Manneville, 2004]. At the leading edge, activated GTP-bound cdc42, recruits regulators of actin nucleation such as formin, N-Wasp, and components of the Arp2/3 complex, for progression of the leading edge and migration [Frantz et al., 2008]. Local activation of cdc42 is mediated by Guanine exchanging factors (GEFs) that are recruited to the cortex through interactions with specific proteins or lipids such as phosphatidylinositol 4,5-bisphosphate (PIP2). In migrating fibroblast, an interesting link between pH regulation, cdc42 activation, and polarity establishment has been put forward throughout subsequent studies (Fig. 2B) [Hooley et al., 1996; Denker and Barber, 2002a; Frantz et al., 2007]. In this system, the conserved sodium/proton exchanger NHE1 promotes fibroblast polarity and migration [Denker and Barber, 2002a]. This transporter, through its regulatory effect on cortical pH, may function in stabilizing at the leading edge the binding of a cdc42 GEF to PIP2 at the plasma membrane (Fig. 2B) [Frantz et al., 2007]. Interestingly, NHE1 recruitment to the leading edge depends on cdc42 activation [Hooley et al., 1996], and thus NHE1, pH regulation and polarity activation work within a positive feedback loop regulating polarity axis establishment in fibroblast migration.

Similar components have been involved in polarized cancer cell invasion. Invasion, which relies on breakage of the extracellular matrix through a specific polarized structure called invadopodia is a hallmark of cancer metastasis [Weaver, 2006]. Formation of a polarized invadopodia depends on the specific timing of the recruitment of actin polymerization regulators. Early steps of polarization include cortactin phosphorylation and detachment of cofilin to generate free barbed ends filaments and de novo actin polymerization followed by invadopodia progression [Oser et al., 2009]. In a recent study, Magalhaes et al. provide evidence that these early steps are associated with the recruitment of NHE1 and local pH gradients [Magalhaes et al., 2011]. In particular, they demonstrate that cortactin phosphorylation leads to the local recruitment of NHE1, which in turn yields local alkalization in the future invadopodia area (Fig. 2A). This local pH increase may trigger unbinding of cofilin from cortactin, by reducing the binding strength between the two proteins, promoting actin polymerization and invadopodia protrusion. Thus, pH regulation through NHE1 may work in reinforcing the definition of a polarity axis and in catalyzing actin polymerization for progression of this subcellular structure. pH deregulation through the sodium/proton exchangers has been implicated in numerous cases of metastasis [Cardone et al., 2005]. pH may directly regulate actin-binding proteins including cofilin, profilin, or talin in vitro and in vivo [McLachlan et al., 2007; Frantz et al., 2008; Srivastava et al., 2008], and thus a similar mechanism may be at play in other actin-based polarization systems.

pH regulation and protein domain charges have also been implicated in planar cell polarity (PCP) pathway regulation in Drosophila epithelial tissues [Simons et al., 2009]. This conserved signaling pathway plays a key role in setting epithelial tissue polarity and architecture in different organisms [Goodrich and Strutt, 2011]. In the Drosophila wing and eye, the pathway serves to define asymmetric recruitment of specific factors within the plane of the tissue. This polarity relies on the recruitment of the transmembrane protein Frizzled (Fz) at cell–cell contact along the tissue axis. Fz binding to Dishevelled (Dsh) activates the recruitment of cytoskeleton elements for cell polarity, growth, and division [Segalen and Bellaiche, 2009; Goodrich and Strutt, 2011]. Fz binding to Dsh requires the targeting of Dsh to the plasma membrane. By performing a genome-wide RNAi screen in drosophila cells, Simons et al. identified the sodium/proton exchanger Nhe2 as a key regulator of Dsh targeting to the

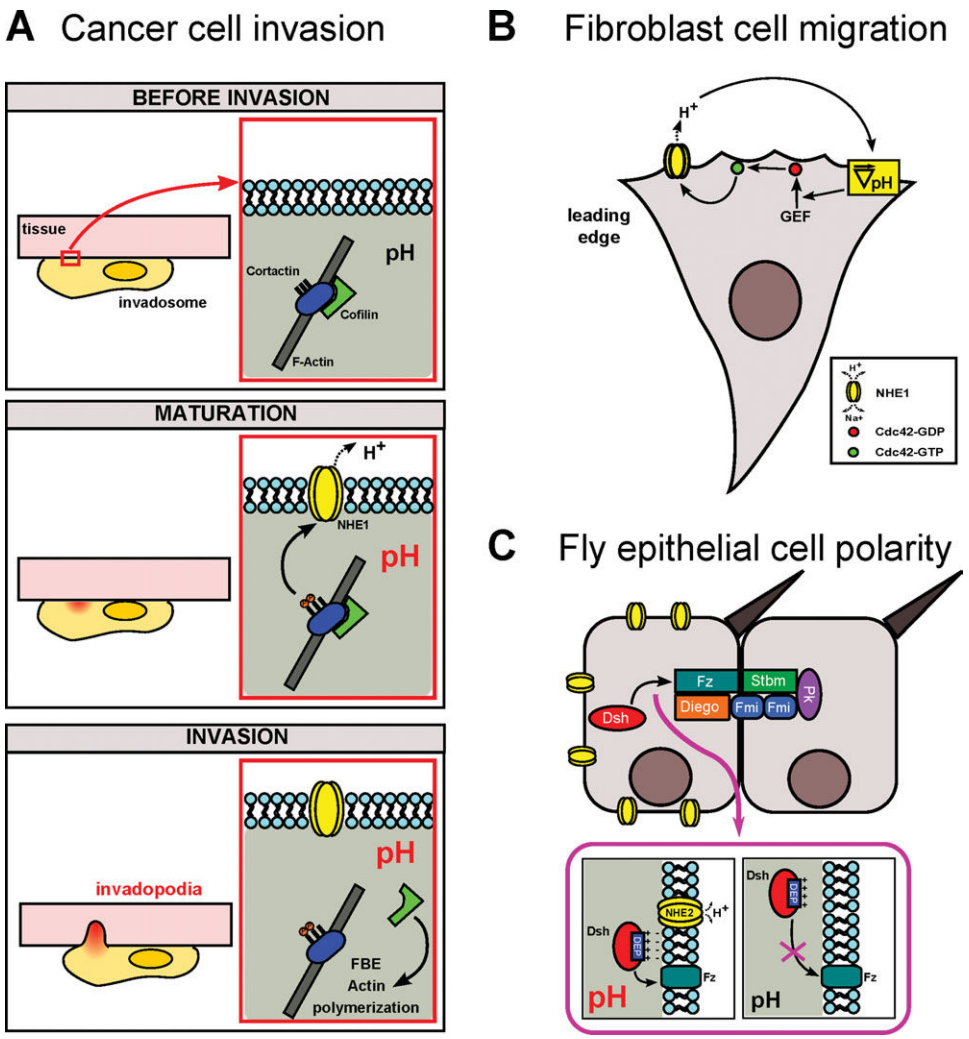

Fig. 2. Electrochemical cues regulating cell polarity. A: Tumor cell invasion. During invadopodia maturation, the sodium/proton exchanger NHE1 is recruited to the invadopodium site by cortactin phosphorylation and generates local pH increase. This change in pH triggers cortactin–cofilin unbinding, de novo actin polymerization and invadopodia progression. **B**: Fibroblast cell migration. NHE1 is localized along the leading edge of a migrating cell, generating a local basic pH that stabilizes GEF interaction with PIPs in the membrane. GEF recruitment mediates cdc42 activation and actin polymerization. Active cdc42 in turn recruits NHE1 to the leading edge, amplifying a positive feedback loop that reinforces polarized migration. **C**: Drosophila epithelial cell polarity. Proton transporters play a role in regulating the asymmetric localization of PCP core proteins to polarized epithelia in the plane of a tissue. The sodium-proton exchanger Nhe2 regulates the recruitment of Dsh to the plasma membrane, through its effect on pH and consequent electrostatic interaction of the positively charged Dsh DEP domain with negatively charged acidic phospholipid groups in the membrane.

membrane. This protein shares homology with the human NHE family, and more particularly with hNHE3. They propose that pH values regulated by Nhe2 influence head phospholipids protonation level (whose pKa are close to neutral) impacting the binding of the polybasic stretch of Dsh DEP (Dishevelled, Egl-10, Pleckstrin) to the plasma membrane inner leaflet. Thus Nhe2 and electrochemical cues regulate Dsh targeting to the membrane, which allows this protein to interact with Fz. In a subsequent study, the same group showed that Fz localization relies on pH regulation, through the action of a V-ATPase proton pump, that extrude protons form organelles and cells by consuming ATP energy [Hermle et al., 2010]. These studies thus demonstrate the importance of proton transporters, pH regulation, and protein charges for the proper stabilization of a polarity axis in a tissue context [Hermle et al., 2011].

Other recent evidences suggest that membrane inner leaflet charges of certain lipids such as phosphatidylserine, may participate in recruiting or stabilizing polarity components in the budding yeast *S. cerevisiae* [Yeung et al., 2008; Fairn et al., 2011; Das et al., 2012]. In the fission yeast, *S. pombe*, the conserved proton ATPase pump pma1p, that regulates membrane potential and intracellular pH in fungi and plants [Sanders et al., 1981], has been shown to regulate polarized growth and cell

morphogenesis [Minc and Chang, 2010]. Transcellular pH gradients exist in large polarized cells such as pollen tubes or fucoid eggs [Gibbon and Kropf, 1994; Feijo et al., 1999], and in fission yeast (our unpublished results). These pH gradients are likely to be cortical or submembranous, since rapid diffusion of protons may impair formation of cytoplasmic gradients. At the cortex, the fast proton extrusion rate by ATPase pumps or ion exchangers coupled with sharp subcellular localization of the channel could explain gradient formation but remains to be explored quantitatively. All together, these data at the single cell and tissue level highlight the importance of electrochemical regulation for polarity. It is likely that pH or membrane potential affect the membrane targeting of different factors or binding strength between proteins.

Yet, these studies suggest some specificity in the polarity pathways activated by the electrochemical cue. Hierarchy in molecular effectors regulating cytoskeletal assembly and polarity pathways coupled with positive feedback loops may allow cells to interpret and use electrochemical cues for specifying and maintaining a polarity axis.

Orienting Cell Polarity to Exogenous Electric Fields

Striking evidences highlighting the electrical aspects regulating polarity, come from electrotactic experiments. In this assay, cells are exposed to small exogenous electric fields (EFs) similar to those found in vivo and orient their polarization with respect to the EF direction [McCaig and Dover, 1991; Rajnicek et al., 1994; Zhao et al., 2006]. EFs can direct division, migration, or polarized growth, and appear as unique universal signals to orient polarity. Cells, ranging from bacteria, fungi to mammalian cells, orient polarity to external EFs. Puzzlingly, different cell types polarize to different directions, some to the anode (positive electrode of the EF), others to the cathode and some even to a direction perpendicular to the EF (Fig. 3). Effects of endogenous EFs on cell polarity are thought to be important for wound healing and development. These effects are used in clinical contexts, for instance in healing therapy and nerve repair [McCaig et al., 2005]. How might cells sense EF signals and reorganize the cytoskeleton and polarity machinery is not well understood. It is generally accepted that the EFs only affect events close to the plasma membrane [Jaffe, 1977]. EFs may influence ion transport and/or membrane potential locally around the cell [Jaffe and Nuccitelli, 1977]. Transmembrane proteins have also been shown to move along the membrane in the presence of EFs through putative electrophoresis mechanisms, potentially leading to the local recruitment or stabilization of downstream polarity factors [Poo and Robinson, 1977; Poo, 1981]. These EF effects may reflect the natural electrochemical organization of ion currents or

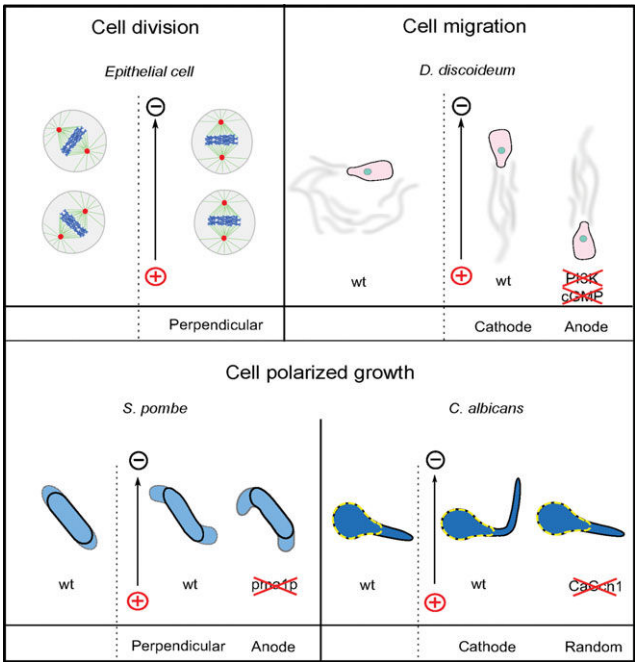

Fig. 3. Directing polarity with exogenous electric fields. A: EF-induced orientation of the division plane: Mitotic corneal epithelial cells position their division plane perpendicular to the EF direction. **B**: WT amoeba *D. discoideum* migrates to the cathode of an applied EF. Mutant cells deficient in the PI3K and cGMP pathway migrate to the anode. **C:** Polarized tip growth in WT fission yeast *S. pombe* cells reorients perpendicular to the EF, but *pma1-1* mutants with impaired proton pumping activity reorient to the anode. The pathogen yeast *C. albicans* grows hyphae to the cathode of the EF, a process that depends on the voltage gated Ca^{2+} channel CaCch1.

membrane domains around a single cell. Recent genetic characterization of such effects have begun to shed light on molecular mechanisms regulating polarity by external EFs and their relevance to natural polarity regulation.

Connections between EF signals and downstream cytoskeletal regulators, including the small GTPase cdc42, the Rho/Rac pathways, integrin signaling and phosphatidylinositol (PIP) signaling, have been suggested in different cellular systems [Pullar et al., 2006; Rajnicek et al., 2006; Zhao et al., 2006; Sato et al., 2009; Minc and Chang, 2010] (Fig. 4). During mammalian wound healing, neutrophils and keratinocytes wound-directed migration depends on PI3K and PTEN which, respectively, positively and negatively regulate PIP2 homeostasis [Zhao et al., 2002, 2006]. Wound-healing relies in part on endogenous EFs generated in the wound, and can be inhibited or accelerated by exogenous application of EFs pointing toward or away from the wound, respectively [Zhao et al., 2006]. In this electrotactic assay, exogenous EFs induce high and sustained phosphorylation of key signaling kinases including, ERK, p38, Src, and Akt. Mutants lacking the catalytic γ-subunit of the PI3K depict impaired activation of Akt and reduced phosphorylation

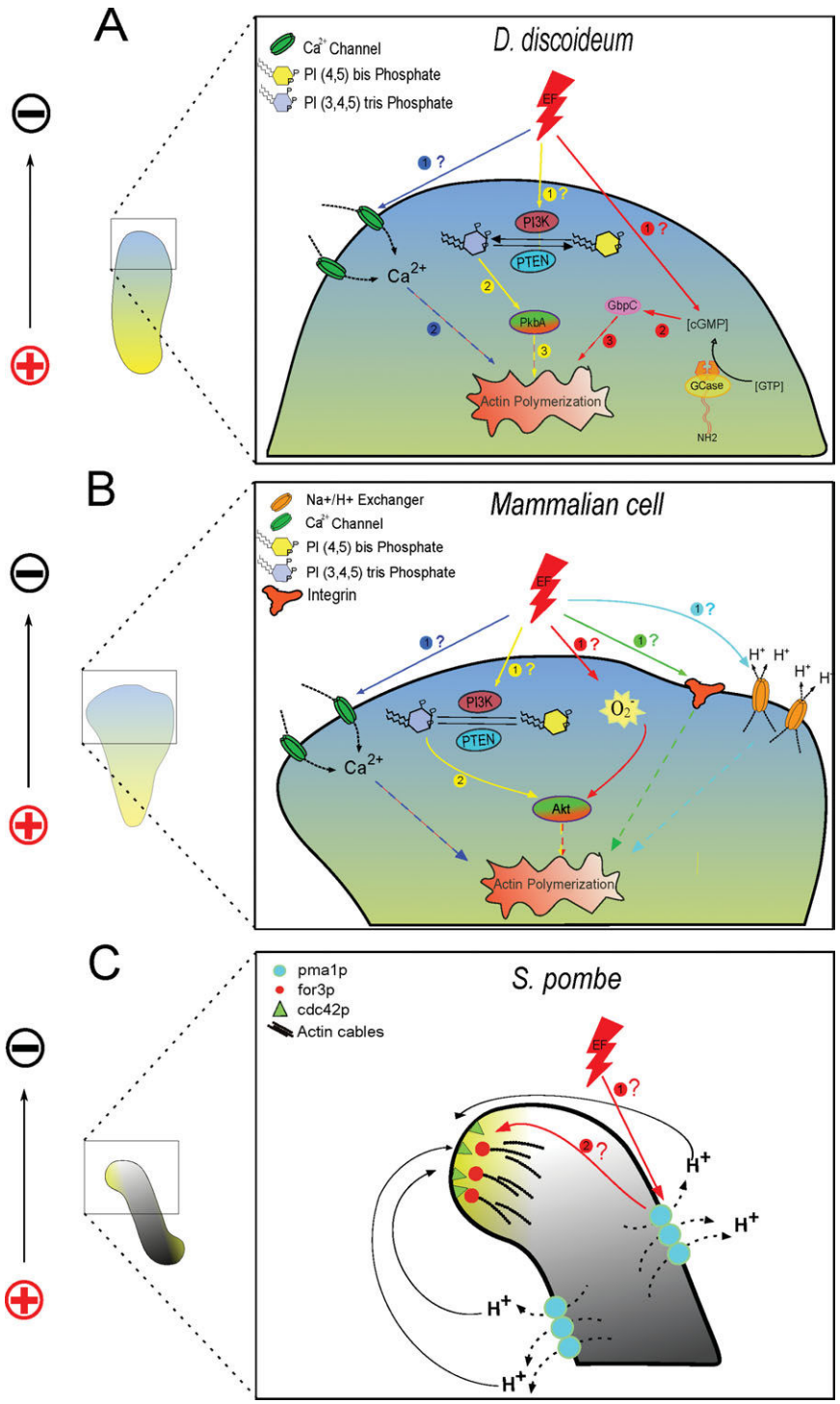

Fig. 4. Pathways regulating electrotactic responses in different cell types. A: *D. discoideum* migration toward the cathode of an exogenous EF involves at least two different pathways: The PI3 kinase and PTEN pathways that lead to a polarized distribution of PIP (in yellow); The cyclic GMP pathway (in red). Upstream EF sensors are not well characterized but Ca^{2+} signaling may be important in this process (in blue). Downstream effectors linking these pathways to actin polymerization may include the protein kinases PkbA and PakA. **B**: In mammalian cells, EF induced migration has been proposed to rely on different pathways. PIP signaling may be important for keratinocytes and neutrophils during wound responses (in yellow). Integrin signaling has been involved in keratinocytes electrotaxis (in green). ROS signaling may be important in cancer cell migration (in cyan). Upstream regulators of EF sensing may include NHE1 (in red), and calcium signaling, although links to downstream effectors are still lacking. Akt and PakA may link PIP and ROS signaling to actin polymerization machinery. **C**: In *S. pombe* cells, reorientation of polarized growth perpendicular to the EF depends on the formin for3p and the small GTPase cdc42p that both regulate polarized actin polymerization. The proton ATPase pump pma1p which regulates pH and is located on the side of the cell may establish putative transcellular proton currents and cortical pH gradients that transduce EF effects to for3p and cdc42p regulation.

of Src, p38, and ERK and display reduced electrotactic migration of neutrophils and keratinocytes and defective wound closure. Conversely, PTEN deletion enhances EF induced Akt and Src phosphorylation and directional migration, and accelerates wound healing. Thus, PIP signaling regulates electrotactic migration of cells in the wounded tissue and proper healing [Zhao, 2009]. It is interesting to note that PIP signaling is also regulating chemotaxis in these cell types. The downstream machinery required for directional migration is thus likely to be similar regardless of the nature of the spatial cue in this situation.

The amoebae *Dictyostelium discoideum* has been instrumental in dissecting molecular mechanisms of directional cell migration [Devreotes and Zigmond, 1988; Parent and Devreotes, 1996; Chen et al., 1996, 1997; Kim, et al. 1997]. When exposed to homogeneous concentrations of cyclic adenosine monophosphate (cAMP) these cells migrate in random directions. In the presence of small EFs, they orient their migration to the cathode of the EF within minutes of EF applications. This EF response is independent of upstream chemotactic receptors [Song et al., 2002]. Downstream signaling modules regulating directional cell migration for instance during chemotaxis include PIP and intracellular cyclic guanosine monophosphate (cGMP) signaling. These effectors promote actin polymerization at the leading edge for migration [Veltman and Van Haastert, 2006; Veltman et al., 2008]. In a recent work, Sato et al. tested the role of these signaling modules in electrotaxis [Sato et al., 2009]. Intracellular cGMP is produced mainly by two enzymes, soluble guanylyl cyclase (sGC) and guanylyl cyclase A (GCA). Mutants lacking the sGC and GCA (gca^-/sgc^-) and mutants lacking the cGMP-binding protein C (*gbpC*), which display reduced levels of cGMP, exhibited attenuated cathodal electrotactic migration. Similar phenotypes were obtained when PIP signaling was repressed through PI3-kinase inhibition. Strikingly, when both PIP2 synthesis and cGMP pathways were knocked down, cells migrated to the opposite direction, to the anode of the EF. These results suggest the existence of parallel pathways participating in regulating electrotaxis and put forward the existence of a third pathway promoting anodal migration [Sato et al., 2009]. sGC may have structural and spatial competing functions in this regulation, as expression of the C terminal catalytic domain of sCG which produces cGMP, can rescue the cathodal migration defects in gca^-/sgc^-cells, while expression of the N terminal domain of sCG which binds the actin cytoskeleton at the leading edge promotes anodal migration. These studies support the role of PIP signaling for electrotaxis in another organism, and provide detailed genetic characterization of the molecular mechanisms involved. Cross talk between EFs and polarity in these systems have been proposed to be mediated by calcium transport and membrane potential [Onuma and Hui, 1988; Pullar and Isseroff, 2005; Shanley et al., 2006; Gao et al., 2011] yet the details of this transduction remain to be established (Fig. 4B).

Reactive oxygen species (ROS) signaling may also mediate electrotactic responses. HT-1080 fibrosarcoma cells display EF-induced migration to the anode of the field and concomitant Superoxide (O_2^-) production [Li et al., 2012]. This O_2^- overproduction may induce the phosphorylation of ERK and downstream signaling components including p38 and AKT for directed migration. Cells overexpressing superoxide dismutase which transform O_2^- into hydrogen peroxide (H_2O_2) display impaired ERK1/2, p38, and AKT phosphorylation and impaired EF anodal migration. ROS signaling has been implicated in wound response to direct leukocytes migration to the wound and could thus represent another regulation layer mediating electrotactic response in this context [Niethammer et al., 2009].

Fungal cells and yeasts are model systems to dissect molecular mechanisms underlying polarity. These nonmigrating cells exhibit polarized growth which involves similar regulatory modules and conserved effectors as higher eukaryotes [Chang and Peter, 2003]. EFs may be present in natural fungal habitat and some fungi and molds have been suggested to target wounds by following ion currents and EFs [van West et al., 2002]. Ion transporters and membrane potential regulators are also widely shared between fungi and higher organisms. Most fungal cells display strong electrotropism (EF directed polarized growth) [Harold et al., 1985; McGillivray and Gow, 1986] (Fig. 3). During filamentous growth, the pathogen *Candida albicans* grows, for instance, its hyphae to the cathode of an exogenous EF [Crombie et al., 1990]. This orientation depends on Ca^{2+} transport mediated by the voltage gated Ca^{2+} channel CaCch1p [Brand et al., 2007]. Fission yeast cells which serve as excellent systems to study polarity [Chang and Martin, 2009], also display electrotactic behavior [Minc and Chang, 2010]. These cells which normally grow into a perfect rod-shape, reorient their growth axis to a direction perpendicular to an applied EF, creating cells with a bent morphology [Minc and Chang, 2010]. Candidate genetic screen for polarity regulators and membrane transporters suggest that this response depends on the formin for3p and the small GTPase cdc42p which regulate aspects of actin polymerization and polarity [Martin et al., 2007; Minc et al., 2009] and on pma1p, a conserved proton ATPase regulating intracellular pH. Surprisingly, mutants in these genes still orient to the EF but to the wrong direction, toward the anode of the EF. These results suggest a key role of pH regulation for proper actin polymerization in electrotactic responses and natural polarity regulation [Minc and Chang, 2010].

All together these genetic dissections in different organisms suggest downstream transduction of EF effects by small GTPase, lipid signaling, and actin regulation factors.

The cross talk between EF and these polarity modules remains to be clearly defined, although some transporters and ions have been specifically identified in these different systems. Calcium and pH regulation may play key roles in mediating EF effects into polarized reorganization of cytoskeletal regulators. Future experiments dissecting the molecular basis of exogenous EF effects are likely to generate novel fundamental understanding in general mechanisms regulating these effects.

Genetic studies in *Dictyostelium* and yeast begin to reveal why different cells may polarize to different directions, and suggest that multiple layer of polarity regulation may be spatially reorganized by EFs, with one predominant mode. When the dominant layer is turned off through mutation, the secondary mode takes over and directs polarity to another direction. These EF experiments are likely to reflect physiological events, in wound healing, neuron organization, and development. They may also begin to reveal the natural electrochemical regulation of polarity and cytoskeletal elements. In that view, the EF effect may bias or exacerbate an existing electrical organization, which yields the polarized reorientation in the EF. A specific cytoskeletal regulator may for instance naturally bind to portions of the plasma membrane with specific charges [Fairn et al., 2011; Das et al., 2012], and the EF-induced perturbation on the membrane potential and membrane charges would induce the relocation of this element to redirect polarity. It has long been a puzzle to understand how such small EFs which perturb only 1% of resting membrane potential could orient polarity in such a striking manner [Jaffe and Nuccitelli, 1977]. Positive feedbacks regulating polarization modules, cytoskeleton, and ion transport may begin to bring answers to these long lasting questions.

Many decades after initial suggestions for a role of "bioelectricity" in orchestrating cells and tissue behavior [Piccolino, 2000], novel functional data begin to unravel mechanisms for their importance in development, tissue architecture, and single cell polarity. Molecular mechanisms regulating and transducing electrochemical signals into cytoskeleton regulation are beginning to emerge, and future work should allow to draw more generic models, and to assess specificity in different cell-types and situations. Genetically encoded fluorescent sensors allowing to measure pH [Miesenbock et al., 1998] and recently developed sensors for quantitatively estimating membrane potential shall bring complementary information of electrochemical patterning in cells, tissues, and embryos [Kralj et al., 2011, 2012]. Optogenetics systems may also serve as powerful tools to locally control electrochemical cues at the level of tissues and cells [Fenno et al., 2011]. These optical tools shall bring important numbers and orders of magnitude that are still missing in the field. Other quantitative approaches, such as systems genetics, microfabrication, and modeling [Minc and Chang, 2010; Li and Lin, 2011], will likely help moving forward in dissecting the crosstalk between electrochemical and biochemical signaling for cell polarity.

Acknowledgments

The authors acknowledge Matthieu Piel for careful reading of the manuscript. N.M. acknowledges financial support from the Agence Nationale de la Recherche (ANR) "retour post-doctorants" grant ANR-10PDOC-003-01 and a European FP7-People-CIG grant. D.B. is supported by an Institut Curie PhD fellowship.

References

Adams DS, Masi A, Levin M. 2007. H+ pump-dependent changes in membrane voltage are an early mechanism necessary and sufficient to induce Xenopus tail regeneration. Development 134(7): 1323–1335.

Bachewich CL, Heath IB. 1997. The cytoplasmic pH influences hyphal tip growth and cytoskeleton-related organization. Fungal Genet Biol 21(1):76–91.

Beane WS, Morokuma J, Adams DS, Levin M. 2011. A chemical genetics approach reveals H,K-ATPase-mediated membrane voltage is required for planarian head regeneration. Chem Biol 18(1): 77–89.

Ben-Chaim Y, Chanda B, Dascal N, Bezanilla F, Parnas I, Parnas H. 2006. Movement of 'gating charge' is coupled to ligand binding in a G-protein-coupled receptor. Nature 444(7115):106–109.

Binggeli R, Weinstein RC. 1985. Deficits in elevating membrane potential of rat fibrosarcoma cells after cell contact. Cancer Res 45(1):235–241.

Binggeli R, Weinstein RC, Stevenson D. 1994. Calcium ion and the membrane potential of tumor cells. Cancer Biochem Biophys 14(3):201–210.

Blackiston DJ, McLaughlin KA, Levin M. 2009. Bioelectric controls of cell proliferation: ion channels, membrane voltage and the cell cycle. Cell Cycle 8(21):3519–3528.

Bohrmann J, Gutzeit H. 1987. Evidence against electrophoresis as the principal mode of protein transport in vitellogenic ovarian follicles of Drosophila. Development 101(2):279–288.

Brand A, Shanks S, Duncan VM, Yang M, Mackenzie K, Gow NA. 2007. Hyphal orientation of Candida albicans is regulated by a calcium-dependent mechanism. Curr Biol 17(4):347–352.

Cardone RA, Casavola V, Reshkin SJ. 2005. The role of disturbed pH dynamics and the Na+/H+ exchanger in metastasis. Nat Rev Cancer 5(10):786–795.

Chang F, Martin SG. 2009. Shaping fission yeast with microtubules. Cold Spring Harb Perspect Biol 1(1):a001347.

Chang F, Peter M. 2003. Yeasts make their mark. Nat Cell Biol 5(4):294–299.

Chen MY, Insall RH, Devreotes PN. 1996. Signaling through chemoattractant receptors in Dictyostelium. Trends Genet 12(2): 52–57.

Chen MY, Long Y, Devreotes PN. 1997. A novel cytosolic regulator, Pianissimo, is required for chemoattractant receptor and G protein-mediated activation of the 12 transmembrane domain adenylyl cyclase in Dictyostelium. Genes Dev 11(23):3218–3231.

Crombie T, Gow NA, Gooday GW. 1990. Influence of applied electrical fields on yeast and hyphal growth of Candida albicans. J Gen Microbiol 136(2):311–317.

Das A, Slaughter BD, Unruh JR, Bradford WD, Alexander R, Rubinstein B, Li R. 2012. Flippase-mediated phospholipid asymmetry promotes fast Cdc42 recycling in dynamic maintenance of cell polarity. Nat Cell Biol 14(3):304–310.

Denker SP, Barber DL. 2002a. Cell migration requires both ion translocation and cytoskeletal anchoring by the Na-H exchanger NHE1. J Cell Biol 159(6):1087–1096.

Denker SP, Barber DL. 2002b. Ion transport proteins anchor and regulate the cytoskeleton. Curr Opin Cell Biol 14(2):214–220.

Devreotes PN, Zigmond SH. 1988. Chemotaxis in eukaryotic cells: a focus on leukocytes and Dictyostelium. Annu Rev Cell Biol 4: 649–686.

Esser AT, Smith KC, Weaver JC, Levin M. 2006. Mathematical model of morphogen electrophoresis through gap junctions. Dev Dyn 235(8):2144–2159.

Etienne-Manneville S. 2004. Cdc42—the centre of polarity. J Cell Sci 117(Pt 8):1291–1300.

Fairn GD, Hermansson M, Somerharju P, Grinstein S. 2011. Phosphatidylserine is polarized and required for proper Cdc42 localization and for development of cell polarity. Nat Cell Biol 13(12): 1424–1430.

Feijo JA, Sainhas J, Hackett GR, Kunkel JG, Hepler PK. 1999. Growing pollen tubes possess a constitutive alkaline band in the clear zone and a growth-dependent acidic tip. J Cell Biol 144(3):483–496.

Fenno L, Yizhar O, Deisseroth K. 2011. The development and application of optogenetics. Annu Rev Neurosci 34:389–412.

Frantz C, Karydis A, Nalbant P, Hahn KM, Barber DL. 2007. Positive feedback between Cdc42 activity and H+ efflux by the Na-H exchanger NHE1 for polarity of migrating cells. J Cell Biol 179(3): 403–410.

Frantz C, Barreiro G, Dominguez L, Chen X, Eddy R, Condeelis J, Kelly MJ, Jacobson MP, Barber DL. 2008. Cofilin is a pH sensor for actin free barbed end formation: role of phosphoinositide binding. J Cell Biol 183(5):865–879.

Gao RC, Zhang XD, Sun YH, Kamimura Y, Mogilner A, Devreotes PN, Zhao M. 2011. Different roles of membrane potentials in electrotaxis and chemotaxis of dictyostelium cells. Eukaryot Cell 10(9): 1251–1256.

Gibbon BC, Kropf DL. 1994. Cytosolic pH gradients associated with tip growth. Science 263(5152):1419–1421.

Goodrich LV, Strutt D. 2011. Principles of planar polarity in animal development. Development 138(10):1877–1892.

Harold FM, Schreurs WJ, Harold RL, Caldwell JH. 1985. Electrobiology of fungal hyphae. Microbiol Sci 2(12):363–366.

Hermle T, Saltukoglu D, Grunewald J, Walz G, Simons M. 2010. Regulation of Frizzled-dependent planar polarity signaling by a V-ATPase subunit. Curr Biol 20(14):1269–1276.

Hermle T, Petzoldt AG, Simons M. 2011. The role of proton transporters in epithelial Wnt signaling pathways. Pediatr Nephrol 26(9):1523–1527.

Hollenhorst MI, Richter K, Fronius M. 2011. Ion transport by pulmonary epithelia. J Biomed Biotechnol 2011:174306.

Hooley R, Yu CY, Symons M, Barber DL. 1996. G alpha 13 stimulates Na+-H+ exchange through distinct Cdc42-dependent and RhoA-dependent pathways. J Biol Chem 271(11):6152–6158.

Hotary KB, Robinson KR. 1992. Evidence of a role for endogenous electrical fields in chick embryo development. Development 114(4): 985–996.

Inaba M, Yamanaka H, Kondo S. 2012. Pigment pattern formation by contact-dependent depolarization. Science 335(6069):677.

Iwashita M, Watanabe M, Ishii M, Chen T, Johnson SL, Kurachi Y, Okada N, Kondo S. 2006. Pigment pattern in jaguar/obelix zebrafish is caused by a Kir7.1 mutation: implications for the regulation of melanosome movement. PLoS Genet 2(11):e197.

Jaffe LF. 1977. Electrophoresis along cell membranes. Nature 265(5595):600–602.

Jaffe LF, Nuccitelli R. 1977. Electrical controls of development. Annu Rev Biophys Bioeng 6:445–476.

Kim JY, Caterina MJ, Milne JL, Lin KC, Borleis JA, Devreotes PN. 1997. Random mutagenesis of the cAMP chemoattractant receptor, cAR1, of Dictyostelium. Mutant classes that cause discrete shifts in agonist affinity and lock the receptor in a novel activational intermediate. J Biol Chem 272(4):2060–2068.

Kline D, Robinson KR, Nuccitelli R. 1983. Ion currents and membrane domains in the cleaving Xenopus egg. J Cell Biol 97(6): 1753–1761.

Kralj JM, Hochbaum DR, Douglass AD, Cohen AE. 2011. Electrical spiking in Escherichia coli probed with a fluorescent voltage-indicating protein. Science 333(6040):345–348.

Kralj JM, Douglass AD, Hochbaum DR, Maclaurin D, Cohen AE. 2012. Optical recording of action potentials in mammalian neurons using a microbial rhodopsin. Nat Methods 9(1):90–95.

Kucerova R, Walczysko P, Reid B, Ou J, Leiper LJ, Rajnicek AM, McCaig CD, Zhao M, Collinson JM. 2011. The role of electrical signals in murine corneal wound re-epithelialization. J Cell Physiol 226(6):1544–1553.

Levin M. 2009. Bioelectric mechanisms in regeneration: unique aspects and future perspectives. Semin Cell Dev Biol 20(5): 543–556.

Levin M. 2012. Molecular bioelectricity in developmental biology: new tools and recent discoveries: control of cell behavior and pattern formation by transmembrane potential gradients. Bioessays 34(3):205–217.

Levin M, Thorlin T, Robinson KR, Nogi T, Mercola M. 2002. Asymmetries in H+/K+-ATPase and cell membrane potentials comprise a very early step in left-right patterning. Cell 111(1): 77–89.

Li F, Wang H, Li L, Huang C, Lin J, Zhu G, Chen Z, Wu N, Feng H. 2012. Superoxide plays critical roles in electrotaxis of fibrosarcoma cells via activation of ERK and reorganization of the cytoskeleton. Free Radic Biol Med 52(9):1888–1896.

Li J, Lin F. 2011. Microfluidic devices for studying chemotaxis and electrotaxis. Trends Cell Biol 21(8):489–497.

Maderspacher F, Nusslein-Volhard C. 2003. Formation of the adult pigment pattern in zebrafish requires leopard and obelix dependent cell interactions. Development 130(15):3447–3457.

Magalhaes MA, Larson DR, Mader CC, Bravo-Cordero JJ, Gil-Henn H, Oser M, Chen X, Koleske AJ, Condeelis J. 2011. Cortactin phosphorylation regulates cell invasion through a pH-dependent pathway. J Cell Biol 195(5):903–920.

Marsh G, Beams HW. 1957. Electrical control of morphogenesis in regenerating Dugesia tigrina. J Cell Comp Physiol 39:191–211.

Martin SG, Rincon SA, Basu R, Perez P, Chang F. 2007. Regulation of the formin for3p by cdc42p and bud6p. Mol Biol Cell 18(10):4155–4167.

McCaig CD, Dover PJ. 1991. Factors influencing perpendicular elongation of embryonic frog muscle cells in a small applied electric field. J Cell Sci 98 (Pt 4):497–506.

McCaig CD, Rajnicek AM, Song B, Zhao M. 2005. Controlling cell behavior electrically: current views and future potential. Physiol Rev 85(3):943–978.

McGillivray AM, Gow NAR. 1986. Applied electrical fields polarize the growth of mycelial fungi. Journal of General Microbiology 132:2515–2525.

McLachlan GD, Cahill SM, Girvin ME, Almo SC. 2007. Acid-induced equilibrium folding intermediate of human platelet profilin. Biochemistry 46(23):6931–6943.

Miesenbock G, De Angelis DA, Rothman JE. 1998. Visualizing secretion and synaptic transmission with pH-sensitive green fluorescent proteins. Nature 394(6689):192–195.

Minc N, Chang F. 2010. Electrical control of cell polarization in the fission yeast Schizosaccharomyces pombe. Curr Biol 20(8): 710–716.

Minc N, Bratman SV, Basu R, Chang F. 2009. Establishing new sites of polarization by microtubules. Curr Biol 19(2):83–94.

Niethammer P, Grabher C, Look AT, Mitchison TJ. 2009. A tissue-scale gradient of hydrogen peroxide mediates rapid wound detection in zebrafish. Nature 459(7249):996–999.

Onuma EK, Hui SW. 1988. Electric field-directed cell shape changes, displacement, and cytoskeletal reorganization are calcium dependent. J Cell Biol 106(6):2067–2075.

Oser M, Yamaguchi H, Mader CC, Bravo-Cordero JJ, Arias M, Chen X, Desmarais V, van Rheenen J, Koleske AJ, Condeelis J. 2009. Cortactin regulates cofilin and N-WASp activities to control the stages of invadopodium assembly and maturation. J Cell Biol 186(4):571–587.

Pai VP, Aw S, Shomrat T, Lemire JM, Levin M. 2012. Transmembrane voltage potential controls embryonic eye patterning in Xenopus laevis. Development 139(2):313–323.

Parent CA, Devreotes PN. 1996. Molecular genetics of signal transduction in Dictyostelium. Annu Rev Biochem 65:411–440.

Piccolino M. 2000. The bicentennial of the Voltaic battery (1800–2000): the artificial electric organ. Trends Neurosci 23(4):147–151.

Poo M. 1981. In situ electrophoresis of membrane components. Annu Rev Biophys Bioeng 10:245–276.

Poo M, Robinson KR. 1977. Electrophoresis of concanavalin A receptors along embryonic muscle cell membrane. Nature 265(5595):602–605.

Prevarskaya N, Skryma R, Shuba Y. 2010. Ion channels and the hallmarks of cancer. Trends Mol Med 16(3):107–121.

Pullar CE, Isseroff RR. 2005. Cyclic AMP mediates keratinocyte directional migration in an electric field. J Cell Sci 118(Pt 9): 2023–2034.

Pullar CE, Baier BS, Kariya Y, Russell AJ, Horst BA, Marinkovich MP, Isseroff RR. 2006. beta4 integrin and epidermal growth factor coordinately regulate electric field-mediated directional migration via Rac1. Mol Biol Cell 17(11):4925–4935.

Rajnicek AM, McCaig CD, Gow NA. 1994. Electric fields induce curved growth of Enterobacter cloacae, Escherichia coli, and Bacillus subtilis cells: implications for mechanisms of galvanotropism and bacterial growth. J Bacteriol 176(3):702–713.

Rajnicek AM, Foubister LE, McCaig CD. 2006. Temporally and spatially coordinated roles for Rho, Rac, Cdc42 and their effectors in growth cone guidance by a physiological electric field. J Cell Sci 119(Pt 9):1723–1735.

Reid B, Zhao M. 2011. Measurement of bioelectric current with a vibrating probe. J Vis Exp 47.

Reid B, Nuccitelli R, Zhao M. 2007. Non-invasive measurement of bioelectric currents with a vibrating probe. Nat Protoc 2(3):661–669.

Robinson KR, Jaffe LF. 1975. Polarizing fucoid eggs drive a calcium current through themselves. Science 187(4171):70–72.

Sanders D, Hansen UP, Slayman CL. 1981. Role of the plasma membrane proton pump in pH regulation in non-animal cells. Proc Natl Acad Sci USA 78(9):5903–5907.

Sato MJ, Kuwayama H, van Egmond WN, Takayama AL, Takagi H, van Haastert PJ, Yanagida T, Ueda M. 2009. Switching direction in electric-signal-induced cell migration by cyclic guanosine monophosphate and phosphatidylinositol signaling. Proc Natl Acad Sci USA 106(16):6667–6672.

Schreurs WJ, Harold FM. 1988. Transcellular proton current in Achlya bisexualis hyphae: relationship to polarized growth. Proc Natl Acad Sci USA 85(5):1534–1538.

Segalen M, Bellaiche Y. 2009. Cell division orientation and planar cell polarity pathways. Semin Cell Dev Biol 20(8):972–977.

Shanley LJ, Walczysko P, Bain M, MacEwan DJ, Zhao M. 2006. Influx of extracellular Ca2+ is necessary for electrotaxis in Dictyostelium. J Cell Sci 119(Pt 22):4741–4748.

Simons M, Gault WJ, Gotthardt D, Rohatgi R, Klein TJ, Shao Y, Lee HJ, Wu AL, Fang Y, Satlin LM, et al. 2009. Electrochemical cues regulate assembly of the Frizzled/Dishevelled complex at the plasma membrane during planar epithelial polarization. Nat Cell Biol 11(3):286–294.

Song B, Zhao M, Forrester JV, McCaig CD. 2002. Electrical cues regulate the orientation and frequency of cell division and the rate of wound healing in vivo. Proc Natl Acad Sci USA 99(21): 13577–13582.

Srivastava J, Barreiro G, Groscurth S, Gingras AR, Goult BT, Critchley DR, Kelly MJ, Jacobson MP, Barber DL. 2008. Structural model and functional significance of pH-dependent talin-actin binding for focal adhesion remodeling. Proc Natl Acad Sci USA 105(38):14436–14441.

Szatkowski M, Mycielska M, Knowles R, Kho AL, Djamgoz MB. 2000. Electrophysiological recordings from the rat prostate gland in vitro: identified single-cell and transepithelial (lumen) potentials. BJU Int 86(9):1068–1075.

van West P, Morris BM, Reid B, Appiah AA, Osborne MC, Campbell TA, Shepherd SJ. 2002. Oomycete plant pathogens use electric fields to target roots. Mol Plant Microbe Interact 15(8): 790–798.

Veltman DM, Van Haastert PJ. 2006. Guanylyl cyclase protein and cGMP product independently control front and back of chemotaxing Dictyostelium cells. Mol Biol Cell 17(9):3921–3929.

Veltman DM, Keizer-Gunnik I, Van Haastert PJ. 2008. Four key signaling pathways mediating chemotaxis in Dictyostelium discoideum. J Cell Biol 180(4):747–753.

Villalba-Galea CA. 2012. New insights in the activity of voltage sensitive phosphatases. Cell Signal 24(8):1541–1547.

Weaver AM. 2006. Invadopodia: specialized cell structures for cancer invasion. Clin Exp Metastasis 23(2):97–105.

Webb BA, Chimenti M, Jacobson MP, Barber DL. 2011. Dysregulated pH: a perfect storm for cancer progression. Nat Rev Cancer 11(9):671–677.

Weick JP, Groth RD, Isaksen AL, Mermelstein PG. 2003. Interactions with PDZ proteins are required for L-type calcium channels to activate cAMP response element-binding protein-dependent gene expression. J Neurosci 23(8):3446–3456.

Weisenseel MH, Nuccitelli R, Jaffe LF. 1975. Large electrical currents traverse growing pollen tubes. J Cell Biol 66(3):556–567.

Wessel GM, Wong JL. 2009. Cell surface changes in the egg at fertilization. Mol Reprod Dev 76(10):942–953.

Woodruff RI, Telfer WH. 1980. Electrophoresis of proteins in intercellular bridges. Nature 286(5768):84–86.

Yeung T, Gilbert GE, Shi J, Silvius J, Kapus A, Grinstein S. 2008. Membrane phosphatidylserine regulates surface charge and protein localization. Science 319(5860):210–213.

Zhao M. 2009. Electrical fields in wound healing-An overriding signal that directs cell migration. Semin Cell Dev Biol 20(6):674–682.

Zhao M, Forrester JV, McCaig CD. 1999. A small, physiological electric field orients cell division. Proc Natl Acad Sci USA 96(9):4942–4946.

Zhao M, Pu J, Forrester JV, McCaig CD. 2002. Membrane lipids, EGF receptors, and intracellular signals colocalize and are polarized in epithelial cells moving directionally in a physiological electric field. FASEB J 16(8):857–859.

Zhao M, Song B, Pu J, Wada T, Reid B, Tai G, Wang F, Guo A, Walczysko P, Gu Y, et al. 2006. Electrical signals control wound healing through phosphatidylinositol-3-OH kinase-gamma and PTEN. Nature 442(7101):457–460.

BIBLIOGRAPHY

Aiba, H., Yamada, H., Ohmiya, R., and Mizuno, T. (1995). The osmo-inducible gpd1+ gene is a target of the signaling pathway involving Wis1 MAP-kinase kinase in fission yeast. FEBS Lett *376*, 199-201.

Akhshi, T.K., Wernike, D., and Piekny, A. (2014). Microtubules and actin crosstalk in cell migration and division. Cytoskeleton (Hoboken) *71*, 1-23.

Alberts B., J.A., Lewis A., Raff M., Roberts K., and Walter P. (2002). Molecular biology of the cell.

Altschuler, S.J., Angenent, S.B., Wang, Y., and Wu, L.F. (2008). On the spontaneous emergence of cell polarity. Nature *454*, 886-889.

Amberg, D.C. (1998). Three-dimensional imaging of the yeast actin cytoskeleton through the budding cell cycle. Mol Biol Cell *9*, 3259-3262.

Andrianopoulos, A. (2002). Control of morphogenesis in the human fungal pathogen Penicillium marneffei. Int J Med Microbiol *292*, 331-347.

Arellano, M., Cartagena-Lirola, H., Nasser Hajibagheri, M.A., Duran, A., and Henar Valdivieso, M. (2000). Proper ascospore maturation requires the chs1+ chitin synthase gene in Schizosaccharomyces pombe. Mol Microbiol *35*, 79-89.

Arellano, M., Coll, P.M., and Perez, P. (1999). RHO GTPases in the control of cell morphology, cell polarity, and actin localization in fission yeast. Microsc Res Tech *47*, 51-60.

Arellano, M., Duran, A., and Perez, P. (1996). Rho 1 GTPase activates the (1-3)beta-D-glucan synthase and is involved in Schizosaccharomyces pombe morphogenesis. EMBO J *15*, 4584-4591.

Arkowitz, R.A., and Iglesias, P.A. (2008). Basic principles of polarity establishment and maintenance. Conference on Mechanisms of Cell Polarity. EMBO Rep *9*, 847-852.

Asnacios, A., and Hamant, O. (2012). The mechanics behind cell polarity. Trends Cell Biol *22*, 584-591.

Bartnicki-Garcia, S. (1968). Cell wall chemistry, morphogenesis, and taxonomy of fungi. Annu Rev Microbiol *22*, 87-108.

Bastmeyer, M., Deising, H.B., and Bechinger, C. (2002). Force exertion in fungal infection. Annu Rev Biophys Biomol Struct *31*, 321-341.

Basu, R., Munteanu, E.L., and Chang, F. (2014). Role of turgor pressure in endocytosis in fission yeast. Mol Biol Cell *25*, 679-687.

Bendezu, F.O., and Martin, S.G. (2010). Actin cables and the exocyst form two independent morphogenesis pathways in the fission yeast. Molecular Biology of the Cell *22*, 44-53.

Bendezu, F.O., and Martin, S.G. (2011). Actin cables and the exocyst form two independent morphogenesis pathways in the fission yeast. Mol Biol Cell *22*, 44-53.

Bendezu, F.O., and Martin, S.G. (2012). Cdc42 oscillations in yeasts. Sci Signal *5*, pe53.

Bendezu, F.O., and Martin, S.G. (2013). Cdc42 explores the cell periphery for mate selection in fission yeast. Curr Biol *23*, 42-47.

Bendezu, F.O., Vincenzetti, V., and Martin, S.G. (2012). Fission yeast Sec3 and Exo70 are transported on actin cables and localize the exocyst complex to cell poles. PLoS One *7*, e40248.

Beneden, E.V. (1883). Recherches sur la maturation de l'oeuf et la fecondation. *Ascaris megalocephala*, Vol 4.

Billings, G., Ouzounov, N., Ursell, T., Desmarais, S.M., Shaevitz, J., Gitai, Z., and Huang, K.C. (2014). De novo morphogenesis in L-forms via geometric control of cell growth. Mol Microbiol *93*, 883-896.

Blaser, H., Reichman-Fried, M., Castanon, I., Dumstrei, K., Marlow, F.L., Kawakami, K., Solnica-Krezel, L., Heisenberg, C.P., and Raz, E. (2006). Migration of zebrafish primordial germ cells: a role for myosin contraction and cytoplasmic flow. Dev Cell *11*, 613-627.

Bonazzi, D., Julien, J.D., Romao, M., Seddiki, R., Piel, M., Boudaoud, A., and Minc, N. (2014). Symmetry breaking in spore germination relies on an interplay between polar cap stability and spore wall mechanics. Dev Cell *28*, 534-546.

Botts, M.R., Giles, S.S., Gates, M.A., Kozel, T.R., and Hull, C.M. (2009). Isolation and characterization of Cryptococcus neoformans spores reveal a critical role for capsule biosynthesis genes in spore biogenesis. Eukaryot Cell *8*, 595-605.

Boudaoud, A. (2003). Growth of walled cells: from shells to vesicles. Phys Rev Lett *91*, 018104.

Boyce, K.J., Hynes, M.J., and Andrianopoulos, A. (2005). The Ras and Rho GTPases genetically interact to co-ordinately regulate cell polarity during development in Penicillium marneffei. Mol Microbiol *55*, 1487-1501.

Brefeld, O. (1872). Untersuchungen aus dem Gesammtgebiete der Mykologie (Leipzig).

Bresch, C., Muller, G., and Egel, R. (1968). Genes involved in meiosis and sporulation of a yeast. Mol Gen Genet *102*, 301-306.

Briza, P., Ellinger, A., Winkler, G., and Breitenbach, M. (1988). Chemical composition of the yeast ascospore wall. The second outer layer consists of chitosan. J Biol Chem *263*, 11569-11574.

Briza, P., Winkler, G., Kalchhauser, H., and Breitenbach, M. (1986). Dityrosine is a prominent component of the yeast ascospore wall. A proof of its structure. J Biol Chem *261*, 4288-4294.

Brownlee, C., and Bouget, F.Y. (1998). Polarity determination in Fucus: from zygote to multicellular embryo. Semin Cell Dev Biol *9*, 179-185.

Brunner, D., and Nurse, P. (2000). New concepts in fission yeast morphogenesis. Philos Trans R Soc Lond B Biol Sci *355*, 873-877.

Bryant, D.M., and Mostov, K.E. (2008). From cells to organs: building polarized tissue. Nat Rev Mol Cell Biol *9*, 887-901.

Bush, D.A., Horisberger, M., Horman, I., and Wursch, P. (1974). The wall structure of Schizosaccharomyces pombe. J Gen Microbiol *81*, 199-206.

Bushart, T.J., and Roux, S.J. (2007). Conserved features of germination and polarized cell growth: a few insights from a pollen-fern spore comparison. Ann Bot *99*, 9-17.

Calonge, T.M., Nakano, K., Arellano, M., Arai, R., Katayama, S., Toda, T., Mabuchi, I., and Perez, P. (2000). Schizosaccharomyces pombe rho2p GTPase regulates cell wall alpha-glucan biosynthesis through the protein kinase pck2p. Mol Biol Cell *11*, 4393-4401.

Campas, O., and Mahadevan, L. (2009). Shape and dynamics of tip-growing cells. Curr Biol *19*, 2102-2107.

Campetelli, A., Bonazzi, D., and Minc, N. (2012). Electrochemical regulation of cell polarity and the cytoskeleton. Cytoskeleton (Hoboken) *69*, 601-612.

Campos, M., Surovtsev, I.V., Kato, S., Paintdakhi, A., Beltran, B., Ebmeier, S.E., and Jacobs-Wagner, C. (2014). A constant size extension drives bacterial cell size homeostasis. Cell *159*, 1433-1446.

Cano, R.J., and Borucki, M.K. (1995). Revival and identification of bacterial spores in 25- to 40-million-year-old Dominican amber. Science *268*, 1060-1064.

Cao, L.G., and Wang, Y.L. (1990). Mechanism of the formation of contractile ring in dividing cultured animal cells. I. Recruitment of preexisting actin filaments into the cleavage furrow. J Cell Biol *110*, 1089-1095.

Castagnetti, S., Behrens, R., and Nurse, P. (2005). End4/Sla2 is involved in establishment of a new growth zone in Schizosaccharomyces pombe. J Cell Sci *118*, 1843-1850.

Chan, Y.F., and Chow, T.C. (1990). Ultrastructural observations on Penicillium marneffei in natural human infection. Ultrastruct Pathol *14*, 439-452.

Chang, E., Bartholomeusz, G., Pimental, R., Chen, J., Lai, H., Wang, L., Yang, P., and Marcus, S. (1999). Direct binding and In vivo regulation of the fission yeast p21-activated kinase shk1 by the SH3 domain protein scd2. Mol Cell Biol *19*, 8066-8074.

Chang, F., and Huang, K. (2014). How and why cells grow as rods. BMC Biol *12*, 54.

Chang, F., and Martin, S.G. (2009). Shaping fission yeast with microtubules. Cold Spring Harb Perspect Biol *1*, a001347.

Chang, F., and Minc, N. (2014). Electrochemical control of cell and tissue polarity. Annu Rev Cell Dev Biol *30*, 317-336.

Chant, J., and Pringle, J.R. (1995). Patterns of bud-site selection in the yeast Saccharomyces cerevisiae. J Cell Biol *129*, 751-765.

Cheng, J., Park, T.S., Fischl, A.S., and Ye, X.S. (2001). Cell cycle progression and cell polarity require sphingolipid biosynthesis in Aspergillus nidulans. Mol Cell Biol *21*, 6198-6209.

Christodoulidou, A., Briza, P., Ellinger, A., and Bouriotis, V. (1999). Yeast ascospore wall assembly requires two chitin deacetylase isozymes. FEBS Lett *460*, 275-279.

Clark, A.G., Wartlick, O., Salbreux, G., and Paluch, E.K. (2014). Stresses at the cell surface during animal cell morphogenesis. Curr Biol *24*, R484-494.

Coll, P.M., Rincon, S.A., Izquierdo, R.A., and Perez, P. (2007). Hob3p, the fission yeast ortholog of human BIN3, localizes Cdc42p to the division site and regulates cytokinesis. EMBO J *26*, 1865-1877.

Coluccio, A., Bogengruber, E., Conrad, M.N., Dresser, M.E., Briza, P., and Neiman, A.M. (2004). Morphogenetic pathway of spore wall assembly in Saccharomyces cerevisiae. Eukaryot Cell *3*, 1464-1475.

Coluccio, A., and Neiman, A.M. (2004). Interspore bridges: a new feature of the Saccharomyces cerevisiae spore wall. Microbiology *150*, 3189-3196.

Coluccio, A.E., Rodriguez, R.K., Kernan, M.J., and Neiman, A.M. (2008). The yeast spore wall enables spores to survive passage through the digestive tract of Drosophila. PLoS One *3*, e2873.

Corellou, F., Coelho, S.M., Bouget, F.Y., and Brownlee, C. (2005). Spatial re-organisation of cortical microtubules in vivo during polarisation and asymmetric division of Fucus zygotes. J Cell Sci *118*, 2723-2734.

Cortes, J.C., Carnero, E., Ishiguro, J., Sanchez, Y., Duran, A., and Ribas, J.C. (2005). The novel fission yeast (1,3)beta-D-glucan synthase catalytic subunit Bgs4p is essential during both cytokinesis and polarized growth. J Cell Sci *118*, 157-174.

Cortes, J.C., Ishiguro, J., Duran, A., and Ribas, J.C. (2002). Localization of the (1,3)beta-D-glucan synthase catalytic subunit homologue Bgs1p/Cps1p from fission yeast suggests that it is

involved in septation, polarized growth, mating, spore wall formation and spore germination. J Cell Sci *115*, 4081-4096.

Cosgrove, D. (1986). Biophysical control of plant cell growth. Annu Rev Plant Physiol *37*, 377-405.

Cosgrove, D.J. (2005). Growth of the plant cell wall. Nat Rev Mol Cell Biol *6*, 850-861.

Cottrell, S.F., Getz, G.S., and Rabinowitz, M. (1981). Phospholipid accumulation during the cell cycle in synchronous cultures of the yeast, Saccharomyces cerevisiae. J Biol Chem *256*, 10973-10978.

Cowan, C.R., and Hyman, A.A. (2004). Centrosomes direct cell polarity independently of microtubule assembly in C. elegans embryos. Nature *431*, 92-96.

Csikasz-Nagy, A., Gyorffy, B., Alt, W., Tyson, J.J., and Novak, B. (2008). Spatial controls for growth zone formation during the fission yeast cell cycle. Yeast *25*, 59-69.

Dague, E., Alsteens, D., Latge, J.P., and Dufrene, Y.F. (2008). High-resolution cell surface dynamics of germinating Aspergillus fumigatus conidia. Biophys J *94*, 656-660.

Dalous, J., Burghardt, E., Muller-Taubenberger, A., Bruckert, F., Gerisch, G., and Bretschneider, T. (2008). Reversal of cell polarity and actin-myosin cytoskeleton reorganization under mechanical and chemical stimulation. Biophys J *94*, 1063-1074.

Daniel, R.A., and Errington, J. (2003). Control of cell morphogenesis in bacteria: two distinct ways to make a rod-shaped cell. Cell *113*, 767-776.

Das, M., Drake, T., Wiley, D.J., Buchwald, P., Vavylonis, D., and Verde, F. (2012). Oscillatory dynamics of Cdc42 GTPase in the control of polarized growth. Science *337*, 239-243.

Das, M., and Verde, F. (2013). Role of Cdc42 dynamics in the control of fission yeast cell polarization. Biochem Soc Trans *41*, 1745-1749.

Das, M., Wiley, D.J., Chen, X., Shah, K., and Verde, F. (2009). The conserved NDR kinase Orb6 controls polarized cell growth by spatial regulation of the small GTPase Cdc42. Curr Biol *19*, 1314-1319.

Das, M., Wiley, D.J., Medina, S., Vincent, H.A., Larrea, M., Oriolo, A., and Verde, F. (2007). Regulation of cell diameter, For3p localization, and cell symmetry by fission yeast Rho-GAP Rga4p. Mol Biol Cell *18*, 2090-2101.

de Groot, P.W., Yin, Q.Y., Weig, M., Sosinska, G.J., Klis, F.M., and de Koster, C.G. (2007). Mass spectrometric identification of covalently bound cell wall proteins from the fission yeast Schizosaccharomyces pombe. Yeast *24*, 267-278.

de Medina-Redondo, M., Arnaiz-Pita, Y., Fontaine, T., Del Rey, F., Latge, J.P., and Vazquez de Aldana, C.R. (2008). The beta-1,3-glucanosyltransferase gas4p is essential for ascospore wall maturation and spore viability in Schizosaccharomyces pombe. Mol Microbiol *68*, 1283-1299.

DeBiasio, R.L., LaRocca, G.M., Post, P.L., and Taylor, D.L. (1996). Myosin II transport, organization, and phosphorylation: evidence for cortical flow/solation-contraction coupling during cytokinesis and cell locomotion. Mol Biol Cell *7*, 1259-1282.

Dekker, N., van Rijssel, J., Distel, B., and Hochstenbach, F. (2007). Role of the alpha-glucanase Agn2p in ascus-wall endolysis following sporulation in fission yeast. Yeast *24*, 279-288.

Di Talia, S., Skotheim, J.M., Bean, J.M., Siggia, E.D., and Cross, F.R. (2007). The effects of molecular noise and size control on variability in the budding yeast cell cycle. Nature *448*, 947-951.

Diego-Taboada, A., Beckett, S.T., Atkin, S.L., and Mackenzie, G. (2014). Hollow pollen shells to enhance drug delivery. Pharmaceutics *6*, 80-96.

Dodgson, J., Chessel, A., Yamamoto, M., Vaggi, F., Cox, S., Rosten, E., Albrecht, D., Geymonat, M., Csikasz-Nagy, A., Sato, M.*, et al.* (2013). Spatial segregation of polarity factors into distinct cortical clusters is required for cell polarity control. Nat Commun *4*, 1834.

Drake, T., and Vavylonis, D. (2013). Model of fission yeast cell shape driven by membrane-bound growth factors and the cytoskeleton. PLoS Comput Biol *9*, e1003287.

Drgonova, J., Drgon, T., Tanaka, K., Kollar, R., Chen, G.C., Ford, R.A., Chan, C.S., Takai, Y., and Cabib, E. (1996). Rho1p, a yeast protein at the interface between cell polarization and morphogenesis. Science *272*, 277-279.

Drubin, D.G., and Nelson, W.J. (1996). Origins of cell polarity. Cell *84*, 335-344.

du Roure, O., Saez, A., Buguin, A., Austin, R.H., Chavrier, P., Silberzan, P., and Ladoux, B. (2005). Force mapping in epithelial cell migration. Proc Natl Acad Sci U S A *102*, 2390-2395.

Dumetre, A., Dubey, J.P., Ferguson, D.J., Bongrand, P., Azas, N., and Puech, P.H. (2013). Mechanics of the Toxoplasma gondii oocyst wall. Proc Natl Acad Sci U S A *110*, 11535-11540.

Dyer, J.M., Savage, N.S., Jin, M., Zyla, T.R., Elston, T.C., and Lew, D.J. (2013). Tracking shallow chemical gradients by actin-driven wandering of the polarization site. Curr Biol *23*, 32-41.

Edamatsu, M., and Toyoshima, Y.Y. (2003). Fission yeast synaptobrevin is involved in cytokinesis and cell elongation. Biochem Biophys Res Commun *301*, 641-645.

Endo, M., Shirouzu, M., and Yokoyama, S. (2003). The Cdc42 binding and scaffolding activities of the fission yeast adaptor protein Scd2. J Biol Chem *278*, 843-852.

Engler, A.J., Sen, S., Sweeney, H.L., and Discher, D.E. (2006). Matrix elasticity directs stem cell lineage specification. Cell *126*, 677-689.

Estravis, M., Rincon, S.A., Santos, B., and Perez, P. (2011). Cdc42 regulates multiple membrane traffic events in fission yeast. Traffic *12*, 1744-1758.

Etienne-Manneville, S. (2004). Cdc42--the centre of polarity. J Cell Sci *117*, 1291-1300.

Etienne-Manneville, S., and Hall, A. (2002). Rho GTPases in cell biology. Nature *420*, 629-635.

Fairn, G.D., Hermansson, M., Somerharju, P., and Grinstein, S. (2011). Phosphatidylserine is polarized and required for proper Cdc42 localization and for development of cell polarity. Nat Cell Biol *13*, 1424-1430.

Fang, T.H., Kang, S.H., Hong, Z.H., and Wu, C.D. (2012). Elasticity and nanomechanical response of Aspergillus niger spores using atomic force microscopy. Micron *43*, 407-411.

Fares, H., Goetsch, L., and Pringle, J.R. (1996). Identification of a developmentally regulated septin and involvement of the septins in spore formation in Saccharomyces cerevisiae. J Cell Biol *132*, 399-411.

Farge, E. (2003). Mechanical induction of Twist in the Drosophila foregut/stomodeal primordium. Curr Biol *13*, 1365-1377.

Fay, J.C., and Benavides, J.A. (2005). Evidence for domesticated and wild populations of Saccharomyces cerevisiae. PLoS Genet *1*, 66-71.

Feierbach, B., and Chang, F. (2001). Roles of the fission yeast formin for3p in cell polarity, actin cable formation and symmetric cell division. Curr Biol *11*, 1656-1665.

Felder, T., Bogengruber, E., Tenreiro, S., Ellinger, A., Sa-Correia, I., and Briza, P. (2002). Dtrlp, a multidrug resistance transporter of the major facilitator superfamily, plays an essential role in spore wall maturation in Saccharomyces cerevisiae. Eukaryot Cell *1*, 799-810.

Flor-Parra, I., Bernal, M., Zhurinsky, J., and Daga, R.R. (2014). Cell migration and division in amoeboid-like fission yeast. Biol Open *3*, 108-115.

Freisinger, T., Klunder, B., Johnson, J., Muller, N., Pichler, G., Beck, G., Costanzo, M., Boone, C., Cerione, R.A., Frey, E.*, et al.* (2013). Establishment of a robust single axis of cell polarity by coupling multiple positive feedback loops. Nat Commun *4*, 1807.

Frieser, S.H., Hlubek, A., Sandrock, B., and Bolker, M. (2011). Cla4 kinase triggers destruction of the Rac1-GEF Cdc24 during polarized growth in Ustilago maydis. Mol Biol Cell *22*, 3253-3262.

Fu, Y., Gu, Y., Zheng, Z., Wasteneys, G., and Yang, Z. (2005). Arabidopsis interdigitating cell growth requires two antagonistic pathways with opposing action on cell morphogenesis. Cell *120*, 687-700.

Fukuda, K., Yamada, K., Deoka, K., Yamashita, S., Ohta, A., and Horiuchi, H. (2009). Class III chitin synthase ChsB of Aspergillus nidulans localizes at the sites of polarized cell wall synthesis and is required for conidial development. Eukaryot Cell *8*, 945-956.

Fukui, Y., Kaziro, Y., and Yamamoto, M. (1986). Mating pheromone-like diffusible factor released by Schizosaccharomyces pombe. EMBO J *5*, 1991-1993.

Fukunishi, K., Miyakubi, K., Hatanaka, M., Otsuru, N., Hirata, A., Shimoda, C., and Nakamura, T. (2014). The fission yeast spore is coated by a proteinaceous surface layer comprising mainly Isp3. Mol Biol Cell *25*, 1549-1559.

Gachet, Y., and Hyams, J.S. (2005). Endocytosis in fission yeast is spatially associated with the actin cytoskeleton during polarised cell growth and cytokinesis. J Cell Sci *118*, 4231-4242.

Garcia, I., Tajadura, V., Martin, V., Toda, T., and Sanchez, Y. (2006). Synthesis of alpha-glucans in fission yeast spores is carried out by three alpha-glucan synthase paralogues, Mok12p, Mok13p and Mok14p. Mol Microbiol *59*, 836-853.

Gauthier, N.C., Fardin, M.A., Roca-Cusachs, P., and Sheetz, M.P. (2011). Temporary increase in plasma membrane tension coordinates the activation of exocytosis and contraction during cell spreading. Proc Natl Acad Sci U S A *108*, 14467-14472.

Gerhart, J., Danilchik, M., Doniach, T., Roberts, S., Rowning, B., and Stewart, R. (1989). Cortical rotation of the Xenopus egg: consequences for the anteroposterior pattern of embryonic dorsal development. Development *107 Suppl*, 37-51.

Gierer, A., and Meinhardt, H. (1972). A theory of biological pattern formation. Kybernetik *12*, 30-39.

Goehring, N.W., and Grill, S.W. (2013). Cell polarity: mechanochemical patterning. Trends Cell Biol *23*, 72-80.

Goehring, N.W., Trong, P.K., Bois, J.S., Chowdhury, D., Nicola, E.M., Hyman, A.A., and Grill, S.W. (2011). Polarization of PAR proteins by advective triggering of a pattern-forming system. Science *334*, 1137-1141.

Goldstein, B., and Macara, I.G. (2007). The PAR proteins: fundamental players in animal cell polarization. Dev Cell *13*, 609-622.

Goriely, A., and Tabor, M. (2003). Self-similar tip growth in filamentary organisms. Phys Rev Lett *90*, 108101.

Goryachev, A.B., and Pokhilko, A.V. (2008). Dynamics of Cdc42 network embodies a Turing-type mechanism of yeast cell polarity. FEBS Lett *582*, 1437-1443.

Gouin, E., Welch, M.D., and Cossart, P. (2005). Actin-based motility of intracellular pathogens. Curr Opin Microbiol *8*, 35-45.

Gow, N.A., Brown, A.J., and Odds, F.C. (2002). Fungal morphogenesis and host invasion. Curr Opin Microbiol *5*, 366-371.

Graml, V., Studera, X., Lawson, J.L., Chessel, A., Geymonat, M., Bortfeld-Miller, M., Walter, T., Wagstaff, L., Piddini, E., and Carazo-Salas, R.E. (2014). A genomic Multiprocess survey of machineries that control and link cell shape, microtubule organization, and cell-cycle progression. Dev Cell *31*, 227-239.

Grindstaff, K.K., Yeaman, C., Anandasabapathy, N., Hsu, S.C., Rodriguez-Boulan, E., Scheller, R.H., and Nelson, W.J. (1998). Sec6/8 complex is recruited to cell-cell contacts and specifies transport vesicle delivery to the basal-lateral membrane in epithelial cells. Cell *93*, 731-740.

Gupta, S., and McCollum, D. (2011). Crosstalk between NDR kinase pathways coordinates cell cycle dependent actin rearrangements. Cell Div *6*, 19.

Hamant, O., Heisler, M.G., Jonsson, H., Krupinski, P., Uyttewaal, M., Bokov, P., Corson, F., Sahlin, P., Boudaoud, A., Meyerowitz, E.M.*, et al.* (2008). Developmental patterning by mechanical signals in Arabidopsis. Science *322*, 1650-1655.

Han, K.H., and Prade, R.A. (2002). Osmotic stress-coupled maintenance of polar growth in Aspergillus nidulans. Mol Microbiol *43*, 1065-1078.

Harigaya, Y., and Yamamoto, M. (2007). Molecular mechanisms underlying the mitosis-meiosis decision. Chromosome Res *15*, 523-537.

Harold, F.M. (1990). To shape a cell: an inquiry into the causes of morphogenesis of microorganisms. Microbiol Rev *54*, 381-431.

Harold, F.M. (1991). Biochemical topology: from vectorial metabolism to morphogenesis. Biosci Rep *11*, 347-382; discussion 382-345.

Harold, F.M. (2002). Force and compliance: rethinking morphogenesis in walled cells. Fungal Genet Biol *37*, 271-282.

Hartwell, L.H. (1971). Genetic control of the cell division cycle in yeast. IV. Genes controlling bud emergence and cytokinesis. Exp Cell Res *69*, 265-276.

Hartwell, L.H. (1974). Saccharomyces cerevisiae cell cycle. Bacteriol Rev *38*, 164-198.

Hatanaka, M., and Shimoda, C. (2001). The cyclic AMP/PKA signal pathway is required for initiation of spore germination in Schizosaccharomyces pombe. Yeast *18*, 207-217.

Hatschek, B. (1888). Lehrbuch der Zoologie : eine morphologische Übersicht des Thierreiches zur Einführung in das Studium dieser Wissenschaft.

Hayles, J., and Nurse, P. (2001). A journey into space. Nat Rev Mol Cell Biol *2*, 647-656.

Hayles, J., Wood, V., Jeffery, L., Hoe, K.L., Kim, D.U., Park, H.O., Salas-Pino, S., Heichinger, C., and Nurse, P. (2013). A genome-wide resource of cell cycle and cell shape genes of fission yeast. Open Biol *3*, 130053.

He, B., and Guo, W. (2009). The exocyst complex in polarized exocytosis. Curr Opin Cell Biol *21*, 537-542.

Heckman, D.S., Geiser, D.M., Eidell, B.R., Stauffer, R.L., Kardos, N.L., and Hedges, S.B. (2001). Molecular evidence for the early colonization of land by fungi and plants. Science *293*, 1129-1133.

Heidenhain, M. (1893). Uber kern und protoplasma.

Heisenberg, C.P., and Bellaiche, Y. (2013). Forces in tissue morphogenesis and patterning. Cell *153*, 948-962.

Herman, P.K., and Rine, J. (1997). Yeast spore germination: a requirement for Ras protein activity during re-entry into the cell cycle. EMBO J *16*, 6171-6181.

Hird, S.N., and White, J.G. (1993). Cortical and cytoplasmic flow polarity in early embryonic cells of Caenorhabditis elegans. J Cell Biol *121*, 1343-1355.

Hochstenbach, F., Klis, F.M., van den Ende, H., van Donselaar, E., Peters, P.J., and Klausner, R.D. (1998). Identification of a putative alpha-glucan synthase essential for cell wall construction and morphogenesis in fission yeast. Proc Natl Acad Sci U S A *95*, 9161-9166.

Hohmann, S. (2002). Osmotic stress signaling and osmoadaptation in yeasts. Microbiol Mol Biol Rev *66*, 300-372.

Homble, F., and Leonetti, M. (2007). Emergence of symmetry breaking in fucoid zygotes. Trends Plant Sci *12*, 253-259.

Horio, T., and Oakley, B.R. (2005). The role of microtubules in rapid hyphal tip growth of Aspergillus nidulans. Mol Biol Cell *16*, 918-926.

Houk, A.R., Jilkine, A., Mejean, C.O., Boltyanskiy, R., Dufresne, E.R., Angenent, S.B., Altschuler, S.J., Wu, L.F., and Weiner, O.D. (2012). Membrane tension maintains cell polarity by confining signals to the leading edge during neutrophil migration. Cell *148*, 175-188.

Houk, A.R., Millius, A., and Weiner, O.D. (2009). Compete globally, bud locally. Cell *139*, 656-658.

Howard, J., Grill, S.W., and Bois, J.S. (2011). Turing's next steps: the mechanochemical basis of morphogenesis. Nat Rev Mol Cell Biol *12*, 392-398.

Howard, R.J., Ferrari, M.A., Roach, D.H., and Money, N.P. (1991). Penetration of hard substrates by a fungus employing enormous turgor pressures. Proc Natl Acad Sci U S A *88*, 11281-11284.

Howell, A.S., Jin, M., Wu, C.F., Zyla, T.R., Elston, T.C., and Lew, D.J. (2012). Negative feedback enhances robustness in the yeast polarity establishment circuit. Cell *149*, 322-333.

Howell, A.S., Savage, N.S., Johnson, S.A., Bose, I., Wagner, A.W., Zyla, T.R., Nijhout, H.F., Reed, M.C., Goryachev, A.B., and Lew, D.J. (2009). Singularity in polarization: rewiring yeast cells to make two buds. Cell *139*, 731-743.

Huang, S., and Ingber, D.E. (2005). Cell tension, matrix mechanics, and cancer development. Cancer Cell *8*, 175-176.

Huxley, H.E. (1957). The double array of filaments in cross-striated muscle. J Biophys Biochem Cytol *3*, 631-648.

Huxley, H.E. (1969). The mechanism of muscular contraction. Science *164*, 1356-1365.

Hwang, J.U., Gu, Y., Lee, Y.J., and Yang, Z. (2005). Oscillatory ROP GTPase activation leads the oscillatory polarized growth of pollen tubes. Mol Biol Cell *16*, 5385-5399.

Iden S, C.J. (2008). Crosstalk between small GTPases and polarity proteins in cell polarization

Nat Rev Mol Cell Biol *9*, 846-859.

Iden, S., and Collard, J.G. (2008). Crosstalk between small GTPases and polarity proteins in cell polarization. Nature Reviews Molecular Cell Biology *9*, 846-859.

Irazoqui, J.E., Gladfelter, A.S., and Lew, D.J. (2003). Scaffold-mediated symmetry breaking by Cdc42p. Nat Cell Biol *5*, 1062-1070.

Ishiguro, J. (1998). Genetic control of fission yeast cell wall synthesis: the genes involved in wall biogenesis and their interactions in Schizosaccharomyces pombe. Genes Genet Syst *73*, 181-191.

Jeffries, P., Robinson-Boyer, L., Rice, P., Newsam, R.J., and Dodd, J.C. (2007). Ultrastructure of spore development in Scutellospora heterogama. Mycorrhiza *17*, 395-403.

Johnson, J.M., Jin, M., and Lew, D.J. (2011). Symmetry breaking and the establishment of cell polarity in budding yeast. Curr Opin Genet Dev *21*, 740-746.

Jose, M., Tollis, S., Nair, D., Sibarita, J.B., and McCusker, D. (2013). Robust polarity establishment occurs via an endocytosis-based cortical corralling mechanism. J Cell Biol *200*, 407-418.

Joseph-Strauss, D., Zenvirth, D., Simchen, G., and Barkai, N. (2007). Spore germination in Saccharomyces cerevisiae: global gene expression patterns and cell cycle landmarks. Genome Biol *8*, R241.

Jun, S., and Taheri-Araghi, S. (2015). Cell-size maintenance: universal strategy revealed. Trends Microbiol *23*, 4-6.

Kelly, F.D., and Nurse, P. (2011a). De novo growth zone formation from fission yeast spheroplasts. PLoS One *6*, e27977.

Kelly, F.D., and Nurse, P. (2011b). Spatial control of Cdc42 activation determines cell width in fission yeast. Mol Biol Cell *22*, 3801-3811.

Kemphues, K.J., Kusch, M., and Wolf, N. (1988). Maternal-effect lethal mutations on linkage group II of Caenorhabditis elegans. Genetics *120*, 977-986.

Kirschner, M., and Mitchison, T. (1986). Beyond self-assembly: from microtubules to morphogenesis. Cell *45*, 329-342.

Kishida, M., and Shimoda, C. (1986). Genetic mapping of eleven spo genes essential for ascospore formation in the fission yeast Schizosaccharomyces pombe. Curr Genet *10*, 443-447.

Knop, M., and Strasser, K. (2000). Role of the spindle pole body of yeast in mediating assembly of the prospore membrane during meiosis. EMBO J *19*, 3657-3667.

Koch, A.L. (2001). Bacterial Growth and Form.

Kondo, S., and Miura, T. (2010). Reaction-diffusion model as a framework for understanding biological pattern formation. Science *329*, 1616-1620.

Kono, K., Matsunaga, R., Hirata, A., Suzuki, G., Abe, M., and Ohya, Y. (2005). Involvement of actin and polarisome in morphological change during spore germination of Saccharomyces cerevisiae. Yeast *22*, 129-139.

Kono, K., Saeki, Y., Yoshida, S., Tanaka, K., and Pellman, D. (2012). Proteasomal degradation resolves competition between cell polarization and cellular wound healing. Cell *150*, 151-164.

Kopecka, M., Fleet, G.H., and Phaff, H.J. (1995). Ultrastructure of the cell wall of Schizosaccharomyces pombe following treatment with various glucanases. J Struct Biol *114*, 140-152.

Kortholt, A., Keizer-Gunnink, I., Kataria, R., and Van Haastert, P.J. (2013). Ras activation and symmetry breaking during Dictyostelium chemotaxis. J Cell Sci *126*, 4502-4513.

Kovar, D.R., Sirotkin, V., and Lord, M. (2011). Three's company: the fission yeast actin cytoskeleton. Trends Cell Biol *21*, 177-187.

Kozubowski, L., Saito, K., Johnson, J.M., Howell, A.S., Zyla, T.R., and Lew, D.J. (2008). Symmetry-breaking polarization driven by a Cdc42p GEF-PAK complex. Curr Biol *18*, 1719-1726.

Kuo, C.C., Savage, N.S., Chen, H., Wu, C.F., Zyla, T.R., and Lew, D.J. (2014). Inhibitory GEF phosphorylation provides negative feedback in the yeast polarity circuit. Curr Biol *24*, 753-759.

Layton, A.T., Savage, N.S., Howell, A.S., Carroll, S.Y., Drubin, D.G., and Lew, D.J. (2011). Modeling vesicle traffic reveals unexpected consequences for Cdc42p-mediated polarity establishment. Curr Biol *21*, 184-194.

Lecuit, T., and Lenne, P.F. (2007). Cell surface mechanics and the control of cell shape, tissue patterns and morphogenesis. Nat Rev Mol Cell Biol *8*, 633-644.

Lecuit, T., Lenne, P.F., and Munro, E. (2011). Force generation, transmission, and integration during cell and tissue morphogenesis. Annu Rev Cell Dev Biol *27*, 157-184.

Li, C.H., Cervantes, M., Springer, D.J., Boekhout, T., Ruiz-Vazquez, R.M., Torres-Martinez, S.R., Heitman, J., and Lee, S.C. (2011). Sporangiospore size dimorphism is linked to virulence of Mucor circinelloides. PLoS Pathog *7*, e1002086.

Li, J., Ning, Y., Hedley, W., Saunders, B., Chen, Y., Tindill, N., Hannay, T., and Subramaniam, S. (2002). The Molecule Pages database. Nature *420*, 716-717.

Li, R., and Bowerman, B. (2010). Symmetry breaking in biology. Cold Spring Harb Perspect Biol *2*, a003475.

Li R, G.G. (2008). Beyond polymer polarity: how the cytoskeleton builds a polarized cell. Nat Rev Mol Cell Biol *9*, 860-873.

Li, R., and Gundersen, G.G. (2008). Beyond polymer polarity: how the cytoskeleton builds a polarized cell. Nat Rev Mol Cell Biol *9*, 860-873.

Lichius, A., Berepiki, A., and Read, N.D. (2011). Form follows function -- the versatile fungal cytoskeleton. Fungal Biol *115*, 518-540.

Lichius, A., Goryachev, A.B., Fricker, M.D., Obara, B., Castro-Longoria, E., and Read, N.D. (2014). CDC-42 and RAC-1 regulate opposite chemotropisms in Neurospora crassa. J Cell Sci *127*, 1953-1965.

Lindner, P. (1893). Schizosaccharomyces Pombe n. sp., ein neuer Gährungserreger. Wochenschrift für Brauerei *10*, 1298-1300.

Liu, J., Tang, X., Wang, H., and Balasubramanian, M. (2000). Bgs2p, a 1,3-beta-glucan synthase subunit, is essential for maturation of ascospore wall in Schizosaccharomyces pombe. FEBS Lett *478*, 105-108.

Lo Presti, L., Chang, F., and Martin, S.G. (2012). Myosin Vs organize actin cables in fission yeast. Mol Biol Cell *23*, 4579-4591.

Lockhart, J.A. (1965). An analysis of irreversible plant cell elongation. J Theor Biol *8*, 264-275.

Lynn, R.R., and Magee, P.T. (1970). Development of the spore wall during ascospore formation in Saccharomyces cerevisiae. J Cell Biol *44*, 688-692.

Madden, K., and Snyder, M. (1992). Specification of sites for polarized growth in Saccharomyces cerevisiae and the influence of external factors on site selection. Mol Biol Cell *3*, 1025-1035.

Maeda, Y., Kashiwazaki, J., Shimoda, C., and Nakamura, T. (2009). The Schizosaccharomyces pombe syntaxin 1 homolog, Psy1, is essential in the development of the forespore membrane. Biosci Biotechnol Biochem *73*, 339-345.

Marco, E., Wedlich-Soldner, R., Li, R., Altschuler, S.J., and Wu, L.F. (2007). Endocytosis optimizes the dynamic localization of membrane proteins that regulate cortical polarity. Cell *129*, 411-422.

Marks, J., Hagan, I.M., and Hyams, J.S. (1986). Growth polarity and cytokinesis in fission yeast: the role of the cytoskeleton. J Cell Sci Suppl *5*, 229-241.

Marshall, W.F. (2011). Origins of cellular geometry. BMC Biol *9*, 57.

Marshall, W.F., Young, K.D., Swaffer, M., Wood, E., Nurse, P., Kimura, A., Frankel, J., Wallingford, J., Walbot, V., Qu, X.*, et al.* (2012). What determines cell size? BMC Biol *10*, 101.

Martin, S.G., and Berthelot-Grosjean, M. (2009). Polar gradients of the DYRK-family kinase Pom1 couple cell length with the cell cycle. Nature *459*, 852-856.

Martin, S.G., and Chang, F. (2005). New end take off: regulating cell polarity during the fission yeast cell cycle. Cell Cycle *4*, 1046-1049.

Martin, S.G., Rincon, S.A., Basu, R., Perez, P., and Chang, F. (2007). Regulation of the formin for3p by cdc42p and bud6p. Mol Biol Cell *18*, 4155-4167.

Martin, V., Garcia, B., Carnero, E., Duran, A., and Sanchez, Y. (2003). Bgs3p, a putative 1,3-beta-glucan synthase subunit, is required for cell wall assembly in Schizosaccharomyces pombe. Eukaryot Cell *2*, 159-169.

Martin, V., Ribas, J.C., Carnero, E., Duran, A., and Sanchez, Y. (2000). bgs2+, a sporulation-specific glucan synthase homologue is required for proper ascospore wall maturation in fission yeast. Mol Microbiol *38*, 308-321.

Mata, J., Lyne, R., Burns, G., and Bahler, J. (2002). The transcriptional program of meiosis and sporulation in fission yeast. Nat Genet *32*, 143-147.

Mata, J., and Nurse, P. (1997). tea1 and the microtubular cytoskeleton are important for generating global spatial order within the fission yeast cell. Cell *89*, 939-949.

Matsuo, Y., Fisher, E., Patton-Vogt, J., and Marcus, S. (2007). Functional characterization of the fission yeast phosphatidylserine synthase gene, pps1, reveals novel cellular functions for phosphatidylserine. Eukaryot Cell *6*, 2092-2101.

Matsuo, Y., Tanaka, K., Matsuda, H., and Kawamukai, M. (2005). cda1+, encoding chitin deacetylase is required for proper spore formation in Schizosaccharomyces pombe. FEBS Lett *579*, 2737-2743.

Matsuo, Y., Tanaka, K., Nakagawa, T., Matsuda, H., and Kawamukai, M. (2004). Genetic analysis of chs1+ and chs2+ encoding chitin synthases from Schizosaccharomyces pombe. Biosci Biotechnol Biochem *68*, 1489-1499.

Meinhardt, H., and Gierer, A. (1974). Applications of a theory of biological pattern formation based on lateral inhibition. J Cell Sci *15*, 321-346.

Meinhardt, H., and Gierer, A. (2000). Pattern formation by local self-activation and lateral inhibition. Bioessays *22*, 753-760.

Meitinger, F., Khmelinskii, A., Morlot, S., Kurtulmus, B., Palani, S., Andres-Pons, A., Hub, B., Knop, M., Charvin, G., and Pereira, G. (2014). A memory system of negative polarity cues prevents replicative aging. Cell *159*, 1056-1069.

Mellman, I., and Nelson, W.J. (2008). Coordinated protein sorting, targeting and distribution in polarized cells. Nature Reviews Molecular Cell Biology *9*, 833-845.

Merlini, L., Dudin, O., and Martin, S.G. (2013). Mate and fuse: how yeast cells do it. Open Biol *3*, 130008.

Minc, N., Boudaoud, A., and Chang, F. (2009a). Mechanical Forces of Fission Yeast Growth. Current Biology *19*, 1096-1101.

Minc, N., Bratman, S.V., Basu, R., and Chang, F. (2009b). Establishing new sites of polarization by microtubules. Curr Biol *19*, 83-94.

Minc, N., and Chang, F. (2010). Electrical control of cell polarization in the fission yeast Schizosaccharomyces pombe. Curr Biol *20*, 710-716.

Mirabet, V., Das, P., Boudaoud, A., and Hamant, O. (2011). The role of mechanical forces in plant morphogenesis. Annu Rev Plant Biol *62*, 365-385.

Mitchell, P. (1963). Molecule, group and electron translocation through natural membranes. Biochem Soc Symp *22*, 142-169.

Mitchison, J.M., and Nurse, P. (1985). Growth in cell length in the fission yeast Schizosaccharomyces pombe. J Cell Sci *75*, 357-376.

Mitrossilis, D., Fouchard, J., Pereira, D., Postic, F., Richert, A., Saint-Jean, M., and Asnacios, A. (2010). Real-time single-cell response to stiffness. Proc Natl Acad Sci U S A *107*, 16518-16523.

Mogilner A, O.G. (1996). Cell motility driven by actin polymerisation. Biophys J *71*, 3030-3045.

Monshausen, G.B., and Gilroy, S. (2009). Feeling green: mechanosensing in plants. Trends Cell Biol *19*, 228-235.

Mori, Y., Jilkine, A., and Edelstein-Keshet, L. (2008). Wave-pinning and cell polarity from a bistable reaction-diffusion system. Biophys J *94*, 3684-3697.

Moseley, J.B., Mayeux, A., Paoletti, A., and Nurse, P. (2009). A spatial gradient coordinates cell size and mitotic entry in fission yeast. Nature *459*, 857-860.

Munro, E., Nance, J., and Priess, J.R. (2004). Cortical flows powered by asymmetrical contraction transport PAR proteins to establish and maintain anterior-posterior polarity in the early C. elegans embryo. Dev Cell *7*, 413-424.

Nakamura, T., Abe, H., Hirata, A., and Shimoda, C. (2004). ADAM family protein Mde10 is essential for development of spore envelopes in the fission yeast Schizosaccharomyces pombe. Eukaryot Cell *3*, 27-39.

Nakaseko, Y., Niwa, O., and Yanagida, M. (1984). A meiotic mutant of the fission yeast Schizosaccharomyces pombe that produces mature asci containing two diploid spores. J Bacteriol *157*, 334-336.

Neiman, A.M. (1998). Prospore membrane formation defines a developmentally regulated branch of the secretory pathway in yeast. J Cell Biol *140*, 29-37.

Neiman, A.M. (2005). Ascospore formation in the yeast Saccharomyces cerevisiae. Microbiol Mol Biol Rev *69*, 565-584.

Nelson, W.J. (2003). Adaptation of core mechanisms to generate cell polarity. Nature *422*, 766-774.

Nurse, P. (1975). Genetic control of cell size at cell division in yeast. Nature *256*, 547-551.

O'Rourke, S.M., Herskowitz, I., and O'Shea, E.K. (2002). Yeast go the whole HOG for the hyperosmotic response. Trends Genet *18*, 405-412.

Oda, Y., and Fukuda, H. (2012). Initiation of cell wall pattern by a Rho- and microtubule-driven symmetry breaking. Science *337*, 1333-1336.

Orlando, K., and Guo, W. (2009). Membrane Organization and Dynamics in Cell Polarity. Cold Spring Harbor Perspectives in Biology *1*, a001321-a001321.

Orr, A.W., Helmke, B.P., Blackman, B.R., and Schwartz, M.A. (2006). Mechanisms of mechanotransduction. Dev Cell *10*, 11-20.

Osherov, N., and May, G.S. (2001). The molecular mechanisms of conidial germination. FEMS Microbiol Lett *199*, 153-160.

Osumi, M. (2012). Visualization of yeast cells by electron microscopy. J Electron Microsc (Tokyo) *61*, 343-365.

Osumi, M., Sato, M., Ishijima, S.A., Konomi, M., Takagi, T., and Yaguchi, H. (1998). Dynamics of cell wall formation in fission yeast, Schizosaccharomyces pombe. Fungal Genet Biol *24*, 178-206.

Ozbudak, E.M., Becskei, A., and van Oudenaarden, A. (2005). A system of counteracting feedback loops regulates Cdc42p activity during spontaneous cell polarization. Dev Cell *9*, 565-571.

Pahlman, A.K., Granath, K., Ansell, R., Hohmann, S., and Adler, L. (2001). The yeast glycerol 3-phosphatases Gpp1p and Gpp2p are required for glycerol biosynthesis and differentially involved in the cellular responses to osmotic, anaerobic, and oxidative stress. J Biol Chem *276*, 3555-3563.

Paluch, E., Piel, M., Prost, J., Bornens, M., and Sykes, C. (2005). Cortical actomyosin breakage triggers shape oscillations in cells and cell fragments. Biophys J *89*, 724-733.

Paluch, E., Sykes, C., Prost, J., and Bornens, M. (2006a). Dynamic modes of the cortical actomyosin gel during cell locomotion and division. Trends Cell Biol *16*, 5-10.

Paluch, E., van der Gucht, J., and Sykes, C. (2006b). Cracking up: symmetry breaking in cellular systems. J Cell Biol *175*, 687-692.

Pan, K.Z., Saunders, T.E., Flor-Parra, I., Howard, M., and Chang, F. (2014). Cortical regulation of cell size by a sizer cdr2p. Elife *3*, e02040.

Park, H.O., and Bi, E. (2007). Central roles of small GTPases in the development of cell polarity in yeast and beyond. Microbiol Mol Biol Rev *71*, 48-96.

Perez, P., and Ribas, J.C. (2004). Cell wall analysis. Methods *33*, 245-251.

Perez, P., and Rincon, S.A. (2010). Rho GTPases: regulation of cell polarity and growth in yeasts. Biochem J *426*, 243-253.

Podila, G.K., Rogers, L.M., and Kolattukudy, P.E. (1993). Chemical Signals from Avocado Surface Wax Trigger Germination and Appressorium Formation in Colletotrichum gloeosporioides. Plant Physiol *103*, 267-272.

Pollard, T.D., and Borisy, G.G. (2003). Cellular motility driven by assembly and disassembly of actin filaments. Cell *112*, 453-465.

Pollard, T.D., and Cooper, J.A. (1986). Actin and actin-binding proteins. A critical evaluation of mechanisms and functions. Annu Rev Biochem *55*, 987-1035.

Proctor, S.A., Minc, N., Boudaoud, A., and Chang, F. (2012). Contributions of turgor pressure, the contractile ring, and septum assembly to forces in cytokinesis in fission yeast. Curr Biol *22*, 1601-1608.

Pruyne, D., Gao, L., Bi, E., and Bretscher, A. (2004). Stable and dynamic axes of polarity use distinct formin isoforms in budding yeast. Mol Biol Cell *15*, 4971-4989.

Qadota, H., Python, C.P., Inoue, S.B., Arisawa, M., Anraku, Y., Zheng, Y., Watanabe, T., Levin, D.E., and Ohya, Y. (1996). Identification of yeast Rho1p GTPase as a regulatory subunit of 1,3-beta-glucan synthase. Science *272*, 279-281.

Qin, Y., and Yang, Z. (2011). Rapid tip growth: insights from pollen tubes. Semin Cell Dev Biol *22*, 816-824.

Rabl, C. (1885). Über Zelltheilung.

Ragni, E., Coluccio, A., Rolli, E., Rodriguez-Pena, J.M., Colasante, G., Arroyo, J., Neiman, A.M., and Popolo, L. (2007). GAS2 and GAS4, a pair of developmentally regulated genes required for spore wall assembly in Saccharomyces cerevisiae. Eukaryot Cell *6*, 302-316.

Ram, A.F., Kapteyn, J.C., Montijn, R.C., Caro, L.H., Douwes, J.E., Baginsky, W., Mazur, P., van den Ende, H., and Klis, F.M. (1998). Loss of the plasma membrane-bound protein Gas1p in Saccharomyces cerevisiae results in the release of beta1,3-glucan into the medium and induces a compensation mechanism to ensure cell wall integrity. J Bacteriol *180*, 1418-1424.

Repass, S.L., Brady, R.J., and O'Halloran, T.J. (2007). Dictyostelium Hip1r contributes to spore shape and requires epsin for phosphorylation and localization. J Cell Sci *120*, 3977-3988.

Riquelme, M., Reynaga-Pena, C.G., Gierz, G., and Bartnicki-Garcia, S. (1998). What determines growth direction in fungal hyphae? Fungal Genet Biol *24*, 101-109.

Rojas, E., Theriot, J.A., and Huang, K.C. (2014). Response of Escherichia coli growth rate to osmotic shock. Proc Natl Acad Sci U S A *111*, 7807-7812.

Rojas, E.R., Hotton, S., and Dumais, J. (2011). Chemically mediated mechanical expansion of the pollen tube cell wall. Biophys J *101*, 1844-1853.

Rotrosen, D., Edwards, J.E., Jr., Gibson, T.R., Moore, J.C., Cohen, A.H., and Green, I. (1985). Adherence of Candida to cultured vascular endothelial cells: mechanisms of attachment and endothelial cell penetration. J Infect Dis *152*, 1264-1274.

Rudall, P.J., and Bateman, R.M. (2007). Developmental bases for key innovations in the seed-plant microgametophyte. Trends Plant Sci *12*, 317-326.

Sahin, O., Yong, E.H., Driks, A., and Mahadevan, L. (2012). Physical basis for the adaptive flexibility of Bacillus spore coats. J R Soc Interface *9*, 3156-3160.

Salbreux, G., Charras, G., and Paluch, E. (2012). Actin cortex mechanics and cellular morphogenesis. Trends Cell Biol *22*, 536-545.

Santo, L.Y., and Doi, R.H. (1974). Ultrastructural analysis during germination and outgrowth of Bacillus subtilis spores. J Bacteriol *120*, 475-481.

Savage, N.S., Layton, A.T., and Lew, D.J. (2012). Mechanistic mathematical model of polarity in yeast. Mol Biol Cell *23*, 1998-2013.

Sawin, K.E. (2009). Cell cycle: Cell division brought down to size. Nature *459*, 782-783.

Schaechter, M., Maaloe, O., and Kjeldgaard, N.O. (1958). Dependency on medium and temperature of cell size and chemical composition during balanced grown of Salmonella typhimurium. J Gen Microbiol *19*, 592-606.

Seale, T. (1973). Life cycle of Neurospora crassa viewed by scanning electron microscopy. J Bacteriol *113*, 1015-1025.

Sharifmoghadam, M.R., de Leon, N., Hoya, M., Curto, M.A., and Valdivieso, M.H. (2010). Different steps of sexual development are differentially regulated by the Sec8p and Exo70p exocyst subunits. FEMS Microbiol Lett *305*, 71-80.

Shimoda, C. (2004). Forespore membrane assembly in yeast: coordinating SPBs and membrane trafficking. J Cell Sci *117*, 389-396.

Siegrist, S.E., and Doe, C.Q. (2007). Microtubule-induced cortical cell polarity. Genes Dev *21*, 483-496.

Slaughter, B., and Li, R. (2006). Toward a molecular interpretation of the surface stress theory for yeast morphogenesis. Curr Opin Cell Biol *18*, 47-53.

Slaughter, B.D., Smith, S.E., and Li, R. (2009). Symmetry breaking in the life cycle of the budding yeast. Cold Spring Harb Perspect Biol *1*, a003384.

Slaughter, B.D., Unruh, J.R., Das, A., Smith, S.E., Rubinstein, B., and Li, R. (2013). Non-uniform membrane diffusion enables steady-state cell polarization via vesicular trafficking. Nat Commun *4*, 1380.

Sleigh, M.A. (1973). Biology of Protozoa (Cambridge, UK: Cambridge University Press).

Smith, A.E., Zhang, Z., Thomas, C.R., Moxham, K.E., and Middelberg, A.P. (2000). The mechanical properties of Saccharomyces cerevisiae. Proc Natl Acad Sci U S A *97*, 9871-9874.

Smith, L.G., and Oppenheimer, D.G. (2005). Spatial control of cell expansion by the plant cytoskeleton. Annu Rev Cell Dev Biol *21*, 271-295.

Suda, Y., Rodriguez, R.K., Coluccio, A.E., and Neiman, A.M. (2009). A screen for spore wall permeability mutants identifies a secreted protease required for proper spore wall assembly. PLoS One *4*, e7184.

Suwannasai, N., Whalley, M.A., Whalley, A.J., Thienhirun, S., and Sihanonth, P. (2012). Ascus apical apparatus and ascospore characters in Xylariaceae. IMA Fungus *3*, 125-133.

Swift, J., Ivanovska, I.L., Buxboim, A., Harada, T., Dingal, P.C., Pinter, J., Pajerowski, J.D., Spinler, K.R., Shin, J.W., Tewari, M.*, et al.* (2013). Nuclear lamin-A scales with tissue stiffness and enhances matrix-directed differentiation. Science *341*, 1240104.

Tanaka, K., and Hirata, A. (1982). Ascospore development in the fission yeasts Schizosaccharomyces pombe and S. japonicus. J Cell Sci *56*, 263-279.

Tatebe, H., Nakano, K., Maximo, R., and Shiozaki, K. (2008). Pom1 DYRK regulates localization of the Rga4 GAP to ensure bipolar activation of Cdc42 in fission yeast. Curr Biol *18*, 322-330.

Taylor, J.W., and Berbee, M.L. (2006). Dating divergences in the Fungal Tree of Life: review and new analyses. Mycologia *98*, 838-849.

TerBush, D.R., Maurice, T., Roth, D., and Novick, P. (1996). The Exocyst is a multiprotein complex required for exocytosis in Saccharomyces cerevisiae. EMBO J *15*, 6483-6494.

Terenna, C.R., Makushok, T., Velve-Casquillas, G., Baigl, D., Chen, Y., Bornens, M., Paoletti, A., Piel, M., and Tran, P.T. (2008). Physical mechanisms redirecting cell polarity and cell shape in fission yeast. Curr Biol *18*, 1748-1753.

Thanbichler, M., and Shapiro, L. (2006). MipZ, a spatial regulator coordinating chromosome segregation with cell division in Caulobacter. Cell *126*, 147-162.

Thompson, D.W. (1945). On Growth and Form (Cambridge : University Press ; New York : Macmillan).

Thomson, D.D., Wehmeier, S., Byfield, F.J., Janmey, P.A., Caballero-Lima, D., Crossley, A., and Brand, A.C. (2014). Contact-induced apical asymmetry drives the thigmotropic responses of Candida albicans hyphae. Cell Microbiol.

Ting, A.E., Hazuka, C.D., Hsu, S.C., Kirk, M.D., Bean, A.J., and Scheller, R.H. (1995). rSec6 and rSec8, mammalian homologs of yeast proteins essential for secretion. Proc Natl Acad Sci U S A *92*, 9613-9617.

Tran, P.T., Marsh, L., Doye, V., Inoue, S., and Chang, F. (2001). A mechanism for nuclear positioning in fission yeast based on microtubule pushing. J Cell Biol *153*, 397-411.

Tucker, S.L., and Talbot, N.J. (2001). Surface attachment and pre-penetration stage development by plant pathogenic fungi. Annu Rev Phytopathol *39*, 385-417.

Turing, A.M. (1990). The chemical basis of morphogenesis. 1953. Bull Math Biol *52*, 153-197; discussion 119-152.

Turner, J.J., Ewald, J.C., and Skotheim, J.M. (2012). Cell size control in yeast. Curr Biol *22*, R350-359.

Ursell, T.S., Nguyen, J., Monds, R.D., Colavin, A., Billings, G., Ouzounov, N., Gitai, Z., Shaevitz, J.W., and Huang, K.C. (2014). Rod-like bacterial shape is maintained by feedback between cell curvature and cytoskeletal localization. Proc Natl Acad Sci U S A *111*, E1025-1034.

Uyttewaal, M., Traas, J., and Hamant, O. (2010). Integrating physical stress, growth, and development. Curr Opin Plant Biol *13*, 46-52.

Vale, R.D. (1987). Intracellular transport using microtubule-based motors. Annu Rev Cell Biol *3*, 347-378.

Vallee, R.B., and Shpetner, H.S. (1990). Motor proteins of cytoplasmic microtubules. Annu Rev Biochem *59*, 909-932.

van der Gucht, J., and Sykes, C. (2009). Physical Model of Cellular Symmetry Breaking. Cold Spring Harbor Perspectives in Biology *1*, a001909-a001909.

Van Etten, J.L., Bulla, L.A., Jr., and St Julian, G. (1974). Physiological and morphological correlation of Rhizopus stolonifer spore germination. J Bacteriol *117*, 882-887.

Verde, F., Mata, J., and Nurse, P. (1995). Fission yeast cell morphogenesis: identification of new genes and analysis of their role during the cell cycle. J Cell Biol *131*, 1529-1538.

Villar-Tajadura, M.A., Coll, P.M., Madrid, M., Cansado, J., Santos, B., and Perez, P. (2008). Rga2 is a Rho2 GAP that regulates morphogenesis and cell integrity in S. pombe. Mol Microbiol *70*, 867-881.

Walkinshaw, C.H., Hyde, J.M., and van Zandt, J. (1967). Fine structure of quiescent and germinating aeciospores of Cronartium fusiforme. J Bacteriol *94*, 245-254.

Wallar, B.J., and Alberts, A.S. (2003). The formins: active scaffolds that remodel the cytoskeleton. Trends Cell Biol *13*, 435-446.

Wedlich-Soldner, R. (2014). A longer life for yeast with good memory. Dev Cell *31*, 391-392.

Wedlich-Soldner, R., Altschuler, S., Wu, L., and Li, R. (2003). Spontaneous cell polarization through actomyosin-based delivery of the Cdc42 GTPase. Science *299*, 1231-1235.

Wedlich-Soldner, R., and Li, R. (2003). Spontaneous cell polarization: undermining determinism. Nat Cell Biol *5*, 267-270.

Wedlich-Soldner, R., Wai, S.C., Schmidt, T., and Li, R. (2004). Robust cell polarity is a dynamic state established by coupling transport and GTPase signaling. J Cell Biol *166*, 889-900.

Wellman, C.H., and Gray, J. (2000). The microfossil record of early land plants. Philos Trans R Soc Lond B Biol Sci *355*, 717-731; discussion 731-712.

Wendland, J. (2001). Comparison of morphogenetic networks of filamentous fungi and yeast. Fungal Genet Biol *34*, 63-82.

Wendland, J., and Philippsen, P. (2000). Determination of cell polarity in germinated spores and hyphal tips of the filamentous ascomycete Ashbya gossypii requires a rhoGAP homolog. J Cell Sci *113 (Pt 9)*, 1611-1621.

Wendland, J., and Philippsen, P. (2001). Cell polarity and hyphal morphogenesis are controlled by multiple rho-protein modules in the filamentous ascomycete Ashbya gossypii. Genetics *157*, 601-610.

Westphal, A.J., Price, P.B., Leighton, T.J., and Wheeler, K.E. (2003). Kinetics of size changes of individual Bacillus thuringiensis spores in response to changes in relative humidity. Proc Natl Acad Sci U S A *100*, 3461-3466.

Wilson, E.B. (1896). The Cell in Development and Inheritance.

Wodarz, A., and Nathke, I. (2007). Cell polarity in development and cancer. Nat Cell Biol *9*, 1016-1024.

Wood, V., Gwilliam, R., Rajandream, M.A., Lyne, M., Lyne, R., Stewart, A., Sgouros, J., Peat, N., Hayles, J., Baker, S.*, et al.* (2002). The genome sequence of Schizosaccharomyces pombe. Nature *415*, 871-880.

Wu, C.F., and Lew, D.J. (2013). Beyond symmetry-breaking: competition and negative feedback in GTPase regulation. Trends Cell Biol.

Yamaoka, T., Imada, K., Fukunishi, K., Yamasaki, Y., Shimoda, C., and Nakamura, T. (2013). The fission yeast synaptobrevin ortholog Syb1 plays an important role in forespore membrane formation and spore maturation. Eukaryot Cell *12*, 1162-1170.

Yao, X., Jericho, M., Pink, D., and Beveridge, T. (1999). Thickness and elasticity of gram-negative murein sacculi measured by atomic force microscopy. J Bacteriol *181*, 6865-6875.

Zajac, A., Sun, X., Zhang, J., and Guo, W. (2005). Cyclical regulation of the exocyst and cell polarity determinants for polarized cell growth. Mol Biol Cell *16*, 1500-1512.

Zhao, L., Schaefer, D., and Marten, M.R. (2005). Assessment of elasticity and topography of Aspergillus nidulans spores via atomic force microscopy. Appl Environ Microbiol *71*, 955-960.